Proceedings of International Conference on

POWER OF ARTIFICIAL INTELLIGENCE AND MACHINE LEARNING FOR HUMAN EMPOWERMENT

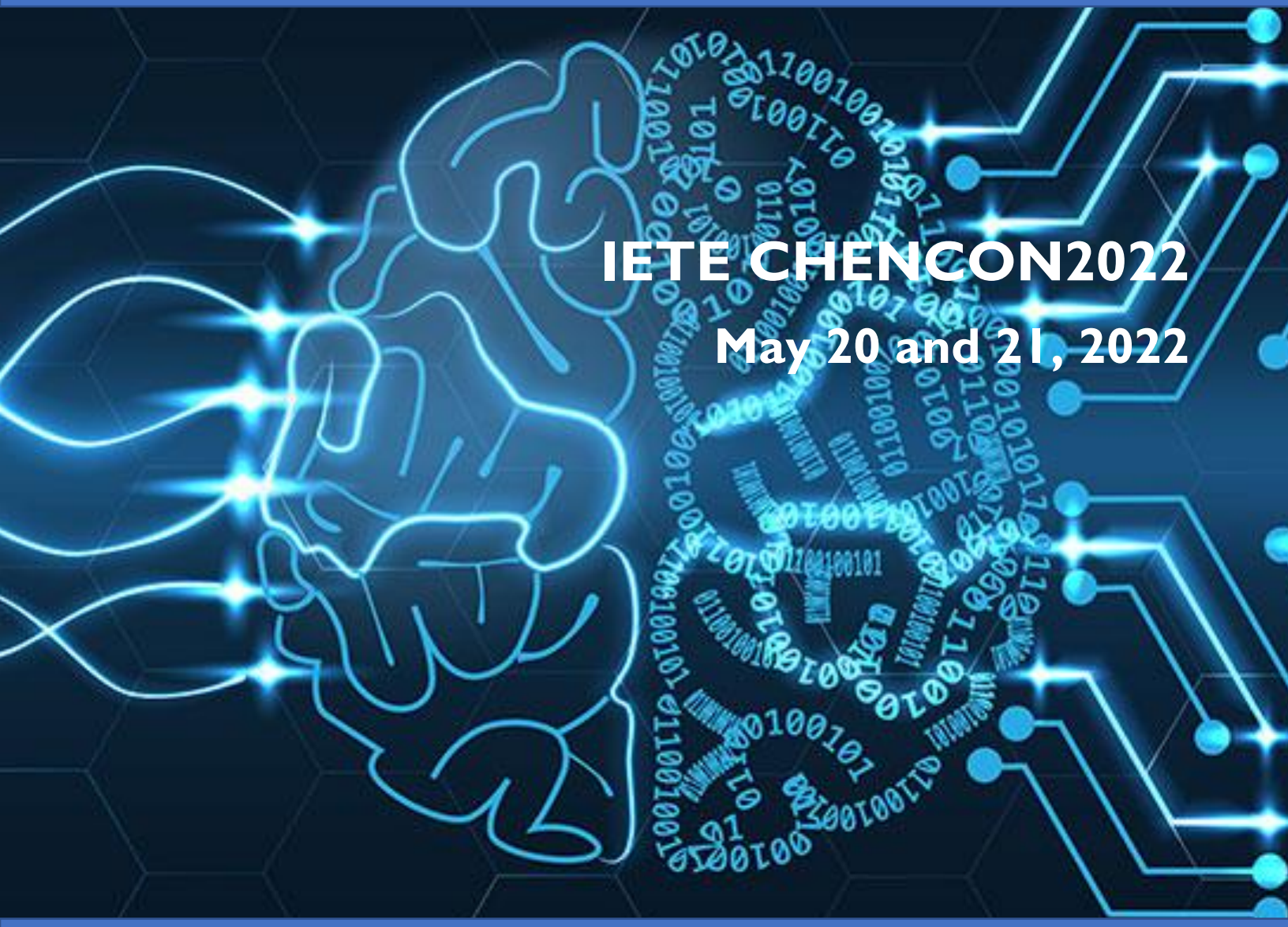

IETE CHENCON2022

May 20 and 21, 2022

THE INSTITUTION OF ELECTRONICS AND TELECOMMUNICATION ENGINEERS

CHENNAI CENTRE

37, Conran Smith Road, Gopalapuram, 600066

Proceedings of International Conference on

POWER OF ARTIFICIAL INTELLIGENCE AND MACHINE LEARNING FOR HUMAN EMPOWERMENT
IETE CHENCON2022

May 20 and 21, 2022

THE INSTITUTION OF ELECTRONICS AND TELECOMMUNICATION ENGINEERS

CHENNAI CENTRE

37, Conran Smith Road, Gopalapuram, Chennai-600066

Prof (Wg Cdr) P Prabhakar (Retd)

President, IETE

PRESIDENT MESSAGE

I am happy to note that the Institution of Electronics and Telecommunication Engineers, Chennai Centre is organizing the IETE Chennai Conference CHENCON-2022 on the “Power of Artificial Intelligence and Machine Learning for Empowering Humans”. IETE has provided the Chennai branch with an outstanding opportunity to host this prestigious conference.

The mission behind this conference is to support collaboration and help generate value to society by becoming one of the cornerstones of new fields of research such as AI Technologies, AI/ML infrastructure, Emerging applications of AI and ML in Communications and Industry applications of AI/ML.

I believe that the IETE is a place of novelty and collaboration, and we hope to be part of the ongoing revolution to integrate AI and ML into the day to day lives to help develop a beautiful relationship between man and machine. I congratulate the organizers of the Conference and wish all the students, engineers, and researchers a very rewarding professional interaction and experience.

DR. V. KAMAKOTI

Director, IIT Madras

MESSAGE FROM THE CHIEF GUEST

Artificial Intelligence/Machine Learning (AI/ML) are the new emerging areas with abundant research and employment opportunities.

I am happy that the Sri Venkateswara College of Engineering is hosting the International Conference on Power of Artificial Intelligence and Machine Learning for Human Empowerment under the aegis of IETE CHENCON 2022, that covers this important emerging area that is believed to improve quality of human lives.

I with the Conference all Success.

SHRI V. VENKATESAN

Programme Director, SAMEER-Chennai

MESSAGE FROM PROGRAMME DIRECTOR SAMMEER

It gives me immense pleasure to welcome you to the IETE CHENCON 2022, International conference on power of Artificial intelligence and Machine Learning for Human Empowerment.

The recent spike in the usage of AI/ML based technologies has provided an ample platform for new research opportunities and niches. The conference provides a platform for discussing and observing technical developments, in the presence of research experts and Industrialists from each domain. The delegates will exchange and discuss advancements, marketability and problems faced by the advent of AI/ML into their respective domains. The IETE CHENCON will be an enriching experience for learners, researchers, and industry professionals altogether. I wish all the participants and the organizers a fruitful and beneficial experience.

DR. N. VENKATESWARAN

Chairman, IETE Chennai Center

MESSAGE FROM THE CONFERENCE CHAIR, CHENCON 2022

I am happy to note that the grand success of IETE CHENCON 2021 during the summer of last year we are excited to welcome you all to the next iteration of IETE's CHENCON concentrating on the Power of AI/ML in empowering Humans.

Last year's conference was held on the online mode, and it was a grand success in lieu of the participation we received from across the globe but also the efforts put in by the Organizing committee. The main objective of IETE CHENCON is to help provide a platform to advance and exchange ideas in the torch bearing technologies of machine learning and artificial intelligence and how these can be used to better improve the lives of humans, thus enabling us to concentrate on larger problems.

Several invited talks from world renowned researchers form part of the technical program. I hope the conference can act as a hub for researchers and professionals to share their knowledge and experience in the community and have a very fruitful event. I am sure that all the delegates will update their knowledge from this Conference, with the array of Invited Lectures, panel and paper sessions planned. I congratulate the organizing committee for the excellent work done and I welcome the esteemed guests and delegates to IETE CHENCON 2022.

MS. T.J. JEYAPRABHA

Hony. Treasurer, IETE Chennai Center

MESSAGE FROM THE CO-CHAIR, CHENCON 2022

I would like to thank my organizing team members of the IETE CHENCON 2022 - International Conference under the theme, "**Power of Artificial Intelligence and Machine Learning for Human Empowerment**" for bringing together various researchers, students, faculty, and industry professionals in a hybrid mode on account of the prevailing pandemic. Hybrid platforms connect the researchers to share their ideas wherever they are.

It gives me immense pleasure that IETE Chennai Centre is able to organize various technical activities like Seminars, Project Competitions, Hack-a-thons, and Paper Presentations for the benefit of the student community. I am sure that this conference will serve as a platform for researchers, professionals, and academicians to develop knowledge in Artificial Intelligence and Machine Learning and share innovative ideas and their implementation aspects in this domain.

This forum would help researchers across the globe to come up with societal challenges and address their solutions for the same. The proceedings of this conference will benefit the participants to understand ongoing research areas and help them to come up with different ideas for existing problems.

I wish the conference IETE CHENCON 22 a great success.

MR. M. ARUN

Executive Committee Member, IETE Chennai Center

MESSAGE FROM THE CO-CHAIR, CHENCON 2022

It is a great honour and privilege to host this IETE ChenCon2022 - International Conference on Power of Artificial Intelligence and Machine Learning for Human Empowerment during 20 and 21 May, 2022. The prime focus of this conference is cantered towards Specialists, Researchers, Experts, Teachers and Students to share their experience, creative thoughts, issues, late patterns and future bearings in the field of Engineering and Technology.

The purpose of this conference is to provide a forum for the exchange of creative thoughts, specialized mastery for innovative headways, latest technical information, the dissemination of high-quality research papers and discourses for shaping future developments. It is truly a pleasure to welcome you all. I sincerely hope that this meeting will deliberate and discuss all the different facets in Engineering and Technology. I am confident that you will enjoy a stimulating conference and your presence and participation will help contribute to this vibrancy and enrich discussions around the theme Power of Artificial Intelligence and Machine Learning for Human Empowerment developing professional knowledge, exchange insights and collaborations.

I also appreciate the efforts taken by the conference organizing team. I take this opportunity to thank all the delegates, supporting institutes/industry and above all, volunteers without whose efforts, the conference would not have been possible. I hope all the participants will have a fruitful and beneficial experience. I wish the conference a grand success.

KEYNOTE SPEAKERS

DR. P. VIJAYALAKSHMI

Speech technology – challenges of a learning machine

Dr. P. Vijayalakshmi received B.E (ECE) degree, first-class, with distinction from Bharathidasan University. She Completed M.E (Communication systems) from Regional Engineering College, Trichy (currently NIT, Trichy). She earned her Ph.D. degree from IIT Madras and worked as a doctoral trainee for a year at INRS – EMT, Montreal, Canada. During her Ph.D, she developed various speech recognition systems and a novel approach for detection and assessment of disordered speech such as hypernasal and dysarthric speech apart from analyzing normal speech. During her Ph.D she had an opportunity to work with Prof. Douglas O'Shaughnessy at National Institute of Scientific Research (INRS), Montreal, Canada as a doctoral trainee for a period of one year in a project titled "Speech recognition and analysis".

She has published over 100 research publications in refereed international journals and in proceedings of international conferences. As a principal investigator she is currently involved in DST-TIDE funded project. As a co- investigator she has completed projects funded by DeitY, MCIT, New Delhi, and Tamil Virtual Academy, a Government of Tamil Nadu organization, and as a principal investigator completed one AICTE funded project and two projects funded by SSN Trust. She is a recognized supervisor of Anna University and currently guiding three fulltime and one part-time Ph.D scholar in the field of speech technology. Her areas of research include speech enhancement, statistical parametric speech synthesis and speech enabled assistive technology, voice conversion, polyglot speech synthesis, speech recognition.

Dr. P. Vijayalakshmi is a AICTE nominated **Margdarshak** under Margdarshan scheme to mentor Insitutes for NBA accreditation.

Abstract

Starting from statistical machine learning algorithms to deep learning, there are various challenges handled by the researchers in building a speech based human computer interaction systems. This talk will give an overview of various challenges starting from data collection to handling dialect variations in speech and building assistive technology devices for people with speech disorders.

DR. HEMPRASAD YASHWANT PATIL

Applications of Deep Learning for Image Classification

Dr. Hemprasad Yashwant Patil has completed his Ph.D. from Visvesvaraya National Institute of Technology, (NIT) Nagpur, India. He is currently working as Assistant Professor (Sr.) at Vellore Institute of Technology, Vellore. He has published more than 35 research articles related to artificial intelligence and computer vision in various National/International conferences and journals. He has authors two books in the domain of Artificial Intelligence and Internet of Things. He has presented his research work at IPTA which was held at Paris, France which was fully sponsored by Government of India. Also, He has published three Indian patents. He is a recipient of JTF award from CICS India. He was one of the finalists who prepared working prototypes out of their research at TITAN Hosur plant.

Abstract

Deep Learning and Machine Learning are becoming increasingly indispensable tools and methods for learning from data to make decisions and interact with our environment. Convolutional Neural Networks (CNNs) are key to several popular applications of deep learning such as image perception, speech recognition, etc. The increasing usage of CNNs in various applications on mobile devices and data centres have led the researchers to explore application specific hardware accelerators for CNNs which typically consist of a number of convolution, activation and pooling layers of which convolution layers is most intensive computationally. We will be discussing Basics of CNN and will see the demonstration to identify the bank currency notes using deep learning.

MR. SRINIVASA RAGHAVAN PARTHASARATHY

Harnessing the power of AI and ML- the Smart Way

Shri. Srinivasa Raghavan is an experienced Silicon Valley test architect and leader who has developed several end-to-end test solutions for both IC chips and consumer electronic products. His core expertise is in Design For Test (DFT), increasing the intensity of design while simplifying manufacturing and factory tests to appeal to business economics. He is also a Product Manager, defining features and specifications for Information Security Products. Raghavan is currently with Apple Inc., working from its headquarters in Cupertino, California since 2015. Before that, with Qualcomm Inc.,Singapore, he formed and led its first ever Product Test Engineering team outside the USA, focusing on snapdragon processors. Prior to Qualcomm, Raghavan developed numerous test solutions for programmable ICs at Xilinx & StatsChippac, Singapore and SPIC Electronics, India. Raghavan holds a Bachelor's degree in Electronics and Communication from India, Master of Science in Consumer Electronics from Singapore, and an MBA in Corporate & International Finance from the USA, besides being a certified Project Management Professional (PMP). A constant learner, he is now pursuing an advanced PG diploma on AIML from Purdue University, USA. He has received numerous awards in both academics and the corporate world for excellence in technology, management, and leadership. There are many innovations to Raghavan's name, including a patent for his DFT design and numerous other industry trade secrets that are silently but extensively used in many products today. Raghavan has now started formulating ways for businesses to harness from AIML and he hopes to leave a positive impact on as many people as possible in this way.

Abstract

Artificial intelligence is the technology to create intelligent systems that can simulate human intelligence. Machine learning is a subfield of AI, that enables machines to learn without *explicit* programming. AIML is the brainchild of these two fields, one of the greatest breakthroughs in technology. It is growing to be a trend, a permanent fixture in our world, changing our fundamental approach to solving problems and providing solutions that we humans cannot conceive. Looking into the future, the biggest challenge we face is on how businesses can harness the power of AIML efficiently. While it is difficult to discuss AIML in generic terms, the presenter, an

expert in consumer electronics product development, attempts to cover the essence of this field. As a background, our speaker will go over an example of a Design For Test (DFT) problem resolved using conventional or traditional means and elude to an 8-step plan to harness the benefits of AIML to enhance business performance. It all starts with a clear problem statement and ROI to drastically improve the probability of reaching the right solution. Though AIML is incredibly powerful, not every problem fits into its domain. Upon confirmation, thorough planning is followed by Proof Of Concept (POC) builds to gain confidence and momentum with this approach prior to implementing with the right task force. There is no single AIML algorithm that applies to all issues, but there is generally an agreed approach to direct us to the right model for a particular project. Unlike conventional solutions that rely on strong underlying principles and science, performance of AIML is limited by the training data provided and trends discovered. When future data starts to drift, AIML models trained with earlier data could become vulnerable and lose accuracy. Future proofing becomes key to ensure lasting success. Finally, the solution needs to be validated thoroughly to make sure every possible corner case gets addressed. While this field and topic are inevitably complex and multifaceted, the keynote speaker attempts to provide specific details on every step mentioned to allow businesses to harness the power of AIML: the force determined to stay and conquer.

DR. RAM PRASAD KRISHNAMOORTHY

Advanced Deep Neural architectures

Dr Ram Prasad received his Ph.D degree in Computer Science Engineering from Autonomous University of Madrid, Spain, and pursued his postdoctoral research work at Dublin City University, Ireland. His doctoral and postdoctoral research works were funded by the prestigious European Union Marie-Curie Fellowship. His doctoral research work got nominated for the prestigious European Biometrics and Research Award. He was a visiting researcher at University of Twente, The Netherlands, and University of Halmstad, Sweden. He graduated in Computer Science from Chennai Mathematical Institute, India.

His expertise is in the areas of classical machine learning, deep learning, computer vision, biometrics, software developments and algorithm design. He was the founder and director of Vision Cog Research and Development Private Limited, India and managed commercial R&D works in the domain of computer vision and biometrics. Currently he is an Assistant Professor of Computer Science at Shiv Nadar University Chennai. His primary research interests are in the Mathematical Optimizations for Machine Learning and Computer Vision.

Abstract

Many state of the art results in Computer Vision and Natural Language Processing are currently achieved using an advanced deep learning architecture referred to as Transformers. It is a neural network architecture solely based on self-attention mechanism and is highly parallelizable in nature. Transformers handle variable size inputs using stacks of self-attention layers. It doesn't make assumptions about the temporal or spatial relationships across the data. It can learn long-range dependencies. In this tutorial, we will dive into conceptual insights and mathematical intuitions behind this advanced architecture.

DR. ARUN P V

Machine Learning for Empowering Agriculture: A case study of using machine learning and remote sensing in smart farming

Dr. Arun is currently an Asst. Professor in CSE at the Indian Institute of Information Technology, Sri City, Chittoor. He is also the programme leader for the M.Tech (AIML) programme and the co-principal incharge for the CCMT 2022. His area of interest includes deep learning, computer vision, explainable image & signal processing, remote sensing and precision agriculture. Prior to joining IIIT Sri City, he served in Huawei R&D as a research scientist. He completed his postdoc from Ben-Gurion University, Israel and PhD from IIT Bombay.

He has published in around 15 high impact SCI indexed journals and has around 300 citations. He also served as a reviewer for IEEE TPAMI, IEEE TNLS, Information Fusion, Pattern Recognition, etc and has several conference publications. He collaborates with national and international agencies.

Abstract

Agriculture is getting highly impacted by climate and environmental changes. Machine Learning and related techniques should be explored to cater to the needs of individual crops. In this regard, this talk presents some case studies and applications of the use of ML & RS for smart farming. The use of deep learning and remote sensing for crop monitoring and other related applications will be highlighted. The talk will discuss the studies conducted in these areas in Israel and India.

DR. GANAPATHY KRISHNAMURTHI

Deep Learning with Limited Annotations

Dr. Ganapathy Krishnamurthi is an Associate Professor in the Department of Engineering Design at IIT-Madras and PI of the Medical imaging and Reconstruction Laboratory. He got his PhD from Purdue University (USA) followed by postdoctoral stints at Case Western Reserve University and Mayo Clinic. His research interests are in Medical Image analysis and reconstruction. Specifically his lab works on applying Deep Learning and Machine Learning techniques to problems in medical image analysis.

Abstract

Deep learning with limited annotations refers to techniques and heuristics that can train deep learning models with state-of-the-art performance or near state of the art without using large, labelled datasets. This is very relevant to the medical imaging community because it is difficult to collect high quality labelled data for a large number of patients given the diversity of imaging modalities and patient populations, especially in India. High quality labelling requires that experts annotate data and the costs involved are not affordable. Also in many cases disease data can be rare since vast majority of medical scans turn out to be normal scans. In this scenario a variety of methods have been explored wherein deep learning models have been trained with limited data with high performance. The talk will provide an overview of some of these methods and briefly discuss prospects of deep learning methods in medical imaging.

Ms. Gnanapriya C

From Complexity to Possibility, How AI can unleash the potential of 5G?

Ms. Gnanapriya (Priya) is Associate Vice President, Unit Technology Officer, Global Head of Technology & Architecture Practice - Communications, Media & Entertainment, Energy, utilities & Services Business Unit (ECS). Priya has 28+ years of experience in Telecom & IT. She contributes to unit strategy, drives technology adoption for business solutions across varied programs globally.She has been driving Digital Transformation, Enterprise Architecture, IT roadmap, Micro Services, Cloud migration, Open Source Adoption, 5G / Edge, 5G Use Cases & Industry solutions, emerging technologies themes like Blockchain solutions & Software Marketplaces, Data Modernization, Legacy & Technology Modernization, Innovation, guiding varied transformation & modernization programs for ECS global clients and part of org level core team.

She got 'Outstanding Achievement' Award under Disruptor category of "Global Women in Telco & Tech" Awards for 2020. She holds bachelor's degree in Electronics & Communication Engineering, Masters degree specializing in Communications Engineering, Business Administration. Under her guidance & drive, Infosys has won 13 Outstanding Catalyst Team Awards in TM Forum, she received Individual Recognition Award @ Industry TM Forum, serving as TMF Collaboration Sub-committee member. She had contributed to TMForum OpenAPIs, ODA, Edge, Software Marketplaces, Blockchain, technology reports, reference architectures.

She is a speaker in multiple Industry and Technology Forums. She received 'Best Technical Presentation' award in SPE. She is a Senior IEEE member, IEEE ComSoc member, Execom member of Bangalore Chapter. She has co-authored book on Digital Signal Processing I, II editions published by McGraw Hill, International edition and translated to Mandarin.

The Institution of Electronics and Telecommunication Engineers
Chennai Centre
International Conference on Power of Artificial Intelligence and Machine Learning for Human Empowerment
IETE CHENCON 2022
Inaugural Session Programme

May 20, 2022
Venue: Conference Hall, Library Building,
Sri Venkateswara College of Engineering, Pennalur, Sriperumbudur.
Join Online Link: https://meet.google.com/utg-pduc-rsg

9:00am - 9:30 am	Registration	
9:30am - 9:32 am	Invocation	
9:32am - 9:35 am	Lightening Kuthuvilaku	
9:35am - 9:40am	WELCOME Address	**Ms. T. J. Jeyaprabha,** Associate professor, Sri Venkateswara College of Engineering, Honorary Treasurer, IETE Chennai Center
9:40am - 9:45am	About the Conference IETE - CHENCON2022	**Dr. N. Venkateswaran** Professor, Sri Sivasubramaniya Nadar College of Engineering, Chairman-IETE Chennai Center
9:45am - 10:00am	Address by CHIEF GUEST	**Dr. V. Kamakoti** Director, Indian Institute of Technology Madras
10:00am - 10:15am	PRESIDENTIAL ADDRESS	**Prof (Wg Cdr) P Prabhakar (Veteran)** President, The Institution of Electronics and Telecommunication Engineers (IETE), New Delhi
10:15am - 10:20am	Address by GUESTS OF HONOUR	**Shri V. Venkatesan** Programme Director, SAMEER-Chennai, Tamil Nadu
10:20am - 10:25am	Address by GUESTS OF HONOUR	**Dr. S. Muthukumar,** HOD-ECE, Sri Venkateswara College of Engineering, Pennalur, Sriperumbudur
10:25am - 10:30am	Vote of Thanks	**Shri. M. Arun** Assistant Professor, Panimalar Institute of Technology, Chennai. Member – Executive Committee, IETE Chennai Center
10:30am - 10:45am	Morning break with refreshments	

International Conference on Power of Artificial Intelligence and Machine Learning for Human Empowerment CHENCON2022

Keynote Talks and Technical Sessions

Venue: Sri Venkateswara College of Engineering (SVCE), Pennalur, Sriperumbudur.

Date & Time		Details	
Day 1: Friday, 20th May, 2022	09.00 – 09.30	**Registration**	
	09.30 – 10.30	**CHENCON 2022 – Inauguration** **Join Online Link: https://meet.google.com/utg-pduc-rsg**	
	Morning break with refreshments		
	10.45 – 11.45	**Keynote Talk (PMKT) -1**	**Dr. P. Vijayalakshmi,** **Professor and HoD, ECE,** **Sri Sivasubramaniya Nadar College of Engineering, Chennai** **Speech technology – Challenges of a learning machine**
	11:45 - 12:45	**Keynote Talk (PMKT) -2**	**Dr. Hemprasad Yashwant Patil** **Assistant Professor Senior Grade 1** **School of Electronics Engineering - Embedded Technology, VIT University, Vellore.** **Applications of Deep Learning for Image Classification**
	Lunch Break		
	13:30 - 15:30	**Technical Session**	**OMTS 1: AI Enabled technologies** **Paper IDs: IC -12,13,20,25,28** **https://meet.google.com/gdo-srvv-bxb**
			OMTS 2: AI / ML Infrastructure **Paper IDs: 10,11,40,49,57** **https://meet.google.com/isg-dnbu-try**
			OMTS 3: Emerging applications of AI in Communication **Paper IDs: 08,15,17,26,42** **https://meet.google.com/dfi-bqmm-dfo**
			PMTS 1: **Paper IDs: IC-56,60,61,76 Venue: Conference Hall**
	18:30 - 19:30	**Keynote Talk OMKT -1**	**Mr. Srinivasa Raghavan Parthasarathy** **Product Manager and Platform Test Design Lead** **Apple, Pleasanton, California, United States** **Harnessing Power of AI and ML – The Smart Way** **https://meet.google.com/utg-pduc-rsg**

Date & Time		Details	
Day 2: Saturday, 21st May, 2022	09.00 – 10.00	Keynote Talk (PMKT) - 3	**Dr. Ram Prasad Krishnamoorthy,** Assistant Professor, Department of CSE, Shiv Nadar University - Chennai. Emerging Deep learning models
	Morning break with refreshments		
	10.10 – 11.10	Keynote Talk (PMKT) - 4	**Dr. Arun P V,** Asst. Professor Computer Science and Engineering, Indian Institute of Information Technology, Sri City Machine Learning for Empowering Agriculture: A case study of using machine learning and remote sensing in smart farming
	11.15 – 12.15	Keynote Talk (PMKT) - 5	**Dr. Ganapathy Krishnamurthi,** Assistant Professor Robert Bosch Centre for Data Science and AI Department of Engineering Design,IIT Madras. Deep Learning with Limited Annotations
	Lunch break		
	13:00 - 14:30	Technical Session	OMTS 4: AI Enabled technologies Paper IDs: IC -14,30,35,43,51 https://meet.google.com/gdo-sryv-bxb
			OMTS 5: Industry Applications of AI Paper IDs: 44,45,47,59,63 https://meet.google.com/isg-dnbu-try
			OMTS 6: Emerging applications of AI in Communication Paper IDs: IC -19,68,73,74,78 https://meet.google.com/dfi-bqmm-dfo
			PMTS 2: Paper IDs: IC-7,31,53,54 Venue: Conference Hall
	18:30 - 19:30	OMKT -2	**Ms.C. Gnanapriya,** Associate Vice President, Infosys, Bengaluru From Complexity to Possibility- How AI can unleash the potential of 5G? https://meet.google.com/utg-pduc-rsg
	14.30 - 15.15	Valedictory Function	

The Institution of Electronics and Telecommunication Engineers

Chennai Centre

International Conference on Power of Artificial Intelligence and Machine Learning for Human Empowerment

IETE CHENCON 2022

Valedictory Session Programme

May 21, 2022

Venue: Conference Hall, Library Building,
Sri Venkateswara College of Engineering, Pennalur, Sriperumbudur.

https://meet.google.com/utg-pduc-rsg

2:30pm - 2:35 pm	Invocation	
2:35pm - 2:40pm	Welcome Address	**Ms.T.J.Jeyaprabha,** Associate professor, Dept. of ECE, Sri Venkateswara College of Engineering, Honorary Treasurer, IETE Chennai Center
2:40pm - 2:55pm	President Address	**Prof (Wg Cdr) P Prabhakar (Veteran)** President, The Institution of Electronics and Telecommunication Engineers (IETE), New Delhi
2:55pm - 3:00pm	Address by Guest of Honour	**Dr. S. Ganesh Vaidyanathan** Principal, Sri Venkateswara College of Engineering
3:00pm - 3:10pm	Prize and Certificate distribution	**Dr.P.Jothilakshmi,** Professor, Department of ECE **Dr.G.A.Sathish Kumar,** Professor, Department of ECE, Sri Venkateswara College of Engineering
3:10pm - 3:15pm	Vote of Thanks	**Shri.M. Arun** Assistant Professor, Dept. of ECE, Panimalar Institute of Technology, Chennai. Member – Executive Committee, IETE Chennai Center

National Anthem

IETE CHENCON 2022

International Conference on Power of Artificial Intelligence and Machine Learning for Human Empowerment

May 20 & 21, 2022

Technical Program at a Glance

May 20, 2022, Time: 13.30 – 15.30
OMTS 1: AI Enabled technologies
https://meet.google.com/gdo-sryv-bxb

May 20, 2022, Time: 13.30 – 13.50
Paper ID: IC 12

A Review of Deep Learning-Based Models For Automatic Modulation Recognition
Surendiran R, Kalaichelvi G, Bhadru Amgothu, Sujitha Sathiyamoorthy, Kishan J
SAMEER-CEM

May 20, 2022, Time: 13.50 – 14.10
Paper ID: IC 13

Channel Selection by Using Fuzzy C Means Clustering Under Lower SNR
Subhabrata Dhar, Sabyasachi Chatterjee
GURU NANAK INSTITUTE OF TECHNOLOGY

May 20, 2022, Time: 14.10 – 14.30
Paper ID: IC 20

Analysis of Twitter Data Using Machine Learning Algorithms
Sanchana.R, Nithya Devi.S, Mercy.P,Bhavani Sree.S K, Swetha.S
SRI SAI RAM INSTITUTE OF TECHNOLOGY

May 20, 2022, Time: 14.30 – 14.50
Paper ID: IC 25

Solving Partial Differential Equations Using Deep Learning
Sneha S, Shweta Srikanth, Vikram Venkat Krishnan, W Jinohans, N Padmapriya
SRI SIVASUBRAMANIYA NADAR COLLEGE OF ENGINEERING

May 20, 2022, Time: 14.50 – 15.10
Paper ID: IC 28

A Survey on Diabetic Retinopathy Detection Using Deep Learning
Shreya G Gawande, Ajay P Thakare, Bhushan V Wakode
SIPNA COLLEGE OF ENGINEERING & TECHNOLOGY, AMRAVATI

May 20, 2022, Time: 13.30 – 15.30
OMTS 2: AI / ML Infrastructure
https://meet.google.com/isg-dnbu-try

May 20, 2022, Time: 13.30 – 13.50
Paper ID: IC 10

Data Transmission Through LI-FI in Underwater
Dr. C. Padmaja, Kurra Pallavi
G Narayanamma Institute of Technology and Sciences (For Women)

May 20, 2022, Time: 13.50 – 14.50
Paper ID: IC 11

Design of Dual-Band Microstrip Antenna for Bandwidth Enhancement Using Slotted DGS
Surendra Kumar P, Siva Prasad A, Sandhya G, Devasena G, Sri Krishna K, Meena Manogna G
BAPATLA ENGINEERING COLLEGE, BAPATLA, AP , INDIA

May 20, 2022, Time: 14.10 – 14.30
Paper ID: IC 40

Feasibility of Brain Computer Interface (BCI) and Internet Of Things (IOT) in Assisting Elderly and Disabled People
Monisha B, Sruthi Vrindha R, Subashini U, Dr.K.Sumathi
SRI SAIRAM ENGINEERING COLLEGE

May 20, 2022, Time: 14.30 – 14.50
Paper ID: IC 49

Design And Implementation of CPW fed MLDA Antenna for Wireless Personal Area Networks
Kanniyappan N, Amali C
SRM Valliammai Engineering College

May 20, 2022, Time: 14.50 – 15.10
Paper ID: IC 57

Microstrip Antenna For 5G Sub-6Ghz and X-Band Wireless Communication Applications
Dr. J. Chandrasekar Rao, P. Bhargav, N. Harik, N. Vyshnavi
BAPATLA ENGINEERING COLLEGE

May 20, 2022, Time: 13.30 – 15.30
OMTS 3: Emerging applications of AI in Communication
https://meet.google.com/dfi-bqmm-dfo

May 20, 2022, Time: 13.30 – 13.50
Paper ID: IC 08

Complexity Analysis of Channel Decomposition Schemes In Multi-User Mimo Precoder
Markkandan S, Venkateswaran N
SRM TRP Engineering College

May 20, 2022, Time: 13.50 – 14.10
Paper ID: IC 15

Color Image Restoration From Low Resolution Based On Multiscale Decomposition
Abdur Rahman. A, Adhithya Ner. P.V., Bathri. D, Charavanan. V, Abinaya. B, Senthil Kumar. K
Rajalakshmi Engineering College

May 20, 2022, Time: 14.10 – 14.30
Paper ID: IC 17

Bio-Metric Authentication Using Dorsal Hand Vein Pattern
Shanthi C, Ayswariah S S, Latha K
MIT CAMPUS, ANNA UNIVERSITY CHENNAI

May 20, 2022, Time: 14.30 – 14.50
Paper ID: IC 26

Smart Assistant For Visually Impaired Using Computer Vision
Abinav Narayanan S, Abishek Viswanath P, Bhooshan V, Sreeja B S
SSN College of Engineering

May 20, 2022, Time: 14.50 – 15.10
Paper ID: IC 42

Soil Nutrient Analysis Using IOT For Yield Prediction
Dr. M. Selvi, Dr. C. Sheeba Joice, Dr. J. Jeffin gracewell
Saveetha Engineering College

May 20, 2022, Time: 13.30 – 15.30
PMTS 1: ALL Tracks

May 20, 2022, Time: 13.30 – 13.50
Paper ID: IC 56

A Novel Analysis Of Nd:Yag Photon Materials Usage In The Modern Era
T.Suresh, T.D.Subha, Shri Abijith.M, T.Shanmugaesh
R.M.K. ENGINEERING COLLEGE

May 20, 2022, Time: 13.50 – 14.10
Paper ID: IC 60

A Study Of A Gradient Monitoring System Using Wireless Sensor Network
B.Jeyapoornima, T.D.Subha, L.Kavya, K.Jaithri
R.M.K ENGINEERING COLLEGE

May 20, 2022, Time: 14.10 – 14.30
Paper ID: IC 61

Analysis Of Wireless Electronic Traffic Mirror Using Dynamic Map Based System
N.M.Jothi Swaroopan, T.D.Subha, Swathi M., Subhashini. E, Snehaa. S
R.M.K. ENGINEERING COLLEGE

May 20, 2022, Time: 14.30 – 14.50
Paper ID: IC 76

For MIMO OFDM Systems, The Design of A New MRMDF Structure-Based FFT Processor
Nancy W, Deepika V, Shobana L, Sai Tharun Kb, Satvika V
JEPPIAAR INSTITUTE OF TECHNOLOGY

May 21, 2022, Time: 13.00 – 14.30
OMTS 4: AI Enabled technologies
https://meet.google.com/gdo-sryv-bxb

May 21, 2022, Time: 13.00 – 13.20
Paper ID: IC 14

Neighbour Vehicle Monitoring In V2i Using Dedicated Short-Range Communication
Reshma P, V Sudha
NATIONAL INSTITUTE OF TECHNOLOGY TIRUCHIRAPPALLI

May 21, 2022, Time: 13.20 – 13.40
Paper ID: IC 30

AI Based Smart Interaction System For Computer Management

Bala Avanthiga B, Divya P, Hariharan B
SSN COLLEGE OF ENGINEERING

May 21, 2022, Time: 13.40 – 14.00
Paper ID: IC 35

Work Prediction On Cloud Computing Using Long Short Term Memory Algorithm

Dr. M.Ayyadurai, Ganesh BS, Shivani Devi, Shiva Prakhash
SRM Institute of Science and Technology

May 21, 2022, Time: 14.00 – 14.20
Paper ID: IC 43

CNN Based Food Calorie Recognition For Dietary Assessment

Dr. Pavithra Guru, Sai Vamsi Gorle, Srinivas Jayavarapu, Srimounisha Dadi
SRMIST, Ramapuram

May 21, 2022, Time: 14.20 – 14.40
Paper ID: IC 51

Artificial Intelligence And Machine Learning Based Wireless Localization

Charu Jain, Indu Subramanian, Meghna Govind and Venkateswaran N
SSN College of Engineering

May 21, 2022, Time: 13.00 – 14.30
OMTS 5: AI / ML Infrastructure
https://meet.google.com/isg-dnbu-try

May 21, 2022, Time: 13.00 – 13.20
Paper ID: IC 44

An Automatic Emergency Ventilator For Covid Patients

Surendhar A, Sushma R, Venmughil Vannan R, Yobishiya Stefi W J
SRM VALLIAMMAI ENGINEERING COLLEGE

May 21, 2022, Time: 13.20 – 13.40
Paper ID: IC 45

A Comprehensive Review of Anemia Detection Methods

Vinit P. Kharkar, Ajay P. Thakare
SIPNA COLLEGE OF ENGINEERING AND MANAGEMENT, BADNERA

May 21, 2022, Time: 13.40 – 14.00
Paper ID: IC 47

3-BIT All-Optical Binary to Gray Code Converter Using 2D Photonic Crystal Design

Ms. Monica Philo s, Ms. Nandhini S, Ms. Rakshitha V S, Ms. Santhiya S, Mr. S Syedakbar, Ms. S Geerthana, Dr. T Sridarshini
K. RAMAKRISHNAN COLLEGE OF TECHNOLOGY

May 21, 2022, Time: 14.00 – 14.20
Paper ID: IC 59

Smart Agriculture

Amara Deepika, A. Vijayalakshmi, M. Meena, G. Nixon Samuel Vijayakumar
R.M.K. ENGINEERING COLLEGE

May 21, 2022, Time: 14.20 – 14.40
Paper ID: IC 63

Forecasting The Sea Level Rise Using Arima Model

Ms. M.Methini, T.R. Mohana Priya, M. Sruthika, S. Suryadharshini
SRI SAIRAM ENGINEERING COLLEGE

May 21, 2022, Time: 13.00 – 14.30
OMTS 6: Emerging applications of AI in Communication
https://meet.google.com/dfi-bqmm-dfo

May 21, 2022, Time: 13.00 – 13.20
Paper ID: IC 19

Direction-of-Arrival Estimation of Multiple Closely Spaced Signals Using MVDR-CSVR Approach

Ashok C, Vaddi Lakshmi Satya Sai Sarojini, N. Venkateswaran
St. Joseph's College of Engineering

May 21, 2022, Time: 13.20 – 13.40
Paper ID: IC 68

A New Paradigm of Covid Chamber Using Raspberry PI

Mahalakshmi V, Sasikala G, Sai Venkata Raghavan N, Nasir SK, Veerendranath R
Vel Tech Rangarajan Dr.Sagunthala R&D Institute of Science and Technology

May 21, 2022, Time: 13.40 – 14.00
Paper ID: IC 73

Depiction of User Clustering Algorithm In MIMO - NOMA For 5g And Beyond

Elayaraja C, Amali C
Dhaanish Ahmed College of Engineering, ANNAUNIVERSITY

May 21, 2022, Time: 14.00 – 14.20
Paper ID: IC 74

A Review of Data Security Challenges In Wireless Sensor Networks(WSN)

R.K.Sharma
UNITED UNIVERSITY

May 21, 2022, Time: 14.20 – 14.40
Paper ID: IC 78

An Eminent Role of Zeolites in Purification Of Solutions

Amara Deepika, A. Vijayalakshmi, M. Meena, G. Nixon Samuel Vijayakumar
R.M.K. ENGINEERING COLLEGE

May 21, 2022, Time: 13.00 – 15.20
PMTS 2: All Tracks

May 21, 2022, Time: 13.00 – 13.20
Paper ID: IC 07

Automated Visual Inspection System For Production Line Using Kinect

Aravind Mohan, Sudarsan V. S. Ranganathan, Vivek Hari Sankaran and N. Venkateswaran
Sri Sivasubramaniya Nadar College of Engineering

May 21, 2022, Time: 13.20 – 13.40
Paper ID: IC 31

Diagnosis of Stages of Acute Lymphoblastic Leukemia Using Image Processing and Deep Learning

Krishi Divya Dharshini V, Nethra Prakash K, Shafiya Sidrath A, Venkateswaran N
Sri Sivasubramaniya Nadar College of Engineering

May 21, 2022, Time: 13.40 – 14.00
Paper ID: IC 53

Video Surveillance Based Congestion Avoidance System During Evacuation

Dr.Dinesh Anton Raja.P, T.D.Subha, Rajalakshmi.D, Priyadharshini.V,
R.M.K. ENGINEERING COLLEGE

May 21, 2022, Time: 14.00 – 14.20
Paper ID: IC 54

Digital Jewellery

Sivasubramanian R, Suraj Sk, Saalini D, Sangeeth Kanna P, T J Jeyaprabha
Sri Venkateswara College of Engineering

May 21, 2022, Time: 14.20 – 14.40

Paper ID: IC 91

Fingerprint Based Person Authentication System Using Siamese Resnets

J. Jeffrey Joan, Naveen Sriram R., Uma Maheshwari D., Prithiviraj V.S., Dr. Veluchamy
Department of Electronics and Communication Engineering and Computer Science Engineering, Sri Venkateswara College of Engineering

May 21, 2022, Time: 14.40 – 15.00

Paper ID: IC 92

Secured Dynamic Substitution box Design using Linear Trigonometric Transformation

B. Sarala, G.A. Sathish Kumar, A. Shalini, A. Subhapriya, T. Thivya
Department of Electronics and Communication Engineering, Sri Venkateswara College of Engineering, Sriperumbudur, Kancheepuram District, Tamil Nadu, India

May 21, 2022, Time: 15.00 – 15.20

Paper ID: IC 93

UI Based Solution for XSS Vulnerability Detection and Report Analysis

Yukesh Kumar S, Sneha S, Sujitha R, Sakthi M, Vaishnavi M, Sathya Priya S, T.J. Jeyaprabha
Department of Electronics and Communication Engineering, Sri Venkateswara College of Engineering, India

TABLE OF CONTENTS

Automated Visual Inspection System for Production Line using Kinect

Aravind Mohan[1], Sudarsan Vasista Srinivasan Ranganathan[2], Vivek Hari Sankaran[3], N. Venkateswaran[4]
[1-4]Department of Electronics and Communication Engineering, Sri Sivasubramaniya Nadar College of Engineering, Kalavakkam, Kanchipuram, Tamil Nadu, India
[1]ara.mohan@gmail.com, [2]sudarsanvsr2005@gmail.com, [3]vivu91@gmail.com, [4]venkateswarann@ssn.edu.in

***Abstract*—Automated visual inspection system (AVIS) is a non-destructive testing (NDT) system used in analysing, classifying and detecting defects a production line. Existing systems are generally expensive and product specific and use data from an RGB colour camera alone. In this paper is proposed a system that performs (i) depth image processing and (ii) colour image processing using Microsoft Kinect™, a low cost device that provides access to depth and colour data of a subject. Suitable pre-processing, segmentation and feature extraction techniques are employed to enhance accuracy. Support vector machine (SVM) expert system is used to improve classification accuracy and help design an intelligent system.**

***Keywords*—automated visual inspection system, Microsoft Kinect, non destructive testing, support vector machines**

I. INTRODUCTION

A. Automated Visual Inspection System using Kinect

Visual inspection is an NDT technique used in industries where every manufactured component is checked visually to ensure conformance to specifications. Automated visual inspection is the process of testing parts visually without using manpower and using a computer alone [1]. This increases the throughput of the system and avoids human error. Due to the long set-up time for inspection systems, AVIS are suited for tasks where many products of the same type are made in a production line environment. There are three main application areas for AVIS. Firstly, it is used in mark identification where marks such as bar codes, printed characters, etc. on products can be checked. Secondly, dimensional analysis can be performed. Thirdly, defects can be detected by testing for cracks, missing teeth and colour variation.

The various steps in the implementation of AVIS using Kinect include the following. Image enhancement techniques are used to pre-process the images. Integral to the process of AVIS is segmentation, which decomposes an image into constituent objects or regions. From each of the segmented objects, a set of features is extracted to describe the object. This set of features is called a feature vector, which is presented to a classifier to identify the type of the object. It is important that a suitable feature vector is chosen, as this is the only data passed to the classifier. In classification, a feature vector is taken and the type, or class, of the object that the vector represents is determined.

B. Motivation

The aim of the work is to develop a new system which can isolate any object under study using a single procedure with a three-dimensional (3D) view of the object. Obtaining a depth map is a costly affair with normal time of flight cameras. In February 2011, Microsoft KinectTM was introduced. This is a gaming device used to recognize skeletons of players by using infrared speckle pattern imaging, a patented technology developed by PrimeSense [2]. The low cost depth mapper sparked interest in research and several innovative applications [3, 4] were developed using the Kinect. In this paper is proposed the use of Kinect in an AVIS which can be employed in a production line for classification of objects through computer vision. The system is designed to provide information like dimensions, surface correctness, etc. of a product. The paper presents conceptual procedure with proof of working for detecting various faults. It explains (i) depth image processing using Kinect for dimensional analysis and (ii) colour image processing for detection of defects.

II. THE SYSTEM

A. Functional Description

This section describes the production line setup, along with its functional block diagram. An intermediate setup is used due to unavailability of a production line setup. The work is divided into (i) depth image processing and (ii) colour image processing as shown in Fig. 1. The test specimen used is a brass synchronizer, which is a component used in manual transmissions of cars.

Depth image processing involves processing of data acquired from the depth sensor of Kinect camera. The depth image undergoes pre-processing and segmentation before it is used in performing the following functions:

1. Measurement of thickness of a part
2. Measurement of diameter of a part

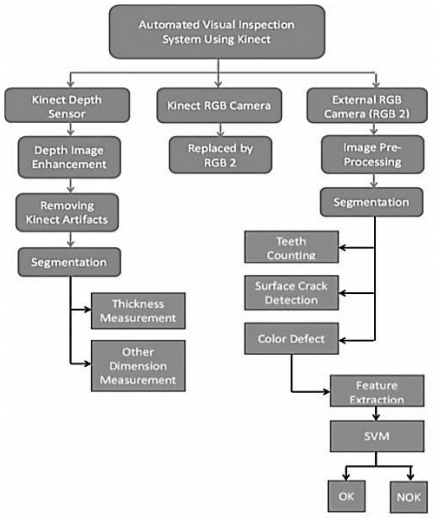

Fig. 1 Automated visual inspection system using Kinect – Functional blocks

A secondary red green blue (RGB) camera is used in lieu of the Kinect RGB camera. The reason for this substitution is explained in Section III. Colour image processing of the acquired colour image is carried out to perform the following functions:

1. Detection of number of teeth in a grooved part
2. Detection of cracks
3. Detection of colour variation in a good part.

NDT testing techniques such as acoustic resonance testing (ART) cannot detect these defects because there is no change in the resonance spectrum of the object.

Later, in February 2012, Microsoft released the official software development kit (SDK) with better compatibility. This was also accompanied by the release of the improved Kinect hardware that included near field viewing. VC++ was used for coding to interface with MATLAB. An external RGB camera was used to improve the image.

B. Depth Map and Problems Faced in Using a Depth Map

A depth map comprises an array of 3D coordinates, including a depth (Z) coordinate value of the body surface at each point (X, Y) within a predefined field of view. The processor present in the Kinect computes the 3D coordinates of points on the surface of the object by triangulation, based on transverse shifts of spots in the pattern. This technique is referred to as pattern-based depth mapping. An example of a depth map is shown in Fig. 3.

C. Proposed Production Line System

The Kinect is placed at a distance, generally around 90 to 100cm, from the object. This lies within the optimum range of functioning of the Kinect. The older version of Kinect for Xbox has a constraint that it can measure depth accurately only beyond 80cm. The newer version of Kinect however has near field viewing which allows the Kinect to be positioned even as close as 40cm. Three sets of LED arrays (or more if required) are positioned above the Kinect, and directed towards the object for proper illumination. The plane containing the dimension of the object to be measured is aligned perpendicular to the axis of the Kinect camera, i.e., the production line and the Kinect should be perfectly parallel. There is a processor and a control system to control the whole system. As the parts pass through the production line, they will be tested and based on the decision taken, they will be thrown into accept or reject bay by the control system.

III. MICROSOFT KINECT

A. The Device

Fig. 2 shows the Microsoft Kinect used for this work. It is a low-cost motion sensing device that combines powerful, yet simple technology to render high quality depth images and colour images. There is enough literature that specifies the specifications and functionalities of Kinect. The technology behind Kinect has been explained in references [5,6]. It was developed by PrimeSense, Tel Aviv and patented by them.

B. Interfacing the Kinect

The Microsoft Kinect was originally designed to work with the Microsoft Xbox. Several unofficial open source drivers to interface the Kinect with a computer through the USB port were then made available.

Fig. 2 Microsoft Kinect

Fig. 3 Depth map

The Kinect is a low cost device and it is inaccurate at providing depth map at times. *One problem with Kinect is that it does not provide a "dense depth map" — there are lots of holes (black) where the Kinect infrared (IR) sensor cannot "see". This is due to faulty lighting, objects being out of range, reflection, transparency and objects absorbing and not reflecting infrared light.* These black holes are known as occlusions and have been shown in Fig. 4 in the form of white patches. *The problem is overcome and the*

accuracy of the depth data is enhanced by using simple mean and median filters across multiple depth frames.

Another problem encountered with the Kinect is the occurrence of vertical banding. In smooth regions vertical lines or 'vertical bands' of values are present. Standard methods to overcome vertical banding include using mean, median and Gaussian filters. They smoothen the data by averaging the pixels across the neighbors. Fig. 5 (a) shows vertical banding around the region of interest in the image.

(a) *(b)*

Fig. 4 (a) Image with occlusion (b) Mean and median filtered output image

(a) (b)

Fig. 5 (a) Before non-local mean filtering (b) After non-local mean filtering

The noise is removed, but leads to smoothing of edges and blurring near sharp changes in contrast. To overcome this problem non-local means filtering as in [7, 8] has been done to filter the depth image. The result is shown in Fig. 5(b).

D. Segmentation using KINECT

Depth data processing and colour image processing can be integrated in a way that segmentation in colour image can be performed using the depth image. This narrows down the area of interest of search for an object by isolating it from the background using a simple thresholding procedure.

IV. Classifier Systems

A. Support Vector Machines

SVM is a learning method developed by Vapnik and his co-workers as in [9] and can be used in a production line to classify faults. SVMs [10] are systems used for training linear learning machines defined in the Kernel induced feature space and are designed to be optimum based on general optimization theory. An important advantage of SVMs is that they result in sparse dual representation of the hypothesis which produces highly efficient algorithms due to the Karush-Kahn-Tucker conditions. Another advantage is that they do not have local minima and are convex optimization problems. The general equation for an SVM using kernel is given in equation 1.

$$f(x) = \sum_{i=1}^{l} \alpha_i y_i \langle \phi(x_i) \bullet \phi(x) \rangle + b \qquad (1)$$

The SVM is used in this system to improve the accuracy of the classifier to detect defects and to make the system intelligent. It also makes training the system for new components easier and quicker. It is used to detect the variation in colour in components and is trained using a suitable size sample set.

V. Measurements Using The Setup

This section describes the three functions that were performed making use of the depth data. There is a global variable background depth which is the distance to the background or the production line. This is constant throughout the process. Fig. 6 shows the experimental setup required to find out the distance to the background and also to the object. A indicates the point where Kinect is present. BC is the line segment drawn across the width of an object placed along Kinect's axis.

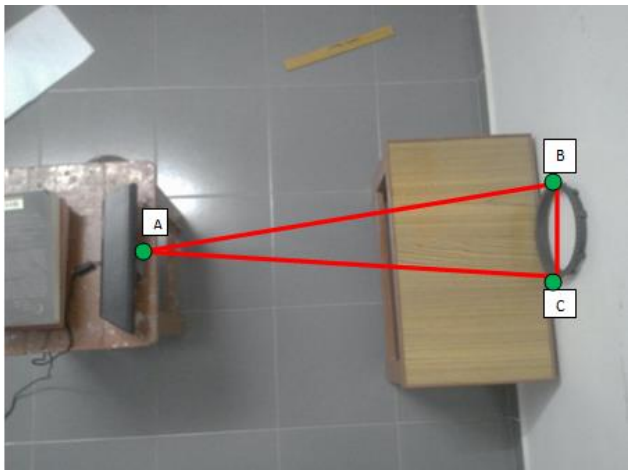

Fig. 6 Experimental Setup

Using colour images, 3 specific functions are to be performed, namely (i) crack detection, (ii) teeth counting in a grooved part and (iii) colour defect detection using SVM.

A. Thickness Measurement

A part (with a uniform surface on top) comes in front of the Kinect and the distance to its surface is found out from Kinect as 'objdepth'. The thickness of the object is then

$$\text{thickness} = \text{objdepth} - \text{bgdepth} \qquad (2)$$

B. Diameter Measurement

The Kinect data is thresholded to obtain the object edges as required and the pixel count of the object across its diameter is found out. Using triangular trigonometric operations, the diameter of the required part is obtained. The diameter BC is found out as

$$BC^2 = AB^2 + AC^2 - 2*AB*AC*\cos(a) \qquad (3)$$

where 'a' is the angle opposite side BC. AB and AC are known depth measurements. Angle a is established by relating the pixel count of diameter BC and the Kinect field of view (in degrees).

C. Crack Detection

An algorithm to detect surface cracks for a specific industrial part namely brass synchronizer ring, has been

devised. The algorithm is based on colour image processing principles. Also, the algorithm can be extended to any other industrial part with appropriate pre-processing for every part. The brass synchronizer (Fig. 7 (a)) is a component present in manual transmissions of cars. Fig. 7 (b) shows a crack formed during production process. Fig. 8 shows the crack detection flowchart.

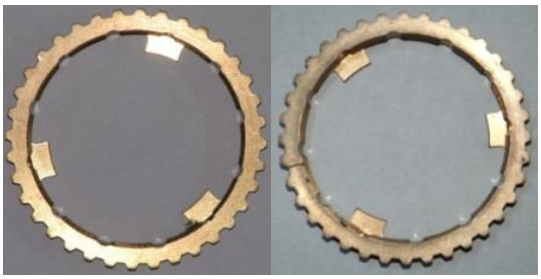

(a) (b)

Fig. 7 Brass synchronizer rings – (a) Part without crack (b) Part with crack

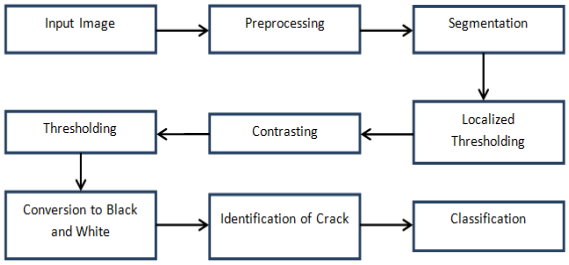

Fig. 8 Crack Detection – Flowchart

Reconstruction, alteration or changes in intensities of pixels, etc. to make cracks on a pavement surface from the background of the rest of the image, along with noise reduction/removal have been performed already. The usage of median filtering and linear regression techniques for preprocessing were described in [11]. This method uses thresholding and then median filtering process is suggested in [12]. To minimize the speed and effort for crack detection, another method was proposed by Mould [13]. Finally the method to be used has been narrowed to pre-processing followed by localized thresholding and conversion of image to black and white. Localized thresholding was also explained in [14].

The input image is a symmetrical circular synchronizer ring and a crack is present across the surface of the ring. In this case it is enough to feed a circular ring section of the image to detect presence of crack in the part. The circular Hough transform [15, 16], a segmentation technique, is applied to the input image to detect the center of the inner circle of the synchronizer ring. The radius of the part (in pixels) is fed as a constant input to the algorithm. Once the center of the ring has been detected, Hough transform algorithm will find the most potential candidate center pair. A portion of the ring (predefined thickness as required) is then cut using the center and used for further processing.

The image is then filtered to remove all noise. First the crack is isolated from the background using standard deviation between R, G and B components and average intensities of image blocks. The whole image is divided into $sx \times sy$ sized blocks initially. The values sx and sy depend on the resolution of the image.

$$block(l,m) = \begin{cases} background & \text{if } thresh(l,m) \geq 10 \\ & \& \; thresh(l,m) > threshold(image) \\ crack & otherwise \end{cases} \quad (4)$$

where *threshold(image)* is the average intensity of the entire image, *threshRGB(l,m)* is the standard deviation of means of R, G, B components in a block and *thresh(l,m)* is the average intensity of the block. There are l*m blocks in the image totally. After isolating the background, the next step is to verify the continuity of blocks. Each block should be complemented by other neighboring blocks that have already been erased. The erased blocks are white in colour. In other words, the average intensity of the neighboring blocks has to be 255 in a gray scale image. In the event that there are not as many erased blocks, the block is retained. If the block has more than three erased neighboring blocks, the block is erased. Optimum accuracy in extracting the region of interest can be obtained.

$$block(l,m) = background \text{ if } count > 3 \quad (5)$$

where *count* is the number of neighboring blocks that are part of the background already.

Localized thresholding can identify potential crack pixels by using the classical thresholding mechanism local to a smaller area of the image. The motive of this method is to facilitate the classification of pixels by contrasting the intensities of potential crack pixels from the rest. The threshold values are localized and are stored separately in an array.

For every block of the g^{th} row and h^{th} column,

$$Threshold\ T(g,h) = \left(\sum_{i=1}^{sx}\sum_{j=1}^{sy} I((x*a)+i),(y*b)+j)\right) / sx*sy \quad (6)$$

Using a localized threshold alone to classify the pixels is inaccurate. If it becomes the only criteria for classification, then it is possible that every block would contain potential crack pixels. Therefore, other conditions could be specified for pixels to be considered crack pixels. The advantage of this process is that the crack pixels which are usually of much lesser intensity than the other pixels are identified with less noise when compared to global thresholding. This is due to the possibility that initially more than 50% of pixels could have had a lesser intensity than the intensity of the threshold. For example, one high value among a set of 6 pixels is likely to change the mean value completely and might eventually result in the mean value being higher than the remaining 5 pixels, which leads to inconsistency. Localized thresholding separates the crack pixels from the rest of the pixels. This gap can further be widened by raising the contrast between the crack pixels and the rest. By identifying a localized threshold, one can separate the pixels of smaller intensity from those with a relatively higher intensity. The contrast is achieved by pulling apart the histogram of the image about the localized threshold. The histograms in Fig. 9 show the intensities of pixels in the image before and after contrasting.

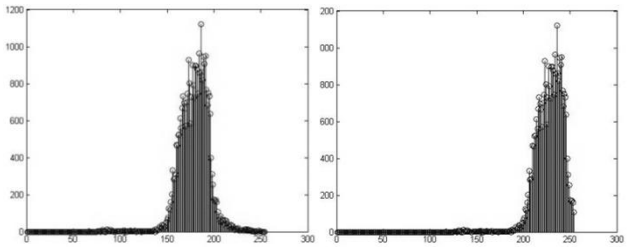

Fig. 9 Histograms of image before (left) and after contrasting (right)

After processing the image, it is converted into black and white for the final stage of crack detection. Identification of final threshold value is one of the major steps in conversion to black and white. The mean of the pixel values can be used as the threshold value to convert the gray scale image into black and white image. But there can be a possibility that the number of pixels lying in the null region is too high. This is in contrast to the mean thresholding process. But this case is avoided in the present application because there will be only 2 ranges of values in intensities after contrast stretching.

The final stage in thresholding is done with respect to the following points:

1. Any block with threshold value greater than the latest threshold value belongs to the background

$$block(l,m) = background \text{ if } thresh1(l,m) > threshimage \quad (7)$$

2. For the non-zero blocks deviations from the latest average intensity value, threshimage, are calculated and

$$difference(l,m) = threshimage - thresh1(l,m) \quad (8)$$

3. The mean of all deviations is then calculated

$count1 = 0$

Loop:

$$meandiff = (\sum_{g=1}^{rnum} \sum_{h=1}^{cnum} thresh1(g,h) \forall thresh1(g,h) \neq 0) \quad (9)$$

$count1 = count1 + 1$ if $thresh1(g,h) \neq 0$

Loop Ends

$meandiff = meandiff / count1$

4. For the remaining non-zero blocks, they are identified to be a part of the background or crack as follows. The output is shown in Fig. (10).

When the image is converted back into black and white (Fig. 10(b)), there might be an inaccuracy in identifying the threshold for conversion. A minimum number of pixels in the neighborhood must be cracks for a pixel to be considered as a crack pixel. The rest of the pixels that do not satisfy the criteria are to be removed. By verifying through this step, further the cracks are enhanced. The final output is shown in Fig. 11.

$$block(l,m) = \begin{cases} background \text{ if } difference(l,m) / \max(\max(difference)) < 0.5 \\ background \text{ if } difference(l,m) / \max(\max(difference)) > 0.5, \\ \quad abs(\max(\max(difference)) - meandiff) < meandiff * 2, \\ \quad difference(l,m) < meandiff \\ crack \quad otherwise \end{cases} \quad (8)$$

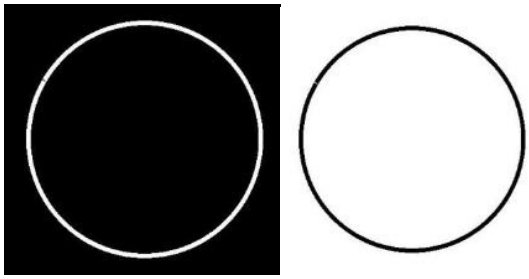

(a) (b)

Fig. (10) (a) Final stage of thresholding– OutputI2 (b) Conversion into black and white– OutputI3

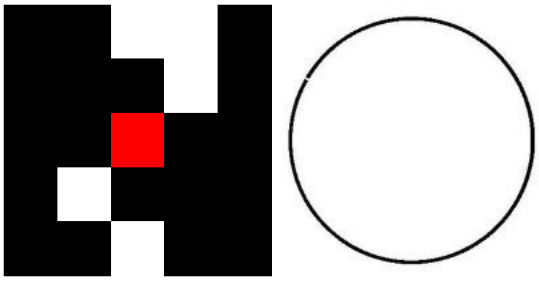

(a) (b)

Fig. 11 Continuity verification of crack– Red pixel indicates discontinuity (b) Continuity verification of crack– OutputI4

Cracks can be identified based on the number of areas that are supposed to be present in the image. If there is a crack in the part, in the final image, the area around the ring and within the ring will combine together as one through the crack. By using 8-connectivity one can identify all the connected regions in a black and white image.

$$crack = \begin{cases} 1 \text{ if } \max(\max(bwlabel(I4))) \neq 2 \\ 0 \quad otherwise \end{cases} \quad (9)$$

where bwlabel returns the number of 8-connected regions in the final black and white image I5 and crack returns 1 if there is a crack detected. The logic behind the step is that, if there are no cracks in the part there will be 3 regions totally in the final image. The first region is the ring which is black, the second and the third regions are the inner and outer regions around the ring. If there is a crack in the part, the inner and the outer regions around the ring will become one 8-connected region through the crack and hence the number of regions will reduce by one. The command bwlabel returns the number of regions numbering them through 0, 1, 2…n-1, where n is the total number of regions present in the image.

D. Teeth Counting

In geared automotive components one of the problems found to occur is the absence of teeth in gears. The teeth in the component break during forging either due to internal material flaw or external force. Thus this method is accompanied by a manual visual inspection. The part is inspected manually for colour variation and missing teeth defects.

The approach followed starts with isolating the object accurately from the background. The next step is to detect the centre of the ring using circular Hough transform. Then the object is cut out leaving only the teeth behind. The number of connected regions are then identified and counted to be the number of teeth present in the component. As

shown in Fig. 12, the output of the algorithm isolates the teeth as blobs which can be counted using binary morphological 8-connectivity test.

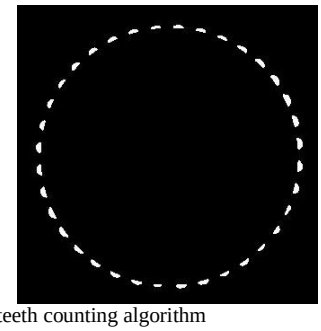

Fig. 12 Output of teeth counting algorithm

E. Colour Defect Detection

In forged automotive components, a defect is observed to occur as the variation in colour of the component. This change is due to the change in the internal composition of the alloy during forging and is accompanied by a change in the mechanical properties of the component. Thus the component is a defective component and needs to be removed from the line. Fig. 13(a) below is an example of a non-defective part and Fig. 13(b) is an example of a defective part. As can be seen, the defective part has a pink tinge due to a change in composition of the alloy during forging.

(a) (b)

Fig. 13 (a) Non-defective component (b) Coloured component (defective) with pink tinge

The algorithm uses an RGB camera to capture the image of the object and an SVM to detect the colour variation. The crack detection and the colour variation algorithms share the pre-processing stage and the output of the final stage of the crack detection algorithm is fed as input to the colour variation detection code. This is used to extract a strip of pixels which represent the part as a whole and takes into account the variation in illumination at different points on the part. The pre-processed image obtained from the crack detection algorithm is shown in Fig. 14.

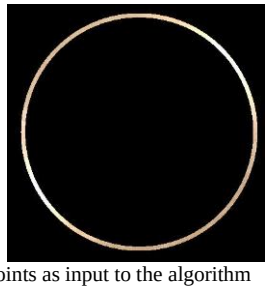

Figure 14 Non-zero points as input to the algorithm

RGB and YCbCr values of these pixels are identified. The illumination component is not separate in the RGB model. It results in large values in R, G and B values depending on the lighting. For example, a white patch would have a large red component as well. However the idea is to detect a pinkish tinge in the component. This can be identified by an increase in the red component of the part. Thus there is a need to consider the YCbCr model also. In this model the illumination is removed from the chroma component and it helps to make the system more robust to the illumination variation. Also this separates the red component and thus an increase in the red component can be easily identified. The image is converted from RGB to YCbCr. The RGB and YCbCr values of the non-zero pixels are stored in an array and returned from the crack detection module.

The array containing the RGB and YCbCr values are used to calculate the mean and standard deviation of the R, G, B, Y, Cb and Cr components. These are the feature vectors chosen as input to the SVM.

A training set is generated by taking a suitable number of samples for defective and non-defective parts. A feature vector is generated by calculating the mean and standard deviation. A suitable kernel is chosen based on the requirements and the input. Once the network is trained with a number of samples, it can be used to classify the components by feeding it with the feature vector of the component under test.

VI. Experimental Results

A. Dimensional Analysis

This section provides experimental results of the tests. Fig. 15 shows the values of '*bgdepth*' and '*objdepth*' for one run of a part. Table 1 shows the experimental results of dimensional analysis for different industrial parts that were tested for conformity with the interim experimental setup shown in Fig. 6. It can be seen that the results for measured subjects are fairly accurate.

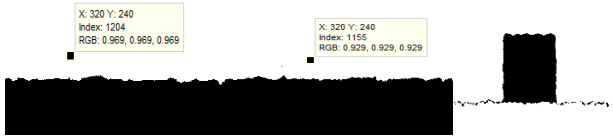

Fig.15 Depth images of wall, object (box) and the object isolated using the difference in depth (from left)

Table I. Experimental Results Of Dimensional Analysis

Object	Actual diameter (cm)	Measured diameter (cm)	Actual thickness (cm)	Measured thickness (cm)
Ring	15.8	15.7	2	1.8
Disc	17.1	16.8	1.8	1.8
Wheel	20	19.78	1.2	1.3

B. Colour Image Processing

The setup was as explained earlier and the test was carried out on 20 samples. The results were found to be accurate and the methods were found to be effective to detect cracks, colour variation and to count the number of teeth in a part.

VII. Summary and Conclusions

Automated visual inspection system has been implemented to classify parts in a production line. The cost of the system is very low since it uses just a Kinect and a desktop personal computer (PC). The accuracy of the Kinect camera is still subject to improvement. Since the Microsoft Kinect is a product which is continuously under development, any improvement to the hardware automatically results in improvement in the accuracy of the AVIS. The system can be extended to perform works in other inspection fields as well and can also be used for object detection and classification. It could be combined into a single hardware specific module using an embedded system in combination with a digital signal processor making it ideal for the industrial environment.

References

[1] D.T. Pham, and R.J. Alcock, "Smart Inspection Systems: Techniques and Applications of Intelligent Visual Inspection Systems", Elsevier, 2002.

[2] Primesense LTD., "Method and system for object reconstruction", International Publication Number WO 2007/043036.

[3] S. Moretti,,"Doctors use Xbox Kinect in cancer surgery", CHealth, March 2011, http://tinyurl.com/4ym6866.

[4] J.L. Raheja, A. Chaudhary, and K. Singal, "Tracking of fingertips and centers of palm using Kinect", 2011 Third International Conference on Computational Intelligence, Modelling and Simulation, pp 248-252.

[5] "Kinect and MRPT | The Mobile Robot Programming Toolkit", Mrpt.org, Retrieved 16th March 2011.

[6] Microsoft Kinect Forum – http://kinectforwindows.org

[7] A. Buades, B. Coll, and J.-M. Morel, "A non-local Algorithm for image denoising", Proc. IEEE Conference on Computer Vision and Pattern Recognition (CVPR), 2005, vol II, pp 60-65

[8] B. Huhle, T. Schairer, P. Jenke, and W. Straßer, "Robust non-local denoising of coloured depth data", Proceedings of the IEEE Computer Society Conference on Computer Vision and Pattern Recognition Workshops, 2008, pp. 1–7.

[9] V. N. Vapnik, "Statistical Learning Theory", ISBN 0-4761-03003-1, John Wiley & Sons, 1998.

[10] N. Cristianini and J. S. Taylor, "An Introduction to Support Vector Machines and Other Kernel-Based Learning Methods", Cambridge University Press, 2000.

[11] H. Rababaah, J. Wolfer, D. Vrajitoru, "Asphalt pavement crack classification: A comparison of GA, MLP, and SOM", Proceedings of the Genetic and Evolutionary Computation Conference (GECCO'05 and SIGEVO 1), Washington, DC, June 25-29, 2005, Late breaking papers.

[12] A. Georgopoulos, A. Lozios, A. Flouda. "Digital image processing for pavement distress evaluation", Elsevier Science B.V. ISPRS Journal o Photogrammetry and Remote Sensing, vol. 50, issue 1, 1995, pp. 23-33

[13] D. Mould, "Image-based editing and image-based animation" Proceedings of Graphics Interface 2005 Victoria, British Columbia Session, pp 219 – 226.

[14] N. Katakam, "Pavement Crack Detection System through Localized Thresholding", Thesis, The University of Toledo, Dec. 2009.

[15] J. R. Jen, M. C. Shie and C. Chen, "A circular Hough transform hardware for industrial circle detection applications", IEEE 1st Conference on Industrial Electronics and Applications, May 2006, pp. 1-6.

[16] N. Guil, E.L. Zapata, "Lower order circle and ellipse Hough transform", Technical Report No: UMA-DAC-97/22, J. Pattern Recognition, vol. 30, no. 10, October 1997, pp 1729-1744.

Complexity Analysis of Channel Decomposition Schemes in Multi-User MIMO Precoder

Markkandan S[1] and Venkateswaran N[2]

[1]Department of ECE, SRM TRP Engineering College, Trichy, India.
[2]Department of ECE, SSN College of Engineering, Chennai, India.

[1]markkandan@gmail.com, [2]venkateswarann@ssn.edu.in

***Abstract*— As Multiple Input and Multiple Output (MIMO) channel attains amplified transmission rate by separating the input stream in to a multitude of parallel data streams that are transmitted in parallel. Precoding at the transmitter goals to decompose the channel in to an uncorrelated sub channels, whereas the data streams will be fed in parallel independent subchannels. In this proposed work, the performances of MIMO precoder using numerous channel decomposition algorithms are related and its computational complexity is examined. The channel decomposition schemes measured are, LDL^H, L [1], Geometric Mean Decomposition (GMD) [2], Schur [3], Singular Value Decomposition (SVD) [4], [5] QR [6] and Jordan decomposition. The simulation results authorize that precoding for MIMO channel decomposed by QR scheme outstrips all the other precoding methods based on channel decomposition in the light of BER (Bit Error Rate) performance and involves relatively lesser number of FLOPs.**

***Keywords*— Precoding, Channel decomposition, MIMO, Subchannel.**

I. INTRODUCTION

Matrix decomposition achieves the factorization of the matrix into a product of matrices. Matrix decomposition is an essential theme in linear algebra and applied statistics consuming both scientific and engineering significance. The aim of matrix decomposition characteristically includes two features: computational convenience and analytic simplicity. When, the information carrying matrix found by using the decomposition methods is used as the input, BER can be enhanced. Few of the decomposition techniques existing are:

- QR decomposition
- SVD decomposition
- GMD decomposition
- Cholesky decomposition
- LU decomposition

The decomposition methods in addition to the proposed LLL based precoders in Massive MU-MIMO deliver an improved BER and less Complexity.

II. SYSTEM ANALYSIS

Use of the channel decomposition methods, provides the ability to MIMO channel to get decomposed into parallel independent channels. Independent data streams in each subchannel can be transmitted to enable increase in throughput without using any additional bandwidth. In the diversity mode, the same data stream is transmitted in each subchannel. In the channel decomposition, precoding the channel gain matrix is subject to decomposition and generates the information matrix, which can be used along with the precoding techniques for reducing the BER performance. Fig. 2.1 displays the System Model for Massive MU-MIMO with decomposition methods.

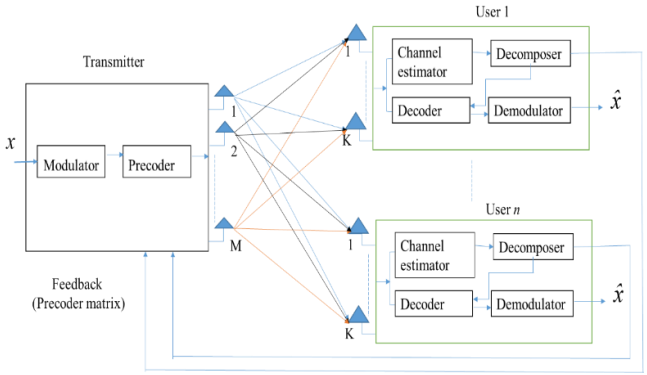

Fig. 2.1 System Model for Massive MU-MIMO with decomposition technique

Precoding at the transmitter requires CSI at the transmitter. In order to obtain CSI at the transmitter, the channel should be fixed (non-mobile) or approximately constant over a reasonably duration. If CSI is available at the transmitter, the transmitted symbols, either for a single-user or for multiple users, can be separated by means of pre-equalization at the transmitter. Generally, SVD is used for decomposing the MIMO channel into parallel Eigen modes and wide range of singular values are obtained. These large variations in the singular values (diagonal elements) affect the uniformity of sub channel gain. Literature provides information relating to many SVD based decomposition schemes for the improvement of uniformity in subchannel gain [7], [8], [9]. Among them, Geometric Mean Decomposition (GMD) and Uniform Channel Decomposition (UCD) are widely used. Uniformity of sub channel gain is maintained in these SVD based schemes.

The Geometric Mean Decomposition (GMD) algorithm is a popular approach in the development of a precoding scheme for joint Multiple-Input–Multiple-Output (MIMO)

transceiver designs. Joint transceiver designs, which call for coordination between the transmitter and the receiver, have attracted much attention in Multiple-Input Multiple-Output (MIMO) communication systems. The MIMO channel matrix *H* can be decomposed using QR as

$$H=QRP^{H} \quad (1)$$

Where *Q* and *P* are unitary matrices and *R* is an upper triangular matrix.

A. QR Decomposition

The rudimentary goal of the QR decomposition is to feature a matrix as a product of two matrices like, *Q* and *R*. QR decomposition is the Gram-Schmidt procedure functional to the columns of the matrix. In the QR decomposition, the R term transmits the information and Q is an orthogonal matrix of the channel gain information.[10]

$$H=Q \times R \quad (2)$$

1) Linear and Non-Linear Precoders with QR decomposition

- MMSE Precoding

The decomposed channel matrix used as the input to the MMSE Precoding. The precoding matrix is,

$$W_k = R_k^H (R_k R_k^H + \beta I_k)^{-1} \quad (3)$$

- Vector perturbation precoding

The decomposed channel matrix used as the input to the Vector perturbation precoding. The transmitted vector is given as

$$x_n = \sqrt{\frac{P}{\Gamma}} R^{\dagger}(S_n + \tau Z_n^*) \quad (4)$$

- Vector perturbation precoding with LLL technique

The decomposed channel matrix is used as the input to the Vector perturbation precoding with LLL technique. The transmitted vector is given as

$$x_n = \sqrt{\frac{P}{\Gamma}} R^{\dagger}(TT^{-1})(S_n + \tau Z_n^*) \quad (5)$$

The received signal represented as

$$y = Q^H H W_x + n \quad (6)$$

Where, Q^H is used as decoder at the receiver.

III. Simulation Results

A. Simulation Results of Linear and Non-Linear Precoders with QR Decomposition

Simulation is used to study the performance of Linear and Non-Linear Precoders with QR decomposition beneath perfect and Imperfect CSI for large MIMO systems. The number of receivers is 10 with 4 antennas each. The number of transmitting antennas ranges from 100 to 400 throughout simulation. The Signal to Noise Ratio vs. BER[11] using Perfect Channel State Information with QR decomposition technique for MMSE Precoder and Signal to Noise Ratio vs. BER using Perfect Channel State Information with QR decomposition technique for VP-MMSE Precoder. The Signal to Noise Ratio vs. BER using Perfect Channel State Information with QR decomposition technique for MMSE Precoder and Signal to Noise Ratio vs. BER using Perfect Channel State Information with QR decomposition technique for VP-MMSE Precoder depicted in Fig. 3.1 and 3.2 respectively.

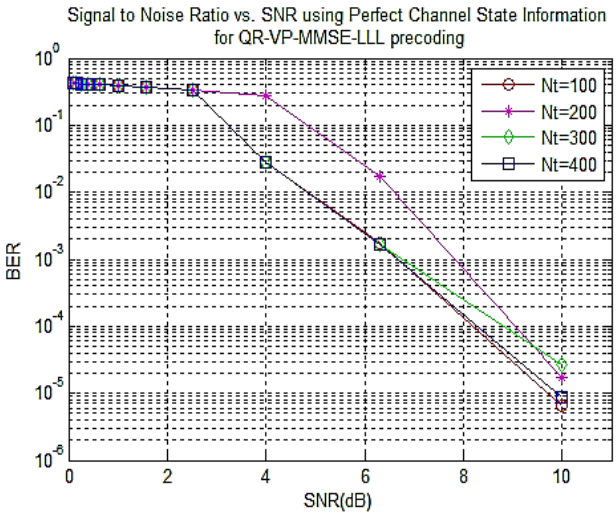

Fig. 3.1. Signal to Noise Ratio vs. BER using Perfect Channel State Information with QR decomposition technique for MMSE Precoder

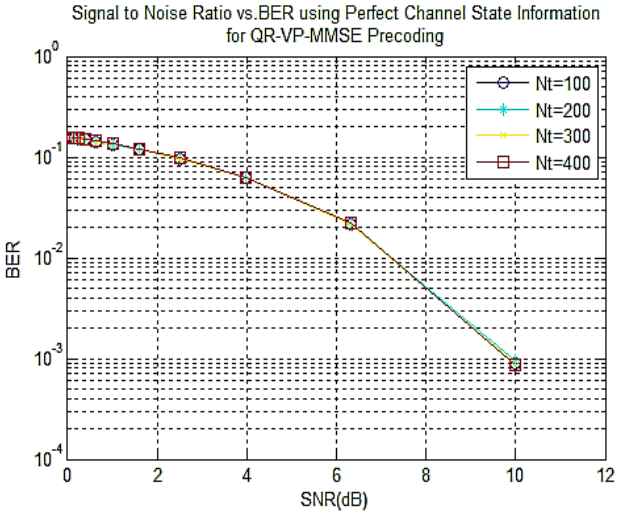

Fig. 3.2. Signal to Noise Ratio vs. BER using Perfect Channel State Information with QR decomposition technique for VP-MMSE Precoder

The Signal to Noise Ratio vs. BER using Perfect Channel State Information with QR decomposition technique for VP-MMSE-LLL Precoder and Signal to Noise Ratio vs. BER using Perfect Channel State Information with QR decomposition technique for VP-ZF Precoder is depicted in Fig. 3.3 and 3.4 respectively.

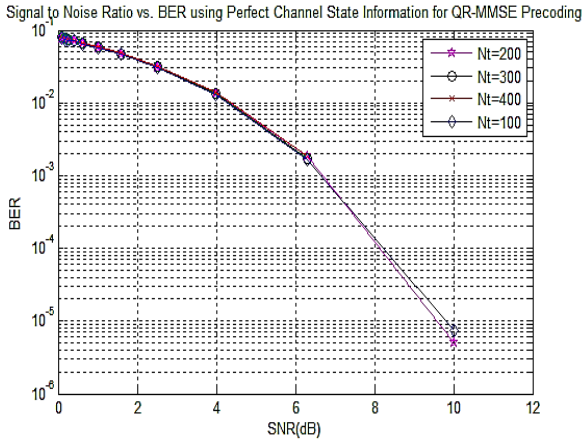

Fig. 3.3. Signal to Noise Ratio vs. BER using Perfect Channel State Information with QR decomposition technique for VP-MMSE-LLL Precoder

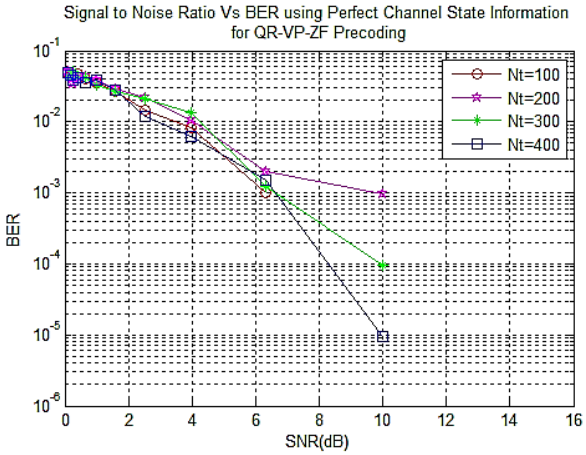

Fig. 3.4. Signal to Noise Ratio vs. BER using Perfect Channel State Information with QR decomposition technique for VP-ZF Precoder

The Signal to Noise Ratio vs. BER using Perfect Channel State Information with QR decomposition technique for VP-ZF-LL Precoder and Signal to Noise Ratio vs. BER using imperfect Channel State Information with QR decomposition technique for MMSE Precoder is depicted in Fig. 3.5 and 3.6 respectively.

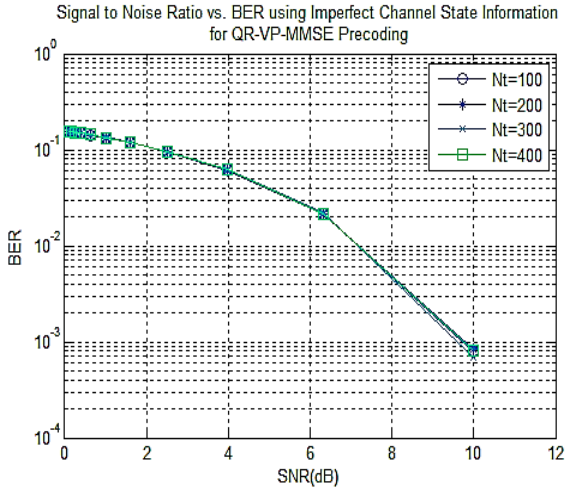

Fig. 3.5. Signal to Noise Ratio vs. BER using Perfect Channel State Information with QR decomposition technique for VP-ZF-LL Precoder

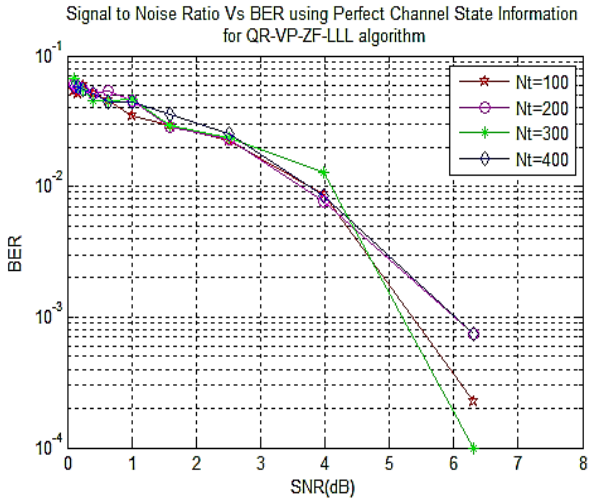

Fig. 3.6. Signal to Noise Ratio vs. BER using imperfect Channel State Information with QR decomposition technique for MMSE Precoder

The Signal to Noise Ratio vs. BER using imperfect Channel State Information with QR decomposition technique for VP-MMSE Precoder and Signal to Noise Ratio vs. BER using imperfect Channel State Information with QR decomposition technique for VP-MMSE-LLL Precoder was analysed and plotted in Fig. 3.7 and 3.8 respectively.

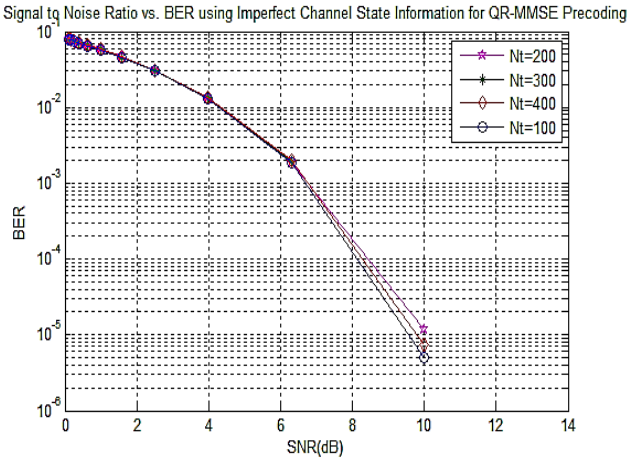

Fig. 3.7 Signal to Noise Ratio vs. BER using imperfect Channel State Information with QR decomposition technique for VP-MMSE Precoder

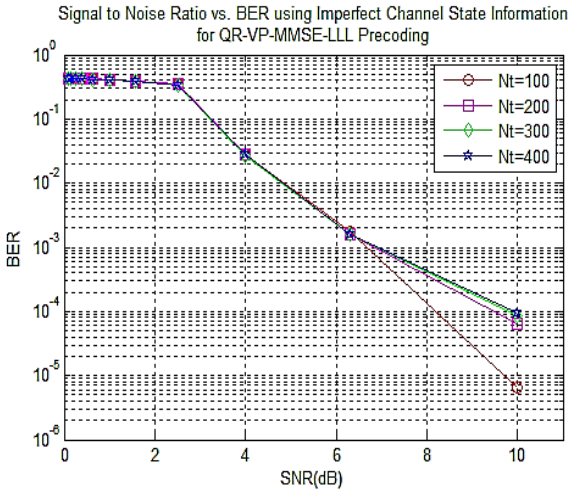

Fig. 3.8 Signal to Noise Ratio vs. BER using imperfect Channel State Information with QR decomposition technique for VP-MMSE-LLL Precoder

The Signal to Noise Ratio vs. BER using imperfect Channel State Information with QR decomposition technique for VP-ZF Precoder and Signal to Noise Ratio vs. BER using imperfect Channel State Information with QR decomposition technique for VP-ZF-LLL Precoder is compared and plotted in Fig. 3.9 and 3.10 respectively.

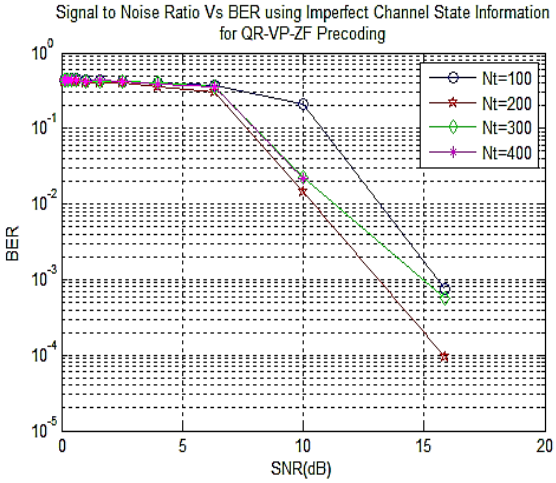

Fig. 3.9 Signal to Noise Ratio vs. BER using imperfect Channel State Information with QR decomposition technique for VP-ZF

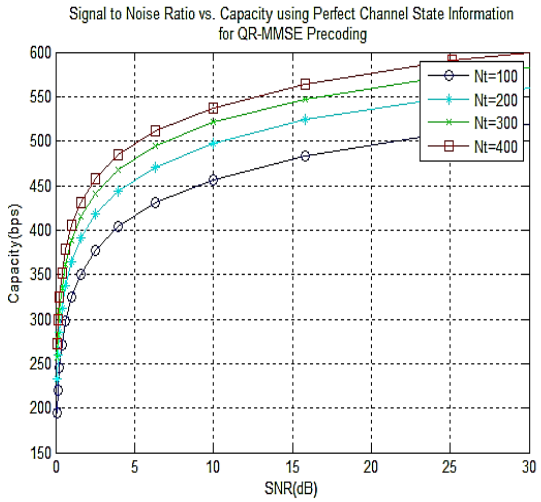

Fig. 3.10 Signal to Noise Ratio vs. BER using imperfect Channel State Information with QR decomposition technique for VP-ZF-LLL Precoder

The Signal to Noise Ratio vs. capacity using perfect Channel State Information with QR decomposition technique for MMSE Precoder and Signal to Noise Ratio vs. capacity using perfect Channel State Information with QR decomposition technique for VP-MMSE Precoder are depicted in Fig. 3.11 and 3.12 respectively.

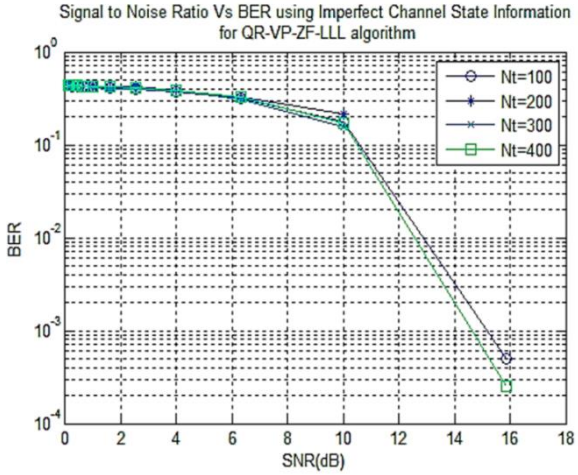

Fig. 3.11 Signal to Noise Ratio vs. capacity using perfect Channel State Information with QR decomposition technique for MMSE Precoder

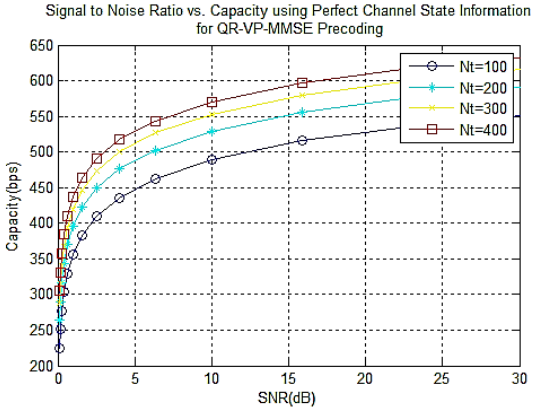

Fig. 3.12 Signal to Noise Ratio vs. capacity using perfect Channel State Information with QR decomposition technique for VP-MMSE Precoder

The Signal to Noise Ratio vs. capacity using perfect Channel State Information with QR decomposition technique for VP-MMSE-LLL Precoder and Signal to Noise Ratio vs. capacity using perfect Channel State Information with QR decomposition technique for VP-ZF Precoder is depicted in Fig. 3.13 and 3.14 respectively.

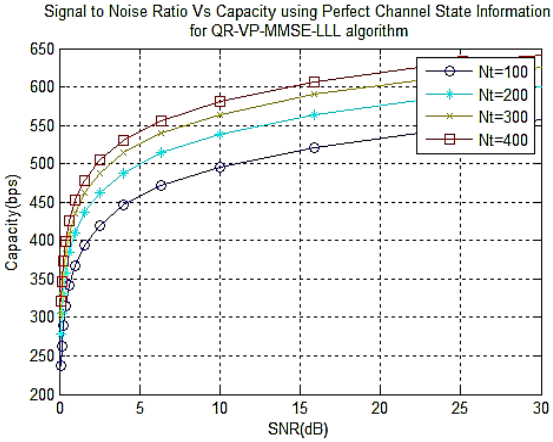

Fig. 3.13. Signal to Noise Ratio vs. capacity using perfect Channel State Information with QR decomposition technique for VP-MMSE-LLL Precoder

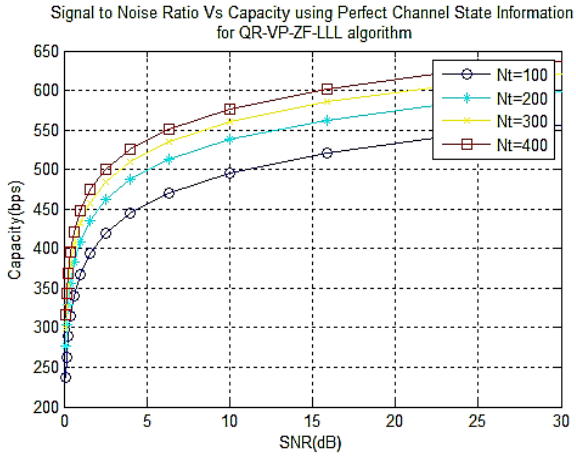

Fig. 3.14 Signal to Noise Ratio vs. capacity using perfect Channel State Information with QR decomposition technique for VP-ZF Precoder

The Signal to Noise Ratio vs. capacity using perfect Channel State Information with QR decomposition technique for VP-ZF-LLL Precoder and Signal to Noise Ratio vs. capacity using imperfect Channel State Information with QR decomposition technique for MMSE Precoder is depicted in Fig. 3.15 and 3.16 respectively.

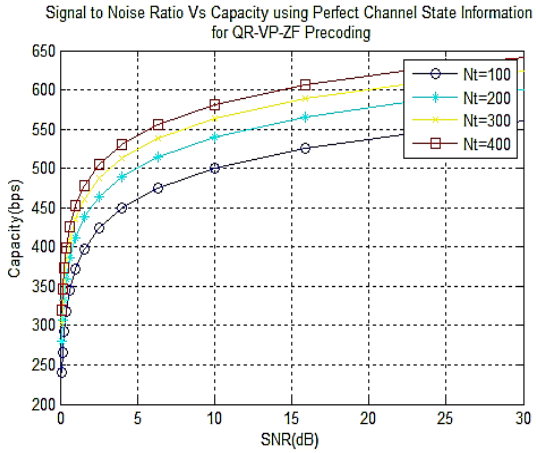

Fig. 3.15. Signal to Noise Ratio vs. capacity using perfect Channel State Information with QR decomposition technique for VP-ZF-LLL Precoder

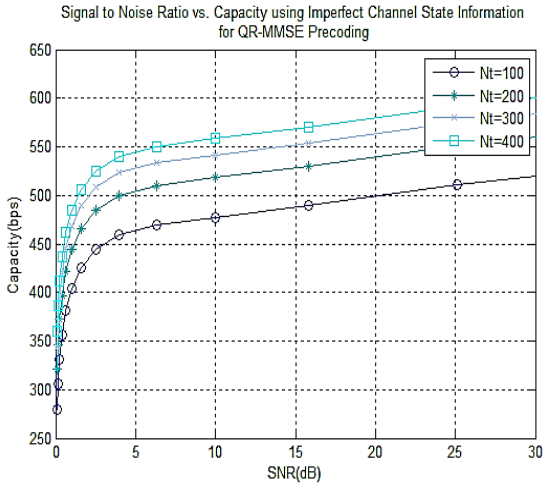

Fig. 3.16 Signal to Noise Ratio vs. capacity using imperfect Channel State Information with QR decomposition technique for MMSE Precoder

The Signal to Noise Ratio vs. capacity using imperfect Channel State Information with QR decomposition technique for VP-MMSE Precoder and Signal to Noise Ratio vs. capacity using imperfect Channel State Information with QR decomposition technique for VP-MMSE-LLL Precoder is depicted in Fig. 3.17 and 3.18 respectively.

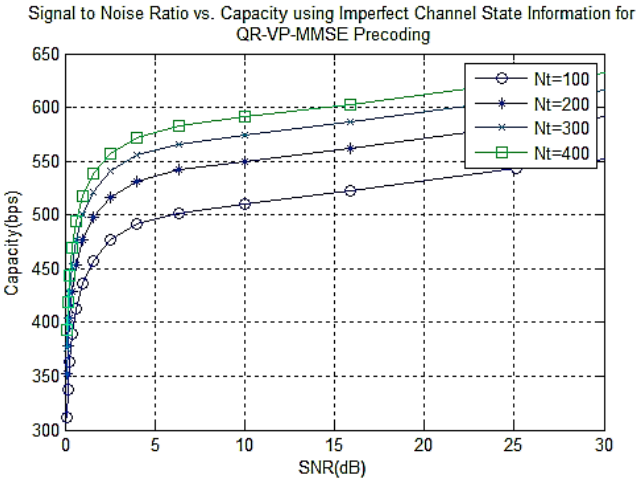

Fig. 3.17 Signal to Noise Ratio vs. capacity using imperfect Channel State Information with QR decomposition technique for VP-MMSE Precoder

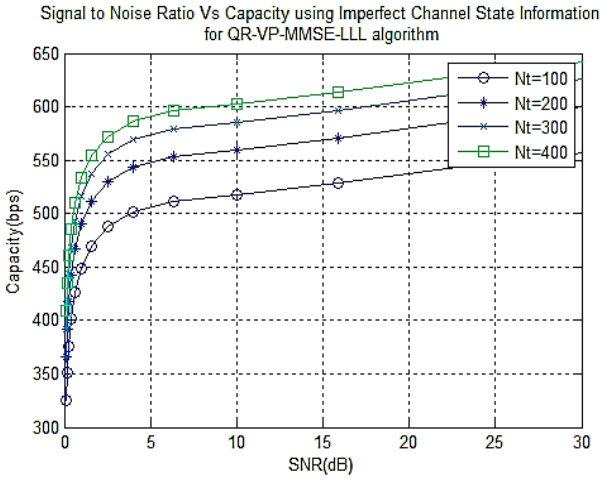

Fig. 3.18 Signal to Noise Ratio vs. capacity using imperfect Channel State Information with QR decomposition technique for VP-MMSE-LLL Precoder

Comparison of QR, SVD, GMD technique along with various precoders has been presented in table 3.1. Since THP is not suitable for massive MIMO channel matrix, the decomposition algorithms are not applied. From analysis VP-ZF-LLL precoder outperforms with all channel decomposition schemes.

Comparison of QR, SVD, GMD technique along with various precoders under imperfect channel state information has been presented in table 3.2. From analysis MMSE based precoder outperforms with all channel decomposition schemes.

B. Complexity Analysis:

The computational complexity of all the seven decomposition schemes has been plotted in Fig. 3.19, for a m×n channel matrix. The computational complexity is measured in terms of flops. The plot shows the following:

1. The minimal complexity of QR decomposition is reflected by its requirement of the computation of a single unitary matrix for decoding.
2. SVD necessitates the computation of two unitary matrices.

3. GMD which is a combination of SVD and QR decomposition suffers from a high computational complexity.
4. LU, QR decomposition schemes offers low complexity.

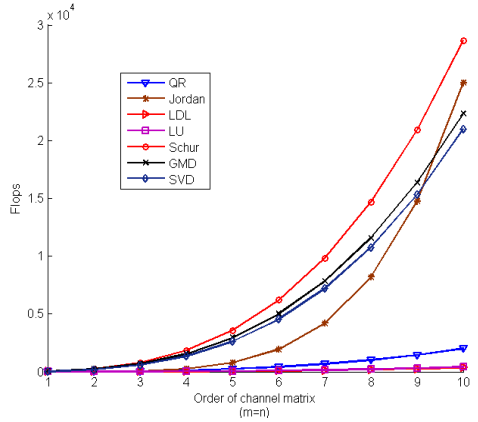

Fig.. 3.19 Computational Complexity of decomposition algorithms

It is evident that the number of operations required for Schur scheme is relatively high and low for the LDL scheme among all decompositions. Similarly, LU decomposition requires additional operations compared to LDL. Though not immediately perceivable, Jordan decomposition is computationally heavy compared to LU decomposition

TABLE 3.1 BER COMPARISON OF VARIOUS PRECODING TECHNIQUES WITH AND WITHOUT DECOMPOSITION TECHNIQUES UNDER PERFECT CSI

Precoder	MMSE	Block diagonalization	THP	VP-MMSE	VP-MMSE-LLL	VP-ZF	VP-ZF-LLL
Without decomposition	5.20×10^{-3}	1.25×10^{-1}	2.00×10^{-3}	3.78×10^{-3}	5.62×10^{-3}	4.44×10^{-3}	$\mathbf{4.05\times10^{-3}}$
QR	5.61×10^{-3}	-	-	3.86×10^{-2}	8.70×10^{-3}	3.30×10^{-3}	$\mathbf{1.76\times10^{-3}}$
SVD	5.61×10^{-3}	1.59×10^{-1}	-	4.04×10^{-3}	3.75×10^{-3}	7.03×10^{-3}	$\mathbf{2.85\times10^{-3}}$
GMD	5.42×10^{-3}	2.80×10^{-1}	-	6.03×10^{-3}	4.79×10^{-3}	4.38×10^{-3}	$\mathbf{8.07\times10^{-3}}$

TABLE 3.2 BER COMPARISON OF VARIOUS PRECODING TECHNIQUES WITH AND WITHOUT DECOMPOSITION TECHNIQUES UNDER IMPERFECT CSI

Precoder	MMSE	Block diagonalization	THP	VP-MMSE	VP-MMSE-LLL	VP-ZF	VP-ZF-LLL
Without decomposition	$\mathbf{5.63\times10^{-2}}$	7.84×10^{-2}	2.02×10^{-1}	3.97×10^{-1}	1.70×10^{-3}	3.89×10^{-3}	4.04×10^{-1}
QR	$\mathbf{5.55\times10^{-2}}$	-	-	3.92×10^{-2}	8.36×10^{-3}	3.89×10^{-3}	3.46×10^{-1}
SVD	$\mathbf{5.41\times10^{-2}}$	7.61×10^{-2}	-	3.52×10^{-1}	3.47×10^{-3}	3.14×10^{-3}	3.88×10^{-1}
GMD	$\mathbf{5.26\times10^{-2}}$	8.46×10^{-2}	-	3.06×10^{-1}	3.45×10^{-3}	3.32×10^{-1}	2.72×10^{-1}

TABLE 3.3 COMPUTATIONAL COMPLEXITY OF CHANNEL DECOMPOSITION ALGORITHMS

Sl. No.	Decomposition Scheme	No. of flops required for ($m\times n$) matrix
1.	SVD	$9m^2+8mn^2+4m^2n$
2.	GMD	*Flops of SVD* + $[(4m+n)m+4nm+4n^2+n]$
3.	LDL^H	$n^3/3$
4.	LU	$n^3/3+n^2-n/3$
5.	Schur	$(86/3)\,n^3$
6.	QR	$2mn^2$
7.	Jordan	$n^3/2 + n^3/2$

IV. CONCLUSION

The performance of Channel Decomposition Algorithms with Linear and Non-Linear precoding with Lattice Reduction using the LLL algorithm considering perfect and imperfect channel state information. The focus is on the assessment of Bit Error Rate (BER) and Capacity compared to Signal to Noise Ratio for Massive MIMO systems with the number of transmitter antennas ranging from 100 to 400. Channel decomposition schemes like QR, SVD, GMD have been analysed for altering channel matrix in to unitary or singular values. MUI cancellation and noise cancellation QR decomposed vector perturbation precoder joint with zero forcing equalization algorithms was providing low BER in perfect CSI. The upright performance of the precoder under imperfect CSI, QR-VP-MMSE was observed. The performance of QR-VP-ZF under perfect CSI and imperfect CSI based on capacity was also observed. The less effect of the channel state information on the performance of capacity was also detected.

REFERENCES

[1] C. P. Wu, and J. M. W decomposition for spatial mul 9th Workshop on Signal Pro Communications, July 2008.

[2] Y. Jiang, W. Hager, and decomposition," Linear Algeb pp. 373-384, Feb. 2005.

[3] Bojanczyk, Adam & Golub, Gene & Van Dooren, Paul. (1996). The periodic Schur decomposition. Algorithms and applications. Proceedings of SPIE - The International Society for Optical Engineering. 1770. 10.1117/12.130915.

[4] Shaowei Lin, W. L. Ho, an Diagonal Geometric Mean Multiuser MIMO Broadcast 2006, pp. 1-5

[5] V. Stankovic, and M. Haardt User MIMO Precoding Ma Commun., vol. 7, no. 3, pp. 95

[6] M. Joham and W. Utschic Harashima Precoding. chap Publishing Corporation, 2005.

[7] Chen, Wei-Da & Hwang, Yin-Tsung. (2013). A Constant Throughput Geometric Mean Decomposition Scheme Design for Wireless MIMO Precoding. Vehicular Technology, IEEE Transactions on. 62. 2080-2090. 10.1109/TVT.2013.2238686.

[8] Jiang, Yi & Li, Jian & Hager, William. (2005). Joint transceiver design for MIMO communications using geometric mean decomposition. Signal Processing, IEEE Transactions on. 53. 3791 - 3803. 10.1109/TSP.2005.855398.

[9] JS Lin, YT Hwang, SH Fang, PH Chu, MD Shieh (2014) Low-complexity high-throughput QR decomposition design for MIMO systems, IEEE Transactions on Very Large-Scale Integration, 2014.

[10] D. Wubben, R. Bohnke, Kammeyer, "Efficient algorit time codes," Electronics Letter Oct. 2001.

[11] N. Wang, and S. D. Blostein "Approximate Minimum BER Power Allocation for MIMO Spatial Multiplexing Systems," IEEE Trans. Commun., vol. 55, no. 1, pp. 180-187, Jan. 2007.

Data Transmission through Li-Fi in Underwater

Kurra Pallavi[1] and C. Padmaja[2]

[1,2]Dept. of Electronics and Communication, G Narayanamma Institute of Technology and Science, Hyderabad, Telangana, India

[1]kurra294@gmail.com, [2]padmaja.chennapragada@gmail.com

***Abstract*—In the present scenario for various industrial, scientific and underwater applications high speed wireless communication is desirable. The existing underwater communication technique such as acoustic communication method has high latency and suffer low data rates, whereas RF frequency communication have high attention of signal underwater. The emerging optical wireless communication techniques have offered high data rates in Gbps and visible light promises low attenuation of signal strength which provides high data density. The proposed method deals with the transmission of data underwater through visible light communication. The proposed method designs data transmission model where it transmits text, audio, image through water. The hardware used in this model are Arduino Nano and the transmitter part in the model is the laser light, whereas the receiver part is made of laser receiver. The transmitter follows On Off Keying (OOK) modulation technique where the blinking of laser on determine1's and off as 0's in this way the data is transmitted via line of sight to the receiver underwater. Li-Fi implementation can be executed to achieve rapid information move. In future, the capacity can be increased as per the requirement to transmit high quality image audio using higher rage lasers and photodiodes.**

***Keywords*—Arduino Nano, laser transmitter, laser receiver, OOK modulation, Li-Fi, visible light communication, underwater optical wireless communication.**

I. INTRODUCTION

In the recent years where technology has been ruling the world with its high-speed internet services, optical wireless communication can play a crucial role in this sector. Optical wireless communication is capable of providing high data rates with low power and mass requirement and is used in various industrial, space and underwater communication applications. Underwater optical wireless links are less explored as it is more challenging where various physical parameters are to be considered for the data transmission as the underwater environments vary from shallow water bodies to deep oceans. The present technology using acoustic waves for underwater communication links has limited performance due to low bandwidth, high transmission losses, time varying multipath propagation, high latency and doppler spread. These factors lead to temporal and spatial variation of acoustic channel which in turn limits the available bandwidth of the system [1]. It can support data rate up to tens of kbps for long distances (ranging in kms) and up to hundreds of kbps for short distances (few meters). All this has led to the conception of underwater optical wireless communication (UOWC), as it provides higher data rates than the traditional acoustic communication systems with significantly lower power consumption and simpler computational complexities for short-range wireless links [2]. UOWC has different potential applications ranging from deep oceans to coastal waters.

Light Fidelity (Li-Fi) is the most reliable means of underwater communication for data transmission. This paper determines the better model for underwater data transmission. This model uses visible light source such as LEDs or laser are used as transmitter and photodiodes like LDR or laser receiver are used as a receiver. The visible light source used in this model is the laser transmitter module and laser receiver on the receiver part. The data to be transmitted is processed through Arduino into 1's and 0's and it follows On Off Keying (OOK) modulation [3]. The blinking of laser on determines 1's and off as 0's, in this way the data is transmitted via line of sight to the receiver underwater. Once the data is received is processed to get the information which can be a text, audio or image. This can be a feasible means of communication between the submarines, autonomous underwater vehicles (AUV) and unmanned underwater vehicles (UUV) as it provides high data rates in the range of Gbps.

II. LITERATURE SURVEY

In the recent years, optical wireless communication is being preferred for terrestrial communications, underwater communications for different applications in various fields due to its high-speed data transfer and low equipment requirement. Acoustic waves are widely used for the underwater communication links [4]. Though acoustic communication has improved over the years for better communication in underwater for long distances but it's relatively low data rates, highly varying multipath and propagation delay makes acoustic networks less reliable [5]. The Radio Frequency (RF) communication has high data rates in the terrestrial links. The RF communication in underwater is not preferable as the RF waves get absorbed in the water and the signal gets attenuated [6]. These disadvantages paved a way for the optical wireless underwater communication which succeeds in high data rates, low signal attenuation and less equipment requirement [2]. The visible light is used for the communication in the optical wireless communication called as visible light communication. The visible light spectrum wavelength

doesn't get absorbed in the water which is the major reason for low signal attenuation and high-speed data rate in the range of Gbps [3]. Generally, the LED or laser light are used for the visible light communication in the underwater on the transmission side and received by the photodiodes [7]. Since light is used for the communication link, it is called as Li-Fi technology. For longer range and to prevent scattering, laser light is best for the data transmission [8]. Laser light is highly directional, monochromatic and coherent and it doesn't scatter in the water travelling around 100m range. Hence laser light is highly preferable. The proposed technique uses laser transceiver for the communication link in the water [9].

III. System Design

The proposed underwater wireless communication system model uses laser transceiver for the communication and a microcontroller for the data processing. The below fig. 1 is the block diagram of the proposed underwater communication link.

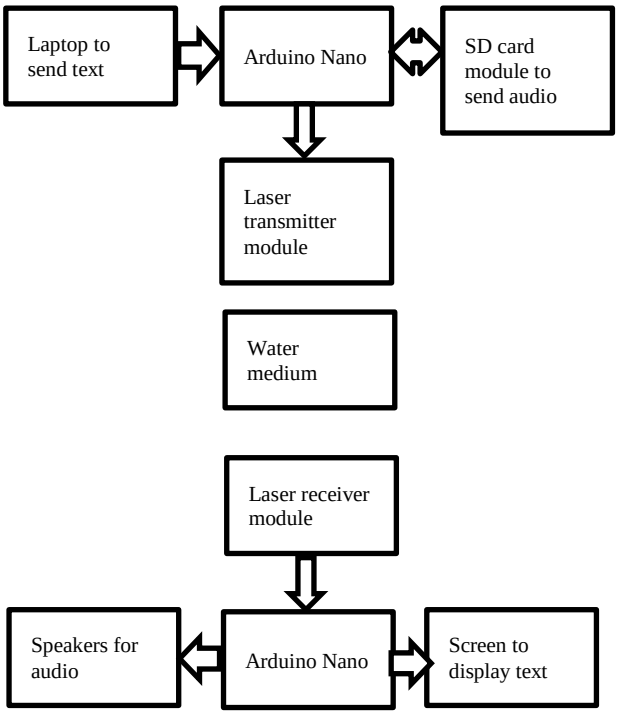

Fig. 1. Block Diagram of the proposed Underwater wireless communication model.

As stated in Fig. 1 the main blocks of the system are:

A. Arduino Nano

The microcontroller used in the proposed model is the Arduino Nano. The conversion of text or audio to bits is done here.

B. Laser Transmitter Module

It is a three pin module consisting of VCC, OUT and GND. The wavelength of the laser module used is 650nm.

The bits 1's is represented by high output i.e., on of the laser light and 0's as low, off of the laser light. In this way on off keying (OOK) modulation technique is implemented.

C. Laser Receiver Module

It is also a three pin module consisting VCC, OUT and GND. It is non modulated receiver. The contact of the laser light on the photodiode represents high and no contact as low. In this way the bits are sent to the receiver microcontroller.

D. SD Card Module

The audio is stored in the SD Card. The SPI SD card module is interfaced with the Arduino Nano. The audio is sent to the Arduino through the Sd Card module.

E. Speakers

The AUX speakers are used for the audio output. The give the better audio output.

IV. Working

A. Text Transmission

The text transmission design flow is shown in the Fig. 2.

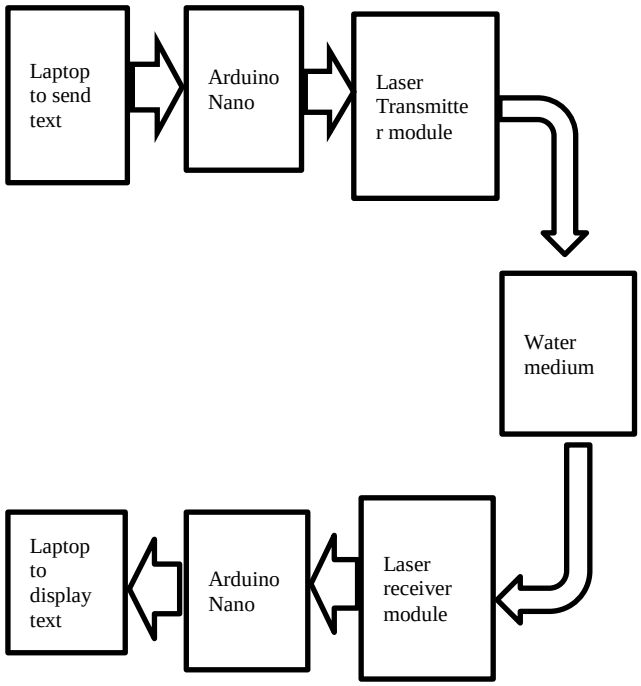

Fig. 2. Block diagram of Text Transmission.

- The text is converted into bits and sent byte by byte in the transmitter Arduino Nano to the laser transmitter.
- The on off keying modulation is done at the laser transmitter where the bits are sent as on and off of the laser light for 1's and 0's respectively through the water medium.
- The receiver depicts the contact of laser light as 1 and without contact as zero.
- The received 1's and 0's are read byte by byte and converted to characters in the receiver Arduino Nano.

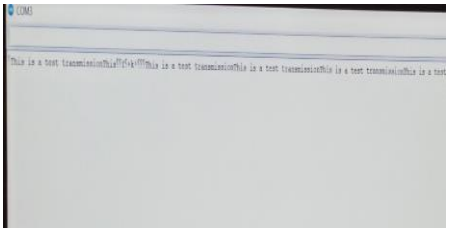

Fig. 3. Text received displayed on the screen.

The above Fig. 3 depicts the output of the text received through the water medium.

B. Audio Transmission

The below Fig. 4 shows the design flow of the audio transmission.

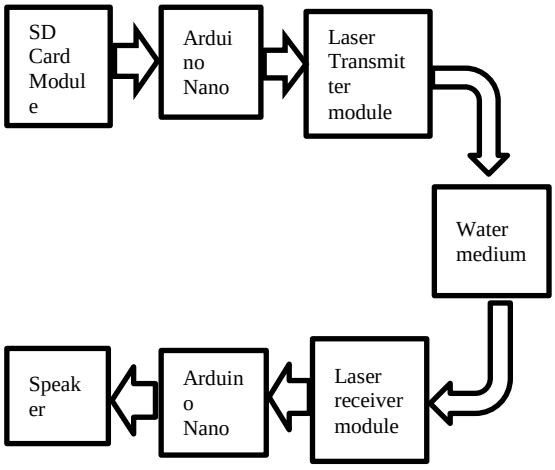

Fig. 4. Block Diagram of the Audio Transmission.

- First the audio is converted to the .wav format using the online converter tool.
- The converted audio file is stored in the SD Card. The SPI SD Card module is interfaced to the Arduino Nano.
- This audio file converted to bits and are sent to the laser transmitter where the bits are sent serially.
- The receiver depicts the contact of laser light as 1 and without contact as zero.
- The Arduino Nano at the receiver process the received bits and get back the audio file.
- The output audio file is played through the speakers at the receiver.

V. RESULTS

The data transmission model using Li-Fi technology for underwater wireless optical communication is designed. The text and audio are transmitted as shown in Fig. 5.

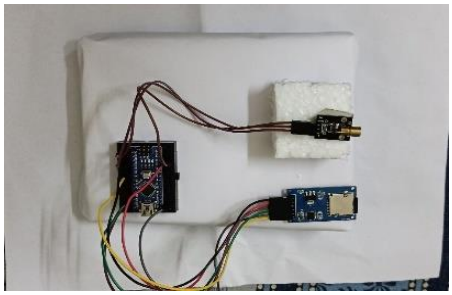

Fig. 5. Data Transmission Model.

The data transmitted is received on the laser receiver module and data is processed in the receiver Arduino Nano. The data receiver model for the underwater wireless data communication is shown in Fig. 6.

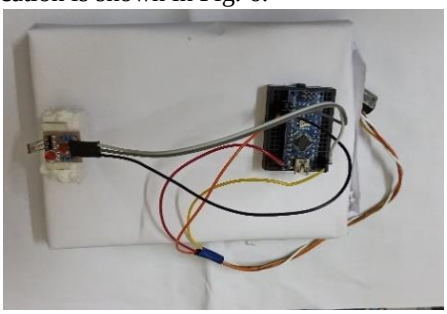

Fig. 6. Data Receiver Model.

VI. CONCLUSION AND FUTURESCOPE

The underwater Li-FI data transmission and reception model using laser transceiver is designed, where data like text and audio are transmitted using visible light communication. This provides high data rates and high data density. This model can be used for speech transmission between divers in underwater, communication between two submarines etc.

Further the utilization of underwater wireless optical communication is being developed for various applications where it can be IoT based as described in the following:

- Providing information to fishermen about the various under water species available.
- Providing the information on the pollution levels in the water to the environmental organizations.
- Providing information to the naval bases of the anonymous AUV vehicle intrusions at the water borders. Further it can be developed for video transmission in underwaters.

REFERENCES

[1] D.B. Kilfoyle, A.B. Baggeroer, "The state of the art in underwater acoustic telemetry," *IEEE Journal of Oceanic Engineering* , vol. 25, no. 1, pp. 4 - 27, 2000.

[2] Hemani Kaushal, Georges Kaddoum, "Underwater Optical Wireless Communication," *IEEE Access*, vol. 4, pp. 1518 - 1547, 2016.

[3] Georgios N. Arvanitakis, et al., "Gb/s Underwater Wireless Optical Communications Using Series-Connected GaN Micro-LED Arrays," *IEEE Photonics Journal* , vol. 12, no. 2, 2020.

[4] J. R. Apel, Principles of Ocean Physics, Academic Press, 1987.

[5] E M Sozer, M Stojanovic, J G Proakis, "Underwater acoustic networks," *IEEE Journal of Oceanic Engineering*, pp. 72-83, 2000.

[6] A.I. Al-Shamma'a, A. Shaw, S. Saman, "Propagation of electromagnetic waves at MHz frequencies through seawater," *IEEE Transactions on Antennas and Propagation*, vol. 52, no. 11, pp. 2843 - 2849, 2004

[7] Chunxiao Han, Xiaozhou Sun, Shigang Cui, "Design of 100Mbps white light LED based visible light communication system," in 2017 4th International Conference on Systems and Informatics (ICSAI), Hangzhou, China, 2017.

[8] C. Shen, "Laser-based high bit-rate visible light communications and underwater optical wireless network," in 2020 Photonics North (PN), Niagara Falls, Canada, 2020.

[9] Syed Agha Hassnain Mohsan, Abid Hussain, Nawaf Qasem Hamood Othman, Hussain Amjad, "Investigation and Design of Laser Diode based Diver-to-Diver Optical Communication System," in 2020 IE2020 IEEE MTT-S International Conference on Numerical Electromagnetic and Multiphysics Modeling and Optimization (NEMO), Hangzhou, China, 2020.

Design of Dual-Band Microstrip Antenna for Bandwidth Enhancement Using Slotted DGS

Surendra Kumar Painam[1], Devasena G[2], Siva Prasad A[3], Sri Krishna K[4], Sandhya G[5], Meena Manogna G[6]

[1-5]Dept. Electronics and Communication Enginering, Bapatla Engineering College, Bapatla, AP, India

[1]mailtosurendra@gmail.com, [2]devasena712@gmail.com, [3]sivaprasadaraja7@gmail.com,
[4]srikrishnakolla@gmail.com, [5]sandhyag34585@gmail.com, [6]meenamanogna111@gmail.com

***Abstract*—Microstrip patch antenna is used in different applications. Narrow bandwidth is one of the main disadvantage of microstrip patch antenna. In this work, we are improving the bandwidth of the Rectangular Microstrip patch antenna [RMPA] by using a slotted Defected Ground Structure [SDGS]. An RMPA is designed which operates at 2.4GHz. It is considered as a reference antenna. By introducing asymmetric, shape DGS we got a dual-band antenna, which resonates, at two different frequencies. The bandwidth is increased, the return loss and VSWR are in an acceptable range. The bandwidth obtained is used for various applications such as Bluetooth and WLAN (Wireless Local Area Network). The design and simulation is done by using HFSS software.**

***Keywords*—Dual-band, HFSS, microstrip, slot antenna, DGS.**

I. INTRODUCTION

The antenna is defined as a metallic for radiating or receiving radio waves and it is called Arial [1]. It is the transitional structure between free space and guiding device (transmission line or coaxial cable or waveguide). The guiding device is used to transport electromagnetic energy from the transmitting source to the antenna or from the antenna to the receiver. It act like radiation transducer and sensor. Antenna functions consist of the conversion of electrical current into electromagnetic wave at transmitting end and vice-versa at receiving end. Antenna directs radiating energy into desired direction and used as the impedance matching device. For the future wireless communications, more data rates are required to fulfill the bandwidth requirements. So antenna play a crucial role for this requirement. Some of the antenna performance parameters are bandwidth, return loss and gain. To improve bandwidth, they are several ways such as increase substrate thickness, decreases dielectric constant and different feeding positions [2][3].The most popular technique for bandwidth improvement is DGS technique. Now this technique is modified as slotted DGS (SDGS).

Nowadays Microstrip Patch Antenna are widely used because of its advantages like low cost, ease to fabricate, and portable [4]. One of the major drawback is narrow bandwidth. This disadvantage is overcome by different techniques. And it should be capable to operate multiple frequencies simultaneously [5].Microstrip Patch antenna are used in many applications fields like RFID (radio frequency identification devices), mobile communication, GPS systems and healthcare [6]. By using different slotted techniques one can overcome disadvantage and to increase the bandwidth. Microstrip patch antenna consists of a pair of parallel conducting layers a dielectric medium referred as substrate FR-4. It is most commonly used as an electrical insulator and possessing considerable mechanical strength [7]. The patch or upper conducting layer is the source of radiation where electromagnetic energy fringes off the edges of the patch and into the substrate, the lower conducting layers acts as perfectly reflecting ground plane bouncing energy back through the substrate and into free space physically, the patch is conducting that is an appreciable fraction of a wavelength in extent. The patch, which has resonant behavior, which is responsible to achieve adequate bandwidth. One technique to construct a multiband antenna is by applying fractal shape in to antenna geometry [8]. It is the transitional structure between free space and guiding device (transmission line or coaxial cable or waveguide) [9]. For dual-band, reactive loading technique is also used for designing microstrip patch antenna [10]. There are many aspects that affect the performance of the antenna such as dimensions, the shape of patch, slots, feeding technique, substrate [11].

II. PROPOSED ANTENNA DESIGN

The proposed rectangular microstrip patch consists of the ground plane and radiating patch is etched on other sides of the substrate. The substrate is used in this FR-4 epoxy. The length and breadth of the substrate are 58mm, 66mm and substrate thickness is 1.6mm. The software used for the design of antenna is High Frequency Structure Simulator (HFSS). The defected ground structure technique (DGS) is used in this proposed antenna, asymmetric shape is introduced in the ground plane for increasing the bandwidth. Defected Ground Structure (DGS) is more popular among all the techniques reported in the literature for enhancing the bandwidth due to its simple structural design. Removing the radiating part on the ground plane is referred as Defected Ground Structure. The removed parts may be Single or

multiple on the ground plane may be considered as DGS. Nowadays DGS is in demand extensively for various applications. DGS has been used in the field of microstrip antennas for enhancing the bandwidth and gain of microstrip antenna and to suppress the higher mode harmonics, mutual coupling between adjacent element, and cross-polarization for improving the radiation characteristics of the microstrip antenna. DGS. DGS is comparably easy to design and fabricate. Defects or etched slots on the ground plane of microstrip circuits is known as Defected Ground Structure. Single or multiple deformity on the ground plane can be considered as DGS. Nowadays DGS is more popular in the field of future wireless communication applications. It has been used in the field of microstrip antennas for improving bandwidth and gain of microstrip antenna and to suppress the higher mode of harmonics, cross polarization and mutual coupling between adjacent elements. DGS is easy to design and fabricate.

TABLE I. PARAMETERS OF THE ANTENNA

S. No	Parameter	Value
1.	Length of Substrate (L_g)	58 mm
2.	Width of Substrate (W_g)	66 mm
3.	Thickness of Substrate (t)	1.60 mm
4.	FR-4 Epoxy dielectric (ϵ_r)	4.4
5.	Length of Patch (L_p)	29.40 mm
6.	Width of Patch (W_p)	38 mm
7.	Length of feed line (L_1)	29 mm
8.	Width of feed line (W_1)	3mm

The dimensions of the antenna are calculated using the following equations

The width of the rectangular patch is given by

$$W = \frac{c}{2*fr}\sqrt{\frac{2}{\varepsilon r+1}} \quad (1)$$

The effective dielectric constant is

$$\varepsilon reff = \frac{\varepsilon r+1}{2} + \frac{\varepsilon r-1}{2}\sqrt{1+12\frac{h}{w}} \quad (2)$$

The effective length is calculated from

$$Leff = \frac{c}{2fr\sqrt{\varepsilon reff}} \quad (3)$$

The length of extension is given as,

$$\Delta L = 0.412h\frac{(\varepsilon_{eff}+0.3)(\frac{W}{h}+0.264)}{(\varepsilon_{eff}-0.258)(\frac{W}{h}+0.8)} \quad (4)$$

The actual length of top patch is obtained by using expression,

$$L = L_{eff} - 2\Delta L \quad (5)$$

The input resistance within the patch at distance from patch edge is calculated as,

$$R_{in}(y = yo) = \frac{1}{2(G_1 \pm G_{12})}cos^2(\frac{\pi}{L_p}yo) \quad (6)$$

A. Design Procedure:

Step-1: First, we need to calculate the length and width of the patch by using below mentioned formulas.

Step-2: Designing of antenna starts by creating a ground plane which is a two dimensional structure.

Step-3: In the proposed antenna, FR-4 epoxy (flame radiant) is used as a substrate. This is placed over a ground plane with the same dimensions of a ground plane. The thickness of a substrate is 1.6mm.

Step-4: Patch is a conducting material placed over the surface of a dielectric material. While designing an antenna different shapes of patches are used like rectangular, square, circular, hexagonal, triangular or elliptical in shapes. The functionality of an antenna depends on the shape of the patch used. In the proposed antenna the shape of the patch is rectangular. The calculated length and widths are used while creating the patch.

Step-5: In order to give input to the antenna, a feedline is needed. A feedline is created to the patch. The importance of the feedline is to match the input impedance of antenna. Location of feedline impact input impedance of the antenna. The design procedure is presented in Fig.1 to Fig. 5.

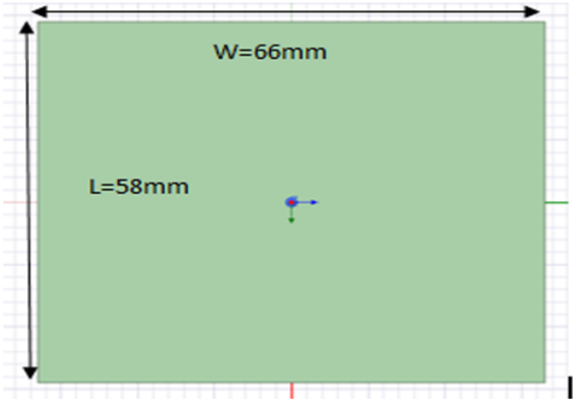

Fig. 1. Design procedure Step:1.

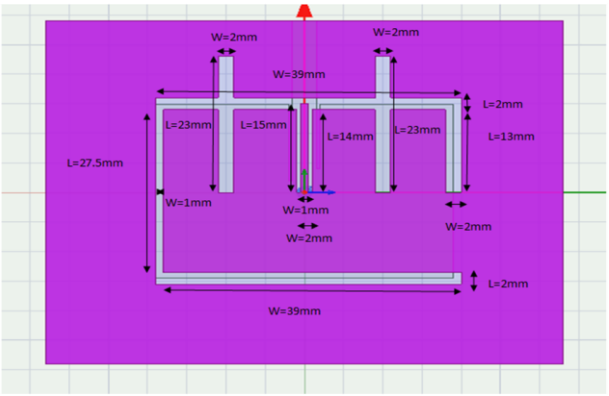

Fig. 2. Design procedure Step:2.

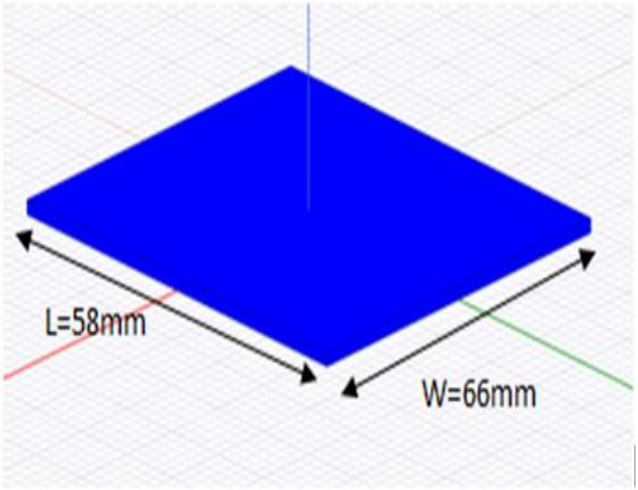

Fig. 3. Design procedure Step:3.

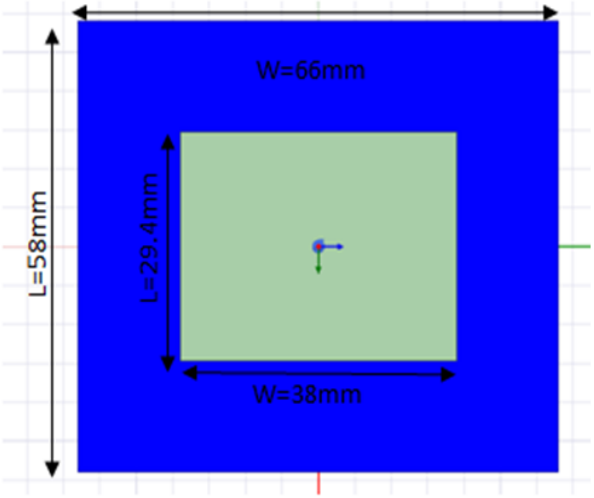

Fig. 4. Design procedure Step:4.

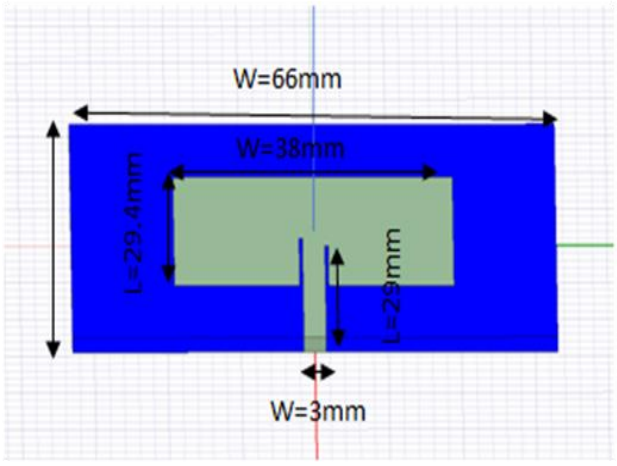

Fig. 5. Design procedure Step:5

III. Simulation Results

The proposed dual-band slotted antenna is designed with the help of Ansys HFSS Software. The below figures are the results of the simulations done on Ansys HFSS Software based on the specifications presented in Table 1. A very low cost FR4 substrate material with a standard thickness of 1.6mm is used to simulate the dual-band design. The resultant parameters are return loss (dB), bandwidth (MHz), VSWR, Gain (dBi) and fractional bandwidth (%).

A. *Return Loss*

The antenna should maintain the input-output relationship between ports which is described by return loss or S_{11} curve. S_{11} represents how much power is reflected from the antenna. For a better antenna performance, S_{11} should always be less than -10 dB. The return loss indicates the ratio of rejected and accepted radio waves arriving at the antenna. From Fig. 6 we get three parameters bandwidth fractional bandwidth and return loss. For proposed antenna return loss is 18dB and 25.93 dB at 2GHz and 2.43GHz respectively. Bandwidth is 120MHz and 6% fractional bandwidth.

B. *VSWR*

Voltage-standing wave ratio (VSWR) is a quantity that tells how best the impedance of the antenna is matched [9]. Smaller the VSWR, better the impedance matched. For better performance, VSWR reading should be near to 1. The VSWR of the proposed dual band microstrip antenna at 2 GHz and 2.43 GHz frequencies are about 1.3471 and 1.0977 respectively. This qualifies the theoretical limit of VSWR given by VSWR≤2.

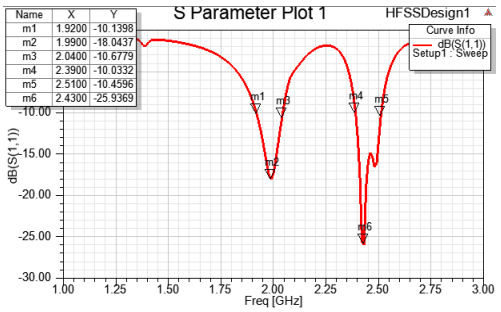

Fig. 6. Return loss vs frequency Plot.

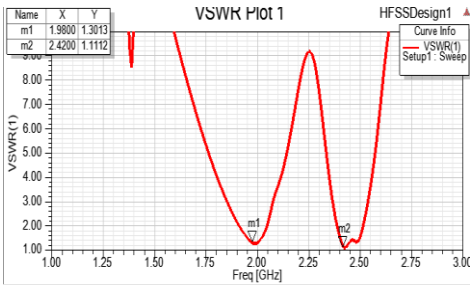

Fig. 7. VSWR plot for the proposed design

.

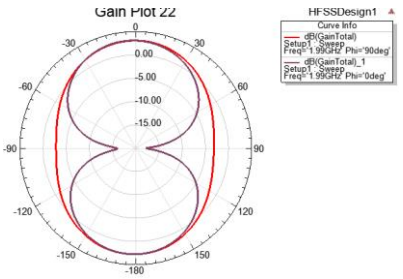

Fig. 8. 2D radiation pattern at 2 GHz

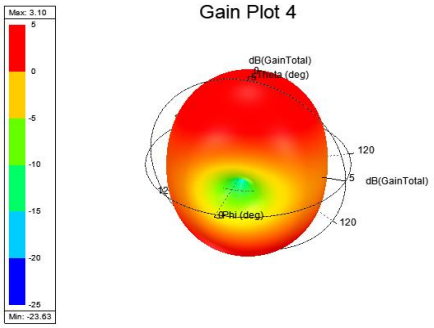

Fig. 9. 3D radiation pattern at 2 GHz

VSWR indicates the amount of mismatch between an antenna and the feed line connecting to it. The VSWR of proposed antenna is 1.20 (average of two bands).

C. *Radiation Pattern*

The radiation pattern describes the relative strength of the radiated field in various directions from the antenna at a constant distance. It also describes the receiving properties of the antenna. The radiation pattern is of both two-dimensional and 3-dimensional.

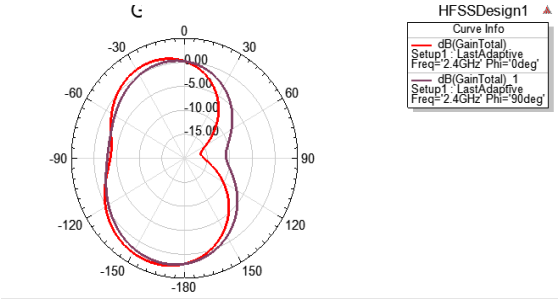

Fig .10. 2D radiation pattern at 2.4 GHz

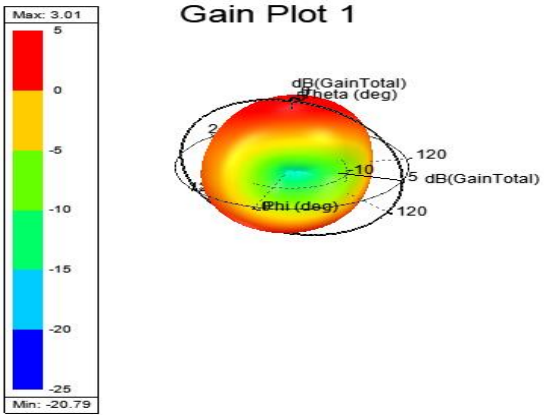

Fig. 11. 3D radiation pattern at 2 GHz.

4. Antenna gain is the ratio of power transmitted in a certain direction with a specific reference point. The proposed antenna gain is 3.025dBi.

TABLE II. SIMULATED RESULTS OF PROPOSED ANTENNA

Parameters	Values (Band1)	Band 2	Average values
Frequency	2.00GHz	2.43GHz	2.215GHz
Return loss	-18.043dB	-25.93dB	-21.98dB
Bandwidth	120MHz	120MHz	120MHz
FBW	6%	6%	6%
VSWR	1.3	1.11	1.20
Gain	3.10dBi	3.01dBi	3.05dBi

TABLE III. COMPARASION OF PROPOSED ANTENNA WITH EXISTING WORKS

Ref	Frequency (GHz)		Return loss (dB)		Bandwidth (MHz)		Avg BW
[8]	1.8	2.44	-18.7	-16.3	33	21	27
[9]	1.66	2.7	-24.59	-16.44	36.1	53.9	90
[10]	2.4	5.2	-19.6	-17.5	115	110	112.5
[11]	2.4	3.6	-22.29	-14.24	140	90	115
Pro	2.0	2.43	-18.0	-25.9	120	120	120

IV. CONCLUSION

The presented work shows the bandwidth enhancement of MPA by using asymmetric shape DGS. The bandwidth of RMPA without DGS is 60MHz.By using asymmetric shape DGS we got dual band antenna, which resonates, at two frequencies 1.99GHz and 2.43GHz. We got Bandwidth of 120MHz at two resonant frequencies. From the simulated results and comparison we can see that the how narrow bandwidth is transformed to wide band RMPA without changing its physical dimension. The proposed antenna is used for WLAN applications. The proposed antenna is designed on very low cost substrate material and easy to integrate with other devices in the communication system. To make the compact design the single design resonates at dual frequencies. By using slotted DGS (SDGS) one can extent the dual band design to triple band design.

REFERENCES

[1] Zain Ul Abedin and Zahid Ullah," Design of a Microstrip Patch Antenna with High Bandwidth and High Gain for UWB and Different Wireless Applications",(IJACSA) International Journal of Advanced Computer Science and Applications,Vol. 8, No. 10, 2017.

[2] Balanis.C.A,"Antenna+++Theory-Analysis and Design".John wiley and sons,New York.1997.

[3] BahlandP.Bhatia.I.,"Microstrip Antennas".Artech House Inc.IN.1982.

[4] Zachou.V,"Transmission line model design formula for Microstrip Antenna with slots",IEEE.2004.

[5] Kumar Gand Ray K.P, "Broadband Micro strip antennas", Artech House, USA.2003

[6] R.Mishra,"An Overview of Microstrip Antenna", HCTL open international journal of technology innovations and research(IITIR).vol.21.pp.2-4,August 2016.

[7] Jain, K., and Sharma, S. (2013). Dual Band Rectangular Microstrip Antenna for Wireless Communication Systems. International Journal of Innovations in Engineering and Technology (IJIET), 2(4), 235-246.

[8] Jacob Abraham, Mr. Aju John K K and Dr. Thomaskutty Mathew," Microstrip Antenna Based on Duder Pentagon Fractial Patch for multiband wireless applications",International Conference on Information Communication & Embedded Systems (ICICES 2014).

[9] Arun Singh Kirar, Veerendra Singh Jadaun, Pavan Kumar Sharma" Design a Circular Microstrip Patch Antenna for Dual Band",International Journal of Electronics Communication and Computer Technology (IJECCT) Volume 3 Issue 2 (March 2013).

[10] Jeffrey C. Saturday, 2Kufre M. Udofia, 3Afolayan J. Jimoh" Design of Dual Band Microstrip Antenna Using Reactive Loading Technique" Mathematical and Software Engineering, Vol. 2, No. 2 (2016), 114-121.

[11] Soundarya S, Meghana S, Shanthi P" Design of Dual Band Micro Strip Antenna for 2.4 Ghz And 3.6 Ghz"International Journal of Recent Technology and Engineering (IJRTE) ISSN: 2277-3878, Volume-8, Issue-1, May 2019.

A Review of Deep Learning-based Models for Automatic Modulation Recognition

Surendiran R[1], Sujitha Sathiyamoorthy[2], Kalaichelvi G[3], Kishan J[4], Bhadru Amgothu[5]

[1-5]Digital Signal Processing Division, SAMEER-CEM, Chennai, India

[1]surendiranr1995@gmail.com, [2]sujiheera@gmail.com, [3]kalai.sameer@nic.in,
[4]kishanj.dev@gmail.com, [5]amgothubhadru.sameer@nic.in

***Abstract*—This paper aims to review the Deep Learning (DL) architectures for modulation recognition of unstructured In phase (I) and Quadrature phase (Q) time series data at different Signal to Noise Ratio (SNR) values. Practically all the signals extracted from over the air are low power having low SNR values. Hence, the objective is to determine an optimal model, which performs well even in low SNR values and extract features to classify the signal even in high noise scenarios. This work is a comprehensive comparison of four DL models namely Resnet (Residual Neural Networks), CLDNN (Convolutional Long short-term memory Deep Neural Networks), CGDNN (Convolutional Gated recurrent unit Deep Neural Networks) and CBLDNN (Convolutional Bi- Long short-term memory Deep Neural Networks) with respect to automatic signal modulation recognition. Various metrics and parameters of the DL models trained on RadioML 2018.01A dataset like prediction accuracy at different SNR values, number of trainable parameters and training time are tabulated. The results indicate that CLDNN gives the best metrics in terms of prediction accuracy. In addition, CLDNN is trained on other two datasets and confusion matrices are plotted for analyzing the effect of dataset size and generalization of the model.**

***Keywords*—Automatic Modulation Recognition, Deep Learning, Convolutional Neural Networks, Recurrent Neural Networks, LSTM, GRU, Resnet, CLDNN, CGDNN, CBLDNN**

I. INTRODUCTION

Modulation recognition plays a major role in cognitive radio applications and is in demand for spectrum monitoring, interference detection and mitigation in both military and civilian applications. In the previous decade, modulation recognition has been done by using two approaches namely likelihood based and Feature Based (FB). Now with the evolution of faster processors and computational power, artificial intelligence based approaches such as machine learning and deep learning had become feasible, human interference is reduced and feature extraction processes are automatically carried out by neural networks. A large set of raw I/Q data is enough for a deep learning algorithm to effectively find patterns and complex features to classify the modulation categories of signals. Modulation classification is not such a complex task as image classification for the neural networks. The neural networks can extract enough features even with simpler designs.

II. BACKGROUND

Likelihood based methods make a decision by evaluating a likelihood function of the received signal and comparing the likelihood ratio with a predefined threshold. Likelihood based classifiers are optimal in minimizing the probability of false classification but they suffer from high computational complexity.

Feature based approaches target on extracting features from the signal of interest such as instantaneous amplitude, frequency, phase, higher order moments, constellation, time-frequency relation etc. Conventional FB approaches heavily rely on expert knowledge, which performs well on specialized solutions but exhibits poor performance when solving general problems and its time consuming.

Machine Learning (ML) methods have come into account, which maintains good accuracy and performance. ML classifiers for example support Vector Machines (SVM), K Nearest Neighbours also require feature engineering to some extent and accuracy depends on expert experience. The new evolved Deep Learning (DL) architecture has self-learning ability, which is easily adaptable to new environments and gives desirable performance on accuracy and efficiency.

Some of the notable literature for automatic modulation recognition using deep learning are enumerated below.

Hui Han et.al. proposed a feature fusion scheme which fuses different features of input signal for a stable and efficient representation of signal modulation classes. Here the time series signals are converted to frequency domain and Convolutional Neural Network (CNN) and Stacked Auto Encoder (SAE) are used for feature extraction [1].

Kai Liu et.al. illustrates that a deep complex network can be used to extract the amplitude and phase information of the signal. By cascading a bidirectional, Long Short-term Memory (LSTM) layer the contextual information of the signals can be extracted. The long-term dependence problem can also be addressed using the Bi-LSTM network [2].

Shunjun Wei et.al. also used the Bi-LSTM network with

their self attention mechanism to improve the recognition accuracy of low SNR radar signals [3].

Xiaosong Xie et.al proposed a network structure, which uses DenseNet (Densely connected neural networks), and BILSTM to extract more time series features which deepen the neural network without overfitting the model [4].

Zhuangzhi Chen et.al. developed a framework called sigNet where the original signal is converted to a square matrix with a signal to matrix (S2M) operator followed by a CNN for classification. The classification accuracy and efficiency is further improved by integrating a one-dimensional convolutional layer before matrix conversion operation [5].

Jialang Xu and Chunbo Luo proposed a three stream deep learning framework which extracts the features from the I/Q symbols individually and also in combined format. Integrated one dimension convolutional, two dimension convolutional and LSTM layers are used to effectively extract the features [6].

Ruolin Zhou et. al. reviewed the most recent deep learning algorithms for classifying a wireless signal. Models like CNN, Recurrent Neural Network (RNN) based LSTM, some of the hybrid types are covered, and performance is evaluated. They demonstrated the feasibility of classifying over the air wireless signals using Mathworks deep learning toolbox with Universal Software defined Radio Peripheral (USRP) and Pluto SDR (Software Defined Radio) [7].

Rui Zhang et. al discussed a hybrid method with a parallel structure which uses CNN to extract the spatial features and GRU (Gated Recurrent Unit) to extract the temporal features. An additive margin softmax function is used for the classification at the output [8].

Ke Bu et.al insist on reducing the training data size while maintaining a better accuracy. Most existing deep learning methods are suitable for data of the same distribution. In practical scenarios, data is distributed with varying sampling frequency. An Adversarial Transfer learning Architecture (ALTA) which incorporates a knowledge transfer method to address the challenges [9].

Xiaofan Li et.al discussed most of the effective machine learning and deep learning algorithms for signal classification such as ANN (Artificial Neural Networks), KNN (K nearest neighbours), SVM (support vector machines), Naive Bayes classifier, HMM (Hidden Markov model), fuzzy classifier, polynomial classifier, DNN (Deep Neural Network), DBN (Deep Belief network), CNN, LSTM, Auto encoder network, GAN (Generative Adversarial Networks) and more [10].

Omar S Mossad et.al proposed a CNN model, which outperforms the previous CNN, and CLDNN models in terms of classification accuracy. Experiments with different models have been done using python programming and Tensorflow, a deep learning framework [11].

According to Ruiyan Du et.al most existing modulation recognition algorithms have better accuracy only at high SNR. In disaster areas and battlefields, the SNR may lower to -10dB or less. The low SNR performance was improved with the help of a bidirectional RNN, which motivates us to use bidirectional LSTM [12].

Timothy James O'Shea et.al generated a dataset using SDR with 24 modulation types, which consists of both normal classes and practically significant difficult classes. The synthetic dataset was trained using a Resnet (Residual Network) model. They also used a USRP setup to transmit and receive the modulated signals to add over the air effects and channel impairments. The trained model is also evaluated using the OTA (Over the Air) signals and showed an improved effect of transfer learning [13].

III. Organization of the Paper

The paper is organized as follows, in the section 2 the background briefing the traditional methods and recent literatures on modulation recognition are discussed and the section 4 briefs about various signal datasets available and used for comparison of performance of models under consideration. In Section 5, the DL architectures with the basic description of CNN and RNN and the recent models used for review are discussed. The experimental results such as confusion matrices, Accuracy vs SNR graph for reviewed models and a table representing parameters, accuracy and training time are detailed in section 6.The challenges and future directions are portrayed in the section 7 and finally the concluding remarks are presented in section 8.

IV. Signals Datasets

Complex signals are of great use when it comes to signal processing techniques like modulation.

A complex signal m(t) is represented as

$$m(t) = m_R(t) + j\, m_I\,(t) \tag{1}$$

Where $m_R(t)$ is the real component and $m_I\,(t)$ is the imaginary component. These two orthogonal synchronously sampled parameters are known as I/Q samples.

For training, validation and testing of the deep learning networks signal datasets have more significance. In the literature a significant amount of work implemented deep learning models trained on publicly available benchmark datasets, however some of the authors used their own simulated datasets or in combination of both. Some of the publicly available datasets are briefed as follows.

A. RadioML 2016.10A

A synthetic dataset generated with GNU Radio with 11 modulation types which includes 3 analog modulations namely WB-FM, AM-SSB and AM-DSB and 8 digital modulations namely 8PSK, BPSK, CPFSK, GFSK, PAM4, QAM16, QAM64 and QPSK. Data is stored in pickle format with 220K examples, each 128 samples long. There are 20 different SNR levels from -20dB to +18dB. Simulated channel effects such as CFO (Carrier Frequency offset),multipath fading and some more effects are also included in this dataset.

B. RadioML 2018.01A

A strictly validated dataset, which includes both synthetic, simulated channel effects and over-the-air recordings of 24 analog and digital modulation types, is available for research. The modulation types are as follows:

16APSK, 32PSK, 32QAM, GMSK, 32APSK, 8ASK, OQPSK, FM, BPSK, 8PSK, AM-SSB-WC, AM-SSB-SC, 4ASK, 128APSK, 16PSK, 64APSK, 128QAM, AM-DSB-

SC, 64QAM,AM-DSB-WC, QPSK, 256QAM, OOK, 16QAM.

Data is stored as complex floating-point values in hdf5 format, with approximately 2 million examples, each 1024 samples long [13]. There are 26 SNR levels from -20dB to +30dB. Each modulation class, SNR pair, has 4096 training samples. A total of 2.56 Million I/Q time series examples are present in the dataset.

C. MIGOU-MOD

This dataset consists of over the air measurements of 11 different modulated radio signals. The signals were generated with GNU Radio, transmitted with USRP B210 and received using MIGOU, a low power experimental platform for IOT. Data is stored in pickle format with 8.8 million examples, each 128 samples long. It consists of two SNR measurements 'OTA1m' and 'OTA 6m', which corresponds to 37dB and 22 dB respectively [19].

V. DL Architectures

Deep learning is considered as a subfield of machine learning that structures algorithms layer by layer to create an Artificial Neural Network (ANN) that can learn to make intelligent decisions on its own. Deep learning is more suitable for unstructured data. Choosing or designing the right architecture might be challenging as the performance depends on many variables. Hyper-parameters are variables that determine the network structure, such as a number of hidden layers and units, activation functions, optimizer with correct learning rates, etc. and they can affect the network's performance and size a lot. Some of the significant architectures that work well with modulation recognition tasks are discussed here.

A. CNN

CNN's are designed for working on data with grid-like topology. They use convolution instead of general matrix multiplication in at least one of their layers. Image data can be seen as a 2-Dimensional grid of data and time series data have a single dimensional structure and therefore can be used in convolutional networks as well. CNN consists of arranging the combination of three basic layers such as a convolutional layer, a pooling layer and a fully connected layer. The fully connected layer, also called a dense layer, is used at the end of the network to map features into labels. The final layer is an N - dimensional vector, where N is the number of target classes from the dataset. The last dense layer is commonly activated with a softmax function, which assigns the best predicted class to the input.

B. RNN

While CNN's are good at processing data with spatial information,RNNs are designed to work with sequential information as well. They are well known for applications concerning text data in natural language processing but can work with any other sequential data such as audio signals, stock price forecasting etc.

A simple recurrent layer has a problem with vanishing gradient, which makes it harder to learn dependency during long time steps. The LSTM and GRU helps to solve this problem.

Since RNN remembers the features learned through time they make a good case for use in time-series prediction and classification. The LSTM, RNN persists the information by creating a network with loops in them [18]. This loop structure allows the network to take the sequence of input.

LSTM and GRU layers work similarly, and both save the information during the training and prevent older signals from gradually vanishing. Both LSTM and GRU have self-loop gates, which are controlled by a hidden unit, which allows the gradient to flow for a long duration.

C. Models

1) Resnet

A Residual neural network is a kind of artificial neural network. [14] This architecture was used to train Deep Neural Networks (DNN). Adding more layers to a DNN will cause overfitting, accuracy degradation and increases the validation error. Shortcut connections are inserted into the plain network to make a residual structure, Resnet is found to have considerably lower training and validation error compared to a plain network. Also the number of parameters are the same as that of its plain counterparts. The network performs well for image recognition tasks.

2) CGDNN

CGDNN network combines the use of GRU and CNN modules. CNN is good at extracting the spatio-temporal features. The model consists of a one-dimensional convolutional layer followed by a maximum pooling layer. Gaussian dropout is used to turn off random neurons to prevent overfitting. GRU module is used to trace the long term dependency as discussed in the earlier section [17]. Two GRU layers are used with dropouts in between and finally a fully connected layer with softmax activation is used for classification at the output.

3) CLDNN

The combination of convolutional and recurrent networks combines the partial feature extraction from the convolutional layer and a long-term memory coherence from the LSTM layers [15]. One convolutional layer, a max-pooling layer followed by two LSTM layers are used. In addition, two dropout layers are added in between that prevents overfitting of the model to the training data. The final layer is a dense layer activated with a softmax function, which maps to the predicted modulation classes. The layers of CNN, CLDNN and CGDNN are clearly depicted in fig. 1.

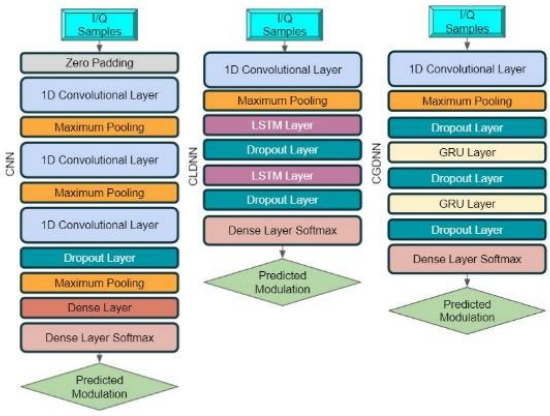

Fig. 1. Layers of CNN, CLDNN and CGDNN

4) CBLDNN

The layer arrangement in CBLDNN is the same as in CLDNN except the LSTM layers. Here the LSTM layers are replaced with Bi-LSTM [2]. Bi-LSTM is a neural network model used to process sequence information by putting two independent RNN's together. It is a combination of forward and backward LSTM networks used for taking information from input in forward and backward directions respectively. When replacing the two LSTM layers with bidirectional LSTM the number of parameters become high and the low SNR performance was not satisfactory.

VI. Experimental Results and Discussion

The state of art models mentioned in the recent literature are taken for review and trained using three open source datasets and evaluated for performance in different SNR values. The models are implemented on a computer with 3.70GHz Intel Core i9 10900X processor, NVIDIA Quadro RTX 5000 16GB computer graphics card and 64GB of RAM. The models were framed, trained and validated using python programming. Some of the important python packages used for this experiment are H5py, Tensorflow, Keras, Matplotlib, Numpy, Pandas etc. Jupyter notebook is used as an IDE (Integrated Development Environment).

A low SNR (-6dB) and a high SNR (+18dB) is chosen from the available range of SNR values in both RadioML 2016 and RadioML 2018 dataset for comparison. Since Migou-mod does not have a low SNR data only the high SNR (+ 22dB), which is closer to the other compared datasets is chosen.

Table I. Comparison of Parameters and Accuracy for Reviewed Models

DNN Model	No. of Trainable Parameters	Accuracy at -20dB	Accuracy at 0 dB	Accuracy at +30dB	Training Time in Minutes* (No. of Epochs)
CLDNN	847,488	0.35181	0.69108	0.94469	880 (48)
CBLDNN	3,714,136	0.21312	0.63038	0.95009	120 (60)
CGDNN	643,024	0.12024	0.53130	0.93605	36 (35)
Resnet-60	238,840	0.04375	0.49973	0.91916	119 (55)

The table I shows the parameters, training time and accuracy for very low, medium, high SNR values for different models whose input, and output layers have been modified to fit RadioML 2018 dataset. From the above table the advantages and disadvantages of the models can be inferred. While CGDNN has, the lower training times compared with the rest and has less parameters thus the size. Even Though Resnet has less parameters its performance is satisfactory only at high SNR and is not suitable for practical scenarios. The CBLDNN, also a hybrid model, gives a better performance only after CLDNN but the number of trainable parameters is high and requires powerful computational resources to train making it less attractive.

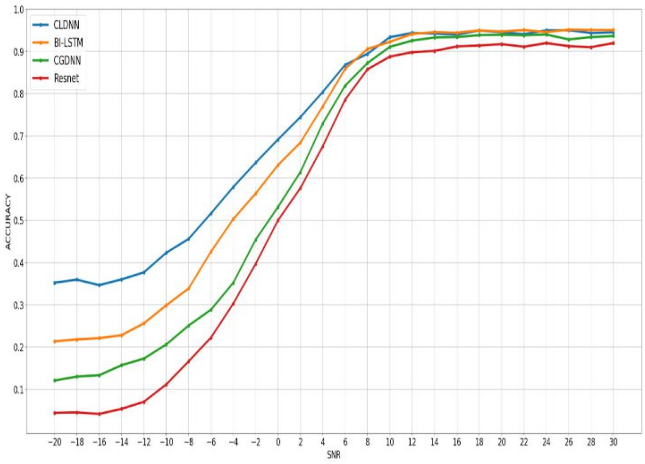

Fig. 2. Accuracy vs SNR graph of DL models trained and tested using RadioML 2018.01A dataset

From the Fig. 2, we can infer that CLDNN model with tuned hyper parameters outperforms the other models even in the lower SNR values and gives 70 percent accuracy in zero SNR value. In addition, Resnet seems to be a better model but its performance is poor when it is deployed in a low SNR environment, and it misclassifies every modulation type to be 128 QAM. Therefore, it is clear that Resnet cannot be used for practical low SNR applications.

In order to evaluate the influence of datasets on the top performing model, the results in the form of confusion matrix for CLDNN model trained and tested on three available datasets is presented below. The confusion matrix for CLDNN model trained on RadioML 2016 dataset at -6dB and +18dB SNR is shown in Fig. 3 and Fig. 4 respectively.

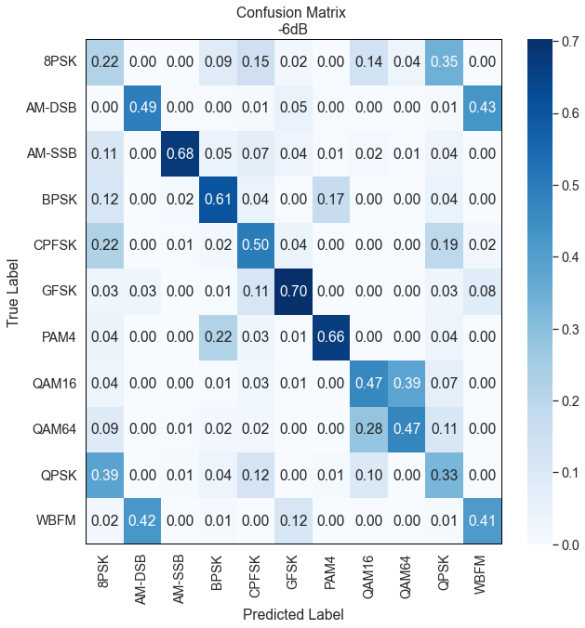

Fig. 3. Confusion matrix of CLDNN model for RadioML 2016 dataset at -6dB SNR

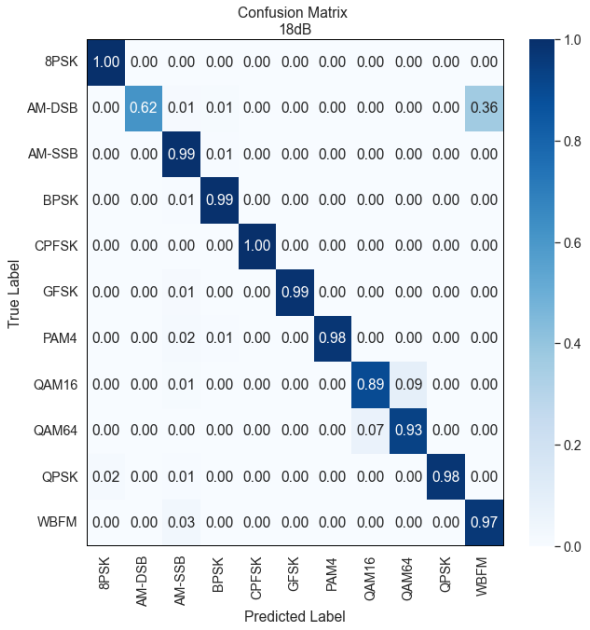

Fig. 4. Confusion matrix of CLDNN model for RadioML 2016 dataset at +18dB SNR

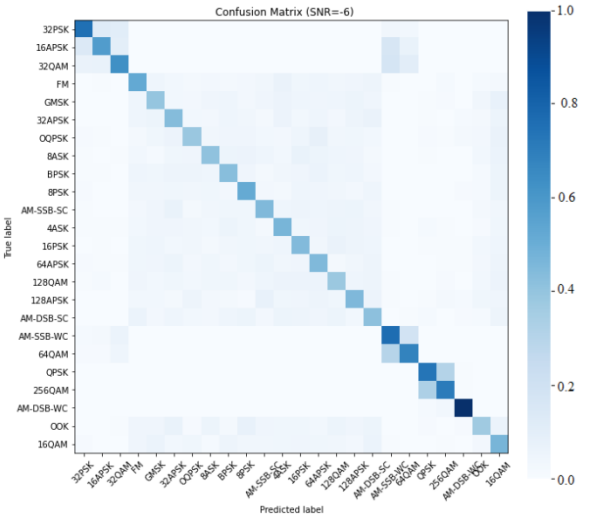

Fig. 5. Confusion matrix of CLDNN model for RadioML 2018 dataset at -6dB SNR

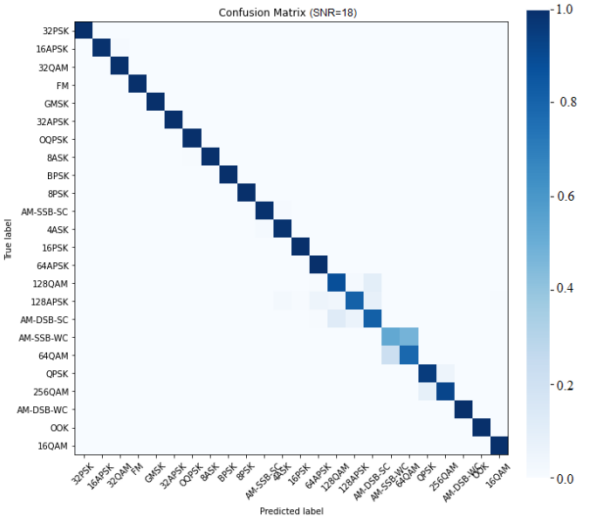

Fig. 6. Confusion matrix of CLDNN model for RadioML 2018 dataset at +18dB SNR

The confusion matrix for CLDNN model trained and tested on RadioML 2018 dataset at -6dB and +18dB is shown in Fig. 5 and Fig. 6 respectively. From the above results, it is observed that the CLDNN model trained on RadioML 2016 and 2018 datasets gives good classification accuracy for majority of modulation schemes, even in low SNR.

The results in low SNR shows a significant improvement when trained on RadioML 2018 dataset compared to 2016 dataset. It can be attributed that the size of the 2018 dataset is vastly larger than the 2016 dataset and quality of the dataset played a major role in training a deep learning model.

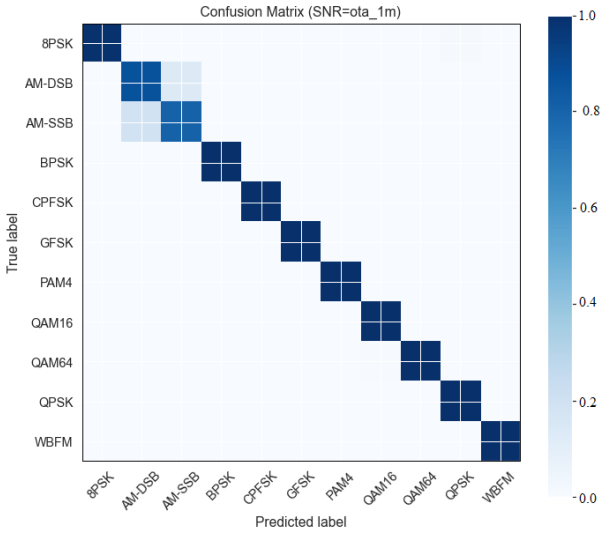

Fig. 7. Confusion matrix of CLDNN model for Migou-mod dataset at ota_1m equivalent to 22dB SNR

In the migou-mod dataset the stated SNR values are 22 dB (OTA_6m) and 37dB (OTA_1m).The model is trained on the entire dataset. Since there is no significant difference between the two SNR values, the confusion matrix for 22 dB is plotted in Fig. 7.

VII. Challenges and Future Research Directions

When it comes to deep learning, a high quality dataset is required in addition with a good fitting model because deep learning architectures are basically data driven. The performance of the model depends on the features learned from the input training data and if certain real-life conditions are ignored in the dataset, the trained model might not generalize well.

It is imperative that we choose the model depending on the practical application as it is inferred from the above results that different models give different performance on a particular SNR range. Hence, a single model cannot achieve best results for every SNR and a trade off between performance and desired SNR has to be done. As the dataset used for training and validation are synthetic, practical signals may have some different features. Hence, the models should be adaptive and robust enough to classify the signals. Radio channel is not only limited to these 24 modulation schemes and day by day efficient modulation schemes are evolving and also tending to be more complex in nature. The model can be extended to train any other new modulation techniques. Modulation recognition is not the only attribute

for wireless signal identification. Deep learning has constantly been evolving and there is an open research area for wireless signal recognition in defense applications. Spectrum monitoring devices such as RF sensors are capable of acquiring wireless signal's I/Q components in a detailed manner, storage of such data on distributed sensing devices is often infeasible due to resource constraints. Hence, more optimal model with less storage requirements need to be framed.

VIII. Conclusion

In this work, recently evolved deep learning models for automatic modulation recognition are reviewed and the performance are evaluated. A deep insight on the performance of the CLDNN model on three different datasets for different SNR scenarios is presented. During validation using RadioML 2018 dataset, at -20 dB SNR CLDNN gives 14% higher prediction accuracy than CBLDNN, 23% higher than CGDNN and 31% higher than Resnet. It is observed that the quality of the dataset and the model's architecture are vital to obtain satisfactory performance. As stated earlier deep learning is robust for complex problem solving like the automatic modulation recognition. However, the Deep Learning model is only as good as the data it is trained on. A major challenge is to see how the trained models performs in the real time scenario. Hence, efforts are needed to ensure the progress obtained translates to real time applications.

References

[1] Han H., Ren Z., Li L., Zhu Z. Automatic Modulation Classification Based on Deep Feature Fusion for High Noise Level and Large Dynamic Input. Sensors. 2021; 21:2117. doi: 10.3390/s21062117.

[2] Kai Liu, Wanjun Gao, and Qinghua Huang Automatic Modulation Recognition Based on a DCN-BiLSTM Network. Sensors. 2021;21:1577. doi: 10.3390/s21051577.

[3] S. Wei, Q. Qu, X. Zeng, J. Liang, J. Shi and X. Zhang, "Self-Attention Bi-LSTM Networks for Radar Signal Modulation Recognition," in IEEE Transactions on Microwave Theory and Techniques, vol. 69, no. 11, pp. 5160-5172, Nov. 2021, doi: 10.1109/TMTT.2021.3112199.

[4] X. Xie, G. Yang, M. Jiang, Q. Ye and C. -F. Yang, "A Kind of Wireless Modulatio Recognition Method Based on DenseNet and BLSTM," in IEEE Access, vol. 9, pp. 125706-125713, 2021, doi: 10.1109/ACCESS.2021.3111406.

[5] Z. Chen et al., "SigNet: A Novel Deep Learning Framework for Radio Signal lassification," in IEEE Transactions on Cognitive Communications and Networking, doi: 10.1109/TCCN.2021.3120997.

[6] J. Xu, C. Luo, G. Parr and Y. Luo, "A Spatiotemporal Multi-Channel Learning Framework for Automatic Modulation Recognition," in IEEE Wireless Communications Letters, vol. 9, no. 10, pp. 1629-1632, Oct. 2020, doi: 10.1109/LWC.2020.2999453.

[7] R. Zhou, F. Liu and C. W. Gravelle, "Deep Learning for Modulation Recognition: A Survey With a Demonstration," in IEEE Access, vol. 8, pp. 67366-67376, 2020, doi: 10.1109/ACCESS.2020.2986330.

[8] Zhang, R.; Yin, Z.; Wu, Z.; Zhou, S. A Novel Automatic Modulation Classification Method Using Attention Mechanism and Hybrid Parallel Neural Network. Appl. Sci. 2021, 11, 1327. https://doi.org/10.3390/app11031327

[9] K. Bu, Y. He, X. Jing and J. Han, "Adversarial Transfer Learning for Deep Learning Based Automatic Modulation Classification," in IEEE Signal Processing Letters, vol. 27, pp. 880-884, 2020, doi: 10.1109/LSP.2020.2991875.

[10] X. Li, F. Dong, S. Zhang and W. Guo, "A Survey on Deep Learning Techniques in Wireless Signal Recognition", Wireless Communications and Mobile Computing, vol. 2019, 2019.

[11] Mossad, Omar S., ElNainay, Mustafa, Torki, Marwan "Modulations Recognition using Deep Neural Network in Wireless Communications", 2nd Europe - Middle East - North African Regional Conference of the International Telecommunications Society (ITS), 2019, International Telecommunications Society (ITS), Calgary.

[12] Du, Ruiyan & Liu, Fulai & Xu, Jialiang & Gao, Fan & Hu, Zhongyi & Zhang, Aiyi. (2021). Modulation Recognition Based on Denoising Bidirectional Recurrent Neural Network. 10.21203/rs.3.rs-325033/v1.

[13] T. J. O'Shea, T. Roy and T. C. Clancy, "Over-the-Air Deep Learning Based Radio Signal Classification," in IEEE Journal of Selected Topics in Signal Processing, vol. 12, no. 1, pp. 168-179, Feb. 2018, doi: 10.1109/JSTSP.2018.2797022.

[14] K. He, X. Zhang, S. Ren and J. Sun, "Deep Residual Learning for Image Recognition," 2016 IEEE Conference on Computer Vision and Pattern Recognition (CVPR), 2016, pp. 770-778, doi: 10.1109/CVPR.2016.90.

[15] N. E. West and T. O'Shea, ''Deep architectures for modulation recognition,'' in Proc. IEEE Int. Symp. Dyn. Spectr. Access Netw. (DySPAN), Mar. 2017, pp. 1–6.

[16] F. A. Gers, "Learning to forget: Continual prediction with LSTM", Proc. 9th Int. Conf. Artif. Neural Netw. (ICANN), pp. 2451-2471, 1999.

[17] S. N. Tran, A. D. Garcez, T. Weyde, J. Yin, Q. Zhang and M. Karunanithi, "Sequence classification restricted Boltzmann machines with gated units", IEEE Trans. Neural Netw. Learn. Syst., vol. 31, no. 11, pp. 4806-4815, Nov. 2020.

[18] D. Hong, Z. Zhang and X. Xu, "Automatic modulation classification using recurrent neural networks", Proc. 3rd IEEE Int. Conf. Comput. Commun. (ICCC), pp. 695-700, Dec. 2017.

[19] Utrilla, Ramiro (2020), "MIGOU-MOD: A dataset of modulated radio signals acquired with MIGOU, a low-power IoT experimental platform", Mendeley Data, V1, doi: 10.17632/fkwr8mzndr.1

Channel Selection by using Fuzzy C Means Clustering under lower SNR

Subhabrata Dhar[1] and Sabyasachi Chatterjee[2]

[1]Assistant Professor, Guru Nanak Institute of Technology, Kolkata, India
[2]Assistant Professor, Heritage Institute of Technology, Kolkata, India

[1]subhabratadhar1992@gmail.com, [2]sabyasachi.chatterjee@heritageit.edu

***Abstract*— Channel selection plays an essential role in uninterrupted and efficient cognitive communication. However, the reliable channel selection in real-time may be affected severely due to variation of the operational parameters. Therefore, we have implemented the learning-based sensing and allocation mechanism to enhance channel sensing in the cognitive radio network. An analytical data prediction model has been proposed in this paper for channel prediction. The proposed ADP model has reduced the transmission delay to a great extent. The packet loss ratio and transmission delay have been considered as selection parameters. The Fuzzy C means clustering algorithm has been applied to enhance the accuracy of the proposed model. The modified model detects available channels even under lower signal-to-noise ratio conditions.**

***Keywords*—Cognitive Radio Network; Transmission Delay; Modified Analytical Data Prediction; Fuzzy C Means Clustering; Lower Signal to Noise Ratio.**

I. INTRODUCTION

During the last few years, globally, there are rapid growths of wireless communication devices. The limited radio spectrum is widely used by various mobile technologies such as wireless local area network (WLAN), Global systems for mobile communication (GSM), military and commercial services over large geographical regions. Therefore, the spectrum becomes overloaded due to the limited allocation of the spectrum. This problem leads to spectrum scarcity [1]. Cognitive radio (CR) technology [2] is established to mitigate the problem of spectrum inefficiency. The CR is a promising technology that is capable to gather information from the surrounding radio frequency (RF) environment, learning from it, and making firm decisions about proper utilization of spectrum [2]. Therefore, channel sensing and selection are salient features in cognitive radio networks (CRN) [3]. In CRN, licensed users or primary users (PUs) are allowed to transmit data on the licensed spectrum. But unlicensed users or secondary users (SUs) always try to access those licensed spectrums opportunistically [4]. Sometimes, cognitive radio users (CRUs) act as SUs that continuously observe the behavior of PUs by various sensing techniques. Proper spectrum sensing by SUs can lead to efficient utilization of spectrum. However, there is a high probability of interferences between PUs and SUs that can effectively degrade the performance of PU [5]. Therefore, channel selection and allocation need to be enhanced to improve the spectrum access reliability of licensed bands.

Several channel sensing and selection techniques have been performed to monitor the presence of PUs in CRN. The Markovian model [6] was implemented to determine the best free spectrum for proper secondary allocation. However, with the help of the Markovian model [6], SUs fail to indicate whether PUs is already present in the spectrum or not. Therefore, the hidden Markov model (HMM) has been incorporated in [7] to avoid channel detection problems. But, HMM has failed to control the uncertainty problems when two or more users are present in the spectrum due to the shadowing effect. Hence, a centralized cooperative spectrum (CCS) mechanism has been implemented to solve the uncertainty problems [8]. The CCS technique helps users to share information among them and take proper decisions to improve the quality of the spectrum. But, all these methods are unable to reduce the transmission delay and interference problems that degrade the performance of CRN. Hence, an analytical data prediction (ADP) model has been incorporated in this paper to minimize the computational as well as transmission delay problem in CRN. The ADP model is very much efficient to select free channels by distinguishing between free channels and busy channels. The proposed ADP model implements a learning-based channel selection mechanism by machine learning (ML) technology. ML can gather information from past data, learn from it and adapt itself based on the acquired knowledge [9]. In our proposed work, multi-slot channel sensing has been performed where transmission delay and packet loss ratio of the channel has been considered as operating parameters in learning-based channel selection.

The fuzzy C means clustering (FCM) algorithm has been implemented in our work to enhance the accuracy rate of the ADP model under a lower signal-to-noise ratio (SNR). The FCM algorithm [10] is an efficient ML-based technology that can significantly mitigate the interference problem under lower SNR conditions. Hence, the channel selection mechanism can be enhanced to a great extent under lower SNR.

The significant contributions of this paper are as follows:

- The proposed ADP model is established to reduce the

computational delay through efficient channel selection.

- The proposed model also can mitigate the transmission delay problem in the network.
- The FCM algorithm has been incorporated to enhance the accuracy level of the proposed ADP model.
- The modified ADP (MADP) model can perform efficient channel selection even under lower SNR.

The rest of the paper categorizes as followers: Section 2 explains the channel selection model, section 3 exhibits result and analysis and finally section 4 concludes this paper.

II. Channel Selection Models

In this work, we have performed simulation of n channels in m different time slots to exhibit a channel selection scheme by using an analytical data prediction (ADP) model.

In the proposed ADP model, the set of channels has been represented as $p,\ p \in \{1,2,3,....n\}$, where n is the total number of channels. Algorithm 1 shows the channel prediction scheme in the cognitive radio network (CRN). The linear regression scheme [11] has been applied in our proposed ADP model.

The best fit line of linear regression can be depicted in eq.1 as

$$y = c_0 + c_1 x + e \tag{1}$$

where, y is the predicted variable, x is the data samples, c_o is the intercept, c_1 is the slope of the line and e is the prediction error.

The slope c_1 is defined in eq.2 as

$$c_1 = \frac{P_{xy}}{P_{xx}} \tag{2}$$

where, P_{xy} is the regression coefficient of x and y variables and P_{xx} is the regression coefficient of two x variables.

Here, $$P_{xy} = \sum_{p=1}^{n} (x_p - \bar{x})(y_p - \bar{y}) \tag{3}$$

and $$P_{xx} = \sum_{p=1}^{n} (x_p - \bar{x})^2 \tag{4}$$

where, $\bar{x}$ is the mean of data samples, $\bar{y}$ is the mean of predicted variables and n is the total number of channels.

Replacing values of P_{xy} and P_{xx} in eq.2, we get,

$$c_1 = \frac{\sum_{p=1}^{n} \left(x_p - \bar{x}\right)\left(y_p - \bar{y}\right)}{\sum_{p=1}^{n} \left(x_p - \bar{x}\right)^2} \tag{5}$$

The eq.5 is the final derived equation of the slope of the line.

The final derived equation of prediction error (e) can be expressed in eq.6 as

$$e = c_1 (x - \bar{x}) \tag{6}$$

The prediction error e is actually the vertical distances from each data point projected to the best fit line. In our proposed ADP model, we have considered the threshold prediction error as 0.05. The threshold transmission delay of channels has also been assumed as 3.5 ms. If the prediction error as well as the delay of channels are less than 0.05 and 3.5 ms respectively, then the channel has been considered as free channel for secondary allocation. Otherwise, the channel is partially filled channel that means PUs are already present in the channel. In our proposed ADP model, our main objective is to minimize the delay of channels as well as the summation of the squares of vertical distances $\sum d_n^2$ where n is represented as number of channel data points. In case of free channels, if delay of channels decreases, then packet loss ratio of channels also get minimized. This can improve the learning based channel selection to a great extent. However, sometimes in case of high signal to noise ratio (SNR), secondary users (SUs) fail to monitor the location of primary users (PUs). Therefore, learning based sensing mechanism gets degraded. Hence, in our work, the fuzzy c means clustering (FCM) algorithm has been implemented under lower SNR conditions to enhance the channel sensing accuracy of the proposed ADP model. So, a modified ADP model has been established by using FCM algorithm.

Fig.1 exhibits the schematic representation of FCM algorithm. The FCM is the clustering based machine learning (ML) technique that performs by initializing membership value to each data samples [10]. Here, data samples are channels in each time slot. The set of channels has been abbreviated as $p,\ p \in \{1,2,3,....n\}$, where n is the number of channels. Channels in each time slot have been categorized into several clusters. Each cluster comprises of center point or centroid. The set of cluster centers has been represented as $c,\ c \in \{1,2,3,...g\}$, where g is the total number of cluster centers. In our simulation, we have considered two clusters. The fuzzy membership value β varies based on the euclidean distance between the data point and the centroid.

The fuzzy membership value (β) can be represented in eq.7 as

$$\beta = \left[\sum_{c=1}^{g} \left(h_{cp}^2 / h_{pa}^2 \right)^{1/z-1} \right]^{-1} \tag{7}$$

Here, h_{pa} is the euclidean distance between p^{th} data and a^{th} cluster center. z is the fuzziness parameter (generally considered as 2 or 3). In our work, we have taken z as 2.

The cluster center (χ_a) can be calculated in eq.8 as

$$\chi_a = \sum_{p=1}^{n} \left(\beta_{cp}^z * x_c \right) / \sum_{p=1}^{n} \beta_{pc}^z \tag{8}$$

where, $a \in \{1,2,...g\}$ and x_c is the c^{th} data point.

The fuzzy membership value as well as cluster center must be updated after each iteration to obtain better results. Here, in our work, we have executed 20 iterations to get

accurate results. In FCM, objective function must be reduced to acquire good membership values.

The objective function can be demonstrated in eq.9 as

$$F(p,a)=\sum_{p=1}^{n}\sum_{a=1}^{q}\left(\beta_{pa}\right)^{z}\left\|x_p-\chi_a\right\|^2 \tag{9}$$

If the distance between p^{th} data variable and a^{th} cluster center decreases, then overlapping of clusters occur. Therefore, there is a high probability that the data point can belong to more than one cluster. The overlapping of cluster leads to accurate results.

Here, in our simulation, the lower threshold of β has been considered as 0.5 whereas upper threshold of βhas been considered as 0.6 to obtain overlapped data points. Therefore, learning based channel selection can be enhanced under lower signal to noise (SNR) conditions. Fig.2 depicts flow chart representation of MADP algorithm.

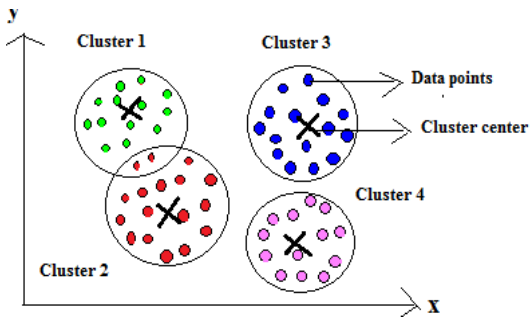

Fig. 1: Fuzzy C Means Clustering Algorithm [10]

ALGORITHM 1 : MODIFIED ANALYTICAL DATA PREDICTION MODEL

1. Initialize set of channels by p, where $p \in \{1,2,3,4,....n\}$, where n is the total number of channels.
2. Assign p channels in m slots. Assign slot number as $l, l \in \{1,2,...m\}$.

Secondary user senses each channel in each time slot to identify whether the channel is free or busy.

3. ***While*** $l \le m$ ***do*** {
4. ***for*** (p =1 to n) {
5. Estimate best fit line by using equation $y = c_0 + c_1 x + e$, where y is the packet loss ratio of channels and x is the delay of channels.
6. Initialize vertical distance as $d_p, \forall p$.
7. Estimate $\sum d_p^2 \ \forall p$.
8. Calculation of computational error e.
9. $e \leftarrow$ min $\left|\sum d_p^2\right|$
10. Calculate slope of the best fit line $(c_1)$by using equation 6.
11. Calculate intercept $(c_0)$of the best fit line by using equation 8.
12. Put values of c_0, c_1 and e in step 5 for obtaining the predicted output.
13. ***if*** $(e \le 0.05)$
    if $(x < 3.5)$ **then**
    Free channels $\leftarrow p$

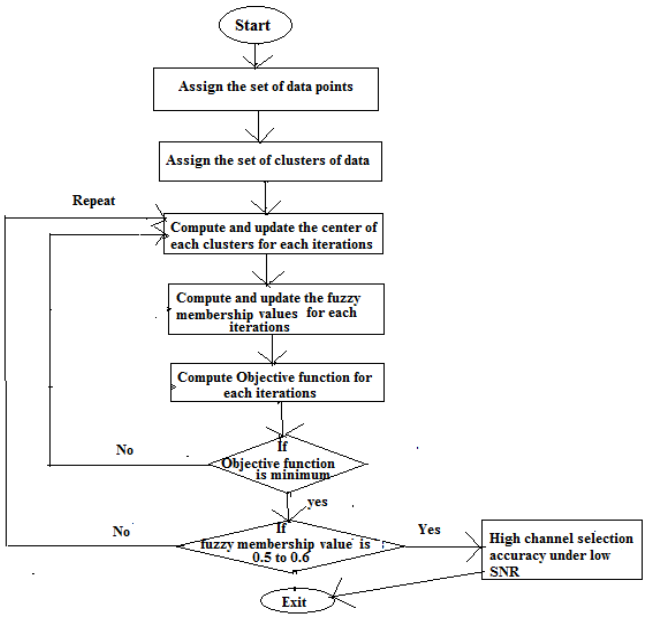

Fig. 2: Flow chart representation of MADP algorithm

III. RESULT SECTION

In the proposed analytical data prediction (ADP) model mentioned in algorithm 1, we have performed a simulation to select reliable free channels for secondary allocation. In the proposed system model, eighteen channels have been considered with three-time slots. A group of six channels has been applied for each time slot. These channels in each time slot have been abbreviated as ch1, ch2, ch3, ch4, ch5, and ch6. Three parameters have been analyzed to estimate the channel performance.

A. Channel Detection by using the proposed ADP model

In fig.3 depicts a multi-slot channel selection scheme. The Channels belonging to the first, second, and third time slots have been indicated by red, black, and blue colors, respectively. The threshold limit of delay for all channels has been kept within 3.5 ms. The graphical analysis exhibits that channels (ch2, ch3, ch4, ch5, ch6) of the first time slot except ch1 are suitable for secondary user allocation since squared vertical distances of channel points (ch2, ch3, ch4, ch5, ch6) from the best-fit regression line are less than 0.05[as per algorithm 1]. Vertical distance represents deviations or computational errors. However, the delay of channels (ch3 and ch4 of slot1) is more than the threshold limits (3.5 ms). Therefore, ch3 and ch4 of the first time slot have been considered as partially filled channels. In the case of slot2, all channels are suitable for secondary user allocation [as per algorithm1]. Here, the delay of channels has not exceeded the threshold limit (3.5 ms). Therefore, all channels in slot2 have been considered as free channels. Similarly, in the case of the third time slot, ch1, ch3, ch4, ch5, and ch6 are suitable for secondary allocation, whereas channel ch2 of slot 3 is partially suitable for allocation due to high delay (more than 3.5 ms) [as per algorithm 1]. Table I shows the summary of free channels, partially filled channels, and busy channels for each time slot.

However, in case of free channels, there is less channel interference due to lower transmission delay and packet loss ratio. Therefore, signal to noise ratio (SNR) of channels also get increased [12]. For these reasons, data transmission of channel enhances that improves the signal quality to a great extent. But, sometimes high SNR can degrade the signal quality of the cognitive radio network (CRN). Therefore, SNR with lower value has been taken into consideration to improve accuracy of our work. Therefore, fuzzy c means clustering (FCM) algorithm has been implemented in fig.4. By the help of FCM, we have obtained free channels with lower SNR value.

TABLE I. SUMMARY OF FREE CHANNELS, PARTIALLY FILLED CHANNELS AND BUSY CHANNELS

Time Slot	Free Channels	Partially Filled Channels	Busy Channels
1	Ch2, Ch5, Ch6	Ch3, Ch4	Ch1
2	Ch1, Ch2, Ch3, Ch4, Ch5, Ch6	No Channels	No Channels
3	Ch1, Ch3, Ch4, Ch5, Ch6	Ch2	No Channels

B. Improved Channel Detection under lower SNR value

The graphical analysis of fig.4 depicts the enhanced channel detection under lower SNR value with the help MADP algorithm [refer to fig.2]. Here, channels in each time slot have been divided into two clusters (Cluster 1 and Cluster2). Channels in first slot, second slot and third slot have been highlighted with green color, blue color and magenta color respectively. Each cluster has a cluster center (or centroid). The FCM algorithm works by assigning membership values to each channel points. The membership value depends on the distance between cluster center and channel points. The membership value varies from 0 to 1. If the membership value is 0.5, then there is probability that a channel point belongs to two clusters. The overlapping data gives good prediction and high accuracy. In fig.4, we can observe that if the membership value is kept between 0.5 and 0.6, then accuracy level increases. In slot1, channels (ch3, ch4) have membership values of 0.5424, 0.598 respectively. Although, ch3 of slot 1 has been considered as the partially filled channel, it can be considered for secondary allocation due to good membership value and high accuracy. Therefore, ch3 and ch4 of slot1 have more accuracy level with lower SNR value. Similarly, in slot2, it has been detected that channels (ch3 and ch4) have membership values of 0.562 and 0.59 respectively. Again, in slot3, channels (ch3 and ch4) have membership values of 0.585 and 0.572 respectively. Therefore, channels (ch3 and ch4) suffer less interference problems. The SNR has been considerably reduced due to this phenomenon.

In fig.5, we have depicted the variation of SNR with different membership values of channels. It has been clearly visualized from the fig.3 that the SNR value becomes less within the range of 0.5 and 0.6 of membership value. Therefore, prediction accuracy increases under lower value of SNR. In case of slot 1, channels ch3 and ch4 have SNR values of 16.4 and 18.4 dBm for membership values of 0.5424 and 0.598 respectively. Similarly, in slot 2, channels ch3 and ch4 have SNR of 17.2 and 18.1 dBm for membership values of 0.562 and 0.59 respectively. Again, in slot3, we have observed that channels ch3 and ch4 have SNR of 17.8 and 17.92 dBm for membership values of 0.585 and 0.572 respectively. Therefore, we can conclude that these channels are very ideal for secondary allocation in

lower SNR value. Table II summarizes list of channels under lower SNR values.

Fig.6 depicts the SNR behavior of the k-means clustering algorithm [13]. The fig.6 shows that the membership value is high for both lower as well as high SNR. The SNR also fluctuates abruptly for different membership values. Therefore, the channel selection efficiency has been reduced. However, in the case of the FCM algorithm, the membership value remains below 0.6 for a lower SNR value. Hence, the MADP algorithm performs more efficiently than the k- means clustering algorithm. Table III depicts a comparative study on the established MADP model with the k means clustering algorithm based on channel selection accuracy.

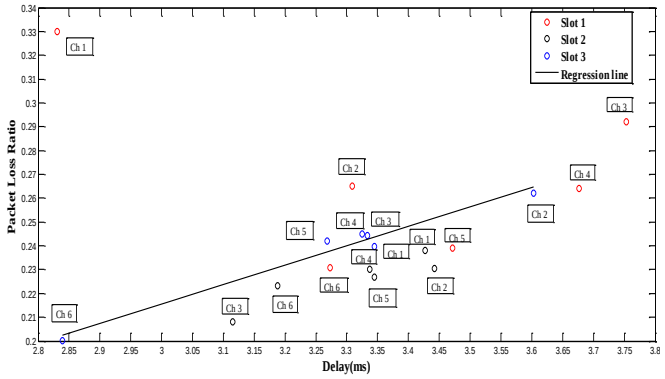

Fig.3: Channel Detection with the help of proposed ADP model

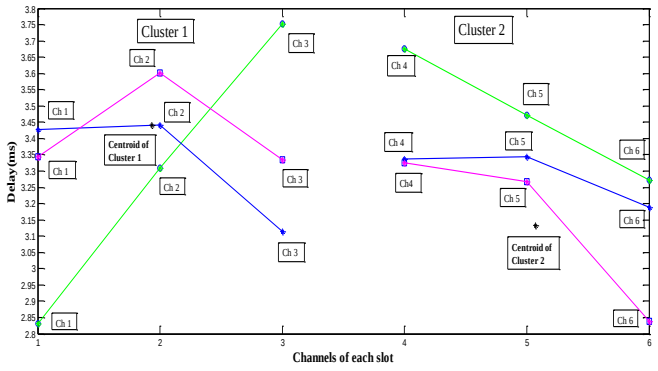

Fig.4: Enhanced Channel Detection by using MADP model

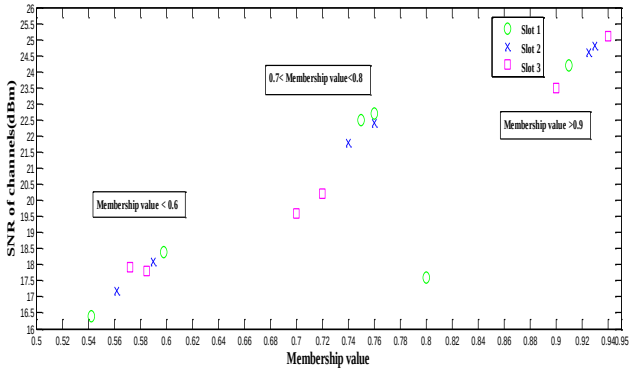

Fig.5: Variation of SNR with respect to membership value of channel by using MADP Algorithm

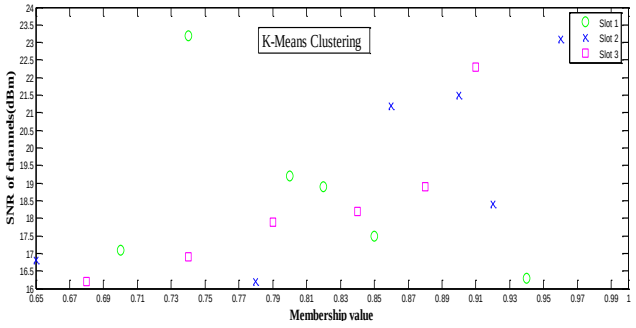

Fig.6: Characteristics of SNR with respect to membership value of channel by using K -Means Clustering Algorithm [13]

TABLE II. LIST OF CHANNELS WITH DIFFERENT SNR VALUES

Channels	Slot	Membership value (β)	SNR (dBm)
Ch 3	1	0.5424	16.4
Ch4		0.598	18.4
Ch 3	2	0.562	17.2
Ch 4		0.59	18.1
Ch3	3	0.585	17.8
Ch 4		0.572	17.92

TABLE III. COMPARISON OF ALGORITHMS WITH RESPECT TO ACCURACY

Algorithms	Accuracy (%)	Features
Modified ADP model	99.1	Channel sensing in lower SNR in Cognitive Radio Network.
K-Means Clustering [13]	86.5	

IV. CONCLUSIONS

A learning-based channel selection model has been incorporated in this paper to enhance the CRNs' performance. The ADP model has been proposed to perform reliable channel selection for secondary communication. The proposed ADP model has considerably reduced the computational as well as transmission delay in the network. The efficiency of the proposed model has been enhanced by applying the FCM algorithm under lower SNR conditions. It has been observed that the channel selection accuracy has been improved under lower SNR with the modified model. The graphical analysis states that channels (ch3, ch4 of the first slot, ch3, ch4 of the second slot, and ch3, ch4 of the third slot) are suitable for secondary allocation with a prediction rate of 99.1%. MATLAB and Radio Frequency simulators have been applied to execute network simulations in this paper. In the future, the proposed model may be implemented for the successful deployment of orthogonal based 5G cognitive cellular network.

REFERENCES

[1] Tlouyamma, J., & Velempini, M. (2021). Channel Selection Algorithm Optimized for Improved Performance in Cognitive Radio Networks. *Wireless Personal Communications*, *119*(4), 3161-3178.

[2] Develi, I. (2020). Spectrum sensing in cognitive radio networks: threshold optimization and analysis. *EURASIP Journal on Wireless Communications and Networking*, *2020*(1), 1-19.

[3] He, X., Song, Y., Xue, Y., Owais, M., Yang, W., & Cheng, X. (2022).Resource Allocation for Throughput Maximization in Cognitive Radio Network with NOMA. *CMC-COMPUTERS MATERIALS & CONTINUA*, *70*(1), 195-212.

[4] Hlophe, M. C., Maharaj, B. T., & Hamouda, S. (2017, September).Distributed spectrum sensing for cognitive radio systems using graph theory. In *2017 IEEE AFRICON*, 267-272.

[5] Zhao, J., & Wang, X. (2012, October). Channel sensing order in multi-user cognitive radio networks. In *2012 IEEE International Symposium on Dynamic Spectrum Access Networks*, 397-407.

[6] Loganathan, J., & Janakiraman, S. (2016, March). Improved history based channel allocation scheme for cognitive radio networks. In *2016 World Conference on Futuristic Trends in Research and Innovation for Social Welfare (Startup Conclave)*, 1-8.

[7] Chatziantoniou, E., Allen, B., Velisavljevic, V. (2013). An HMM-based spectrum occupancy predictor for energy efficient cognitive radio. In: IEEE 24th International Conference on Personal Indoor and Mobile Radio Communications, 601–605.

[8] Sharma, V., & Joshi, S. (2018, June). A Literature Review on Spectrum Sensing in Cognitive Radio Applications. In *2018 Second International Conference on Intelligent Computing and Control Systems (ICICCS)*, 883-893.

[9] Rehman, K., Ullah, I., & Habib, M. (2019, March) Detail Survey of Cognitive Radio Communication System.

[10] Paul, A., & Maity, S. P. (2017, March). On energy efficient cooperative spectrum sensing using possibilistic fuzzy c-means clustering. In *International Conference on Computational Intelligence, Communications, and Business Analytics* (382-396).

[11] Uyanık, G. K., & Güler, N. (2013). A study on multiple linear regression analysis. *Procedia-Social and Behavioral Sciences*, *106*, 234-240.

[12] Atapattu, S., Tellambura, C., Jiang, H., & Rajatheva, N. (2014). Unified analysis of low-SNR energy detection and threshold selection. *IEEE Transactions on vehicular technology*, *64*(11), 5006-5019.

[13] Marquez, H., Salgado, C., & Hernández, C. (2017). Multichannel assignment using K-Means in cognitive radio networks. *Tecnura*, *21*(52), .68-78.

NEIGHBOUR VEHICLE MONITORING IN V2I USING DEDICATED SHORT-RANGE COMMUNICATION

Reshma P[1] and V. Sudha[2]
[1,2]Department of ECE, National Institute of Technology, Tiruchirappalli

[1]408121005@nitt.edu, [2]vsudha@nitt.edu

***Abstract*—Future transport implants with automatic driving vehicles, where the practical challenge is detecting traffic and reducing vehicle to vehicle and vehicle to infrastructure communication delay. These problems can be solved using image processing and RADAR based approaches. However, the vehicle at a certain distance, out of line of sight. Therefore, to provide a solution to identify out of LOS range vehicles, vehicles communication modules with short-range communication were implemented as the future communication between the vehicle to vehicle and vehicle to infrastructure communication process. Here in this paper, vehicle to vehicle and vehicle to infrastructure communication was implemented. vehicle to everything modules implementation results in vehicles' connectivity and their communication was established using the 802.11e module based dedicated short-range communication for effective and efficient. This approach also helps the driver of the vehicle to learn the streamline of traffic and roadways. To travel very safely and reduce delay communication which is an important barrier of the communication system was minimized using the proposed vehicle to everything communication system.**

***Keywords*—V2V, V2I, DSRC, communication, wireless communication, transportation systems.**

I. INTRODUCTION

India is perhaps the busiest country on the planet as far as street traffic. The auto business across the south Asian nation turned into the fourth biggest on the planet in 2017. In 2019, there were just about 3,000,000 new vehicle enlistments in the country. The Indian Street organization, crossing more than 5,000,000 kilometres, conveyed right around 90% of the country's traveller traffic and around 65% of the products.

V2V (Vehicle to Vehicle) is a correspondence innovation that encourages in minimizing accidents and regulates the traffic density. It utilizes VANETs (vehicular ad-hoc networks), data incorporates speed, position, slowing down, soundness, the course of movement, among others. This communication module utilizes DSRC. The principal objective of a V2V communication is to eliminate lives cost and hazardous car accidents.

Industry pioneers expect that associated V2X will find a fault in the remote communication with vehicles, and infrastructure.

The main uses of the V2X communication include:

- Personalized help of street and side of the road
- Real-time traffic update
- Monitoring autos and change of places of roadways
- Emergency cautions to caution drivers about out of the path floating
- Slowdown of vehicles while recognizing any hindering in its closeness of reach

This paper considers a single direction, bi-directional avenue (e.g., thruway) for effortlessness as shown in Figure 1, Drivers overlook the width of paths accepting the width is immaterial compared to the road period; thus, the vehicle closer to each route can be seen as a one-dimensional point degree. As indicated, [9-11] the vehicles on a throughway can be demonstrated as a Poisson Point Process. Everyone should not forget the vehicles that are suited for V2V & V2I (Vehicle to Infrastructure) communication and do not leave the roadway earlier than arriving at the goal RSU (Road Side Unit) as it were. Drivers can appraise vehicles' considering the above situations and apply a diminishing method to the car turning degree. Characterize a set as the automobile where the vehicles are going similar way, and each pair of vehicles within the bunch is associated through both single-path and multi-soar way.

In a set, the vehicle nearest to RSU is characterized as the Cluster Head (CH). RSUs that can be handled using Internet are placed alongside the road. Each RSU can communicate with automobile units in the correspondence range utilizing V2I. An automobile unit has an inner communication that helps to communicate with RSU can straightforwardly switch through a V2I interface; else, it wishes to use V2V connection to lower the inactiveness.

Drivers make the accompanying presumptions (that have been broadly utilized inside the past works, e.g., [9], [11], [13]). Vehicles can accumulate the statistics, including nearby RSUs, the car pace and density of the current road element, and trading records with specific vehicles and RSUs. V2I has a higher information rate and larger inclusion of transmission data that allows to communicate using V2V. An applicable MAC layer (e.g., [1], [6]) is utilized so automobiles can transmit the faraway channels on hand for V2V transmission efficaciously.

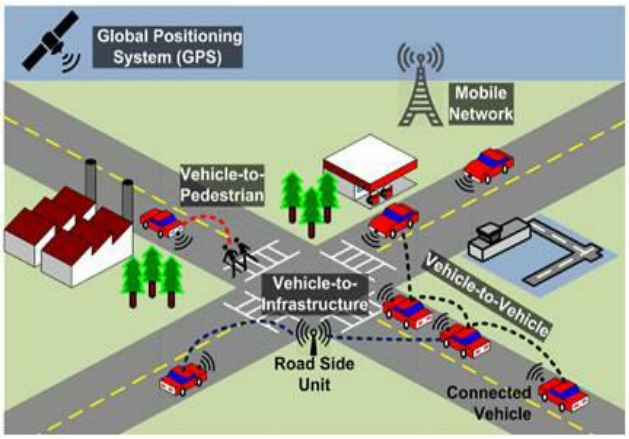

Figure 1 System Model

II. Mathematical Modeling Of Proposed Method

Hence, to construct a viable scientific model, to solve the problem anticipating the constant V2I/V2V facts pay and state of no activity for every V2I/V2V transmission, separately, and information may get delay that might lead to crashes otherwise channel blurring are unimportant. The proposing approach may consider the below point as suppositions

- Brake without Lane Changing (cars intersection)
- Conservative Lane Change
- Performance Lane Change
-

To deploy the proposed approach, it is necessary to learn how a transportation system works with associated vehicles differs from an ordinary one. Every driver conveys their objectives (for example, securely make the objective in 60 minutes) and displays various qualities (for example, response time, wanted speed, and course inclination). The driver's thinking insight and their objectives and attributes are joined with the apparent world to settle on driving choices, for example, target course, lane-keeping, and driving pace. Thus, these choices are completed as activities and executed on the vehicle. Subsequently, the vehicle moves powerfully as the driver coordinates. In the interim, this vehicle and different vehicles' movement adjust the actual world powerfully reflected in the driver's apparent world, which triggers the above interaction cycle. Their front, the above cycle, can be summed up as a driver vehicle climate shut circle approach.

Interestingly, in a transportation framework with associated vehicles, the driver's capacities are altogether upgraded because of V2V and V2I DSRC:

- The apparent world turns into a more successive example of the actual world, particularly at crucial points in time since the associated vehicle innovation can help the driver to continually screen the actual world and draw their consideration as the need emerges.
- The apparent world turns into a more precise figure of the actual world since the associated vehicle innovation gives the driver more exact data about the actual world.
- The apparent world covers a bigger extent of the actual world since V2V and V2I DSRC broadens the driver's situational mindfulness past their insight limit.
- There is less vulnerability in the driver's dynamic since their apparent world approximates the actual world nearer.

Accurate data requires less an ideal opportunity for the driver to react, and diminished vulnerability diminishes discernment response fluctuation.

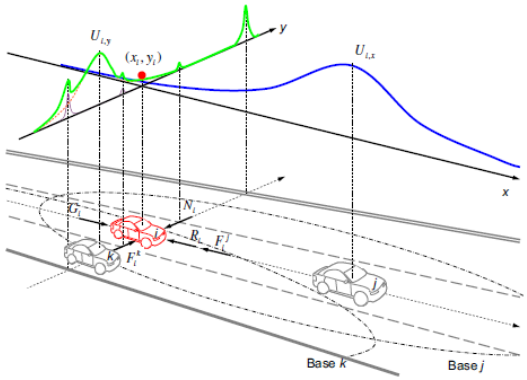

Figure 2 Roadways with RSU and V2V connection

Vehicles can each be tended to as a possible field. Above Figure 2 addresses two such fields clear by a driver: one for vehicle j and the other for vehicle k, the two of which show up with slants perceptible for what it's worth and related bases on the ground. The vehicle i interface with j and k far off intervened by their corresponding fields. For instance, vehicle j impedes i by spurning power while k drives i to avoid another force F_i^k, where F_i^j and F_i^k can be gotten from their relating fields. Note that driver characteristics and the related vehicle effects can be brought into the meaning of these fields. Even more unequivocally, such fields' shapes and sizes might vary when seen by different drivers or a comparable driver at different running conditions and other situational care. For example, an intense driver will recognize more restricted after distances. Therefore, the obvious field between vehicles covers a more unassuming base. On the other hand, a driver helped by related vehicle advancement knows the state of their neighbour decisively and might respond quickly so that the evident field may be more hidden than that of a driver without such assistance.

A driver's perspective on forwarding roads supplements compactness and security (gains) while avoiding accidents and encroachment of traffic rules (setbacks). Such a procedure can be tended to use an overall potential field U_i containing fragment fields, such as moving bodies U_i^B, roads U_i^R, and traffic light contraptions U_i^c.

$$U_i = U_i^B + U_i^R + U_i^c \quad (1)$$

If U_i is viewed as a mountain range whose tallness means the risk of hardships, the driver's framework investigates the mountain range along its valley, for instance, the most un-upsetting course. For example, Figure 2 addresses two sections of such a field. As the scene driver i, the longitudinal x piece of the field, $U_{i,x}$, is overpowered by vehicle j since it is the solitary bordering vehicle centrally. The vehicle I tended to as a ball that rides on the tail of twist

$U_{i,x}$ since the vehicle is inside vehicle j's field. Like this, the vehicle I is reliant upon a rebuffing power F_j^i, which is gotten from $U_{i,x}$ as

$$F_j^i = -\frac{\partial U_{i,x}}{\partial x} \quad (2)$$

The impact of F_j^i is to push vehicle i back to be careful distance. By consolidating the driver's unsatisfied craving for versatility $(G_i - R_i)$, the net power apparent by driver i the x way can be resolved as

$$m_i x_i = \sum F_{i,x} = G_i - R_i - F_i^j = (m_i g_i - R_i) + \frac{\partial U_{i,x}}{\partial x} \quad (3)$$

The segment of U_i in the parallel y bearing, $U_{i,y}$ (strong bend), is the amount of two segments: the cross-part of the field because of vehicle k (ran bend) and that because of the street field (dabbed bend). The previous outcomes in a repulsing power F_i^kmake vehicle I avoid vehicle k, and the last creates a remedy power Ni should vehicle I leave its path community. Subsequently, the net impact can be communicated as

$$m_i y_i = \sum F_{i,y} = -N_i + F_i^k = \frac{\partial U_{i,x}}{\partial x} \quad (4)$$

The above strategically arrangement of conditions summarizes Field Theory in nonexclusive terms and contains the principal law that supervises a driver's functional control (for instance, controlling and accelerating/deceleration) of their vehicle on roads.

As shown Figure 3, driver help empowered by associated vehicle innovation can upgrade driver capacities, for example, driver attributes Q and situational mindfulness X. In this manner, Q and X are data elements that V2V and V2I DSRC achieve. For instance, upheld by human factor contemplates [2] the insight response season of a standard driver (without driving help), a driver with driving help and as tests various appropriations The contrasts between normal helped and robotized vehicles can be reflected in these basic dispersions.

Driving conduct demonstrating captures the communication between cars, especially the automobile's reaction to the vehicle in front, for example, the F_i^jexpression. This term can be streamlined as a security rule: at any second, a car ought to depart sufficient area earlier than it to have the choice to prevent securely behind its riding car if the primary automobile applies crisis slowing down. Two cars following each other. A Driving vehicle with ID I-1 is located x_{i-1} with speed $x_{i-1}(t)$ and quickening. The situation automobile i is at position x_i with velocity $x_i(t)$ and increasing speed$x_i(t)$. The safe base distance has to permit the concerned vehicle to stop behind the main vehicle after a perception reaction time s_i and a deceleration interplay at an ok degree piece.

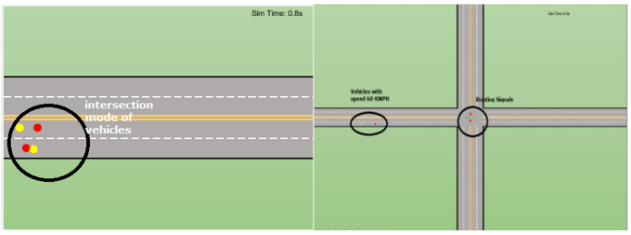

Figure 3 V2V or V2I connectivity with 2-way lane and 4-way lane with signals

After some math, the security rule may be formed as

$$S_i(t) = x_{i-1}(t) - x_i(t) \geq l_{i-1} + x_i\tau_i - l_{i-1} - \frac{x_i^2(t)}{2b_i} + \frac{x_{i-1}^2(t)}{2B_{i-1}} \quad (5)$$

S_i is the isolating between the two vehicles, B is the best acceleration applied by the actual vehicle, and l is the primary vehicle's length. Under congruity conditions, vehicles will, for the most part, continue reliably and, this way, lose their characters. After choking time t, the partitioning becomes

$$S \geq l + x\tau - \frac{x^2}{2b} + \frac{x^2}{2B} = \left(\frac{1}{2B} - \frac{1}{2b}\right)x^2 + \tau x + l \quad (6)$$

To ensure security from accidents, an extra defer q to s offers additional assurance for the subject vehicle, so the above disparity becomes

$$S \geq l + x(\tau + \theta) - \frac{x^2}{2b} + \frac{x^2}{2B} = \left(\frac{1}{2B} - \frac{1}{2b}\right)x^2 + (\tau + \theta)x + l \quad (7)$$

Hence, a non-maintaining distance cover between the vehicle is unequivocally communicated as an element of speed (under balance conditions, it is additionally the traffic pace) with boundaries s, q, B, b, and l. Among the entirety of the boundaries, s and q address drivers' conduct and are fair of speed v and dividing S, B, b, and l are vehicle houses and can be expected as constants. To comprehend that density k is related to dispersing S

$$k = \frac{1}{S^0} \quad (8)$$

the traffic flow q is acquired by displacing k the stream q is arranged by displaced k and v into the crucial connection:

$$q = kv = \frac{v}{Gv^2 + \tau' v + l'} \quad (9)$$

In this connection, v can be seen as the essential information. v and s^0 are autonomous factors. Therefore, the most extreme feasible q is of interest. To track down the most extreme q (meant q_m), addressing the condition:

$$\frac{dq}{dv} = \left| -\frac{G - \frac{1}{v^2}}{Gv + \tau' + \frac{l}{v}} \right|_{v_m} = 0 \quad (10)$$

get the root:

$$V_m = \sqrt{\frac{l}{G}} \tag{11}$$

and correspondingly:

$$q_m = \frac{1}{2\sqrt{Gl}+\tau'} \tag{12}$$

To confirm that q_m is undoubtedly a most as v shifts, one can likewise test the second side project of q at v_m. Again, it appears to be that this is real.

III. RESULTS

In figure 4 the neighbouring connection error analysis was performed on different lane mode of operations. Figure 4(a) indicates 6 vehicles communication for simulation time in same lane same direction was plotted. Figure 4(b) indicates 6 vehicles communication for simulation time in two lanes in equal share with opposite direction was plotted. Figure 4(c) indicates 6 vehicles communication for simulation time in four lanes with random vehicle allocation in all 4 directions was plotted. Figure 4(d) indicates 6 vehicles communication for simulation time in four lanes with random vehicle share with random lane selection along with traffic signal-based direction plotted.

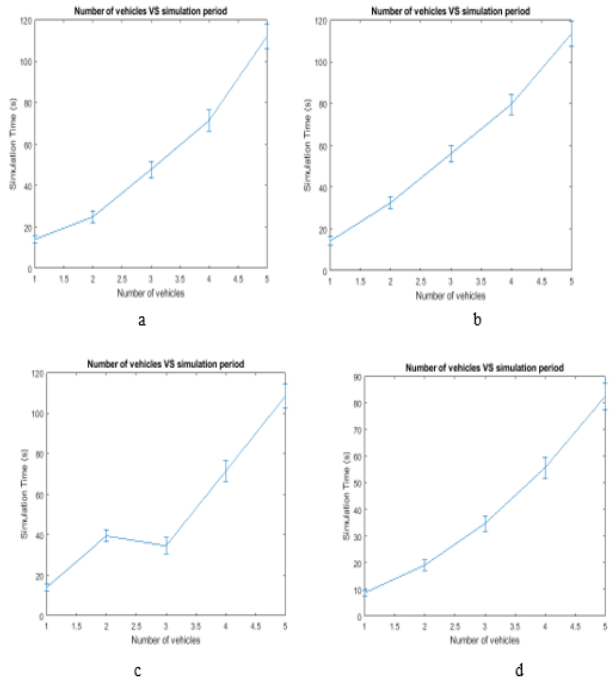

Figure 4 Error analysis for simulation with respect to number of vehicles

In figure 5 connectivity with respect to neighbouring connections with respect to 3rd vehicle, for a 50m distance with average vehicle speed 60 KMPH as per Indian roads shown in figure 5(a), as per time of 30 sec limit-based traffic density and connection of vehicles with respect to 3rd vehicle for a 50 meter of distance. In figure 5(c) average duration for same connection with 30 sec continuous time was plotted. In figure 6 a graphical representation of simulation was implemented and by accessing 802.11p technology based V2I and V2V communication was plotted.

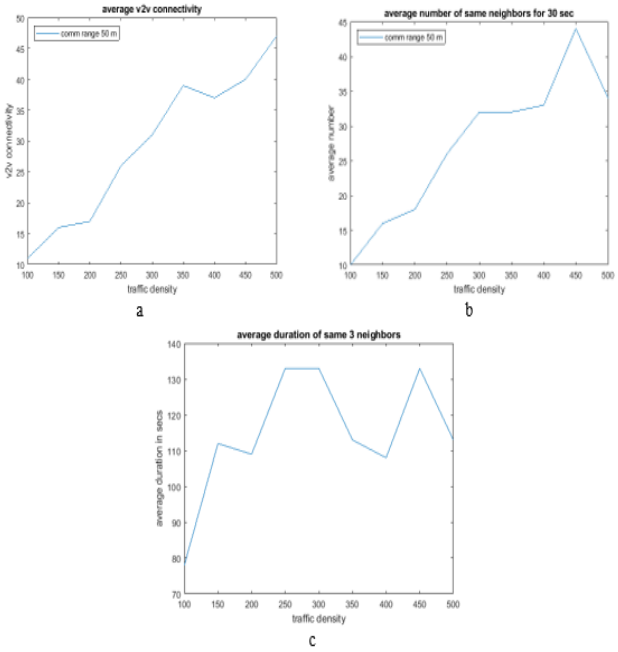

Figure 5 Average duration of neighbour connections with respect to traffic density.

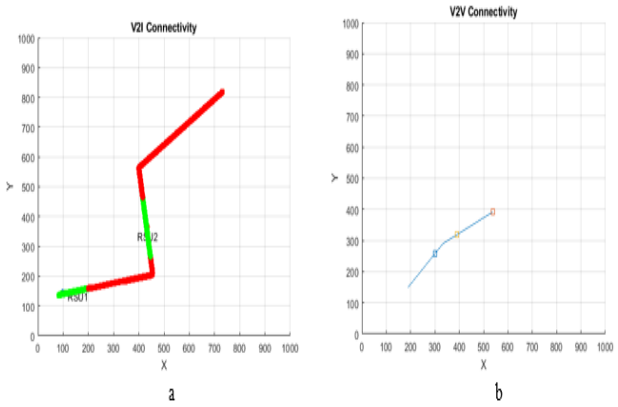

Figure 6 V2I and V2V connectivity with respect to RSU.

TABLE 1 PERFORMANCE COMPARISON BETWEEN DSRC 3GPP AND DSRC LTEA AT 6HZ MESSAGE FREQUENCY

Traffic density	DSRC 4G	DSRC 5G
100	20	17
200	30	19
300	35	21
400	39	26
500	52	34

In table 1, it was showcased the comparison between DSRC 4G and DSRC 5G communication difference for time delay on different traffic ranges.

IV. CONCLUSION

The sector's extensive graduation of normalized IEEE 802.11p, which has just been very well inspected, may want likewise to undergo the price of a dependable framework for overseers of traffic basis, such as visitors' signals, and armadas, i.e., crisis administrations and constructing website automobiles. In that manner, statistics on traffic move, mishaps, avenue works, and different critical conditions and occasions may be reputedly made available inside the

neighbourhood. From the above resultant car associations, it becomes confirmed that an unattended vehicle can be associated with 60 different cars, but the mistake was expanding as the affiliation receives multiplied. In addition to that LTEA or 3GPP based methodologies, the supply is probably stepped forward contrasted and 802.11p calculation. Moreover, underpins the correspondence altogether forms of the route without misuse of data switchability to use and upgrades QoS's presentation, such as delay, energy usage, parcel conveyance proportion, packet drop in each high-density and low-density traffic situation.

REFERENCES

[1] Arul Jothy, M.K. and Murugesan, D. (2016) 'An enhanced self-scheduled access control in vehicular ad hoc networks (VANET)', *International Conference on Information Communication and Embedded System* (*ICICES 2016*).

[2] Avcil, M.N., Gurle, M.C. and Soyturk, M. (2016) 'Collision resolution MAC algorithm for vehicular ad hoc networks', *IEEE*, 978-1-5090-2558-9/16/$31.00.

[3] Balador, A., B¨ohm, A., Calafate, C.T. and Cano, J-C. (2016) 'A reliable token-based MAC protocol for V2V communication in urban VANET', *IEEE 27th Annual IEEE International Symposium on Personal, Indoor and Mobile Radio Communications* – (*PIMRC*): *MAC &Cross-Layer Design*.

[4] Barkouk, H. and En-Naimi, E.M. (2016) 'Development of an alert message dissemination protocol based on LEACH protocol to improve VANET road safety', 978-1-5090-0751-6/16/$31.00.

[5] Cao, Y. and Wang, N. (2016) 'Towards efficient electric vehicle charging using VANET-based information dissemination', 0018-9545.

[6] Chen, Y., Fang, M., Shi, S., Guo, W. and Zheng, X. (2016) 'Distributed multi-hop clustering algorithm for VANETs based on neighborhood follow', *EURASIP Journal on Wireless Communications and Networking* (2015) 2015:98.

[7] Fekair, M.E.A., Lakas, A. and Korichi, A. (2016) 'An efficient QoS-compliant routing scheme for VANET', *5th International Conference on Electronic Devices, System and Application* (*ICEDSA*), DOI: 10.1109/ICEDSA 2016.7818499.

[8] Gandhi, M. and Khan, M.A. (2014) 'Performance analysis of metrics of broadcasting protocols in VANET', *International Conference on Innovative Applications of Computational Intelligence on Power, Energy and Controls with their Impact on Humanity* (*CIPECH14*).

[9] Guo, C., Li, D., Zhang, G. and Cui, Z. (2016) 'Data delivery delay reduction for VANETs on Bidirectional roadway', *IEEE*, 2169-3536.

[10] K. A. Hafeez, A. Anpalagan and L. Zhao, "Optimizing the Control Channel Interval of the DSRC for Vehicular Safety Applications," in IEEE Transactions on Vehicular Technology, vol. 65, no. 5, pp. 3377-3388, May 2016, doi: 10.1109/TVT.2015.2440994.

[11] Hassan, A., Ahmed, M.H. and Rahman, M.A. (2016) 'Performance evaluation for multicast transmissions in VANET', *IEEE CCECE 2011–001108*.

[12] Hubballi, P., Sutagundar, A.V. and Belagali, R. (2016) 'Agent based dynamic clustering for hybrid VANET (ADCHV)', *IEEE International Conference on Recent Trends in Electronics Information Communication Technology*, India, 20–21 May.

[13] Jiang, X. and Du, D.H.C. (2016) 'PTMAC: a prediction-based TDMA MAC protocol for reducing packet collisions in VANET', *IEEE*, 10.1109/TVT.2016.2519442.

[14] Kopp, C., Tyson, M. and Pose, R. (2016) 'Tomographic reconstruction of RF propagation to aid VANET routing in urban canyons', *Transactions on Vehicular Technology*, Vol. 65, pp.9888–9901.

Color Image Restoration from Low Resolution Based on Multiscale Decomposition

Abdur Rahman A[1], Charavanan. V[2], Adhithya Ner. P.V.[3], Abinaya B[4], Bathri D[5], Senthil Kumar K[6]

[1–3,5,6]Department of ECE, Rajalakshmi Engineering College
Chennai, India

[4]Department of ECE, St. Joseph College of Engineering, Chennai, India

[1]abdurrahman.a.2019.ece@rajalakshmi.edu.in, [2]charavanan.v.2019.ece@rajalakshmi.edu.in,
[3]adhithyaner.pv.2019.ece@rajalakshmi.edu.in, [4]abisankari84@gmail.com,
[5]bathri.d.2019.ece@rajalakshmi.edu.in, [6]senthilkumar.kumaraswamy@rajalakshmi.edu.in

***Abstract*— A successful method for improving the clarity of dim light image that has been compromised by unbalanced lightning is to evaluate and compress the lightning portion. Due to inaccurate calculation, some previous approaches like edges are affected in improved image. The weighted least square multi scale image decomposition model's goal is to separate the light layer as effectively as possible. Later enhancement effect is obtained by adjusting the illumination layer. The proposed decomposition model is used to the value channel in HSV space in order to avoid colour artefacts caused by illumination adjustments and reduce computing complexity. Experiments reveal that the advance approach works well with an outspread range of dim images.**

***Keywords*— Dim light, contrast enhancement, multi scale decomposition, illumination, weighted least square, reflectance**

I. INTRODUCTION

In dim-light situations, digital imaging technologies have historically performed poorly due to a shortage of natural light sources, resulting in low contrast and image blurring. Many devices have an LED light, which is useful when the subject is close to the camera. To counteract this, devices with dual LED flash, i.e. twice the brightness, have begun to emerge, despite the fact that light energy diminishes exponentially with time. Aim of improving image quality is to make low-contrast aspects more visible. It increases the image's digital output. Locally differing statistics, different edges, and smoothness are all present in the image.

Dim-light conditions cause every surface's detail information to be lost. When a dim–light scene is enhanced, the noise in the dark area is also amplified. As a consequence, simply increasing the contrast of a dim-light image would not suffice. The lack of contrast creates a concern with human visual visibility. To solve this problem, we need to improve the contrast of dim-light for extracting input image's clarity. Dim light can be affected by a variety of factors. It may be caused by a lack of illumination, a shadow cast by an object, or the fading of bright light under low luminance.

This paper presents multiscale picture deterioration creation tracks and directs a few investigations to show the viability of the recommended decay process for contrast upgrade. Without presenting clear curios, the proposed approach will forestall over-improvement in splendid regions and increment the enlightenment of dull regions.

II. RELATED WORKS

The decay of enlightenment and reflectance layers is utilized to improve images using Retinex-based contrast enhancement methods. The methodologies depending on the Poisson condition expect that the light is spatially smooth. Picture inclinations can be delegated either the reflectance layer or the enlightenment layer dependent on their size [1-3]. Filtering-based decomposition methods are built on the same premise. The distinction is in the illumination estimation filter. The illumination layer is estimated using a Gaussian filter in SSR and MSR [4, 5]. However, since the illumination can shift dramatically around sharp edges, they will cause halo artifacts in the enhanced image. As a result, Ref. [6] recommended the crown antiquities with a two-sided channel. Sadly, these methodologies produce more obscure brightening than reflected enlightenment, implying that the surface ingests more light than it gets. [7] proposed a splendid pass channel that actions the light by a weighted normal of its more brilliant neighbors to restrict the reflectance values in the range [0; 1]. Liang et al. recently suggested using a nonlinear diffusion filter with surround suppression to improve diffusive intensity in textural areas [8]. The resulting light has sharp variations around the border and is smooth in textural regions.

III. PROPOSED METHODOLOGY

This section will cover the proposed multiscale decomposition-based contrast enhancement process. Next, the suggested method's structure is represented. Multiscale image decomposition and illumination adjustment are the two main modules.

A. Overview of Proposed Method

Figure 1 depicts the proposed technique framework. The proposed contrast enhancement method is based on the following measures:

- We begin by converting an information shading picture I into a HSV portrayal.
- Following stage is to find, the worth (V) channel picture is decayed into lighting (L) and reflectance (R) layers utilizing the proposed multiscale picture disintegration model.
- Third, the Gamma mapping feature is used to change the L layer, resulting in an adjusted L layer, defined by La.
- The improved V channel image Ve is then generated by multiplying the modified La by the reflectance layer R.
- At last, the improved Hue Saturation Value image is converted to pixels, resulting in the final outcome I_e.

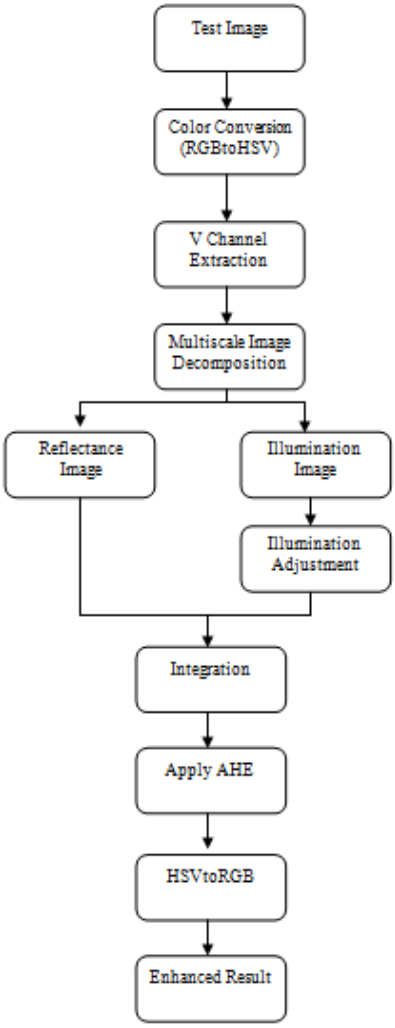

Fig. 1. Overall Framework of Proposed Method.

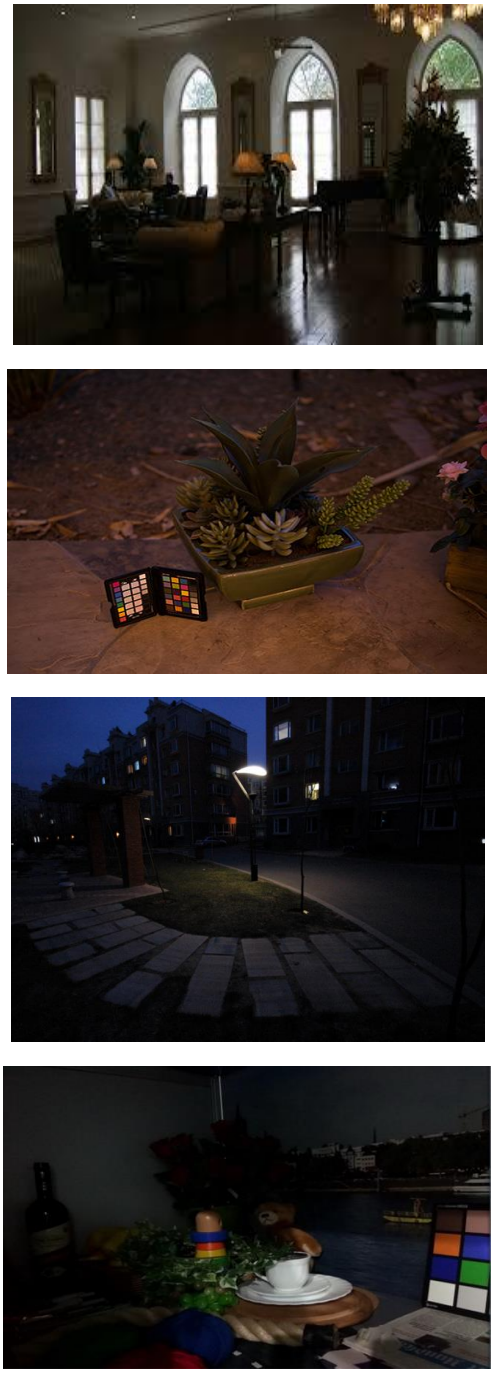

Fig. 2. Sample Dim Light Images.

B. Multiscale Image Decompsition

The suggested algorithm begins with a shading space change from pixels to Hue Saturation Value, followed by a reverse conversion. The V channel is separated from Hue Saturation Value image for further processing. During the multiscale image decomposition process, the V channel is dissected into the lighting part L and the reflectance part R.

$$I = LR \tag{1}$$

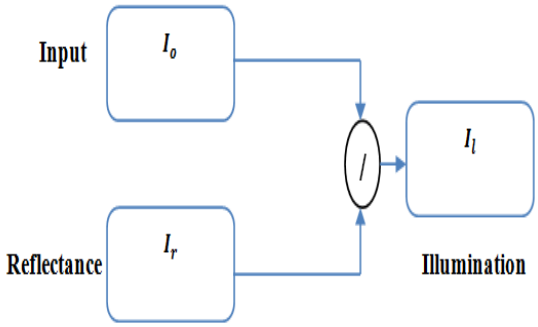

Fig. 3. WLS Decomposition Process.

S = WLS (I_o,λ,τ) performs WLS smoothening (reflectance part) of input image I_o, with parameters of smoothness weight lambda and rate kappa. The Smoothing parameter lambda governs the degree of smoothness. Kappa is in control of the rate. The smaller the kappa, the more iterations there are and the sharper the edges. The illumination part I_l can then be obtained using reflectance part.

$$I_l = \mathrm{Io}/\, I_r \qquad (2)$$

where I_o is input image and I_r is reflectance image.

Fig. 4. Reflectance Part by WLS.

Fig. 5. Illumination Part by WLS.

C. *Illumination Adjustment*

After computing R & L layers, the next step is to modify the illumination values to increase image information. Commonly used functions include log, sigmoid, and gamma. They can, however, compact intensities in light environments, minimizing the variance of high intensities. The Log and Sigmoid functions, in particular, can suffer from a lack of information in bright areas.

In our tests, γ is set to 2.2. As a result, the decomposed reflectance R is multiplied by the modified illumination, yielding the improved V channel image Ve. The enhanced result is denoted by V_{e1}. The final result is created by converting the improved HSV image to pixels I_e.

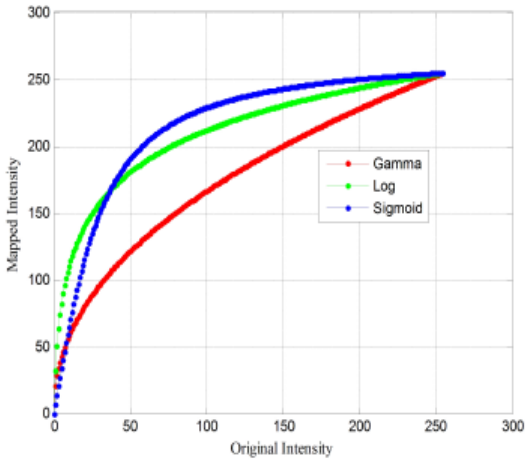

Fig. 6. Mapping Functions.

Fig. 7. Illumination Adjusted Image using Gamma Function.

Fig. 8. Enhanced Result using AHE.

IV. Experiment Outcome

The proposed multiscale decomposition based contrast improvement implementation result has been shown in this part. Proposed work would suitable to different image size. It has been implemented in MATLAB software.

Table I. Image Quality Analysis based on Proposed Method

Metrics	Sample Image 1	Sample Image 2	Sample Image 3
MSE	4.2765e+03	2.5935e+03	6.8215e+03
PSNR	27.2164	32.2176	22.5469
SSIM	0.9508	0.9490	0.9550
NC	0.3983	0.3809	0.4475
NAE	0.6018	0.6192	0.5532
Time	16 s	14 s	17 s

The proposed method based obtained result of contrast enhanced image quality analysis is shown in Table I. PSNR and SSIIM are significant picture quality investigation measurements.

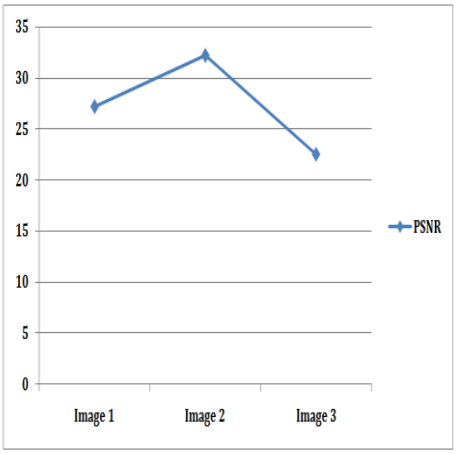

Fig. 9. PSNR Analysis.

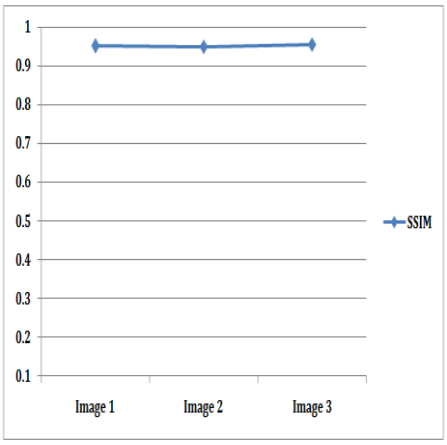

Fig. 10. SSIM Analysis.

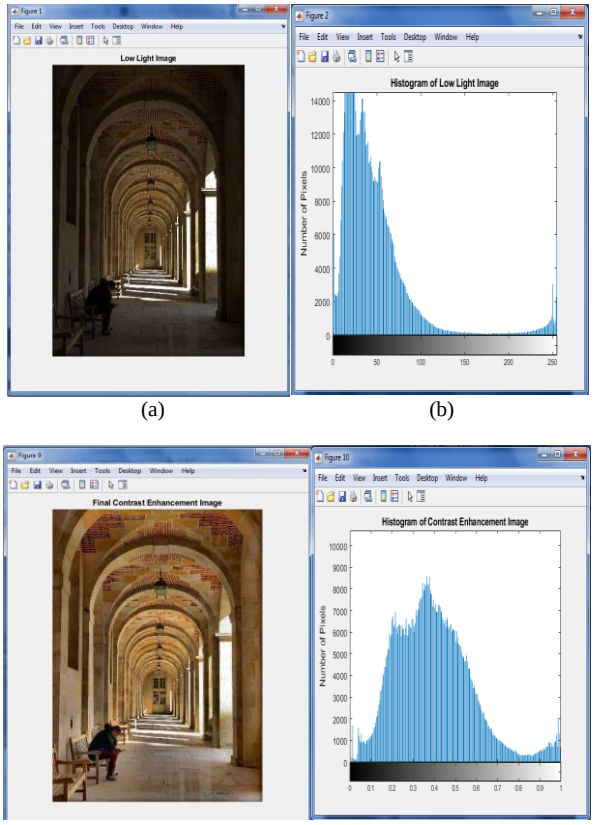

(a) (b)

(c) (d)

Fig.11 Contrast Enhancement Result by Proposed Method (Sample Image 1); (a). Dim light image, (b). Histogram of dim light image, (c). Final contrast improved image, (d). Histogram of improved image.

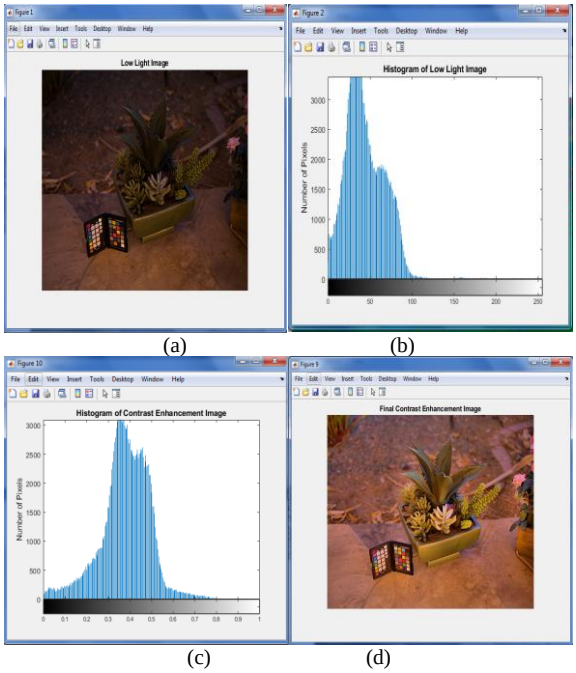

(a) (b)

(c) (d)

Fig.12 Contrast Enhancement Result by Proposed Method (Sample Image 2); (a). Dim light image, (b). Histogram of Dim light image, (c). Final contrast enhanced image, (d). Histogram of enhanced image.

V. CONCLUSION

In this article, we suggest using a multiscale image decomposition model involves estimating R & L layers to improve images. Later apply AHE to further improvements. In terms of image enhancement, our model exceeds image decay approaches, and development strategy, according to experimental data, produces the most noteworthy abstract and objective result for a wide assortment of pictures.

REFERENCES

[1] H. Sawant and M. Deore, A comprehensive review of image enhancement techniques, International Journal of Computer Technology and Electronics Engineering, vol. 1, no. 2, pp. 39–44, March 2010.

[2] C. Wang and Z. Ye, Brightness preserving histogram equalization with maximum entropy: a variational perspective, IEEE Transactions on Consumer Electronics, vol. 51, no. 4, pp. 1326–1334, December 2005.

[3] H. Ibrahim and N. S. P. Kong, Brightness preserving dynamic histogram equalization for image contrast enhancement, IEEE Transactions on Consumer Electronics, vol. 53, no. 4, pp. 1752–1758, November 2007.

[4] D. Menotti, L. Najman, J. Facon, and A. d. A. Ara´ujo, Multi-histogram equalization methods for contrast enhancement and brightness preserving, IEEE Transactions on Consumer Electronics, vol. 53, no. 3, pp. 1186–1194, October 2007.

[5] A. M. Reza, Realization of the contrast limited adaptive histogram equalization (clahe) for real-time image enhancement, Journal of VLSI Signal Processing Systems for Signal, Image and Video Technology, vol. 38, no. 1, pp. 35–44, August 2004.

[6] S.-H. Yun, J. H. Kim, and S. Kim, Contrast enhancement using a weighted histogram equalization, in Consumer Electronics (ICCE), 2011 IEEE International Conference on. IEEE, Las Vegas, March 2011, pp. 203–204.

[7] K. Gu, G. Zhai, X. Yang, W. Zhang, and C. W. Chen, Automatic contrast enhancement technology with saliency preservation, IEEE Transactions on Circuits and Systems for Video Technology, vol. 25, no. 9, pp. 1480–1494, September 2015.

[8] K. Gu, G. Zhai, W. Lin, and M. Liu, The analysis of image contrast: From quality assessment to automatic enhancement, IEEE Transactions on Cybernetics, vol. 46, no. 1, pp. 284–297, January 2016.

Biometric Authentication Using Dorsal Hand Vein Pattern

Shanthi C[1], Ayswariah S S[2], Latha K[3]

[1-3]Department of Instrumentation Engineering, Madras Institute of Technology, Chennai, India

[1]cgshanthi@gmail.com, [2]ayswariahnec@gmail.com, [3]lat_padhu@yahoo.com

***Abstract*—Biometric authentication is a method of identifying the individuals based on their unique biological traits. In this paper, Convolutional Neural Network (CNN) and image search engine algorithms are proposed for the biometric authentication using dorsal hand veins. Various pre-processing methods were done to segment the vein pattern from the raw images. The ResNet- 18 and image descriptor are used for the extraction of feature vectors. The authentication and matching process are carried out based on the threshold values obtained from the distance metric method. The matched image is also retrieved using image search engine algorithm. The results indicated that the image search engine algorithm can be used as the most effective method for the authentication process.**

***Keywords*— Deep learning, ResNet-18, Image search engine, image segmentation, feature vector extraction and Euclidean distance**

I. INTRODUCTION

Existing biometrics like fingerprints [1], palm prints can be easily forged by applying any stickers over the prints, hard work and physical activities in some occupations can cause people to lose their fingerprints.

The retina / iris biometric [2] requires specific cameras, hardware which make it cost higher. The face biometrics can also get confused between identical twins.

To overcome these disadvantages, hand veins pattern [3] are used for the biometric authentication. The veins in the hand consist of two parts, the dorsal and ventral side. The ventral veins are more difficult to distinguish from the dorsal side of the hand, because it has denser tissue. Hence dorsal hand vein pattern is used for biometric. The dorsal hand vein pattern is unique, non-contact type, pattern differs between identical twins and difficult to forge.

An improved method which makes combination of dorsal hand vein pattern, hand geometry and shape clues that makes the authentication process more effective [4].

Local feature-based approach by matching the key-points of the dorsal vein using Harris, Hessian and DOG [5] which compares the result based on the accuracy and is time consuming.

Improved visibility of thermal images of the vein pattern using Gabor filter and Wavelet transforms [6] have been used for the texture-based feature extraction which achieved accuracy of 97%.

Fractal technique [7] used for feature extraction which is advanced and complex. The fractal regions of the pattern are calculated by box counting method. It gives a promising and optimistic results.

Feature extraction are done using various deep learning networks and classified using SVM [9],[10],[12]. It uses the combination of convolution and max pooling layers which gives accuracy of about 96.63%.

Image search algorithms [14],[15] are used for the retrieval of the image from the dataset along with the authentication.

In this paper, deep neural network and image search algorithm based biometric authentication using dorsal hand vein pattern has been reported.

II. METHODOLOGY

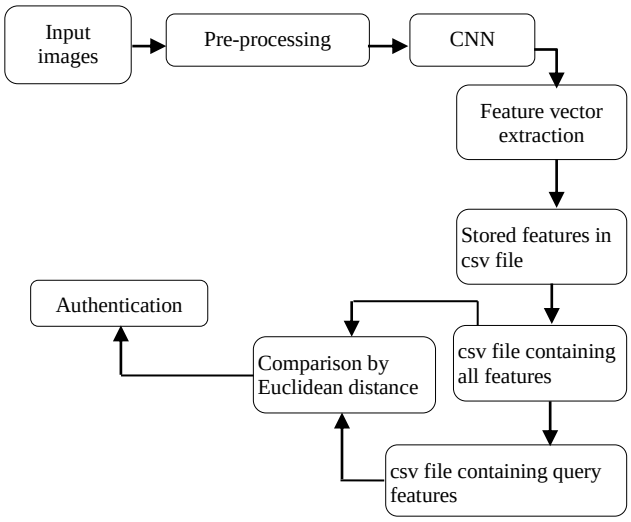

Fig.1. Block diagram of biometric authentication using ResNet-18

Fig.1. shows the block diagram of the biometric authentication using CNN, in which the input images are pre-processed and given to the CNN networks. From that the feature vectors of the images are extracted and then uploaded in the csv file with all the 1500 images using Euclidean distance. According to the threshold the authentication is done.

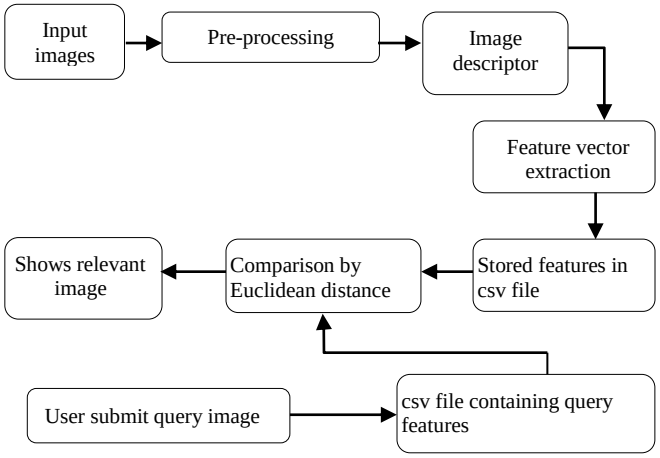

Fig.2. Block diagram of biometric authentication using Image search engine algorithm

Fig.2. shows the block diagram of biometric authentication using image search engine algorithm in which the input is pre-processed and sent to the image descriptor. From that the feature vector are extracted and loaded in the csv file. At the same time, it asks for the user to submit the name of the query image. Then it compares the features by Euclidean distance and shows the matched image from the database.

A. Image acquisition

The dataset consists of 1500 infrared images of dorsal hand vein pattern from Suas and Bosphorus university.

B. Image pre-processing

Image pre-processing consists of various techniques to extract the useful information from the images. The image is first converted into grayscale image and then the particular image is cropped using Region of Interest (ROI). The cropped images are then enhanced using adaptive histogram equalization.

C. Image segmentation

The enhanced images are then segmented using thresholding methods, dilation, erosion and thinning to extract the skeleton pattern from the images. Different dataset consists of different thresholding techniques like binary adaptive and global methods based on the pixel intensity.

D. Feature extraction

The feature vector of the image is extracted using the network and they are stored in the csv file for further processing.

E. Authentication

The matching of the images is done using distance metric methods. In this paper Euclidean distance is considered as a metric for authentication. According to the dataset the threshold value is fixed. If the Euclidean distance is above the limit it is said to be different person.

III. RESULTS AND DISCUSSION

This section consists of the results from Image pre-processing to authentication. Image pre-processing includes Grayscale conversion, ROI, enhancement and segmentation using thresholding, dilation, erosion and thinning. The feature vectors of segmented image are extracted using CNN / image search engine algorithm. Finally, the authentication is done using distance metrics and their Euclidean distance are compared.

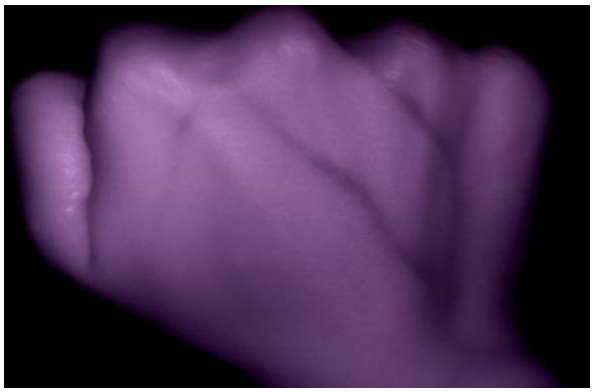

Fig..3. Dorsal hand vein image1

Fig.3. shows the sample image of dorsal hand vein pattern which is taken under infrared light and collected dataset of about 1000 images of different persons (suas dataset).

Fig. 4. Dorsal hand vein image 2

Fig.4. shows the sample image of dorsal hand vein pattern which is taken under infrared light and collected dataset of about 500 images of different persons (Bosphorus dataset).

Fig.5. Grayscale conversion of dorsal vein images

Fig.5. shows the sample gray scale image of the dorsal hand vein pattern which is converted from dataset consists of infrared images

(a)

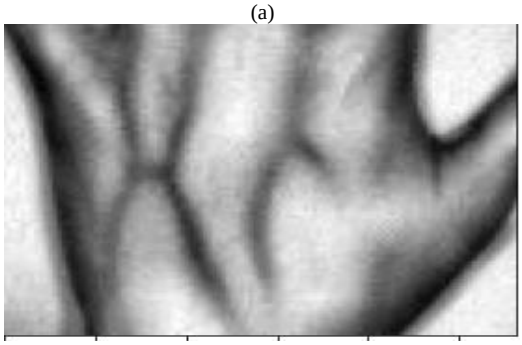

(b)

Fig.6. Adaptive histogram equalisation method

Fig.6. (a) shows the sample image before enhancement, (b) shows the adaptive histogram equalization based enhanced image.

Fig.7. Thresholding method

Fig.7. shows the binary image obtained after thresholding in which the background becomes lighter and veins become darker.

Fig.8. Thinning method

Fig.8. shows the image after thinning process followed by erosion, in which the veins get brighter and the background gets darker. By using these segmentations methods, the veins are extracted without any noise.

TABLE I. FEATURES EXTRACTED USING THE CNN

Name of the image	Features		
Image_01	0.033	0.082	……. ,0.193
Image_02	0.002	0.055	……..,0.067
Image_03	0.004	0.059	……..,0.019
Image_04	0.011	0.049	……..,0.034
Image_05	0.001	0.042	……..,0.256

Table I. shows the extracted sample features of the five images in the csv file for further analysis.

TABLE II. AUTHENTICATION USING EUCLIDEAN DISTANCE

Name of the image	Extracted features
First image (image_01)	[0.033379, 0.08233453,..,0.19342345]
Second image (image_156)	[0.16471794,0.22003083, …,0.07929542]
Distance between images	0.49
Authentication	Not Matched

Table II. shows the Euclidean distance between two different images from extracted feature vector.

QUERY IMAGE

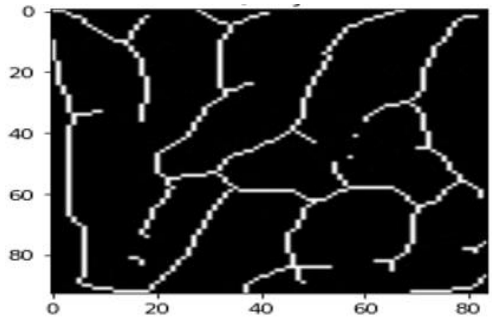

(a)

RESULT

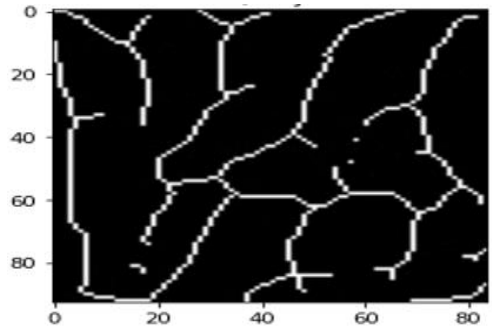

(b)

Fig.9. Query image matched with database

Fig.9. (a) shows the query image which is given by the user, (b) shows the resultant image retrieved from the database which is matched with the given query image.

IV. CONCLUSION

The biometric authentication is done using ResNet-18 and image search engine algorithm with the obtained dataset of dorsal hand vein pattern. Various pre-processing techniques were applied to extract the pattern clearly, so that the lighting effect in or at background of the images is neglected. The ResNet-18 gives good Euclidean distance from the extracted features but consumes more time and memory space. In this paper, new method named "Image search engine algorithm" is used which require less time to extract the features of the images and consumes less memory space. Along with the Euclidean distance, the matched image is also retrieved from the database.

ACKNOWLEDGMENT

Authors would like to thank SUAS University and BOSPHORUS University, Turkey for providing the infrared images of dorsal hand veins.

REFERENCES

[1] F. Liu, G. Liu, Q. Zhao, and L. Shen, ''Robust and high-security fingerprint recognition system using optical coherence tomography,'' neurocomputing, vol. 402, pp. 14–28, Aug. 2020

[2] M. Trokielewicz, A. Czajka, and P. Maciejewicz, ''Post-mortem iris recognition with deep-learning-based image segmentation,'' Image Vis. computer., vol. 94,Art. no. 103866, Feb. 2020.

[3] Chih-Lung Lin, Kuo-Chin Fan, "Biometric verification using thermal images of Palm dorsal vein patterns" IEEE Transactions Circuit and system for Video Technology volume:14, issue:2. 2004.

[4] Di huang, Xiangrong Zhu, Yunhong Wang and David,"Dorsal hand vein recognition via Hierarchical Combination of Texture and Shape Clues" Neurocomputing ELSEVIER SCIENCE DIRECT vol.214, pp.815-828, 2016.

[5] Di Huang, Yinhang Tang, Liming Chen,"Hand dorsa vein recognition by the matching local features of multisource keypoints" IEEE Transactions On Cybernetics Volume: 45,issue : 9, 2014.

[6] Amioy Kumar, M. Hanmand and H. M. Gupta,"Online biometric authentication using hand vein patterns" IEEE Symposiumon computational Intelligence in Security and Defense Applications, 2009.

[7] Murat Erhan Cimen, Omer Boyraz, Mustafa Zahid Yildiz, Fuat Boz,"A new dorsal hand vein authentication system based fractal on the dimension box counting method" International Journal For Light and Electron Optics ELSEVIER, Vol.226,part 1.2021

[8] Puneet Gupta and Phalguni " Multibiometric Authentication system Using slap Fingerprints, Palm Dorsal Vein and Hand Geometry" IEEE Transaction On Industrial Electronics Volume: 65, Issue: 12.2018

[9] Rafat Jamal Tazim, Md. Messal Monem Miah, Sanzida Sayedul Surma and Mohammad Tariq Islam "Biometric Authentication Using CNN Features of Dorsal Vein Pattern Extracted from NIR Image"International Journal of Innovative Research in Science, Engg and Technology, Vol. 5, Issue 9.2018.

[10] Sanchit, Ramalho and Luis Dulca soares,"Biometric identification through palm and dorsal hand vein patterns" IEEE EUROCON,2011.

[11] Sandip Joardar, Amitava Chatterjee, Sanghamitra Bandyo padhyay and ujjwal maulik, "Multi size patch based collaborative representation for Palm Dorsa Vein Pattern recognition by enhanced ensemble learning with modified interactive artificial bee colon algorithm" ELSEVIER, vol.60, pp.151- 163,2017.

[12] Alashik K.M, Yildirim.R, (2021) "Human identity verification from biometric dorsal vein images using the DL Methods" IEEE ACCESS, vol 9, pp.74194-74208.

[13] Wei Jiaa, Wei Xia, Bob Zhang, Yang Zhao, Lunke Fei e, et al.," A Survey On Dorsal Hand Vein Biometrics" Pattern Recognition, ELSEVIER, Volume 120,2021.

[14] Aditya Mishra, Ashish Kumar, Ayush Yadav, Aurangajeb Ansari and Nidhi Gupta. Image Search Engine. International Research Journal of Engineering and Technology (IRJET),2020.

[15] Pei yin and liang zhang, "Image recommendation algorithm based on the deep learning" Gigapixel Panoramic Video with Virtual Reality, IEEE ACCESS, vol. 8,2020.

Direction-of-Arrival Estimation of Multiple Closely Spaced Signals using MVDR-CSVR Approach

Ashok C[1], Vaddi Lakshmi Satya Sai Sarojini[2], N. Venkateswaran[3]

[1,2]Department of Electronics and Communication Engineering, St. Joseph's College of Engineering Chennai-119, India

[3]Department of Electronics and Communication Engineering, SSN College of Engineering, Chennai-110, India

[1]ashokc@stjosephs.ac.in, [2]vaddisathya@gmail.com

***Abstract*—In this paper, the problem of estimating the direction of arrival (DOA) of signals from multiple closely spaced sources is researched. A new approach, by combining minimum variance distortionless response (MVDR) and complex support vector regression (CSVR) called MVDR-CSVR is proposed. The proposed approach detects the number of sources using MVDR and computes the DOAs from a nonlinear mapping function, which relates the received signal with its associated DOAs. The nonlinear mapping function is approximated using the CSVR model. The proposed method successfully resolves the closely spaced sources with the minimum number of sensor elements and snapshots compared to the classical beamformer and subspace-based methods. From the simulation results, it is observed that the proposed approach exhibits superior estimation performances in resolving closely spaced sources.**

***Keywords*—Direction of arrival (DOA) estimation, minimum variance distortionless response (MVDR), complex support vector regression (CSVR).**

I. INTRODUCTION

There has been a growing interest in the estimation of the direction of arrival (DOA) of signals from multiple sources. In wireless communication system development for fifth-generation (5G), target detection and many other applications have DOA estimation of signals as significant consideration [1], [2]. Recently, machine learning algorithms have been widely employed in many signal processing applications. Mostly, machine learning algorithms have the inherent capability to solve nonlinear problems such as regression and classification [3]. From the machine learning perspective, the DOA estimation problem can be viewed as a nonlinear mapping, that relates the received signal with its associated DOAs [4]. In the DOA estimation problem, the received signals are complex-valued. However, most of the machine learning algorithms do not operate in complex domains directly instead consider the complex-valued data as two independent real-valued data and operate separately [4].

For DOA estimation, several methods have been reported in the literature. The subspace-based DOA estimation methods are more popular than the conventional beamformer [5] and maximum likelihood (ML) methods [6]. The Multiple signal classification (MUSIC) [7] and estimation of the signal parameter via rotational invariance techniques (ESPRIT) [8] are the two most widely used subspace methods. Several modified versions have been proposed for both MUSIC and ESPRIT methods. These include Root-MUSIC, beamspace Root-MUSIC, spatially smoothed MUSIC and beamspace ESPRIT [9]-[11]. It is well known that subspace methods result in poor DOA estimates for signals from multiple sources with very small angular separations [4]. Machine learning-based methods have also been proposed for DOA estimation such as radial basis neural network (RBNN) [4], [12] and support vector machine (SVM) [13],[14]. It is observed that the machine learning-based methods are advantageous in terms of computational complexity over the subspace-based methods. The support vector regression (SVR) based method proposed in [15],[16] for DOA estimation requires a large number of sensor elements. In addition, it also requires exhaustive offline training. Furthermore, it handles the received complex signal values as two real values for approximating the nonlinear mapping function. The recently proposed complex support vector machines (CSVM) algorithm [17] is capable of dealing the complex quantities directly, without considering them as two individual real forms. In [17], both complex support vector regression (CSVR) and complex support vector classification frameworks have been derived. This paper focuses on the estimation of DOA of multiple closely spaced signals with the CSVR framework. The proposed model helps in the reduction of hardware complexity for practical implementation. In this paper, we combine the minimum variance distortionless response (MVDR) and complex support vector regression (CSVR) techniques for the estimation of DOAs of multiple closely spaced signals. The

proposed approach called MVDR-CSVR consists of two stages. In the first stage, the angular region of interest (ARoIs) and the number of sources present in the received signal are computed by using the minimum variance distortionless response (MVDR). After that, a complex support vector regression (CSVR) algorithm approximates the nonlinear mapping function over the ARoIs, to compute the DOAs of multiple sources.

The main contribution of the paper is summarized as follows

1. Estimation of DOAs of multiple sources with very small angular separations, ranging from 1 degree to 5 degrees.
2. The proposed method achieves superior estimation performances with the minimum number of sensor elements and snapshots.
3. The proposed approach has good generalization capability by operating directly on the complex domain.

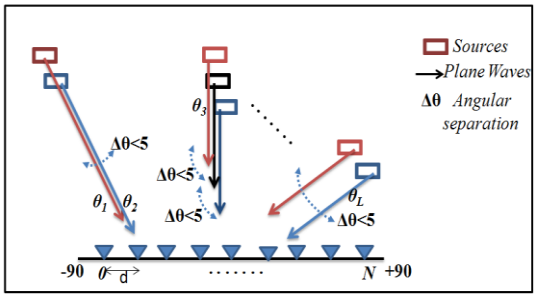

Fig.1. A linear array of N elements with L incoming signals

II. Array Signal Model

Let an L narrowband plane waves with unique DOAs θ_k, $0 \leq k \leq L-1$ impinges on the uniform linear array (ULA) of N elements. The received signals are binary phase-shift keying (BPSK) modulated. As shown in Fig 1. the element of the array is spaced by half a wavelength i.e., $d = \frac{\lambda}{2}$, where λ is the wavelength of the incoming signals. The signal received by i^{th} element at n^{th} instant of the array is given by

$$x_i[n] = \sum_{k=0}^{L-1} s_k[n]\, a(\theta_k) + v_k[n] \quad (1)$$

where $i = 0,1,2,\ldots,N-1$, The matrix form of Equation (1) can be represented by

$$\mathbf{x}[n] = \mathbf{A}(\theta)\, \mathbf{s}[n] + \mathbf{v}[n] \quad (2)$$

where

$\mathbf{x}[n] = [x_0[n], x_1[n], \ldots, x_{N-1}[n]]^T$
$\mathbf{v}[n] = [v_0[n], v_1[n], \ldots, v_{N-1}[n]]^T$
$\mathbf{s}[n] = [s_0[n], s_1[n], \ldots, s_{L-1}[n]]^T$
$\mathbf{A}(\theta) = [a(\theta_0)\; a(\theta_1) \ldots a(\theta_{L-1})]$

where T indicates the transpose, $\mathbf{s}[n]$ is L x 1 signal vector of the incoming signal, $\mathbf{v}[n]$ is N x 1 vector of additive white Gaussian noise with zero mean and variance of $\sigma^2$and $\mathbf{A}(\theta)$ is L x N steering matrix of the incoming signal and $a(\theta_k) = [1,\, e^{-j\pi cos\theta_k}, \ldots,\, e^{-j(L-1)\pi cos\theta_k}]^T$ is L x 1 steering vector of the incoming signal.

III. Proposed MVDR-CSVR Method

A. Angular Region of Interest (ARoIs) and detection of the number of sources

Most of the high-resolution DOA estimation methods, operate over the entire angular region i.e., -90^o to $+90^o$. The proposed approach initially determines the angular region of interests (ARoIs) from the received signal. The ARoIs give the range of angular regions for which the signal is present. Then the number of sources present in ARoIs is being computed by an approximation method. The DoAs of multiple closely spaced signals is computed from the nonlinear mapping functions constructed over the ARoIs. The minimum variance distortionless response (MVDR) is utilized to compute the ARoIs from the received signals. In MVDR, the peaks of the power spectrum indicate the presence of a signal within the angular region. The power the spectrum of the MVDR is given by

$$\hat{f}_{MVDR}(\theta) = \frac{1}{\mathbf{a}^H(\theta)\, \hat{\mathbf{R}}_{xx}^{-1}\, \mathbf{a}(\theta)} \quad (3)$$

where $\hat{\mathbf{R}}_{xx}^{-1}$ is the inverse of the sample covariance matrix $\hat{\mathbf{R}}_{\mathrm{xx}}$ on the received signals and it is expressed as

$$\begin{aligned}\hat{\mathbf{R}}_{\mathrm{xx}} &= \frac{1}{K}(\mathbf{x}[n]\mathbf{x}^{\boldsymbol{H}}[n]) \\ &= \mathbf{A}(\theta)\, \boldsymbol{E}\{\mathbf{s}[n]\boldsymbol{s}^{\boldsymbol{H}}[n]\}\mathbf{A}^{\boldsymbol{H}}(\theta) + \boldsymbol{E}\{\mathbf{v}[n]\mathbf{v}^{\boldsymbol{H}}[n]\} \\ &= \mathbf{A}(\theta)\boldsymbol{P}\, \mathbf{A}^{\boldsymbol{H}}(\theta) + \sigma^2 \boldsymbol{I}\end{aligned} \quad (4)$$

where K represents the number of snapshots i.e., the number of observations required to find the covariance matrix, $\boldsymbol{P}$ gives the signal covariance matrix, $\boldsymbol{I}$ represent the unit matrix and H indicates the complex conjugate transpose.

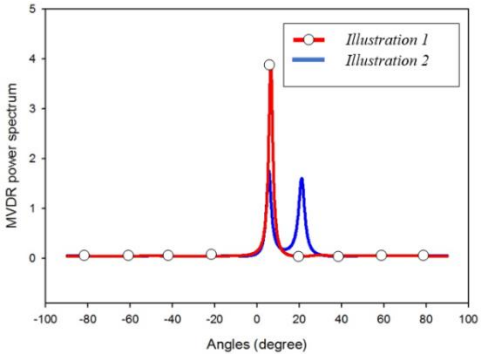

Fig.2. The MVDR power spectrum

In ARoIs, the lower bound and upper bound angles are represented by θ_L and θ_U. The lower and upper bound is computed from the half-peak width of the power spectrum. In a case where the power spectrum results in multiple peaks due to signals coming from multiple sources as shown in Fig.2, then the θ_L and θ_U are computed for each peak in the power spectrum is given by $\{(\theta_{L1}, \theta_{U1}), (\theta_{L2}, \theta_{U2}), \ldots, (\theta_{LQ}, \theta_{UQ})\}$, where Q indicates the total number of peaks present in the power spectrum. To present the significance of the above approach, two simple illustrations are listed below

Illustration 1: when signals coming from multiple sources with an angular separation of about 1 degree say $\theta_1 = 5^o$,

$\theta_2 = 6^o$, $\theta_3 = 7^o, \theta_4 = 8^{o\cdot}$. *The MVDR results in a power spectrum with a single peak* ($Q = 1$) *in the range of the above angles. The* θ_{L1} *and* θ_{U1} *are computed by the above approach.*

Illustration (case) 2: when signals coming from multiple closely spaced sources with an angular separation of about 1 degree and 2 degrees say $\theta_1 = 5^o$, $\theta_2 = 6^o$, $\theta_3 = 20^o$, $\theta_4 = 22^o$. *The MVDR results in a power spectrum with two peaks* ($Q = 2$) *in the range of the above angles. Then the* $\{(\theta_{L1}, \theta_{U1}), (\theta_{L2}, \theta_{U2})$ *are computed by the above approach.*

Generally, in most of the DOA estimation methods, the number of signals present in the received signal is known priori. Even in SVR based DOA estimation method, the number of signals that impinges on the ULA is known as apriori. An approximation has been derived from the MVDR power spectrum for determining the number of sources

$$L = \sum_{q=1}^{Q} \hat{f}_{MVDR}(q) \tag{5}$$

From Fig.2. It is evident that, for the first case, the MVDR power spectrum peaks result in a magnitude, which is approximately equal to 4, indicating the number of sources present in the received signal ($L = 4$). Likewise, for the second case, the magnitude sum of the MVDR power spectrum peaks approximately equal to 4, indicating the number of sources present in the received signal is ($L = 4$).

B. DOA Estimation using Complex Support Vector Regression (CSVR)

In this stage, an unknown nonlinear mapping function that relates the received signal with its associated DOAs is computed by a complex support vector regression (CSVR) model. The unknown nonlinear function parameters are computed by proper training with several known received signals and its associated DOA pairs. Finally, the DOAs are computed from the nonlinear mapping function. The training samples of the form $(\boldsymbol{z}, \theta)$, where $\boldsymbol{z}$ is complex-valued and θ is real-valued DOA are generated based on the ARoIs and the number of sources (L) present in the received signal. For the training phase, the source angles are θ_1^q, $\theta_2^q, \ldots, \theta_L^q$ and it can be represented as

$$\begin{aligned} \theta_1^q &= (\theta_L - 1) + q \\ \theta_2^q &= \left(\theta_1^q - 1\right) + \Delta\theta \\ \theta_L^q &= \left(\theta_{L-1}^q - 1\right) + \Delta\theta \end{aligned} \tag{6}$$

where $q = 1,2,\ldots,\theta_U - \theta_L$ and $\Delta\theta$ be angular separation. The received signal for the above-known DOAs is computed using Equation (1). Then the training data set is defined as

$$\left\{ \left(\begin{pmatrix} \theta_1^1 \\ \theta_2^1 \\ \cdot \\ \cdot \\ \theta_L^1 \end{pmatrix}, \mathbf{x}^1 \right), \left(\begin{pmatrix} \theta_1^2 \\ \theta_2^2 \\ \cdot \\ \cdot \\ \theta_L^2 \end{pmatrix}, \mathbf{x}^2 \right), \ldots, \left(\begin{pmatrix} \theta_1^q \\ \theta_2^q \\ \cdot \\ \cdot \\ \theta_L^q \end{pmatrix}, \mathbf{x}^q \right) \right\}$$

where $\mathbf{x}^q$ be the received signal for the associated training DOAs. The feature vector required for CSVR training is obtained by computing the sample covariance matrix on the received signals $\mathbf{x}$ as given in Equation (4). The sample covariance matrix is organized in an array $\boldsymbol{G}$, given by

$$\boldsymbol{G} = [r_{12}, r_{13}, .., r_{1N}, r_{23}, r_{24}, \ldots, r_{(N-1)N}] \tag{7}$$

where $r_{ij} = [\hat{\mathbf{R}}_{\mathrm{xx}}]_{ij}$, $i, j = 1,2,..,N$.The feature vector $\boldsymbol{G}$ is normalized to get $\boldsymbol{z}$ is given by

$$\boldsymbol{z} = \boldsymbol{G}/_{||\boldsymbol{G}||} \tag{8}$$

To compute the L DOAs, L estimators have to be constructed by the CSVR model. The training set used to obtain the CSVR model is given by

$$\begin{aligned} &\{(\boldsymbol{z}^1, \theta_1^1), (\boldsymbol{z}^2, \theta_1^2), \ldots, (\boldsymbol{z}^q, \theta_1^q)\} \\ &\{(\boldsymbol{z}^1, \theta_2^1), (\boldsymbol{z}^2, \theta_2^2), \ldots, (\boldsymbol{z}^q, \theta_2^q)\} \\ &\{(\boldsymbol{z}^1, \theta_L^1), (\boldsymbol{z}^2, \theta_L^2), \ldots, (\boldsymbol{z}^q, \theta_L^q)\} \end{aligned} \tag{9}$$

The CSVR model for DOA estimation of L sources is given by

$$\begin{aligned} \widetilde{\theta_1} &= \langle w_{\boldsymbol{1}}, \boldsymbol{\Phi}(\boldsymbol{z}) \rangle + b_{\boldsymbol{1}} \\ \widetilde{\theta_2} &= \langle w_{\boldsymbol{2}}, \boldsymbol{\Phi}(\boldsymbol{z}) \rangle + b_{\boldsymbol{2}} \\ \widetilde{\theta_L} &= \langle w_{\boldsymbol{L}}, \boldsymbol{\Phi}(\boldsymbol{z}) \rangle + b_L \end{aligned} \tag{10}$$

where $\boldsymbol{\Phi}$ is the feature map that transforms the signal vector from original space χ to higher dimensional space $\mathcal{H}$, w gives the orientation of the regression, b gives the position of the regression, $\langle .,. \rangle$ denotes the scalar product. The parameters of CSVR model are computed in the training phase, by minimizing the regression risk function [17]

$$R_{reg} = \frac{1}{2}||w|| + C \sum_{i=0}^{q-1} c(z^i, \theta_L^i) \tag{11}$$

where C is a tradeoff constant between the tolerance of estimation and flatness of the solution and $c(z^i, \theta_L^i)$ is the insensitive loss function [18]. The above constraint optimization problem can be recast into an unconstraint problem by introducing Lagrangian multipliers. The dual form for the above problem can be derived as

$$\begin{aligned} &\underset{\alpha^+, \alpha^-}{maximize} \begin{cases} -\varepsilon \sum_{i=1}^{L} (\alpha_i^+ + \alpha_i^-) + \sum_{i=1}^{L} \theta_1^i (\alpha_i^+ - \alpha_i^-) \\ -\frac{1}{2} \sum_{i,j=1}^{L} (\alpha_i^+ + \alpha_i^-)(\alpha_i^+ - \alpha_i^-) \boldsymbol{\Phi}(\boldsymbol{z}^i, \boldsymbol{z}^j) \end{cases} \\ &subject\ to\ \sum_{i=1}^{L} (\alpha_i{}^+ - \alpha_i{}^-) = 0 \text{ and } \alpha^+, \alpha^- \in [0, C/L] \end{aligned} \tag{12}$$

where $\alpha^+, \alpha^-$are the Lagrange multipliers, The orientation of the regression w is given by

$$w = \sum_{i=1}^{L} (\alpha_i{}^+ - \alpha_i{}^-) \boldsymbol{\Phi}(z^i) \tag{13}$$

TABLE I. STEPS OF THE PROPOSED METHOD

Step 1	The ARoIs and number of sources (L) are computed from the MVDR spectrum using Equation (5).
Step 2	The training samples are generated based on the ARoIs and L using Equations (6),(7),(8) and (9).
Step 3	The CSVR model is computed with known training samples from step 2 using Equations (12), (13) and (14).
Step 4	Estimation of DOAs for the normalized received signal is obtained by Equation (10).

The position of the regression b is computed by exploiting the Karush-Khun-Tucker (KKT) condition [19][20]. Finally, the nonlinear mapping function for DOA estimation can be given by

$$\tilde{\theta}(\boldsymbol{z}) = \sum_{i=1}^{L}(\alpha_i{}^{+} - \alpha_i{}^{-})\langle \boldsymbol{\Phi}(\boldsymbol{z}^i), \boldsymbol{\Phi}(\boldsymbol{z})\rangle + b$$
$$= \sum_{i=1}^{L}(\alpha_i{}^{+} - \alpha_i{}^{-})k_{\mathbb{C}}(\boldsymbol{z}^i, \boldsymbol{z}) + \mathrm{b} \quad (14)$$

where $k_{\mathbb{C}}(\boldsymbol{Z}^i, \boldsymbol{Z})$ is the complex Gaussian kernel [17] with free positive parameter t, the exp (.) is the extended exponential function in the complex domain defined as

$$k_{\mathbb{C}}(\boldsymbol{z}^i, \boldsymbol{z}) = exp(-t\sum_{i=1}^{L}(\boldsymbol{z}^i - \boldsymbol{z}^*)^2) \quad (15)$$

where * denotes complex conjugate. The summary of the steps in the proposed approach is given in Table I.

IV. Simulation Results

In this section, the validation of the proposed approach is discussed with numerical computer simulations. The simulation setup used for the validation is described as follows: A uniform linear array (ULA) with half-wavelength spacing for each sensor element is used for receiving multiple signals for DOA estimation. The signals are narrowband digitally modulated Binary phase shifting keying (BPSK) is considered. The incoming signals are assumed to be corrupted by additive complex white Gaussian (AWGN) noise with variance σ^2. The implementation is performed in MATLAB. The signal to noise ratio (SNR) used in the simulation is defined as

$$SNR = 10\,log\left(\frac{S}{\sigma^2}\right) \quad (16)$$

where S is the maximum signal power and σ^2 is the average noise power. In simulation scenario 1, four uncorrelated signals with equal power from angles $\theta_1 = 9^o$, $\theta_2 = 10^o$, $\theta_3 = 11^o$and $\theta_4 = 12^o$ is received using a ULA with $N = 10$ elements. A snapshot of $K = 100$ is used for sample covariance matrix computation. The SNR of the received signal is kept as $5dB$ and 100 independent trails are used for the DOA estimation. The proposed approach initially computes the ARoIs range of the received signal as $\theta_L = 8^o$ and $\theta_U = 13^o$. It is observed that the proposed approach results in good estimation accuracy for estimating the DOAs of four sources, each with an angular separation of 1 degree as shown in Table II.

Again, the simulation is repeated for the case of $L = 6$ signals arriving from angles $\theta_1 = 4^o$, $\theta_2 = 5^o$, $\theta_3 = 6^o$, $\theta_4 = 7^o$, $\theta_5 = 20^o, \theta_6 = 22^o$. Initially, the ARoIs are computed as $\theta_{L1} = 2^o$, $\theta_{U1} = 13^o$ $\theta_{L2} = 18^o$, $\theta_{U2} = 24^o$. The estimated DOAs shown in Table II indicate that the proposed approach results in good estimation accuracy. The performance of the proposed approach is validated in comparison with existing classical beamformer, MVDR and subspace methods such as MUSIC, ESPRIT, and Min-Norm. Here, three situations are considered such as *situation 1:* signals arriving from 2 sources at an angle $\theta_1 = 15^o$ and $\theta_2 = 16^o$. *Situation 2:* signals arriving from 3 sources at an angle $\theta_1 = 20^o$,$\theta_2 = 21^o$ and $\theta_3 = 23^o$. *Situation 3:* signals arriving from 5 sources at an angle $\theta_1 = 35^o$, $\theta_2 = 36^o$, $\theta_3 = 37^o$, $\theta_4 = 50^o$and $\theta_5 = 53^o$. All the situations are evaluated with $N = 10$, $K = 100$ and $SNR = 5dB$. From Fig.3 and Fig.4 and Table III, it can be clearly seen that the proposed method successfully resolves the closely spaced sources whereas the existing method fails to resolve. Moreover, the proposed approach shows good estimation accuracy over the existing methods.

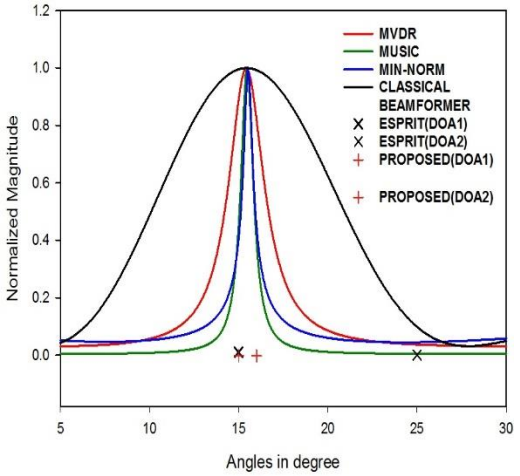

Fig.3. Estimation comparison of methods for the case $L = 2$ sources from $\theta_1 = 15^o$ and $\theta_2 = 16^o$

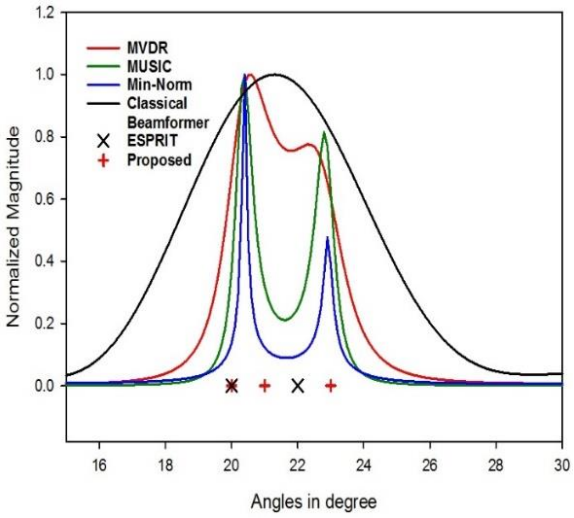

Fig.4. Estimation comparison of methods for the case $L = 3$ sources from $\theta_1 = 20^o$, $\theta_2 = 21^o$ and $\theta_3 = 23^o$

TABLE II Detection and Estimation Results of the Proposed Method

Case for $L = 4$ sources from $\theta_1 = 9^o$, $\theta_2 = 10^o$, $\theta_3 = 11^o$and $\theta_4 = 12^o$	
Number of sources	4
ARoIs	$\theta_L = 8^o, \theta_U = 13^o$
Estimated DOAs	$\widetilde{\theta_1} = 9.8^o, \widetilde{\theta_2} = 10.8^o, \widetilde{\theta_3} = 11.5^o$and $\widetilde{\theta_4} = 12.3^o$
Case for $L = 6$ sources from $\theta_1 = 4^o$, $\theta_2 = 5^o$, $\theta_3 = 6^o$, $\theta_4 = 7^o$, $\theta_5 = 20^o$ *and* $\theta_6 = 22^o$.	
Number of sources	6
ARoIs	$\theta_{L1} = 2^o, \theta_{U1} = 13^o$ $\theta_{L2} = 18^o, \theta_{U2} = 24^o$
Estimated DOAs	$\widetilde{\theta_1} = 4.3^o$, $\widetilde{\theta_2} = 5.5^o$, $\widetilde{\theta_3} = 6.1^o$, $\widetilde{\theta_4} = 7.2^o$, $\widetilde{\theta_5} = 20^o, \widetilde{\theta_6} = 22^o$

TABLE III. COMPARISON OF DOA ESTIMATION METHODS

Case for $L = 5$ sources from $\theta_1 = 35^o$, $\theta_2 = 36^o$, $\theta_3 = 37^o$, $\theta_4 = 50^o$ and $\theta_5 = 53^o$	
Methods	Estimated DOAs
MUSIC	$\widehat{\theta_1} = 36.05^o, \widehat{\theta_2} = 51.52^o$
ESPRIT	$\widehat{\theta_1} = -4.10^o$, $\widehat{\theta_2} = 8.17^o$, $\widehat{\theta_3} = 32.59^o$, $\widehat{\theta_4} = 33.69^o$ and $\widehat{\theta_5} = 29.90^o$
CSVR (Proposed)	$\widehat{\theta_1} = 34.5^o$, $\widehat{\theta_2} = 35.5^o$, $\widehat{\theta_3} = 376.3^o$, $\widehat{\theta_4} = 49.9^o$ and $\widehat{\theta_5} = 52.9^o$

V. CONCLUSION

A new approach for estimating the DOAs of signals from multiple closely spaced sources was presented. The proposed approach was found to be advantageous in terms of the number of sensor elements and snapshots required for DOA estimation. The proposed method does not require prior knowledge of the number of sources present in the received signal, unlike the existing SVR method. The computational complexity is considerably reduced for hardware implementation due to the reduced requirement of snapshots for computing the sample covariance matrix. The consistency of the proposed approach was validated through numerical simulation results. The MVDR-CSVR approach is believed to be well suited for compactly designed DOA estimation systems. This approach has the potential to be extended to the estimation of DOAs of moving sources as well.

REFERENCES

[1] L. Pucci, E. Paolini and A. Giorgetti, "System-Level Analysis of Joint Sensing and Communication based on 5G New Radio," *IEEE Journal on Selected Areas in Communications*, 2022 (Early access).

[2] M. Koivisto, J. Talvitie, E. Rastorgueva-Foi, Y. Lu and M. Valkama, "Channel Parameter Estimation and TX Positioning with Multi-Beam Fusion in 5G mmWave Networks," *IEEE Transactions on Wireless Communications*, 2021 (Early access)

[3] Bishop C, Pattern Recognition and Machine Learning, *New York: Springer*, 2006.

[4] A.H.El Zooghby, C. G. Christodoulou, and M. Georgiopoulos, "Performance of radial-basis function network for direction arrival estimation with antenna arrays," *IEEE Transactions on Antennas and Propagation*, vol. 45, no. 11, pp. 1611-1617, Nov. 1997

[5] J. Capon, "High resolution frequency-wavenumber spectral analysis," *Proceedings of the IEEE*, vol. 57, pp. 1408–1518, Aug. 1969.

[6] I. Ziskind and M. Wax, "Maximum likelihood localization of multiple sources by alternating projection," *IEEE Transactions on Acoustics, Speech, Signal Processing*, vol.36, pp. 1553–1560, Oct. 1988.

[7] R. O. Schmidt, "Multiple emitter location and signal parameter estimation," *IEEE Transactions on Antennas and Propagation*, vol. AP-34, pp. 276–280, Mar. 1986.

[8] R. Roy and T. Kailath, "ESPRIT — Estimation of signal parameters via rotational invariance techniques," *IEEE Transactions on Acoustics, Speech, Signal Processing*, vol.37, pp. 984–995, July 1989.

[9] A. J. Barabell, "Improving the Resolution Performance of Eigenstructure-based Direction Finding Algorithms," in *Proceedings of the IEEE International Conference on Acoustics, Speech and Signal Processing*, pp. 336–339, 1983.

[10] M. D. Zoltowski, G. M. Kautz, and S. D. Silverstein, "Beamspace ROOT-MUSIC," *IEEE Transactions on Signal Processing*, vol. 41, no. 1, pp. 344–364, Feb. 1993.

[11] G. Xu, S. D. Silverstein, R. H. Roy, and T. Kailath, "Beamspace ESPRIT," *IEEE Transactions on Signal Processing*, vol. 42, no. 2, pp. 349–356, Feb. 1994.

[12] A. H. El Zooghby, C. G. Christodoulou, and M. Georgiopoulos, "A neural network-based smart antenna for multiple source tracking," *IEEE Transactions on Antennas and Propagation* vol. 48, no. 5, pp. 768–776, May 2000.

[13] M. Donelli, F. Viani, P. Rocca, and A.Massa, "An innovative multiresolution approach for DOA estimation based on a support vector classification," *IEEE Transactions on Antennas and Propagation*, vol. 57, no. 8, pp. 2279–2292, Aug. 2000

[14] M. Pastorino and A. Randazzo, "The SVM-based smart antenna for estimation of the directions of arrival of electromagnetic waves," *IEEE Transaction on Instrumentation and Measurement.*, vol. 55, pp. 1918–1925, Dec. 2006.

[15] Matteo Pastorino, Andrea Randazzo, "A smart antenna system for direction of arrival estimation based on support vector regression," *IEEE Transactions on Antennas and Propagation*, vol. 53, pp. 2161–2168, Jul. 2005.

[16] A.Randazzo et al, "Direction of arrival estimation based on support vector regression: Experimental validation and comparison with MUSIC," *IEEE Antennas and Wireless propagation letters*, Vol.6, 2007.

[17] P. Bouboulis, S. Theodoridis, C. Mavroforakis and L. Evaggelatou-Dalla, "Complex Support Vector Machines for Regression and Quaternary Classification," *IEEE Transactions on Neural Networks and Learning Systems*, vol. 26, no. 6, pp. 1260-1274, Jun. 2015.

[18] A. J. Smola and B. Schölkopf, "A tutorial on support vector regression," *Statistics and Computing*, vol. 14, no. 3, pp. 199–222, Aug. 2004.

[19] Cortes, C., Vapnik, V., "Support Vector Networks," *Machine Learning*, Vol. 20, pp. 273-297, 1995

[20] V. Vapnik, *Statistical Learning Theory*, *New York: Wiley*, 1998.

Analysis of Twitter Data Using Machine Learning Algorithms

Sanchana R[1], Nithya Devi S[2], Mercy P[3], Bhavani Sree SK[4], Swetha S[5]

[1-5]Department of Information Technology, Sri Sairam Institute of Technology

[1]sanchana.it@sairamit.edu.in, [2]sit19it062@sairamtap.edu.in, [3]sit19it052@sairamtap.edu.in, [4]sit19it039@sairamtap.edu.in, [5]sit19it083@sairamtap.edu.in

***Abstract*—Sentiment analysis is one among the distinguished fields of knowledge and pattern mining that deals with the identification and analysis of sentiment within the text. The main challenges in sentiment analysis are word ambiguity and multi polarity. The problem of word ambiguity is to define polarity because the polarity for words is context dependent. The tweets are initially preprocessed. The preprocessing includes the removal of stop words, and lower case conversion. The tweets are then passed to the feature extraction techniques. Then the data is splitted as training and testing data. The trained data is passed to the different machine learning algorithm like Naive Bayes. Support Vector machine, Random forest, and Decision Tree and k-NN algorithm. The accuracy obtained using the Naive Bayes. Support Vector machine, random forest, and Decision Tree, k-NN and Logistic regression algorithm is 80%, 77%, 72%, 61% ,56% and 78%. The naïve bayes algorithm has achieved a better accuracy when compared to the other algorithm.**

Keywords—SVM, Naive bayes, Decision tree, Random forest

I. INTRODUCTION

Natural language processing utilizes two main principal strategies they are syntax and semantic analysis. The arrangement of words in a sentence to make grammatical sense is called syntax analysis. Natural language processing uses syntax analysis techniques to assess meaning from a language based on grammatical rules. Syntax structure procedures incorporate parsing, word segmentation, sentence breaking, morphological segmentation, and stemming. Semantic uses a calculation to comprehend the importance and structure of a sentence. The techniques that NLP uses with semantics include word sense disambiguation, named entity recognition, and natural language generation. The word sense infers the importance of the word dependent on the specific situation. Named entity recognition decides whether the words can be categorized into groups. Natural language generation utilizes a database to decide the semantics behind the word. NLP uses a rule-based approach where machine learning techniques are used to train the models. The models are trained in such a way that when words and phrases appear in the particular text and are given a response when those particular phrases appear in the text. The primary use case for NLP is sentiment analysis. The sentiment analysis used by the data scientist can assess comments via web-based networking media to perceive how their business image is performing.

The challenging task in natural language processing is semantic analysis. NLP does not pick up sarcasm easily since it requires an understanding of the words being used and the context in which the words are being used. Natural language processing is additionally a difficult task by the means that language, and therefore the manner in which individuals use it, is persistently evolving. NLP makes use of a data engine that processes language and facial expression in order to monitor president trump's emotional state. Sentiment analysis is combined with image recognition to enhance accuracy. Image recognition techniques break down the image connected with the tweet, and then machine learning processes them together with the language to tell the actual emotionality of an image. Sentiment analysis is the process of determining whether or not the polarity in particular text is positive, negative or neutral. Sentiment analysis is one among the distinguished fields of knowledge and pattern mining that deals with the identification and analysis of sentiment within the text. Sentiment analysis is referred to as opinion mining. Opinion mining combines natural language processing and machine learning techniques to assign weighted sentiment scores to each and every entity. The types of sentiment analysis are generally classified into fine-grained, emotion detection, aspect-based sentiment analysis, and intent analysis. Fine grained sentiment analysis provides different flavors of polarity by identifying the actual text as positive or negative sentiment. The text is related to a particular feeling such as anger disappointment or worries (negative feelings) or happiness; love (positive feelings). Emotion detection is used to detect emotions like happiness, anger, and sadness. The words that generally express anger may also express happiness depending on the context of the words being used. The aspect-based sentiment analysis breaks down the text into aspects. Each aspect is assigned with sentiment values as positive negative and neutral**.**

For instance "The battery lifetime of this camera is simply too short" The above example is expressing a negative opinion regarding the camera, but precisely it describes the battery life which is the explicit feature of the camera. The intent analysis refers to the text rather than the people say with the text. For example **"**I would like to know how to replace the things". The above example can be inferred from

the text, but in many cases, inferring the text requires some contextual knowledge. Multilingual sentiment analyses are often troublesome task since it needs a lot of preprocessing techniques and preprocessing makes use of wide range of resources.

The main challenges in sentiment analysis are word ambiguity and multi polarity. The problem of word ambiguity is to define polarity because the polarity for words is context dependent. For example “The story of the movie is unpredictable” [1] “The steering wheel of the automotive is unpredictable” [2]. The primary example defines the polarity of the word “unpredictable” as positive. The second example defines the polarity of the word “unpredictable” as negative.

For instance **“**The audio quality of my phone is so cool however the display colors are not too good” Multi-polarity sentiment analysis model can assign a negative or a neutral polarity to the particular instance defined above. The overcome this drawback, every sentence must be assigned with polarity; here “audio” is assigned with positive polarity and “display” is assigned with negative polarity. Sentiment analysis provides a quantitative and qualitative data through which we can assess the success of the market campaign. Sentiment analysis plays a vital role in

Monitoring the customers and spotting the negative comments early which will help the business parties to overcome the critical situation. The biggest advantage of sentiment analysis is to increase the sales revenue which in turn improves the products/service quality and customers services. Sentiment analysis is employed across a variety of applications and for multiple purposes. One such application is the prediction of election results. Sentiment analysis has been utilized by political candidate to observe overall opinion concerning policy changes enabling them to fine-tune their approach and to better relate to voters. In brand reputation management application, sentiment analysis enables brands to identify peaks in overall brand sentiment so enabling companies to make improvement absolutely with client demands.

II. LITERATURE SURVEY

A Twitter sentiment analysis study by Go et al does a two-classed (negative and positive) classification of tweets. The training data was preprocessed before it was used to train the classifier. The Preprocessing techniques include removing the user names and actual URLs and converting the classes into equivalence classes like 'URL' and 'USERNAME' respectively. To select useful uni-grams, they used such feature selection algorithms. The feature selection algorithm is frequency, mutual information, and chi-square method. Multinomial Naive Bayes, maximum entropy and support vector machines (SVM) are the three supervised techniques used for analysis. The accuracy of 84% was obtained with multinomial Naive Bayes using uni-gram features selected on the basis of their MI score. The accuracy was low when the tweets are processed using the bi-gram approach. The experiment did not recognize and they were not able to handle neutral tweets. To take into account neutral tweets, they collected tweets about a term that do not have emoticons. Nearly 33 tweets were manually annotated and they are used as test data. The manually annotated tweets where labeled as neutral. They merged these two datasets with the training data and test data used in the above two-classed classification. They trained a three-classed classifier and tested it, and achieved an accuracy of 78% .

Sentiment analysis on ensemble learning classifier was proposed by Ankit et al., (2018), focusing on ensemble classifier which combines the base learning classifier to form a single classifier that aims in redesigning the performance and accuracy of sentiment classification. The Ensemble approach takes the positive and negative scores of the tweet. The positive score is higher than the negative score then the score of sentiment tweet is positive. The negative score is higher than the positive score then the sentiment score is negative. If the positive and negative scores are equal then the system calculates the cosine similarity of that tweets. The cosine similarity of the tweets is in contrast with the testing data and identifies the most similar tweets. Then calculates the positive and negative score identified tweets. It failed to calculate the values of neutral tweets which incorporate neither positive nor negative sentiment.

Twitter sentiment analysis using the hybrid cuckoo search method was proposed by Avinash Chandra Pandey et al., (2017), a heuristic technique that is based on k-means and cuckoo search. The heuristic method is used to find the optimum cluster heads from the sentimental contents of the Twitter dataset. K-means data clustering method groups n data points in k clusters and distance can be calculated either by using Euclidean distance or cosine measures. K-means can be used for initial clustering which is the major drawback. The generated cluster need to be further analyzed therefore cuckoo search method is used for further optimization of the cluster-heads. The cuckoo search approach makes use of a random initialization method that increases the number of iterations to converge and also stuck to some local solution. The process of the cuckoo search method results in faster convergence and better optimum solutions. The cuckoo search method modifies the initialization from k-means which resolves the problem of random initialization.

Twitter sentiment analysis was proposed by Barbosa and Feng (2010) used a two-phased approach for sentiment analysis. The two phases are: 1) classifying the dataset into objective and subjective classes (subjectivity detection) and 2) classifying subjective sentences into positive and negative classes (polarity detection). Suspecting that the use of n-grams for Twitter sentiment analysis might not be a good strategy since Twitter messages are short, they use two other features of tweets: Meta information about tweets and syntax of tweets. For meta-information, they use Parts of speech tags and mapping words to prior subjectivity (strong and weak), and prior polarity (negative, positive and neutral). The prior polarity is reversed when a negative expression precedes the word. For tweet syntax features, they use #, @, retweets, link, punctuations, emoticons, capitalized words, etc. SVM has achieved a better accuracy compared to the other machine learning techniques. For test data, 1000 tweets were manually annotated. The tweets are annotated as Positive, negative, and neutral tweet. The

highest accuracy obtained was 81.9% on subjectivity detection followed by 81.3% on polarity detection.

III. ARCHITECTURE

The following figure 3.1 represents the architecture diagram of the Twitter data analysis using different machine learning algorithms. The dataset is collected from Twitter. The tweets are pre-processed to clean and transform the data for feature extraction. The tweets are initially pre-processed. The pre-processing includes the removal of stop words and lower case conversion. The tweets are then passed to the feature extraction techniques. Then the data is split as training and testing data. The trained data is passed to different machine learning algorithms like Naive Bayes. Support Vector Machine, Random Forest, Decision Tree, and k-NN algorithm. The precision, recall, and accuracy score are calculated and finally, the data are visualized in the graphical format.

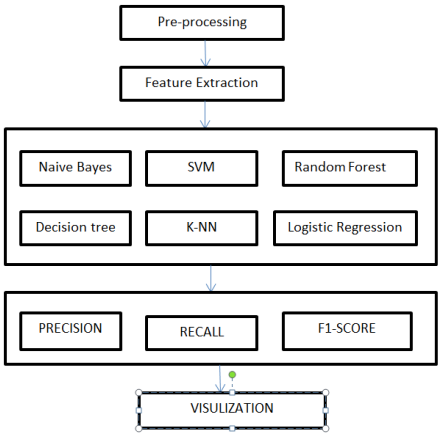

Figure 1. Architecture Diagram of twitter data analysis

A. Data pre-processing

The data preprocessing includes the lower case conversion and stop words removal. The lower case conversion is done mainly because these words will be represented in two dimension vector spaces. The stop words are removed because these words occupy a unnecessary memory spaces and these words are not used during the analysis since they do not provide any meaning to the context.

B. Feature Extraction

Feature extraction plays a vital role in the part of text classification. It is based on vector space model. The feature extraction is an approach to minimize the quantity of resources required to describe a dataset. Analysis with a massive range of variables requires a large amount of memory and more computational power. The classification algorithm overfit the training sample and generalizes to new samples. Hence the feature extraction technique is essential while dealing with classification problems with a large number of variables. The multiple features are compared and different accuracy scores are achieved for different features. The vector space model views the text as a dot in the N-dimensional space. The different feature extraction techniques are bag of words, n-gram, TF-IDF. Bag of words is mainly used in the document classification. Document classification mainly uses each word as a feature for training the classifier. The main disadvantage of the model is that the order of occurrence of each word is lost because for each word it creates a vector of tokens in randomized order. In order to overcome this problem we go for an approach called N-gram. The N-gram approach works based on how often the word sequences occur in the corpus text.

Input: preprocessed tweet

Output: tokenized tweet
Step 1: Token = tokenization of the word
Step 2: Polygram = gram (token, 10)
Step 3: analysis = analyze the tweet using get sentiment function
Step 4: Gram input= [text, analysis]

C. Classification

One of the supervised learning techniques is Classification. It specifies the class to which the data element belongs to and it is used once the output has finite and distinct values. The sentiment analysis in social media has two potential outcomes, positive or negative.

"The best economy in our lifetime"
"The Obama administration built the cages not the Trump administration"

Classification techniques will categorize the data as positive, negative or neutral. The above example "the best economy in our life time" is categorized as a positive class label. "The Obama administration built the cages not the Trump Administration" is categorized as a negative label.

D. 3.1 Naive Bayes Algorithm

Naive Bayes is a classification technique. The principle behind the Naive bayes algorithm is Bayes theorem. Bayes theorem defines the independence among predictors. There are two types of implementations – Bernoulli and Multinomial. The difference between the models is the way in which the features are extracted from the document. According to Bayes model the conditional probability can be calculated as

$$p\left(\frac{y}{x}\right) = p\left(\frac{x}{y}\right).p(y)/p(x) \qquad [3.1]$$

[3.4] Represents a very large number of p(y/x) is the posterior probability of the class given attribute. The prior probability of the class is represented using P(y). P (x) is the prior probability of the attribute. P (x|y) is the likelihood which determines the probability of the attributes given class.

$$p(y|x1, x2 \ldots\ldots xn) = p(y)\pi p(x_i|y) \qquad [3.2]$$

We have to find the probability of the given set of inputs for all possible values of the class y and the output which has the maximum probability. The main drawback of naive Bayes classifiers is highly scalable. The naive bayes model requires a large number of variables (features/predictors) in a learning problem. Naive bayes model is easy to build and particularly useful for handling large datasets. Naive Bayes is easy to implement and needs less training data.

Positive tweet analysis:

$$p(tweet_{positive}) = \frac{p(totalcount_{positive})}{p(total_{tweetcount})} \quad [3.3]$$

Negative tweet analysis:

$$p(tweet_{negative}) = \frac{p(totalcount_{negative})}{p(total_{tweetcount})} \quad [3.4]$$

Neutral tweet analysis:

$$p(tweet_{neutral}) = \frac{p(totalcount_{neutral})}{p(total_{tweetcount})} \quad [3.5]$$

Naive bayes method is a popular basic method to categorize the text. It uses frequencies of words in document as the feature for classification. The advantage of Naive Bayes classifier is its high scalability as it requires parameters in proportion to the number of features or variables and that too linearly. Naive bayes requires a small set of data for training the classifier.

E. Support Vector Machine

SVM is a supervised machine learning algorithm. Support vector machine may be used for both classification and regression. SVM performs classification by finding the hyper-plan that differentiates the categories that are premeditated in an n-dimensional area. The algorithm works comparatively well once there's a clear margin of separation between categories. SVM is more efficient in high dimensional space.

Prediction score:

$$prediction_{svm} = predict(test\ ) \quad [3.6]$$

Accuracy score:

$$accuracy_{score} = predict_{testy}*100 \quad [3.7]$$

F. Decision Tree

The decision tree is the most popular algorithm used for classification and prediction. The decision tree follows a tree-like structure that contains internal nodes, branch, and leaf nodes. The internal node represents an attribute, the branch represents an outcome and the leaf node holds the information about the class label. The decision tree is initially constructed by splitting the dataset into a subset based on the attribute. The process is repeated on the derived subset in a recursive manner. The main advantage of the decision tree is the construction of the tree does not require any domain knowledge. A decision tree can handle both continuous and categorical variables. The main disadvantage of using the decision tree - generates more errors in classification problems since we use a small number of training datasets.

G. Logistic Regression

Logistic regression is the machine learning algorithm that comes under the supervising learning techniques. In logistic regression, the outcome must be a categorical or a discrete value. The output of the logistic regression is a categorical dependent variable. The dependent variable can be predicted from the given set of independent variables. The logistic regression uses a cost function called the sigmoid function. The sigmoid function is mainly used to map the predicted values corresponding to their probabilities. The linear regression classifier combines the weight of the input features. The weighted input features are passed as an input to the sigmoid function. The sigmoid function transforms the input into a number. The transformed input values should lie between 0 and 1.

H. K-NN Algorithm

The k-nearest algorithm is supervised machine learning. K-NN is also known as a non-parametric or lazy learner algorithm. The k-NN does not learn from the training set. The K-NN stores the training dataset and then classifies the data. The classified data is then grouped. The K-NN algorithm works by selecting the k neighbors. Then the Euclidean distance is calculated for the K number of neighbors. Take the k nearest neighbors from the Euclidian distance calculated. In each category count the number of data points. The new data points which are calculated are assigned based on the number of neighbors is maximum. Finally, the model is ready for evaluation. The main advantages of using the K-NN algorithm are more effective when the training dataset is large. The disadvantage of using the algorithm is to determine the k value which may be complex. The cost of calculating the distance between the data points for all the training datasets is high.

I. Random Forest Algorithm

The Random forest is a machine learning algorithm that can be used to solve both classification and regression based problems. Random forest algorithm belongs to a supervised learning technique. Random forest works based on the concept of ensemble learning technique. The ensemble method solves a complex problem by combining multiple classifiers in order to improve the performance of the model. The random forest contains a number of decision trees. The decision tree is classified based on the various subsets of the given datasets. Finally the average is taken in order to improve the predictive accuracy of the dataset. The number of trees constructed in the forest is greater leads to higher accuracy and preventing the problem of overfitting. The random forest algorithm works by selecting the random data points K from the training dataset. The decision tree is constructed based on the selected data points. If there are only few data points then find the predictions of each decision tree. Then assign the new data point to the category which has majority votes. The advantage of the random forest model improves the accuracy and resolves the problem of overfitting. The random forest algorithm is not more suitable for the regression-based problem.

IV. Result And Discussion

A. Naive Bayes Algorithm

The following table 5.1 represents the precision-recall and f1-score achieved using the Naive Bayes algorithm. The naïve Bayes algorithm is calculated against two values i.e. 0 or 1. The precision, recall, and f1-score achieved using the positive tweets are 80%, 69%, and 82%. The precision, recall, and f1-score achieved using the negative tweet is 78%, 87%, and 82%.

TABLE 5.1 PRECISION, RECALL AND F1-SCORE USING NAIVE BAYES

	Precision	Recall	F1-score	Support
0	0.78	0.87	0.82	4500
1	0.80	0.69	0.74	3543

The following figure 5.1 represents the confusion matrix obtained using the Naive Bayes algorithm. The confusion matrix is plotted against the true negative, false positive, false negative and true positive values. The true negative value is 3912, the false positive value is 588, the false negative value is 1116 and the true positive value is 2427.

Figure 2. Confusion matrix using Naive bayes

B. *Decision Tree*

The following figure 5.2 represent the construction of the decision tree with the given set of input data.

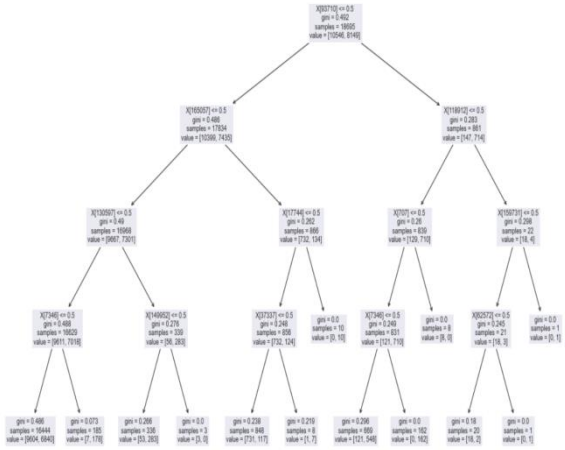

Figure 3. Decision Tree Constructions

The following table 5.2 represents the precision recall and f1-scoreachieved using the decision tree algorithm. Decision tree algorithm is calculated against two values i.e. 0 or 1. The precision, recall and f1-score achieved using the positive tweets are 86%, 25% and 25%. The precision, recall and f1-score achieved using the negative tweet is 59%, 98% and 74%.

TABLE 5.2 PRECISION, RECALL AND F1-SCORE USING DECISION TREE

	Precision	Recall	F1-score	Support
0	0.59	0.98	0.74	4500
1	0.86	0.25	0.25	3543

The following figure 5.3 represents the confusion matrix obtained using the Decision tree algorithm. The confusion matrix is plotted against the true negative, false positive, false negative and true positive values. The true negative value is 4420, the false positive value is 80, the false negative value is 3032 and the true positive value is 511.

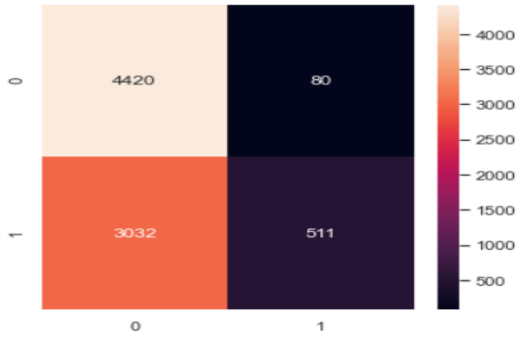

Figure 4. Confusion matrix using Decision tree

C. *Support Vector Machine*

The following table 5.3 represents the precision recall and f1-score achieved using the support vector algorithm. Support vector algorithm is calculated against two values i.e. 0 or 1. The precision, recall and f1-score achieved using the positive tweets are 80%, 64% and 71%. The precision, recall and f1-score achieved using the negative tweet is 76%, 87% and 81%.

TABLE 5.3 PRECISION, RECALL AND F1-SCORE USING SUPPORT VECTOR MACHINE

	Precision	Recall	F1-score	Support
0	0.76	0.87	0.81	4500
1	0.80	0.64	0.71	3543

The following figure 5.3 represents the confusion matrix obtained using the Support vector machine algorithm. The confusion matrix is plotted against the true negative, false positive, false negative and true positive values. The true negative value is 3918, the false positive value is 582, the false negative value is 1263 and the true positive value is 2280.

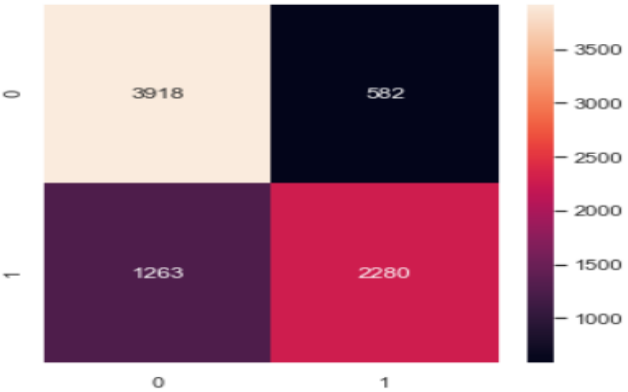

Figure 5 Confusion matrix using Support Vector Machine

D. *Logistic Regression*

The following table 5.4 represents the precision recall and f1-score achieved using the logistic regression algorithm.

Logistic regression algorithm is calculated against two values i.e. 0 or 1. The precision, recall and f1-score achieved using the positive tweets are 81%, 65% and 72%. The precision, recall and f1-score achieved using the negative tweet is 76%, 88% and 82%.

TABLE 5.4 PRECISION, RECALL AND F1-SCORE USING LOGISTIC REGRESSION

	Precision	Recall	F1-score	Support
0	0.76	0.88	0.82	4500
1	0.81	0.65	0.72	3543

The following figure 5.4 represents the confusion matrix obtained using the Logistic Regression algorithm. The confusion matrix is plotted against the true negative, false positive, false negative and true positive values. The true negative value is 3969, the false positive value is 531, the false negative value is 1255 and the true positive value is 2288.

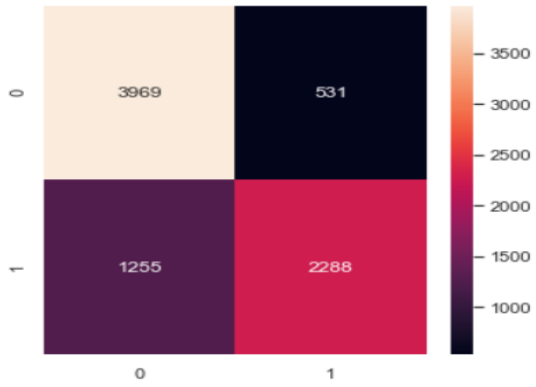

Figure 6 Confusion matrix using Logistic Regression

E. *Random Forest*

The following table 5.4 represents the precision recall and f1-score achieved using the Random forest algorithm. Random forest algorithm is calculated against two values i.e. 0 or 1. The precision, recall and f1-score achieved using the positive tweets are 82%, 47% and 60%. The precision, recall and f1-score achieved using the negative tweet is 69%, 92% and 79%.

TABLE 5.5 PRECISION, RECALL AND F1-SCORE USING RANDOM FOREST

	Precision	Recall	F1-score	Support
0	0.69	0.92	0.79	4500
1	0.82	0.47	0.60	3543

The following figure 5.5 represent the confusion matrix obtained using the random forest algorithm. The confusion matrix is plotted against the true negative , false positive, false negative and true positive values. The true negative values is 4139, the false positive value is 361,the false negative value is 1887and the true positive value is 1656.

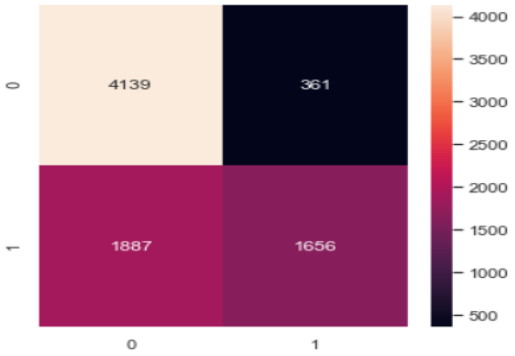

F. *KNN*

The following table 5.4 represents the precision recall and f1-score achieved using the logistic regression algorithm. Logistic regression algorithm is calculated against two values i.e. 0 or 1. The precision, recall and f1-score achieved using the positive tweets are 66%, 50% and 25%. The precision, recall and f1-score achieved using the negative tweet is 57%,97%,72%.

TABLE 5.6 PRECISION, RECALL AND F1-SCORE USING LOGISTIC REGRESSION

	Precision	Recall	F1-score	Support
0	0.57	0.97	0.72	4500
1	0.66	0.50	0.25	3543

The following figure 5.6 represent the confusion matrix obtained using the random forest algorithm. The confusion matrix is plotted against the true negative, false positive, false negative and true positive values. The true negative values are 4237, the false positive value is 201, false negative value is 3311 and the true positive value is 264.

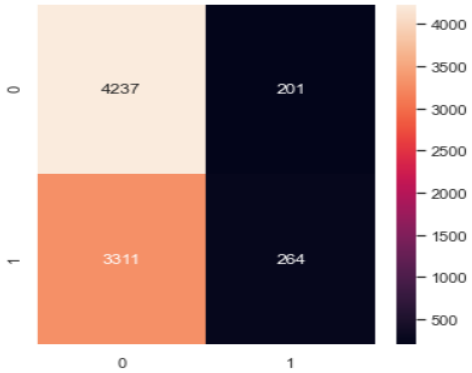

Figure 7. Confusion matrix using Random Forest

G. *Testing Accuracy*

The input data is splitted as training and testing data. The training data is nearly 70% of the dataset which is used to teach the machine learning models. The test data is 20% of the given dataset where it is used to test the data for the given input, the outputs are derived correctly. The following table 5.7 represent the accuracy obtained using the test data.

TABLE 5.7 ACCURACY OF TEST DATA

Algorithm	Accuracy of test data
Naive Bayes	80%
K-NN	56%
Random Forest	72%

Decision Tree	61%
Logistic Regression	78%
Support Vector Machine	77%

H. Graphical Representation

The graph is plotted against the different machine learning model and their corresponding accuracy. The x axis contains the accuracy and the y-axis is plotted against the different machine learning models. The following figure 5.7 represents the graphical representation of different machine learning model.

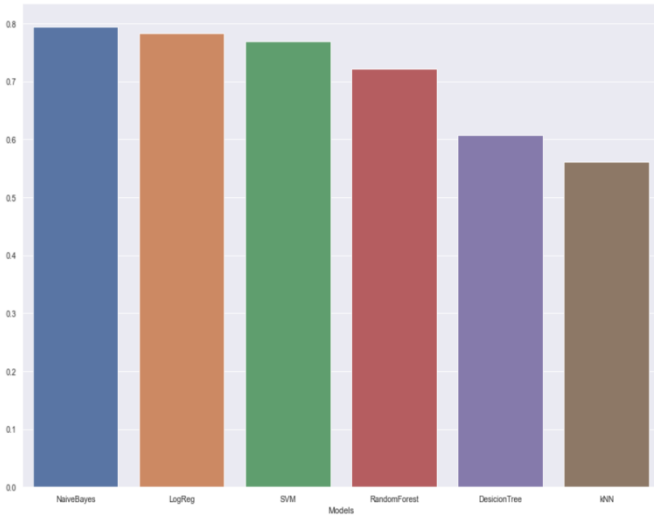

Figure 8. Graphical representations of different machine learning models

V. Conclusion

The proposed work analyzed the information spread over social networks like Twitter. Sentiment analysis is a uniquely powerful tool for the analysis of election results that is looking to measure attitudes, feelings, and emotions. Nevertheless, the evolution of social media analysis regarding politics is still considered to be in its infancy, despite the importance of the topic for political science. The dataset is collected from Twitter. The tweets are pre-processed to clean and transform the data for feature extraction. . The tweets are then passed to the feature extraction techniques. Then the data is split as training and testing data. The trained data is passed to different machine learning algorithms like Naive Bayes. Support Vector Machine, Random Forest, Decision Tree, and k-NN algorithm.

The accuracy obtained using the Naive Bayes. Support Vector machine, random forest, and Decision Tree, k-NN and Logistic regression algorithm is 80%, 77%, 72%, 61% ,56% and 78%. The naïve bayes algorithm has achieved a better accuracy when compared to the other algorithm.

VI. Future Work

There is a vast future scope in this research area as it is not only interesting but also challenging in the real world. In the future, sarcasm can be detected in text. Many tools and algorithms rely on the polarity of the words and the scoring is dependent on polarity. This means that accuracy drops since the semantics of the complete sentence are lost. To measure the polarity of the sentence on each and every individual words the semantics of the sentence. The semantics of the sentences make it difficult to identify the polarity. For instance, the financial industry has its own language which means completely differs from the Entertainment industry. This makes it hard for the tool to predict the emotion or semantics of the sentence.

References

[1] Ahmad S, Asghar MZ, Alotaibi FM, Awan I(2018), ”Detection and classification of social media-based extremist affiliations using sentiment analysis techniques” Vol.9,pp.1-24.

[2]

[3] Alotaibi FM, Awan I (2016), “American presidential election. Journal of Internet Services and Applications” Vol.9, pp.1-18.

[4]

[5] Budiharto & Meiliana, M. (2018), “Prediction and analysis of Indonesia Presidential election from Twitter sentiment analysis”.Vol.5, pp.1-51.

[6] Budiharto W, MeilianaM (2018),”Prediction and analysis of Indonesia Presidential election from Twitter using sentiment analysis”. Journal of Big Data. Vol.1, pp.5-51.

[7] Caetano JA, Lima HS, Marques-Neto HT(2017), ”sentiment analysis using twitter” Vol.5, pp.8-24.

[8]

[9] Santos MF (2018), “Using sentiment analysis to define twitter political users classes and their homophily during the American presidential election”-Journal of Internet Services and Applications Vol.8,pp.70-77.

[10]

[11] Nakov, P., Ritter, A., Rosenthal, S., Sebastiani, F., & Stoyanov, V. (2016),”Sentiment analysis in Twitter. In Proceedings of the 10th international workshop on semantic evaluation Vol.5, pp.1-18.

[12] Pandey, A.C., Rajpoot, D.S. and Saraswat, M (2017), “Twitter sentiment analysis using hybrid cuckoo search method. Information Processing & Management” Vol.53 (4), pp.764-779.

[13]

[14] Saif, H., He, Y., & Alani, H. (2012), “Semantic sentiment analysis of twitter. In International semantic web conference” Vol.5,pp. 508-524.

Solving Partial Differential Equations Using Deep Learning

Sneha S[1], Shweta Srikanth[2], Vikram Venkat Krishnan[3], W. Jino Hans[4], N Padmapariya[5]

[1-4]ECE Department, Sri Sivasubramaniya Nadar College of Engineering, Chennai, India

[5]Department of Mathematics, Sri Sivasubramaniya Nadar College of Engineering, Chennai, India

[1]snehasathish17@gmail.com, [2]shwetasrikanth6@gmail.com, [3]krishnan.vikram13@gmail.com, [4]jinonhansw@ssn.edu.in, [5]padmapriyan@ssn.edu.in

***Abstract*—Partial differential equations are ubiquitous in mathematically-oriented scientific fields, such as physics and engineering. Due to this presence, there is a wide spectrum of such equations and multiple methodologies have been developed to solve these equations. The recent advancements in computational technology using deep learning can be utilized to solve these equations efficiently. The proposed work attempts to solve a partial differential equation, Burger's equation, by comparing the solutions obtained by an artificial neural network and a physics-informed neural network.**

***Keywords*—partial differential equations, deep learning, physics informed neural networks, Burger's equation**

I. INTRODUCTION

A partial differential equation (PDE) is a mathematical equation that involves two or more independent variables, an unknown function (dependent on those variables), and partial derivatives of the unknown function with respect to the independent variables [1]. They play a prominent role in engineering, physics, economics, biology and other disciplines[2]. PDEs are used to mathematically formulate, and thus aid the solution of physical and other problems involving functions of several variables, such as the propagation of heat and sound, fluid flow, elasticity, electrostatistics, electrodynamics etc. Therefore, to study these phenomena, solving PDEs is of significance. Since analytical solutions can often be impossible to compute, several numerical methods have been used in the past. These include finite difference method, finite element method, finite volume method, etc [3-4]. However, a few drawbacks of such numerical solutions are they require discretisation and the complexity of finding close formed solutions increases with the system's linearity. Developments of computing resources and advancements in data driven methods in recent years have led to application of machine learning and deep learning methods to solve PDEs. Lagaris et al. [5] illustrated a method to solve a variety of ordinary and partial differential equations using artificial neural networks and present comparisons with solutions obtained from the Galerkin finite element method. Although this idea was proposed in the 90's, it has started to have a big impact in recent times. Wu et al. [6] proposed a deep learning framework for recovering/approximating unknown time-dependent PDE using its solution data. Another deep learning approach was introduced by Han et al. [7] where PDEs are reformulated using backward stochastic differential equations and the gradient of the unknown solution is approximated by neural networks. Sirignano et al. [8] proposed a Deep Galerkin Method (DGM) , the algorithm which is similar in spirit to Galerkin methods, with the solution approximated by a neural network instead of a linear combination of basis functions. Amongst the many deep learning frameworks being studied, the physics informed neural network(PINNs) methodology proposed by Raissi et al. [9] is of significance. PINNs are those that are trained to solve learning tasks while respecting any given laws of physics described by general nonlinear partial differential equations. It seamlessly integrates data and mathematical physics models, even in uncertain and high-dimensional contexts and implements them through neural networks. PINNs have been further extended for various applications such as solving Huxley equation [10] and Biot's equation[11]. Pang et al. [12] compared the performance of PINNs against physics-informed Gaussian processes. Bleschmidt et al. [13] presented an expository review and contrasted three recent approaches for solving PDEs: physics-informed neural networks, methods based on the Feynman–Kac formula, and methods based on the solution of backward stochastic differential equations.

In the following sections, Section II introduces the proposed system, Section III includes the implementation and Sections IV and V provide the results and conclusions respectively

II. PROPOSED SYSTEM

Burger's Equation has a crucial role to play in the field of Engineering [14]. The equation is a fundamental partial differential equation occurring in various areas of applied mathematics, fluid mechanics and has applications in nonlinear underwater acoustics and in studying the propagation of nonlinear shallow-water waves.

$$\partial_t u + u\partial_x u - (0.01/\pi)\partial_{xx} u = 0,\ (t,x) \in (0,1] \times (-1,1) \quad (1)$$

$$u(0,x) = -\sin(\pi x), x \in [-1,1] \quad (2)$$

$$u(t,-1) = u(t,1) = 0, t \in (0,1] \quad (3)$$

where x is the spatial coordinate; t is the temporal coordinate and

This work aims to implement a deep learning model making use of Physics-Informed Neural Networks (PINNs) to solve the Burgers Equation, by regularizing the training of the model on a small data set. PINNs attempt to solve physical systems which can be written as

$$\partial_t u(t,x) + \mathcal{N}[u](t,x) = 0, x \in R^D, t \in R \quad (4)$$

where $\mathcal{N}[u(t, x); \lambda]$ is an underlying differential operator describing the physical system, parameterised by λ, and u(t, x) represents the solution of the system. The basic idea of PINNs is to use a neural network Λ(t, x; θ), parameterised by θ, to approximate the solution of the physical system u(t, x) and to use Equation 1 as a constraint when training the network. Importantly, the network is a direct functional approximation of u(t, x). It is trained using a loss function which includes both a boundary condition and the underlying equation, given by

$$L = \frac{1}{N_u}\sum_{i=1}^{N_u} ||u(t_i,x_i) - \Lambda(t_i,x_i)||^2 + \frac{1}{N_\Lambda}\sum_{j=1}^{N_\Lambda} ||\mathcal{N}[\Lambda(t_j,x_j;\theta);\lambda]||^2 \quad (5)$$

The first term refers to the data loss while the second term refers to the physics loss.

In general, while neural networks accurately model the physical process within the vicinity of the experimental data, it fails to generalize away from this training data. However, while making use of Physics-Informed Neural Networks the second term in the loss function can be seen as an unsupervised regulariser and thus the network is likely to have better generalization performance outside of the boundary data than one trained with just the boundary loss. Another notable benefit of this approach is that it does not require discretisation, in contrast to traditional numerical methods, and can be used to solve variants of nonlinear PDEs.

Thus, the methodology to solve Burgers equation using PINN begins with the generation of a training dataset, also known as collocation points, based on the equation and its initial and boundary conditions. This is followed by setting up the appropriate network architecture and deriving the loss function which is to be minimized as a sum of data loss and physics loss. The network is then trained and optimized using the loss function after which the solution for Burger's Equation can be plotted and the loss plot can be assessed. Figure 1 summarizes the methodology as discussed above

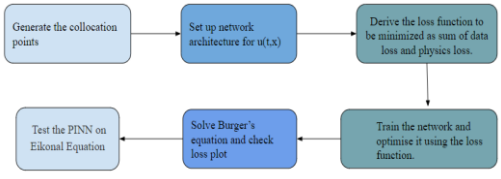

Fig 1: Block Diagram of Proposed System

III. Implementation

A. Data Set Generation

As mentioned earlier, acquiring data for physical systems is prohibitive. Hence random collocation points have been generated to train the model. These points have been sampled from a uniform distribution of data and are bounded by initial and boundary conditions. Cumulatively 10100 collocation points have been generated, of which 10000 points are residual data points represented by the red dots, 50 are initial condition points represented by the multi-coloured crosses and 50 are boundary condition points represented by the blue crosses in Figure 2.

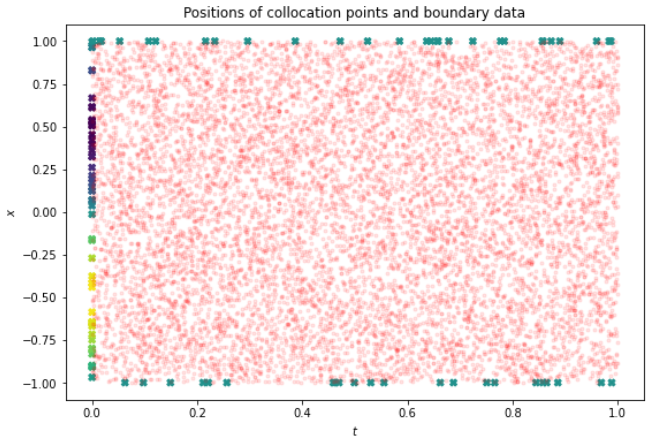

Fig 2: Position of Collocation Points

B. Network Architecture

As mentioned earlier, acquiring data for physical systems is prohibitive. A feed forward network as shown in Figure 3 was constructed.

- Input is scaled element wise to lie in the interval [-1,1].
- Eight fully connected layers each having 20 neurons and each followed by a hyperbolic tangent activation function and one fully connected layer.
- This results in a network with 3021 trainable parameters.

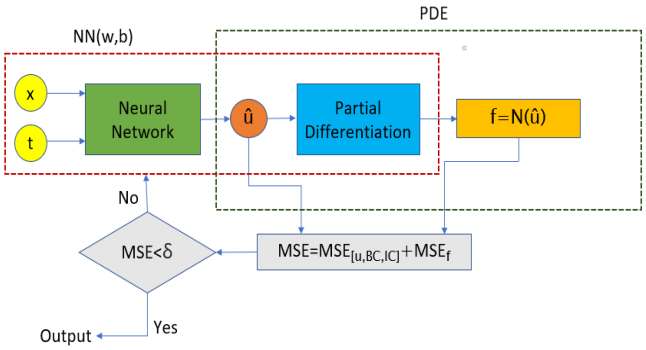

Fig 3: Network Architecture

The loss equations used to optimise the model is

$$\phi_\theta(X) := \phi_\theta{}^r(X^r) + \phi_\theta{}^0(X^0) + \phi_\theta{}^b(X^b) \quad (6)$$

where

$$\phi_\theta{}^r(X^r) := \frac{1}{N_r}\sum_{i=1}^{N_r} |r_\theta\ (t_i{}^r, x_i{}^r)|^2 \quad (7)$$

$$\phi_\theta{}^0(X^0) := \frac{1}{N_0}\sum_{i=1}^{N_0} |u_\theta\ (t_i{}^0, x_i{}^0) - u_0\ (x_i{}^0)|^2 \quad (8)$$

$$\phi_\theta{}^b(X^b) := \frac{1}{N_b}\sum_{i=1}^{N_b} \left|u_\theta\,(t_i{}^b, x_i{}^b) - u_b\,(t_i{}^b, x_i{}^b)\right|^2 \quad (9)$$

Equation (7) corresponds to the physics loss while equation (8) and equation (9) correspond to the data loss. Piecewise decay of learning rate and SciPy optimizer [15] is chosen, and the model is trained for 5000 epochs.

IV. Results

A. *Solution of Burger's Equation*

To understand the importance of a physics-informed neural network, 2 models, a simple feed forward neural network (model 1) and a physics-informed neural network (model 2) have been trained and the results were compared. Model 2 is a feed forward neural network where the partial differential equation of the physical system is included in the cost function and is used to train and optimise the model. Figures 4 and 5 display the predicted solutions for Burger's equation for timestamps t=0.25s, t=0.5s and t=0.75s for Models 1 and 2.

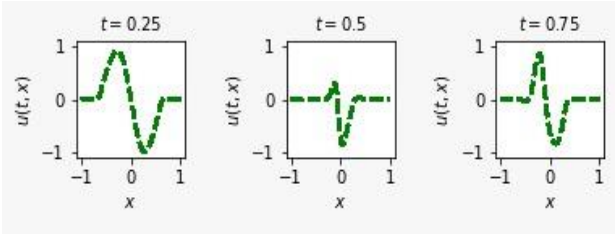

Fig 4: Predicted Solutions for Model 1

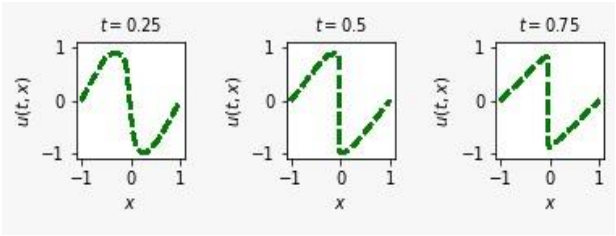

Fig 5: Predicted solutions for Model 2

In order to have a quantitative comparison metric, the loss plot has been plotted. Figures 6 and 7 display the same. The x-axis represents the number of epochs and the y-axis represents the loss.

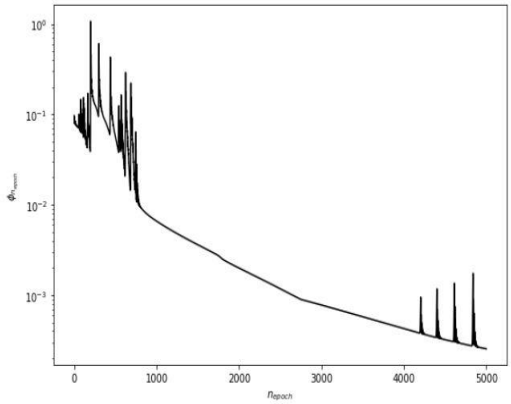

Fig 6: Loss Plot for Model 1

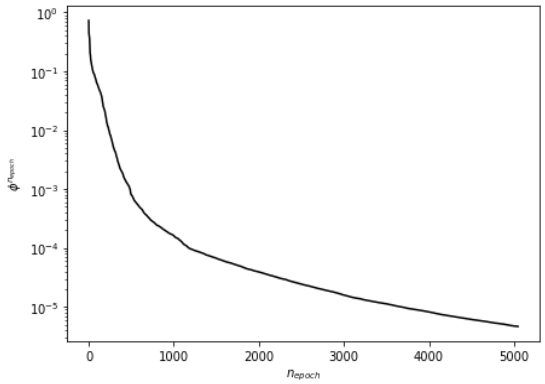

Fig 7: Loss Plot for Model 2

As seen from the loss plots in Figures 6 and 7, incorporating the physics loss in Model 2, depicted by Fig 7 has led to a smooth loss curve, which is steadily decreasing with increase in number of epochs. The comparision of the loss plots shows that PINN's are a preferred method in the context of solving PDE's. Figures 8, 9 and 10 present the comparsions of the expected and predicted solutions for Model 2 for the timestamps t=0.25s, t=0.5s t=0.75s.

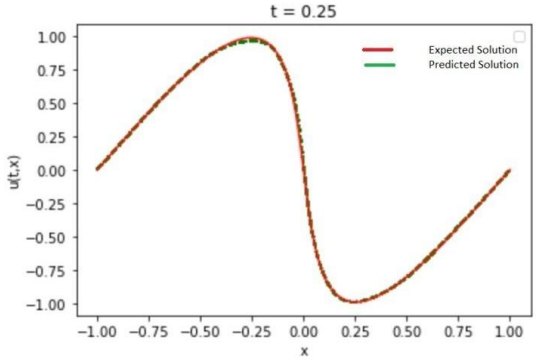

Fig 8: Expected vs Predicted Solution for t=0.25s

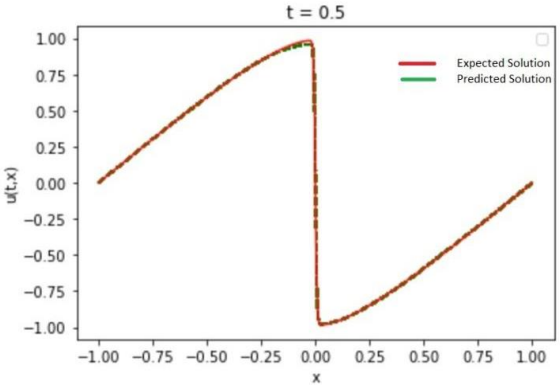

Fig 9: Expected vs Predicted Solution for t=0.5s

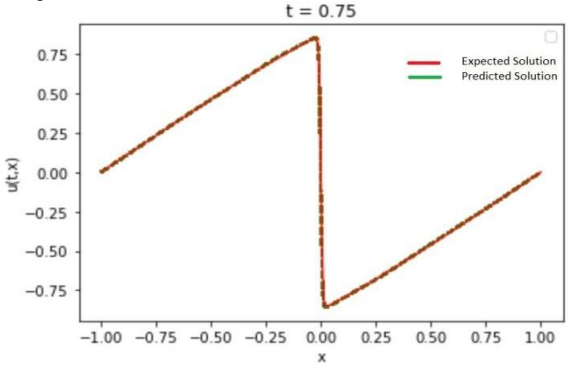

Fig 10: Expected vs. Predicted Solution for t=0.75s

V. CONCLUSION

Recent advancements in computational technology has led to the use of deep learning to solve partial differential equations. Our work emphasizes on the use of PINN's over simple neural network on the context of solving PDE's using Burger's equation as an example. This model can further be used for the solving of other PDE's of similar nature such as Eikonal Equation.

ACKNOWLEDGEMENT:

The authors would like to thank Sri Sivasubramaniya Nadar College of Engineering for their support in this work.

REFERENCES

[1] *Introduction to Partial Differential Equations*. 1995. Accessed: May 03, 2022. [Online]. Available: https://press.princeton.edu/books/hardcover/9780691043616/introduction-to-partial-differential-equations.

[2] M. J. Ghasemi, "Partial Differential Equations for Scientists and Engineers Stanley J. Farlow", Accessed: May 03, 2022. [Online]. Available: https://www.academia.edu/38471963/Partial_Differential_Equations_for_Scientists_and_Engineers_Stanley_J_Farlow.

[3] "Numerical Methods for Partial Differential Equations - 3rd Edition." https://www.elsevier.com/books/numerical-methods-for-partial-differential-equations/ames/978-0-08-057130-0 (accessed May 03, 2022).

[4] A. Quarteroni and A. Valli, *Numerical Approximation of Partial Differential Equations*, vol. 23. Berlin, Heidelberg: Springer, 1994. doi: 10.1007/978-3-540-85268-1.

[5] Lagaris, I. E., Likas, A. & Fotiadis, D. I (1998), 'Artificial neural networks for solving ordinary and partial differential equations', IEEE Trans. Neural Netw., Vol. 9, pp.987–1000.

[6] K. Wu and D. Xiu, "Data-driven deep learning of partial differential equations in modal space," *J. Comput. Phys.*, vol. 408, p. 109307, May 2020, doi: 10.1016/j.jcp.2020.109307.

[7] J. Han, A. Jentzen, and W. E, "Solving high-dimensional partial differential equations using deep learning," *Proc. Natl. Acad. Sci. U. S. A.*, vol. 115, no. 34, pp. 8505–8510, Aug. 2018, doi: 10.1073/pnas.1718942115.

[8] J. Sirignano and K. Spiliopoulos, "DGM: A deep learning algorithm for solving partial differential equations," J. Comput. Phys., vol. 375, pp. 1339–1364, Dec. 2018, doi: 10.1016/j.jcp.2018.08.029.

[9] M. Raissi, P. Perdikaris, and G. E. Karniadakis, "Physics-informed neural networks: A deep learning framework for solving forward and inverse problems involving nonlinear partial differential equations," *J. Comput. Phys.*, vol. 378, pp. 686–707, Feb. 2019, doi: 10.1016/j.jcp.2018.10.045.

[10] Y. Bai, T. Chaolu, and S. Bilige, "Solving Huxley equation using an improved PINN method," *Nonlinear Dyn.*, vol. 105, no. 4, pp. 3439–3450, Sep. 2021, doi: 10.1007/s11071-021-06819-z.

[11] T. Kadeethum, T. M. Jørgensen, and H. M. Nick, "Physics-informed neural networks for solving nonlinear diffusivity and Biot's equations," *PLOS ONE*, vol. 15, no. 5, p. e0232683, May 2020, doi: 10.1371/journal.pone.0232683.

[12] "Physics-Informed Learning Machines for Partial Differential Equations: Gaussian Processes Versus Neural Networks | SpringerLink." https://link.springer.com/chapter/10.1007/978-3-030-44992-6_14 (accessed May 03, 2022).

[13] J. Blechschmidt and O. G. Ernst, "Three ways to solve partial differential equations with neural networks — A review," *GAMM-Mitteilungen*, vol. 44, no. 2, p. e202100006, 2021, doi: 10.1002/gamm.202100006.

[14] S. Kutluay, A.R. Bahadir, A. Özdeş, Numerical solution of one-dimensional Burgers equation: explicit and exact-explicit finite difference methods,Journal of Computational and Applied Mathematics,Volume 103, Issue 2,1999,Pages 251-261,ISSN 0377-0427.

[15] D. C. Liu and J. Nocedal, "On the limited memory BFGS method for large scale optimization," *Math. Program.*, vol. 45, no. 1, pp. 503–528, Aug. 1989, doi: 10.1007/BF01589116.

Smart Assistant for Visually Impaired Using Computer Vision

S. Abinav Narayanan[1], B. S. Sreeja[2], P. Abishek Viswanath[3], V. Bhooshan[4]

[1–4]Electronics and Communication Engineering, Sri Sivasubramaniya Nadar College of Engineering (Anna University), Chennai, India

[1]abinav1805@ece.ssn.edu.in, [2]sreejabs@ssn.edu.in, [3]abishek1806@ece.ssn.edu.in, [4]bhooshan18032@ece.ssn.edu.in

***Abstract*—There are many systems that aid in solving the navigation problem faced by the visually impaired, most of them are not capable of giving the user a sense of vision, in its complete sense. With the intention of giving the visually impaired a complete sense of vision to the best possible extent a model that is lightweight and could be worn for longer periods of time was designed. It uses the image recognition algorithm Mobile Net SSD to detect the object/obstacle in front of the wearer, while simultaneously tracking the distance from the object using ultrasonic sensors. The output of the image recognition algorithm is converted to speech and given as an audio output, with low latency making it a real time solution. The design has incorporated ultrasonic sensors placed at strategic points, to detect objects/obstacles approaching from any side. The ultrasonic sensors are wired to buzzers, designed to raise alarm if the distance between the wearer and the obstacle becomes too close.**

***Keywords*—computer vision, image recognition, MobileNet-SSD, object detection, Raspberry Pi**

I. Introduction

Based on the review conducted by British Journal Ophthalmology in 2012 it was found that the number of people of all ages visually impaired is estimated to be 285 million, of whom 39 million are blind, with uncertainties of 10-20%. It was also found that 65% and 82% of visually impaired and blind respectively are of people above 50 years [1]. A product that is not heavy and could be worn at all times with relative ease, and tries to provide a complete sense of vision should be the prime requirements and design considerations. The solution offered by us is motivated by a desire to deliver a product that can act as “an eye” for the visually impaired and make them integrate better into the working society. Image recognition algorithms are put to use along with computer vision tools to detect the obstacle in front of the camera. The computationally fast and lightweight algorithm used here allows real time object recognition. The use of ultrasonic sensors provides the user a complete awareness of their surroundings, in which they can navigate with a sense of comfort and safety. The product is designed in such a way that the camera is placed at angle that gives the maximum field of view possible, and the lightweight nature allows it to be worn for extended periods without the worry of feeling burdened by the product.

II. Related Works

The existing systems each have their own approaches in solving this problem. DRISHTI, a wireless pedestrian navigation system for the visually impaired and differently abled, emphasizes on enhancing the navigation experience of visually impaired people by focusing on contextual awareness. However, even after much effort it was not possible to completely integrate this system, thus the components could not be optimized fully [2]. TYFLOS system focused on integrating different navigation technologies such as a wireless computer, cameras, natural language processor, microphone, range sensors, GPS sensors, text-to-speech device, etc., and methodologies such as region-based segmentation, fusion, range data conversion, etc., to allow more independence during navigation and reading. The drawback of this system was that it was not tested on blind people so it did not have any real feedback to improve on its hardware and software integration [3]. NAVBELT is an obstacle avoidance system that uses a mobile robot consisting of ultrasonic range sensors, a computer and earphones. The disadvantage of this system was that it exclusively used audio feedback and was also very bulky for the users. Moreover, the users required extensive training to operate this system [4].

III. System Design

The system designed is a wearable device which the visually impaired person can wear and successfully navigate indoor surroundings. The wearable device consists of sensors/buzzers, piCamera module, and Raspberry Pi. The detailed specifications of items used, and their placements on the cap are explained below.

A. Hardware Components

To provide an increased awareness of the surroundings, two HC-SR04 ultrasonic sensors along with

two passive 5V buzzers are used. HC-SR04 sensors can measure distances up to 4m, while buzzers generate a 2kHz tone with 3-12V peak-to-peak voltage. The specifications of HC-SR04 sensors are given in Table I:

TABLE I

Working Voltage	DC 5V
Working Current	15 mA
Working Frequency	40Hz
Maximum Range	4m
Minimum range	2cm
Measuring Angle	15°
Trigger Input Signal	10uS TTL pulse
Echo Output Signal	Input TTL lever signal and the range in proportion
Dimension	45 x 20 x 15mm

The specifications of the 5V buzzers are given in Table II:

The wearable device shall also have Raspberry Pi Camera which captures and sends images to the device. The camera is placed on the front side of the cap and faced outwards. The piCamera 1.3 can capture images of resolution of 5 megapixels and send it to Raspberry Pi at a high data rate via the CSI cables.

The Raspberry Pi 3 Model B uses a Broadcom BCM2837 SoC with a 1.2 GHz 64-bit quad-core ARM Cortex-A53 processor, with 512 KB shared L2 cache. Raspberry Pi is known for its small form factor but high performance.

The piCamera captures and feeds images real-time to Raspberry Pi which contains modules like OpenCV and TensorFlow. With the help of these modules, objects in images can be detected and recognized. The recognized objects will be outputted in the form of an array which is again fed into a text-to-speech module like *txtts*, this array output will be converted to speech and will be sent to the speaker. The block diagram of the entire process is shown below (Fig. 1):

TABLE II

Diameter	11.9mm / 0.47″
Weight	1g
Frequency	2 kHz
Height	8.4mm / 0.33”
Voltage	3 - 12V

B. Software Components

The software implementation of the system can be divided into two components – object detection and speech conversion part, and sensors and buzzers part

1) Object detection and text-to-speech conversion part:

Image capturing, object detection, text-to-speech conversion is done using Python modules like OpenCV, TensorFlow Lite, and *txtts* respectively. The use of TFLite allows us to achieve lightweight, but highly efficient model with relatively low latency. The MobileNet-SSD model is a Single-Shot multi-box Detection (SSD) network intended to perform object detection. The model input is a blob that consists of a single image and outputs a typical vector containing the tracked object data. It is trained on the COCO SSD dataset which is a large-scale object detection, segmentation and captioning dataset provided by Microsoft.

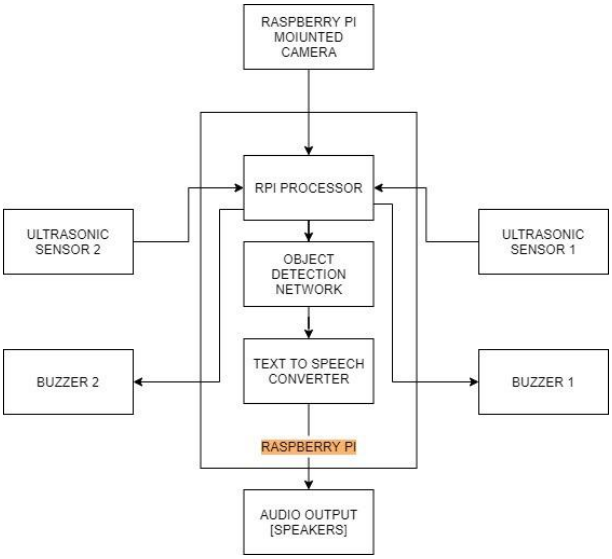

Figure 1

2) Sensors/buzzers part:

There is a single *.py* file that controls the behavior of the ultrasonic sensors and the buzzers. In this Python file, required modules like *RPi.GPIO* and *time* are imported. *RPi.GPIO* is the interface through which data and commands flow from/to the sensors. *time* module is used to time the ultrasonic sensors for estimating distance. The most important part of obstacle detection, i.e., threshold value is present in this code file.

IV. RESULTS

The system is implemented as shown below (Fig. 2): When the Raspberry pi is connected to a display device, outputs can be visualized as shown below (Fig. 3):

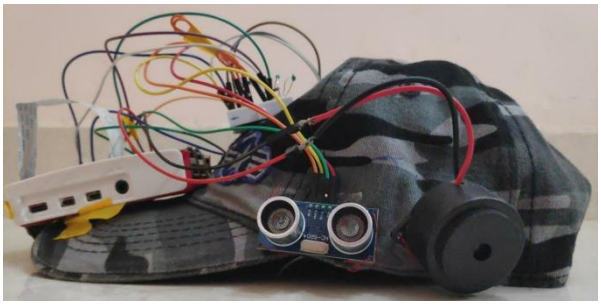

Figure 2.

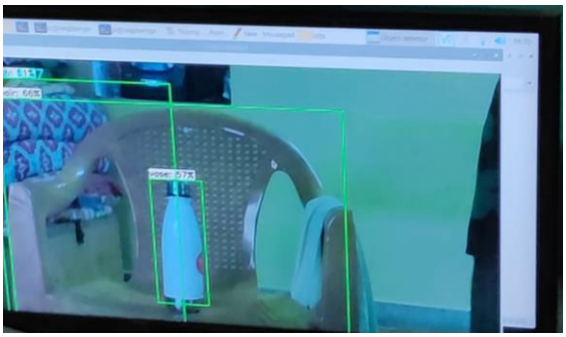

Figure 3.

To compare with other Object Detection Networks, we use the measures latency, idle current and peak current. Comparison of latency and peak current on different platforms is shown in the tables below (Table III, and Table IV).

From the table, it is observed that the use of RPi TFLite for object detection corresponds to low values of latency allowing the user to achieve real-time processing without putting burden on power-supply and processor. Thus, it could be concluded that the use of MobileNet SSD algorithm on TFLite platform allows us to design a low-cost, light-weight and wearable device for visually impaired.

V. LIMITATIONS

The biggest drawback of the SSD framework is the fact that its performance is directly proportional to object sizes meaning that it doesn't fare too well on object categories with small sizes as compared to other approaches such as the family of R-CNNs [5][6]. This is because small objects may not contain any useful information in the top layers of the network that can be fruitfully used for detection.

TABLE III

Platform	**Latency (MobileNet SSD v1) (ms)**	**Latency (MobileNet SSD v1) (ms)**
Nvidia Jetson Nano (TF)	276.0	309.3
RPi TF	480.3	654.0
RPi TFLite	***271.5***	379.6

TABLE IV

Platform	**Idle Current (mA)**	**Peak Current (mA)**
Nvidia Jetson Nano (TF)	450	1220
RPi TF	58	74
RPi TFLite	***64***	***78***

REFERENCES

[1] Pascolini D, Mariotti SPM. Global estimates of visual impairment: 2010. British Journal Ophthalmology Online First published December 1, 2011 as 10.1136/bjophthalmol-2011-300539.

[2] A. Helal, S. E. Moore and B. Ramachandran, "Drishti: an integrated navigation system for visually impaired and disabled," Wearable Computers, 2001. Proceedings. Fifth International Symposium on, Zurich, 2001, pp. 149-156.

[3] Dakopoulos and N. G. Bourbakis, "Tyflos: Wearable Obstacle Avoidance Electronic Travel Aids for Blind: A Survey," in IEEE Transactions on Systems, Man, and Cybernetics, Part C (Applications and Reviews), vol. 40, no. 1, pp. 25-35, Jan. 2010.

[4] Shraga Shovel, Iwan Ulrich, and Johann Borenstien, "NavBelt and the Guide Cane", IEEE Transactions on Robotics & Automation, Vol.10, No.1, pp. 9-20, March 2003.

[5] Liu, W. et al. (2016). SSD: Single Shot MultiBox Detector. In: Leibe, B., Matas, J., Sebe, N., Welling, M. (eds) Computer Vision – ECCV 2016. ECCV 2016. Lecture Notes in Computer Science(), vol 9905. Springer, Cham. https://doi.org/10.1007/978-3-319-46448-0_2

[6] Ren, S., He, K., Girshick, R., & Sun, J. (2015). Faster r-cnn: Towards real-time object detection with region proposal networks. Advances in neural information processing systems, 28

A survey on Diabetic Retinopathy Detection Using Deep Learning

S G Gawande[1], A P Thakare[2], B V Wakode[3]

[1-3]Electronics & Telecommunication Department, SIPNA College of Engineering and Technology, Amravati, India

***Abstract*—Diabetic Retinopathy (DR) is an ocular complication occurs due to damages to blood vessels of retina. DR affects up to 80% of population suffering from diabetes. If not diagnosed at early stages Diabetic Retinopathy is serious complication which can lead to visual loss. Early diagnosis and treatment is a key to slow down progression of DR in order to avoid blindness. Diagnosis of DR at early stages by manual process is difficult and error-prone task for physicians. However machine learning and deep learning based computing systems are developed to assist physicians for early detection of DR. Recently Convolution Neural Networks are widely used for DR fundus image detection and classification. This paper summarizes state of the art methods for DR detection using deep learning approaches. Furthermore available DR datasets and performance metrics for DR detection are discussed.**

***Keywords*—Diabetic Retinopathy, Deep Learning, Machine earning, Convolution Neural Network**

I. INTRODUCTION

Diabetic Retinopathy is an eye complication occurs in prople suffering from diabetes. It is the leading cause of blindness worldwide. Every year DR accounts for about 12% of new class of blindness. The main cause for DR is high level of blood sugar which damages blood vessels of retina [1]. The retina is the light-sensitive layer of cells at the back of the eyes Non-proliferative diabetic retinopathy (NPDR) and proliferative diabetic retinopathy (PDR).

Non-proliferative diabetic retinopathy- is the early stage of diabetic retinopathy. In this stage tiny blood vessels leaks which leads to swelling of retina. Generally, four types of lesions are diagnosed in NPDR as Micro-aneurysms (MA), hemorrhages (HM), exudates (EX) and Cotton Wool. Early phase of DR starts with balloon-like swelling of blood vessels of retina known as Micro-aneurysms. It grows gradually which leads to hemorrhages. This is the lesion which occurs when retinal vascular tree starts blood leakage. At later stage exudates occur. In case of exudates yellow white color plasma starts leaking from blood capillaries. Last lesion in case of NPDR is Cotton Wool which appears next to exudates.

Proliferative diabetic retinopathy is advanced stage of diabetic retinopathy in which retina starts growing new blood vessels. This is also known as neovascularization [2]. The newly formed abnormal blood vessels starts bleeding which is main cause of visual problems such as blurriness, reduced field of vision, and some time complete blindness.

Diabetic Retinopathy detection consist of identifying 5 phases which are, no DR, mild DR, moderate DR, severe DR and proliferative DR [3] [4]. Manual DR detection is difficult and error-prone task for physicians. However, computing system can be developed to assist physicians in screening and diagnosis of DR so as to minimize their workload and improve the precision level. Recent developments in CAD systems have capability in making proper decisions with high precision.CAD systems will reduce time, cost and human resource early detection of DR. Researchers are adopting deep learning approaches [5] for identifying, detecting and classifying diabetic fundus images. Amongst the diverse DL techniques [6] [7], the CNNs are trained to improve the performance by self learning and correction.

This paper reviews the recent developments in automated diabetic retinopathy detection using deep learning techniques. This paper is organized as follows: Section 2 presents various retinal fundus image datasets, while Section 3 explains various deep learning models for DR detection. Performance measures are presented in Section 4 while Section 5 covers the discussion part.

II. DIABETIC RETINOPATHY DATASET

A. Kaggle EyePACS

Kaggle EyePACS is the most widely used and largest public dataset available for Diabetic Retinopathy classification, it consist of more than 80000 fundus images. Dataset was designed for Diabetic Retinopathy Detection competition sponsored by California Healthcare Foundation [8]. Retinal images were provided by EyePACS, which a free platform for the Diabetic Retinopathy screening. This dataset consist of high resolution retinal images of the retina of both eyes, which were taken under a variety of imaging conditions. Images provided in the dataset are labeled with subject id and also marked as either left or right.

B. Messidor & Messidor2

Methods to Evaluate Segmentation and Indexing Techniques in the field of Retinal Ophthalmology (Messidor) have been designed for facilitating the studies on computer assisted diabetic retinopathy detection. The primary goal of Messidor dataset was to compare and evaluate different segmentation algorithms developed for lesion detection in color retinal images. The Messidor dataset consist of 1200 fundus color images acquired by three different ophthalmic departments. Images are captured using 8 bits per color plane at 1440*960, 2240*1488 or 2304*1536 pixels [9].

C. IDRiD

Indian Diabetic Retinopathy Image Dataset (IDRiD) [10] is the first dataset representative of an Indian population. It consist of 516 color fundus images divided into train set (413 images) and test set (103 images). The images were acquired at an ophthalmology clinic in Maharastra, India using a Kowa VX - 10α FUNDUS CAMERA. The dataset constitutes typical diabetic retinopathy lesions and normal retinal structures annotated at a pixel level. It provides image level grading information on the disease severity and diabetic macular edema for each image. The dataset is useful for development and evaluation of image analysis algorithms in order to detect diabetic retinopathy at early stage.

D. DDR

The DDR [11] fundus image dataset consist of 13673 images collected from 147 hospitals from 2016 to 2018 covering 23 province in China. Near about 9598 patients were examined for acquiring fundus images. It is largest dataset for lesion segmentation. DDR dataset is primarily designed for DR classification, DR object detection and DR semantic segmentation.

E. E-ophtha

The E-Ophtha [12] dataset consist of 463 color fundus images generated from the OPHDIAT Tele-medical network for DR screening. Dataset includes 268 healthy subjects, 148 patients with micro-aneurysms or other small red lesions and 47 with exudates. The E-ophtha dataset is generally used for segmentation algorithms instead of classification because of less number of images.

F. DIARETDB1

DIARETDB1 [13] consists of 89 fundus images of which 84 consist of mild non proliferative sign of DR while 05 does not contain any sign of DR. All the images are collected from Kuopio University under a controlled environment and were graded by 4 experts. The images contain a varying amount of imaging noise, but the optical aberrations and photometric accuracy are the same. This data set is referred to as "calibration level 1 fundus images".

III. Deep Learning Approaches

Deep learning refers to a “subfield of machine learning composed of algorithms that use a cascade of multilayered artificial neural networks for feature extraction and transformation” [14] [15]. Deep learning has been highly exploited to be capable of automated screening and diagnosis of diabetic retinopathy. There are many DL-based methods such as restricted Boltzmann Machines, convolutional neural networks (CNNs), auto encoder, and sparse coding. Convolutional Neural Network are most widly used method for DR detetion. This section gives an overview of various deep learning approaches used for DR detection.

Michael Chi Seng Tang et al. [16] has proposed a method for neovascularization detection based on transfer learning. Neovascularization is the condition in which new blood vessels are formed in the optic disk. They are of two types as neovascularization at the optic disk (NVD) and neovascularization elsewhere (NVE). Both are responsible for growth of hemorrhages which ultimately leads to vision loss. In order to detect the neovascularization the proposed model preprocesses the input fundus images and divide it into patches for network training. Based on transfer learning pre-trained CNN like AlexNet, GoogLeNet, ResNet18, and ResNet50 are evaluated. Authors proposed a method which is based on combination of ResNet18 and GoogLeNet. As ResNet18 and GoogLeNet are smaller networks computation power is conserved in this approach. Various metrics used for performance evaluation are accuracy, sensitivity, specificity, and precision. The results shows that proposed methodology achieved 91%,85%,97.44% and 97.1% accuracy, sensitivity, specificity, and precision respectively

Tieyuan Liu et al 2021 [17] proposed a novel method to detect the microaneurysms (MAs) and hard exudates (HEs) based on deep symmetric convolution neural network. The symmetric convolutional structure increases the depth and width of the network in order to overcome the imbalance of the number of positive and negative samples and avoid the overfitting of the model. This method is trained and tested on the public database DIARETDB1. Different overfitting structurs such as convolution, max-pooling, ave-pooling are used for detection of accuracy of the objects. The accuracy achived is 92.0%, 93.2%, 93.6%, when using different over-fitting structures. The results showed that ave-pooling layer can improve the microneuroysms detection while max-pooling layer can improve the detection of hard exudates.

Binhua Yang et al. 2022 [18] used Global Channel Attention (GCA) mechanism for DR severity classification. In order to update GCA module parameters adaptive one-dimensional convolution kernel size calculation method is introduced. GCA-EfficienttNet (GENet) model is proposed by the the authors which is combination of GCA and EfficientNet. The proposed model is evaluated on Kaggle Dataset. The GENet model divides the dataset into training set and validation set in the ratio 8:2. The image resolution is set as 224 *224 and cross-entropy loss function is used. The model was trained for 100 epochs and performance is compared with classical DCNN. The results showd that GENet achives 0.956 accuracy, 0.956 precision, 0.956 sensitivity and 0.989 specificity.

Muhammad Mateen et al. 2022 [19] Proposed a novel and efficient deep CNN-based approach for microaneurysms detection and classification. VGG-19 and Inception-v3 pretrained CNN models are used for early detection of microaneurysms using a hybrid feature embedding approach. The proposed model initially performs Data Pre processing to discriminate microaneurysms followed by pathch genration. Patch-based images are then fed into VGG-19 and Inceptionv3 for feature extraction. Extracted features are fed into the softmax classifier for the final result. The proposed model is evaluated through benchmark datasets E-Optha and DIARETDB1. The performance shows that the proposed model achived 96% accuracy, 95% specificity and 87% sensitivity for micronurasysm detection and classification.

Zubair Khan et al. 2021 [20] proposed a highly nonlinear scale-invariant model VGG-NiN. The transfer learning model is Vgg16 model fed to new network model Network-

in- Netwok(NiN). The proposed model has benefits of VGG16 [21], SPP [22], and NiN [24]. The convolutional layers of the trained VGG network are frozen using transfer learning AND THE he NiN part of the model is initialized by the Xavier method. For the purpose of performance evaluation imbalanced version of Kaggle dataset is used. The results shows that model can classify DR different stages with lowest possible learnable parameters to speed up the training and model convergence.

Harshit Kaushik et al. 2021[25] proposed a methodology based on stacked generalization of convolution neural networks. In order to eliminate color aberrations and irrelevant illuminations in fundus images stacked deep learning technique is used. To improve the overall image quality the gray world color constancy algorithm is used. Three different submodels of CNNs are fed into a single meta-learner classifier for feature extraction. The fusion strategy of the stacking model is based on the weighted majority from each of the sub-model for generating better features for classification. Data augmentation technique is also applied to improve the diversity of images in the dataset. Finally, the meta-learner classifier produces the diagnostic result as healthy (No DR) or unhealthy (DR). For evaluation of proposed methodology Kaggle dataset provided by EyePACS is used. The proposed stacked model reports an overall test accuracy of 97:92% (binary classication) and 87:45% (multi-class classication)

Manuel et al. 2017[26] have developed a technique, which recognized the existence of haemorrhages and Micro-aneurysms (MA) by means of supervised classification models. In this context, assessment was carried out on different patients, who were affected with DR and evaluation was performed for identifying the existence or nonexistence of the disease. The investigational outcomes have offered an enhanced level of sensitivity that was almost equal to the one accomplished by the experts.

In 2020, Kumar et al. [27] have established enhanced approach for haemorrhages detection and MA that contributed on the overall enhancement in the earlier recognition of DR. In this work, an enhanced segmentation technique was presented for segmenting the blood vessels and optic disc. Consequently classification was done via the NN framework that was trained by means of the MA features. Finally, simulated outcomes have illustrated the betterment of the introduced technique in terms of accuracy and so on.

Shanthi and Sabeenian 2019 [28] have introduced a scheme that concerned on the fundus image classification using Convolution Neural Network (CNN) model. Accordingly, the CNN scheme has classified the images depending on the harshness of the disease, by which higher accurateness was attained. In the end, the classification accuracy of the presented model was established from the attained outcomes.

Thomas et al. 2016 [29] have introduced a scheme that determined the rate of success of gradable images that were generated for identifying DR in kids who were under the age of 18. Moreover, the images considered for screening DR has resolved the slight variations like MA. From the simulated outcomes, half of the kids have accomplished complete success; on the other hand, only six percentage of the initial DR detection was unproductive, thus exhibiting its betterment in treating DR in kids.

Mona Leeza et al. 2019 [29] have proposed a model for detecting the severity level of DR. They used Bag of Features model which is a dictionary based approach. Bag of Features is adaptive approach for storing images. This approach is used in classification of images in computer vision. The proposed system uses k-means clustering algorithm for dictionary generation. Coding and Polling is applied before processing by SVM. The proposed system grades the severity of DR into different levels.

IV. Performance Metrics

The performance of deep learning classification methods is measured as Type I and Type II measures. Type I measures are positive measures like Accuracy, Sensitivity, Specificity, Precision, Negative Predictive Value (NPV), F1Score and Mathews correlation coefficient (MCC), and Type II measures are negative measures like False positive rate (FPR), False negative rate (FNR), and False Discovery Rate (FDR). These are the performance measures used for performance analysis.

V. Conclusion

Diabetic Retinopathy is retinal complication occurred in patients suffering from diabeties. If not diagnosed and treated at early stages it can damage retina and even loss of vision. In recent years use of Deep learning in detecting diabetic retinopathy has increased noticeably. The performance achvied by DL models is quite high and in some cases it surpasses the human expertise. In this paper, efforts are made to review most notable work in the area of DR detection using DL. Various available datasets for DR detection are also reviewd along with metrics for performance evaluation. It is observed that various methods of DR detection are introduced by the researchers.

Each method has its own benefits and shortcoming. As evaluation measures applied and type of dataset used differs from method to method it is complex task to pickup best method for designing DR screening system. However, deep learning has paved the way for more accurate results for early detection of diabetic retinopathy. To achieve higher performance researchers need has to overcome some challenges such as lack of high-quality labeled data, diversity in data, lack of interpretability and poor generalization performance.

References

[1] Lakshminarayanan V, Kheradfallah H, Sarkar A, Jothi Balaji J. Automated Detection and Diagnosis of Diabetic Retinopathy: A Comprehensive Survey. J Imaging. 2021 Aug 27;7(9):165.

[2] Ghazal, Mohammed, et al. "Accurate detection of non-proliferative diabetic retinopathy in optical coherence tomography images using convolutional neural networks." IEEE Access , pp. 34387-34397, August 2020

[3] Tien Y. Wong, Jennifer Sun, Ryo Kawasaki, Paisan Ruamviboonsuk, Neeru Gupta, Van Charles Lansingh, Mauricio Maia, Wanjiku Mathenge,Sunil Moreker, Mahi M.K. Muqit, Serge Resnikoff, Juan Verdaguer,Peiquan Zhao, Frederick Ferris, Lloyd P. Aiello, and Hugh R. Taylor.Guidelines on Diabetic Eye Care. Ophthalmology, 125(10):1608–1622, October 2018.

[4] Sunil Mamtora, Yun Wong, Dugald Bell, and Teresa Sandinha. Bilateral Birdshot etinochoroiditis and Retinal Astrocytoma. Case Reports in Ophthalmological Medicine, 2017:1–4, February 2017.

[5] Nivetha Murugesan, Tuna Üstunkaya, and Edward P. Feener. Thrombosis and Hemorrhage in Diabetic Retinopathy: A Perspective from an Inflammatory tandpoint. Seminars in Thrombosis and Hemostasis, 41(6):659–664, September 2015.
[6] Elaheh Imani, Hamid-Reza Pourreza, Touka Banaee, "Fully automated diabetic retinopathy screening using morphological component analysis", Computerized Medical Imaging and Graphics, vol. 43, pp. 78-88, July 2015.
[7] Manuel E. Gegundez-Arias, Diego Marin, Beatriz Ponte, Fatima Alvarez, Jose M. Bravo, "A tool for automated diabetic retinopathy pre-screening based on retinal image computer analysis", Computers in Biology and Medicine, vol. 88, pp. 100-109, Sept. 2017.
[8] Arnon Blum, Nina Pastukh, Dorina Socea, Hanin Jabaly, " Levels of adhesion molecules in peripheral blood correlate with stages of diabetic retinopathy and may serve as bio markers for microvascular complications", Cytokine, vol. 106, pp. 76-79, June 2018.
[9] https://www.adcis.net/en/third-party/messidor
[10] Prasanna Porwal, Samiksha Pachade, Ravi Kamble, Manesh Kokare, Girish Deshmukh, Vivek Sahasrabuddhe, Fabrice Meriaudeau, Indian diabetic retinopathy image dataset (IDRiD): a database for diabetic retinopathy screening research, Data 3 (3) (2018), https://doi.org/10.3390/data3030025. ISSN 23065729.
[11] Tao Li, Yingqi Gao, Kai Wang, Song Guo, Hanruo Liu, Hong Kang, Diagnostic assessment of deep learning algorithms for diabetic retinopathy screening, Inf. Sci., 511–522.
[12] https://www.adcis.net/en/third-party/e-ophtha
[13] Kauppi, T.; Kalesnykiene, V.; Kamarainen, J.; Lensu, L.; Sorri, I. DIARETDB0 : Evaluation Database and Methodology for Diabetic Retinopathy Algorithms. Mach Vis Pattern Recognit Res Group, Lappeenranta Univ Technol Finland. 2006.
[14] Wejdan L. Alyoubi, Wafaa M. Shalash,Maysoon F. Abulkhair. "Diabetic retinopathy detection through deep learning techniques:A review", Informatics in Medicine Unlocked,2020
[15] Retinopathy Detection Using Optimization Assisted Deep Learning Model: Outlook on Improved Grey Wolf Algorithm", International Journal of Image and Graphics, 2021
[16] M. C. S. Tang, S. S. Teoh, H. Ibrahim and Z. Embong, "A Deep Learning Approach for the Detection of Neovascularization in Fundus Images Using Transfer Learning," in IEEE Access, vol. 10, pp. 20247-20258, 2022,
[17] T. Liu et al., "A Novel Diabetic Retinopathy Detection Approach Based on Deep Symmetric Convolutional Neural Network," in IEEE Access, vol. 9, pp. 160552-160558, 2021.
[18] B. Yang, T. Li, H. Xie, Y. Liao and Y. -P. P. Chen, "Classification of Diabetic Retinopathy Severity Based on GCA Attention Mechanism," in IEEE Access, vol. 10, pp. 2729-2739, 2022.
[19] M. Mateen, J. Wen, M. Hassan, N. Nasrullah, S. Sun and S. Hayat, "Automatic Detection of Diabetic Retinopathy: A Review on Datasets, Methods and Evaluation Metrics," in IEEE Access, vol. 8, pp. 48784-48811, 2020
[20] Z. Khan et al., "Diabetic Retinopathy Detection Using VGG-NIN a Deep Learning Architecture," in IEEE Access, vol. 9, pp. 61408-61416, 2021
[21] B. Yang, T. Li, H. Xie, Y. Liao and Y. -P. P. Chen, "Classification of Diabetic Retinopathy Severity Based on GCA Attention Mechanism," in IEEE Access, vol. 10, pp. 2729-2739, 2022
[22] K. Simonyan and A. Zisserman, ``Very deep convolutional networks for large-scale image recognition," 2014,
[23] K. He, X. Zhang, S. Ren, and J. Sun, ``Spatial pyramid pooling in deep convolutional networks for visual recognition," IEEE Trans. Pattern Anal. Mach. Intell., vol. 37, no. 9, pp. 1904-1916
[24] M. Lin, Q. Chen, and S. Yan, ``Network in network," 2013
[25] H. Kaushik, D. Singh, M. Kaur, H. Alshazly, A. Zaguia and H. Hamam, "Diabetic Retinopathy Diagnosis From Fundus Images Using Stacked Generalization of Deep Models," in IEEE Access, vol. 9, pp. 108276-108292, 2021
[26] Manuel E. Gegundez-Arias, Diego Marin, Beatriz Ponte, Fatima Alvarez, Jose M. Bravo, "A tool for automated diabetic retinopathy pre-screening based on retinal image computer analysis", Computers in Biology and Medicine, vol. 88, pp. 100-109, September 2017.
[27] Shailesh Kumar, Abhinav Adarsh, Basant Kumar, Amit Kumar Singh, "An automated early diabetic retinopathy detection through improved blood vessel and optic disc segmentation", Optics & Laser Technology, vol. 121, January 2020.
[28] T. Shanthi, R. S. Sabeenian, "Modified Alexnet architecture for classification of diabetic retinopathy images", Computers & Electrical Engineering, vol. 76, pp. 56-64, June 2019.
[29] Thomas C. Gräsbeck, Sophia V. Gräsbeck, Päivi J. Miettinen, Paula A. Summanen, "Fundus Photography as a Screening Method for Diabetic Retinopathy in Children With Type 1 Diabetes: Outcome of the Initial Photography", American Journal of Ophthalmology, vol. 169, pp. 227-234, September 2016.
[30] M. Leeza and H. Farooq, "Detection of severity level of diabetic retinopathy using Bag of features model," in IET Computer Vision, vol. 13, no. 5, pp. 523-530, August 2019.

AI Based Smart Interaction System for Computer Management

Bala Avanthiga B[1], Divya P[2], Hariharan B[3], Rajavel R[4]

Department of ECE, Sri Sivasubramaniya Nadar College of Engineering,
Kalavakkam, Chennai, 603110

[3]hariharanbalaji023@gmail.com

Abstract – Human-Computer Interaction (HCI), a man-machine interaction where communication between man and computer happen naturally and intuitively. Nearly, all the researched topic in this field is hand gesture recognition, where hand movements are used to control computers. The project has been come up with an interactive computer system which promotes the man-machine interaction and can operate without the help of input devices (physical keyboard and mouse). Input feed is taken from the webcam using OpenCV from where the hand is detected with the help of python package mediapipe. Points are plotted and landmarks are obtained respectively. By hand gestures, functions of physical keyboard and mouse have been done virtually. Both virtual keyboard and mouse has been integrated and is converted to an application using pyinstaller.

***Keywords*—Human-Computer Interaction (HCI), Hand Gestures, Virtual Keyboard, Virtual Mouse.**

I. INTRODUCTION

In this modern world, there are various developed technologies to come in contact with computer. However, there is a trouble in communicating and interacting with computer for few people. People had made up their mind with other jobs as they break down to connect with computer.

Most significant for human interface is the hand gestures where physical behavior and emotional expression is a key-symbol of gesture. The significant role in Human-Computer Interaction is played by keyboard and mouse [4]. Smart interface which is the gesture-based interface are fast, intuitive and give use of full controlled interface without any complications [7]. It is easy to represent ideas and actions naturally by using the different hand shapes and being identified by gesture recognition technique is the gestures using hands where more natural bond to the system has been provided [2]. Virtual keyboard is sustainable because of its minimal resource utilization and is simple and manageable which can be effectuated using a digital camera and a paper keyboard [8]. Actions of mouse are controlled by gestures and webcam where OpenCV captures data for the function of virtual Mouse by using Hand signal identification [10].

The proposed project work aims to advance an AI/Machine Learning based system to associate with computer easily using hand movements. Instead of using physical mouse and keyboard, one can interact with computer using hand signs that will be recognized by webcam.

The primary intention of the work is to take the system to the next level by replacing keyboard and mouse using a camera. As the world is more virtual and touch screen is used worldwide, the new age development which is the hand action detection will be widely used soon. Developing a model which could combine virtual keyboard and mouse using hand signals and also be efficient in many sectors like classroom teaching, office presentations, futuristic shopping models and much more. The model replaces wireless keyboard and mouse, acting as easy and comfortable to access with minimum space requirement making it more portable and cost efficient since it can last a lifetime.

Mode of living will be difficult to function without technology i.e., Smartphones, Tablets, Computers. In a very short span of time, technology has exploded, and people cannot imagine a life without it. Today's world is travelling between virtual and real world frequently. The easiness and comfortness have been brought by the virtual world which has already become part of our lifestyle. Keeping these in mind, the project is being developed.

The following section of the paper gives the clear view of Human-Computer Interaction. Section II explains the task of the project in a stepwise manner. In section III, problems in creating the project, numbers of attempts taken, and the experimental results have been explained. Section IV concludes the project and highlights the future scope of the design.

II. PROPOSED SMART INTERACTION SYSTEM FOR COMPUTER MANAGEMENT

Human computer interactions are becoming more advantageous in today's world. Making devices easy-to-use and operational with minimum physical contact have been focused now-a-days. Following is the model represents the schematic workflow of the proposed project where touchable keyboard and mouse were replaced by artificial real keyboard and mouse using gestures.

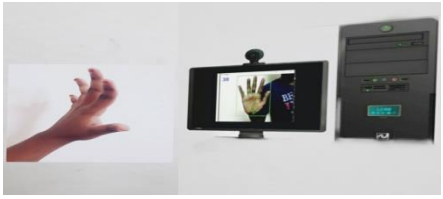

Fig. 1. Schematic representation of the proposed model of the project.

Initially, getting input from the camera feed and process the feed image to detect hand using Open CV library and the python package mediapipe. Furthermore, using autopy, pynput and keyboard package, the hand tracking input is given as the system input.

The proposed model is to use physical input devices virtually. Here, Hand gesture are given as input which is accessed using camera. The received input is processed as image and hand detection takes place. Later the landmarks are detected, and a choice is given to preferably choose between keyboard or mouse. Once the function is chosen, the respectful action takes place. Thus, the computer is managed with the help of a camera virtually. The functional flow of each and ever stages in the proposed computer management system is explained in Fig. 2. An equivalent flowchart characterization of the same system in another aspect is illustrated in Fig. 3.

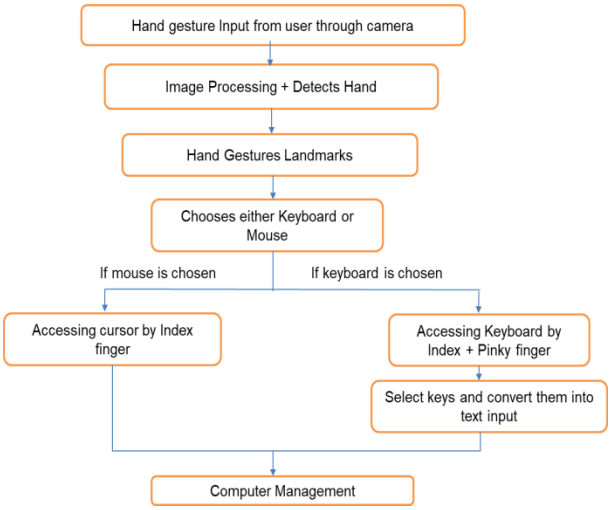

Fig. 2. Functional flow of the smart interaction system for computer management

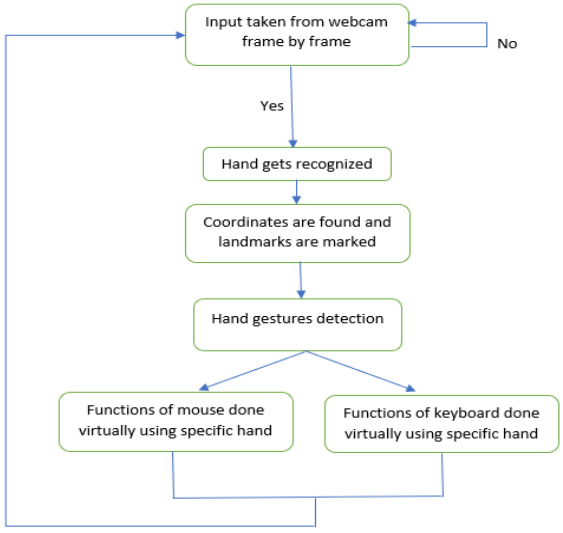

Fig. 3. The flow chart of the project which represents each process in step-by-step.

III. Experimental Results And Discussion

The project is to set up an interactive keyboard and mouse system so that the users can approach the computer through webcam and their hands. The input is taken from the webcam and the feed image is processed to detect and track hand. Then it is given as the input to the system.

First, the camera is accessed using OpenCV and image is obtained. From the obtained image, hand is detected with mediapipe. Once the hand gets recognized, the landmarks are plotted at the keypoints. By performing specific hand signs, a particular action takes place.

On-screen keyboard is displayed which has been pre-created using OpenCV. The on-screen keyboard contains symbols, numbers and alphabets. The interaction between hardware and software is done using pynput and keyboard package. Using detected hand, the input is derived by interacting with on-screen keyboard.

Once the hand gets recognized, the required landmarks are plotted which are the 21 points and the respective coordinates are printed as shown in figure 4. Using these landmarks, the input is detected.

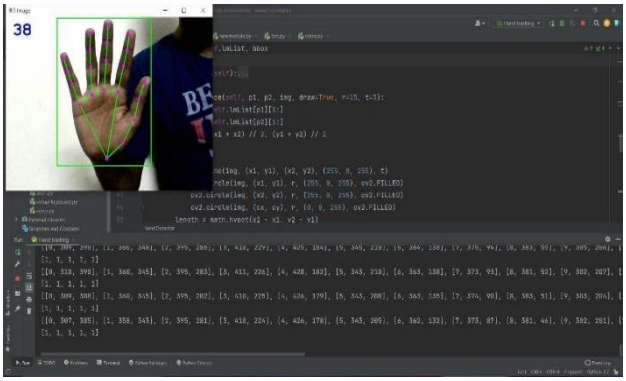

Fig. 4. Using mediapipe and OpenCV hand tracking is done and the landmarks are plotted.

The on-screen keyboard is displayed with alphabets and options to switch to numbers and symbols as shown in figure 5. Similarly, it is done for the on-screen keyboard displayed with symbols and numbers as shown in figure 6 and 7. User can move the finger in front of the webcam on the respective letter of the on-screen keyboard and perform the assumed gestures which finally replaces the functions of the input devices. As a specific action is assigned for selecting letters, the output gets displayed in the selected window.

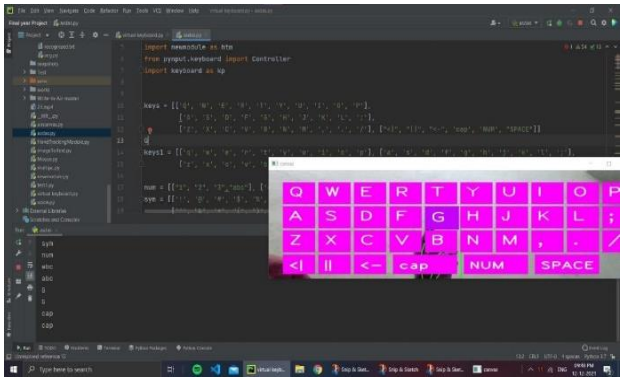

Fig. 5. The On-screen keyboard for alphabets.

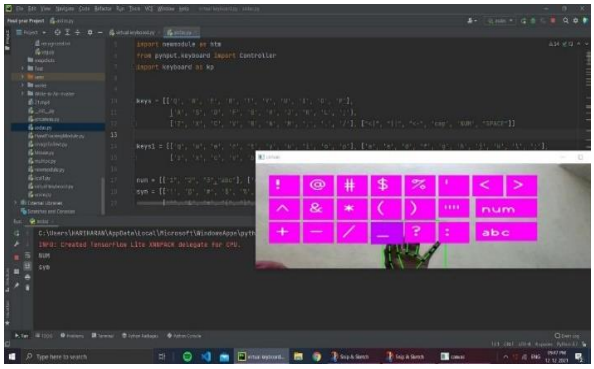

Fig. 6. The On-screen keyboard for symbols.

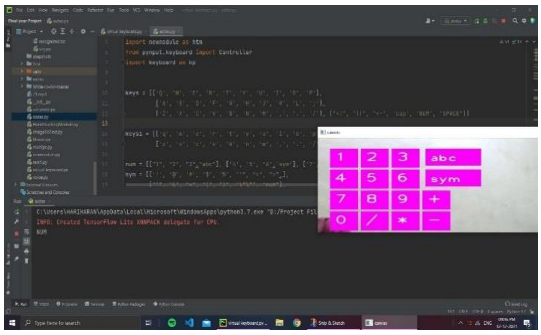

Fig. 7. The on-screen keyboard for numbers.

The keyboard functions and the mouse cursor function have been controlled by hand gestures instead of using a input devices. Cursor movement function of mouse has been performed by assigning specific hand sign as shown in figure 8.

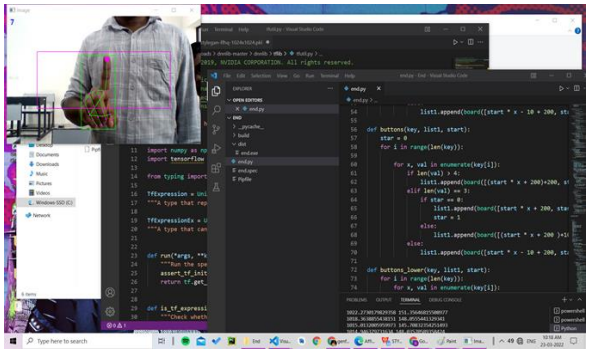

Fig 8. Cursor movement function of the mouse.

Similarly, the right click function and drag function of the mouse have been done by assigning different signs as shown in figure 9 and 10.

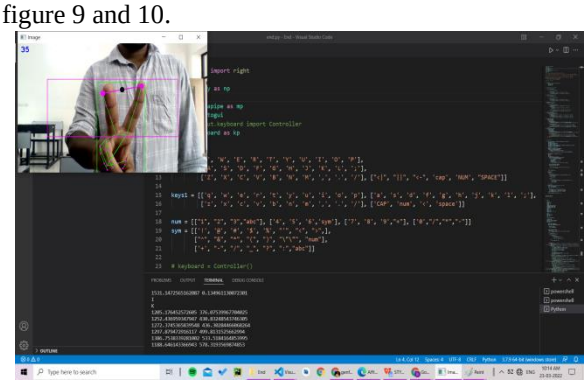

Fig 9. Right click function of the mouse.

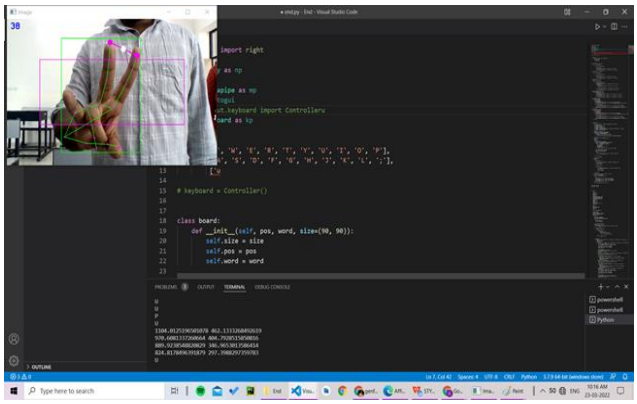

Fig 10. Drag function of the mouse.

From these results, a virtual system can be developed where people can interface with the computer without the usage of input devices. The concepts of object detection and image processing for the implementation has proved to be practically successful and the function of keyboard and mouse is achieved with good accuracy.

In the project, there is a complication in creating hand detection module. Google has been brought into play as source documentation for every packages. After overcoming, another problem arose in finding hand gestures using limited variables and finding the point position of the finger which is to be related to digital screen. The process had been failed more than 50 times. Debugging the code line-by-line helps to understand where the problem originates. After this, a problem in converting a python file to .exe file (executable file) had been faced. Breaking a complex model to sub-complex sort of such that makes the code run efficient and faster.

IV. Conclusion and Future Scope

Computers can recognize, process, and react to human emotions to develop emotionally intelligent information systems. Gesture recognition and object recognition are becoming increasingly important in Human-Computer Interaction. The keyboard functions and the mouse cursor function have been controlled by using the assumed signs of the hand instead of using input devices. The proposed system can be accomplished by using a webcam or a built-in camera which detects the hand and processes these frames to achieve the specific functions.

As of now, the implementation of artificial realistic keyboard and mouse has been done in the project. Both virtual keyboard and virtual mouse were integrated. Using pyinstaller, the integrated system will be converted to an application. Once an application is developed, a hardware system which contains the integrated system as a major interaction system will be developed using Jetson board. This system will be a route to new level of Human-Computer Interaction which does not require physical contact with other devices.

The task will be accomplised to bring interaction between computing systems and human more thoughtful of multi-dimensional nature of everyday interrelation.

REFERENCE

[1] T. Murase, et al. (OCT-2011) "Gesture keyboard requiring only one camera", Proc. of the 24th Annual ACM Symposium Adjunct on User Interface Software and Technology, Santa Barbara, USA, pp. 9-10.

[2] M. Panwar. (2012) "Hand gesture recognition based on shape parameters", International Conference on Computing, Communication and Applications, pp. 1-6.

[3] M. Hagara and J. Pucik. (2013) "Fingertip detection for virtual keyboard based on camera", 23rd International Conference Radioelektronika (RADIOELEKTRONIKA), pp. 356-360.

[4] Zhi hua Chen, Jung Tae Kim, Jianning Liang, Jing Zhang, Yu Bo Yuan. (2014) "Real Time Hand Gesture Recognition Using Finger Segmentation", National Nature Science Foundation of China (Grant no. 61370174 and Grant no. 61300133) and the Fundamental Research Funds for the Central Universities, pp. 1-9.

[5] Farah Farhana Mod Ma asum and Suhana Sulaiman and Azilah Saparon. (2015) "An Overview of Hand Gest ures Recognition System Techniques", IOP Conference Series: Materials Science and Engineering, Vol. 99, pp. 012012.

[6] Manasa Srinivasa H S, Laxmi Tyapi, Suresha H S. (2015) "Online Hand Gesture Recognition Using OpenCV", International Journal of Emerging Technologies and Innovative Research (www.jetir.org), Vol.2, Issue 5, pp.1635-1637.

[7] R. Agrawal and N. Gupta. (2016) "Real Time Hand Gesture Recognition for Human Computer Interaction", IEEE 6th International Conference on Advanced Computing (IACC), pp. 470-475.

[8] Y. Zhang, W. Yan and A. Narayanan. (2017) "A virtual keyboard implementation based on finger recognition", International Conference on Image and Vision Computing New Zealand (IVCNZ), pp. 1-6.

[9] Wiley, Victor & Lucas, Thomas. (2018) "Computer Vision and Image Processing: A Paper Review", International Journal of Artificial Intelligence Research, Vol. 2, pp. 22-22.

[10] K. S. Varun, I. Puneeth and T. P. Jacob. (2019) "Virtual Mouse Implementation using Open CV", 3rd International Conference on Trends in Electronics and Informatics (ICOEI), Vol. 7, Issue. 6, pp. 825- 829.

[11] Zhang, Fan & Bazarevsky, Valentin & Vakunov, Andrey & Tkachenka, Andrei & Sung, George & Chang, Chuo-Ling & Grundmann, Matthias. (2020) "MediaPipe Hands: On-device Real-time Hand Tracking".

[12] Sai Mahitha, Gummadi & Revanth, Banala & Geetha, Gaddam & Sirisha, Ramavath. (2021) "Hand Gesture Recognition to Implement Virtual Mouse Using Open Source Computer Vision Library: Python", Proceedings of International Conference on Advances in Computer Engineering and Communication Systems, pp. 435-446.

Diagnosis of Stages of Acute Lymphoblastic Leukaemia using Image Processing and Deep Learning

Krishi Divya Dharshini V[1], Nethra Prakash K[2], Shafiya Sidrath A[3], Venkateswaran N[4]

Department of Electronics and Communication Engineering, Sri Sivasubramaniya Nadar College of Engineering (Autonomous) Chennai, India

[1]krishi19050@ece.ssn.edu.in, [2]nethra19067@ece.ssn.edu.in, [3]shafiya19096@ece.ssn.edu.in, [4]venkateswarann@ssn.edu.in

***Abstract*—Acute Lymphoblastic Leukemia (ALL) is the most common type of childhood cancer and accounts for about 25% of the pediatric cancers. Leukemia and other conditions usually cause abnormal counts of blood cells, but immature cells are not usually distinguishable by the human eye. Previous works related to the detection of Leukemia using Deep Learning based Computer Aided Diagnosis (CAD) systems only deal with a binary classification of Leukemic and non-leukemic cells in a Peripheral Blood Smear image. Our aim is to develop a multi class classifier to diagnose the stages of the leukemic blast cells to simulate a more real, life like diagnosis which assists clinicians in early administration of necessary treatments. We have split our problem into two modules. The first module is the segmentation of the affected cells, which are achieved by color thresholding the image in the HSV scale. The second module is the classifier module which has been realized using several deep learning classifiers. We have compared the use of state-of-the-art Vison Transformer model, Shallow CNN models and DenseNet architectures. We have proposed a Light-DenseNet model which has the same functionalities as the DenseNet architecture as well as train with lesser parameters, making the training more efficient and testing and validation accurate. The algorithm is implemented in Python3.7 and an accuracy of 97.00% was obtained on unseen data.**

***Keywords*—Image processing, ALL Blasts, Deep learning, Diagnosis, PBS images, Light-DenseNet**

I. INTRODUCTION

In recent years, thanks to the growing computational abilities and the amount of data, artificial intelligence is proving to be an efficient assistant for the physicians and the radiologists as a diagnosis tool. Image processing techniques and deep learning models have proved to give an edge to the medical practitioner in the course of treatment and help them draw inferences by understanding the necessary feature markers. Real world microscopic images tend to contain some staining noise and illumination errors which is possible to correct by pre-processing techniques. The task of identifying immature cancer cells from normal cells under the microscope is not only time consuming, expensive and invasive test but can also be challenging due to the morphological similarities and the inability to focus on key pointers. Moreover, the examination of the peripheral blood smear images used in this study is riddled with problems such as diagnostic error because of the non-specific nature of ALL signs and symptoms often lead to misdiagnosis.

Leukaemia is broadly classified as acute and chronic based on the rapidity with which they spread as acute and chronic. Acute leukaemia develops and spreads rapidly whereas chronic leukaemia doesn't spread that rapidly and the mature lymphocytes are able to carry out some normal cellular functions. Acute lymphoblastic leukaemia (ALL) is the most common type of paediatric cancer. It is a type of cancer of blood and bone marrow, the word ‘acute’ comes from the fact that the tumour spreads rapidly. Under this condition the bone marrow produces immature blood cells instead of mature ones, these immature cells develop into leukemic white blood cells called lymphoblasts, these cells affect haematopoiesis causing difficulty in breathing, cellular diffusion, oxygen transportation and blood clotting. Acute lymphocytic leukaemia occurs when a bone marrow cell has a mutation in its DNA.

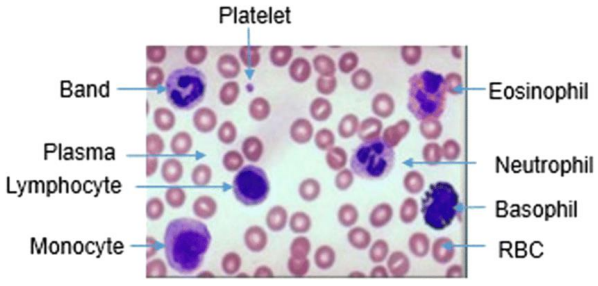

Fig. 1. Labelled Peripheral Blood Smear. [9]

Trained and experienced physicians can detect chronic Leukaemia in a regular blood test, but study shows that not all kinds leukaemia allows the leukaemia cells to spread in the blood. Traditionally, before the advent of artificial intelligence and automation, Acute Lymphoblastic Leukaemia (ALL) can be diagnosed by the following four methods [15]:

- Blood Test: They reveal the number of RBCs and platelets. A blood test also can also reveal the presence

of blast cells. Blast cells are immature cells that are found in the bone marrow.

- Bone Marrow Test: A sample for biopsy is taken from the breast bone or hip bone and the sample is sent to the lab for detection of leukaemia. The lab tests help to classify the cells based on their size, shape and molecular features. They also tell if the leukaemia cells began from T lymphocytes or B lymphocytes.
- Imaging test: X-ray, a computerized tomography (CT) scan or an ultrasound scan will help to find whether the cancer has spread to other parts such as brain or the spinal cord.
- Spinal Fluid Test: Here the spinal fluid that surrounds the spinal cord and the brain is collected to test whether leukaemia cells are present or not.

The above-mentioned traditional methods do not always point out the key markers to identify the leukaemia cells. The early diagnosis of the Leukaemia blast will allow early intervention and administration of necessary treatments. Hence, this paper focusses on the problem of multiclass classification of tumours and also to detect early-stage cancer cells. Tumours can be broadly classified into two groups - benign (non-cancerous) and malignant (cancerous). Benign tumours do not spread and grow slowly whereas malignant tumours tend to spread faster. The malignant class can be further classified into 3 subtypes such as – Early, Pre, Pro. Many signs of the disease mimic that of a viral fever. Timely treatment plays a crucial role in curing this disease.

The field of medical imaging is expanding and new age technologies are employed to achieve automation in detecting Leukaemia in the early stages from microscopic peripheral blood smear (PBS) images. The conventional pipeline is as follows- pre-processing, cell segmentation, feature extraction and cell classification. Beevi et al. [4] have concluded that marker-controlled watershed algorithm yields better result than other cell segmentation techniques. Aljaboriy et al [10] have enhanced the PBS images by shifting them to a different colour domain to highlight particular features of the image, hence better feature extraction abilities. It is also noted in [18] that the identification of WBC is possible with conversion to the CMYK model, it is noted that the leukocytes have a higher contrast in the Y component because of the absence of the colour in the WBCs. The Tranh et al. in [11] have proposed some simple data augmentation techniques to overcome the challenge of lack of data in the field of medical imaging. Implementation of a deeper CNN architecture showed better results for the augmented data. In the work done by Ibrahim et al. [14], the model classified the normal microscopic images from the ones which contained ALL blasts, but the immature cells were not studied here.

Existing models have used binary classifiers for classifying the sample images as cancer and non-cancerous. This binary approach to medical problems is not realistic and does not reflect the real-life complexity of pathological diagnosis. We have proposed a multi-class classifier which classifies the sample into benign, malignant, pre and pro cancer, thus enabling more efficient diagnosis. The main contribution of our proposed work are as follows:

1. Formulation of a technique to segment the white blood cells of interest by employing thresholding processes.
2. A robust automated multi class classifier system which successfully segments the input microscopic
3. A user interface to have the developed model at the backend and to which an unprocessed PBS image can be uploaded to return the stage of the lymphoblastic cell.

This paper consists of 7 sections. The Section 2 briefly discusses the dataset and works that have been carried out on it, Section 3 shortly describes our problem statement, Section 4 describes our solution and proposed approach, Section 5 includes details about experimental results and simulations carried out, Section 6 includes our conclusions and the areas of improvement of this project and the paper ends with Section 7, a list of all references and links that aided to construct this paper.

II. DATASET

The Dataset used in this study is available for public use in the famous dataset repository, Kaggle [7,16]. The dataset contains 3256 peripheral blood smear images collected from 89 patients suspected of ALL along with 25 healthy individuals (hematogone). Each microscopic image was skilfully stained and hand labelled by experienced laboratory technicians. The dataset is broadly classified into two groups namely benign and malignant. The malignant subgroup has three subtypes which tells us about the stage at which the tumour is. The subtypes are as follows: Early, Pre-B, Pre-B, and Pro-B malignant lymphoblasts. The resolution of the images is 224x224 given in the RGB colour space. As a pre-processing step, the images are uniformly reshaped, transformed to the HSV colour space, colour thresholding is done to extract the lymphoblastic cells.

These PBS images were collected from the bone marrow laboratory of Taleqani Hospital (Tehran, Iran). The images were captured using the Zeiss camera in a microscope with a 100x magnification. The images were later classified and labelled by a specialist by using a flow cytometry tool. This dataset also provided segmented image for each of the classes for ease of processing. The repository contains two folders—Original and Segmented, each of the folder containing four folders for each subtype. Each image has a specific naming convention, ‘WBC’ followed by the type of tumour (benign or malignant), subtype of the tumour (Benign, Early, Pre, Pro) and the sample number. The images are of jpg format. For example, an image from the Original Folder, from the Early subtype would have the following name: WBC-Malignant-Early-001.jpg. This image will have a corresponding segmented image in the Segmented folder as well.

The original image and the corresponding segmented images are shown in Fig 1. Vasuki et al. in [17], elaborated on the methods of segmentation of lymphoblasts from the microscopic image. It is observed that the lymphocytes being immature WBCs, have a higher contrast in the HSV colour space.

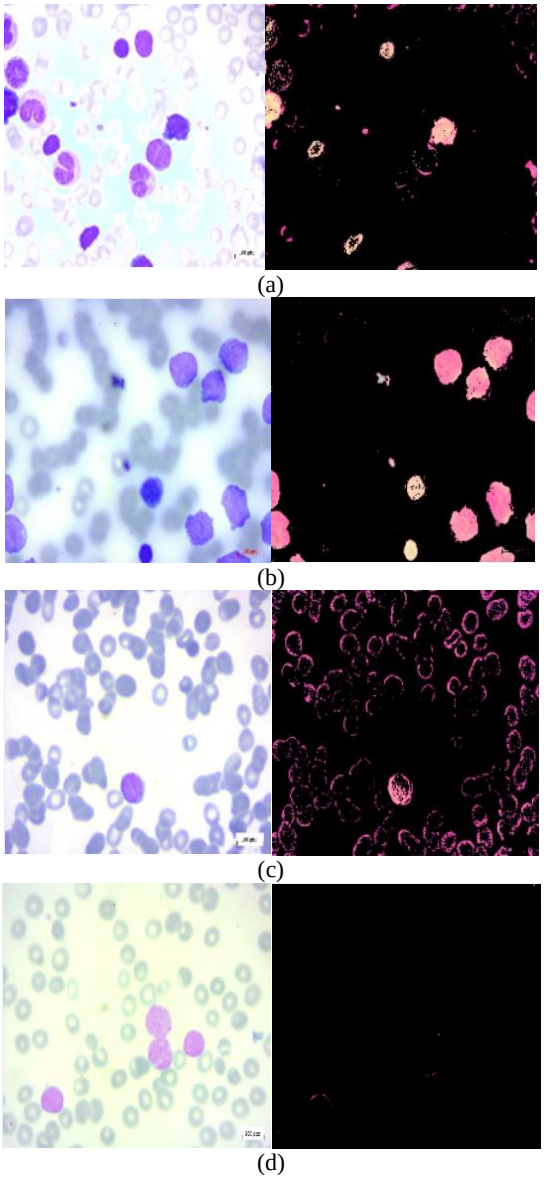

Fig. 2. Sample images from each class – (a)Benign, (b)Early, (c)Pre, (d)Pro and the corresponding segmemted images (right)

A. *Data Augmentation techniques:*

The images are augmented before passing on to the transformer. The peripheral blood smear images are resized to (128,128) and normalized as well. The images are augmented randomly by flipping it horizontally and rotating the images. These processes are carried out by the Keras pre-processing layers such as Resizing, Rescaling, RandomFlip, and RandomRotation [19]. This process is done sequentially and saved in run time and passed on to the models for compilation and training.

Two main factors which are to be taken into account while preparing the dataset for the process of classification are: there maybe manual errors during the process of preparation of the blood smear slide, one needs enough experience to prepare a blood smear. Hence, inaccuracies may rise from here. In addition to this, the experience of the person analysing the smear may also affect the result. Hence, data augmentation and more images are included to make our model more accurate and robust to such discrepancies.

III. PROPOSED SOLUTION

Once, the images for training are prepared, the output labels have to be properly encoded as we are dealing with multi-class classification problem. We have followed the categorically encoded for the neural network to learn. We have four classes each with an already encoded label: [0,1,2,3]. This class vector (integers) is converted to a binary class matrix. Keras provides a Numpy utility library, from which the method to_categorical() is employed. This function returns a matrix of binary values ('0' or '1'). It has number of rows equal to the length of the input vector and number of columns equal to the number of classes [13].

Several architectures for classification were synthesized but one of the major concerns among the scientific community arise when the CNN go deeper. The information path becomes longer, hence the extracted features might get vanished before reaching the other side. We developed a vanilla CNN model whose accuracy was obtained as 89%, trained using the categorical cross entropy loss function, trained for 20 epochs. Keeping this metric as a baseline value, we will be moving forward through the section. Hence, in our work we have implemented the classification process using a Vison Transformer (ViT) model, DenseNet-121 and DenseNet-201 architecture.

A. *Vision Transformer:*

Vision Transformer is an image classification technique that supposedly performs better than CNN for large datasets. It applies transformer like operations over the patches. An image is divided into fixed-size patches, which are then linearly embedded, position embeddings added, and the resulting vector sequence given to a conventional Transformer encoder. The ViT is a visual model based on a transformer's architecture. The ViT model represents an input image as a series of image patches, similar to how word embeddings are represented in text when employing transformers, and predicts class labels for the image directly. The entire flow of the transformer network is visualized in Fig 7.

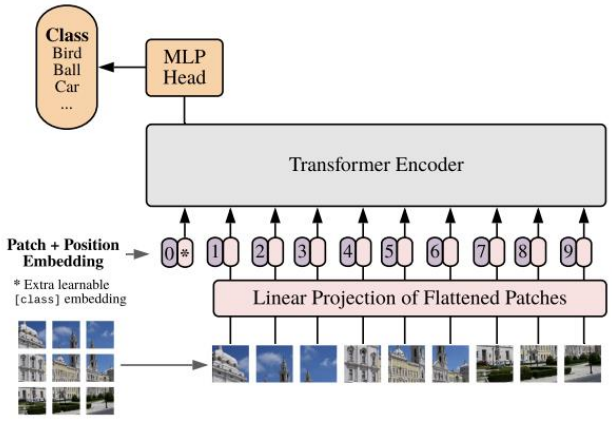

Fig. 3. Visual Transoformer (ViT) [6]

The similar architecture was adopted for our problem and the classification was trained for 100 epochs while employing the categorical cross entropy loss function and the AdamW optimization algorithm. The results of the above deep learning models are tabulated (Table 5).

B. DenseNet Architecture:

Huang et al. [8] in the year 2018, proposed a densely connected convolutional neural network, where each layer is connected to every other layer in the network. With such dense connections, fewer parameters are used and high accuracy is achieved as compared to ResNet. Here, the information is consequently passed to each successive layer using the composite function operator. The composite function consists of convolution layer, pooling layer, batch normalization and non-linear activation function. Since the information is continuously is received, the architecture is thinner and compact. Hence, it shows better computational as well as memory efficiency.

For L layers, there are L(L+1)/2 direct connections. For each layer, the feature maps of all the preceding layers are used as inputs, and its own feature maps are used as input for each subsequent layer. DenseNets essentially connect every layer to every other layer. The input of a layer inside DenseNet is the concatenation of feature maps from previous layers. DenseNets have several compelling advantages: they alleviate the vanishing-gradient problem, strengthen feature propagation, encourage feature reuse, and substantially reduce the number of parameters. The dense nature of the architecture can be visualized with the help of Fig. 4. The images were trained on the DenseNet-121 and the DenseNet-201 architectures.

The numbers 121 and 201 in the above notations essentially specify the depth of the models. The values can be calculated as follows:

5 + (6+12+24+16)*2 = 121 for DenseNet-121 and

5 + (6+12+48+32)*2 = 201 for DenseNet-201

TABLE 1. LAYER-WISE REPRESENTATION OF DEEP LEARNING ARCHITECTURES (SECTION III)

Hidden Layers	Output Size	DenseNet - 121	DenseNet – 201	Light-DenseNet
Convolution	112 x 112	7 x 7 conv, stride 2		
Pooling	56 × 56	3 x 3 max pool, stride 2		
Dense Block (1)	56 × 56	[1 x 1 conv, 3 x 3 conv] x 6		[1 x 1 conv, 3 x 3 conv] x 6
Transition Layer (1)	56 x 56 28 x 28	1 x 1 conv 2 x 2 average pool, stride 2		
Dense Block (2)	28 x 28	[1 x 1 conv, 3 x 3 conv] x 12		[1 x 1 conv, 3 x 3 conv] x 6
Transition Layer (2)	28 x 28 14 x 14	1 x 1 conv 2 x 2 average pool, stride 2		
Dense Block (3)	14 x 14	[1 x 1 conv, 3 x 3 conv] x 24	[1 x 1 conv, 3 x 3 conv] x 64	
Transition Layer (3)	14 x 14 7 x7	1 x 1 conv 2 x 2 average pool, stride 2		
Dense Block (4)	7 x 7	[1 x 1 conv, 3 x 3 conv] x 16	[1 x 1 conv, 3 x 3 conv] x 48	
Classification Layer	4 x 4	7 x 7 global average pool 4D fully-connected, softmax		

Where 5 is split between a convolution, pooling layer and 3 transition layers. The second part of the sum shows the repetitions of the dense layers owing to the dense nature of the architecture. Each dense block in the architecture has 2 layers. Hence, the multiplication by 2. Every layer is tabulated and represented in Table 1, and the classification results are discussed in future sections.

The highly dense number of connections make the visualizations more complex. Fig 4 shows a simple visual representation of the architecture used. It helps in understanding the structure and the connectivity.

It should also be noticed that as we go deeper into the network, the number of features is not exploding as anticipated because of the transition layers, which leads to the reduction in the size of the feature maps hence making the architecture sustainable. To sum up, we have employed the DenseNet architecture in the work for the following reasons:

1. Parameter Efficiency: Only limited number of parameters are passed on to the consecutive layers.
2. Dense Connectivity: Input feature maps from previous layers – minimal loss of information.
3. Transition Layers: Feature maps are reduced.

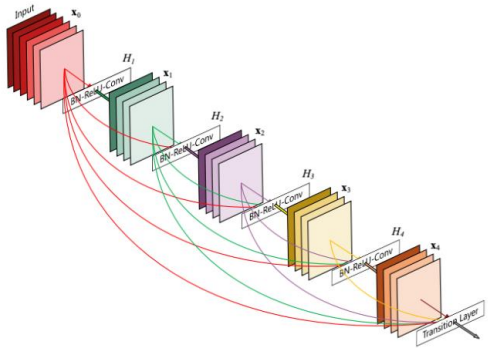

Fig. 4. Architecture of DenseNet. [8]

C. Light-DenseNet:

It was observed that the accuracy difference between the vanilla CNN and the DenseNet was not correlating with the complexity and the cost of the networks. Hence, a lighter

version of the DenseNet is proposed. The basic layer-wise structure is visualized in Table 3. The number of parameter used for training is significantly reduced to 6,796,346. The number of layers in this architecture is illustrated: 5 + (6+12)*2 = 41 for Light-DenseNet. The results and the accuracy are elaborated on following sections.

IV. Results And Discussion

The dataset for testing is curated by considering 500 images from each of the class to create a balanced dataset and to avoid bias. The model was implemented in Python3.7 using the TensorFlow library. The Google Colaboratory environment was used, the NVIDIA Tesla K80 GPU was accessed using this environment and the models were run on the virtual environment and the results were observed.

A. Performance analysis:

The identification task was performed using Vision Transformers, DenseNet-121, DenseNet-201 and a proposed modified DenseNet architecture. The vision transformer models do not yield expected results. So, the DenseNet architectures were employed. The major drawback observed while implementing the Dense Architecture was that, the number of trainable parameters were extremely high. 30,676,356 parameters for DenseNet-201 and 6,966,020 parameters for DenseNet-121. Even though DenseNet-121 is computationally less expensive, was compromised on the accuracy. Hence, we developed an architecture which is computationally less expensive as well as resulting in better classification.

Table 2. Comparative Study

Architecture	Accuracy (in %)	Parameters Used
Vanilla CNN	89.68	656,020
Vision Transformer	90.83	21,660,612
DenseNet-121	91.67	6,966,020
DenseNet-201	95.03	30,676,356
Proposed Architecture	97.00	1,302,532

From Table 2, we can understand that the proposed architecture yielded the best result and the performance metrics for the same are analyzed in the following subsection.

A. Performance metrics:

The Receiver Operator Characteristic (ROC) depicts the performance of a classification model at all classification thresholds. It tells how well the model is able to distinguish between the classes. The ROC curve was also plotted for each of the classes and it is shown in Fig 5.

Additionally, amongst many evaluation metrics for image classification problems, we have chosen Precision and Recall and the results are visualized using a confusion matrix.

Precision gives the percentage of the predictions that are correct i.e., measures how accurate your predictions are. Recall measures how good the detector identifies the positives in the dataset The mathematical definition of the metrics is given below,

$$\text{Precision} = \frac{TP}{TP+FP}$$

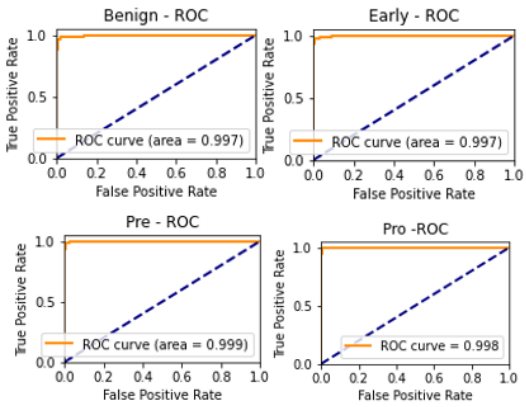

Fig. 5. Reciever Operator Characteristic Curve for the four classes.

$$\text{Recall} = \frac{TP}{TP+FN}$$

$$\text{F1 score} = 2*\frac{Precision * Recall}{Precision + Recall}$$

Where, TP = True Positive, TN = True Negative, FP = False Positive, FN = False Negative

Table 3. Confusion Matrix of the Results Obtained

Confusion Matrix	Precision	Recall	F1 Score
Actual: BENIGN	0.98	0.96	0.97
Actual: EARLY	0.94	0.97	0.95
Actual: PRE	0.95	0.98	0.96
Actual: Pro	1.00	0.96	0.98

B. Experimental Comparison:

The curated dataset is divided into training, testing and validation sets. The learning rate was set to 0.0002, training batch size to 64 and the categorical cross entropy loss function and the AdaMax optimization algorithm is employed in the training process. The accuracy and the parameters used are tabulated in Table 2

The loss and accuracy data for the models are stored in the history object. The Loss and validation loss against epochs and the training accuracy and validation accuracy against the number of epochs is plotted in Fig 6. The training was performed and the weights at the end of 50 epochs were downloaded and stored as .h5 files. This enables us to resume training from a specific point instead of restarting the entire procedure and test the model. The DenseNet-201 being a deeper architecture with many more layers proved to be more effective in the stage detection of the lymphoblastic cell. The Denser architecture performed better for our data because of the strong feature propagation mechanism. We have shown the confusion matrix for the results obtained from the DenseNet-201 architecture in Table 4.

Table 4. Confusion Matrix of the Results Obtained

Confusion Matrix	Predicted: BENIGN	Predicted : EARLY	Predicted: PRE	Predicted: PRO
Actual: BENIGN	155	5	1	0
Actual:	1	135	3	0

EARLY				
Actual: PRE	0	3	142	0
Actual: Pro	2	0	4	150

II. CONCLUSION:

The proposed model was able to classify and detect the various stages of Leukemia from the peripheral blood smear images. Our work aims to be an assistive device for effective classification and allows to correlate the results deduced from the traditional methods and our model. The lymphoblastic cells are effectively segmented from the background by employing image processing techniques and passed on to the Model. The model achieves an average accuracy of 97% at the end of just 30 epochs. The augmentation techniques employed has made the model more robust as the orientation of the peripheral blood smear images are not pre-defined. As we are dealing with medical image classification, even the minute errors in classification may incur high costs. From the Table 3, we can see that all the leukemic cells have been successfully detected but there is a minor misclassification only in the stage of the cancer. Hence, our model proves to be a good classifier and allows medical practitioners start appropriate treatments as soon as possible. Only major drawback of the model was that, there are several benign samples which were misclassified, which would result in a waste of resources. Future work would employ more robust methods for WBC segmentation which can handle any manual errors made while the preparation of the blood smear itself. A GUI is currently in development to make real-time detection much easier, enabling the clinical practitioners to use it effectively for early diagnosis and onset of treatment.

REFERENCES

[1] Sheeba, Feminna, et al. "Detection of poor quality peripheral blood smear images used in detection of leukocytes and erythrocytes." 2017 Fourth International Conference on Image Information Processing (ICIIP). IEEE, 2017.

[2] T. TTP, G. N. Pham, JH. Park, KS. Moon, SH. Lee, and KR. Kwon, "Acute Leukemia Classification Using Convolution Neural Network in Clinical Decision Support System," in Proc. 6th International Conference on Advanced Information Technologies and Applications (ICAITA 2017), Sydney, 2017

[3] Tran, T. & Vununu, Caleb & Atoev, Sukhrob & Lee, Suk-Hwan & Kwon, Ki-Ryong. (2018). Leukemia Blood Cell Image Classification Using Convolutional Neural Network. International journal of computer theory and engineering. 10. 54-58. 10.7763/IJCTE.2018.V10.1198.

[4] Ansha Beevi, Remya R.S., "An Overview on Acute Lymphocytic Leukemia Detection using Cell Image Segmentation", IOSR Journal of Computer Engineering (IOSR-JCE) 2014

[5] https://ai.googleblog.com/2019/05/efficientnet-improving-accuracy-and.html

[6] https://towardsdatascience.com/are-you-ready-for-vision-transformer-vit-c9e11862c539

[7] Mehrad Aria, Mustafa Ghaderzadeh, Davood Bashash, Hassan Abolghasemi, Farkhondeh Asadi, and Azamossadat Hosseini, "Acute Lymphoblastic Leukemia (ALL) image dataset." Kaggle, (2021). DOI:10.34740/KAGGLE/DSV/2175623

[8] Gao Huang.Zhuang Liu , Laurens van der Maaten, Kilian Q. Weinberg, "Densely Connected Convolutional Networks" Jan 2018

[9] Hegde, Roopa & Prasad, Keerthana & Hebbar, Harishchandra & Singh, Brij Mohan. (2019). Development of a robust algorithm for detection of nuclei of white blood cells in peripheral blood smear images. Multimedia Tools and Applications. 78. 10.1007/s11042-018-7107-x.

[10] Aljaboriy, S., Sjarif, N., and Chuprat, S. (2019). Segmentation and detection of acute leukemia using image processing and machine learning techniques: a review. AUS 26, 511–531. doi: 10.4206/aus.2019.n26.2.60

[11] Ahmed N, Yigit A, Isik Z, Alpkocak A. Identification of Leukemia Subtypes from Microscopic Images Using Convolutional Neural Network. Diagnostics. 2019; 9(3):104. https://doi.org/10.3390/diagnostics9030104

[12] https://towardsdatascience.com/understand-the-architecture-of-cnn-90a25e244c7

[13] https://towardsdatascience.com/target-encoding-for-multi-class classification-c9a7bcb1a53

[14] Ibrahim, I., & Abdulazeez, A. (2021). The Role of Machine Learning Algorithms for Diagnosing Diseases. Journal of Applied Science and Technology Trends, 2(01), 10-19.

[15] https://www.mayoclinic.org/diseases-conditions/acute-lymphocytic-leukemia/diagnosis-treatment/drc-20369083

[16] Ghaderzadeh M, Aria M, Hosseini A, Asadi F, Bashash D, Abolghasemi H. "A Fast and Efficient CNN Model for B-ALL Diagnosis and its Subtypes Classification using Peripheral Blood Smear Images" XXX 2021;23(4):e27468 URL: https://www.---.org DOI: - PMID: -

[17] J. Kanimozhi, Dr. P. Vasuki, R. Preethi, 2016, Blood Vessel Segmentation for Fundus Images by Active Contour Method, INTERNATIONAL JOURNAL OF ENGINEERING RESEARCH & TECHNOLOGY (IJERT) ICETET – 2016 (Volume 4 – Issue 16)

[18] Ajay Mittal, Sabrina Dhalla, Savita Gupta, and Aastha Gupta. 2022. Automated analysis of blood smear images for leukemia detection: a comprehensive review. ACM Comput. Surv. Just Accepted (January 2022). DOI:https://doi.org/10.1145/3514495

[19] https://www.tensorflow.org/api_docs/python/tf/keras/layers

[20] R. Agrawal, S. Satapathy, G. Bagla and K. Rajakumar, "Detection of White Blood Cell Cancer using Image Processing," 2019 International Conference on Vision Towards Emerging Trends in Communication and Networking (ViTECoN), 2019, pp. 1-6, doi: 10.1109/ViTECoN.2019.8899602.

[21] Vo, Quyen Hoang, Xuan-Hieu Le, and Thanh-Hai Le. "A deep learning approach in detection of malaria and acute lymphoblastic leukemia diseases utilising blood smear microscopic images." Vietnam Journal of Science, Technology and Engineering 64.1 (2022): 63-71.

[22] Das, Pradeep Kumar, Biswajit Nayak, and Sukadev Meher. "A lightweight deep learning system for automatic detection of blood cancer." Measurement 191 (2022): 110762.

[23] Sabry, Hend & Omar, Rowan & Saeed, Nermeen & Essam, Ali & Ayman, Nada & Mohiy, Taraggy & AbdelRaouf, Ashraf. (2018). Automated detection of white blood cells cancer diseases. 48-54. 10.1109/IWDRL.2018.8358214.

[24] Zhang, Jing, et al. "Computerized detection of leukocytes in microscopic leukorrhea images." Medical physics 44.9 (2017): 4620-4629.

[25] Ali Abdullah Yahya, Jieqing Tan, Min Hu, "A Novel Model of Image Segmentation Based on Watershed Algorithm", Advances in Multimedia, vol. 2013, Article ID 120798, 8 pages, 2013. https://doi.org/10.1155/2013/120798

Workload prediction on cloud computing using long short term memory algorithm

M. Ayyadurai[1], Ganesh BS[2], Shivani Devi[3], Shiva Prakhash[4]

[1–4]Department of Electronics and Communications Engineering, SRM Institute of Science and Technology, Chennai
[1]ayyadurm@srmist.edu.in, [2]bg5873@srmist.edu.in, [3]sd3799@srmist.edu.in, [4]ss4400@srmist.edu.in

***Abstract*— Great guide control may be extremely important within the cloud, and responsibility expectation is critical for achieving the right guide control. While it is far more plausible to anticipate the jobs of long-running liabilities based entirely on the irregularity of their notable jobs, it is far more difficult to accomplish this for obligations that do not have such ongoing responsibility designs. We examine an excellent response for undertaking responsibility forecasting in this paper. Rather than using the notable responsibility of one Endeavor to predict the predetermination responsibility of another, we can use information to predict the latest job. A reasonable responsibility for calculating supplier serves as the heart of this hybrid distributed computing model.**

In this cloud platforms work forecasting is the key to successful resource management. Finding work in initial tasks for work in focus on their earlier workload is difficult; however, identifying work for activities they've observed without a workload pattern is much more difficult. This time, we'll utilize a different method to forecast workload. Rather than using existing workload to forecast future workload, we will employ the long short term memory(LSTM) technique. This hybrid cloud estimation model is built on an intelligent workload factoring service that is calculated for proactive workload management.

***Keywords*— workload prediction, multiple clusters, neural networks, cloud computing**

I. Introduction

Cloud computing has more scope and has become the primary computing method in recent years. It has many advantages and some drawbacks also. Cloud computing has two major objects are memory consumption and processor. This method has become costly and inefficient. We can use workload prediction method to improve efficiency and operational costs of a cloud. Previous approaches are not able to give accuracy. So, to improve this we developed a solution in this project by employing more efficient algorithms and neural models. To begin, the responsibilities of existing errands are divided into groups. Then, a brain network is used to become acquainted with the characteristics of each group's jobs. The clever responsibility considering administration's central innovation is a quick successive information thing location calculation, which enables calculating approaching solicitations on volume as well as on information content, based on a changing application information prominence. Watchwords: responsibility forecasting, large groups, brain organizations, and distributed computing. Introduction Cloud registering has grown in popularity, and it is now one of the most popular methods of calculating. Despite its numerous advantages, it also has some drawbacks. The processor and memory utilization are two of the most difficult aspects of distributed computing. These variables cause a cloud framework to emerge.

II. Literature Survey

The authors of [1] developed the RL algorithm, in which the (BSs) are recorded in the historical data in many stacks, reducing prediction time consumption and enhancing knowledge ability. The authors of [2] paper proposed a multi-layer data-flowing procedure model to efficiently use the computing capacity of the entire system. For the modelling and study, a standard IOT solicitation pictures absorbing and face identification are being used, and the results show that the Edge Flow can effectively reduce latency and recovery rates than earlier distributed frameworks. Here, the workload on infrastructures is reduced to a minimum. The researchers of [3]article focused at a compute sharing challenge in MEC. The purpose of a compute sharing system model is to keep down power depletion and task lag when offloading work sections in order to maintain control overhead steady and find attractive outcomes. Traditional Qos does not compensate for the user's mobility and dependence, that creates a shift in the monitoring result. The authors present the ghBSRM-MEC in this[4] article (Gaussian hidden Running time of the Monitor for the MEC). During execution, it combines the KNN algorithm with some operations to dynamically change to Qos mobility, leading in verifiable results.

Now, [5] The NFV and MEC are the new top technologies that are leading the nation to the next step, supporting novel applications and services with short processing times and greater required resources, such as autonomous vehicles and augmented reality, among other technologies. Depending on the different scenarios of the problem, the authors use NP-hard and implemented an Integer Programming (IP). Which is extremely effective when working with complex issues. The authors propose a cloud-guided feature extraction approach for mobile image retrieval in [6] article, and the experimental data shows that it reduces network traffic by nearly 93 % and makes better recoupment accuracy by more or less 6.9% as compared to the previous MEC image retrieval methods. The author of [7]article presented an expense sub structure for the MEC and cloud to allocate computing capabilities and assets in order to bolster business ratios. Even so, the system has

proven ineffective, and the subject also significantly increases the complication of the problem, When the advent of computing tasks surpasses the maximum capacity of the MEC, the concept still need more debate for admission control systems. The authors of the [8]article launch an investigation peer of loading plans in MEC-enabled small cell which possibilities to work patterns are properly considered within both spatial - spectral domains They created open, an online peer offloading architecture that employs the Lyapunov approach to maximize edge computing performance with minimal energy supplies contributed by particular SBSs while avoiding the need for future system dynamics insights.. This system is opportunistic and uncontrollable, spite of the fact that it streamlines the implementation process. The amount of iteration estimates in the network is huge. The aim of this [9] The goal of this paper is to combine dynamic caching, resource allocation, and compute offloading to improve the long-term averages of the objective functions, which includes energy consumption, delay, and cache contents fetching costs in a cache-assisted multi-user MEC system. The authors had researched on a dynamic scheduling scheme for a while now. that combines DRL (Deep Reinforcement Learning) and the DDPG method (Deep Deterministic Policy Gradient). It has led to the reduction in calculation time, and also a faster and more efficient decision-making approach. The aim of this [10] article is to improve the system utility for leveraging throughput and fairness by finding an optimal offloading plan for optimization. Based on the Karush-Kuhn-Tucker condition, an increment-based greedy approximate algorithm was proposed, and the results indicate that the algorithm can achieve effective utility and accuracy performance, although the model is expensive to train. [11] The proposed results do not rule out the possibility of deploying HLA as a Grid service.[12] This article introduces a method that combines LSTM and (Recurrent Neural Network) RNN to develop a clever calculation that can set out not to gain proficiency with a similar-asset distribution system and improve learning productivity. This is an algorithm that aids in avoiding learning the same resource allocation and efficiently improves learning. [13-17] These articles provide such a method for managing the forecast on a particular time, ahead to the anticipated time point, to allow enough time for task scheduling based on the expected workload. That article introduced a clustering-based workload prediction technique, in which the tasks are first grouped and then a prediction model for the appropriate is developed.

Another article proposes an integrated deep learning method for time series prediction. It also includes system models, such as bi-directional and grid long short-term memory networks, to assist with workload prediction and resource management. This article outlines a workload-prediction framework that combines a neural network and a self-adaptive differential evolution algorithm to learn the best suitable variation strategy as well as the best acceptance rate.

III. Related Work

In the Literature Survey found many insignificance let us discuss about the joint errand, range and send power assignment issue, for a remote organization is investigated, where portable edge figuring is provided to base stations(BS's) and (MEC) waiters that offer correspondence administrations and estimation to clients is investigated. Each client has the option of requesting one of three different sorts of computational work. Every computing work is variable in size, and when the size of the task changes, the BSs must adjust their assets, such as send power and subcarrier, as well as errand designation plans, to provide the best service to the customers. They planned to improve the drawbacks with the aim to reduce the transmission and maximum computational delay between the clients. To address this problem, a multi-stack support learning method was developed.

The usage of MEC servers in base stations to jointly deliver communication and computational services to consumers is being researched. In this paper, we will look upon cloud network that has memory and CPU usage allocation problem. Each user has the option of requesting three computing tasks. They are having different size of estimation task, the BSs must adjust their task allocation and resource such as memory allocation and cores in a good manner to serve the users. We have devised a strategy to reduce transmission and computational latency for all users. For this problem, a multi-stack support learning (RL) technique is being developed. In several prediction research publications, the Deep Belief Network algorithm (DBN) is being used. It has a trouble dealing with several datasets while executing the DBN. When compared to the resources of load collation, the accuracy is detected less. When the matrix probability technique is used, it is not supported, and it is acutely susceptible to missing and noisy data.

IV. Proposed System

In the related work had discussed many in significance and significance of the forecast so to overcome this come up with a methodology for anticipating workload forecast examples of new assignments utilizing a collection of verifiable undertakings execution profiles to form the undertaking pool, we pick tasks from various platforms and log them. One way of making use of the information from the errand pool is to build a gaining model that learns from all of the assignments in the pool and use the model to help with the forecast. In any case, this coarse-grained data may not have enough information to improve responsibility forecast precision further. It contains reasonable information on applications that execute using various resources. The proposed LSTM algorithm has been implemented, and it has the ability to predict forecasts as well as more exact and clear forecasting work. This has been used in many other fields like sales and Stock markets. and also imported many packages and used many visualizing tools. Then by these essential network and algorithm from information that collected will be visualized by each and every information like values ,memory and CPU usage.

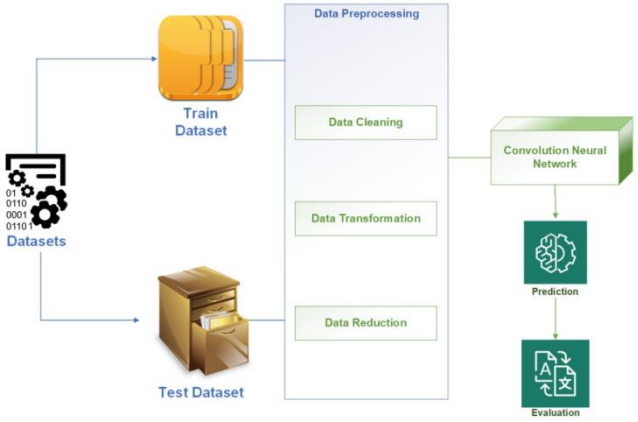

Fig. 1. Proposed Model

The source codes modified for different cloud specialist organizations are freely accessible We are positive that it recommends open doors for new capacity applications with decreased analysis arrangement overheads. In this research, we show how a Neural Network model can be used to recognize a Cloud responsibility expectation module for Cloud vendors. Fig 1 clearly explains about the each and every process that are implemented in the proposed model We present the forecast in light of the NN model and assess its precision of future responsibility expectation utilizing genuine hints of solicitations to web server.

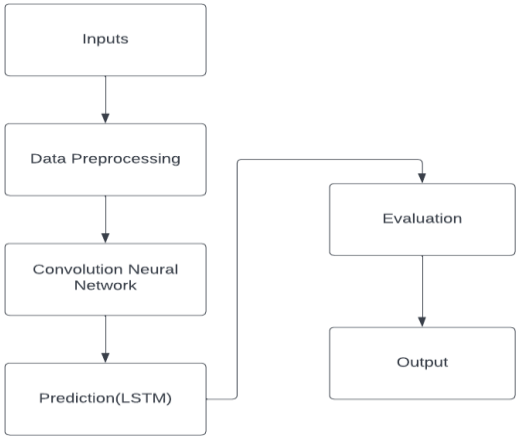

Fig. 2. Work Load Prediction Flowchart

Collected the inputs from the various sources then Data preprocessing will applied to the information that collected and CNN is implemented to understand the outliers and function . LSTM is the used for the prediction and the evaluation.Fig 2 that explains about the frame work of the model that clearly says the input are collected in the step 1 .In step 2 data preprocessing are implemented on that inputs. In step 3 CNN is used to undersatnd the outliers.In step 4 LSTM is used for the forecast a. At final step evaluation and output.

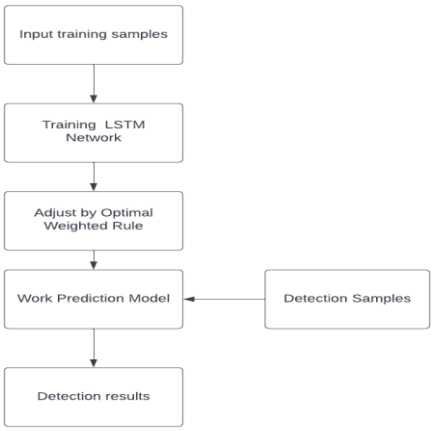

Fig. 3. Working Flow of the cloud computing work prediction model based on DBN and LSTM.

The inputs get trained by the DBN and LSTM then information is optimized by the Weighted rule then the model will get the Detection samples and the Detection results. In Fig 3 explains the process of the model collecting the input from various platforms. Training the models by the LSTM network. Adjusting by the optimal Weight rule and forecasting the model by the detecting the results and the input samples.

V. Description Experiment

A. Proposed ALgorithm:

The LSTM Algorithm was utilized. It's a kind of repeated brain network that's good for learning request reliance in issues of succession expectation. This is typical behaviour in complex issue areas such as machine interpretation and discourse acknowledgment, and the sky is the limit from there. LSTMs are an enigma in the field of deep learning. The key benefits of these calculations are as follows Unstructured data is used to the greatest extent possible, and Feature Engineering data is eliminated and furthermore the capacity to bring High-Quality outcome. Further developed energy structure forecast model Rationality of the design expectation is extraordinarily worked on High achievability of the model Radial premise work is adapted Ease of moving information starting with one model then onto the next in view of areas and errands. As given the inputs and adjusted by the optimal weight rule from the y_t ,the calculation of the hidden layer g_t and the state of cell C_t in LSTM

Step (i) $A_t = \sigma(W_a . [g_{t-1}, y_t] + c_f)$
Step (ii) $h_t = \sigma(W_h . [g_{t-1}, y_t] + c_i)$
Step (iii) $\tilde{C}t = \tanh(W_c . [g_{t-1}, y_t] + c_c)$
Step (iv) $C_t = g_t * C_{t-1} + i_t * \tilde{C}t$
Step (v) $q_t = \sigma(W_o . [g_{t-1}, y_t] + b_o)$
Step (vi) $g_t = q_t * \tanh(C_t)$

In step (i) Wa, Step(ii) W_h, Step(iii) Wc ,Step(v) Wo, all these indicates the weight matrixes and Step (i) C_f,Step (ii) C_i, Step(iii) Cc are the three gates of the biases and the state of cell. sigmoid function σ and the hyper tangent-tanh.

Then for the final prediction of the value, the first layer and second layers is calculated by the

g(x)= max(αy,y)

α is the updated parameter with the training process. T Then the unique form of the parameter α is changed to 0.02 and the third layer that forecast the value between the 0.0 to 1and it get assigned by sigmoid function.

$$X = f(y) = \frac{1}{1+ e^{-\theta x}}$$

The final forecast value of the future is predicted by the value x.

No.of. Virtual Machine	Actual Value by DBN/10^2	Predicted Value by LSTM/10^2
1	412.43	409.27
2	583.56	585.70
3	232.25	234.32
4	558.57	560.67
5	263.23	265.87
6	312.98	309.53
7	530.52	533.02
8	662.97	657.32
9	142.76	140.64
10	643.36	639.65

The Actual values have been calculated by the equations and forecasted the values in each and every step and the accuracy that had produced in the average is 0.931.

B. *Datasets:*

We collected the datasets from the various fields like Kaggle and from the many references papers, after collecting we will train the datasets like the removing unwanted and null values once that is over we will clean the data and we will take the data which is essential for the project .This datasets have many fields like CPU Capacity provisioned for the overall storage secondly comes the CPU usage thirdly comes the Memory usage, Memory Capacity and also read the Disk ,Disk write and finally the Network experience the outturn and Network transmitted outturn. After the cleaning and collected the data we will start to visualize according the needs.

C. *Experimental Setup:*

Hardware Requirements:

The processor of Minimum i3 Dual-Core with Ethernet association (LAN) OR a remote connector (Wi-Fi) and Hard Drive with a limit of Minimum 100 GB.

Software Requirements:

Python, Anaconda, Jupiter Notebook, and TensorFlow.

VI. Results And Discussion

A. *Graph:*

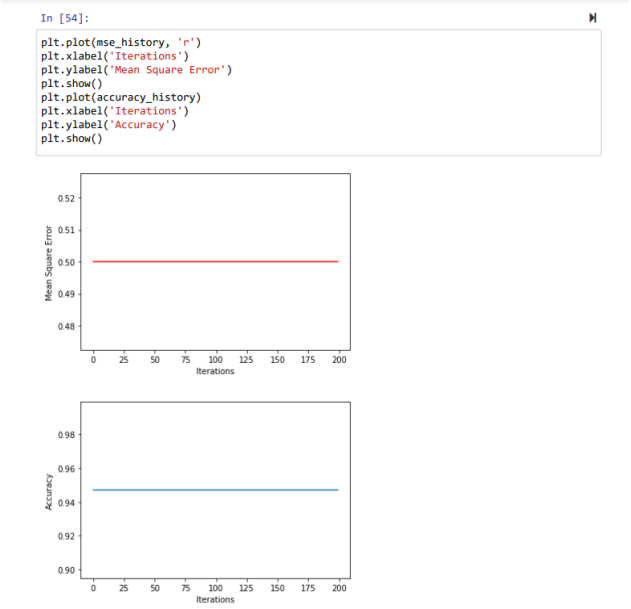

Fig. 4. Iterations and Accuracy

The Graph plots the mse_history the information that collected and the Mean Square Value and the Iterations of the predictons and the Accuracy_history in the second graph.

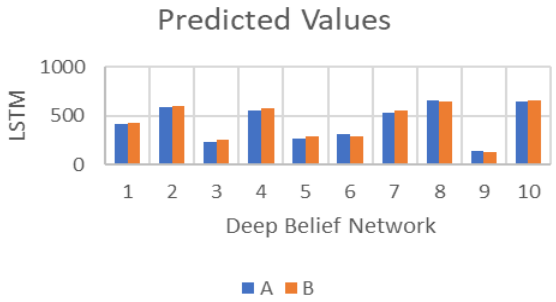

Fig. 5. Prediction value of graph

The Fig 5 tells the complete details about the forecast values of the DBN and LSTM Algorithm.The values are slightly changed when compared to the DBN..

B. *Result Pictures:*

Fig. 6. Importing the packages and connecting the dataset.

Fig. 7. Value Count in index

```
In [43]:
def model_neural_network(x, weigths, biases):
    layer_1 = tf.add(tf.matmul(x, weigths['h1']), biases['h1'])
    layer_1 = tf.nn.sigmoid(layer_1)
    layer_2 = tf.add(tf.matmul(layer_1, weigths['h2']), biases['h2'])
    layer_2 = tf.nn.sigmoid(layer_2)
    layer_3 = tf.add(tf.matmul(layer_2, weigths['h3']), biases['h3'])
    layer_3 = tf.nn.sigmoid(layer_3)
    layer_4 = tf.add(tf.matmul(layer_3, weigths['h4']), biases['h4'])
    layer_4 = tf.nn.sigmoid(layer_4)
    output_layer = tf.matmul(layer_4, weigths['out']) + biases['out']
    output_layer = tf.nn.relu(output_layer)
    return output_layer
```

Fig. 8. Implementing Convolution Neural Network

```
In [55]:
correct_prediction = tf.equal(tf.argmax(y, 1), tf.argmax(output, 1))
accuracy = tf.reduce_mean(tf.cast(correct_prediction, tf.float32))
print("Test Accuracy: ", (sess.run(accuracy, feed_dict={input_data: test_x, output: test_y}
Test Accuracy:  0.9310345
```

Fig. 9. The Test Accuracy of the Prediction

C. Module 1 -Data Preprocessing:

The foremost and important step to build this model is Data Preprocessing In this there are a lot of steps to do firstly data cleaning the dataset that collected from various platforms and exist models may have many incorrect values ,missing values and also the null values so by this process the all unwanted information will be eliminated .The collected information may also have the duplicate and inaccurate values all these are corrected in this process, quality data should have the validity which means understand the model requirements and constraints then collect the information. Accuracy make sure that the information are accurate and true values. Completenesss process is all about to make sure the information is known and related to the model. Consistency check the information are have the consistent within and across the all information. Uniformity in this information is measured using the same unit. By using the data cleaning tools the according to the model the information is filtered and make it accurate.

Secondly Data Transformation the process is all about to changing the format and values of the collected information. extract the information from the multiple sources and convert it all into a helpful format and save it to any one of the known destination all this process is called as ETL (Extract ,Load, Transform). Before joining the data from various steps are taken to prepare the dataset in that all scaled values are ranged between 0.1-0.8 by the scaler values of smaller value to larger value.

$$Yi=HWH+yi-y_{min}(VPM-HWH)/y_{max}-y_{min}$$

Where the minimum and maximum values of dataset are y_{min} and y_{max} .that reach the range up to the range between 0.1-0.8. Data Transformation has the Data Discovery in this where all the information is identified and transform all to its source format according to the model need then the Data Mapping in this phase the whole transformation process is confirmed. Review in this where the all information is formatted exactly to the need.

Finally the Data Reduction in this where the collected information will be reduced but it have the quality of the original information, there are several methods they are Data Cube Aggregation in this information will be aggregated after this process completion easily the information will be summarized. Dimension Reduction in this data size will be reduced and it eliminate the outdated and redundant information. Data Compression in this technique the size of the information is reduced using different encoding methodology. This whole process is implemented in the dataset that we collected and created for the model in CSV file.

D. Module 2-Convolution Neural Networks:

Convolution is also known as ConvNets. CNN is basically known as the machine learning model which comes under the Deep Learning. The usage of the CNN is it work more efficiently when we use big data and also it shows us the extraordinary accuracy as we expect. ConvNets is mainly used for the classification, processing and segmentation, for the feature engineering process it takes less time priorly using the ConvNets in applications. Backpropagation algorithm is used to the network architecture and gradient descent is familiar from the artificial brain networks but the modification of this is little for the several types of layers . CNN contains many layers so each layers have the function of activating several components then that are sent to other layers. First layer do the work of pull out the basic features which contains the horizontal and vertical edges, then this sent to next layer it identify the complex features. Stride which measure the count and the distance of the input that we provide and also tells the whether it is a large or smaller outline. Pooling layer is same as convolution Layer it duty is to reduce the size of computational power which is needed for processing the data. This pooling have two sub parts average pooling this layer returns the average of values where as the max pooling play the role of Noise Suppressant and also do the de-noising. Fully connected layer as the name mentioned the each and every single node is connected to all. This does the task of categorizing based on the features pulled out from the before layers and all their several filters. FC layers are usually do the soft max activation function to categorize the several inputs according to the instructions.

The ConvNets have the ability to understand the model how it function and predict the outliers. It helps to tune the hyperparameter and also pop out the failures of the model then gives complete information why they have failed to achieve the process. It tells about the all commitment to the users. The drawback is the that they gives the highly accurate categorized outputs when they trained with many information. Once all these have implemented in the graphs and data has been visualized according to the instructions that we given.

E. Module 3 - Model Prediction & Evaluation:

The previous modules have almost completed the process of the model in this module remaining process of prediction and evaluation is going to proceed. In the Data Pre processing the information that we collected are reduced to our requirement and filtered the all other values. In the CNN the data has been imported and made the various visualization and made the graphs, then by applying the proposed algorithm which has the ability to predict the model with accuracy. According to the study, the best model prediction should have the criteria like Multiple Data sets in this criteria the information will be collected from various platforms which relevant to the model and start the other process. Data Collating means which have data insights of the collected information and also make sure to avoid the all problems and accurate forecast are required. Correct Data Analysis even the most of the situations the lot of complex problems have been explained through the visualization by displaying the large data into graphs and charts according to the requirements. Accurate Data Validation in this where the information that we collected and made them into the certain models their outcome and that will be compared to various sources from that report the results should satisfy the conditions finally the model gets validated, When the model satisfy the all the stages then the model is predicted with Excellent accuracy. In our model the data collected and tested then by applying the CNN and the data has been started to predict the work Load after this by using LSTM algorithm the outcome of the prediction have been predicted with excellent accuracy.

Evaluation is the final stage of the model. The Evaluation have the different criteria where it uses the many evaluation methods to get a model performance and it clearly explains about the significance and insignificance. This evaluation is the most important asset to predict the efficiency of the model in the starting stages and also have the important play in the model monitoring. Evaluation have many category to satisfy the model initially the Accuracy in this they measure the prediction of the model with the all other exist prediction of the models and make them as excellent model. Precision is the stage where it checks the predicted results are truly justified to the model and this is quality choice of the model evaluation. Confusion Matrix it clearly explains the details about the incorrect categorization for each and every stage of the modules using this matrix the can get the complete distinction between the module. The proposed model had gone through the every stages and the outcome had evaluated and then compared, then our proposed model have evaluated successfully.

The dataset for the work load prediction in cloud computing has been collected from various platforms like Kaggle and many other sectors of cloud computing collected and tested according to the project is more efficient and accurate by using the Long Short Term Memory Algorithm when compare to algorithms like Deep belief network and many other existing algorithms.

VII. CONCLUSION AND FUTURE WORK

The new developed model that we build form the proposed methodology and algorithm are more efficient and accurate when we compared with other existing model so, finally we conclude that the model that we build is predict the work on cloud with expected accuracy and efficiency. In upcoming days, we intend to incorporate into the design a responsive module that can go about as a second line of safeguard against poor QoS by repaying mistakes in the forecast with improvement choices on powerful provisioning.

REFERENCES

[1] S. Wang, M. Chen, X. Liu, C. Yin, S. Cui, and H. Vincent Poor, "A Machine Learning Approach for Task and Resource Allocation in Mobile-Edge Computing-Based Networks," *IEEE Internet of Things Journal*, vol. 8, no. 3. pp. 1358–1372, 2021. doi: 10.1109/jiot.2020.3011286.

[2] "Joint Task Assignment, Transmission, and Computing Resource Allocation in Multilayer Mobile Edge Computing Systems." https://ieeexplore.ieee.org/document/8493145 (accessed Apr. 27, 2022).

[3] "Multi-Objective Computation Sharing in Energy and Delay Constrained Mobile Edge Computing Environments." https://ieeexplore.ieee.org/document/9091902 (accessed Apr. 27, 2022).

[4] "Mobility and Dependence-Aware QoS Monitoring in Mobile Edge Computing." https://ieeexplore.ieee.org/document/9366770 (accessed Apr. 27, 2022).

[5] "Reliability-Aware Virtualized Network Function Services Provisioning in Mobile Edge Computing." https://ieeexplore.ieee.org/document/8758846 (accessed Apr. 27, 2022).

[6] "A Cloud-Guided Feature Extraction Approach for Image Retrieval in Mobile Edge Computing." https://ieeexplore.ieee.org/document/8851250 (accessed Apr. 27, 2022).

[7] "Efficient Computing Resource Sharing for Mobile Edge-Cloud Computing Networks." https://ieeexplore.ieee.org/document/9046758 (accessed Apr. 27, 2022).

[8] "Computation Peer Offloading for Energy-Constrained Mobile Edge Computing in Small-Cell Networks." https://ieeexplore.ieee.org/document/8392534 (accessed Apr. 27, 2022).

[9] "Deep reinforcement learning for dynamic computation offloading and resource allocation in cache-assisted mobile edge computing systems." https://ieeexplore.ieee.org/document/9310745 (accessed Apr. 27, 2022).

[10] "Utility aware offloading for mobile-edge computing." https://ieeexplore.ieee.org/document/9147161 (accessed Apr. 27, 2022).

[11] M. Urkia Kortabarria, "Web Service Performance on Heterogeneous Systems : A performance comparison between J2EE and .NET on heterogeneous systems," 2013. Accessed: Apr. 27, 2022. [Online]. Available: https://www.diva-portal.org/smash/get/diva2:636008/FULLTEXT01

[12] J. Brownlee, *Long Short-Term Memory Networks With Python: Develop Sequence Prediction Models with Deep Learning*. Machine Learning Mastery, 2017.

[13] "Machine Learning Based Workload Prediction in Cloud Computing." https://ieeexplore.ieee.org/abstract/document/9209730 (accessed Apr. 27, 2022).

[14] "Integrated deep learning method for workload and resource prediction in cloud systems," *Neurocomputing*, vol. 424, pp. 35–48, Feb. 2021.

[15] "Workload prediction in cloud using artificial neural network and adaptive differential evolution," *Future Gener. Comput. Syst.*, vol. 81, pp. 41–52, Apr. 2018.

[16] K. L. LaCurts and Massachusetts Institute of Technology. Department of Electrical Engineering and Computer Science, *Application Workload Prediction and Placement in Cloud Computing Systems*. 2014.

[17] sihua wang,Mingzhe Chen, Xuanlin Liu Student member,Changchuan Yin Senior member July 2020 "A Machine Learning Approach for Task and Resource Allocation in Mobile Edge Computing Based Networks"

Feasibility of Brain Computer Interface (BCI) and Internet of Things (IoT) in assisting Elderly and Disabled people

Monisha B[1], Sruthi Vrindha R[2], Subashini U[3], K Sumathi[4]

[1–4]Electronics and Communication Engg., Sri Sairam Engineering College, Chennai, India

[1]e8ec096@sairamtap.edu.in, [2]e8ec083@sairamtap.edu.in, [3]e8ec156@sairamtap.edu.in, [4]sumathik.ece@sairam.edu.in

***Abstract*—Brain-computer interface (BCI) is an active area of research which provides a smart solution for the accessibility challenges faced by the elderly or the disabled who are the main potential targets. A brain-computer interface (BCI) is a new communication channel between the human brain and a digital computer. Different brain states are the result of different patterns of neural interaction. These patterns lead to waves characterized by different amplitudes and frequencies caused by the neural interactions. Every interaction between neurons creates a minuscule electrical discharge. A brain wave sensor is used to collect those brain wave signals which are then divided into packets. The packet data is transmitted through Bluetooth to the laptop/PC which is connected to the brain wave sensor. Different patterns of brain activities are taken as commands. The wave measuring unit will receive the brain wave raw data and convert it into a signal using the MATLAB platform. Then the instructions are sent to the controller section to operate the modules. An additional feature of controlling the devices using voice command is also integrated using bluetooth.**

Keywords : Brain Computer Interface (BCI) , Electroencephalographic (EEG), MATLAB, Bluetooth, Neurosky mind wave sensor, Arduino.

I. INTRODUCTION

Brain computer interface is often called a mind-machine interface (MMI), is a direct communication pathway between the brain and an external device [1] . BCIs are often directed at assisting, augmenting, or repairing human cognitive or sensory-motor functions. Brain Computer Interface (BCI) device transforms the EEG (Electroencephalographic) signals produced by brain activity into control signals which can be used for controlling the interfaced modules. A BCI system detects the presence of specific patterns in a person's ongoing brain activity that relates to the person's intention to initiate control.

People with visual or locomotive imparities and elderly people have problems with their day - to - day activities which makes them to depend on others. Sometimes it will reduce their self confidence. One of them is operating their home appliances which makes them feel inefficient due to dependency. The goal is to give motivation to the differently abled and elderly people to operate home systems independently which will boost their confidence. People with speech impairment are mostly benefited as it does not involve any voice commands. In this system sensing is done by a Brain wave sensor instead of placing a camera for detection. An additional feature of controlling the devices using voice command is also proposed. The proposed system is designed involving two domains, Iot (Internet of Things) and BCI (Brain Computer Interface).

Riera et al proposed the Unobtrusive Biometric System Based on Electroencephalogram Analysis [2]. Rapid and unobtrusive authentication methods were presented that used 2 frontal electrodes referenced to another one placed at the ear lobe. In this system we used a multistage fusion architecture which improves the system performance.

D. La Rocca presented Human Brain Distinctiveness based on EEG Spectral Coherence Connectivity [3]. The use of EEG biometrics, for the purpose of automatic people recognition, has received increasing attention in recent years. Most of the current analyses rely on the extraction of features characterizing the activity of single brain regions, like power spectrum estimation, thus neglecting possible temporal dependencies between the generated EEG signals. However, important physiological information can be extracted from the way different brain regions are functionally coupled. Brigham and B. V. K. Vijaya Kumar presented Subject Identification from Electroencephalogram (EEG) Signals During Imagined Speech [4].

In the proposed system, a novel approach is proposed that fuses spectral coherence-based connectivity between different brain regions as a possibly viable bio-metric feature.

II. PROPOSED SYSTEM

The first part of the system is automation using BCI. Voice command is widely used for most of the automations but can't be effectively used in noisy environments. Hence Brain Computer Interface (BCI) is proposed that uses brain wave signals for the control of devices by using an electrode. The frequency band of the brain waves, frequency and status of brain waves is shown in the table given below.

TABLE 1 : BRAIN WAVES FREQUENCY BAND

Frequency band	Frequency	Brain states
Gamma (γ)	35 Hz	Concentration
Beta (β)	12–35 Hz	Anxiety, dominant, active, external attention, relaxed
Alpha (α)	8–12 Hz	Very relaxed, passive attention
Theta (θ)	4–8 Hz	Deeply relaxed, drowsiness, inward focused
Delta (δ)	0.5–4 Hz	Sleep

An electroencephalogram is a measure of the brain's voltage fluctuations as detected from scalp electrodes. It is an approximation of the cumulative electrical activity of neurons. Electroencephalography (EEG) is the most studied potential non-invasive interface, mainly due to its fine temporal resolution, ease of use, portability and low set-up cost. But as well as the technology's susceptibility to noise, another substantial barrier to using EEG as a brain–computer interface is the extensive training required before users can work the technology. There are several types of brain waves generated from the user's brain. Each type of wave is generated when a certain operation is performed.

Table 1 shows different brain waves generated from the human brain with respect to different actions performed. Neurosky mindwave sensor (Fig.1) is the best option as the headband is fast to attach and works on dry skin without any gels. It only needs electrical contact on the forehead and earlobe. NeuroSky devices measure attention and meditation, eye blinks, as well as the raw brainwave data from the user's brain. Various waveforms generated from various brain signal patterns and eye blinks are studied from various references taken and the results are obtained based on the data collected.

The second part of the system deals with automation using voice commands by arduino UNO, Bluetooth module and a smartphone.

A. Neurosky Mindwave

The Mind Wave sensor from NeuroSky (Fig. 1), is a headset that uses EEG technology to safely measure and transfer the brain waves from the user's brain (alpha waves, beta waves, etc.) as data via Bluetooth module to wireless communication to PC.

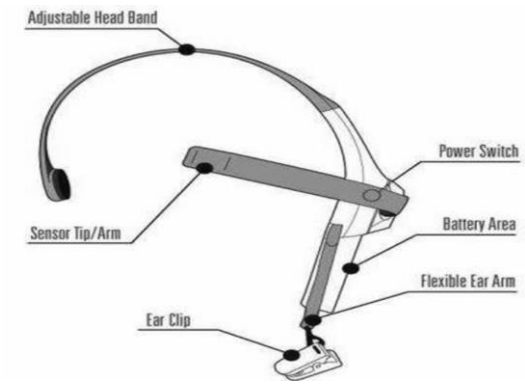

Figure 1 Neurosky Mindwave sensor (Image Courtesy: Neurosky)

III. METHODOLOGY

The first part of the proposed system is shown in Fig.1. The system involves components like Neurosky mindwave sensor, PC, Arduino and a Bluetooth module. The software used is Neurosky Mindwave driver, MATLAB software and Arduino IDE. MATLAB 32 bit programming and Embedded C.

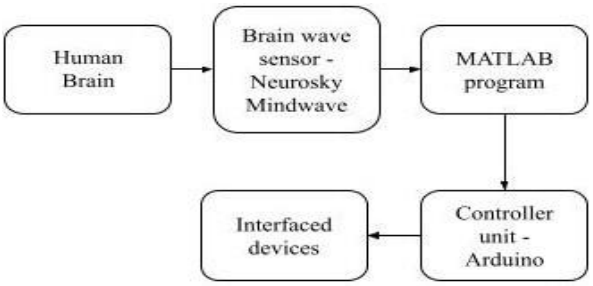

Figure 2 Proposed system Block Diagram (BCI)

1. Extraction of raw brain wave data from the neurosky mind wave and transferred to laptop/PC via Bluetooth.
2. Development of an algorithm for control of the module.
3. Matlab will be used for simulation of the algorithm.
4. Control of the module with the brain wave data using arduino.

The system is designed to control four different operations : turning on and off the light, turning on and off the fan which meets the basic needs of a disabled person. In addition a DC motor is added which can be implemented in wheelchair movement setup. The detailed block diagram is shown in Fig.3 which explains the flow of the system implemented.

The brain wave sensor is placed on the head to collect the brain wave signals (raw data) which occur due to the minuscule electrical discharge caused by the interaction of neurons. The brain wave sensor is connected to the laptop/PC through the Bluetooth module. The commands used are brain waves generated by our attention and meditation level like alpha and beta waves and eye blinking and they are fed to the MATLAB program. The inputs are shown in Fig.4 flow diagram.

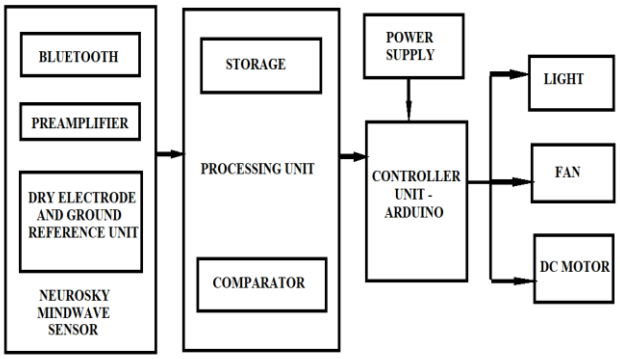

Figure 3 Detailed Block Diagram

The raw data is extracted from the signal and processed using the MATLAB platform which is the part of the data processing unit using the amplitude and time period of the brain wave signal. Each action has a specific amplitude and time period range specified in the program to perform the

required action. The data from this is given to the controller unit to control and operate the interfaced modules.

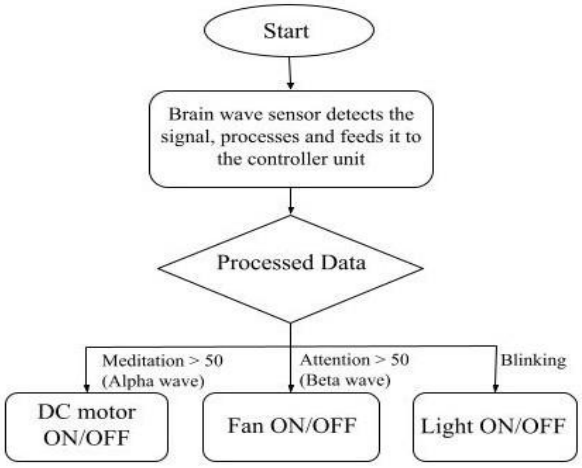

Figure 4 Flow diagram of the operation of the system

The proposed system could be used for the differently abled and elderly people to control appliances from a place. It requires no voice command required so can also be used in noisy environments and will be very useful for dumb people. Independent control over the home operations like switching on/ off of home appliances. Highly configurable, more versatile and accessible. Simple, cost efficient and can be implemented easily.

It will be quite difficult to acquire proper signals for a good classification as BCI is still under research and development. The user's condition and the environment be proper as it is very important to receive proper signals for the classification. From this proposed BCI system further improvements can be made to make a wheelchair movement setup by adding further commands.

The second part of the system deals with automation using voice commands. Arduino UNO is made to serially communicate with the HC-05 Bluetooth module and a smartphone for sending voice commands to Bluetooth module. For receiving voice commands we are using the "Arduino Bluetooth Voice Controller" android app which can be downloaded from the play store. The commands are coded in the arduino which is transmitted via bluetooth from the receiver. The block diagram of this system is given in Fig 5.

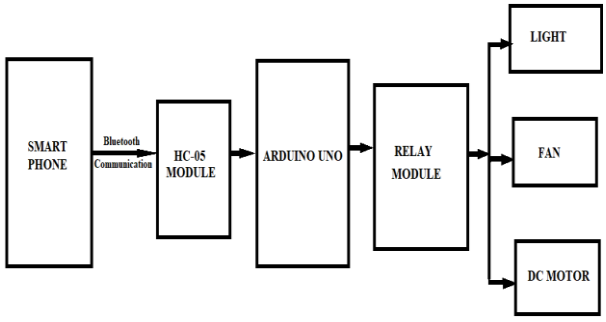

Figure 5 Proposed system block diagram (voice command)

IV. Results and Discussion

The BCI part of the proposed system is implemented by controlling the interfaced devices by turning on/off the fan, light and Dc motor and the desired results obtained are shown. The entire module setup is shown in Fig.6 and the sensor we used is the Neurosky mindwave v1.0 EEG headset which is shown in Fig.7.

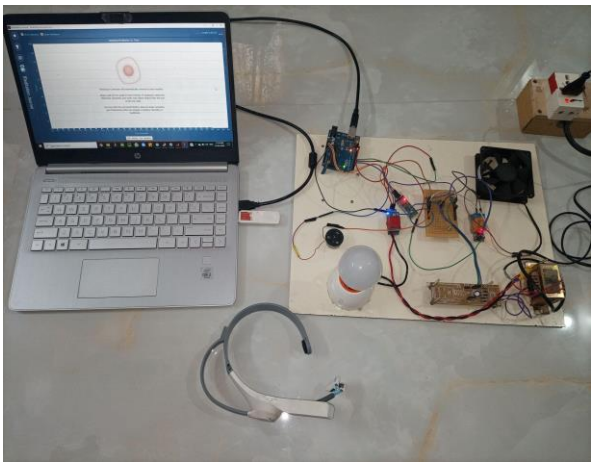

Figure 6 Module setup

Figure 7 Neurosky Mindwave v1.0 EEG Headset

The electrode is placed on the forehead which senses the brainwaves. The blinks and attention, meditation levels are sensed by the brain wave sensor, waveform generated and the data is sent to laptop/PC via Bluetooth and processed in the Matlab platform. The data is then sent to the arduino and the devices are controlled.

The graph representing the waveform in MATLAB software is the Time vs Attention/Meditation/Blink level graph. The attention and meditation waveforms shows how the user is attentive and focussed with respect to the time. The red waveform represents attention, the blue waveform represents meditation, the black waveform represents the blink level with respect to time .

- Attention level is high --> Beta Waves
- Meditation level is high --> Alpha Waves

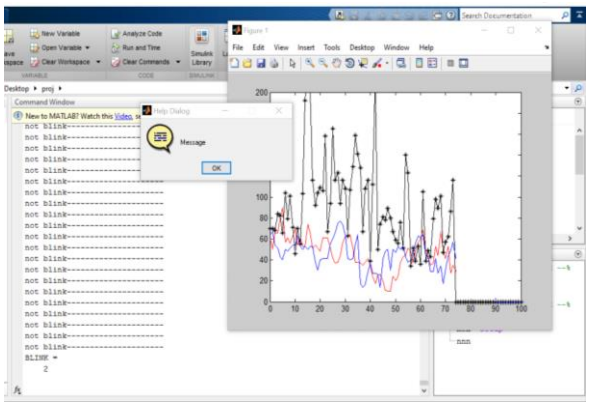

Figure 8 Output simulated from Matlab when blinking

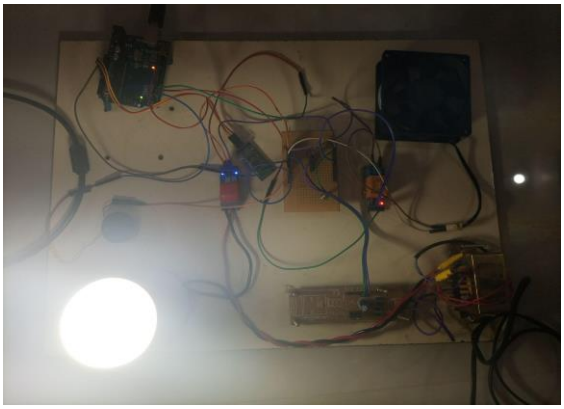

Figure 9 Light turned ON

The matlab simulated output when the blinking is detected is shown in Fig. 8. When blinking is detected the light is turned ON/OFF as shown in Fig. 9

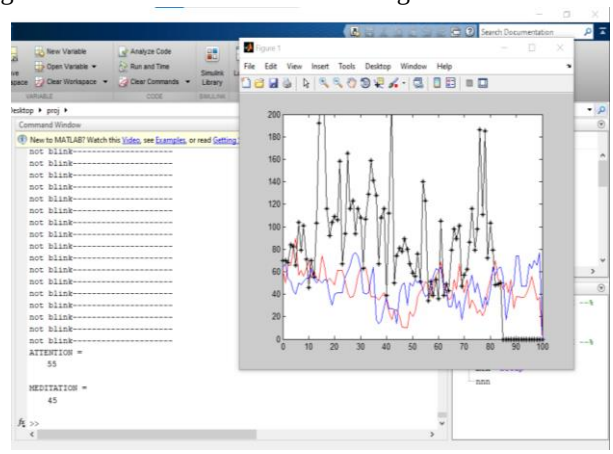

Figure 10 Output simulated from Matlab when attention level is above 50 (Beta wave)

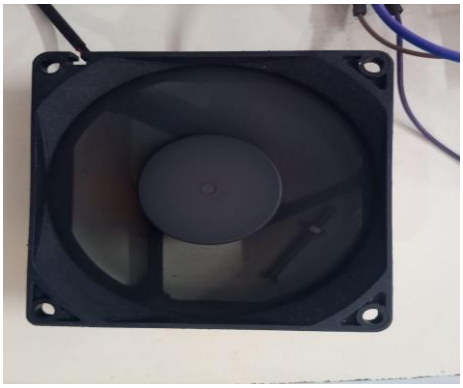

Figure 11 Fan turned ON

The matlab simulated output when attention and meditation levels are above 50 as coded are shown in Fig.10 and Fig. 12. When attention level is above 50 the fan gets turned on as shown in Fig.11. When meditation level is above 50 then the dc motor runs as shown in Fig.13

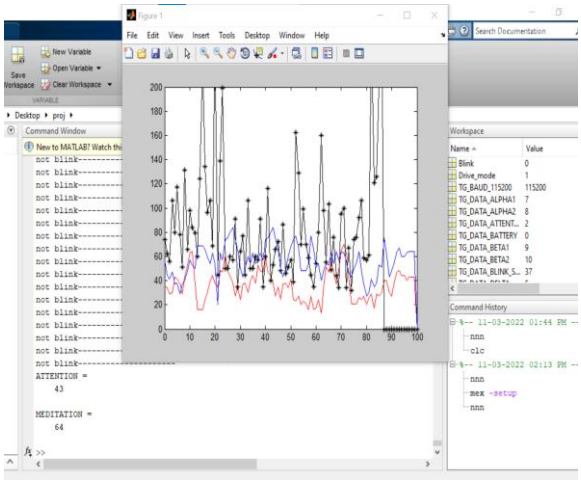

Figure 12 Output simulated from Matlab when meditation level is above 50 (Alpha wave)

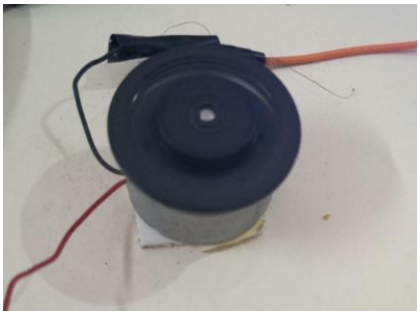

Figure 13 DC motor turned ON

The additional part of the system using voice command is also implemented by controlling the above mentioned devices by the voice commands “Light ON/OFF”, “DC fan ON/OFF”, “Motor ON/OFF” which are taken as input as coded in the arduino.

V. Conclusion

In this work, the Brain Computer Interface (BCI) is introduced in which brain wave signals are used to control devices. The control of devices is solely based on brain signals received from the user. The BCI senses the brain signal by eye blinks and attention, meditation levels to control the modules from a place without moving which will be very useful for people like differently abled and elders who are mostly dependent on operating these systems. Thus the results are obtained and implemented

VI. Future Work

The proposed method may be used for Implementation of Music Controller, Improvement in the Model Architecture Mobile , Implementation of the System, Scaling the Project to Deployment Level, Controlling the movement of the robot by dividing the direction in forward, backward, left and right side. Automotive Applications such as thoughts to accomplish a number of tasks like finding a parking spot etc. Industrial Applications can be used to perform operations without involving any human intervention. Remote controls can be replaced with Brain Computer Interface (BCI).

REFERENCES

[1] Shih, J.J., Krusienski, D.J. and Wolpaw, J.R., 2012, March. Brain-computer interfaces in medicine. In *Mayo clinic proceedings* (Vol. 87, No. 3, pp. 268-279). Elsevier.

[2] A. Riera, A. Soria-Frisch, M. Caparrini, C. Grau, and G. Ruffini, "Unobtrusive biometric system based on electroencephalogram analysis," *EURASIP J. Adv. Signal Process*, January 2008.

[3] D. La Rocca, P. Campisi, B. Vegso, P. Cserti, G. Kozmann, F. Babiloni, and F. De Vico Fallani, "Human brain distinctiveness based on eeg spectral coherence connectivity," *IEEE Transactions on Biomedical Engineering*, no. 9, 2014.

[4] Brigham and B. V. Kumar, "Subject identification from electroencephalogram (EEG) signals during imagined speech," in Proceedings of the IEEE Fourth International Conference on Biometrics: Theory, Applications and Systems (BTA10), 2010.

[5] D. La Rocca, P. Campisi, and G. Scarano, "On the repeatability of EEG features in a biometric recognition framework using a resting state protocol," in *BIOSIGNALS 2013*, 2013.

[6] P. Campisi and D. La Rocca, "Brain waves for automatic biometric based user recognition," *Information Forensics and Security, IEEE Transactions on*, vol. 9, no. 5, pp. 782–800, May 2014 .

[7] Kostilek and J. Stastny, "EEG biometric identification: Repeatability and influence of movement-related EEG," in IEEE International Conference on Applied Electronics, 2012.

[8] B. Armstrong, M. Ruiz-Blondet, N. Khalifian, K. Kurtz, Z. Jin, and S. Laszlo, "Brainprint: Assessing the uniqueness, collectability, and permanence of a novel method for ERP biometrics," *Neurocomputing*, vol. 5, 2015.

[9] Branislav Mados, Norbert Adam, Jan Hurtuk, Marek Copjak "Brain-Computer Interface and Arduino Microcontroller Family Software Interconnection Solution" in *IEEE International Conference on Applied Electronics*, 2016.

[10] V. K. K. Shivappa, B. Luu, M. Solis and K. George, "Home automation system using brain computer interface paradigm based on auditory selective attention," *2018 IEEE International Instrumentation and Measurement Technology Conference (I2MTC)*, 2018

[11] M. Rajmohan, S. C. H. Vali, A. Raj and A. Gogoi, "Home Automation using Brain Computer Interface (BCI)," *2020 International Conference on Power, Energy, Control and Transmission Systems (ICPECTS)*, 2020

[12] Simoens, P., Ingelbinck, T., Gent, B., De Coninck, E., and Vervust, T. (2014). "Vision : smart home control with head-mounted sensors for vision and brain activity," in *The 12th International Conference on Mobile Systems, Applications, and Services*

[13] Andre Ferreira, Wanderley C Celeste, Fernando A Cheein, Teodiano F Bastos Filho, Marai Sarcinelli Filho and Ricardo Carelli (2008): "Human-Machine interfaces based on EMG and EEG applied to robotic systems", *Journal of Neuroengineering and rehabilitation*

[14] K. Kiguchi and Y. Hayashi (2015): "Motion Estimation based on EMG and EEG Signals to Control Wearable Robots", *IEEE International Conference on Systems, Man and Cybernetics*

[15] S. Marcel and J. D. R. Millan, "Person authentication using brainwaves (EEG) and maximum a posteriori model adaptation," *IEEE Transactions on Pattern Analysis and Machine Intelligence*, vol. 29, no. 4, pp. 743– 748, 2006.

[16] M. N*a*¨pflin, M. Wildi, and J. Sarnthein, "Test-retest reliability of resting EEG spectra validates a statistical signature of persons," *Clinical Neurophysiology*, vol. 118, no. 11, pp. 2519 – 2524, 2007.

Soil Nutrient Analysis Using Iot for Yield Prediction

Selvi M[1], Sheeba Joice C[2], Jeffin Gracewell J[3]

[1–3]*Saveetha Engineering College, Chennai*

Abstract—Site Specific management (SSM) with IoT is one of the novel agricultural practices followed recently to increases farmers crop yield and gain more profits. It involves soil mapping, which is the soil- nutrient analysis to find the suitability of the soil to increase the crop yield. With the increase in demand for food products globally, technology based agricultural practices has been a potential research topic. In this work, an automatic moisture motoring system is highlighted, where the water content present in the soil on the farm field is monitored for better yield prediction. This system introduces sensor technology along with the microcontroller to control the watering of farm field by turning the motor pump ON/OFF. The soil moisture sensor connected along with the IoT based Arduino UNO (microcontroller) senses the soil characteristics like moisture, present in the soil and transmits the information via microcontroller. The temperature and humidity sensor (DHT11) monitor the system and makes the soil suitable of the better agricultural yields. On experimental prototype evaluation using hardware, reveals that the results are found to be promising and can be extended for further real-time implantations. The primary application of this system is mainly for farmers, where they water the farm field to maintain the soil moisture and nutrient content of the soil for higher yields.

***Keywords*—Smart agriculture, IoT, Soil Nutrient, yield prediction**

I. INTRODUCTION

Farms fields with smaller size, are easy for farmers to monitor and take necessary control measure. With the demand for agricultural needs, technology-based Site-Specific management (SSM) is widely referred for better crop monitoring purposes. Soil nutrient content and water levels in the farm fields are the primary essentials for crop production [1-5]. Efficient SMM techniques also reduces water logging issues, and helps with the optimum usage of water resources for agricultural practices. Water is the elixir of life, a valuable resource that mankind cannot exist without it. It is estimated that 70% of the total available fresh Water is being used for agriculture purpose. Earlier days only less amount of water was used for this purpose since the global population was less. But now the demand for water resources is increased as there are about 7 billion people living in the world. By the increase in global population it is appraised that it will reach 9 billion people by the year 2050. With the advancement of electronics and technology, lives of human beings have become much easier and simpler. Everything has become automatic, reducing the human efforts and activities. In countries like India where agriculture is our backbone efforts must be taken to save water in an efficient way. The climatic conditions are isotropic where we cannot predict the requirement of water by the plants at regular intervals and here comes the sensor technology. Based on the method highlighted, a microcontroller along with the soil moisture sensor are used which senses the moisture present in the soil and the motor pump is switched ON/OFF depending on the requirement of the plants. When we don't water the plants, it leads to the mineral loss in the soil and ends up with rotting the plants. As a traditional method farmer use manual control sprinklers, flood type feeding system to alter the moisture water content in the soil. During this process more water is being absorbed by the soil and thus remains wet for long time producing infections on plants which gets dried. With water deficiency, fungal infections take place in plants. These problems can be rectified by using Automatic monitoring technology. In addition to soil moisture sensor we have used temperature and humidity sensor (DHT11) which helps to monitor the plant when the soil moisture sensor fails to work.

Based on literature review few works have already been carried out on soil moisture monitoring. In [6] M. F. Xing et al has developed surface soil moisture retrieval algorithm for vegetation-covered by defining the Dubois model to describe the backscattering from the underlying soil. Here, a novel modified Water Cloud Model (MWCM) was used to achieve the efficiency. In [7], H. Wang et al, studied the two-component polarimetric decomposition at C-band for soil moisture retrieval over agricultural fields for certain crops such as wheat corn, soybean and canola. In [8], A. Gorrab, et al, proposed a soil moisture estimation based on an empirical change detection approach. Based on their study, improvements soil moisture estimation is found when changes in temporal variations in roughness is introduced. With the amount of work carried out, the major challenge lies with the issues in hardware implementation of the soil moisture estimation in real time. This proposed work highlights the development if the prototype for hardware implementation of the soil moisture estimation and necessary controlled actions based on the estimated parameters.

II. MEHODOLOGY

The main working principle behind this system is in using the soil moisture sensor along with the Arduino UNO which is also connected to other electronic components. Measurement of the soil moisture is done by the soil moisture sensor which forwards the information and

parameters regarding it to the microcontroller (Arduino UNO). The microcontroller then controls the pump by turning the switch ON. If the moisture present in the soil is below the threshold level then the micro controller sends the signal to the relay module which in turn runs the pump and water is supplied to the plants. The buzzer produces a beep sound to indicate that water is supplied to the plants. Once enough water is supplied the pump stops working.

A. Hardware Overview Description

The components used in this work involves the following.

- Arduino UNO,
- Soil moisture sensor(LM 393),
- DHT 11 sensor,
- Servo motor,
- Water pump,
- Relay module,

The power supply to the Arduino must range between 7v-12v.The soil moisture sensor is been connected to the analog pin of the Arduino UNO such that the exact value of the moisture present in the soil is obtained. When the soil moisture sensor fails to work the DHT 11(temperature and humidity sensor) monitors the watering of the plants. The sensor integrated with the IoT device, detects the temperature and the humidity of the surrounding environment and transmits the signal to the micro controller which in turn sends the command to the relay as well as the pump which is connected with the servo motor to carry out automated irrigation system. The value of these sensors and the status of the motor pump is displayed on the LCD screen.

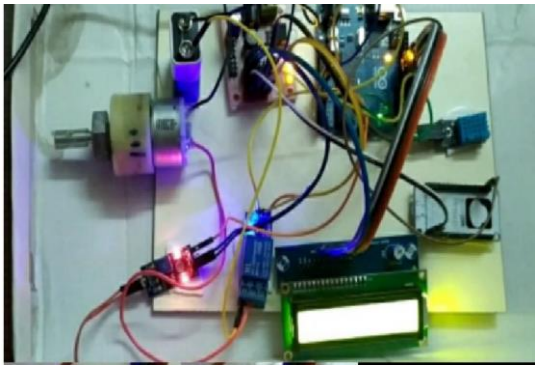

Figure 1: Overview of the hardware Architecture.

B. Prototype for Soil Nutrient Analysis

To monitor the nutrient content of the soil, manual tests were carried out. The testing kit consisted of a capsule system, to detect the amount of nutrient content in the soil. The procedure followed here is to take a sample of soil, mix with water, transfer some of the solution to the color comparator, add powder from the capsule, shake and watch the color develop. Based on the color chart the nutrient content present in the soil can be determined. For better yield, the soil nutrient conditions are to be tested periodically throughout the growing season for the crop. Fig 2 shows the Capsules and test tubes used for Soil testing and. Fig 3 shows the color comparator Chart for measurement of the nutrient content.

Figure 2 Capsules and test tubes used for Soil testing

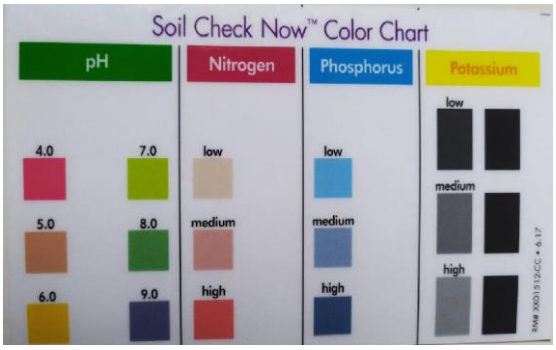

Figure 3 Color comparator Chart for measurement

III. RESULTS & DISCUSSION

A. Analysis On Ground Water Resources

The rainfall in Tamil Nadu is seasonal. According to the recent survey by Tamilnadu (TN) water supply and drainage board The annual rainfall in the state is 960 mm. Approximately 33% from south west monsoon and 48% from north east monsoon.

TABLE1: CHART HIGHLIGHTING THE SEASONAL RAINFALL IN TN

Season	**Month**	**Average rainfall in mm**
Winter rain	Jan-Feb.	47
Summer rain	May	138
SW monsoon	June-sept.	322
NE monsoon	Oct-Nov.	470-970

The total surface water potential of the river basins of Tamilnadu is assessed as 853 TMC.

- 39000 tanks with storage capacity-347 TMC.
- 79 reservoirs with storage capacity-243 TMC.
- Others states -2 TMC.

The average run off (surplus flow) to the sea from the 17 basins of TN state is computed as 177.12 TMC.[14]

By the recent survey of TN-ENVIS, the total ground water available is 22,423 MCM (million cubic metre) and the net ground water draft i.e., the quantity of water withdrawn is 13,558 MCM. Thus, the available balance for use is 8875 MCM. Over the past five years, the percentage of safe blocks has been declined from 35.6% to 25.2%. Over exploitation has already occurred in more than a third of the block (35.8%) and eight blocks (2%) have become saline [15]

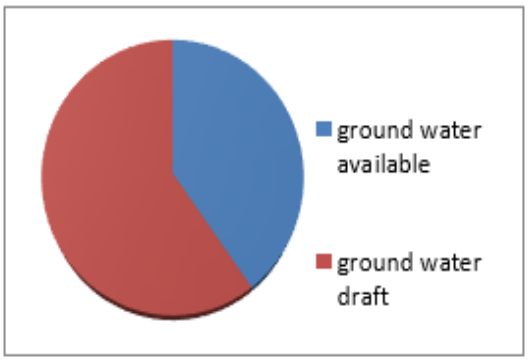

Figure 4 Ground Water availability

This analysis shows that both seasonal rainfall and the surface water couldn't satisfy the demands of the people. The farmers on the farm land are solely dependent on rain and bore wells for irrigation but at most of the times they do not get the adequate water for their agricultural activities. We fail to preserve the surplus water that runs off to the sea. As the population grows and more food is required, better water management is essential. This proposed project will make the farmer to use water in an efficient way.

B. Evaluation on Soil-Nutrient content

With the help of the capsules, the colour content of the water mixed with the soil changes. On finding the similarity measure of the colour content with the colour chart, the measure of nutrient content can be determined. Table 2 shows the test result of nutrient content, Fig 5, Fig 6 and Fig 7 depicts the results for the manual test carried for determining the Nitrogen, Phosphorus, and the Potassium content.

TABLE2: INTERPRETING NUTRIENT TEST RESULTS

		Field	Garden	Field	Garden
		kg/hectare	g/m2	lb/acre	oz/10 ft2
Nitrogen (N)	low	45	5	40	0.1
	medium	179	18	160	1.6
	high	359	36	320	1.2
Phosphorus (P)	low	9	1	8	0.03
	medium	22	2	20	0.1
	high	72	7	64	0.2
Potassium (K)	low	45	5	40	0.1
	medium	90	9	80	0.3
	high	179	18	160	0.6

Figure 5 Similarity measure check to determine the Nitrogen content

Figure 6 Similarity measure check to determine the Phosphorus content

Figure 7 Similarity measure check to determine the Potassium content

C. Evaluation of The Hardware Setup

The Fig 8 depicts the experimental setup and the results obtained for different value of the moisture content. Whenever a need for water moisture was recognized by the sensor, microcontroller sends the signal to the pump to start watering the crop land until enough quantity of water is supplied to the soil. This has been tested and applied in the roof gardens and the system was under observation to the test the stability of the system for a longer period. This helps in minimizing the manual intervention of the farmers and also prevents the excessive loss of water.

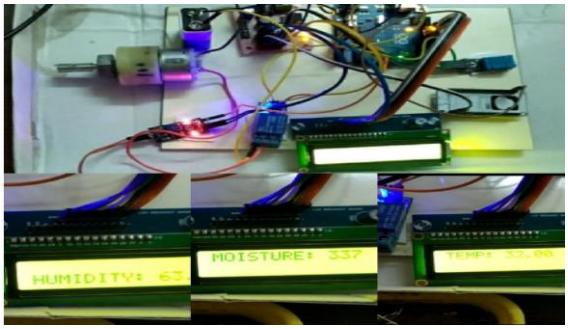

Figure 8 Experimental setup and the results obtained

IV. SCOPE FOR FUTURE WORK

As a part of future work, it involves, building an AI based recommendation system that recommends the best possible information for soil conditioning for better yield and productivity. Content based filtering is used to build the recommendation system which gives the specification requirements details for soil conditioning. The initial data collection to build the recommendation system is obtained from the online resources and also from the data obtained from the preliminary investigation which were done earlier.
The work can be extended to implement a hardware architecture for weed detection using vison-based algorithms. Vision based semantic segmentation is used to detect the weeds from the high-resolution ground imagery

obtained from the farm field.

V. Conclusion

In this article, a recent challenge faced by farmers for better agricultural practices is addressed. With the global demand for food production, technology-based precision agricultural practices are the need of the hour. Agriculture backbone of our country, India this work enlight to envision on the hardware implementation of soil nutrient analysis using IoT for better yield prediction. Further, AI based recommendation systems and weed detection system are to be carried our as a part of our future work.

References

[1] P. Chivenge and S. Sharma, ‘‘Precision agriculture in food production: Nutrient management,’’ in Proc. Int. Conf. ICTs Precis. Agricult., 2019, p. 12.

[2] A. Viña, A. A. Gitelson, A. L. Nguy-Robertson, and Y. Peng, ‘‘Comparison of different vegetation indices for the remote assessment of green leaf area index of crops,’’ Remote Sens. Environ., vol. 115, no. 12, pp. 3468–3478, Dec. 2011.

[3] R. E. Plant, ‘‘Site-specific management: The application of information technology to crop production,’’ Comput. Electron. Agricult., vol. 30, nos. 1–3, pp. 9–29, Feb. 2001.

[4] P. S. Thenkabail, J. G. Lyon, and A. Huete, Advanced Applications in Remote Sensing of Agricultural Crops and Natural Vegetation. Boca Raton, FL, USA: CRC Press, 2018.

[5] A. Viña, A. A. Gitelson, A. L. Nguy-Robertson, and Y. Peng, ‘‘Comparison of different vegetation indices for the remote assessment of green leaf area index of crops,’’ Remote Sens. Environ., vol. 115, no. 12, pp. 3468–3478, Dec. 2011.

[6] B. He, M. Xing, and X. Bai, “A synergistic methodology for soil moisture estimation in an alpine prairie using radar and optical satellite data,” Remote Sens., vol. 6, no. 11, pp. 10966–10985, Nov. 2014.

[7] M. F. Xing et al., “Retrieving surface soil moisture over wheat and soybean fields during growing season using modified water cloud model from Radarsat-2 SAR data,” Remote Sens., vol. 11, no. 16, Aug. 2019, Art. no. 1956.

[8] H. Wang, R. Magagi, and K. Goita, “Potential of a two-component polarimetric decomposition at C-band for soil moisture retrieval over agricultural fields,” Remote Sens. Environ., vol. 217, pp. 38–51, Nov. 2018.

[9] A. Gorrab, M. Zribi, N. Baghdadi, B. Mougenot, P. Fanise, and Z. L. Chabaane, “Retrieval of both soil moisture and texture using TerraSAR-X images,” Remote Sens., vol. 7, no. 8, pp. 10098–10116, Aug. 2015.

[10] C. Tong et al., “Soil moisture retrievals by combining passive microwave and optical data,” Remote Sens., vol. 12, no. 19, 2020, Art. no. 3713.

[11] Gracewell, J., John, M. Dynamic background modeling using deep learning autoencoder network. Multimed Tools Appl 79, 4639–4659 (2020). https://doi.org/10.1007/s11042-019-7411-0

[12] https://www.hackster.io/neetithakur/automatic-plant-watering-system-using-arduino-uno-8764ba

[13] http://www.circuitstoday.com/arduino-irrigation-plant-watering-using-soil-moisture-sensor

[14] https://www.researchgate.net/publication/283230079_Implementation_of_an_automated_irrigation_system_Smart_irrigation_system_paper_subtitle

[15] http://www.twadboard.gov.in

[16] http://tnenvis.nic.in/Database/TN-ENVIS_791.aspx

CNN Based Food Calorie Recognition for Dietary Assessment

R. Pavithra Guru[1], G. Sai Vamsi[2], J. Srinivas[3], D. Sri Mounisha[4]

[1]Department of Electronics and Communication and Engineering,SRM Institute of Science and Technology, Ramapuram Campus, Chennai-89

[2,3,4]Department of Computer Science and Engineering,SRM Institute of Science and Technology, Ramapuram Campus, Chennai-89

Abstract: In recent years, people tend to consume excess junk food and are unaware of the amount of calories taken. To have a healthy diet, people need to calculate the calorie count before eating. We have developed a calorie management system using deep learning algorithms from images provided by users to enable users to track their daily calorie intake. It can be used for daily calorie tracking for health enthusiasts. It can also provide information about food ingredients. This model uses the Gray Level Co-occurrence Matrix and the Discrete Wavelet Transform.The Time Complexity of this model has been reduced in order to deliver the quickest results, which is its primary benefit. Using this model, people can determine how many calories they need to eat each day in order to avoid health problems. People who consume an excessive amount of calories can use this model to learn about their food intake's nutritional value.

***Keywords*—Gray Level Co-occurrence Matrix, Discrete Wavelet Transform, Deep learning, food calories,ingredients.**

I. INTRODUCTION

Calorie tracking has become one of the important aspects of a healthy lifestyle today especially during the pandemic. People are more concerned about how many calories they consume on a daily basis, but tracking calories is not an easy task or requires you to manually track calories by weighing food ingredients. Alternatively, people must use a fitness tracking device. Using this method suggested by this model will make this process more tedious. Users simply take a picture of the food and the developed algorithm determines how many calories the food contains.This model uses deep learning, GLCM and DWT to track and manage calories.

Deep learning is a subset of machine learning and artificial intelligence that includes neural networks. This neural network mimics the human brain. Neuronal networks are composed of three layers: the "input," "hidden," and "output" layers, which are all interconnected with one another and with the outside world. There are three layers: the input layer, the hidden layer for prediction, and the output layer for conveying the outcomes.

A Statistical method of studying textures considering the spatial attitude of pixels is a crushing matrix. The gray profile (GLCM) is also known as a spatial dependent gray matrix.The GLCM function generates GLCM in the spatial relationship in the image and then extracts statistical measurements from this matrix to characterise image textures. It is a pair of pairs with a specific value. (The texture filter function described in calculation of texture statistical action can not provide information about the spatial relationship of the image of the image).

A Discrete Wavelet Transform is a transform technique that uses a set of wavelet scales to change the conformity to specific rules. This method divides the signal into orthogonal sets of wavelets, which distinguishes it from the continuous wavelet transform or its discrete time sequence implementation, which is also known as the discrete time continuous wavelet transform.

II. RELATED WORK

Chen & Li, 2021, proposed Deep Recipes, a predictive model for extracting ingredient quantities from online text recipes. Based on the name of a recipe and the ingredients listed, this model predicts the amount of ingredients. To train the data set, they employed SVM, Random tree classifier, and K-means clustering to predict the ingredients to a collection of recipes that yields the proper calorie count. Turmchokkasam & Chamnongthai, 2018, proposed a methodology for detecting calories and ingredients in food using nutritional knowledge and heat information. In this method, the food image is initially identified as a food type, and the food ingredients identified are collected from the input dataset, along with nutritional information and brightness patterns. The image is separated into material candidate limits, and each limit is categorised as a material using fuzzy logic based on thermal models. Finally, using the area ratio to total calories and nutritional information, classifying ingredients from all limits are computed. Hu & Zhang, 2020, calculated the calorie values of various popular Chinese and Western cuisines using object recognition. Several image-based calorie estimation methods have been created based on input photos and predefined nutritional data. This allows users to correctly identify the titles of various dishes while also providing nutrition plans. To identify a dish, a single-shot multi-box detector is employed for real-time object recognition and categorization. A computer application called "labelling" is used to name each dish. Ankitha & Pragati, 2017, developed a neural network-type model that guesses the contents of the food from the given input image and displays the estimated calories of the discovered food. To do this, they produced a

dataset of approximately 23,000 photos, as well as 23 different food categories, and trained CNNs using Inception V3 features.Balbin & Valiente, 2019, proposed effective methods for measuring and managing patients' and nutritionists' daily food intake. The system uses image processing, segmentation, and classification to calculate the nutritional and calorie content of food. The proposed system will undoubtedly improve and promote existing calorie measurement methods. We'll use the Food Part Recognition System to calculate calories and nutritional value in this article. Mokshada and Jyoti, 2020 proposed a model based on still images that employs a thermal camera in a hardware system to predict the ingredient and calorie count of food, focusing on chicken and fish. Convolutional neural networks (CNNs) were built-in algorithms that were used to identify food in images. Ayon & Mashrafi, 2021, Created a cloud-based calorie consumption report generation system, as well as a canteen ordering system that allows customers to place orders at any time and from any location. This system was created in response to issues in the food industry.

III. PROPOSED SYSTEM

Input image includes food recipes. The captured image is then re-sized as in line with the requirement. Image is scaled into 200 * 200 dimensions after which eliminates needless distortions in image pixels. This guarantees correct prediction. The image obtained from the above technique is transformed from RGB to HSV. This technique converts Red, Blue, and Green shades to Hue Saturation Values. After color conversion, function extraction is done. The technique of translating uncooked records into numerical capabilities that may be processed at the same time as preserving the data with-inside the authentic records set is known as function extraction. It produces higher consequences than simply making use of device studying to uncooked records. Gray-Level Co-Occurrence Matrix and Discrete Wavelet Transform are utilized in function extraction. The GLCM capabilities outline an photograph`s texture through calculating how regularly pairs of pixels with given values and in a particular spatial courting seem in an photograph, producing a GLCM, after which extracting statistical measures from this matrix. After you've got created the GLCMs with graycomatrix, you could use graycoprops to get a whole lot of records from them. These records provide data on an photograph's texture. This numerical uncooked records from function extraction is similarly dispatched to neural networks. A neural community is a hard and fast of algorithms that tries to hit upon underlying relationships in a batch of records the use of a method just like how the human mind works. A neural community includes 3 different of

Layers: input layer, hidden layer, and output layer. Input layer takes the uncooked records and hidden layers are used for mathematical operations this residue enables us to discover meals with-inside the image and energy of meals with-inside the photograph. Output layer offers the calorie rely of the meals recipe. Figure 1 describes the architecture diagram of this model.

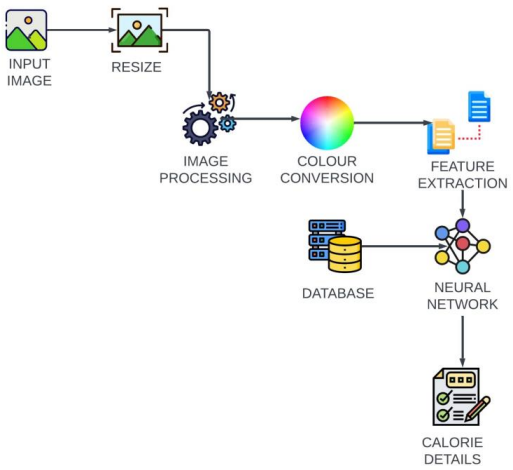

Figure 1 : Architecture Diagram

IV. MODULES

A. *Preprocessing*

Preprocessing is the fundamental step in training the images in the data set, allowing the algorithms to be applied to the image. This module employs a digital image processing method that eliminates unnecessary distortions in each and every pixel of the image. Digital image processing improves image sharpness and provides the best visual quality. That image will be used in a subsequent process to apply algorithms and various methods to it. This process does not increase the image's data but rather decreases it if unwanted data is present.The below figure 2 represents the Digital Image Processing.

Figure 2: Digital Image Processing

B. *Color Conversion*

The primary colours in any image are red, green, and blue, which are referred to as RGB. In this method, the RBG colours are converted to hue, saturation, and value shades in order to make the image match with the input database. The hue saturation process is applied to the red, green, and blue colors in the image and will convert them into tint, shade, and tone variations before sending the image to be processed further.In order to convert into the hue saturation area, each colour type requires a unique formula.

Red-Green Sector:

$$for\ 0^\circ < H \le 120^\circ$$

$$b = \frac{1}{3}\left(1 - S\right),\ r = \frac{1}{3}\left[1 + \frac{S\cos(H)}{\cos(60^\circ - H)}\right],\ g = 1 - \left(r + b\right) \quad (1)$$

Green-Blue Sector:

$$for\ 120^\circ < H \le 240^\circ$$
$$r = \frac{1}{3}\left(1 - S\right),\ g = \frac{1}{3}\left[1 + \frac{S\cos(H)}{\cos(60^\circ - H)}\right],\ b = 1 - \left(r + b\right) \quad (2)$$

Blue-Red Sector:

$$for\ 240^\circ < H \le 360^\circ$$
$$g = \frac{1}{3}\left(1 - S\right),\ b = \frac{1}{3}\left[1 + \frac{S\cos(H)}{\cos(60^\circ - H)}\right],\ r = 1 - \left(r + b\right) \quad (3)$$

Equation (1,2,3) helps to achieve the correct color conversion.

C. Feature Extraction

Gray-Level Co-occurrence Matrices are used in this module to convert the pixel data of the input image into digital raw data. It will be represented in matrix form. The pixel data will be referred to as grey levels in this manner, and the number of grey levels will determine the size of the matrix.Figure 3 potrays the GLCM Feature Extraction.

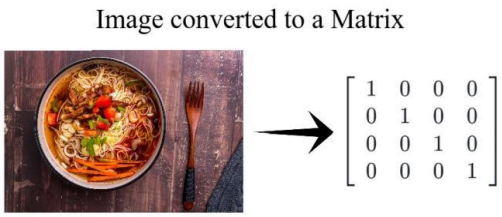

Figure 3: Gray Level Co-occurrence matrix

D. Prediction:

The final phase of our model is to use deep learning algorithms to predict the ingredients and calories of the given food recipe in the supplied input image. The convolutional neural network is a deep learning algorithm that is utilized in the prediction process. It makes a comparison between the input image and the input data set.The below figure 4 represents the prediction.

Figure 4: Detection

V. Result And Discussion

The output displays the ingredients and calorie count of the food recipe shown in the input image. The accuracy was quite satisfactory. The graph below depicts the method's accuracy. Below are some examples of input and output images. The input is a food recipe, and the output is a list of the ingredients used in the recipe as well as their respective calories. Figure 5 and 6 represents the input and output images.

Figure 5: Input

noodles

	Serving	Ingredient	Calories
0	10 tsp	vegetable oil	1240
1	20.95 g	onion springs	8
2	1/2 gram	ginger & garlic sauce	7
3	0.13 gram	chili powder	0
4	0.11 gram	black pepper powder	0
5	0.15 gram	turmeric powder	0
6	0.58 gram	salt	0
7	70 gram	Cabbage chopped	17
8	80 gram	carrot chopped	32
9	1 tsp	soya sauce	3
10	2 tsp	olive oil / sesame oil	5
11	100 gram	noodles	310
12	1 cup	Noodles	1622

>>>

Figure 6: Output

The figure 7 and 8 compares the Support Vector Machine and the Convolutional Neural Network. The current model makes use of the Support Vector Machine, which has a lower accuracy rate than the suggested Convolutional Neural Network model. Convolutional Neural Network outperformed Support Vector Machine in the Performance Graph. Support Vector Machine produced inconsistent results, but Convolutional Neural Network produced consistent and superior results. The Loss Graph clearly shows that the Support Vector Machine has numerous faults when compared to Convolutional Neural Network.

This System needs minimum hardware and software requirements of our system. The system we used consists of Intel i3 dual core and minimum of 8GB RAM . In order to run the model, Python 3.7 with TensorFlow, anaconda prompt and jupyter notebook should be installed on system. Internet is required to download the pre-trained weights without head from cloud. Hard drive of minimum 100gb.

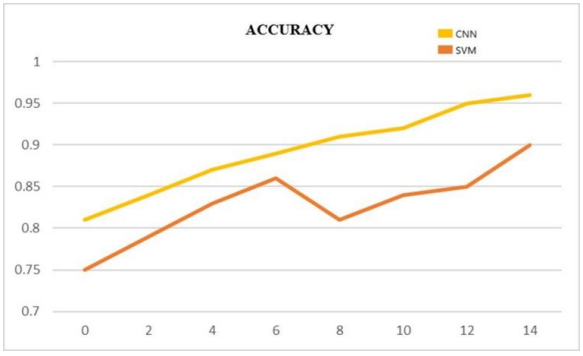

Figure 7: Accuracy Graph

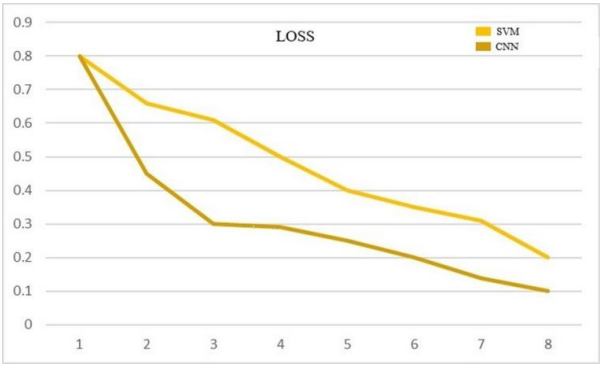

Figure 8: Loss Graph

Many difficulties have arisen as a result of SVM's superior time complexity when compared to CNN. The time complexity of CNN and SVM with different numbers of recipes from the dataset is compared. When compared to SVM, CNN trains the dataset faster. The comparison was done with multiple sets of datasets that included recipe data and the dataset was calculated in seconds, as shown in the Table 1. Complexity, as the name implies, is a measure of how difficult it is to solve a problem. CNN outperforms SVM in this situation.

TIME COMPLEXITY

Dataset (Recipes)	SVM (Seconds)	CNN (Seconds)
100	300	200
50	150	100
25	75	50

TABLE 1: TIME COMPLEXITY TABLE

VI. CONCLUSION

In this model, we demonstrated the implementation of a convolutional neural network and two distinct approaches to detect the ingredients and calorie count. Gray Level Co-occurrence Matrix is a feature extraction module that outperformed current models. When the convolutional neural network and support vector machine algorithms were evaluated, the convolutional neural network performed better than the existing approach, support vector machine. In the future, this model could be integrated into a mobile application that performs better than current model. In the future, the proposed method will be a full mobile application based on this algorithm. A mobile application can make a positive difference in people's lives by assisting them in tracking their daily calorie intake.

REFERENCES

[1] Ankitha, A., & Pragati, D. (2017). Image-Based Food Calories Estimation Using Various Models of Machine Learning. International Journal of Advanced Research in Computer and Communication Engineering, 243-248. DOI 10.17148/IJARCCE.2017.6146

[2] Ayon, S. A., & Mashrafi, C. Z. (2021). FoodieCal: A Convolutional Neural Network Based Food Detection and Calorie Estimation System. National Computing Colleges Conference (NCCC), 1-6. 10.1109/NCCC49330.2021.9428820

[3] Balbin, J. R., & Valiente, L. D. (2019). Determination of Calorie Content in Different Type of Foods using Image Processing. International Conference on HNICEM , 1-6. 10.1109/HNICEM48295.2019.9073397

[4] Chen, Y., & Li, H. (2021). DeepRecipes: Exploring Massive Online Recipes and Recovering Food Ingredient Amounts. IEEE Access,9,67859-67873.10.1109/ACCESS.2021.3077645

[5] Hu, H., & Zhang, Z. (2020). Image Based Food Calories Estimation Using Various Models of Machine Learning . ICMCCE, 1874-1878. 10.1109/ICMCCE51767.2020.00411

[6] Mokshada, D., & Jyoti, K. (2020). CLOUD BASED CALORIE CONSUMPTION REPORT GENERATION IN CANTEEN ORDER SYSTEM. Journal of Emerging Technologies and Innovative Research (JETIR), 7(9), 559-566. http://www.jetir.org/

[7] Turmchokkasam, S., & Chamnongthai, K. (2018). The Design and Implementation of an Ingredient-Based Food Calorie Estimation System Using Nutrition Knowledge and Fusion of Brightness and Heat Information. IEEE Access, 6, 46863-46876. 10.1109/ACCESS.2018.2837046

An Automatic Emergency Ventilator For Covid Patients

Surendhar A[1], Sushma R[2], Venmugil Vannan R[3], Yobishiya Stefi W.J.[4], N. Usha Bhanu[5]

[1-5]Student, Department of Electronics and Communication Engineering, SRM Valliammai Engineering College

Abstract—COVID-19 is a pandemic viral outbreak. All the existing preventing methodologies for COVID have some shortcomings and are short-lived. This system is proposed with the view of achieving a long-term solution for this issue and would help to connect the doctors with the patient without physical contact. It consists of an automatic system. The according to the SPO_2 sensor data the system is function. when the oxygen value is decreased then the proposed system is to perform desired task. This system consists of an ardunio uno and can be controlled remotely by whole system. The SPO_2 sensor can detect the patient's oxygen level and LCD display is used to display the patient's oxygen level . The DC motor can give the pressure to the ambu bag and it will produce the oxygen to breather mask. Thus, this system reduces direct contact among people and would be helpful in reducing the spreading of the deadly virus.

***Keywords*—**COVID, Arudino uno ,SPO2 sensor, DC motor,Ambu bag

I. INTRODUCTION

The recent outbreak of COVID-19 was discovered in 2019 and it is caused by the SARS COV-2 or Severe Acute Respiratory Syndrome. Scientists researched and announced the arrival of a slowly growing pandemic. Now, 208 countries all over the world were fighting with this deadly virus. The medical team is trying its best to find its cure ,it is an individual duty to help them by following the safety measures like wearing masks, following social distancing, and washing hands-on frequent intervals, etc. The doctors and nurse who treated the patients get direct contact with the patient by manually attaching the ventilators. In the second Wave tons of people were affected by the lack of Oxygen,Even the hospitals also had the limited amount of cylinders, Considering all these existing issues, A system is designed which performs automatic ventilation via a device operated using Arduino and dc motor, the Oxygen level is monitor with the help of LCD Display. The system will reduce Oxygen shortages and avoid a direct contact, which in turn reduces the spreading of virus and makes management of COVID more effective and simpler.

II. LITERATURE REVIEW

There are various issues faced by doctors and patients in management of COVID. This alarming pathetic scenario motivated to search for an idea to develop a system which provides solution to all the existing issues and various proposals have been studied to develop this system. Balamurugan et,.al[1] proposed an Design of Ventilator Using Arduino for Covid Pandemic . This ventilator is made with push mechanism in each breath.The entire system is controlled with Arduino and if the oxygen level is low the buzzer is ring and The Motor is used to give the pressure to the ambu bag. When oxygen level count is low this mechanism is performed.From which we gained an idea to construct an motor mechanism to pressures the ambu bag.Leonardo Acho et.al[2]., proposed an Low-Cost, Open Source Mechanical Ventilator with Pulmonary Monitoring for COVID-19 Patients.The construction of low-cost, open-source mechanical ventilator. It demonstrates a numerical approach for monitoring a patient's pulmonary condition using a pressure sensor and an Arduino board to gather data from the sensor and send it to a Raspberry Pi. The raspberry pi instructs the acutor and breathing bag to compress in the appropriate manner.From this,an idea to setup the LCD display is used to monitoring the patients with help of SPO_2 sensor . Sazzad Hossain Sazal[3], proposed an Design and developed a low-cost portable ventilator.This low-cost ventilator delivers breaths by compressing a conventional Bag Valve Mask (BVM) or Ambu bag with a motor drive mechanism, eliminating the need for a human operator.The machine had invasive and non-invasive features, and supports 500-600 mL tidal volume,12 Respiratory rate (RR)/min can provide the patient with the required amount of tidal volume.From this a concept for building a motor mechanism without need of human operation .Rajeev Chauhan,et.al[4].,proposed an Automatic AMBU bag operating device.The principle of an electric linear actuator which converts the rotary motion into a linear motion. A standard adult AMBU was attached to the designed gadget. The frequency of respiratory rate (ranging from 12 to 20 squeezes per minute) for providing the air oxygen mixture into the patient's lungs is modulated by the speed regulator on this DC motor. The Ambu bag can automatically squeeze according to the set parameters. The ambu bag is automatically inflated by the DC motor based on the patient's oxygen level. The goal of this project is to limit corona virus spread by developing an autonomous ventilator for covid patients that does not require human intervention.

III. PROPOSED SYSTEM

Fig 1 depicts the proposed system's block diagram. Arduino uno is used to control the system.The input block consists of SPO_2 sensor which is usually capable to read the oxygen level. The data is then sent to Arduino. Based on the data provided by the SPO_2 sensor, Arduino controls the output block. The data is sent from the Arduino to the LCD display, which displays the value measured by the sensor.The output block consist of DC motor,motor

driver,pressure rod,ambu bag,oxygen mask.

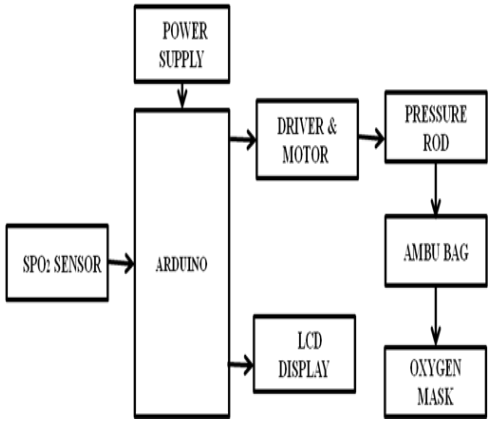

Fig. 1 The proposed system's block diagram

Control circuits work at low current signal whereas motor needs high current signal to work. So, motor driver is required in the circuit. It transforms a low-current signal into a high-current signal and drives the motor. When the mechanical rod is pressed against the ambu bag, oxygen is produced and sent to the breathing mask. Fig 2 depicts the bag value mask or ambu bag. The arduino uno is the project's brain, reading sensor data and controlling I/O devices. Then a DC motor and motor driver are connected to the Arduino, with the motor driver controlling the speed and direction of the motor. The patient's oxygen level and motor speed are displayed on an LCD display. Thus, the device reduces doctor-patient contact and helps in reducing viral spreading of corona. The proposed system's display unit is depicted in Fig 3.

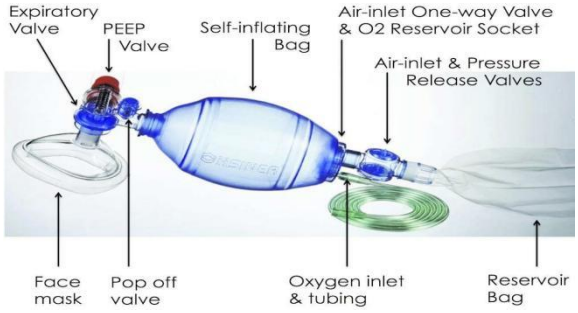

Fig. 2 The bag value mask or ambu bag

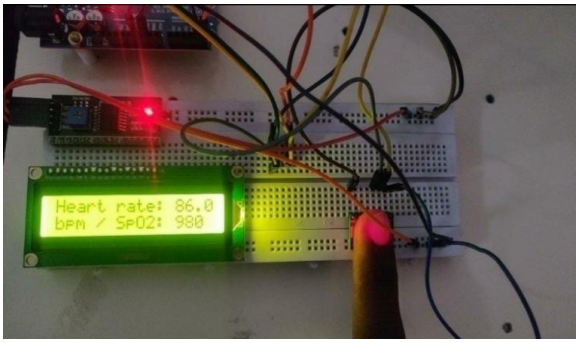

Fig. 3 The Display unit of the proposed system

IV. METHODOLOGY

The Arduino uno is used for remote device access.First, The SPO_2 sensor is attached to an Arduino Uno, and the connections between the Arduino and the LCD display are made using an I2C connector module.Dc motor and motor driver are connected with ardiuno uno and the motor driver is used to control the motor's speed and direction.The pressure rod connected with DC motor, thus DC motor is rotating an rod can be applied the pressure to the ambu bag,this bag is known as manual resuscitators and as self-inflating resuscitation system and it has a various size. The oxygen reservoir, which has two one-way values and an oxygen flow rate equal to or more than the patient's minute volume, permits 100 percent oxygen to be provided to the breather mask and ambu bag, resulting in 12 breaths per minute.By using the LCD display can be easily monitoring patients.

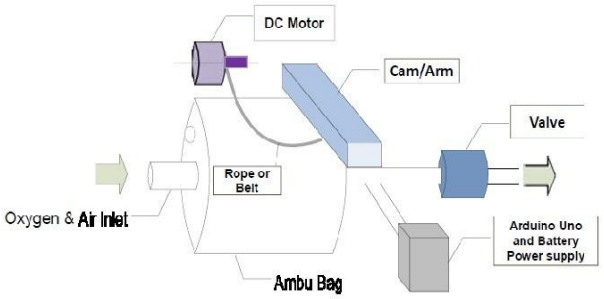

Fig .4 The Motor's Working Mechanism

SPO_2 sensor reads the data , If the oxygen level is less than 90, the motor will rotate at a certain speed; if the oxygen level is less than 80, the motor will rotate at a different speed.

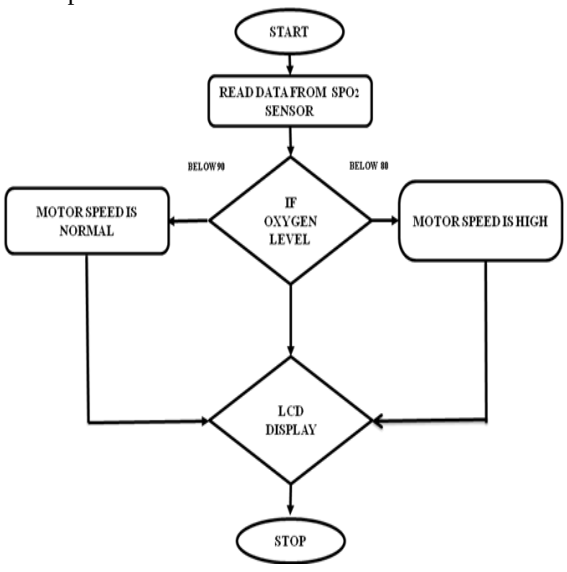

Fig 5. Flowchart of the Proposed system

To the Arduino UNO board, upload the source code for a 2 second forward and 3 second reverse spin.

TABLE 1.RESPIRATORY RATE OF HUMAN BEING

Age limit	range
Adult (More than 18 years)	12 – 20 minutes of breathing
Child (1 – 12 month)	30 - 60 minutes of breathing
Pediatric (6 – 11 years)	18 – 25 minutes of breathing

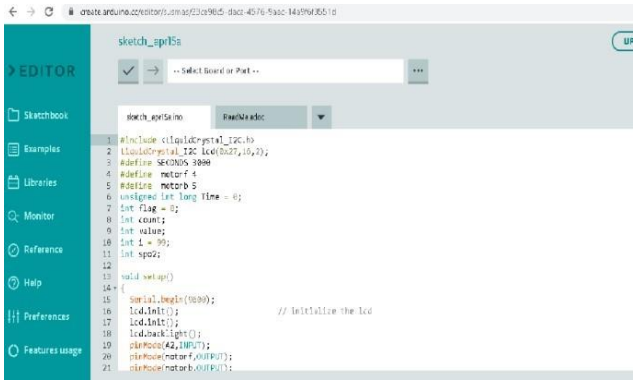

Fig .6 Arduino IDE Software page

V. Results And discussion

The Arduino IDE is used to generate the source code, which is then uploaded to the Arduino Uno.The code is designed by using embedded C. A motor driver is used to provide the necessary power to the motor while run the code the motor will rotating continuously and it provides the oxygen to the breather mask with help of mechanical rod .Initially When the SPO2 sensor reads the data from the patients, the proposed system will run according to the oxygen level read by the sensor. When the oxygen level is normal, the proposed system will turn off. Fig 7 depicts the DC motor pressures on the ambu bag in images of the system's hardware output.

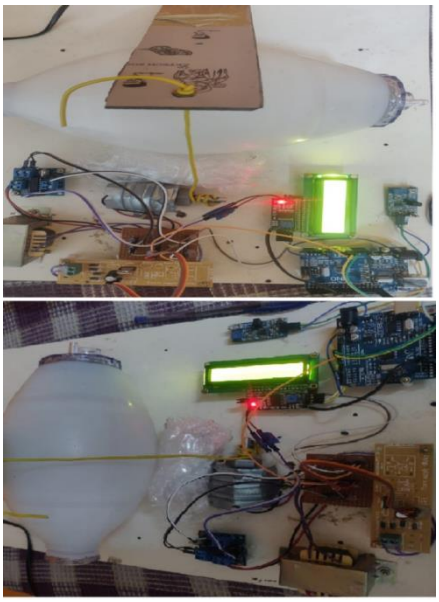

Fig. 8 The system's hardware output

VI. Conclusion

There is clear technical potential for alleviating ventilator shortages during this and future pandemics using open source ventilator designs that can be rapidly fabricated using distributed manufacturing. It is a low - cost construction. Future work is required to realise the full potential of this approach, including developing policies, updating regulations, and securing funding mechanisms for the development and testing of open source ventilators for the current COVID19 pandemic, as well as future pandemics and everyday use in low-resource settings.

Acknowledgment

We thank the Department of ECE, SRM VEC for their Support and laboratory facilities for completion of the project.

References

[1] 'Balamurugan, C. R., Kasthuri, A., Malathi, E., Dharanidharan, S., Hariharan, D., Kishore, B. V., & Venkadesh, T. (2021). Design of Ventilator Using Arduino for Covid Pandemic. Annals of the Romanian Society for Cell Biology, 14530- 14533.

[2] 'Acho, L., Vargas, A. N., & PujolVázquez, G. (2020, September). LowCost, Open-Source Mechanical Ventilator with Pulmonary Monitoring for COVID-19 Patients. In Actuators (Vol. 9, No. 3, p. 84). Multidisciplinary Digital Publishing Institute.

[3] 'Design And Development Of A Low cost Automatic Ventilator by Sazzad Hossain Sazal, B. Tech. in ME (JNTU-A, India) M.Sc. Engg student & TA Dept. of Mechanical Engineering, KUET, Khulna - 9300 on April 2020.

[4] 'Automatic AMBU bag operating device: creating

[5] a boon for high volume centers in low income countries" by RajeevChauhan, Raman Sharma, Nidhi Chauhan on July 2020.

[6] Ardunio nano R3 based ventilator by Anuvind Ashok 2020.

A Comprehensive Review of Anemia Detection Methods

Vinit P. Kharkar[1] and Ajay P. Thakare[2]

[1,2]Department of Electronics & Telecommunication Engineering Sipna College of Engineering & Technology, Amravati

[1]vinitkharkar27@gmail.com, [2]apthakare40@rediffmail.com

***Abstract*—In recent year, anemia emerges as a major health concern among the children and pregnant woman in developing countries like India. The National Family Health Survey data also shows a spike in the anemia prevalence in Children & Women across most states in India. The low concentration of hemoglobin in the blood is the major indicator of anemia in an individual. Considering this fact, extensive research is carried out in the field of anemia detection. This paper gives the review of the research work in this field. Effect of various factors such as age, gender, etc. on hemoglobin levels is also discussed in this research article. This paper gives the brief overview of various data collection and preprocessing methods. It also gives comprehensive analysis of technologies used to detect anemia with the help of hemoglobin estimation. Study of performance measures used for evaluation of results is covered while reviewing existing research work. This paper provides the input for the novel research to be carried out for anemia detection with help of state-of-the-art approached in this domain.**

***Keywords*—Anemia, Hemoglobin, Invasive, Non-invasive**

I. INTRODUCTION

Anemia, defined as low hemoglobin concentration, arises as a global public health concern which affect major populations with varying degree of severity in recent years. According to world health organization (WHO), it is estimated that 42% of children less than 5 years of age and 40% of pregnant woman worldwide are anemic. global nutrition targets endorsed by the Health Assembly includes 50% reduction of anemia in women of reproductive age by the year 2025[1]. National Family health survey (NFHS-5) findings reveal increase in Anemia prevalence in Children & Women across most states in India [6]. Anemia refers to health condition in which the number of red blood cells or hemoglobin concentration in the blood falls below the normal level. Anemia is a sign of malnutrition as well as ill health. Anemia can have further social and economic consequences for individuals and families, including poor educational progress in children and reduced work productivity in adults.

The hemoglobin concentration level in the blood is the major factor determining the severity of anemic condition in population. The table below shows Hemoglobin levels to diagnose anemia [5]. The anemia cutoff presented in the table were presented by study group on nutritional anemia while the cutoff determining mild, moderate and severe anemia were first presented in 1989 guide preventing and controlling anemia through healthcare and then modified for pregnant women, nonpregnant women, and children less than five years of age in the management of nutrition in major emergencies.

TABLE I: HEMOGLOBIN LEVEL TO DIAGNOSE THE ANEMIA (IN GM/DL)

Population	Non-Anemia	Anemia		
		Mild	*Moderate*	*Severe*
Children 6 - 59 months of age	11.0 or higher	10.0 – 10.9	7.0 - 9.9	lower than 7.0
Children 5 - 11 years of age	11.5 or higher	11.0 – 11.4	8.0 - 10.9	lower than 8.0
Children 12 - 14 years of age	12.0 or higher	11.0 – 11.9	8.0 - 10.9	lower than 8.0
Non-pregnant women (15 years of age & above)	12.0 or higher	11.0 – 11.9	8.0 - 10.9	lower than 8.0
Pregnant women	11.0 or higher	10.0 – 10.9	7.0 - 9.9	lower than 7.0
Men (15 years of age & above)	13.0 or higher	11.0 – 12.9	8.0 - 10.9	lower than 8.0

Hemoglobin measurement is one of the most frequently performed diagnostic test for anemia detection as well as in trauma settings. There are two major ways of hemoglobin estimation, Invasive and Non-Invasive. This paper gives detailed review of methods implemented for hemoglobin estimation for anemia detection. Marcel E. Salive, et al. [9] studied anemia and hemoglobin levels in older people in relation to their age, gender, and health status. Even after controlling for demographic variables and health status, they discovered that age is connected with both hemoglobin levels and anemia, with a greater effect in men than in women. The discovery of anemia in an older person should elicit adequate clinical treatment due to the reduction of hemoglobin and concurrent increasing anemia. However, Nitin Raisinghani et. al. [10] claims that the average hemoglobin level did not differ significantly with increasing age. They also suggest doing a population-based study to better understand the frequency and causes of anemia in asymptomatic older people.

The paper is organized into two major parts. The first part is related with the review of existing invasive and non-invasive analysis. It is subdivided into overview of data collection and preprocessing methods and analysis of

methodologies used of anemia detection. The second part is related with performance of existing systems for hemoglobin estimation with both invasive and non-invasive approaches. This section also explains the research gap in the existing implementations. This will also help to overcome the limitation of conventional methods. The objective of this review paper is to study database of existing systems for proposing a quick, valid and reliable method for estimation of hemoglobin status which is vital to detect anemia in the population at risk.

II. Review Of Literature

A. Data collection and Preprocessing

The photoplethysmography (PPG) signal is one of most widely used parameter to estimate the hemoglobin in the blood. By using PPG signal, putut dewantaro et. al. [32] put describes a non-invasive approach for determining hemoglobin levels in the blood. Clamping the PPG sensor, which consists of four LEDs and one photodiode, yields the PPG signal. Prior to signal processing and Hb level computation, PPG signal conditioning is performed. The noise removal from the PPG signal is done by using bandpass filtering with bandwidth of 0.1-3.8 Hz. Dinesh Kumar et. al. [22] put forward a hemoglobin sensing device for anemia detection. They conducted their investigation using a non-invasive method. To solve the issues associated with multi wavelength jaw type finger probes, they adopted point light source architecture. Researchers have developed a method for measuring incident light intensity without being influenced by light source deterioration. The proposed device architecture is based on the operation concept of Beer Lambert's law. The hemoglobin measurement method is based on PPG signals. The overall approach proposed in this paper concentrates around the single point light source and incident intensity. Noninvasive method [27] is based on Modulation ratio (R). The light absorption by oxyhemoglobin and deoxyhemoglobin in blood determines the modulation ratio (R). The PPG wave signal can be different parts of body. The fingertip was chosen since it is said to be the most precise spot in the body for measuring PPG when compared to other places. A probe containing two light sources of 660 nm and 940 nm, as well as a photodiode, was used to record PPG signals. The participants were informed to insert their index finger into the input probe until all of the relevant data was gathered. The average of three attempts, each with a 1.5-minute break between them.

Smartphone camera-based methods also proposed by the researchers [10, 15] to estimate the Hb in blood. The image of conjunctiva captured with the help smartphone camera were used for estimation and analysis purpose [15]. With and without built-in flash, the same image was captured in RAW and Joint Photographic Experts Group (JPEG) formats. The Massey score was calculated visually using a conventional skin tone chart, and the results were entered into the database. The researchers [10] used a conventional back-facing camera on a smartphone under ambient illumination to acquire a photo of the anterior conjunctiva of the eye. For this purpose, they have also developed an android application for capturing the images. The captured image preprocess with the help of MATLAB software. Another approach based on study of the diagnosis of anemia due to eyelid conjunctiva the authors have used hyperspectral images [18]. The advantage of hyperspectral image over normal image is reproducibility of colors and independency from spectral characteristics of light source. a special study to detect anemia in pregnant woman is carried out by the researchers [23]. They employed a method based on conjunctival digital photographs of the eye taken with a smartphone camera with a resolution of 13 MP. The photos were then reduced in size before being converted from RGB colour space to HSV and Grayscale images. The region of interest was determined based on the size of the palpebral conjunctiva.

The HemaSmart system [24] is based on the principle of color difference of blood which causes due to the variation of Hemoglobin level. This non-invasive system simplifies the process of sample collection by selecting appropriate camera and designing the lighting system with the help of white color LED.

The video processing technique have been employed by Asma Z. Yamani et.al. [31] to detect the anemic condition based on hemoglobin value estimation. research team captures close-up videos of the fingertip with the data collection application with a smartphone camera. The another set of videos captured in presence of IR LED and white LEDs in sequential order with gap of 15 seconds for each. In the preprocessing stage video frames are extracted and processed with segmentation to produce histogram as per RGB values.

Based on the blood flow in the palm, the palm colour analysis is also used to assess hemoglobin. The researchers proposed a noninvasive method of measuring hemoglobin based on the redness of the skin of the palm. The setup comprises of a camera that records video of a human subject's palm before and after blood flow is confined to the palm with a sphygmomanometer cuff in the forearm near the wrist. The video continues until the blood flow is restored following the abrupt and quick release of cuff pressure. The required reading for processing is obtained by measuring the redness of the skin colour after occlusion and after the return of blood flow to the palm.

[13] The minimally invasive approach was also used by the for counting the red blood cells for detection of anemia and leukemia. The proposed system uses the microscopic images available at ALL IDB dataset which is one of most widely used dataset for automated identification, counting and classification of blood cell using computer system. The researchers from mapua university [20] utilizes approach based on RBC counting and grading approach for analyzing anemic condition in the patient. Their research employs the SVM algorithm to classify RBCs and their forms, such as normal RBCs and those linked with anemia, such as Target Cells and Elliptocytes. They used a database of local medical institutes to conduct research. Classification of RBC from peripheral blood smear images is another way to be implemented for diagnosis of anemia, leukemia and other disorders [18]. The authors have collected the peripheral blood smear images (PBS) of multiple steins from medical college and also from the internet sources. These images of PBS are preprocessed with adaptive histogram for constant

contrast and illumination.

As proposed by Andrey Azarov et al. [26], hemoglobin can also be determined by assessing the iron amount in the blood. The proposed system works by changing the optical transparency of tissue under the influence of an external magnetic field. It is based on concept that tissue is saturated with iron-containing blood. The property of iron as a ferromagnetic to be attracted by a magnetic field was proposed by the authors. External measuring unit, optical source, optical receiver, and magnetic field source make up the system.

A. Methodology

In this section, the details analysis of methodology used for the hemoglobin estimation is discussed. This will help to understand the scope of different technologies for anemia detection. The most recent development is application of machine learning algorithm to estimate the hemoglobin content of blood [18, 31]. The algorithms are implemented using python and MATLAB. The texture features of manually segmented images are extracted using Gray Level Co-occurrence Matrix (GLCM). These extracted features are fed to the Machine Learning algorithms such as Naive Bayes classifier, K-means clustering Decision Tree (DT), logistic regression, random forest, K-Nearest Neighbors (KNN), Artificial Neural Network (ANN) and support vector machine (SVM). Asma Z. Yamani et.al. uses the values of the RGB histogram for each LED will be entered through multiple regression algorithm in order to predict the Hemoglobin concentration. They have also developed the mobile application for the prototype purpose. Jayakodi et al. [24] devised a Neural Network-based platform that can recognize any input image and calculate the hemoglobin value. The algorithm was created using TensorFlow. The technique was implemented by comparing the hemoglobin value of each image. Instead of using a feed-forward network, the researchers used a convolutional neural network (CNN). The prototype is developed along with mobile application for the final implementation. The use of Machine learning algorithm for processing PPG signal is proposed by Acharya et.al. [28]. The researchers used filtered PPG signal to extract features for the training dataset. Attenuation, sum of Hb moieties, pairwise ratio parameters, age, and pregnancy status are some of the characteristics that will be used as input to the machine learning system. To train a Stacked Regressor Model, different regression models were employed. The complete dataset was divided into training and testing data sets at random. Statistical metrics, Bland-Altman graphs, and Error Grid Analysis were used to assess the suggested algorithm's performance. The accuracy is calculated based on difference between the actual and obtained Hb value.

The methodology based on digital image processing methods as discussed by Amir Aslan Aslani et. al. [13] includes canny edge detection technique, Hit or miss transform to create the marginal image and endpoint sets and application of Hough Transform. Shaharin ahmed et al. [19] present the whole study on measuring blood hemoglobin level from finger nail images for. The finger nail was detected by the researchers using morphological image processing. The RGB values of the pixels that fall within the ROI are retrieved and used to determine the mean. In order to determine the value of Hb, these collected features are fed into a linear regression model.

The processing the conjunctiva image for anemic condition is one the major technique used by the researchers. [23, 15, 21, 10]. The different approached involves stepwise regression analysis [15], estimating color absorption component of tissue using Lambert's law [21], KNN based classification approach [23] and with thresholding technique [10]. The classification approach is used to detect the anemia in pregnant woman [23]. The feature used for study includes first order statistical parameters. The features are extracted for grayscale and RGB image, HSV color space. The features are provided as input to K-Nearest Neighbor (KNN) classification method based on pre-classified learning data that has the closest distance to the test sample. In regression analysis approach [15] used for conjunctival image uses general linear model to estimate Hb. The Phase 1 data of 142 patient is used to develop predictive model for estimated hemoglobin from the conjunctiva. The Phase 2 of 202 new patients is used to improve the predictive model using k-folds testing iteration. The anemic condition in the patient can also be diagnosed by color intensities of green plane and red plane of RGB image of conjunctival pallor [10]. Histograms of the red and green spectrum is used for this purpose. To decide the anemic state of the patient the algorithm is developed for comparing mean red color intensity and mean green color intensity. The threshold is used to determine whether the patient is anemic or not. This is one of the simplest approaches used for anemia detection.

Different researchers have used different methods to process PPG signal. Beer Lambert's law, which deals with the loss of propagating light intensity, is widely utilized by researchers. The modulation ratio is defined by the researchers [27] as the ratio of AC to DC components of a Photoplethysmogram (PPG) signal collected at two distinct wavelengths. The study is based on the fact that the wavelength of incident light affects the absorption of light by blood and tissues, specifically oxy-hemoglobin and deoxyhemoglobin. For the analysis, a nonlinear model including R and gender was used, which was done using the MATLAB 2019 software. A microcontroller-based system is being developed based on the study to forecast and display the risk of anemia. Some methods proposed [37] to determine hemoglobin non-invasively based on a couple of PPG signals acquired from the finger by using two monochromatic light at 660nm (Red) and 940nm (IR). Pulse oximetry is used in the procedure described in this article. The Design of amplifier circuit has signal acquiring and processing circuit and signal conditioning circuit. The clip-on sensor is attached to one of the patient's extremities (finger). Both red and IR light are radiated into the finger via the LED Driver Circuit. A photo-detector detects and collects reflected light, which is then amplified and conditioned. The obtained signals collected through the data Acquisition system and analyzed with LABVIEW software.

Another hardware-based approach is used by putut dewantaro [32] in which OP-AMP MPC 6002 and ATmega328PP-AU plays a vital role in signal conditioning and signal processing. Exponential Moving Average (EMA)

is the approach used to modify the PPG signal, making it smoother than it was previously. The AC and DC components at each wavelength can be calculated using the linear regression approach to determine hemoglobin level. The device will connect to a smartphone through Bluetooth Low Energy 4.0 and save the measured hemoglobin levels. The hardware prototype based on raspberry-pi is put forward by rosemary et.al. [20]. The prototype consists of 5MP camera meant to be attached to the microscope eyepiece to capture the blood smear images. The system takes shape features of target RBC to be given as an input the algorithm. SVM Multiclass Classifier is used for the training and testing purposes.

When determining the iron level in blood for hemoglobin detection, two key issues must be addressed. [32]. The first is the issue of iron magnetization in the human body, and the second is the issue of optical radiation receiver sensitivity. For system design purpose, the authors have utilized pulse generator, synchronous detector, modulator, optical source of radiation, high-pass filter, Low frequency amplifier, transducer and microcontroller.

III. Performance Measures And Research Gap

The accuracy is common performance measure parameter used by most of the researchers. The graph shown below gives the comparison between different methods used for Hemoglobin estimation for anemia detection against the accuracy of that method. Various performance metrics are used for performance analysis are MAE (mean absolute error), Residual sum of squares (MSE), Root mean squared error (RMSE), Relative squared error (RSE), R-squared(R^2). These parameters are mainly used for regression analysis.

After the detailed review it has been found that data collection process needs to be more accurate in order to get more accurate results. A standard operating procedure is required to be designed for collecting the data sample by both approaches i.e. by minimally invasive and non-invasive approach. The sensors are normally used in the non-invasive methods should have good calibration and precision otherwise it may lead to a false reading. Whereas, in case of invasive methods, the amount of blood sample, technical specifications of camera, amount of illumination used while capturing an image of Hb sample, distance between sample and camera, resolution of the microscope are found out to be main parameters to be considered. The use of recent technologies such as machine learning, deep learning is preferred since they are more accurate and less time consuming as compared to conventional methods During the review work, it has also been found that the various factors such as age, gender health status, stress, genetic variations and pregnancy etc. have major impact on hemoglobin level of an individual which needs to considered while developing the system for anemia detection with the help of technology. This will ensure the more accurate determination of anemic condition of an individual. It is need to make sure that the proposed system should able to be used for remote places also.

IV. Conclusion

In this paper, the comprehensive study of anemia detection methods is carried out. It has been discovered that the majority of approaches are used to estimate hemoglobin levels in the blood. The majority of the population in developing countries, such as India, lives in rural areas, where basic diagnostic facilities, such as blood chemistry analysis, are not readily available to the average person. As a result, there is a pressing need for a technique for measuring Hb in human blood that is simple, accurate, and easy to apply in rural regions. Patients with mild or moderate anemia are more likely to develop a more severe anemia condition if they are diagnosed and treated promptly. This review effort will aid in the establishment of a system for early detection of anemia, allowing for a control and management mechanism to take care of the patients.

With this review literature, it can be concluded that in this digital era of technology, providing advance solutions to the existing medical methods with the help of latest technology is beneficial for diagnostic and therapeutic purpose. These technological solutions are not meant to replace existing systems; rather, they are intended to assist them in making faster, better, and more precise assessments in order to improve patient care.

References

[1] WHO, Haemoglobin concentrations for the diagnosis of anaemia and assessment of severity. Vitamin and Mineral Nutrition Information System. Geneva, World Health Organization, 2011 (WHO/NMH/NHD/MNM/11.1) (http://www.who.int/vmnis/indicators/haemoglobin. pdf, accessed [24 march 2022]).

[2] Global nutrition targets 2025: policy brief series, WHO reference number: WHO/NMH/NHD/14.2, Available at https://www.who.int/publications/i/item/WHO-NMH-NHD-14.2 accessed [24 march 2022])

[3] WHO, Global nutrition targets 2025: anaemia policy brief, WHO reference number: WHO/NMH/NHD/14.4 Available at https://www.who.int/publications/i/item/WHO-NMH-NHD-14.4 accessed [24 march 2022])

[4] WHO, UNICEF, UNU. Iron deficiency anaemia: assessment, prevention and control, a guide for programme managers. Geneva, World Health Organization, 2001. Available at http://www.who.int/nutrition/publications/micronutrients/anaemia_iron_deficiency/WHO_NHD_01.3/en/index.html

[5] Nutritional anaemias. Report of a WHO scientific group. Geneva, World Health Organization, 1968.

[6] (WHO Technical Report Series, No. 405). Available at http://whqlibdoc.who.int/trs/WHO_TRS_405.pdf

[7] Government of India, Ministry of Health and Family Welfare, National Family Health Survey - 5, 2019-21. [online] Available at: http://rchiips.org/nfhs/NFHS-5_FCTS/India.pdf [Accessed 23 March 2022].

[8] D. P. Lokwani, “Red Blood Cells” in The ABC of CBC: Interpretation of complete Blood Count & Histograms,1st ed., Jaypee Brothers Medical Publishers Ltd, New Delhi, India, 2013, pp 8-9

[9] Marcel E. Salive, Joan Cornoni-Huntley, Jack M. Guralnik, Caroline L. Phillips, Robert B. Wallace, Adrian M. Ostfeld, Harvey J. Cohen, “Anemia and Hemoglobin Levels in Older Persons: Relationship with Age, Gender, and Health Status”, Journal of American Geriatrics Society, Volume 40, Issue 5, pp 439-548, May 1992

[10] Raisinghani N, Kumar S, Acharya S, Gadegone A, Pai V. “Does aging have an impact on hemoglobin? Study in elderly population at rural teaching hospital”, Journal of Family Medicine and Primary Care, Volume 8, Issue 10, Pp 3345-3349, October 2019.

[11] A. Tamir et al., "Detection of anemia from image of the anterior conjunctiva of the eye by image processing and thresholding," 2017 IEEE Region 10 Humanitarian Technology Conference (R10-HTC), 2017, pp. 697-701, doi: 10.1109/R10-HTC.2017.8289053.

[12] Andrey Azarov, Elena Shirokova, Igor Shirokov, “Non-Invasive System for Determining the Level of Iron in the Blood”, IEEE East-West Design & Test Symposium (EWDTS), September 2019, doi: 10.1109/EWDTS.2019.8884467.

[13] Bikash Santra, Dipti Prasad Mukherjee, Dipankar Chakrabarti, “A Non-Invasive Approach for Estimation of Hemoglobin Analysing

Blood Flow in Palm". IEEE 14th International Symposium on Biomedical Imaging (ISBI 2017), April 2017, pp 1100-1103, doi: 10.1109/ISBI.2017.7950708.

[14] A. Aslani, M. Zolfaghari and H. Sajedi, "Automatic Counting Red Blood Cells in the Microscopic Images by EndPoints Method and Circular Hough Transform," 2022 16th International Conference on Ubiquitous Information Management and Communication (IMCOM), 2022, pp. 1-5, doi: 10.1109/IMCOM53663.2022.9721754.

[15] S. Ghosal, D. Das, V. Udutalapally, A. K. Talukder and S. Misra, "sHEMO: Smartphone Spectroscopy for Blood Hemoglobin Level Monitoring in Smart Anemia-Care," in IEEE Sensors Journal, vol. 21, no. 6, pp. 8520-8529, 15 March15, 2021, doi: 10.1109/JSEN.2020.3044386.

[16] Suner S, Rayner J, Ozturan IU, Hogan G, Meehan CP, et al. (2021) Prediction of anemia and estimation of hemoglobin concentration using a smartphone camera. PLOS ONE 16(7): e0253495. https://doi.org/10.1371/journal.pone.0253495

[17] M. Rivero-Palacio, W. Alfonso-Morales and E. Caicedo-Bravo, "Mobile Application for Anemia Detection through Ocular Conjunctiva Images," 2021 IEEE Colombian Conference on Applications of Computational Intelligence (ColCACI), 2021, pp. 1-6, doi: 10.1109/ColCACI52978.2021.9469593.

[18] P. S. Wazarkar, A. D. Karnale, D. A. Chhabariya, A. R. Tiwari and R. R. Kandelwal, "Early Disease Detection using Android Application based on Nail's Image," 2021 IEEE Bombay Section Signature Conference (IBSSC), 2021, pp. 1-6, doi: 10.1109/IBSSC53889.2021.9673386.

[19] K. T. Navya, K. Prasad and B. M. K. Singh, "Classification of blood cells into white blood cells and red blood cells from blood smear images using machine learning techniques," 2021 2nd Global Conference for Advancement in Technology (GCAT), 2021, pp. 1-4, doi: 10.1109/GCAT52182.2021.9587524.

[20] S. Ahmed and M. A. Habib, "Automatic Region of Interest Extraction from Finger Nail Images for Measuring Blood Hemoglobin Level," 2021 International Conference on Electronics, Communications and Information Technology (ICECIT), 2021, pp. 1-4, doi: 10.1109/ICECIT54077.2021.9641115.

[21] R. V. Pellegrino, A. C. Tarrobago and D. L. B. Zulueta, "Automated RBC Morphology Counting and Grading Using Image Processing and Support Vector Machine," 2021 IEEE 13th International Conference on Humanoid, Nanotechnology, Information Technology, Communication and Control, Environment, and Management (HNICEM), 2021, pp. 1-5, doi: 10.1109/HNICEM54116.2021.9731937.

[22] N. Kobayashi, A. Yoshino, M. Ishikawa and S. Homma, "Anemia Examination Using a Hyperspectral Camera in Telecare System," 2021 IEEE 3rd Global Conference on Life Sciences and Technologies (LifeTech), 2021, pp. 475-476, doi: 10.1109/LifeTech52111.2021.9391912.

[23] R. D. Kumar et al., "A Novel Noninvasive Hemoglobin Sensing Device for Anemia Screening," in IEEE Sensors Journal, vol. 21, no. 13, pp. 15318-15329, 1 July1, 2021, doi: 10.1109/JSEN.2021.3070971.

[24] Y. N. Fuadah, S. Sa'idah, I. Wijayanto, R. Patmasari and R. Magdalena, "Non Invasive Anemia Detection in Pregnant Women Based on Digital Image Processing and K-Nearest Neighbor," 2020 3rd International Conference on Biomedical Engineering (IBIOMED), 2020, pp. 60-64, doi: 10.1109/IBIOMED50285.2020.9487605.

[25] J. A. D. C. A. Jayakody and E. A. G. A. Edirisinghe, "HemoSmart: A Non-invasive, Machine Learning Based Device and Mobile App for Anemia Detection," 2020 IEEE REGION 10 CONFERENCE (TENCON), 2020, pp. 1401-1406, doi: 10.1109/TENCON50793.2020.9293903.

[26] S. J. Mohammed MOHAMMED, A. A. Ahmed, A. A. Ahmad and M. Sami MOHAMMED, "Anemia Prediction Based on Rule Classification," 2020 13th International Conference on Developments in eSystems Engineering (DeSE), 2020, pp. 427-431, doi: 10.1109/DeSE51703.2020.9450234.

[27] A. Azarov, E. Shirokova and I. Shirokov, "Non-Invasive System for Determining the Level of Iron in the Blood," 2019 IEEE East-West Design & Test Symposium (EWDTS), 2019, pp. 1-4, doi: 10.1109/EWDTS.2019.8884467.

[28] A. A. Ajmal, S. Shankarnath, M. Athif and E. H. Jayatunga, "Non-Invasive Screening Tool to Detect Anemia," 2019 IEEE Healthcare Innovations and Point of Care Technologies, (HI-POCT), 2019, pp. 67-70, doi: 10.1109/HI-POCT45284.2019.8962856.

[29] S. Acharya et al., "Non-Invasive Estimation of Hemoglobin Using a Multi-Model Stacking Regressor," in IEEE Journal of Biomedical and Health Informatics, vol. 24, no. 6, pp. 1717-1726, June 2020, doi: 10.1109/JBHI.2019.2954553.

[30] R. An, M. N. Hasan, Y. Man and U. A. Gurkan, "Integrated Point-of-Care Device for Anemia Detection and Hemoglobin Variant Identification," 2019 IEEE Healthcare Innovations and Point of Care Technologies, (HI-POCT), 2019, pp. 37-40, doi: 10.1109/HI-POCT45284.2019.8962876.

[31] C. C. Hortinela, J. R. Balbin, J. C. Fausto, P. Daniel C. Divina and J. P. T. Felices, "Identification of Abnormal Red Blood Cells and Diagnosing Specific Types of Anemia Using Image Processing and Support Vector Machine," 2019 IEEE 11th International Conference on Humanoid, Nanotechnology, Information Technology, Communication and Control, Environment, and Management (HNICEM), 2019, pp. 1-6, doi: 10.1109/HNICEM48295.2019.9072904.

[32] A. Z. Yamani, F. M. Alqahtani, N. S. Alshahrani, R. M. Alzamanan, N. Aslam and A. S. Algherairy, "A proposed noninvasive point-of-care technique for measuring hemoglobin concentration," 2019 International Conference on Computer and Information Sciences (ICCIS), 2019, pp. 1-4, doi: 10.1109/ICCISci.2019.8716418.

[33] P. Dewantoro, C. E. Gandana, R. O. R. H. Zakaria and Y. S. Irawan, "Development of Smartphone-based Non-Invasive Hemoglobin Measurement," 2018 International Symposium on Electronics and Smart Devices (ISESD), 2018, pp. 1-6, doi: 10.1109/ISESD.2018.8605489.

[34] G. Dimauro, D. Caivano and F. Girardi, "A New Method and a Non-Invasive Device to Estimate Anemia Based on Digital Images of the Conjunctiva," in IEEE Access, vol. 6, pp. 46968-46975, 2018, doi: 10.1109/ACCESS.2018.2867110.

[35] E. J. Wang, W. Li, J. Zhu, R. Rana and S. N. Patel, "Noninvasive hemoglobin measurement using unmodified smartphone camera and white flash," 2017 39th Annual International Conference of the IEEE Engineering in Medicine and Biology Society (EMBC), 2017, pp. 2333-2336, doi: 10.1109/EMBC.2017.8037323.

[36] R. A. Rochmanto, H. Zakaria, R. D. Alviana and N. Shahib, "Non-invasive hemoglobin measurement for Anemia diagnosis," 2017 4th International Conference on Electrical Engineering, Computer Science and Informatics (EECSI), 2017, pp. 1-5, doi: 10.1109/EECSI.2017.8239096.

[37] M. F. Shaik and M. M. Subashini, "Anemia diagnosis by fuzzy logic using LabVIEW," 2017 International Conference on Intelligent Computing and Control (I2C2), 2017, pp. 1-5, doi: 10.1109/I2C2.2017.8321790.

[38] K. -S. Pavithra, X. A. Mary, K. Rajasekaran and R. Jegan, "Low cost non-invasive medical device for measuring hemoglobin," 2017 International Conference on Innovations in Electrical, Electronics, Instrumentation and Media Technology (ICEEIMT), 2017, pp. 197-200, doi: 10.1109/ICIEEIMT.2017.8116834.

[39] Saurabh Mitra, Dr. Shanti Rathore, Dr. Sanjeev Kumar Gupta. "A non- invasive medical tool for anemia disease diagnosis". European Journal of Molecular & Clinical Medicine, 2021, pp.7-8, 5393-5408.

[40] E. Mahmodi Arjmand, M. Saadatmand, M. Reza Bakhtiari, M. Eghbal and A. Balaei, "A Centrifugal Microfluidic Platform to Measure Hemoglobin of Whole Blood," 2017 24th National and 2nd International Iranian Conference on Biomedical Engineering (ICBME), 2017, pp. 330-333, doi: 10.1109/ICBME.2017.8430272.

[41] G. M. T. Ahsan et al., "A Novel Real-Time Non-invasive Hemoglobin Level Detection Using Video Images from Smartphone Camera," 2017 IEEE 41st Annual Computer Software and Applications Conference (COMPSAC), 2017, pp. 967-972, doi: 10.1109/COMPSAC.2017.29.

[42] V. Aparna, T. V. Sarath and K. I. Ramachandran, "Simulation model for anemia detection using RBC counting algorithms and Watershed transform," 2017 International Conference on Intelligent Computing, Instrumentation and Control Technologies (ICICICT), 2017, pp. 284-291, doi: 10.1109/ICICICT1.2017.8342575.

[43] S. S. Krivenko, A. A. Pulavskyi and S. A. Krivenko, "Determination of low hemoglobin level in human using the analysis of symbolic dynamics of the heart rate variability," 2017 IEEE First Ukraine Conference on Electrical and Computer Engineering (UKRCON), 2017, pp. 271-274, doi: 10.1109/UKRCON.2017.8100490.

3-bit All-Optical Binary to Gray code converter using 2D Photonic Crystal Design

Monica Philo S[1], Nandhini S[2], Rakshitha V S[3], Santhiya S[4], S Syedakbar[5], S Geerthana[6], T Sridarshini[7]

[1–7]UG Scholar, Department of Electronics and Communication Engineering,
K. Ramakrishnan College of Technology, Trichy

***Abstract*— We proposed a 3-bit all-optical binary to gray code converter in hexagonal lattice using photonic crystals in two dimensions. The design is implemented through XOR logic gates using silicon rods in an hexagonal lattice with an air background in double T-shaped waveguides. By incorporating the cascaded layout of logic gates with the logic of XOR operation, the output can be arrived at by using interference effect. The layout is designed and analyzed using OptiFDTD software. Hence the simulation and verification of the performance metrics are done using the Finite Difference Time Domain method(FDTD).The design renders a contrast ratio of 12.557 dB for the binary to gray code converter with an enhanced refractive index and optimized silicon rod radius.**

Keywords–All-optical binary to gray code converter, XOR logic gate, T shaped Waveguide, OptiFDTD, interference effect, Finite Difference Time Domain method.

I. INTRODUCTION

Photonic crystals are fascinating optical materials that are employed to regulate and manipulate light flow. Photonic crystals (PhCs) are optical nanostructures in which the refractive index changes periodically and it allows large circuits to operate in contracted areas and enables the optical modules to rival with its electronic counterparts despite the use of long wavelengths of light. Photonic crystals are artificial periodic dielectric structures that have a band gap which prohibits the propagation of a particular frequency range of light. This is known as the photonic band gap (PBG).In order for interference effect to occur, the periodicity of the photonic crystal must be equal to or greater than half the wavelength of light in the medium. Hence, the dielectric constant is varied frequently to direct the transmission of light [1]. Photonic band gaps are wavelength bands that are not permitted [2]. In order to design the photonic crystals appropriately, the position and size of the band gap must be decided carefully using the computational modeling methods like Plane wave expansion method, Finite Difference Time Domain method, Order-N spectral method, KKR method etc,.[3].

Thin-film optics based on 1 dimension are already widely used, with applications ranging from low to excessive reflection coatings on lenses and mirrors to color changing paints and inks. Now the photonic crystals with two dimensions have started to emerge for industrial applications. The three-dimensional counterparts are nonetheless a long way from commercialization, however they offer additional capabilities that lead to new device concepts (e.g. optical computers) once some technological elements like manufacturability and major challenges like disorder are addressed.[4].

In other papers that have been analyzed, we studied the various novel designs for AND,OR, XOR gates with optimized values for radius, lattice constant, refractive indices and other performance metrics and its effect on the contrast ratio[5]. For an optical computing system, optical processors are required to be operated completely in the optical domain and hence for that, the all-optical logic gates are essential which provides a wide range of applications that includes encoding/decoding[6],parity checking[7], numerical calculations, and wavelength conversions etc.[8] Out of all the combinational circuits that it offers, code converter is also one of the circuits that enables two different systems to be compatible even when they use different codes. For a binary to gray code converter, the gray code is cyclic which means the two consecutive codes change only by a single bit which yields a lesser error rate than regular binary coding. Here to design the converter all-optical based XOR is the key component and is known to perform a wide range of applications at on-chip optical networks such as data recognition[9], data encryption/decryption[10], pattern matching[11], different switching operations[12], etc.

In general, detector circuits [13], PSK modulators[14], etc are designed with XOR-based logic gates. the nonlinear Kerr effect with ring resonator have been used to implement the logic gates[15][16] and also with two PhCRR limiters in a waveguide of Y-Shape. But it has a complex structure and is hard to fabricate. Therefore in the previous papers that we analyzed, they have used the beam interference method for implementing the all-optical based logic gates in which the presented design is with XOR based logic gates as reference. Based on the phase angle and path covered by an incident light signal, constructive or destructive interference occurs inside the waveguide. This structure acts as optical AOX logic gates by differencing the phase angles of the incident signals. They have designed with cylindrical silicon rods in the air each with a radius of 0.2a, where ‘a’ is the lattice constant. The value of ‘a’ is 0.6 μm and the refractive index (RI) is 3.46. Because of low loss window of optical transmission, they built the AOX-based logic gates to function at a wavelength of 1550 nm.

In our design, we have constructed an optimized 3-bit all-optical binary to gray code converter which is optimized to

accomplish maximum contrast ratio within compact dimensions. In the following section, the operating principle has been discussed, then in section 3 the experimental setup and procedure are explained in depth, followed by section 4 where simulation results are detailedly analyzed and finally in section 5 the paper is concluded. The references are included at the end of the paper.

II. Principle of Operation:

Bands can be defined as the wavelength ranges which can propagate in the particular direction, and the wavelengths that can propagate in that direction are known as modes. Photonic band gaps are wavelength bands that are repudiated and this property of photonic crystals attracts researchers as it provides high operating speeds and wide bandwidth region for upcoming optical networks. Light is an electromagnetic wave which consists of fluctuating electric and magnetic fields, hence it operates in two modes TE and TM mode. For band gaps in photonics, the dielectric rods suit TM light (E parallel to the rods), and the holes made of air suit the TE light (E running around the holes) [17].

The 2D photonic crystal slabs are mostly utilized in terms of functional defects. [18] [19]. We can engineer point defects (micro cavities) and surface defects/line defects which include changing various parameters like radius, lattice constant etc., to effectively and efficiently control the flow of light by which the expected functionality is achieved.

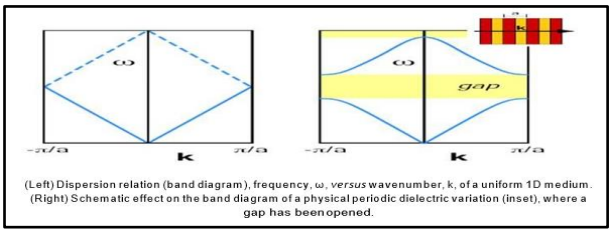

(Left) Dispersion relation (band diagram), frequency, ω, *versus* wavenumber, k, of a uniform 1D medium. (Right) Schematic effect on the band diagram of a physical periodic dielectric variation (inset), where a gap has been opened.

Figure 1. Photonic Band Gap

The band structure is obtained by solving the Maxwell's equation in the simplest form as given below [20],

$$\left\{\nabla \times \frac{1}{\epsilon}\nabla \times\right\}H(r) = \frac{\omega^2}{c^2}H(r) \quad (1)$$

Where, H(r), ω, c and ∈ denote the magnetic field, frequency, the speed of light and dielectric function respectively.

The important equations for the electric and magnetic field are [21],

$$\nabla \cdot E = 0 \quad (2)$$
$$\nabla \cdot B = 0 \quad (3)$$
$$\nabla \times E = -(\partial B/\partial t)) \quad (4)$$
$$\nabla \times H = \partial D/\partial t \quad (5)$$

Where, B denote the magnetic flux and D represents the electric flux density, E is the ∇· and ∇× are the divergence and curl operators, respectively.

To attain the desired logic, the linear interference effect is deployed by properly guiding the light to the necessary output ports. Since linear effects need low input intensities than non linear designs, it produces more energy efficient designs. Generally while using interference method, external phase shifters or additional elements are added for phase control which gives lower contrast ratios and bulky dimensions. But in photonic crystal design, we can achieve proper phase control by simply introducing defects, without the use of external components produces a compact design with better contrast ratios.

Interference effect as per the wave theory occurs when two or more coherent source signals overlap each other at the same point which also has identical wavelengths. If the input signals have a phase difference of an even multiple of π, then it leads to constructive interference else it leads to destructive interference.[22]Constructive interference gives a high output power while destructive interference produce less output power thus producing two distinct logic levels 1 and 0. In our experimental setup we can introduce path difference by varying the dimensions to produce phase difference.

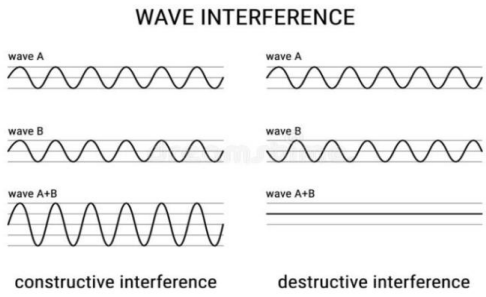

Figure 2 Interference effect

III. Binary To Gray Code Converter (BGCC)

A BGCC converts binary input into gray output code. The conversion steps are given below,

$$G2 = B2 \quad (6)$$
$$G1 = B2 \oplus B1 \quad (7)$$
$$G0 = B1 \oplus B0 \quad (8)$$

Where, ⊕ represents the XOR operator.

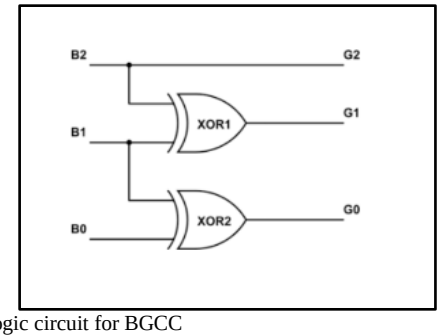

Figure 3 Logic circuit for BGCC

The Most Significant Bit (MSB) remains the same for both the codes. The other bits of the gray code are obtained by implementing the XOR operation between the rests of the adjacent binary bits whose logic circuit is given in the logic diagram.

IV. Experimental Setup and Procedure:

In our proposed method, we present the design for 3-bit

All-Optical Binary to Gray code converter using 2D photonic crystals. The work carried out for the designing of All-Optical Binary to Gray code converter is based on the formerly designed All-Optical based XOR logic gates in a square lattice consisting of cylindrical silicon rods in air. In that design, a radius of 0.2a is considered, with the value of 'a' as 0.6 μm and the refractive index (RI) is 3.46, where 'a' is the lattice constant. It has a maximum contrast ratio of 8.29 dB. Compared to hexagonal lattice, square lattices are simpler but they cannot provide a better band gap as is produced by the hexagonal lattice thus it provides better efficiency and because of which we are implementing the hexagonal lattice in our design.

A. Design for All-Optical Binary to Gray code converter (AOBGCC):

It consists of silicon rods laid out on an hexagonal lattice with an air background. The binary input ports are B1, B2, B3 and the gray output ports are G1,G2,G3 where B3 and G3 represent the Most Significant Bit (MSB) for the binary input and gray output respectively. To permit the equal splitting of input power towards the output port, a Y-shaped waveguide is used at input ports B2 and B3. The main design comprises two all-optical XOR logic gates which have a common input port B2. A direct link is established from port B3 to G3 for the binary to gray code converter as the MSB remains the same. The other bits of the gray code are obtained by implementing the XOR operation between the rests of the adjacent binary bits. Hence the Least Significant Bit (LSB) and the middle bit are obtained at the output of the two all-optical XOR gates.

The proposed design works on the already proposed all-optical XOR logic gate for switching applications which has been modified to the design presented in the existing method. Thus we can create the binary to gray code converter by cascading the XOR logic gate for 3-bits.The structure is designed in virtue of defects. There are two types of defects namely point defects alternatively called micro cavities and line defects. With the application of line and point defects, the linear waveguides have been created by employing the linear interference effect. The layout is realized within 26 × 22 circular silicon rods in a hexagonal lattice with a simple geometry and have not used any non - linear material.

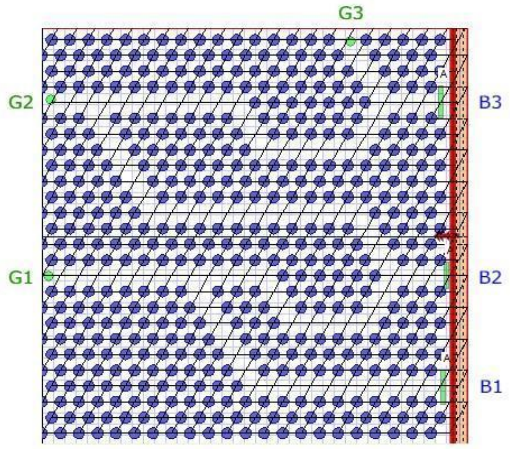

Figure 4. Schematic layout of 3-bit All Optical Binary to Gray Code Converter

V. SIMULATION RESULTS AND DISCUSSION:

The newly designed all-optical code converters were simulated using Two-Dimensional – Finite Difference Time Domain (2D- FDTD) method utilizing OptiFDTD software. A Gaussian modulated continuous wave optical source is kept at all the input ports of the layout with a wavelength of 1550 nm or 1.55 μm and the input power level is set at 1 V/m amplitude. Observation points are placed at each of the output ports to measure the output power level. We compute the simulation results efficiently using the OptiFDTD analyzer which works on the 2D FDTD technique. The electromagnetic waves travel along while the y-axis is the axis of the dielectric rods. The magnetic field polarization and the performance are improved by applying the Perfectly Matched Boundary conditions that minimizes the unnecessary reflections at the boundaries. Since FDTD means Finite Difference Time Domain method, it is based on time domain method and for stable operation the space grids employ the following formula [23],

$$c\Delta t < \frac{1}{\sqrt{\frac{1}{\Delta x^2} + \frac{1}{\Delta z^2}}} \quad (9)$$

Where c→velocity of light in free space
Δt→step time
Δx→space time along x axis
Δz→space time along z axis

In this work logic 1 and logic 0 can be differentiated on the basis of the output power intensity at the output ports. If it is logic 1 then intensity value is P_{IN} else if it is logic 0 then the intensity value is 0 at the input ports. For the output port the distinction for the logic levels is decided by finding whether the intensity range is from 0.5 to P_{IN} then it is considered logic 1 else if the value range is below 0.4 Then it is logic 0.To determine the efficiency and performance of the design, Contrast Ratio (CR) is found using the below formula [24],

$$CR\ (db) = 10\log_{10} P_H/P_L \quad (10)$$

The contrast ratio evaluates the performance by calculating the ratio between the distinct logic levels, i.e, .logic 0(denoted by P_L) and logic 1(denoted by P_H).

TABLE 1 XOR LOGIC GATE TRUTH TABLE

Input		Output
A	B	Y=A⊕B
0	0	0
0	1	1
1	0	1
1	1	0

The truth table for the XOR logic gate is depicted in Table 1.There is one output Y and two inputs A, B. The output for contrast input combinations or logic levels gives logic 1 as output. Whereas, for inputs of the same logic level

combination gives a logic 0 as output. Now Table 2 shows the optical truth table for all-optical XOR logic gate.

TABLE 2 ALL OPTICAL XOR LOGIC GATE TRUTH TABLE

Input A		**Input B**		**Output Y**	
Logic Level	Power Level	Logic Level	Power Level	Logic Level	Power Level
0	0	0	0	0	0
0	0	1	P_{IN}	1	732 P_{IN}
1	P_{IN}	0	0	1	739 P_{IN}
1	P_{IN}	1	P_{IN}	0	0.027 P_{IN}

The All-optical XOR structure has four different combinations of operational states with two inputs, 0 and 1.The power level is given as input and obtained as output in the designed Photonic crystal layout and depending upon the intensity and flow of the incoming light signal the output is set with a certain intensity level, either high or low. The operating bit rate can be approximately computed from the response time. It should be as low as possible for better switching and effectual operation of the device.

TABLE 3 DIGITAL AND OPTICAL TRUTH TABLE FOR 2 BIT BINARY TO GRAY CODE CONVERSION:

INPUT						OUTPUT						CR(db)
B3		B2		B1		G3		G2		G1		
Logic level	Power level	Logic level	Power level	Logic level	Power level	Logic level	Power level	Logic level	Power level	Logic level	Power level	
0	0	0	0	0	0	0	0.009	0	0.003	0	0.003	-
0	0	0	0	1	P_{IN}	0	0.095	0	0.060	1	1.074	12.52
0	0	1	P_{IN}	0	0	0	0.133	1	0.807	1	0.913	10.53
0	0	1	P_{IN}	1	P_{IN}	0	0.129	1	1.060	0	0.328	11.147
1	P_{IN}	0	0	0	0	1	1.076	1	0.751	0	0.034	15.033
1	P_{IN}	0	0	1	P_{IN}	1	1.080	1	1.371	1	1.466	-
1	P_{IN}	1	P_{IN}	0	0	1	1.017	0	0.055	1	0.887	12.669
1	P_{IN}	1	P_{IN}	1	P_{IN}	1	1.031	0	0.239	0	0.365	13.442

The simulation for 3 bit AOBGCC is done using FDTD method in OptiFDTD analyzer and the optical and digital truth table is shown in table 3 as below.

The sample input combinations 000 and 111 are specified in Figure 5 and Figure 6 respectively .In figure 5 , all the input ports have at each input port no power applied hence there is nearly zero or no output obtained at the output ports. Then in figure 6, the input combination 111 is shown where the input ports B3, B2, and B1 has a power intensity of P_{IN} which is set at 1 V/m amplitude for which output gray logic is 100 which is attained correctly as G3 has an intensity of 1.031 and G2 and G1 has a intensity below the range of 0.4 and more close to 0 so it is consequently distinguished as logic 0.

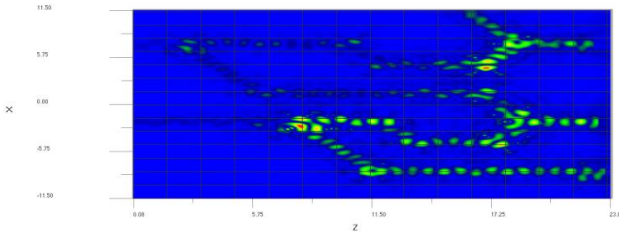

Figure 5. Simulation for input combination 000

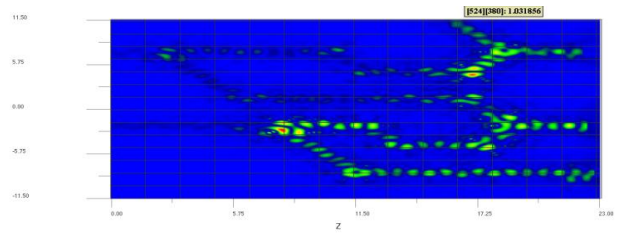

Figure 6. Simulation for input combination 111

The proposed work satisfies all the input combinations as well as shown in Table 3 with clear distinct output intensities and presents an average contrast ratio of 12.557 db for input wavelength of 1550 nm. There are only a few works on All Optical Code Converters using the photonic crystals platform and this work offers a good contrast ratio without utilizing any non linear method. Even though those few other designs show higher contrast ratio, yet it did not have a compact design even at high operating speeds.

VI. CONCLUSIONS

We have designed an All-Optical Binary to Gray Code Converter (or AOBGCC) for 3 bit input combination with 2-D Photonic crystals by employing linear interference phenomena. Using FDTD techniques we have designed it in hexagonal lattice using silicon rods in air. The average contrast ratio of all-optical binary to gray code converter obtained is 12.557 db. Gray codes in optical applications can provide advanced switching, error correction and encryption as well. This design stands useful for satellite communications transmissions, in Wi-Fi devices, wireless communication devices as well as some surveillance systems and weather radar.

REFERENCES

[1] Bao, J., Xiao, J., Fan, L., Li, X.,Hai, Y., Zhang, T. and Yang, C., "All-optical NOR and NAND gates based on photonic crystal ring resonator," Optics Communications, 329, 109-112 (2014).

[2] E. Yablonovitch "Inhibited Spontaneous Emission in Solid-State Physics and Electronics", Phys. Rev. Lett., Vol. 58, 2059 (1987)

[3] Laurent Oyhenart and Valérie Vignéras (2012). Overview of Computational Methods for Photonic Crystals, Photonic Crystals - Introduction, Applications and Theory, Dr. Alessandro Massaro (Ed.)

[4] Photonic Crystals: Optical Properties, Fabrication and Applications, William L. Dahl,Nova Science Publishers, 2011

[5] Design of all-optical AND, OR, and XOR logic gates using photonic crystals for switching applications,Dalai Gowri Sankar Rao, Sandip Swarnakar , Venkatrao Palacharla, Karyabhattu Seeta Rama Raju,Santosh Kumar(2020).

[6] Design of an All Optical Encoder/Decoder using Cross-layered 2D PCRR, Saranya D, Shankar T,2021

[7] All-Optical Non-Inverted Parity Generator and Checker Based on Semiconductor Optical Amplifiers,Bingchen Han ,Junyu Xu ,Pengfei Chen ,Rongrong Guo ,Yuanqi Gu,Yu Ning and Yi Liu,Appl. Sci. 2021

[8] All-optical wavelength conversion for telecommunication mode-division multiplexing signals in integrated silicon waveguides,Zijun Xu, Qiang Jin, Zhihua Tu, and Shiming Gao,2018
[9] All-optical digital logic AND and XOR gates using four-wave-mixing in monolithically integrated semiconductor ring lasers B. Li, D. Lu, M.I. Memon, G. Mezosi, Z. Wang, M. Sorel and S. Yu,2009
[10] An Ultrafast all optical Encryption Decryption Scheme based on XOR logic for secure transmission in Optical Networks ,2021
[11] R. P. Webb, X. Yang, R. J. Manning, G. D. Maxwell, A. J. Poustie, R. P. S. Lardenois, D. Cotter, "42Gbit/s All-optical pattern recognition system," OFC/NFOEC 2008, OTuL2 (2008).
[12] All-Optical XOR Gate Using Single Quantum-Dot SOA and Optical Filter, Evangelia Dimitriadou and Kyriakos E. Zoiros,2013
[13] All-Optical XOR Gate for QPSK In-Phase and Quadrature Components Based on Periodically Poled Lithium Niobate Waveguide for Photonic Coding and Error Detection Applications,Emma Lazzeri,Antonio Malacarne,Giovanni Serafino,A.Bogoni,2013
[14] All-optical XOR gates for QPSK signal based optical networks D. Kong, Y. Li, H. Wang, S. Zhou, J. Zang, J. Zhang, J. Wu and J. Lin,2013
[15] Salmanpour, A., Mohammadnejad, S., Bahrami, A.: All-optical photonic crystal AND, XOR, and OR logic gates using nonlinear Kerr effect and ring resonators. J. Mod. Opt. 62, 693–700,(2015)
[16] Swarnakar, S., Rathi, S., Kumar, S.: Design of all-optical XOR gate based on photonic crystal ring resonator. J. Opt. Commun.,41, 51–56 (2017)
[17] Introduction to Photonic Crystals: Bloch's Theorem, Band Diagrams, and Gaps(But No Defects) Steven G. Johnson and J. D. Joannopoulos, MIT, 3rd February ,2003
[18] O. Painter, R.K. Lee, A. Yariv, A. Scherer, J.D. O Brien, P.D. Dapkus, I. Kim, Two-dimensional photonic bandgap defect mode laser , Science, vol. 284, pp. 1819-1824, 1999.
[19] S. Noda, A. Chutinan, M. Imada, Trapping and emission of photons by a single defect in a photonic bandgap structure , Nature vol. 407, pp. 608-611 (2000).
[20] S. Damodaran, T. Shankar, and R. Anbazhagan, "All optical clocked D flip flop for 1.72 Tb/s optical computing," Microelectron. J., vol. 103, Sep. 2020, Art. no. 104865.
[21] Field Guide to Spectroscopy,Author(s): David W. Ball, Spie Press Book(2006)
[22] Compound transfer matrices:Constructive and destructive interference Petarpa Boonserm (Chulalongkorn University), Matt Visser (Victoria University of Wellington),Journal of Mathematical Physics 53 (2012)
[23] V. Kannaiyan et al., 2D Photonic Crystal-Based Demultiplexer:A Review, Advances in Photonic Crystals and Devices. Boca Raton,FL, USA: CRC Press, 2019, pp. 212–218.
[24] All-optical NOT/OR/XOR Logic Gates Based on Photonic Crystal with Low Response Time and High Contrast Ratio,Bouaouina Mohamed salah Lebbal,Mohamed Redha Bouchemat Touraya Bouchemat Mohamed,2020

Design and Implementation of CPW Fed MLDA Antenna for Wireless Personal Area Networks

Kanniyappan N[1], and Amali C[2]

[1]Department of ECE, Jerusalem College of Engineering, Chennai, India
[2]Department of ECE, SRM Valliammai Engineering College, Chennai, India
[1]kanniyappannallan@gmail.com, [2]amalic.ece@valliammai.co.in

***Abstract*—In this paper, the meander line dipole antenna (MLDA) is proposed for Wireless Personal Area Networks (WPAN) to optimize the responses. The antenna was designed on a FR4 Epoxy substrate with a dielectric constant of 4.4 and a height of 0.5 mm. The designed meander line printed antenna operating at the 2.4 GHz and return loss of -16.6 dB. The proposed antenna is designed and simulated using HFSS Electromagnetic tool. The performance of the antenna was evaluated based on return loss, operational bandwidth, radiation pattern, gain and VSWR characteristics. The fabricated antenna tested using Vector Network Analyzer (VNA) and the prototype antenna merely suitable for WPAN.**

***Keywords*—RFID, MLDA, WPAN, CPW, ISM**

I. INTRODUCTION

In recent days, Radio Frequency Identification (RFID) systems have been gaining a growing interest in the telecommunication system. The capability to mark objects and people with a passive RFID tag that allows easy development of a cost-effective and low power consumption wireless networks[1]. The RFID enables identification from a distance and not in earlier bar-code technology without necessitating a Line of Sight[3]. Recent wireless communication systems require compact size, broadband and multi-band antennas. The possibility to apply these antennas for current wireless communication systems is reinvestigated by applying modifications in their Meander geometrics.

The Meander and spiral antennas are typical reader antennas for conventional case. In some cases, linearly polarized antennas also used for RFID applications. The printed antennas are commonly used in the RFID Tag. The circularly polarized antennas for the tag required in special applications[2]. RFID tag antenna designed with simple impedance transformation in order to matching the chip with special impedance, especially for UHF band applications[4]. In the microwave band, some tag antennas are also designed to integrate with the circuits with 50 ohm impedance. The methods for designing the circularly polarized reader antenna are also presented in the literature [6]. Two ports for the dual circular polarization, the aperture-coupled Meander antenna integrated with the branch line coupler is preferred[5]. Modified Meander line printed dipole method is preferred to achieve the wideband. The meander-line dipole antenna is proposed based on Coplanar Waveguide (CPW) antenna design, a large number of meander antennas for RFID applications have been studied and reported in the literature.

II. RFID ANTENNA TECHNOLOGY

Potential applications of the RFID technology inspired the development of various antennas for the RFID systems. A lot of antennas with high performance for various requirements have been analyzed. The design of RFID antennas was facing many challenges like antenna structure, thickness, size of the antenna, operating frequency, bandwidth, radiation pattern, polarization, mutual coupling between the antennas, and scattering. In the present RFID system, the reader antenna is designed to be a circularly polarized radiation pattern.

TABLE I. FREQUENCY RANGES FOR RFID SYSTEMS

Frequency Range	Remarks	Allowed Tx Power
<135 KHz	Low frequency, Inductive coupling	72dBµA/m
6.765-6.795 MHz	MF Band [ISM],Inductive coupling	42dBµA/m
7.40-8.80 MHz	MF Band, Used for EAS (Electronic Article Surveillance)Only	9dBµA/m
13.553-13.567 MHz	Medium Frequency(13.56MHz,ISM), Inductive coupling, wide spread usage for contact less smart cards (ISO 14443,MIFARE,LEGIC),smart labels(ISO 15693,tag-IT,I-Code) and Item management, (ISO 18000-3)	42dBµA/m
26.957-27.283 MHz	MF Band (ISM, Inductive coupling, special applications only)	42dBµA/m
433 MHz	UHF(ISM),Backscatter coupling, rarely used for RFID as there are more ISM devices working	10-100mW
868-870 MHz	UHF(SRD),backscatter coupling	500mW (Europe)
902-928 MHz	UHF(SRD),backscatter coupling	4 W-Spread spectrum (USA/Canada)
2.4-2.483 GHz	SHF(ISM),backscatter coupling, several systems,(vehicle identification: 2.446-2.454GHz)	4 W-Spread spectrum (USA/Canada)

Table.1 shows the different frequency ranges of RFID Systems, In order to design the antenna for the RFID system, some problems occurs, such as the environmental

effects on RFID tag antennas, especially surrounded by metallic objects, should be considered. Designing the RFID tag antenna, which is mounted on the metallic objects, also faces a challenging task. The EM scattering of the RFID antenna is also introduced and discussed, and relative calculations have been performed. A MLDA with a large dimension working in Industrial Scientific and Medical (ISM) band is proposed. A low power slotted Meander antenna for RFID tag reader applications also preferred. A novel asymmetric cross slotted Meander antenna was proposed in for circular polarized radiation for UHF RFID reader and WiMAX applications which offers better bandwidth and reduction in VSWR[3].

III. Design Of Meander Line Dipole Antenna

The literature survey was carried out for designing the proposed antenna. The design of the meander line antenna will begin from the single element. It is then developed into the five elements and finally the S-parameter, gain and radiation pattern is computed through HFSS Electromagnetic simulation tool. The height of the substrate is given by

$$h_s \leq \frac{0.3c}{2\pi f\sqrt{\varepsilon_r}} \quad (1)$$

where
h_s=height of the substrate
f=frequency in GHz
c=velocity of light in m/s
$\mathcal{E}_r$= Substrate dielectric constant

Also, the length of the Meander can be calculated from the specified equation:

$$L=\frac{c}{2f\sqrt{\varepsilon_{eff}}} - 2\Delta L \quad (2)$$

Where, $\mathcal{E}_{eff}$ = effective permittivity which is given by

$$\varepsilon_{eff}= \left[\frac{\varepsilon_r+1}{2}\right]+\left[\frac{\varepsilon_r-1}{2}\right]\left[\frac{1}{\sqrt{1+\frac{12hs}{wp}}}\right] \quad (3)$$

Or, ΔL = physical length can be calculated from the below

$$\Delta L=h_s\left[\frac{0.412hs(\varepsilon_{eff}+0.3)\left(\frac{wp}{h_s}+0.264\right)}{(\varepsilon_{eff}-0.258)\left(\frac{wp}{h_s}+0.8\right)}\right] \quad (4)$$

The length of the substrate is found by:

$$L=L_p+6h_s \quad (5)$$

Finally, the width of the substrate is found by:

$$W=w_p+6h_s \quad (6)$$

The single element meander line antenna is designed and it will resonate at 2.4 GHz band. The antenna substrate is made on FR4 Epoxy with dimensions are 40 mm x 32 mm x 0.5 mm and coplanar waveguide dimensions are 13 mm x 10 mm. The designed MLDA with coplanar waveguide is shown in Fig. 1.

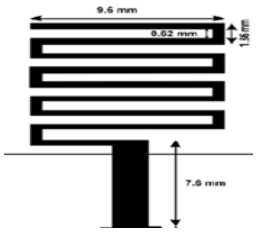

Fig. 1 The MLDA model

The Proposed CPW fed antenna consists of a single conducting circuit printed onto a dielectric substrate with a pair of return conductors and these conductors are on the top plane of the substrate, and hence are coplanar. The main advantage of the CPW fed antenna is the active elements mounted on top of the circuit and it provides a high frequency of operations. The CPW-fed antenna does not require any parasitic discontinuities in the ground plane. The meander line element dimensions are 28 mm and 2 mm with a thickness of 0.035 mm using the dielectric substrate having a relative permittivity of 4.4 with a diameter of 2 mm and the distance between the two meander line elements is 4 mm. The gap between the feed and the coplanar waveguide is 1 mm. The dimensions of the feed are 2 mm x 18 mm with a thickness of 0.035 mm.

IV. Simulated Results

The antenna performance with the coplanar waveguide has examined through HFSS EM simulation tool. HFSS is 3D full wave electromagnetic field simulation tool and it provides E-Fields, H-Fields, currents, S-parameters and near and far field radiation field. The HFSS tool is based on the Finite Element Method (FEM) where it is numerical technique for finding approximate solutions to Partial Differential Equations. In this simulation the meander line antenna operating frequencies from 300 KHz to 3.2 GHz. The simulated results like return loss, VSWR, impedance matching, and higher bandwidth are determined. Fig. 2 shows that three dimensional of MLDA.

A perfect MLDA should have lower return that is below -10 dB. Fig.3 shows the return loss characteristics of the meander line antenna operating at 2.4 GHz and the return loss of -16.6 dB. Meander line antenna operating at 2.4 GHz and the return loss of -16.6 dB.

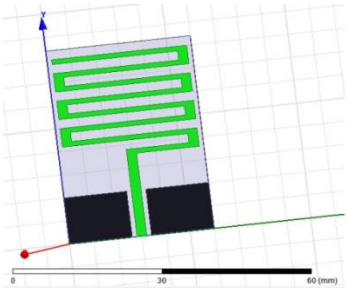

Fig. 2 3D view of proposed MLDA

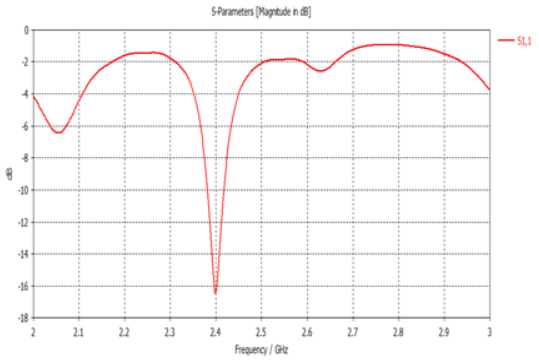

Fig.3 Return loss of MLDA at 2.4GHz

The 2D radiation pattern of the proposed antenna is shown in Fig.4 and in Fig.5 shows the 3D radiation pattern characteristics of proposed antenna. The radiation pattern provides better coverage over far-field network environments. All the graphs are plotted based on the return loss and radiation pattern. The designed MLDA antenna having return loss of -16.6 dB at 2.4 GHz for providing the better coverage for WPAN environments. The designed antenna will be used for mobile handsets, wireless dongles and Bluetooth device.

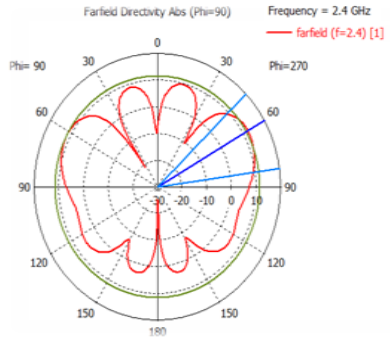

Fig.4 2D radiation pattern of MLDA at 2.4 GHz

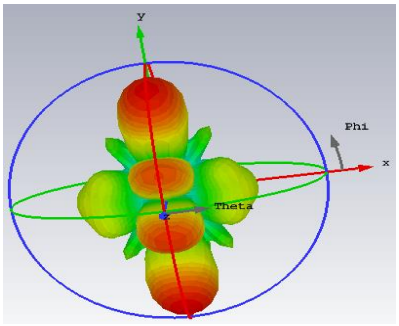

Fig.5 3D radiation pattern of MLDA at 2.4 GHz

V. Experimental Results

The proposed meander-line antenna has been fabricated on a FR4 substrate. The fabricated meander-line antenna is shown in Fig. 6 and their characteristic analyzed by a VNA and it provides better performance over rages of frequencies. Fig.7 shows the return loss (S_{11}) measurement of the given meander-line antenna and its operating spectrum ranging from 300 KHz to 3.2 GHz. The measured results are in good agreement with the simulated ones. The return value at 2.4 GHz is -42.2 dB with respect to the reference point -30 dB.

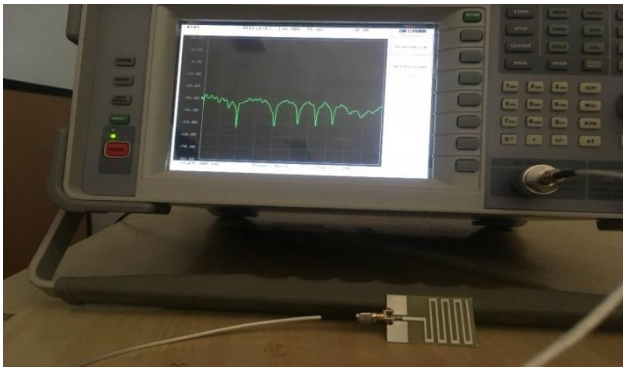

Fig.6 Measurement Setup of fabricated MLDA using VNA

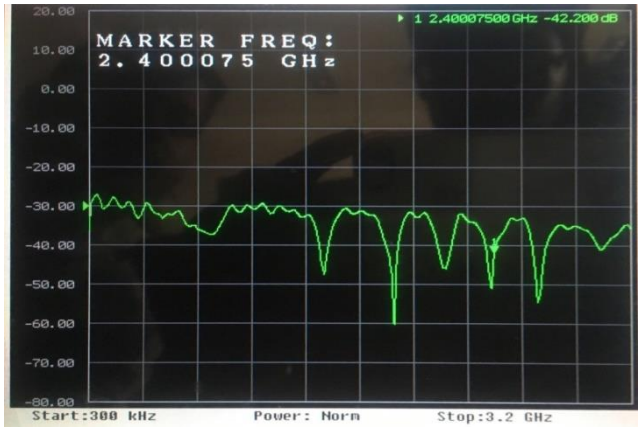

Fig.7 Return Loss (S_{11}) measurement of MLDA using VNA

VI. Conclusion

An electrically small MLDA operating at 2.4 GHz band is designed, fabricated and tested using VNA. The antenna provides enhanced performance at 2.4 GHz with a return loss of -16.6 dB. The MLDA also provides a reflection coefficient, fair radiation pattern and a good gain enhancement of 7.2 dB with return loss of -16.6 dB. The proposed MLDA is working in multiple bands ranging from 1.6 GHz to 3.2 GHz spectrum. The MLDA antenna will be applicable for WPAN, LTE and Bluetooth devices.

References

[1] Mishra, Durga Prasad, Biswajit Dwivedy, Tanmaya Kumar Das, and Santanu Kumar Behera. "MIMO antenna applications: RFID, WLAN, wearable antennas, and IoT." *In Multifunctional MIMO Antennas*, pp. 227-250. CRC Press, 2022.

[2] Paul, Kajol Chandra, and Anis Ahmed. "High Gain Microstrip Patch Array Antenna for Long Range Microwave RFID Applications." *In 2021 5th International Conference on Electrical Information and Communication Technology (EICT)*, pp. 1-6. IEEE, 2021.

[3] Liu, Xinxin, Shaojun Fang, and Hongmei Liu. "A Compact Dual-Band Circularly Polarized RFID Reader/WLAN Antenna." In 2021 9th *International Conference on Communications and Broadband Networking*, pp. 269-273. 2021.

[4] Desai, Arpan, Trushit Upadhyaya, and Merih Palandoken. "Dual band slotted transparent resonator for wireless local area network applications." *Microwave and Optical Technology Letters*, 60, no. 12 (2018): 3034-3039.

[5] Jahanbakshi, Gh.Moradi, R.Sarraf Shirazi, "Design and Simulation of Different Types of Meander Line Antennas with Improved Efficiency", *PIERS Proceedings*, Moscow, Russia, Aug. pp.19-23, 2012.

[6] Chen, Zhi Ning, "Antennas for Portable Devices", Sussex, England: *John Wiley and Sons Ltd*, 2007, pp.20-21.

[7] N.Kanniyappan, Dr. R. Indra Gandhi, "Design and Analysis of Microstrip Patch Antenna Feeding Techniques", *IEEE Proceedings of*

International Conference on Computational Intelligence and Computing Research, 2011, Pages 1268-1273.

[8] Constantine A. Balanis ,"Antenna theory Analysis and Design". *A John Wiley & Sons Inc., Publication*, 3rd Edition, pp. 817-820, 2005.

[9] S.R Best and J.D Marrow, "Limitations of Inductive Circuit Model Representations of meander line antennas", VOL. 1, pp 852-855, *IEEE Trans. Antenna and Propagation Society International Symposium*, June 2003

[10] Inder Bahl, "Lumped Elements for RF and Microwave Circuits", *ArTech House Inc*., 2003, pp. 430.

[11] K.L Wong, "Planar Antennas for Wireless Communications", New York, 2003.

[12] Mohammad S. Shaeawi , Yanal S. Faouri, and Sheikh S. Iqbal, "Design of an electrically small Meander Antenna for LTE Mobile Terminals in the 800MHz Band", *IEEE GCC Conference & Exhibition (GCC)*, Feb. 19-23, UAE, 2001.

[13] Pozar, David. Microstrip Antennas: The Analysis and Design of Microstrip Antennas and Arrays. *United States, Wiley*, 1995.

[14] J.Rashed and C . T. Tai, "A new class of resonant antennas", *IEEE Trans. Antennas propagate*, Vol. 39, pp. 1428-1430, Sept 1991.

Artificial Intelligence and Machine Learning Based Wireless Localization

Charu Jain[1*], Indu S[2], Meghna Govind[3], N. Venkateswaran[4]

[1–4]Dept of ECE, Sri Sivasubramaniya Nadar College of Engineering,
Kalavakkam, Chennai, India – 603110

[1]haru18033@ece.ssn.edu.in

Abstract—Localisation is of great significance in the field of wireless communication. To determine the position of the unknown node, it must use two or three Access Points (APs) that comprise certain positioning information. There are a number of representative range-based methods, including time of arrival (TOA), weighted centroid locating algorithm, received signal strength intensity (RSSI), and time difference of arrival (TDOA) signal, that are received by the receiver. RSSI method uses the signal strength received from the APs to estimate the position of the unknown nodes. RSSI based method has many advantages and is widely used in position tracking. An AI/ML regression model has been devised to predict the latitude and longitude of the unknown node given a set of features. The data was preprocessed through data restructuring, data smoothening, feature selection and data augmentation and the parameters for each of these techniques were optimized individually. The proposed model can be used in a diverse and dynamic environment with good accuracy. The model gave a maximum error of 8.38m and an average error of 4.09m in a 35x15m field and maximum error of 19.25m and an average error of 12.92 in a 50x50m field.

***Keywords*—5G, Beyond 5G, artificial intelligence (AI), Localization, wireless communication systems, machine learning (ML)**

I. INTRODUCTION

Localization is extensively used in Wireless Sensor Networks (WSNs) to identify the current location of the sensor nodes and more so in 5G LANs (Local Area Networks). This is because of the highly increased usage of smart networks in recent times. In most applications, wireless sensor nodes in a WSN are randomly deployed (S. Hara et al [1]). Thus, localisation of these nodes in a Wireless Sensor Network is vital in most applications. Global positioning system (GPS) is the leading stem of localization; however, its accuracy significantly degrades when the number of satellites that can be seen from the receivers decreases or due to the impact of reflection from the structures. An alternative to this is using a Wifi based positioning system. In any WSN, there are fixed nodes which are called Access points or APs and other nodes which randomly join and leave the network whose position is not known. Access points in WSNs obtain their location through GPS modules. Whereas, unknown nodes need to calculate their location by communicating with the anchor nodes using localization algorithms. Localisation can be defined as estimating the position of any node in a network. Localisation can be broadly categorized as range-based and range-free techniques. Received Signal Strength Indicator (RSSI) based localisation is one of the range based localization techniques. The objective is to verify if the AI/ML aided localization utilizing received signal strength indicator (RSSI) observed at the terminal can achieve a similar accuracy as the GPS-based localization. Machine learning algorithms can be used to create a model that can take in RSSI values from the Access points and use these values to predict the location of unknown target nodes, in any given area of interest. There are a plethora of applications of this kind of localisation model. It can be used to monitor pedestrian flows in air terminals and stations, the position of medicines in hospitals for easy access and position of customers in stores and shopping malls. With this positioning system, we can analyze the flow and movement of people around a venue, giving essential insights on the type of layout and areas of improvement to increase sales at stores, monitor passenger flow at stations, minimize wait times at restaurants, or differentiate stand pricing at conventions. This is a good replacement of GPS in places with complex infrastructural environments like multistory buildings, airports, alleys, parking garages, and underground locations and in research.

II. BACKGROUND

Received Signal Strength Indicator is a measure of power level that an RF client device receives from an access point or router. Localisation using RSSI exploits the fact that the received signal power attenuates with distance which can be seen in Fig1.

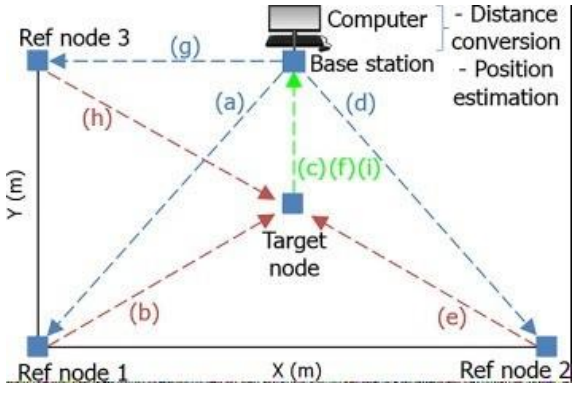

Fig. 1 – RSSI based localisation [2]

The mathematical relationship between RSSI and distance is given by equation 1

$$RSSI = A - 10 \cdot n \cdot (d) \quad (1)$$

where, RSSI - RSSI value of multiple times of measurement, A - the signal strength which is received from reference nodes at the distance d0 n - path attenuation factor in the environment d - signal transmission distance (m) There are multiple other methods that use a distance based location estimation apart from Received Signal Strength (RSS) such as Angle of Arrival (AOA), Time of Arrival (TOA), Time difference of Arrival (TDOA) and so on. Hara et al [1] compared the TDOA and TOA methods in non line of sight and line of sight which led to the conclusion that TOA worked better in LOS dominated environment whereas TDOA worked better in Non - LOS dominated environment. Hara et al [3] yet again compared the RSSI and TDOA based location estimation methods with an experiment and concluded that the RSSI method works better in a crowded Non - LOS (Non line of sight) environment which is an ideal indoor environment. Traditionally, the Maximum Likelihood method was used to solve localization as a complex optimization problem where the distance dependency of the RSSI values were not con sidered. Xu et al [2] proposed a distance based MLE approach which took the distance vs RSSI relationship into account. Mino et al [4,5] used a novel iterative method that used the additional information of RSSI among the target nodes. The log-likelihood function was found to be dependent on the RSSI values from other unknown nodes as well as APs. As the number of target nodes increased, the RMSE error was observed to decrease with higher iterations, which resulted in high complexity. Environmental factors also played a big role in attenuation of the RF signal. The following formula given in equation 2 describes the RF signal power attenuation with distance which has two parameters namely α and β which are assumed depending on the environment.

$$P(d) = \alpha \cdot d^{-\beta} \quad (2)$$

where, P - average received signal power α – parameter proportional to the received signal power at a reference distance from the transmitter, β - parameter b is a path loss exponent To avoid this assumption, Zemek et al [6] proposed a two- stage iterative algorithm which allowed to localize a target node without any prior knowledge of the parameter values. Each stage of the algorithm was implemented using different estimation methods, such as maximum likelihood (ML) and least square (LS) estimation which provides four different combinations. The methods discussed above are channel based models where the RSSI values are fitted into the given theoretical formula. In a real scenario, RSSI values undergo fluctuations due to human crossings and shadowing in the LOS of the transmitter and receiver as shown in Fig 2, which cannot be modeled accurately using the channel based models.

Poulose et al [8] used a more data based approach where a hybrid CNN followed by LSTM model was created. They created the dataset in an indoor environment with training and testing points very close to one another. The raw RSSI data were converted into RSSI heat maps which were fed into the CNN layer. The new testing points were then classified to one of the N training points as we can see in Fig 3 and Fig 4. Adege et al [10] proposed a model for both indoor and outdoor environments using the SVM and DNN hybrid model where they had utilized 35 plus APs. Due to the largeness of the dataset, LDA (Linear Discriminant Analysis) was applied to reduce the features without affecting information.

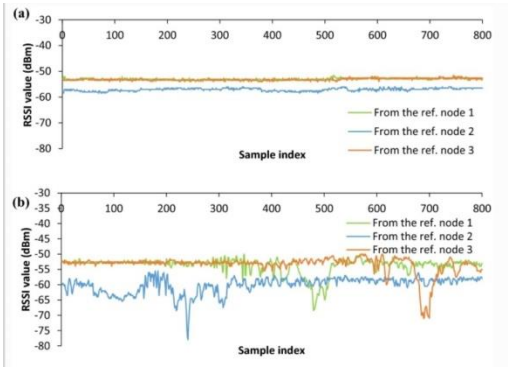

Fig. 2 – Comparing fluctuations in RSSI values without (a) and with (b) humans walking [7]

RSSI Fingerprinting is another common technique to visualize RSSI values, where the signal strength readings are taken at each point of the targeted area's Wireless Local Area Network (WLAN). Thereafter, all the readings observed are stored in a database representing the radio map (RM) of the target area. Khokhar [9] compared the Decision Tree, Random Forest, and Gradient Boosting classifier methods on a RSSI fingerprint of an indoor area. The accuracy and precision for the Random Forest classifier was found to be the highest in comparison. One more important feature to note in the above-mentioned literature is that they used a classification approach where the training data should be available for every point in the area, which is not a practical approach. G. Bhatti [11] formulated a novel way of defining multiple feature vectors to map the localization problem using different machine learning models. They also studied the impact of varying network parameters, such as anchor population, wireless channel quality, and transmitted signal power, on the localization accuracy of the models chosen by them. They also studied the impact of deploying the anchor nodes in a grid based method rather than placing them randomly in the area of interest. The results revealed interesting insights upon the use of multivariate regression model and support vector machine (SVM) regression model. G.Li et al [12] used back propagation neural network optimized by particle swarm optimization (PSO-BPNN) to train the RSSI distance model to reduce the positioning error. The RSSI fluctuations of surrounding Bluetooth nodes were detected using RSSI real-time correction method based on Bluetooth gateway and uploaded to a cloud server. The node whose location had to be determined collected the RSSIs of surrounding Bluetooth nodes and adjusted them by the RSSI fluctuation information stored on the server in real-time.They proposed a method that has better positioning accuracy than the traditional method.

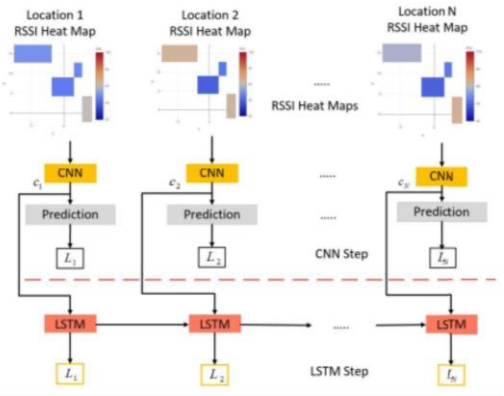

Fig. 3 – Proposed hybrid model [8]

III. AI/ML Based Wireless Localization In 5G

From the literature review it is observed that, in general, two methods of localization are widely used. One is the channel model based method and the other is a data-oriented method. The datasets used are mostly in the form of fingerprinting which is then solved as a classification problem rather than a regression problem. In the traditional localization based on RSSI, it is necessary to have an accurate modeling of the channel model that significantly impacts the localization accuracy. As opposed to treating this localization problem as a classification problem, as done in most of the previous work, here it is treated as a regression problem. Hence, the proposed solution aims to use the data-oriented localization approach and attempt to replace the model-based location with the help of powerful AI/ML techniques.

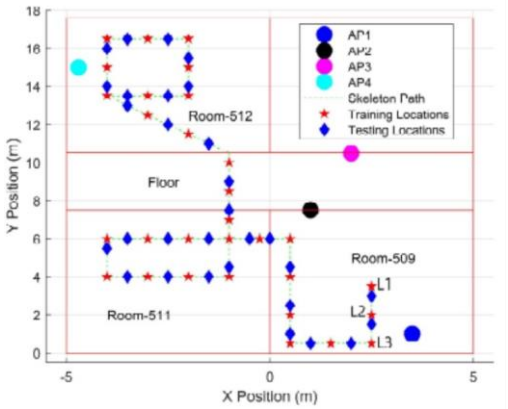

Fig. 4 – Skeleton of dataset topography [8])

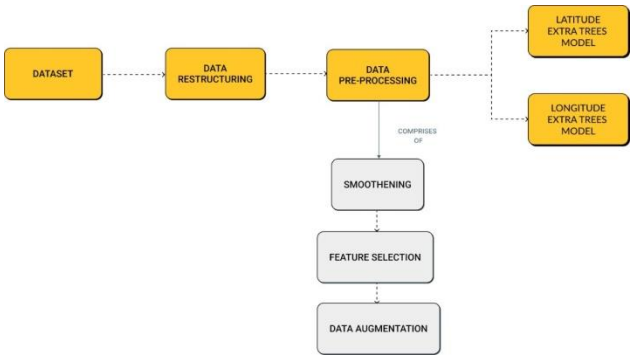

Fig. 5 – Block Diagram of the proposed methodology

The proposed work uses a data-oriented model which incorporates all RSSI fluctuations better than a channel based model. Localisation is solved with regression, where the location of the unknown node is calculated using regression analysis rather than classification to find any of the already existing locations.

Fig 5 represents the block diagram of the proposed methodology. As shown in the diagram, the dataset collected is first restructured and then preprocessed, before feeding it to the regressor model. The following sections talk about the dataset description, analysis and proposed model.

A. *Dataset Description*

The two datasets used for solving the localization problem were taken from the International Telecommunications Union (ITU). These datasets were chosen because they had sufficient datapoints and parameters. The datasets had 4 access points, 13 training and 13 testing nodes. The access points in the datasets are placed at the same height and in an outdoor environment.

As seen in Fig 6, the first dataset has two measurement setups, each with different training and testing data.

Fig. 6 – Measurement setup and location of the first dataset

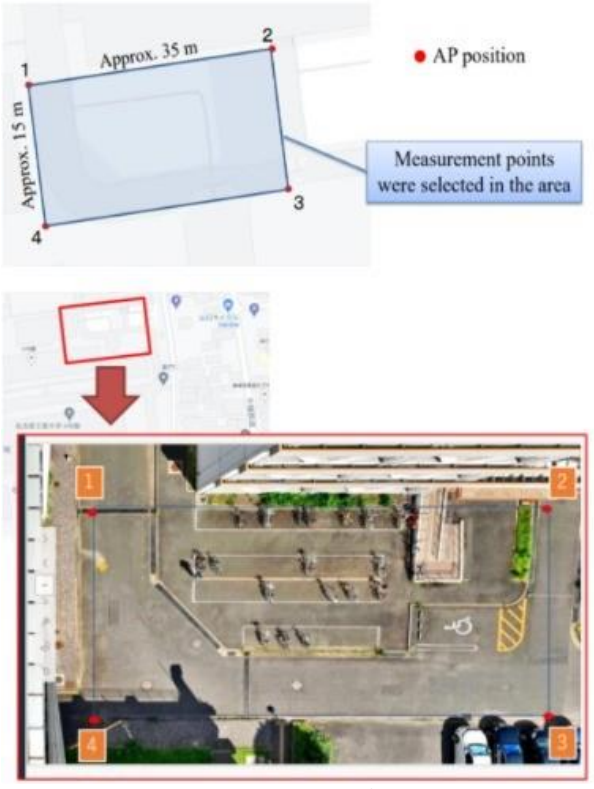

Fig. 7 – Measurement setup and location of the second dataset

So, we have 2 training and 2 testing datasets with 5200 rows each (Fig 8). The features are the same in all the datasets and are as follows: 4 Access Points 13 unknown nodes. Latitude, Longitude of APs Channel number of each

AP Timestamps RSSI (dBm) Details about the Access points are also provided to us (Fig 9).

The second dataset follows the same structure as the first but in a different location and dimension as shown in Fig 7. One significant difference between the datasets as observed from Fig 10 is that the nodes in the wireless network are not confined to the physical area covered by the APs. Due to the differences in topology, dimensions and nature of the nodes in the two datasets, the RSSI patterns vastly differ. The proposed model works well in both of these conditions.

	No.	TimeStamp(UNIX)	Latitude	Longitude	SSID	Channel	RSSI(dBm)
0	1	1631687696	35.157140	136.926306	1	11	-41
1	2	1631687697	35.157140	136.926306	1	11	-41
2	3	1631687697	35.157140	136.926306	1	11	-41
3	4	1631687697	35.157140	136.926306	1	11	-41
4	5	1631687697	35.157140	136.926306	1	11	-41
...	...	...	...	...	...	...	...
5195	5196	1631688763	35.157236	136.926489	4	1	-52
5196	5197	1631688763	35.157236	136.926489	4	1	-52
5197	5198	1631688763	35.157236	136.926489	4	1	-52
5198	5199	1631688763	35.157236	136.926489	4	1	-52
5199	5200	1631688763	35.157236	136.926489	4	1	-52

Fig. 8 – First Dataset

B. Dataset Inference: Regression problem

As observed from the datasets, the sampling period is 100 seconds for an unknown node from one AP, i.e an unknown node observes 100 RSSI values from one AP in this period. The RSSI values given does not always satisfy the RSSI distance relationship as seen in Eq1. The anomalies are as follows: Inferences from the first dataset are drawn as follows:

- In the first dataset, the RSSI values observed at every unknown node are highly dynamic and frequently continue to have the same RSSI value even for subsequent target nodes (Fig 11) . Ideally the RSSI values from one AP to a fixed node should be constant.
- In the second dataset, RSSI values observed at each target node is constant, but two or more target nodes which are different distances from the APs have the same RSSI value.
- From Fig 12 it is observed that the distance between AP4 and unknown node 1 is lesser when compared to the other APs and thus should have the highest signal strength according to the RSSI distance relationship. From Fig 13 we can see that in reality, this is not the case.
- The RSSI values observed at multiple unknown nodes remain the same even though they are in different positions as shown in Fig 14.

The proposed solution models a complex environment as described above with only 400 RSSI values (data points) per node. The model works well in both of these datasets which is bolstered by the low error of our model in both these situations.

IV. DATA PRE-PROCESSING

The dataset has very few data points to model the irregularities. Data preprocessing techniques will help enhance the dataset to get a better accuracy. These preprocessing steps consist of Data restructuring, Data smoothening, Data augmentation and Feature Selection.

AP SSID	Latitude	Longitude	Hight Difference(m)	Indoor/Outdoor
1	35.1573202	136.926447	0	Outdoor
2	35.157347	136.9268074	0	Outdoor
3	35.1572018	136.9268269	0	Outdoor
4	35.157165	136.9264698	0	Outdoor

Fig. 9 – Details of the Access Points (APs) in the first dataset

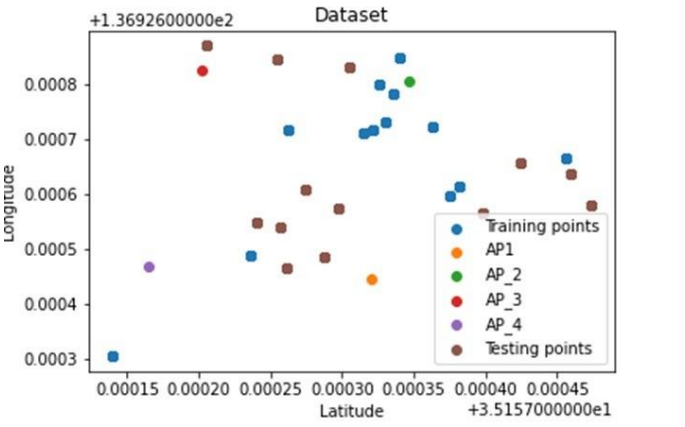

Fig. 10 – Datapoints in the second dataset

A. Data Restructuring

The two datasets which originally contained 5200 rows with 6 features and 8 features respectively were restructured to a dataset of 1300 rows with 12 features as seen in Fig 15. This step in pre-processing is performed so that the model can learn the dataset with ease. The 12 features are RSSI values from all APs, and latitude and longitude of all APs.

B. Data Smoothening

The RSSI values observed by the target nodes are highly dynamic. And in some cases, the RSSI values are similar for 2 or more target nodes, which hampers accurate learning process of the model. This in turn weighs down the accuracy of the model.

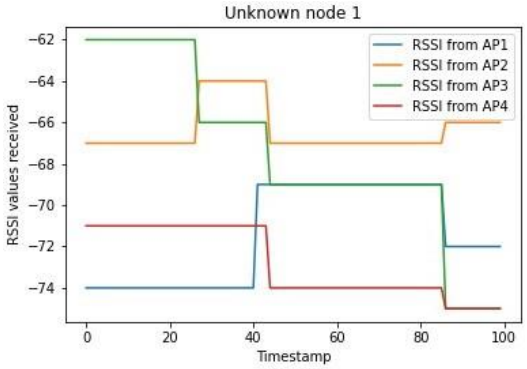

Fig. 11 – RSSI values from APs to unknown node 1 in dataset 1

Therefore, a data smoothening method was formulated called the windowing method. The process is to select a window size 'n' and to determine the average of these values. The weightage of this average value on the current RSSI values is determined by α as demonstrated in equation 3.

$$currval = currval \cdot \alpha + (1 - \alpha) \cdot avgval \quad (3)$$

The smoothening process displayed in Fig 12 has been done utilizing the optimum value of α i.e, 0.2 , to give more weightage to the average of previous values.

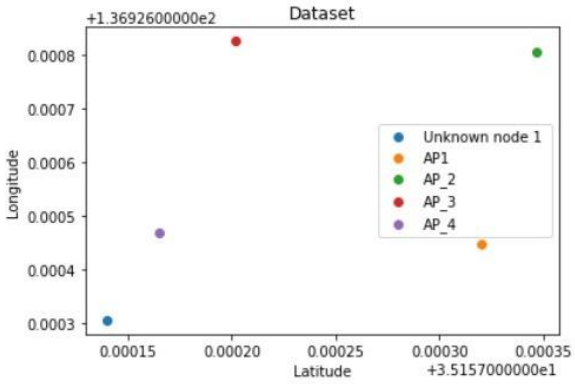

Fig. 12 – Topography of 4 APs and unknown node 1

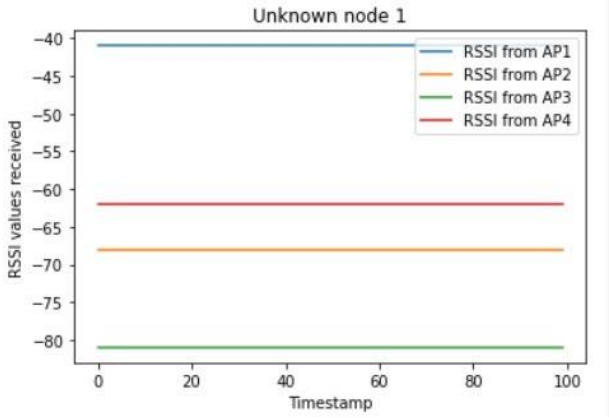

Fig. 13 – RSSI values from APs to unknown node 1

C. *Feature Selection*

Irrelevant or partially relevant features can negatively impact model performance. Having 5 irrelevant features in the data can decrease the accuracy of the model.

Hence, only those features which contribute most to the output are selected. Correlation is a measure of how 2 variables change together. SelectKBest() from scikitlearn machine library uses correlation statistics to provide scores for all features. The scores that are in the negative range or zero are neglected and the scores that fall under the positive range are considered. The scores for the datasets are as shown in Fig 16.

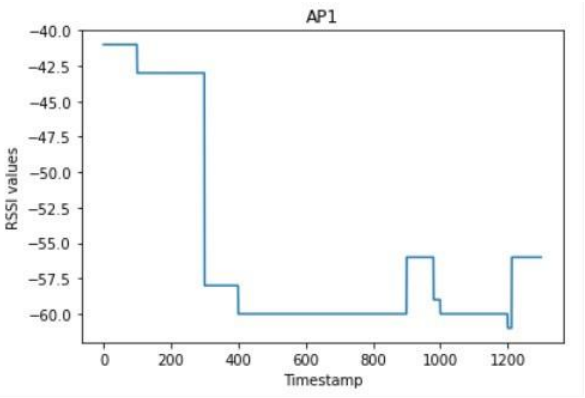

Fig. 14 – RSSI values from AP1 to all 13 unknown nodes

	AP_1	AP_2	AP_3	AP_4	AP1_x	AP1_y	AP2_x	AP2_y	AP3_x	AP3_y	AP4_x	AP4_y
0	-74	-67	-62	-71	35.158465	136.924283	35.158889	136.92435	35.15851	136.923762	35.158931	136.923835
1	-74	-67	-62	-71	35.158465	136.924283	35.158889	136.92435	35.15851	136.923762	35.158931	136.923835
2	-74	-67	-62	-71	35.158465	136.924283	35.158889	136.92435	35.15851	136.923762	35.158931	136.923835
3	-74	-67	-62	-71	35.158465	136.924283	35.158889	136.92435	35.15851	136.923762	35.158931	136.923835
4	-74	-67	-62	-71	35.158465	136.924283	35.158889	136.92435	35.15851	136.923762	35.158931	136.923835
...	...	...	...	...	...	...	...	...	...	...	...	...
1295	-73	-88	-77	-63	35.158465	136.924283	35.158889	136.92435	35.15851	136.923762	35.158931	136.923835
1296	-73	-88	-77	-63	35.158465	136.924283	35.158889	136.92435	35.15851	136.923762	35.158931	136.923835
1297	-73	-88	-77	-63	35.158465	136.924283	35.158889	136.92435	35.15851	136.923762	35.158931	136.923835
1298	-73	-88	-77	-63	35.158465	136.924283	35.158889	136.92435	35.15851	136.923762	35.158931	136.923835
1299	-73	-88	-77	-63	35.158465	136.924283	35.158889	136.92435	35.15851	136.923762	35.158931	136.923835

Fig. 15 – Dataset 1 after restructuring

D. *Data Augmentation*

Data Augmentation is a technique used to increase the amount of data by adding copies of already existing data. A new technique is devised that is used to increase the amount of already existing data. A factor "num" is utilized, which determines by what amount the dataset would increase.

Based on this factor, rows belonging to a particular target node were chosen to be appended to the same node's data points. For every unique target node, "num" number of extra rows were generated. This value is optimized during training. This reduces the risk of overfitting and the accuracy on unseen data is improved.

V. MODEL

Data preprocessing techniques mentioned above prepares the data to be analyzed by the model. The proposed model is a regression based model which is a type of supervised learning task that is used in cases where the value to be predicted is continuous. To predict the Latitude and Longitude of the unknown node, given a set of dependent features, Regression is used. Extra Trees regression model is used to model the given datasets.

The Extra Trees algorithm works by creating a large number of unpruned decision trees from the training dataset. Predictions are made by averaging the prediction of the decision trees in the case of regression. A separate latitude and longitude extra trees model is created.

The training and testing processes are as shown in Fig 18. The values that are to be optimized for data pre- processing are done during the training process.

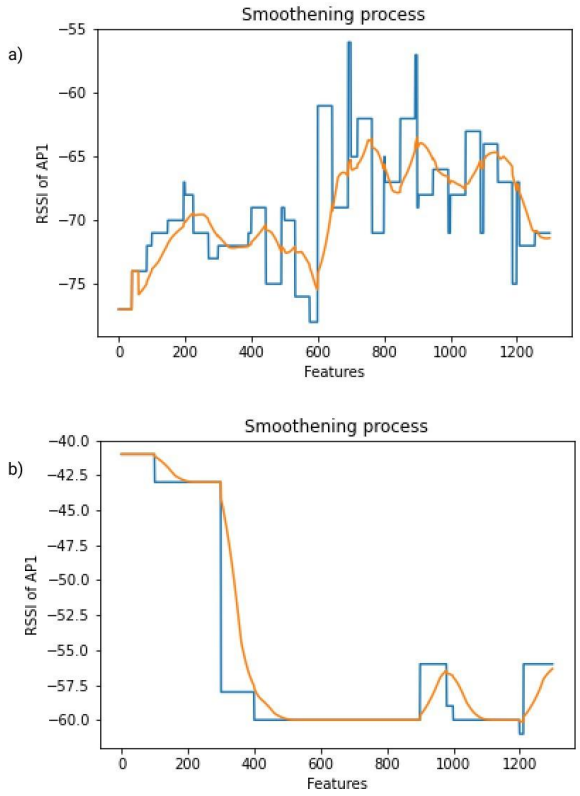

Fig. 16 – Smoothening in a)Dataset 1 and b)Dataset 2

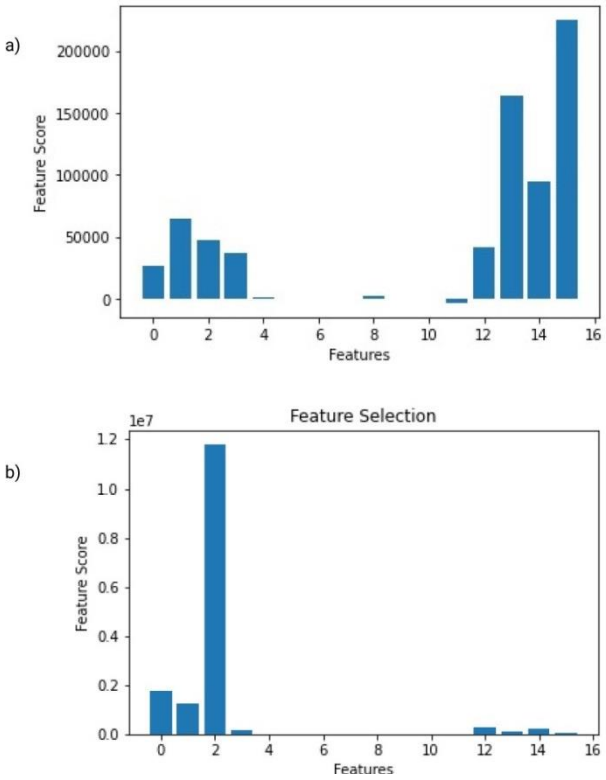

Fig. 17 – Feature scores for a)Dataset 1 and b)Dataset 2

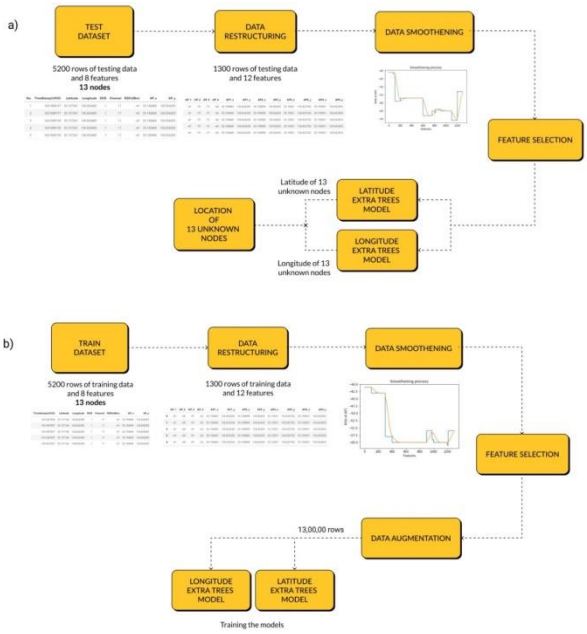

Fig. 18 – a) Training and b)testing block diagram of proposed model

TABLE 1 – RESULTS

	Maximum Error	**Average Error**
Dataset 1	19.25m	12.92m
Dataset 2	8.39m	4.09m

VI. RESULTS

The data from both the datasets was fed to the proposed model and the following evaluation metrics were calculated to measure the efficiency of the model Maximum Error (in metres), Average Error (in metres) and Latency of the model. For the first dataset, as shown in Table 1, a maximum error of 19.25m and average error of 12.92m were obtained for a 50x50 area. For the second dataset, a maximum error of 8.38m and average error of 4.09m were obtained for a 35x15 target location. The latency of the model which utilized the second dataset was measured to be 0.17ms.

VII. CONCLUSION

In this work, an AI/ML method was used to locate a wifi node in a WSN using the RSSI values of the APs. The approach to the localization problem was purely based on regression rather than classification, unlike the case in multiple related works. Hitherto, the data was analyzed and data processing was performed, wherein the data was restructured to increase model learning accuracy and also increased the features from 6 to 12. Furthermore, the problem of RSSI variability was tackled using a smoothening technique wherein, the smoothening parameters were optimized such that the RSSI distribution given in the dataset is intact while removing unnecessary fluctuations causing errors in the learning algorithm. Furthermore, a new augmentation technique was employed which increased the data points in the datasets without interfering with the datasets' variability or distribution. Two models were constructed, one to predict the latitude and the other to predict the longitude. An average average error of 12.92m was obtained in the 50x50m field and an average error of 4.09m was obtained in the 35x15m field.

REFERENCES

[1] S. Hara, D. Anzai, T. Yabu, K. Lee, T. Derham and R. Zemek, "A Perturbation Analysis on the Performance of TOA and TDOA Localization in Mixed LOS/NLOS Environments," in IEEE Transactions on Communications, vol. 61, no. 2, pp. 679-689, February 2013, doi:10.1109/TCOMM.2013.012313.110509.

[2] J. Xu, J. He, Y. Zhang, F. Xu, and F. Cai, "A Distance-Based Maximum Likelihood Estimation Method for Sensor Localization in Wireless Sensor Networks," International Journal of Distributed Sensor Networks, vol. 2016, pp. 1–8, Apr. 2016, doi: 10.1155/2016/2080536.

[3] S. Hara and D. Anzai, "Experimental Performance Comparison of RSSI - and TDOA-Based Location Estimation Methods," in VTC Spring 2008 – IEEE Vehicular Technology Conference , May 2008, pp. 2651–2655. doi: 10.1109/VETECS.2008.581 .

[4] R. Mino et al., "A Belief Propagation-Based Iterative Location Estimation Method for Wireless Sensor Networks," 2006 IEEE 17th International Symposium on Personal, Indoor and Mobile Radio Communications, 2006, pp. 1-5, doi: 10.1109/PIMRC.2006.254179.

[5] R. Mino et al., "A Novel Iterative Technique for Collaborative Location Estimations," in 2006 3rd International Symposium on Wireless Communication Systems, Sep. 2006, pp. 564–568. doi: 10.1109/ISWCS.2006.4362362.

[6] R. Zemek, D. Anzai, S. Hara, K. Yanagihara, and K. Kitayama, "RSSI-based Localization without a Prior Knowledge of Channel Model Parameters," Int J Wireless Inf Networks, vol. 15, no. 3, pp. 128–136, Dec. 2008, doi: 10.1007/s10776-008-0085-6.

[7] Wattananavin, T., Sengchuai, K., Jindapetch, N. et al. A Comparative Study of RSSI-Based Localization Methods: RSSI Variation Caused by Human Presence and Movement. Sens Imaging21,31(2020). https://doi.org/10.1007/s11220-020-00296-1

[8] A. Poulose and D. S. Han, "Hybrid Deep Learning Model Based Indoor Positioning Using Wi-Fi RSSI Heat Maps for Autonomous Applications," Electronics, vol. 10, no. 1, Art. no. 1, Jan. 2021, doi: 10.3390/electronics10010002.

[9] Z. Khokhar and M. Siddiqi, "Machine Learning Based Indoor Localization using Wi-Fi and Smartphone," Journal of Independent Studies and Research Computing - SZABIST, Vol: 18 – Issue: 1, Apr. 2021.

[10] A. B. Adege, H.-P. Lin, G. B. Tarekegn, Y. Y. Munaye, and L. Yen, "An Indoor and Outdoor Positioning Using a Hybrid of Support Vector Machine and Deep Neural Network Algorithms," Journal of Sensors, vol. 2018, p. e1253752, Dec. 2018, doi: 10.1155/2018/1253752.

[11] G.Bhatti, "Machine Learning Based Localization in Large-Scale Wireless Sensor Networks," Sensors (Basel), vol. 18, no. 12, p. 4179, Nov. 2018, doi: 10.3390/s18124179.

[12] G. Li, E. Geng, Z. Ye, Y. Xu, J. Lin, and Y. Pang, "Indoor Positioning Algorithm Based on the Improved RSSI Distance Model," Sensors, vol. 18, no. 9, Art. no. 9, Sep. 2018, doi: 10.3390/s18092820.

Video Surveillance based Congestion Avoidance System during Evacuation

Dinesh Anton Raja P[1], T.D. Subha[2], Rajalakshmi D[3], Priyadharshini V[4]

[1-4]Department of Electronics and Communication Engineering,
R.M.K. Engineering College, Chennai India

[1]pdaraja@gmail.com, [2]tdsubha2010@gmail.com, [3]raja20330.ec@rmkec.ac.in,
[4]priy20326.ec@rmkec.ac.in

***Abstract*—Buildings and infrastructures are becoming progressively complex. Identifying and counting people in a crowded scene is a challenging problem. Situational awareness for crowd control can be increased by providing real-time estimates of the number of individuals entering and alternately exiting a venue. In a serious situation like fire accidents, the exposure to harm is very high and people may not be able to escape from the building safely. Due to increasing human congestion during evacuation the emergency exit numbers have little effect. This project proposes for people counting based on head detection to evaluate the number of people approaching each emergency exit and intimating the safest path to the occupants thus accomplishing the aim of the project.**

Keywords—Blob detection; Markov Random Field Segmentation; Bounding box.

I. INTRODUCTION

In a serious accident like fire in buildings, controlling the crowd becomes extremely important. Detecting people and keeping a count of the people present at each emergency exit helps in directing the crowd to the exits which are relatively less crowded or free. Feature based detection involves integral channel and Haar feature based head detection [5]. They are employed for detecting human heads in a crowd. Analyzing the size and position of the heads detected help in estimating total number of people in a crowd [6]. This method may fail if the area to be observed is very crowded since only few heads can be detected [1], [11]. In Foreground based detection the foreground is extracted first by removing the background from the image with the help of a reference image. The density of crowd is then estimated as a function of the number of foreground pixels [8]. This method however fails when the background changes rapidly over time [2], [12]. Optical Flow and Background Model (OFBM) is based on GEM method and LK optical flow, which is computed for the entire image. OFBM overcomes the limitations of background subtraction and optical flow, such as sensitiveness of changing light and producing accumulate errors [9]. However, the limitation of this model is that it is time consuming [3]. In generative tracking each person's location is estimated and correspondence is done by searching the most similar target candidate with the minimal reconstruction error [10]. It separates the targets from their background with the help of a classifier, and then establishes those targets jointly through correspondences across frames with the help of a target association algorithm [7]. However the disadvantage of these algorithms is that they cannot overcome occlusion [4]. In this paper, blob detection and markov random field segmentation is used for detection of human beings. Using markov random field segmentation, the pixels are classified into different classes. This feature of classifying pixels helps in detecting each person distinctly thus avoiding occlusion. This paper is segmented into four sections. Section I provides description about introduction and previous carried out work on estimation of crowd detection. Section II provides an overview of proposed system. Section III provides working methodology. Section IV provides experimental result. Finally in section V we conclude.

II. SYSTEM OVERVIEW

The figure.1 explains the overview of the system employed to obtain the target result. The fire sensor which is connected to arduino initiates the system working. The embedded vision system is given video input through the camera. The output of the embedded vision system is sent as input back to arduino. The voice playback connected to arduino responds to the signal given by arduino thereby informing people about the congested exit.

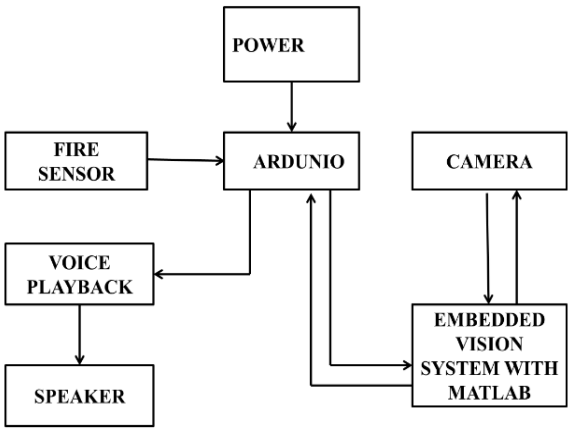

Fig 1: overview of system

When fire is sensed by the fire sensor, the signal is sent to arduino. The arduino responds to the signal and intimates

the people about the fire in the building by sending signal to voice play back and LCD display. The message is conveyed to the people through speakers. As soon as the MATLAB program is run it displays if the path is congested or not. When congestion is observed the information is sent to arduino. Arduino informs people about the congested path through voice playback.

III. WORKING METHODOLGY

The figure 2 explains the algorithm followed to detect the number of people in a frame.

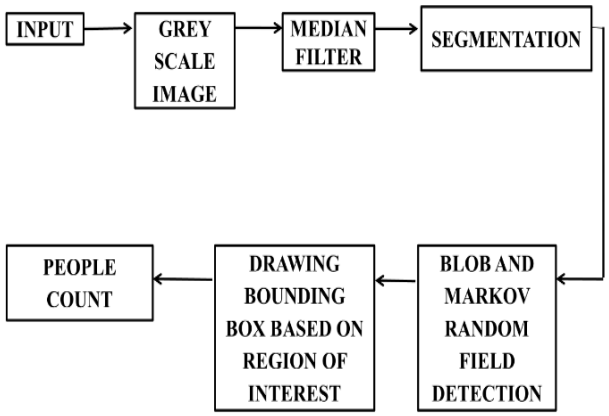

Fig 2: Algorithm of Head Detection

A. *Pre-processing:*

The video having a resolution of 320×240 pixel is taken as input and frames are extracted from the video. After extracting frames, each frame is made to undergo the preprocessing steps. The first step in pre-processing is to convert color image to gray image. This conversion is done to reduce the processing time as time required to process a gray image is less compared to that of color image. The transformation is done using the proposed equation

$$Iy = 0.333Fr + 0.5Fg + 0.1666Fb \quad (1)$$

where, *Fr*, *Fg* and *Fb* represent the intensity of R, G and B component respectively

Ir - intensity of equivalent gray level image of the RGB image.

The nature of the noise naturally added in the image is unknown so a known noise (Salt and pepper noise) is added to the image. The median filter is applied to remove noise from the image. The median filter replaces the pixel value by the median, instead of the average, of all pixels in a neighborhood w

$$y[m,n] = \text{median}\{x[i,j],(i,j)\,\hat{I}\,w\} \quad (2)$$

where w represents a neighborhood defined by the user, centered around location [m,n] in the image.

Noise reduction is performed as a pre-processing step to enhance the results of the image which is processed further.

B. *Segmentation:*

Blob detection is used to detect human blobs. Markov random segmentation is applied to the blobs detected to improve the efficiency and to overcome the problem of occlusion. Before learning about blobs in detail, the definition of blob is necessary. Lindeberg defines a blob as being a region associated with at least one local extreme, either a maximum or a minimum for resp. a bright or a dark blob. Blobs do not have a particular shape and can occur in many shape.The method used for blob detection is automatic scale selection.

C. *Automatic scale selection:*

Lindeberg's method for automatic scale selection is used for most blob detection applications. The main principle used in automatic scale selection is that it assumes a scale level, at which some combination of normalized derivatives assumes a local maximum over scales, reflects the size of the corresponding blob. The scale levels are obtained by performing Gaussian smoothing on them. The Gaussian function provides simpler pictures at course scale. It also ensures that no details are generated when the resolution is decreased. Lindeberg has presented two combinations as basic blob detectors which is used in Gaussian scale-space. They are Monge - Ampere operator and the Laplacian operator. The Laplacian operator is defined as the square matrix of 2nd-order partial derivative of image function which is trace of Hessian matrix. The Laplacian operator is employed to detect the scale-space maxima by performing product of trace and scale parameter. The scale-normalized determinant of Hessian matrix is the Monge-Ampere operator. The scale parameter is multiplied twice to obtain scale invariance. Scaling the image with a constant factor guarantees the transformation with size variations. To formulate blob detection using automatic scale selection, we assume that the points in the scale space at which square of normalized value of Laplacian

$$r^2\text{normal} = t(Lxx + Lyy) \quad (3)$$

assumes a maxima with respect to the scale and the space. These points are called as scale-space extrema of $(r^2\ \text{normal})^2$.

The position, angle and size of heads are detected as blobs using a 3D Look-Up-Table (LUT). Regions that are incorrectly identified as human blobs , are disregarded through markov random field segmentation.

D. *Markov Random Field Segmentation model:*

The image is obtained after applying markov random field segmentation is a cartoon image. This carton image is obtained by labeling image I. The pixel class of each pixel s is obtained using a class label. This class label is modeled as a discrete random variable which takes values in L Z{1, 2,.,L}. The set of labels obtained $W = \{w, s \in \notin\}$ is called the label process. This label process is the random field. The input image features such as color and texture are a realization $f\{fs \mid s \in \$\}$ from another random field, which is actually a function of label process u. Actually, the image process F is the manifestation of its underlying label

process. Finally, the overall segmentation model is made up of the label process u which is hidden and noisy image process F. The goal is to find an optimal labeling ^u which is used to maximize the posterior probability $P(w|f)$,

Estimate

$$W = \arg\max P(f|W)P(w) \quad (4)$$

where U denotes the set of all possible labeling.

E. Bounding Box

The minimum bounding rectangle (MBR), is also known as bounding box or envelope. It is an expression of the maximum extent of a two dimensional object (e.g. polygon, point, line) or set of objects within its (or their) 2-D (x, y) coordinate system, in other words min(x), max(x), min(y), max(y). Bounding box is applied to the output of Markov random segmentation to count the number of people detected. The bounding box is calculated using the formula

$$Y = (P_c, b_x, b_y, b_h, b_w, c) \quad (5)$$

where

c = class of object being detected

p = confidents of an object being present in the bounding box.

b_h = height of the bounding box.

b_w= width of the bounding box.

F. People Count

The number of people in the frame is counted based on the bounding box.

IV. Experimental Result

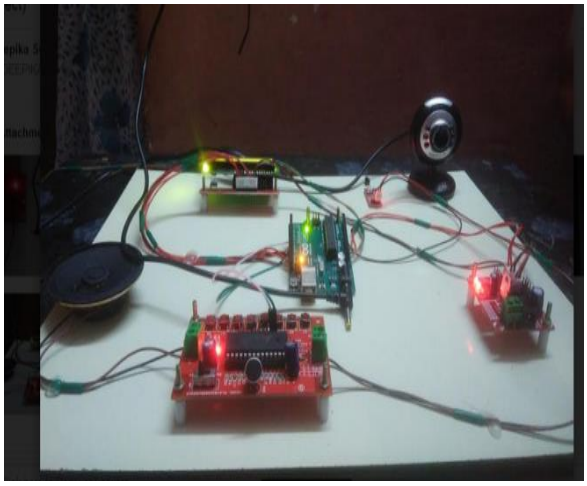

Fig 4.1 Experimental Setup

The figure 4.1 shows the experimental setup of the system. The figures given below show the video with various backgrounds which is used as the input and the output frames which is being tracked. It also contains information about the number of people in the scene.

The frames are obtained from the video. Each frame is processed to detect the number of people present in the frame.

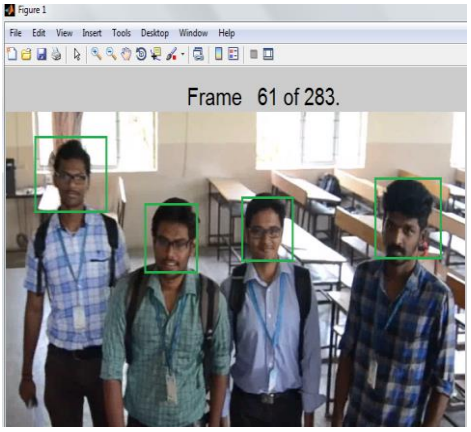

Fig 4.2 Number of People Detected in Dataset

As the people start approaching the exit, the camera located near the exit start counting the people. The figure 4.2 shows that four people are detected in frame 61 of 283.

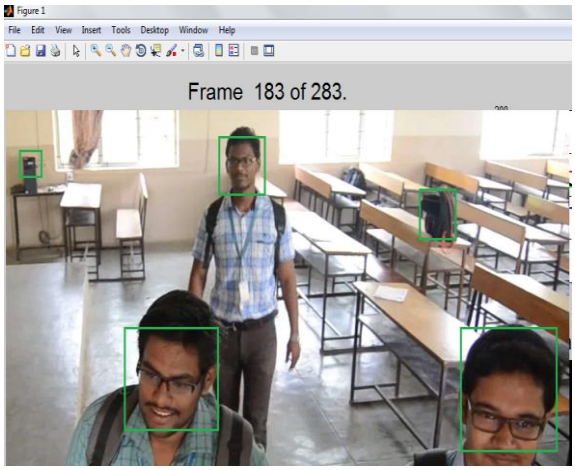

Fig 4.3 Number of People Detected in Dataset

Figure 4.3 shows frame 183 of the video input in which along with the people, bag and CPU is also detected as people

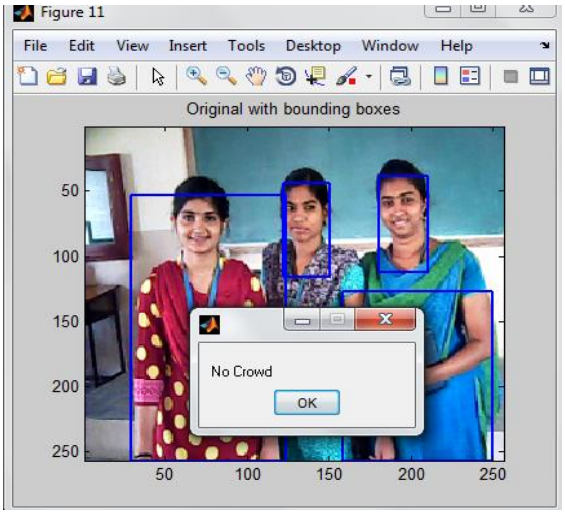

Fig 4.4 Number of People Detected in Real Time

Figure 4.4 shows the people detected with the crowd analysis done. When there are few people in the frame the message is displayed as no crowd.

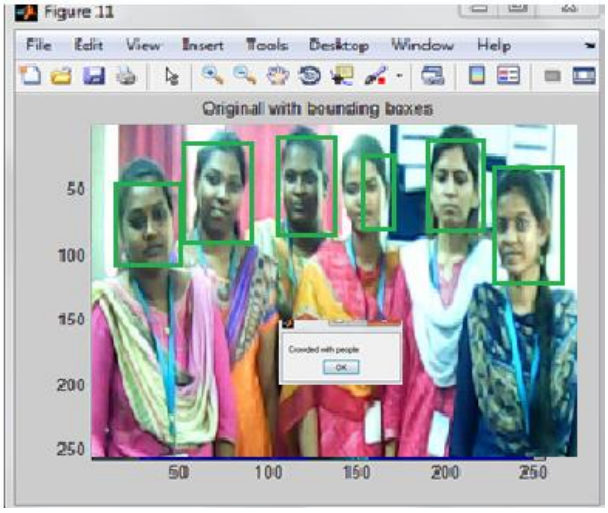

Fig 4.5 Number of People Detected in Real Time

Figure 4.5 shows that 6 people are detected in the input image. When the number of people exceeds the fixed value it displays a message as crowed with people.

TABLE 4.1 OUTCOME TABLE

Frame number	Ground truth	No of people detected
20	0	0
40	1	1
60	3	2
80	4	4
100	2	2
120	5	4
140	7	6
160	3	3

The table 4.1 shows the various objects in addition to people detected in the experiment along with their count.

TABLE 4.2 RELATIONSHIP BETWEEN GROUND TRUTH AND NO OF PEOPLE

	People	Bottle	CPU	Table
People	9	-	1	-
Bottle	1	9	-	-
CPU	4	-	6	-
Table	2	-	-	8

The table 5.2 displays the comparison between the ground truth and the number of people actually detected.

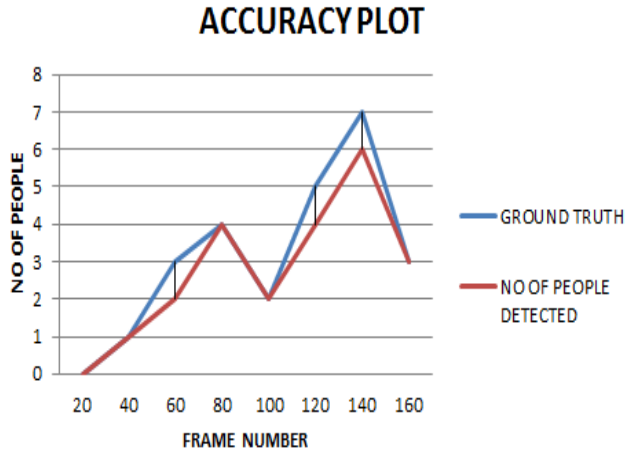

Fig 4.5 Accuracy Graph of Dataset Video

The precision for the above graph 4.5 is calculated using the formula

$$\text{Precision} = \frac{\text{Total number of people detected}}{Ground\ truth}$$

The precision value is 93%

V. CONCLUSION

To conclude we present congestion avoidance based surveillance system that counts the number of people approaching each emergency exit. Our experimental results indicate that there is a significant benefit of using Markov random segmentation to overcome the people detection problem to a certain extent. The system is capable of segmenting groups of people into individuals. Therefore we are, able to count the number of people in a frame with greater accuracy.

VI. FUTURE WORK

The project can be preceded in the future in ways mentioned below. It will be more convenient if research groups build an advance algorithm which can measure and draw circle areas when creating the floor plan. The system evaluates the crowd density by counting the heads in the particular area through a camera. In the present system a separate camera was used rather than the CCTV cameras which are usually present in buildings. In future, taking the input video stream from the existing video surveillance in the building will be more convenient and cost effective. The proposed system takes a rough count of the people just to indicate the relative congestion at each emergency exit. Accurate count of people can be obtained using motion detector. In order to achieve this system has to integrate with motion detector device. In addition to informing users the congested exit, the system can provide the details of the emergency exits which were pre inserted to the database.

REFERENCES:

[1] Dedeoğlu, Yiğithan. Moving object detection, tracking and classification for smart video surveillance. Diss. bilkent university, 2004.

[2] Piccardi, Massimo. "Background subtraction techniques: a review." Systems, man and cybernetics, 2004 IEEE international conference on. Vol. 4. IEEE, 2004.

[3] Zhan, Beibei, et al. "Crowd analysis: a survey." Machine Vision and Applications 19.5-6 (2008): 345-357.
[4] Horn, Berthold KP, and Brian G. Schunck. "Determining optical flow." Artificial intelligence 17.1-3 (1981): 185-203.
[5] Paragios, Nikos, and Visvanathan Ramesh. "A MRF-based approach for real-time subway monitoring." Computer Vision and Pattern Recognition, 2001. CVPR 2001. Proceedings of the 2001 IEEE Computer Society Conference on. Vol. 1. IEEE, 2001.
[6] Conte, Donatello, et al. "A method for counting people in crowded scenes." Advanced Video and Signal Based Surveillance (AVSS), 2010 Seventh IEEE International Conference on. IEEE, 2010.
[7] Wu, Yi, Jongwoo Lim, and Ming-Hsuan Yang. "Online object tracking: A benchmark." Computer vision and pattern recognition (CVPR), 2013 IEEE Conference on. Ieee, 2013.
[8] Jang, Dae-Sik, and Hyung-Il Choi. "Active models for tracking moving objects." Pattern Recognition 33.7 (2000): 1135-1146.
[9] Jang, Dae-Sik, Seok-Woo Jang, and Hyung-Il Choi. "2D human body tracking with structural Kalman filter." Pattern Recognition 35.10 (2002): 2041-2049.
[10] Weng, Shiuh-Ku, Chung-Ming Kuo, and Shu-Kang Tu. "Video object tracking using adaptive Kalman filter." Journal of Visual Communication and Image Representation 17.6 (2006): 1190-1208.
[11] Li, Xin, et al. "A multiple object tracking method using Kalman filter." Information and Automation (ICIA), 2010 IEEE International Conference on. IEEE, 2010
[12] Meshgi, Kourosh, et al. "An occlusion-aware particle filter tracker to handle complex and persistent occlusions." Computer Vision and Image Understanding 150 (2016): 81-94.
[13] Yang, Bo, and Ruoyu Yang. "Interactive particle filter with occlusion handling for multi-target tracking." Fuzzy Systems and Knowledge Discovery (FSKD), 2015 12th International Conference on. IEEE, 2015.
[14] Chu, Chun-Te, et al. "Tracking human under occlusion based on adaptive multiple kernels with projected gradients." IEEE Transactions on Multimedia 15.7 (2013): 1602-1615.
[15] Lu, Shan, et al. "Blob analysis of the head and hands: A method for deception detection." System Sciences, 2005. HICSS'05. Proceedings of the 38th Annual Hawaii International Conference on. IEEE, 2005.

Digital Jewellery

Sivasubramanian R[1], Suraj SK[2], Saalini D[3], Sangeeth Kanna P[4], T J Jeyaprabha[5]

[1–4]Student, Electronics and Communication Engineering, Sri Venkateswara College of Engineering, Chennai.

Abstract—Since the dawn of time, gems have sparked the imagination of people of all ages. We've grown attached to it despite the fact that it serves a moderate motivation of simply improving ourselves. For as long as we can remember, PCs, iPads, and other electronic devices have been present and demonstrated in our advanced society. The most current PC craze has been the ability to wear remote computers. A combination of microcomputer gadgets and rising PC power has enabled a few companies to begin offering design gems with embedded insight, referred to as Digital Jewellery. The entire idea behind it is to have the ability to transmit to others via distant machine means. Another important aspect of this concept is to remain fashionable at the same time. By displaying different wearable gadgets, this study elucidates the concept and ideas behind sophisticated adornments. As a result, "Digital Jewellery" is the name given to these little contraptions.

***Keywords*—Digital Jewellery, Electronics devices, Microcomputer gadgets,iPads.**

I. INTRODUCTION

Changes in technology have resulted in aslew of smaller-than-normal gadgets that make it easier for people to get things done. The ease with which these practical inventions can be put to use, as well as their various functions in assisting people to engage in other beneficial activities, has made the innovation a versatile tool for studying and leisure. Various studies have looked into the capacity of smaller-than-expected gadgets for pervasive learning frameworks, relaxing, and confirming their adequacy, as well as how they affect lives and various areas of human endeavor. An ability to outfit the individual with modified and versatile information: owned, worked, and obliged by the wearer is the key issue in wearable PC.

II. REVIEW OF LITERATURE

The development movement has achieved almost nothing, being flexible and nothing more than ordinary and all-encompassing contraptions worn either externally or inwardly on the body. A combination of shrinking PC gadgets and increasing PC capacity have enabled a few organizations to begin producing structure gems with fixed data. This is the start of the PC's deterioration into small components, as well as new small-scale gadgets that will soon be decorating the human body, and how they will make everyday correspondence and registering much more omnipresent. There are numerous kinds of wearable contraptions that are frequently employed. Eyeglasses, wearable radios, wristwatches, and mechanized diamonds are among the devices employed. Electronic Jewellery is one of the fastest-growing wearable PC areas. A separated segment is a touch of electronic diamonds of the segments in the re-packaged cell phone. The microphone, Receiver, Touchpad, Display, Circuit Board, Antenna, and Battery are the elements of the mobile phone that build each piece of mechanized pearls and make it work as a telephone.

A. Past of Digital Jewellery:

When pocket watches were envisioned in the16th century, the verified setting of wearable PCs was dated. The presence of some moving programming brought in a massive a new epoch of wearable PCs. Edgar Matias and Mike Rucci of the University of Toronto envisaged a wrist PC in 1994. Their wrist PC was introduced to an optional route for managing the creation of a head-up display, notwithstanding amicability reassuring wearable. The framework was developed on an HP 95LX palmtop computer.

B. What is Body-Borne Computer?

A Body-Borne PC is an automated device with a limited scope that is worn by the client under or on articles of clothes. A type of human-PC connected device is a piece that's ready to be worn, available, and beneficial to the consumer on a continuous basis. In this inclusive device, the different activities are reliable to the customer which allows the consumer to enter orders and do without checking. It's an easy-to-use device that fits comfortably on one's body without creating discomfort.

C. What is Digital Jewellery?

A sophisticated decoration is a fashionable jewel with an embedded understanding that helps with the storage of personal information like passwords, realizing a confirmation number, OTP, account information, and so on. It may be substituted for driver's licenses, business cards, Mastercards, medical insurance cards, and corporate security identification additionally. It solves the fundamental problem of forgotten secret keys.

D. Characteristic of Digital Jewellery

Mann (1998) gives numerous characteristics that differentiate digital jewels from other electronic devices such as computers, laptop, mobile phones, PDA etc. Few features are listed below

1 Never OFF: This function allows you to work efficiently with digital jewellery that should still work, ignition, detection and playback. PDA which is a pen, the base should be turned on when needed. It must be easily accessible to the ultimate user: - constantly power-on, accessible, and ready to operate.

2 Portable: The best feature of digital jewellery is that it

can be used roaming or traveling because to his minuscule volume. This special part recognized PC wearables from workstations or other small computers like small CPs.

3 Various types of Sensors: The sensor is the largest part of Digital Jewellery. Users' entries are stored using sensors for their unique features. Such Sensors might consist of Wi-Fi, cameras, Bluetooth, microphones, heart rate monitors, Gyroscopic Sensors, etc.

4 Interaction: It should constantly communicate with users within less time. It can connect to other systems & Mobile Phones.

5 Automated: End – User does not require constant attention or interaction. End-user may do other things while using the wearable computer. It does not cause any inconvenience to the user. The user may around ordrive a car or bike and pass by overcrowded busses.

E. Advantages of Digital Jewellery

1 Constantly connected to the local networking area, bluetooth & infrared.
2 A wireless device of tiny size.
3 It does not depend on externaldevices.
4 No need for any kind of platform or desk.
5 Instantly available to use. No need to turn it on manually.
6 Digital Jewelry can help you solve problems like forgotten passwords and security badges.

F. Limitations

The health risk caused by mobile devices can never be improved. From eye strain and headaches. The high cost makes digital jewelry unavailable for purchase.

III. METHODOLOGY

Various manufacturing companies and individuals have created various digital jewelry from rings to necklaces different designs and designs have been scrutinized to include all these jewelry.

A. Parts of Digital Jewellery

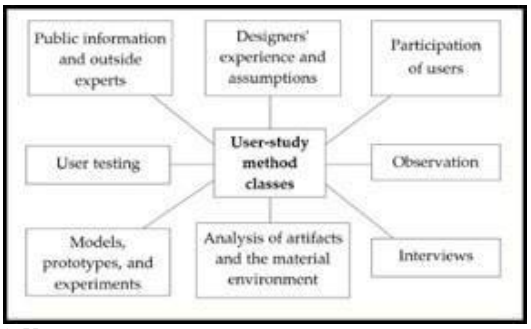

Figure 1: Use-case
Source:https://www.google.com/url?sa=i&url=https%3A%2F%2Fwww.intechopen.com%2Fbooks%2Fdigital- transformation-in-smart-manufacturing%2Fdigital-smart-jewelry-next-revolution-of-jewelry-industry- &psig=AOvVaw0wjHdNYkOqxDCT9AfoMOY5&ust=1646663419297000&source=images&cd=vfe&ved=0CAsQjRxqFwoTCJi5xLXZsfYCFQAAAAAdAAAAABAQ

- **Ring**: This "magic decoder ring," which is perhaps the most exciting part of the phone, is equipped with light-emitting diodes (LEDs) that flash to signify an incoming call. It can also be programmed to flash different colors to signify the significance of a call or to identify a specific caller.
- **Earrings** – The phone's receiver will be embedded with speakers in these earrings.
- **Necklace** – The necklace's inbuilt microphone will be used by users to speak.
- **Bracelet** – The wrist display, which has a video graphics array (VGA) display, and could also be used as a caller identifier, flashing the caller's name and phone number.
- **Hoops** – The telephone's collector will be speakers put into these studs. Bluetooth gadgets in the form of pendants or hoops that people may wear to assist enhance their gadgets are being developed by computerized jewellery companies.

B. Operating of Digital Jewellery

Figure 2: Ring
Source: https://www.google.com/url?sa=i&url=https%3A%2F%2Fwww.amazon.in%2FHoneytecs-Multifunctional-Waterproof-Intelligent-Accessories%2Fdp%2FB08L3S6Y9N&psig=AOvVaw0C-YaWhaGkWGV7ngeB2p67&ust=1646664123898000&source=images&cd=vfe&ved=0CAsQjRxqFwoTCPj-yoPcsfYCFQAAAAAdAAAAABAI

Figure 3: Java Ring
Source: https://www.google.com/url?sa=i&url=https%3A%2F%2Fslideplayer.com%2Fslide%2F4541998%2F&psig=AOvVaw37sD4pDZBbE7ZOGZpT_UOJ&ust=1646664326999000&source=images&cd=vfe&ved=0CAsQjRxqFwoTCIiXseXcsfYCFQAAAAAdAAAAABAs

Figure 4: IBM Ring
Source: https://www.google.com/url?sa=i&url=https%3A%2F%2Fwww.researchgate.net%2Ffigure%2F1-Digital-Jewellery-Set-by-IBMs- Almaden-designLab-1993-Visual-prototype-Source_fig1_341909859&psig=AOvVaw3ykbOPcTmkas3ykpBWw6pg&ust=1646664595141000&source=images&cd=vfe&ved=0CAsQjRxqFwoTCMiWveXdsfYCFQAAAAAdAAAAABAD

Figure 5: Necklace
Source: https://www.google.com/url?sa=i&url=https%3A%2F%2Fwww.pinterest.com%2Fpin%2F638526053407540558%2F&psig=AOvVaw2EMmUI2swrybU488wb1X8j&ust=1646664748212000&source=images&cd=vfe&ved=0CAsQjRxqFwoTCNCo467esfYCFQAAAAdAAAAABAD

C. Java Ring

Celebration School, an innovative K-12 school just outside Orlando, FL, has been testing the Java Ring, which was first introduced at the Java One Conference. Java applets that communicate with host programs on networked systems are programmed into the rings supplied to pupils. Applets are little programs that are designed to operate inside another program. To allow communication between a host system and the Java Ring, the Java Ring is snapped into a reader known as a Blue Dot receptor. The Java Ring is a 16-millimeter (0.6-inch) diameter stainless steel ring that houses an iButton, a one-million-transistor processor. The ring features 134 KB of RAM, 32 KB of ROM, a real-time clock, and a Java virtual machine, which recognizes and translates the Java language for the user's computer system.

D. IBM Ring

Digital Jewellery will alter how we deal with the ever-increasing flood of e-mails, in addition to changing how we make phone conversations. Consider the possibility that the same ring that alerts you to phone calls could also alert you to the fact that e-mail is piling up in your inbox. This flashing notice could potentially reflect the mail's urgency. The mouse and monitor are two of the most easily recognized components of a personal computer. These devices are as common as television sets nowadays.

The IBM mouse-ring will use IBM's Track Point technology to wirelessly move the cursor on a computer monitor display. You're probably most familiar with Track Point as the small button seen on some laptop keyboards. Track Point technology has been applied to a ring that resembles a black pearl ring by IBM researchers.

A little black ball sits atop the ring, which users will swivel to move the cursor, similar to how the Track Point button on a laptop is used.

IV. CONCLUSION

Wearable devices are becoming increasingly popular in today's environment. When you compare the size of electrical devices today to what they were ten years ago, you can see how far technology has progressed. It's possible that by the end of the decade, we'll be wearing our computers rather than sitting in front of them. The core idea behind the Digital Jewellery concept is to combine the ease of wearable, wireless devices with a fashionable appearance. It is hoped that it will be available for purchase soon, however, some issues remain. The ability to charge and the expense are just two of the issues that can arise. Digital Jewellery will be the advancement in digital technology that makes computer elements completely compatible with the human form, designed to supplement the personal computer.

V. FUTURE SCOPE

We are bit by bit moving to the fifth era of electronics which are convenient and tiny to be a piece of individuals' dress. Anyway, these little processing gadgets offer restricted cooperation capacities contrasted with PCs or a telephone." By the finish of this Decade, we would be wearing our PCs as opposed tositting before them."

REFERENCES

[1] Designboom (n.d) Wearable-computers. Retrieved from http://www.designboom.com/weblog/cat/16/view/5586/ wearable-computers.html on 03/03/15

[2] L.Mary Gladence, Shefali Yadav, Roopini.J,“ Digital Jewellery : An Upcoming Technology”, The GRENZE

[3] Scientific Society (GSS) is an international, scholarly, professional organization, 11 February 2017.

[4] N.Rukmini Sai Priya ,“ Digital Jewelry”, 10th International Conference on Recent Trends in Engineering Science and Management Newton's Institute of Science & Technology, Guntur Dist., Andhra Pradesh, India (ICRTESM-17), 13 August 2017.

[5] Miner, Cameron & Chan, Denise & Campbell, Christopher, “Digital jewelry:

[6] wearable technology for everyday life.”, The Association for Computer Machinery Digital Library, 21 January 2001.

[7] Ojo Abosede Ibironke,“ Digital Jewelry: Components and Workability”, International Journal of Life Science and Engineering, Vol.1, No.2, May 2015, 2 April 2015.

[8] https://krazytech.com/technical- papers/digital-jewelry

[9] https://themitpost.com/digital-jewellery/

A Novel Analysis of Nd:YAG Photon Materials Usage in the modern Era

T. Suresh[1], T.D. Subha[2], Shri Abijith M[3], T. Shanmugaesh[4]

[1-4]Department of Electronics and Communication Engineering, R.M.K. Engineering College, Kavaraipettai, Tamil Nadu, India,

[1]hod.ece@rmkec.ac.in, [2]tdsubha2010@gmail.com, [3]shri20408.ec@rmkec.ac.in, [4]shan20406.ec@rmkec.ac.in

Abstract*—The investigation of something like the consequence of Nd:YAG pulse embossing upon that interfaces of photovoltaic devices is described in this research. Substrate smoothing is particularly significant in organic photovoltaic cells production. At standard temperature, the increased energy characteristic impedance of silicon is roughly 1.12ev that also decreases the photovoltaic performance. This process made the silicon to rarely accept the radiation. Traditionally, hydrometallurgical etching is used to rough computer chip surfaces. Hydrothermal method section does not apply for all varieties of crystalline silicon given the diverse crystalline structure. Consequently, in this research, continuous wave Nd:YAG laser would be used for sculpting silicon wafer interfaces. Laser sandblasting is considered although it may be used on different sorts of semiconductor materials but that can exist autonomously while requiring on computer chip attributes admittedly. As beam may develop a picture on polysilicon surfaces however there are a few difficulties of adopting laser structuring. It forms undesirable particles and then it destroys the thin coating with lot of abrasion remnants. This undesirable atoms and remnants must be eliminated in order to minimize surface resonance on photovoltaics. Because after structuring is finalized, the materials are bathed in Pbs solution. Hydroxide solution would be used to eliminate undesirable impurities and to wipe down the tops of semiconductor materials. Following light source exfoliating and postsecondary institution the absorbance data from Colorimetric method is exhibited as a substantial drop with maximum brightness which formed 40 percent to below 10 percent and 20 percent correspondingly. While it has high ruggedness shapes has just been textured due of its poor reflectivity. Continuous Nd:YAG laser embossing is an useful approach for circuit boards but it can be used on a variety of different types of semiconductor materials without requiring any special preparation.

***Keywords*—Photon emission, semiconductor surfaces, silicon layer.**

I. INTRODUCTION

When the sun shines, photon components from the sun are transformed into heat energy, and this is known as a photovoltaic panel. Whenever light shines photovoltaics, light components (particles of light) are captured, and the electricity received is transferred to atoms, resulting in electricity being produced [1]. Electronic components are capable of a wide variety of relevant functions. Transistors having the capacity to transmit electricity in one way above the other, as well as being sensitive to illumination or heat produced and exhibiting impedance (or susceptibility variation). Various photodiodes have been used for switches, multiplication, and power generation, while others are utilised for other purposes. It's indeed common for the susceptibility of a semiconducting material to drop as its operating surface warming. The resistance of a microelectronics can be increased by introducing imperfections through into crystalline phase, which is known as pumping. When a crystalline phase is composed of two sections that have differing doping levels, a superconducting connection can be formed. FIGURE 1 depicts the element transistors with its molecular nucleus.

Fig.1.Silicon.

The particles breakdown respective interactions and form tunnel pairs, which are converted into digital current as well as travel from either the top portion to the rear interaction before being re actually including the hole. While sunlight is shining on the surface of the membrane, the above-mentioned process will continue indefinitely. The doping of electronic components is done under limited circumstances in terms of maintaining the saturation of conjugated polymers inside this p-type as well as n-type portions, which are maintained. Minerals are excellent sources of fiber and are composed of a majority of nations that are only half submerged. Insulation materials, in contradiction to transmission lines, have a limited lot of nations that are only half submerged, and because Recombination frequencies are found within optical band gap because they have a limited impact on electricity domains to possess. As researchers enter the twenty-first generation, designers see several photovoltaic modules molecules, an often generally recognised of that are perovskite - based solar cells, thermoplastic solar cells, polycrystalline sun-spot solar cells, thin-film photovoltaics, dye - sensitized solar cells, but rather tightly packed solar modules. Semiconducting as well

as perovskite cells are included in the category of photovoltaic modules, with the single junction cell being the first photodiode to be developed, in 1981, and the wafer - based cell [2]. Semiconductor is a poor absorber of electromagnetic atmospheric particles, and it is particularly bad at absorbing light with absorption edge, which is very difficult for semiconductor to do. The challenge is to use light capturing during the si wafers production process. Maybe just a tiny monocrystalline silicon cell with a long wavelength range can be maintained using the light trapping approach. Texturing the outer layer of a computer chip would be used to create light entrapment properties. Because the upper section of the circuit board is contoured, the radiation that falls there will not be mirrored carbon into the environment, allowing the upper limit of sun's radiation to cross the membrane to be captured. On a transistor, there is a differential in electrostatic attraction, which results in a non-equilibrium state. This non-equilibrium results in the generation of electron - hole pair throughout the medium. Electrical properties propagation is the term used to describe the migration of electric charges that are oppositely energized to one another, including depletion region. Definite shape and volume are perhaps the most commonly encountered perovskite materials. Researchers should create an insulation communicate by heating up of the dielectric. Although overheating produces energy that causes some protons to cross the absorption coefficient, this is a good thing. FIGURE 3 depicts the lifetime of silicon in its various forms.

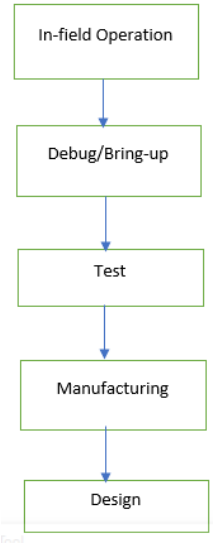

Fig.2 lifecycle of silicon.

Texturing the bottom of something like the si substrate can be executed using a variety of ways. Most of the other processes include chemical precipitation etching, uv exposure sandblasting, and electrical discharge laser cutting, among others [3]. When it comes to the production of photovoltaics, the continuous wave Implying diode is the most widely adopted. It is particularly useful for contaminating, scraping, and layering applications. It is a characteristic of rectifier diodes that they can manage various properties at the same time, but that is for this reason that pulsating laser beams are utilised in the production of solar cells. In Q-switched configuration, a continuous Implying diode is capable of operating at two different temperatures. Two different frequencies are used: one is 532 nm (ecofriendly spectrum) while another is 1064 nm (blue spectrum of light) (infrared). Intermittent photons communicate with the surface of the samples by convection that area through electromagnetic stimulation and interacting with the edges of the cathode [4]. An inorganic compound, also known as a complete dielectric material, has a narrower characteristic impedance to a dielectric and is therefore more efficient. In a particular microfabrication sapphire, designers can always have a large number of p - type semiconductor sectors. The intersections among these zones are able to take responsibility underlying the electrical performance that is conducive to production. The proportion of oxygen vacancies in a superconductive substance fluctuates however when the temperature profile of the component is disturbed. When there is an amount of variation, or when particles enter the network and form electrons and holes, these kinds of changes can take place, for example.

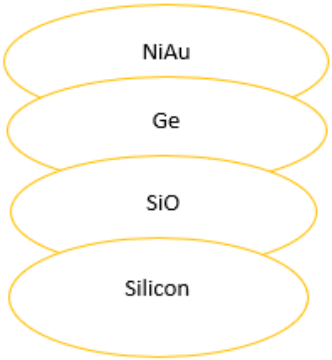

Fig.3.Silicon CMOS devices structure.

The chart illustrates that perhaps the magnesium does indeed have a threshold concentration thickness that seems to be comparable to that of amorphous silicon with wavelengths less than 500 nm. There is an increase throughout the intensity of penetration when the spectrum is more than 500 nm. As a result, it is obvious however that transmittance concentration of transistors has been improved in this case. Since conductivity diameter increases with spectrum, single crystals have the tendency to process a greater number of functional nanoparticles with longer wavelengths, resulting in increased efficiency. In order for the diode to perform on silicon substrate, the infrared beam would have to be crisp when viewed via the objective sensor. When the beam is operated at a given level of power, it reacts with Polycrystalline substrates and generates a small section [5]. Infrared patterning can potentially cause harm to the metal plate. This degraded coating must be evacuated as soon as possible even if it might cause a moderate relatively brief discharge if left in place. The techniques of charge separation synthesis and extermination are referred to as transmission and hybridization, respectively, in science. The carrier concentration characteristics of electronic components differs from that of two or more constituents in a number of ways. In order to determine the impedance of a semiconductor, the percentage of full of liquid states must be considered.

Figure 7 eventually spreading the intensity of photon energy of resulting composites to laser illumination. The transmittance rate is determined in this case through the information of something like the bandwidth. Visually, the Sharepoint Lightweight is depicted in a blue colour. Investigated in this work is the influence of change from baseline sometimes during light source patterning on the photon energy of semiconductor materials, as measured by transmittance measurements [8]. There are numerous information that contain information on ground structuring and how it can be used to promote spectral response. However, it is necessary to investigate the effects of post on this thread sometimes during ultraviolet resurfacing in order to understand the influence of infrared structuring on the associated with each alternative of silicon wafers.

II. Methodlogy Used

It is necessary to employ polycrystalline composite materials with a cross - sectional area of 200 microns, a susceptibility of 20 microns, as well as a dimension of 4 cm x 4 cm. The glass substrates should always be disinfected through using RCA-1 as well as RCA-2 processes, which are described below. It would be necessary to undertake the beam patterning procedure when the cleaning phase is completed. To carry out this investigation, a pulse-pumped Nd: Laser - assisted development agencies to a Q-switched configuration is used. Optical and photovoltaic resources are well depicted in figure 4.

Fig.4.Set-up Representation.

Throughout this investigation, we take into consideration various operating electromagnetic waves: 1064nm and 532nm. It is necessary to blend these two working electromagnetic waves throughout the method of beam embossing to achieve the desired results. The beam utilised in this experiment has a bandwidth of 10 kHz and a sampling rate of less than 0.05 mm at its lowest setting. The mirror of something like the light source could be changed to accommodate to concentrate the light beam together into fine edge. The matlab simulink technology is being used to command the XY transformation spreadsheet in the future [6]. The operational electromagnetic waves that are being investigated are 1064 nm and 532 nm, respectively. In order to accomplish this task of infrared resurfacing, those certain two working frequencies must be used in conjunction [7]. The laser utilised in this experiment has a spectrum of 10 kHz and a depth of penetration of less than 0.05 mm at its lowest setting. The Heterojunction laser has the advantage of allowing the user to manipulate the continuous light source individually [2]. If the workforce dispersion exceeds the threshold value, the Q flipping response is selected, resulting in thermal treatment being directed towards the components. As a result, the laser source incidental on something other than the edge of semiconductor materials can end up receiving increased radiation as a result of the increased wavelength. Whereas during process of beam resurfacing, laser illumination is usually reflected by semiconductor [9].

Once the laser texturing process is done, the textured silicon wafer will undergo further process called post treatment process [10]. It is important to have post treatment so that the laser damage layer can be removed. In order to perform the post treatment process, we use 20% of Potassium Hydroxide solution. The textured silicon wafer will be put into this 20% KOH solution at 80°C temperature. This should be kept for about 5 minutes. During this time, we can observe a layer of bubble on the surface of the silicon wafer [11]. After this 5 minutes process, we can take out the silicon wafer from the solution and it should be washed out under running water. The washed sample need to dried using nitrogen gas [12]. In this experiment, Silicon solar cells produced a good absorption after laser texturing with post-treatment [13]. When Pulsed Nd: YAG laser operated at higher energy, it removed silicon wafer surfaces with a small spot [14]. Comparing the Grid pattern to the series of parallel [15], the great transmittance depth of the Rectangular grid is represented. Due to the general development of a laser degradation layer somewhat on substrate, light impacting on the semiconductor will not be consumed within the piece of silicon [22]. Hence, it is important to remove the laser damage layer after the laser texturing process. The presence of damage layer reduces the absorption depth of silicon. Pulsed laser system connected with Q-switched mode is presented in this study. The two operating wavelengths are 1064 nm (infrared) and 532 nm (green). These two operating wavelengths need to be combined during the process of laser texturing.

The power system as well as comparison arrangement within a week of post-treatment, as shown in SEM micrographs, exhibits a high digestion depth owing to the increase permeability specificity. When viewed from the substrate, the waves of the infrared patterning are now uniformly symmetrical [18]. Depth of penetration of the eliminated material enhances the efficiency of the eradication barrier [19]. If post-treatment is not used, only a low rate of production can be reached. This is due to the presence of a breakdown layer, which collects more light energy and prevents it from passing through the semiconductors. This beam degradation surface is much more than a smear of undesired material that accumulates on the efficiency of solar cells as well as serves no functional purpose. As previously explained, the interface of infrared structuring is covered with something like a liquid layer and during post-treatment process. It is possible to remove this element after 5 minutes beneath running water, resulting in the formation of a glass substrate with a cutting board [20].

The ridges were etched off and the thickness is decreased about 60micron [21].

III. Conclusion

It is possible to make solar cells by the use of selective laser sintering devices. Power source modification, smoothing, and improving over time are just a few of the beam functionalities available for photovoltaics. Treatment usually is more efficient than traditional surface roughness and does not pollute the environment. Nd:YAG light source engraving on polycrystalline surfaces can be accomplished in a relatively short period of time. As a result, laser morphology of the prepared is considered to be an appropriate technology for structuring. Despite the fact that the laser may exist effectively on any solid material surface, it produces a flaw when texturing. This deficiency must be avoided since it diminishes the photoelectric effect within the memory chip, which is undesirable. The greater the amount of light that is absorbed by the hepatocytes, the greater the utilisation. If the comment on this thread is administered in excess, it will result in a diminishment of the electronic structure of the solar photovoltaic cells as a result. For maximum reliability and reasonable electro - optic qualities, it is difficult to maximize thread with surface violence prevention in order to achieve a good proportion. At the end of the day, designers can say that infrared patterning is an excellent option to other methods of obtaining long wavelengths in organic photovoltaic crystals.

References

[1] Takashi Kita, Yukihiro Harada, Shigeo Asahi, Green Energy and Technology: Energy Conversion Efficiency of Solar Cells, Springer Nature Singapore, 2019.

[2] Eugene Peter, T.D.Subash, T.D.Subha, Alsufiyan Nazim, 2020 “Utilizing Radiant Nanoparticles in Silicon for Balanced White Color Adaptors”, International Journal of Silicon, Springer.

[3] José Antonio Luceño-Sánchez, Ana María Díez-Pascual and Rafael Peña Capilla, “Materials for Photovoltaics: State of art and recent developments,” Int. J. Mol. Sci., 2019.

[4] Ali Keyhani, Design of Smart Power Grid Renewable Energy Systems, John Wiley & Sons, 2019.

[5] Nurul Huda Abdul Razak, Kamaruzzaman Sopian, Nowshad Amin, and Md. Akhtaruzzaman "Investigation on the post-treatment after pulsed Nd:YAG laser texturing on silicon solar cells surfaces", Proc. SPIE 11387, Energy Harvesting and Storage: Materials, Devices, and Applications X, 1138717, 18 May 2020.

[6] Mehul C. Raval and Sukumar Madugula Reddy, Industrial Silicon Solar Cells, IntechOpen, 2019.

[7] Abdur-Rahman, E., Alghoraibi, I., & Alkurdi, H., “Effect of isopropyl alcohol concentration and etching time on wet chemical anisotropic etching of low-resistivity crystalline silicon wafer,” Int. J. Anal. Chem., 2017.

[8] Nurul Huda Abdul Razak and Nowshad Amin, “Nd:YAG laser texturization on silicon surface,” 4th International Conference on Advanced Materials Research, ICAMR 2014, Macau., Advanced Materials Research, vol. 894, Trans Tech Publications, Ltd., pp. 201–205, 2014.

[9] Gupta, M., & Carlson, D., Laser processing of materials for renewable energy applications, MRS Energy & Sustainability, vol. 2, E2., 2015.

[10] T.D.Subha, T.D.Subash, K.S.Claudia Jane, Devadharshini.D, Dhanya and Francis, 2020 “Autonomous Under Water Vehicle Based on Extreme Learning Machine for Sensor Fault Diagnosistics”, Elsevier-materials today proceedings-24, pp. 2394-2402.

[11] Arnold, C.B. & Brown, M.S., Fundamentals of lasermaterial interaction and application to multiscale surface modification. Laser Precision Microfabrication, pp. 91-120, 2010.

[12] T.D.Subha, T.D.Subash, K.S.Claudia Jane, Devadharshini.D, Dhanya and Francis, 2020 “Study and Analysis of Suppress of Surface Wave Propagation in Microstrip Patch Antenna”, Elsevier-materials today proceedings-24, pp. 2414-2423.

[13] Ghahremani, A. and Fathy, A.E., High efficiency thin film amorphous silicon solar cells. Energy Sci. Eng., vol. 4, pp. 334-343, 2016.

[14] L. A. Dobranski and A. Drygala, “Surface texturing of multicrystalline silicon solar cells,” J. Achiev. Mater. Manuf. Eng., vol. 31, 2008.

[15] T.D.Subha and V.D.Reshma, 2017 “A study of Non-invasive Heart Rate Monitoring System by using FPGA”, Elsevier-materials today proceedings-4, pp. 4153-4168.

[16] M. Kihl, ”3GPP LTE Downlink Scheduling Strategies in Vehicle-to-Infrastructure Communications for Traffic Safety Applications”, IEEE Symp. Computers and Commun., 2012.

[17] Burnham, Performance of Bifacial Photovoltaic Modules on a Dual-Axis Tracker in a High-Latitude, High-Albedo Environment, 2019 IEEE 46th Photovoltaic Specialists Conference (PVSC), Chicago, IL, USA, 2019, pp. 1320-1327.

[18] Okada, Yoshitaka, Tomah Sogabe, and Yasushi Shoji (2014). "Ch. 13: Intermediate Band Solar Cells". In Arthur J. Nozik, Gavin Conibeer, and Matthew C. Beard (ed.). *Advanced Concepts in Photovoltaics*. Energy and Environment Series. Vol. 11. Cambridge, UK: Royal Society of Chemistry. pp. 425–54. doi:10.1039/9781849739955-00425. ISBN 978-1-84973-995-5.

[19] *Dimroth, Frank; Tibbits, Thomas N.D.; Niemeyer, Markus; Predan, Felix; Beutel, Paul; Karcher, Christian; Oliva, Eduard; Siefer, Gerald; Lackner, David; et al. (2016). "Four-Junction Wafer Bonded Concentrator Solar Cells". IEEE Journal of Photovoltaics. **6** (1): 343–349.*

[20] Collins, R. W.; Ferlauto, A. S.; Ferreira, G. M.; Chen, C.; Koh, J.; Koval, R. J.; Lee, Y.; Pearce, J. M.; Wronski, C. R. (2003). "Evolution of microstructure and phase in amorphous, protocrystalline, and microcrystalline silicon studied by real time spectroscopic ellipsometry". *Solar Energy Materials and Solar Cells*. **78** (1–4): 143.

[21] Kosasih, Felix Utama; Ducati, Caterina (May 2018). "Characterising degradation of perovskite solar cells through in-situ and operando electron microscopy". *Nano Energy*. 47: 243–256.

[22] T.D.Subha, T.D.Subash, Elezabeth Rani and P.Janani, 2020 “LiFi: A Revolution in Wireless Networking”, Elsevier-materials today proceedings-24, pp. 2403-2413.

Microstrip Antenna for 5G Sub-6GHz and X-band Wireless Communication Applications

J. Chandrasekhar Rao[1], P. Bhargav[2], N. Harika[3], N. Vyshnavi[4]

[1-4]Bapatla Engineering College, Bapatla, A.P., India

***Abstract*—A compact multi-slotted microstrip patch antenna for 5G sub-6GHz and X-band wireless communication applications in this paper. The antenna of size 30mmX30mm is designed on FR4-Epoxy dielectric material which is fed by a microstrip antenna. Multiple slots were placed on a circular patch to achieve resonances at the sub-6GHz band from 3.93GHz to 5.8GHz and the X-band from 7.1GHz to 9.1GHz. The S11 of < -25dB and VSWR of below 2 show the good impedance matching properties at the designed bands. The peak gain of >2.5 dBi, the radiation efficiency of more than 95% and stable omnidirectional radiation characteristics manifest that the proposed antenna is suitable for wireless communication applications.**

***Keywords*—Compact, microstrip patch antenna, Sub-6GHz, and wireless communication.**

I. INTRODUCTION

Smartphones and internet of things connections, as well as network speed increases and cellular video consumption, are probable to boost data traffic by several times as the number of mobile users grows [1]. The 2G/3G/4G standard has become extensively used because rapid growth of wireless communication technologies. However, such bandwidth is insufficient to fulfil the recently proposed 5G NR standards, which include n77 (3300-4200 MHz), n78 (3300-3800 MHz), and n79 (4400-5000 MHz. As a result, designing a 5G terminal antenna with wideband performance to fully cover all 2G/3G/4G/5G frequencies is extremely desirable. The FCC separated the frequency spectrum into low-band (up to 1 GHz), mid-band (sub-6 GHz), and high-band (mm Wave- above 6 GHz) to enable 5G. The mmWave delivers data rates of up to 2 Gbps and massive capacity, while the low-band provides good 5G coverage and the midband combines the two. The usage of 5G mmWave spectrum is clearly desirable in order to achieve the goal of ultra-fast data speeds. However, some critical problems must be overcome before mmWave mobile communications may be implemented. Sub-6 GHz 5G communication is appropriate for use in both urban and rural areas since it can transfer high data rates across long distances [2-3]. The 5G antenna should be reliable and capable of operating across several frequency bands. The 5G antenna should be small enough to be integrated inside the portable electronic devices. Furthermore, because sub-6 GHz antenna must coexist with existing long-term evolution (LTE) and other service band antennas, the 5G antenna must support both sub-6 GHz and existing WiMAX, WLAN, and LTE bands. Microstrip patch antennas have become the preferred antenna type because to their appealing characteristics of low-profile, lightweight, low-cost, and ease of integration within microwave integrated circuits (MICs) or monolithic microwave integrated circuits (MMICs). For 5G communication applications, many antennas have already been proposed [4-9]. However, there is a scope for improvement of antenna parameters. In this paper a micro strip patch antenna with several slots for 5G sub-6GHz and X-band wireless communication applications is presented.

The rest of the paper is structured as follows: In Section-II the proposed antenna design is presented. In section-III the results and discussion of the proposed antenna is described. Finally, the conclusions are given in section-IV.

II. ANTENNA DESIGN

A compact slotted microstrip antenna for 5G sub-6GHz and X-band wireless communication applications is proposed in this paper. The antenna having dimensions of 30mmX30mmX1.5mm is designed on low cost FR4-epoxy dielectric substrate as depicted in Fig.1. The substrate having relative permittivity of 4.4, thickness of 1.5mm and loss tangent of 0.02. A circular radiating patch of radius 6mm which is excited by 50-ohm micro strip line feed with dimensions 13.9mmX2mm is placed on top of dielectric substrate as given Fig.1(a).

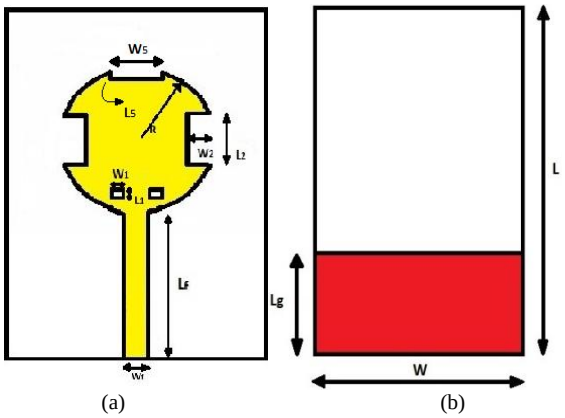

Fig.1: Antenna Topology (a) front view, (b) back view.

A partial ground plane of size 10mmX 20mm is placed on bottom side of the substrate as depicted in Fig. 1(b). To achieve the desired resonating bands at sub-6GHz and X-bands, slots are used on the radiating patch. The S11 and VSWR parameters of the designed antenna are given in Fig. 2(a) and 2(b), respectively. It can be seen from Fig.2 that the designed antenna is working at two bands such as sub-6GHz from 3.9GHz-5.8GHz and X-band from 7.1GHz-9.1GHz.

Also, the VSWR is below 2 at the designed bands.

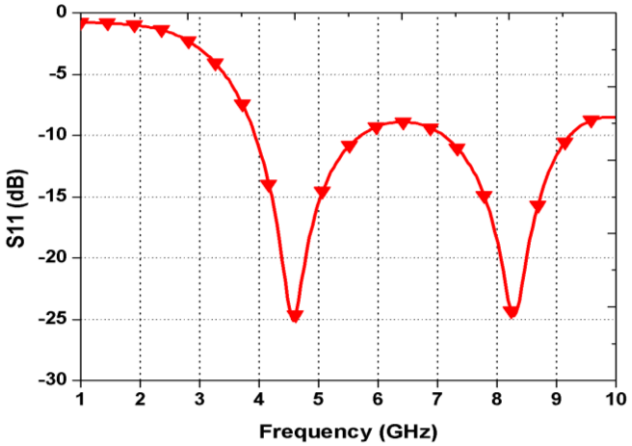

(a)

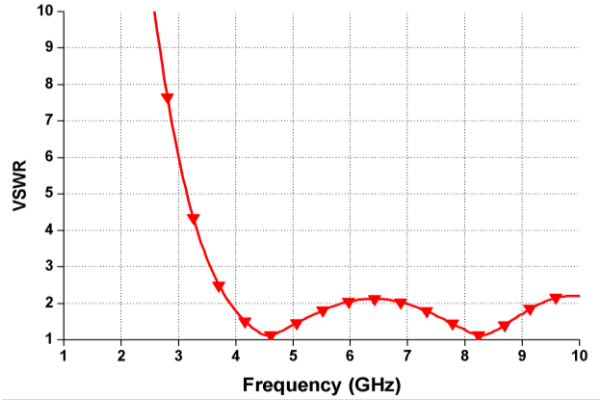

(b)

Fig.2: S11 and VSWR parameters of the proposed antenna.

The detailed design and its analysis is presented in following section III. Table 1 shows the dimensions of the proposed antenna. The presented antenna is designed, simulated and analyzed in Ansoft HFSS.

TABLE 1 DESIGN PARAMETERS OF PROPOSED ANTENNA.

Parameters	Value(mm)	Parameters	Value(mm)
W	20.0	L1	0.6
L	30.0	W2	4
Wp	10	L2	2.1
Lp	18	W3	4
Wf	2.0	L3	2.1
Lf	13.9	W4	4
Wg	20	L4	1.1
Lg	10	W5	4
W1	4	L5	1

III. RESULTS AND DISCUSSION

The evolution of the proposed antenna is presented in Fig. 3(a) through 3(d). The impedance characteristics (S11 and VSWR parameters) of all the antennas are depicted in Fig. 4(a) and 4(b). S11 is an important parameter which describes how much power is reflected from the antenna. The S11 of less than -10dB and the VSWR of 1 to 2 is generally required in practical applications. The basic antenna shown in Fig. 3(a) named Ant.1 is formed with circular radiating patch and partial ground on substrate. The Ant.1 is operating at only one band from 3.98GHz-10GHz with S11 of 26.6dB at 4.6GHz and VSWR of below 2. Fig. 3(b) represents Ant.2 which is obtained by placing couple of slots on patch and each slot having sizes 0.6mm X 1mm. The Ant.2 is working at two bands such as 4.07GHz-7.15GHz and 7.2GHz-10GHz with S11 of 26.1dB at 4.7GHz and 11.28dB at 8.23GHz. The VSWR is below 2 at both the bands. Fig.3(c) shows Ant.3 which is developed by cutting two rectangular slots with sizes 4mm X 2.1mm on left and right sides of the circular patch of Ant.2. The radiation performance is very poor (S11 is 11.28dB) at second band such as 7.2GHz-10GHz.

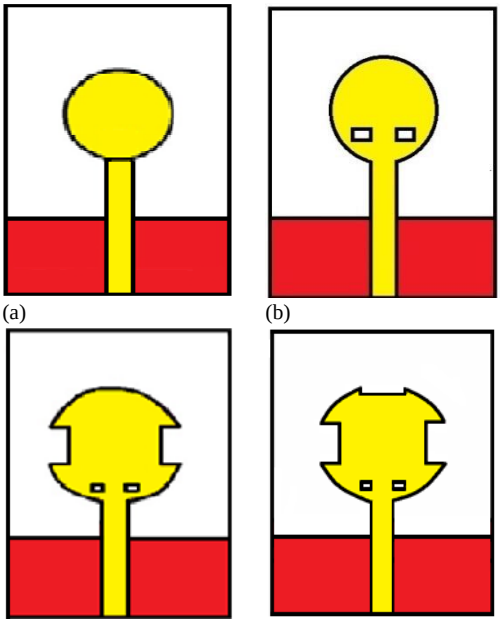

(a) (b) (c) (d)

Fig.3: Evolution of proposed antenna in a step wise manner.

The Ant.3 is resonating at two bands such as sub-6GHz and X-band. The sub-6GHz band is 3.93GHz-5.7GHz and the X-band is from 6.96GHz-9.23GHz with S11 of 24.23dB at 4.52GHz and 23.6dB at 8.19GHz. The VSWR is <2 at these operating bands. The proposed antenna is given in Fig. 3(d). It is formed by adding a slot of dimensions 0.5mm X 4mm at the top of the patch of Ant.3. The desired bands are achieved at sub-6GHz (3.93GHz-5.8GHz) and X-bands (7.1GHz-9.1GHz). The S11 of 25.15dB at 4.52GHz and 24.76dB at 8.28GHz is obtained. Also, the VSWR values are well below 2 at the designated bands. The proposed antenna offers better impedance matching properties (S11 and VSWR values at resonances) when compared with the Ant.2 and Ant.3.

The 2D radiation patterns at 4.6GHz and 8.3GHz of proposed antenna are shown in fig 5(a) and 5(b).It can be observed from the figure that the proposed antenna has Omni-directional H-plane pattern and bidirectional E-plane pattern at both the frequencies and hence it is suitable for wireless communication applications. Figure 6(a) and 6(b) represents the 3D polar plots of proposed antenna at 4.6GHz and 8.3GHz.

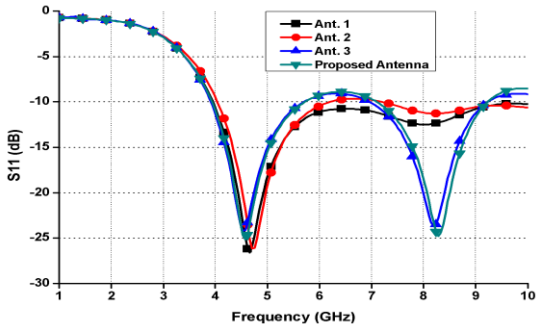

(a)

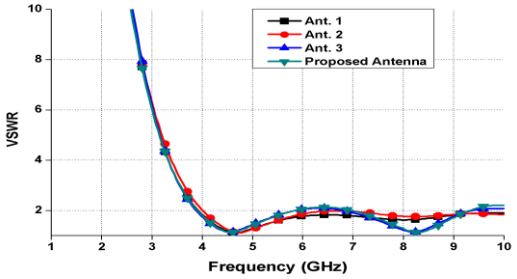

(b)

Fig.4: The S11 and VSWR parameters of all the antennas.

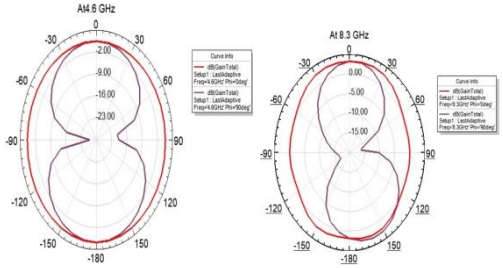

(a) (b)

Fig.5: The 2D radiation patterns at (a) 4.6GHz and (b) 8.3GHz.

The radiation performance of the proposed antenna can also described by using surface current distribution. Fig.6. illustrates the surface current distribution of the proposed antenna at 4.6GHz and 8.3 GHz. It can be identified that the radiation is more at the desired bands such as sub-6GHz and X-band.

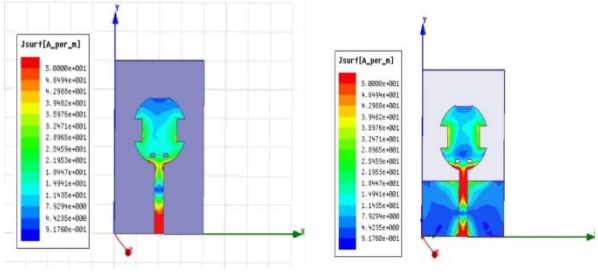

(a) (b)

Fig.6: The surface current distributions at (a) 4.6GHz and (b) 8.3GHz.

The peak gain and radiation efficiency as a function of frequency are given in Fig. 7(a) and 7(b). It is found from the figure that the proposed antenna is offering peak gain of more than 2.5dBi and efficiency of above 95% at the designed bands. Therefore, the proposed antenna has good radiation and impedance matching characteristics hence well fit for wireless applications.

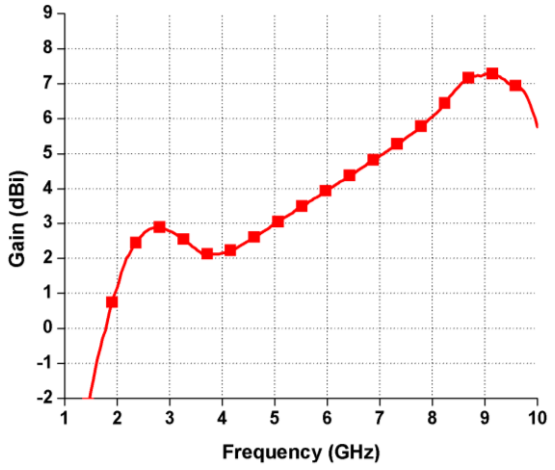

(a)

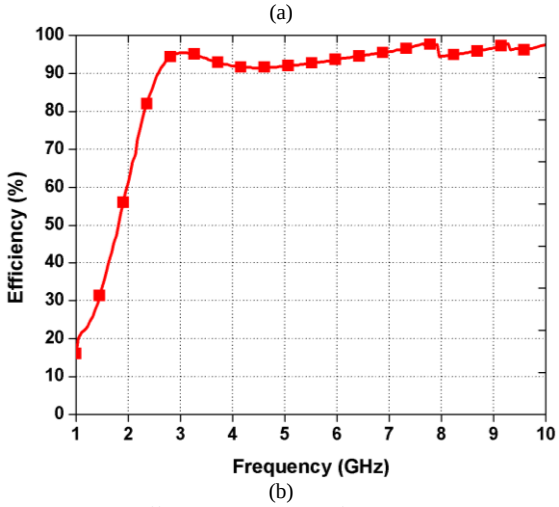

(b)

Fig.7: Peak gain and efficiency parameters of the proposed antenna.

IV. CONCLUSION

In this communication, a compact multi slot micro strip patch antenna for 5G sub-6GHz and X-band wireless communication applications. The antenna is made of a circular radiating patch excited by 50 ohm micro strip line and top of FR4-Epoxy substrate and a partial ground on bottom of it. To achieve frequency bands at sub-6GHz band from 3.93GHz to 5.8GHz and X-band from 7.1GHz to 9.1GHz, multiple slots were etched from circular patch. Moreover, good impedance matching characteristics, acceptable peak gain and radiation efficiency and stable radiation characteristics make the proposed antenna a good choice for 5G sub-6GHz and X-band wireless communication applications.

REFERENCES

[1] Cisco Systems, Mobile Visual Networking Index (VNI) Forecast Project 7-Fold Increase in Global Mobile Data Traffic from 2016–2021. Available at https://newsroom.cisco.com/ press-release-content? articleId=1819296.

[2] Marcus MJ, “5G And IMT for 2020 and beyond [spectrum policy and regulatory issues]”, IEEE Wireless Communications 22, 2–3, 2015.

[3] Rappaport TS, Sun S, Mayzus R, Zhao H, Azar Y, Wang K, Wong GN, Schulz JK, Samimi M and Gutierrez F, “Millimeter wave mobile communications for 5G cellular: it will work,” IEEE Access 1, 335–349, 2013.

[4] Azim R, Meaze AKMMH, Affandi A, Alam MM, Aktar R, Mia MS, Alam T, Samsuzzaman M, Islam MT, “A multislotted antenna for LTE/5G Sub-6 GHz wireless communication applications,” International Journal of Microwave and Wireless Technologies 1–11. https://doi.org/10.1017/ S1759078720001336, 2020.

[5] Arya AK, Kim SJ and Kim S, “A dual-band antenna for LTE-R and 5G lower frequency operations,” Progress Electromagnetics Research Letters 88, 113–119, 2020.
[6] Sekeljic N, Yao Z and Hsu H-H, “5G broadband antenna for sub-6 GHz wireless applications,” IEEE International Symposium on Antennas and Propagation and USNC-URSI Radio Science Meeting, Atlanta, USA.2019.
[7] W, Li Y, Fu H, Ma J, Chen W and Feng B, “Low-profile and wideband microstrip antenna with stable gain for 5G wireless applications,” IEEE Antennas and Wireless Propagation Letters 17, 621–624, 2018.
[8] Ngobese, B. W. and Kumar, P, “A high gain microstrip patch array for 5 GHz WLAN applications,” *Advanced Electromagnetics* 7(3): 93–98, 2018.
[9] An Z and He M, “A simple planar antenna for sub-6 GHz applications in 5G mobile terminals,” Applied Computational Electromagnetics Society Journal 35, 10–15, 2020.

An eminent role of Zeolites in Purification of solutions

Amara Deepika[1], A. Vijayalakshmi[2], G. Nixon Samuel Vijayakumar[3], M. Meena[4]

[1]Information Technology, R.M.K. Engineering College, Kavaraipettai-601206, India

[2-4]Department of Science and Humanities R.M.K. Engineering College, Kavaraipettai-601206, India

[1]amar21105.it@rmkec.ac.in, [2]avl.sh@rmkec.ac.in, [3]gns.sh@rmkec.ac.in, [4]mm.sh@rmkec.ac.in

***Abstract*— Zeolites play a vital role in our day-to-day life. It acts as water softening materials and it is used in water filters. It is having the capability of adsorbing the hardness producing cations such as calcium and magnesium Zeolites are used in odor control and pet litter. Research studies shows zeolites are the effective and active material in removing radioactive material from nuclear waste and heavy metals from the soil. The goal of this investigatory study is to test the efficacy of Zeolites as purifiers of water. Though there may be various methods to filter water, we believe that zeolites are an easy to find and use method of water purification. To investigate, we filtered several types of solutions through a layer of zeolite and checked the purity of the obtained filtrate in standard terms of ppm of solute present in it. The device used to check the purity is a 'Total Dissolved Solids' or a TDS meter.**

***Keywords*— zeolites; water purification; removal of cooking oil from kitchen waste water**

I. Introduction

Physical and chemical properties of certain zeolites are exceptional. They are particularly valuable in a range of applications, including agronomy, ecology, certain manufacturing, industrial processes, medicine, and cosmetics, due to these qualities. A more particular application of clinoptilolite, a naturally occurring zeolite material, has recently been extensively researched in water treatment and human medicine. The use of clinoptilolite-based products in vivo has skyrocketed due to a variety of health benefits, including detoxifying characteristics. However, there have been concerns expressed concerning the safety of clinoptilolite materials for in vivo use.

Humans have been using natural resources to improve quality of life for hundreds of years. We use things in the ways that are accessible in the environment at times, and we develop new and imaginative ways to use them at other times. Sand and charcoal, for example, are both instances of this. These are used as filter medium in water treatment. Zeolites are also employed in the purification of water. The most intriguing aspect of zeolites is their open, cage-like "framework" structure, which allows them to trap other molecules inside.

Everyone is continuously concerned about the quality of the water we use in our everyday lives, from cooking to direct consumption. As a result, water filters are widely used. This was the catalyst for the creation of this project.

Water purifiers use zeolites as part of their comprehensive filtration process. Furthermore, zeolites are readily available at low prices. They could potentially be used to filter water in distant locations where clean drinking water is scarce or unavailable. The micro-pores in the zeolite structure operate as filters, allowing pollutants to be filtered out to some extent. As a result, a bigger number of people will have access to drinkable water.

II. Theory

Zeolites are aluminosilicate minerals with a tetrahedral three-dimensional structure with micro-pores. Through shared oxygen atoms, silicon and aluminium atoms are tetrahedrally coupled with one another. The framework units' micro-pores have sizes ranging from 2 to 8 angstroms, allowing for relatively facile ion movement between cavities.

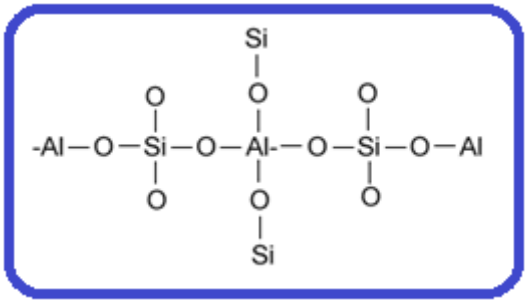

Because of the imbalance generated by the replacement of aluminium for silicon, zeolites have the potential to store a variety of cations. This is what is supposed to be used as the potential material. This feature of zeolites is mainly used in industries.

Zeolites are utilised to adsorb a range of compounds, according to a recent study published by Lentech in 2018. This comprises drying, purification, and separation applications. They can separate isomers and combinations of gases, as well as remove volatile organic compounds from air streams. Zeolites' porous structure can be utilised to "sieve" molecules of specific size and allow them to enter the pores. This feature can be fine-tuned by adjusting the size and number of cations around the pores in the structure.

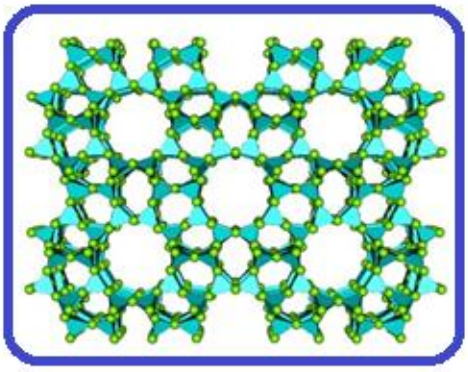

III. EXPERIMENTAL PROCEDURE

A. Removal of ammonium:

- Mix 2g of the Ammonium Chloride in 100ml of distilled water.
- Measure the ppm of the solution using the TDS meter.
- Roll the plastic sheets into thin tubes and fill them with zeolite. Secure the bottom with the thin piece of cloth.
- Suspend the Zeolite filled tube between the burette and conical flask used for collection of the filtrate.
- Pour the acquired solution through the zeolite tube and let it fall drop by drop as slowly as possible and collect the filtrate.
- Now find the TDS meter reading for the filtrate and compare the values before and after the experiment.

B. Removal of cooking oil from kitchen waste water:

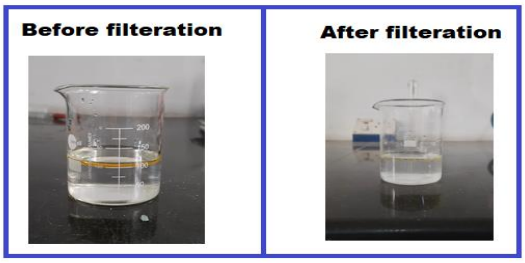

- Mix 10ml of vegetable oil in 100ml of distilled water.
- Roll the plastic sheet's into thin tubes and fill them with zeolite. Secure the bottom with the thin piece of cloth.
- Suspend the Zeolite filled tube between the burette and conical flask used for collection of the filtrate.
- Pour the acquired solution through the zeolite tube and let it fall drop by drop as slowly as possible. Collect the filtrate
- Leave the filtrate undisturbed for some time.
- Now check whether there is any oil left on the surface or not.

C. Removal of Magnesium carbonate:

- To 100ml of distilled water add 1g of Magnesium Carbonate and mix well.
- Roll the plastic sheets into thin tubes and fill them with zeolite. Secure the bottom with the thin piece of cloth.
- Suspend the Zeolite filled tube between the burette and conical flask used for collection of the filtrate.
- Measure the ppm of the solution using the TDS meter.
- Pour the acquired solution through the zeolite tube and let it fall drop by drop as slowly as possible. Collect the filtrate.
- Leave the filtrate undisturbed for some time.
- Now find the TDS meter reading of the filtrate and compare the values before and after the experiment.

D. Removal of sand from water:

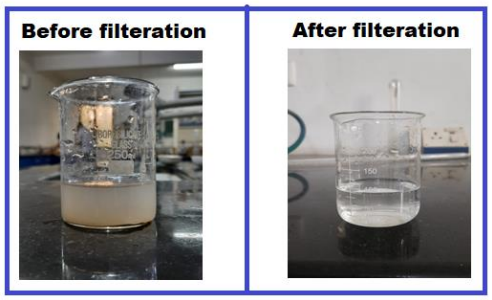

- Mix 5g of beach sand in 100ml of distilled water.
- Roll the plastic sheets into thin tubes and fill them with zeolite. Secure the bottom with the thin piece of cloth.
- Suspend the Zeolite filled tube between the burette and conical flask used for collection of the filtrate.
- Pour the acquired solution through the zeolite tube and let it fall drop by drop as slowly as possible. Collect the filtrate.
- Leave the filtrate undisturbed for some time.
- Observe the filtrate solution.

IV. RESULTS AND DISCUSSION

The observed results are listed in the table.

S.No	Solvent's	Before Filtration	After Filtration	Inference
1	Ammonium Chloride	508 ppm	420ppm	Zeolite filters ammonium
2	Cooking Oil	Distinct separation of layers between oil and water	$3/4^{th}$ of the oil is filtered	Zeolite filters oil
3	Magnesium Carbonate	167 ppm	128 ppm	Zeolite filters magnesium salts
4	Beach Sand	Filled with impurities	Clean solution	Zeolite filters dust and sand particles

V. CONCLUSION

From the above experiments, we can conclude that zeolites can filter and remove ammonium salt from water. For 2 g of ammonium chloride in 100 ml of water, it removes the total dissolved salts from 508 ppm to 420 ppm. Zeolite is used to remove 75% of the oil from water. For 1 g of magnesium carbonate in 100 ml of water, it removes the total dissolved salts from 167 ppm to 128 ppm. Zeolites are used to remove sand particles from water.

REFERENCES

[1] C Martı´nez and A Corma,Zeolites, Comprehensive Inorganic Chemistry II (Second Edition), From Elements to Applications Volume 5, 2013, Pages 103-131.

A Study of a Gradient monitoring Systemusing Wireless Sensor Network

B. Jeyapoornima[1], T.D. Subha[2], Kavya L[3], Jaithri K[4]

[1-4]Department of Electronics and Communication Engineering, R.M.K. Engineering College, Kavaraipettai, Chennai, India

[1]tdsubha2010@gmail.com, [2]bjp.ece@rmkec.ac.in, [3]kavy20225.ec@rmkec.ac.in, [4]jait20218.ec@rmkec.ac.in

***Abstract* — this paper gives out the execution outline of a stable Wireless Sensor Network (WSN) using IEEE802.15.4 (ZigBee) for gradient surveillance. The main aim of this research is to construct a WSN system that can sense and monitor the distortion of the ground caused by calamities in massive regions with sensor and radio equipments. Both environmental and electrical issues must be resolved in order for statistics to be accessed regularly. The methods for dynamical communication mode transformation based on battery capacity, a technique for shielding wireless nodes from lighting, and an enhanced depiction of antenna for WSN are proposed in this paper. The test outcome from the actual test field shows the configuration of a dynamic wireless system. The acquired information from the developed systemcan be used to predict the field's rank.**

***Keywords*—Massive Multiple Input Multiple Output Network System, Dynamic Wireless Network, IoT, IEEE802.15.4 (ZigBee), Sensor, Slope, Wireless Sensor Network (WSN).**

I. INTRODUCTION

Highlands occupy 70% of Japan's overall land area.Slopes surround the pathway and even the city, generating into roughly 1000 geologic perilous occurrences, such as landslides. Preventive maintenance for all of the target locations is problematic to execute due to depopulation and creative commons refers This research research is establishing a low-cost, high-reliability preventive maintenance system. Experts from several professions have been joined to produce a solid preventive maintenance system that reveals bothaspects and the numerous realms of ability. [1]. To generate a database on the causes, wide varieties of physical data must always be analyzed. Due to their low cost, portability, and security, wireless sensor networks (WSNs) are also an incredible resource for a wide range of physical data monitoring.

The long-term ambition of this effort is to stabilise the system. [2]. The solutions of electric and digital problems in WSN, such as power, communication, and other troubles, is crucial to remain the system stable. Therefore, real-time data collection and processing can be utilised to insure record precision. [3]. When compared to boosting models, it grows the model bit by bit and then allows any differentiable loss function to be boosted.

Graphic 1 exhibits a representation of an enormous multiple input multiple output network system.

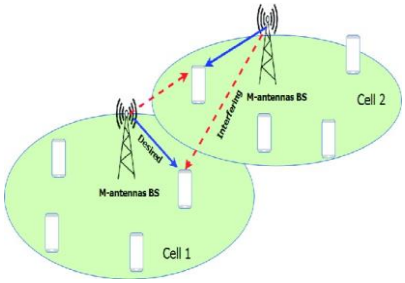

Fig. 1. Model representation of Massive Multiple Input Multiple Output Network System.

A local regularisation mechanism is constructed up of M gradient strengthening iterations (i.e. The quota of trees in the model when the foundation learner is a decision tree). We can diminish the mistake in the training set by enhancing the magnitude of M; however, getting the parameter extremely high may result in curse of density. The prediction error on a different validation data set is analyzed to establish out what the appropriate M value is. In addition to curbing M, alternative regularisation methodologies are also used. Gradientboosting is a mechanism for interpreting data in high-energy physics. In the proposed WSN system, the wireless terminal gets processed separately by the battery and solar pane. As a result, reaching a balance amongst communication rate and energy availability has become a difficulty. Figure 2 represents the extraction and consumption of closed loop CSI measurements.

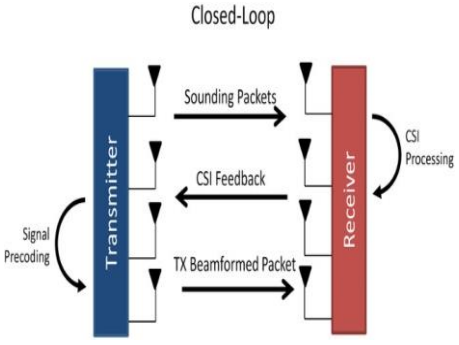

Fig.2. Closed-Loop representation of CSI acquisition andutilization.

corruption Emergency communication systems commonly get and combine the same notification services, but they also comprise two-way communication to aid communication between emergency communications personnel, afflicted citizens, and the central hedger. Another distinguishing feature of the term "communication" is that it entails the ability to convey complex and relevant information about a developing emergency and necessary actions whereas "notification" implies a comparatively simple single-time transference of the existence and frequent nature of an emergency. The fig. 4 represents the solution for maintenance of infrastructure and slopes with telecommunication.

A disaster is an unplanned, catastrophic event that adversely upsets the operation of an environment and causes in considerable losses that are better than the competence to manage using one's own abilities. Developing countries are especially affected by tragedies. More than 95 percent of all deaths through hazards occur in bad democracies and natural-hazard losses in poor countries are 20 times larger (as a proportion of GDP than in industrialised economies. [4]. Gradient boosting is a machine learning (ML) paradigm for grouping and regression problems that generate a prediction model in the form of a combination of weak prediction models, primarily decision trees. When the weak learner is a decision tree, the product practise is known as gradient boosted trees. Random forest is routinely excelled by this strategy. Regardless of the community in which the tragedy occurs, it has a habit of causing changes in the government and social life. Figure 3 depicts the landslide in Japan.

Fig. 3. Landslide in Japan

Regardless despite how tightly information is governed in a society, they have the possibility to modify the course of history by affecting the entire population and exposing dereliction or

Fig.4. Maintenance solution for Infrastructure and Slopes with Telecommunication (MIST).

A natural disaster is a sudden incidence created by forces other than human activity that results in widespread destruction, considerable property damage, or loss of life. [5]. Divergent of gradient boosting Deep Neural Networks (DNN) were adept in emulating the results of non-machine learning techniques of analysis on datasets utilised to determine the Higgs boson at the Large Hadron Collider (LHC). Earthquakes, eruptions, tornadoes, and tsunamis are simply a few of the many natural calamities that wreck chaos on property and landscapes every year. However, as a result of the world population's rising trend and increased concentration, disasters have become more often and severe, particularly in frightening scenarios. Disaster-prone communities are vulnerable due to the hot warmth and swaying landforms, as well as deforestation, accidental overgrowth, and shoddy construction. [6]. Natural accidents threaten inadequate countries as a result of a lack of communication and financial resources to predict and contain disasters. The configuration and flow are clearly shown in fig.5.

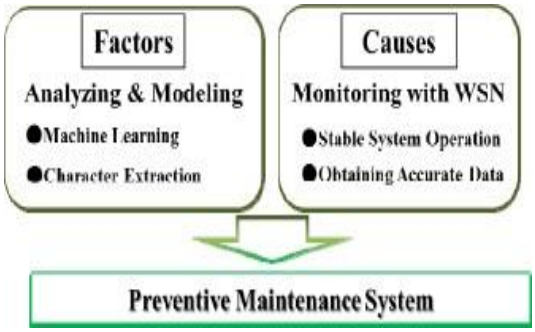

Fig.5. Configuration and Flow.

A distributed wireless network is a mobile ad hoc network (MANET) or a wireless ad hoc network (WANET) [7]. It's known as an ad hoc network because it doesn't rely on pre-existing infrastructure like routers and access points. As a result, each node engages in routing by redirecting data to other nodes, and the conviction of the specific node that redirects data is made on the basis of the routing algorithm and network connectivity in use. The closed-loop motor speed control is shown in fig.6.

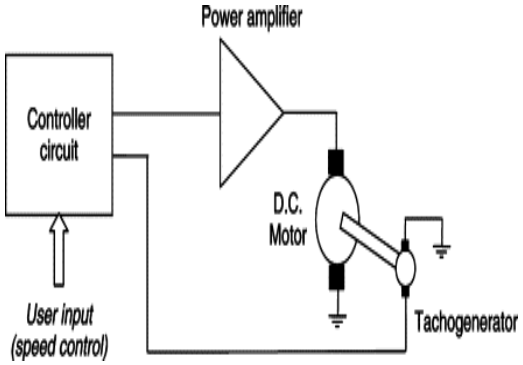

Fig.6. Closed-loop motor speed control.

Ad hoc mode is a communication mode setting in the Windows operating system that allows systems to communicate without a router. The wireless mobile ad hoc

network (WANET) is unlikely to traverse because it is an auto-configuring strongnetwork. These wireless networks do not mandate the development and management of infrastructure, allowing devices to form and join networks "on the go." Every device in a MANET is idle quite so to navigate in any location on its own, therefore it will occasionally replace its link to other devices. [8]. A router should be any device that forwards traffic, regardless of its own purpose. The most difficult component of building a MANET is ensuring that each device keeps the data required to effectively route traffic on a routine basis. This becomes unyielding as the MANET's range expands as a result of:

1. The intent to distribute packets to or through eveynode
2. The percentage of overhead traffic required to sustain an instantaneous routing status.
3. Each node has its own great put to route, unaware to the desires of others.
4. Everyone must share a large supply of communication bandwidth, such as a radio spectrumband.

These networks should either perform independent or as part of a massive Internet. As a result, the configuration becomes extraordinarily powerful andself-determining.

In this paper, some studies for increasing the stability are discussed. The overviews of our system and prototype experiment are detailed in Segments II and III. Sec. IV introduces a software-based dynamic wireless network configuration [9]. In Sec. V, the proposed antenna is for stable wireless communication. In Sec. VI, device protection from lighting is described. In Sec. VII, the analogy of stratum by pore pressure measurement is introduced.

II. Overview

The recommended scheme is titled MIST, which stands for Maintenance Solution for Infrastructure and Slopes with Telecommunication. Figure 3 exhibits a proposed remote monitoring device that utilises ZigBee, an IEEE 802.15.4-based specification for a set of interaction protocols. A coordinator, a router, and an end-device are all part of one of MIST's designs. A ZigBee chip is mounted in each terminal. Individual networks, transmission systems, relay stations, tributary stations, and terminal equipment constitute a communications system, which can be coupled and interoperated to form a credible whole. The contact between two stations, the Transmitter and the Receiver, isdenoted by it. From source to destination, signals or knowledge transfer across a channel. It also illustrates how the signal utilises it to get from point A to point B. The components of a communications system share a single target, are technically compatible, follow common protocols, respond to directions and participate. The role of LR-WPANs isgreatly determined by IEEE 802.15.4. It describes the PLL and MAC for LR-WPANs [10]. This is the foundation for ZigBee, Thread, Wireless HART, 6LoWPAN, and other standards that establish the undefined top layers on top of the IEEE802.15.4 standard.6LoWPAN can be used as a thread in top layers, and it also operates as a binding.. The structure of IEEE 802.15.4 is shown in fig.7. Multiple wireless networking protocols have occurred as a result of the rise of social Media of Things (IoT). For example, ZigBee can manage over 60,000 connections while employing only a limited amount of energy. It is also potential to collect the requisite data while conserving power usage by implementing ZigBee's sleep mode.

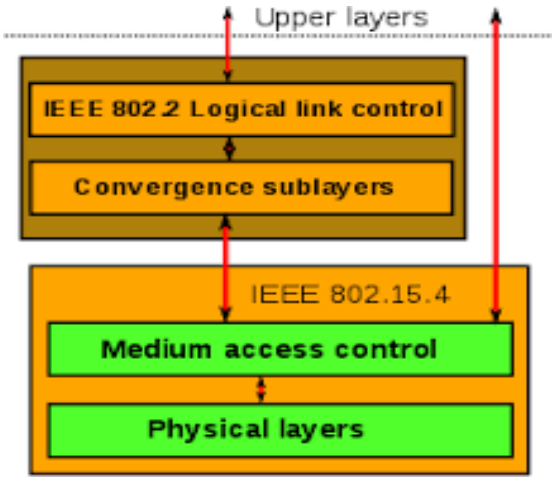

Fig. 7. Structure of IEEE 802.15.4.

Wireless networks are computer networks that are networked without any of the usage of a cable. They are supported by an unique energy source. A radio communication system is composed of many communications subsystems that provide exterior communications capabilities, as well as a transmitting conductor that produces mechanical accelerations or currents and is set up to allow such currents or oscillations to spread through the free storage medium from one point to another. The only medium between the transmitter and receiver in RF communication is air, though in other conditions, such as Sonar, the medium is usually water since sound waves transfer quickly through liquid media. A radio walkie-talkie, which is not relied ona mobile network, is the fastest way to contact The measuring antenna VSR can be seen in the Figure 8.

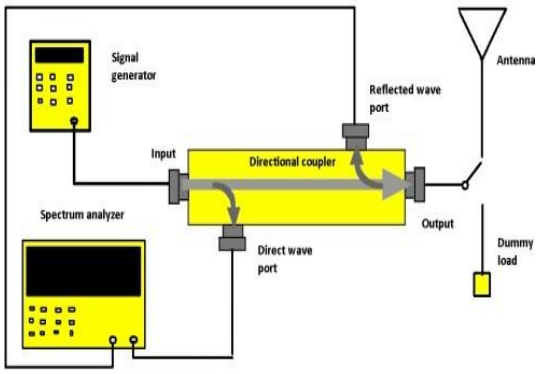

Fig.8. Measuring antenna VSR.

Almost anything can be adopted as a communication channel, from the expanse of the earth to solid globs of metal nonetheless, few mediums are preferred over others. This is the case because different sources flow through subjective media with differing efficiency. These systems utilize numerous input, sensor, and output devices.

Messages are sent from multiple senders to one or more

recipients via a commonly occurring medium. This necessitates the adoption of a channel access scheme that combines a multiplexing mechanism with a media access control protocol. The downlink of a neuronal technology can be thought of as a point-to-multipoint channel. A one-way transmission or broadcast of information about an occurring or pending emergency situation to one or more groups of individuals is what an emergency warning system is. Alarm notification systems include popular siren systems that warn of tornadoes, tsunamis, air defenses, and other disasters, as well as mass automatic dialling services like Cell Broadcast and Reverse 911. The end-device ADC encodes the voltage value supplied by end-device sensors into 16bit data [12]. The data would be sent to the coordinator (master unit) via specific routers (repeaters). This procedure performs itself on a regular schedule, such as every 30 minutes. The coordinator, which is a little microcomputer, forwards all data to the local host machine via the internet (RaspberryPi). The configuration of the terminal system is depicted in Figure 9.

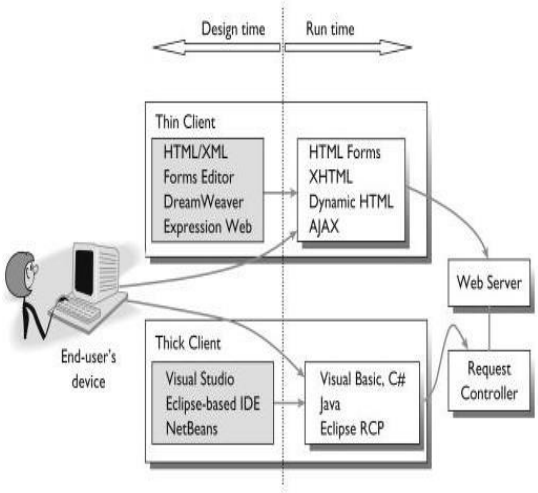

Fig.9. Terminal device structure.

Sensors are connected to end-devices using analogue (ADC) or optical (I2C) connections. Each terminal has its own solar panel and Li-ion battery to power it. As a result, the proposed MIST device will provide real-time analysis as well as remote monitoring of long-distance locations [13]. The datathat has been analysed or the raw data that has been sensed can also be accessed through the internet.

III. Experimental Field

In Nagasaki Region, Japan, the MIST mechanism is now being tested on an experimental field. Artificial land of superior sediment class is also used to create the field. A landslide transpired in a segment of the field four years ago amounting to heavy rain [15]. Even though the landslide hasn't wholly crashed, it's already happening. One of the distributed sensors is a pore water pressure metre for subterranean water level investigations. Similar sensor is a soil moisture metre, which measures changes in saturation and pore pressure near the bottom surface. The presence of precipitation is detected [14]. There are further acceleration, radiation, moisture, and pressure sensors on each terminal. The time domain relationship of the data may be easily investigated while the system's synchronised clock is executing. In fig.10, the wireless sensor node is illustrated graphically, and in fig.11, the MIST device is graphically underscored.

Fig.10. Photo of the wireless sensor node.

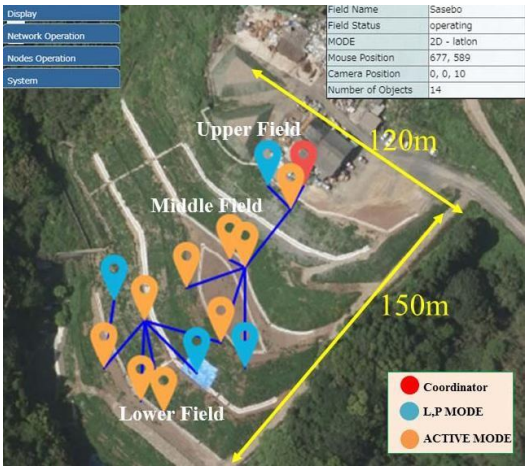

Fig. 11. Actual Screenshot of MIST System

The MIST equipment is the world's foremost autonomous wireless network appliance. On June 28, 2018, a seasonal front flowing west from a non - tropical low near Hokkaido became stationary over Japan [16]. On July 3rd, Typhoon Prairie made touchdown in south-western Japan, bringing severe rainfall and winds. MIST wireless is visible and expandable for indoor location services like signaling.

IV. Wireless Network Configuration

The greatest method of reducing power consumption is to use sleep mode. The terminals, on the other hand, are unable to reconnect to the network if their clocks differ from those of other terminals. As a word, the network has become hazardous. The components needed for effective implementation can vary from one wireless network to the next. In the same way, if the access point's settings are revised to prohibit the use of a specific Wi-Fi channel number, some PCs are now unable to recognize it. The measurement period in relation to battery voltage, whereas Figure12 depicts the dynamic wireless network design.

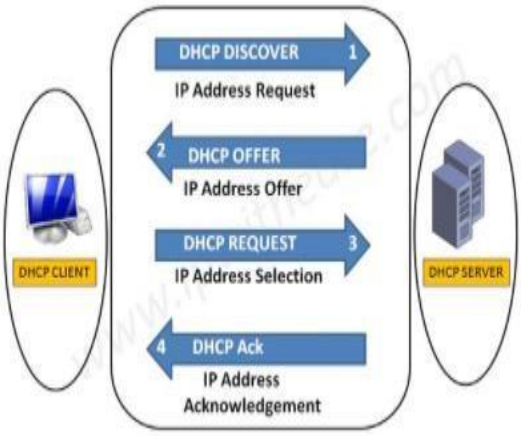

Fig. 12. Dynamic Wireless Network Configuration.

Sensor data is wirelessly communicated via ZigBee. A wireless-based slope stability radar system could be used, even though it is very expensive. On the other side, wireless sensor networks with low cost, low complexity, and two-way communication can be deployed to permanently monitor slopes in open cast mines. Confirm the wireless network key (Wired Equivalent Privacy) settings in Wireless Network Properties, or if the network key is automatically provided for you, allow it.(for example, the key is stored on the wireless network adapter given to you by your administrator), if the key is automatically provided for me, check the box [19]. Addressing the concepts of wireless network configuration is the first and most fundamental stage in the technique. This will reveal how to do everything from cable location to distinct settings. Nodes can be configured symmetrically all across the network, with two nodes in a specified locality classified as a pair, with each node continuing one of two phases (active or low power (L.P) mode). When the battery voltage boundary is set to 3.7V, the practical results are shown in Fig. 7.

V. Proposed Antenna For WSN

The RSSI (Received Signal Strength Indication) was used to analyze the radio wave propagation phenomena in the field. The following things have been clarified as a result of this. Many antennae are positioned on the slope, both vertically and horizontally [20]. Furthermore, the incoming positions of the transmitting wave are unknown. As a result, antennas with a wide beamwidth radiation pattern in all elevation angles are preferred. [21]. For such settings, a radiation pattern with circular polarisation at high elevation angles and vertical linear polarisation at low elevation angles is effective. A horizontal antenna is also better suited for fort-door WSN than a linear antenna when considering the influence of wind and rain. The antenna geometry, whereas Figure 13 indicates the spectral efficiency of several antennas.

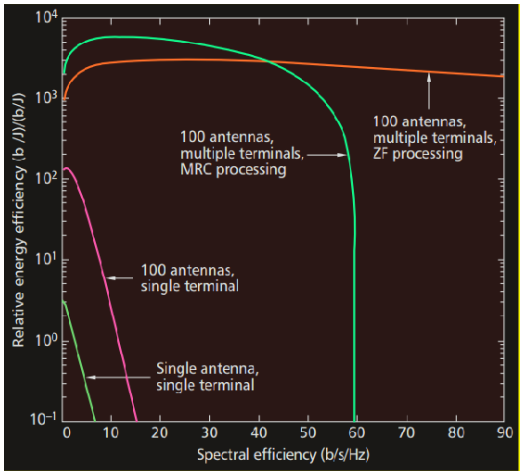

Fig. 13. Spectral Efficiency for various antennas.

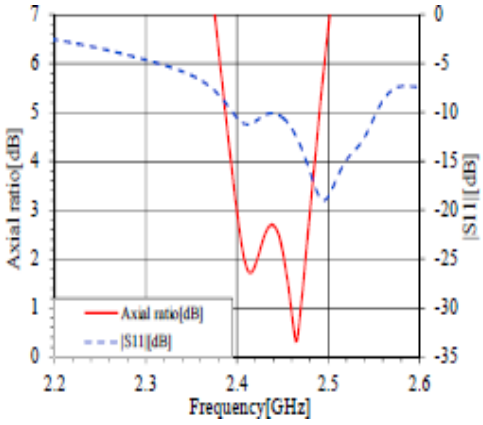

Fig. 14. Simulation curve.

Inserting Crank-shaped slits strengthens the circular bandwidth of circular polarisation. Figure 10 indicates the simulated axial ratio of circularpolarisation and reflection coefficient. In the ZigBee range (2.40 GHz–2.48 GHz), the circularly polarised wave is confirmed to radiate in the direction of [22].

VI. Device Protection From Lighting

When routers and coordinators are situated high in a flat location to promote communication, they are more dangerous to flash floods. [23]. As a result,we're producing a low-cost, simple lightning rod and a lightning protection cage, which is a form of Faraday cage, to secure electronic devices from lightning strikes. The lightning rod image, output voltage, and gain acquired are shown in Figures 15 and 16.

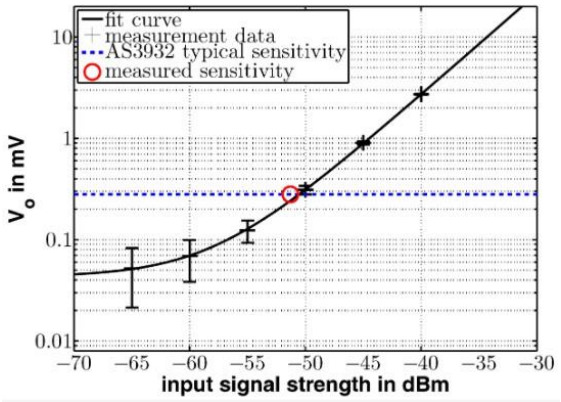

Fig.15. Output voltage.

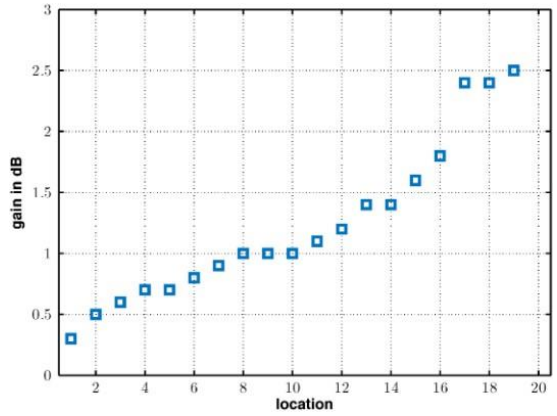

Fig. 16. Gain achieved by the equal-gain diversity.

Figure 11 is a view of a simplified lightning rod. The coordinator is 1.5 metres distant and comes at a height of 2.5 metres. The lightning rod is constructed of wood and a stainless steel pipe with a diameter of12 mm. The lightning protection cage is expected to secure the router from side lightning strokes and upward streamers [24]. The spark cage experimentally demonstrated that lightning hits do not permeate the cage by conducting discharge experiments with a lightning impulse voltage of 100kV.

VII. The Analogy Of Stratum By PorePressure Measurement

The measurement interval is 30 minutes, and the horizontal axis denotes the measurement duration. The output voltage is indicated by the vertical axis, which is measured in the field by a pore-water-pressure sensor with a variation capacity of 0.15 V/m. The output voltage varies from 2.0 V to 3.0 V, as shown in this diagram. As a result, the difference in water level is approximately 6.7 metres. It's also worth referencing that every 5 metres from the sensor's bottom, the water permeability coefficient varies. Similarly, the stratum shifts 5m from the reference position [25]. The system's data can be produced to analyse the stratum composition in the following steps.

VIII. Conclusion

The WSN system was used to produce a remote slope monitoring system. The actual router field monitoring was discovered to have a number ofissues. In order to operate the system for a significant duration, adaptive powering control for the communication terminal has also been offered. The information derived by the proposed system can be applied to forecast the state of the field. It isnecessary to raise communication stability, power supply, and impact on the environment.

References

[1] F. Aliment, V. Palazzi, C. Mariota, P. Monzonite, R. Corrie,
[2] N. B. Carballo, et al., "Smart Hardware for Smart Objects: Microwave Electronic Circuits to Make Objects Smart", *IEEE Microw. Mag.*, vol. 19, no. 6, pp. 48-68, 2018.
[3] G. N. L. Ravi Teja, V. K. R. Harish, N. Mud din K. D.“Land Slide Detection and Monitoring System using “Wireless Sensor Networks (WSN)” International Advance Computing Conference(IACC)2014.
[4] T.D.Subha, T.D.Subash, K.S.Claudia Jane, Devadharshini.D, Dhanya and Francis, 2020 “Study and Analysis of Suppress of Surface Wave Propagation in Microstrip Patch Antenna”, Elsevier-materials today proceedings-24, pp. 2414- 2423.
[5] Hui, Jonathan W.; Culler, David (2004). The Dynamic Behaviour of a Data Dissemination Protocol for Network Programming at Scale. Proceedings of the 2nd International Conference on Embedded Networked Sensor Systems. SenSys '04. New York, NY, USA: ACM. pp. 81–94.
[6] Dave Ta The Chang: “Study of Wireless Sensor Network(WSN) using for slope stability monitoring” Electric Technology and Civil Engineering (ICETCE)2011.
[7] Morteza M. Zanjireh; HadiLarijani (May 2015). A Survey on Centralised and Distributed Clustering Routing Algorithms for WSNs. Conference: IEEE 81st Vehicular Technology Conference: VTC2015-Spring. Glasgow, Scotland. pp. 1–6.
[8] T.D.Subha, T.D.Subash, Elezabeth Rani and P.Janani, 2020 “LiFi: A Revolution in Wireless Networking”, Elsevier- materials today proceedings-24, pp. 2403-2413.
[9] G. DANG and X. CHENG “Application of Wireless SensorNetwork in Monitoring System Based on Zigbee” IEEEWorkshop on Advanced Research and Technology in IndustryApplications (WARTIA) 2014.
[10] Mishra, C. Na and D. Rosenburgh, "On Scheduling Guaranteed Time Slots for Time Sensitive Transactions in IEEE, 802.15.4 Networks," MILCOM 2007 - IEEE Military Communications Conference, Orlando, FL, USA, 2007, pp. 1-7.
[11] T, Fujimoto, T. Tsuruoka, T. Fujishima, Y. Ishizuka, S.Sugimoto, T. Sasamura, “Circularly polarized small microstripantenna for wireless sensor network,” Proc. of InternationalSymposium on Antennas and Propagation 2015.
[12] Silver, H. Ward, ed. (2011). ARRL Antenna Book. Newington, Connecticut: American Radio Relay League. p. 3-2.
[13] T. Fetishism, T. Osaki, S. Macao, T. Frusta, T. Yamashita,S.iSugimoto, T. Fujimoto and Y. Ishizuka, “Trial ofLightning Protection Cage Development for Remote Monitoring,”Pros. in International Conference on Electrical Engineering, (ICEE)2016.
[14] KamilMaslih (15 August 2018). "Malaysia sumbang RM500,000 untukmangsabanjir, strokhaba di Jepun" (in Malay).Utusan Malaysia. Retrieved 22 August 2018.
[15] Emerson, D. T. (1997). "The work of Jagadis Chandra Bose:
[16] 100 years of MM-wave research". IEEE Transactions on Microwave Theory and Research. 45 (12): 2267–2273.
[17] Linebaugh, Kate. "Medical Devices in Hospitals go wireless." Online.wsj. The Wall Street Journal. 23 May 2010. Web. 27 Oct. 2013.
[18] H. Schmeck, C. Müller-Schloer, E. Çakar, M. Mnif, and U. Richter, “Adaptivity and self-organization in organic computing systems,” ACM Transactions on Autonomous and Adaptive Systems, vol. 5, no. 3, 10 pages, 2010.
[19] H. Chan and A. Perrig, “ACE: an emergent algorithm for highly uniform cluster formation,” in Proceedings of the European Workshop on Sensor Networks, pp. 154–171, Berlin, Germany, January 2004.
[20] W. Ye, J. Heidemann, and D. Estrin, “An energy-efficient MAC protocol for wireless sensor networks,” in Proceedings of the 21st Annual Joint Conference of the IEEE Computer and Communications Societies (INFOCOM '02), vol. 3, pp. 1567– 1576, IEEE, New York, NY, USA, June 2002.
[21] K.S.Swetha and T.D.Subha, 2020, “A Novel Approach to White Light Radiation from Silicon Based Tunnel”, Trends in Opto-electro & Optical Communication, vol.10, n0.1, pp.1-13, ISSN:2231-0401.
[22] C. P. Balde, V. Forti, V. Gray, R. Kuehr and P. Stegmann, "The Global E-waste Monitor 2017: Quantities Flows and Resources",

United Nations University International Telecommunication Union and International Solid Waste Association Tech. Rep., 2017.

[23] L. Yu, W. Wang, X. Zhang and W. Zheng, "A review on leaf temperature sensor: Measurement methods and application" in Computer and Computing Technologies in Agriculture IX. CCTA 2015. IFIP Advances in Information and CommunicationTechnology, Cham:Springer, vol. 478, pp. 216-230, 2016.

[24] J. Sjöbergh and Y Tanaka, "Geospatial Digital Dashboard for Exploratory Visual Analytics", Communications in Computer and Information Science Information Search Integration and Personalization, pp. 3-17, 2014.

[25] T.D.Subha, T.D.Subash, K.S.Claudia Jane, Devadharshini.D, Dhanya and Francis, 2020 "Autonomous Under Water Vehicle Based on Extreme Learning Machine for Sensor Fault Diagnosistics", Elsevier-materials today proceedings-24, pp. 2394-2402.

[26] K. Lwin, Y. Sekimoto and W. Takeuchi, "Estimation of Hourly Link Population and Flow Directions from Mobile CDR", ISPRS International Journal of Geo-Information, *vol.*7, no. 11, pp. 449, 2018.

Analysis of Wireless Electronic Traffic Mirror using Dynamic Map Based System

N.M. Jothi Swaroopan[1], T.D. Subha[2], Swathi M[3], Subhashini E[4], Snehaa S[5]

[1-5]Department of Electrical and Electronics Engineering, R.M.K. Engineering College, Kavaraipettai, Chennai, India

[1]jothi.eee@rmkec.ac.in, [2]tdsubha2010@gmail.com, [3]swat20426.ec@rmkec.ac.in, [4]subh20420.ec@rmkec.ac.in, [5]sneh20413.ec@rmkec.ac.in

***Abstract*—When it comes to technological innovation, a consciousness as well as a designed accessibility assistance conceptual model method have been combined primarily with digital technologies that generate integrated quick transportation as well as an adaptability shielding mechanism have been used. In addition to providing updates and transmissions of roadway data collected by roadside sensors to a powerful guide known as a dynamic map (DM), the Intelligent as well as Adaptive Accessibility Benefits Interface also provides increased programmed portability control with high accuracy and reliability. In order to secure the strengthening as well as construction of motorway data to computerized motilities, a Wireless Electronic Traffic Mirror (WETM) has been designed. Watershed information technology (WETM) collects street data, recognises street things, and transfers recognition data into an electronic framework. AMAS would also deliver the external connection that is particularly suitable for transportable in attempt to reach the infrastructure needs of the AWS environment. It is necessary to perform continuous remote connection testing in determining the scope of global communications that are obstructed in order to provide optimal external allocation. Due to the fact that it enables for something like the maintenance of optimal remote dependability, this is a critical responsibility in the AMAS. Throughout this review, the integration of perpetual external take attention away domestic spying in connection with the resulting WETM, and also the indisputable verification of every particular circumstance emergence, together with its meticulousness, is discussed in order to describe the thoughts and ideas behind that one, and also how many of the manifestations, including its asphalt concrete, might have been upgraded, are discussed.**

***Keywords*—Dynamic Map (DM), self-governing, roadway information, wireless electronic traffic mirrors, Deterministic accessibility information (DAI).**

I. Introduction

Self-driving vehicles, drones, agricultural trucks, and robots will all be commonplace sooner rather than later, as autonomous and automatic mobilities continue to increase at a rapid pace. The support of a dependable intelligent transportation system (ITS) is required in order to provide safe movement in this situation. On that basis, several studies and technological improvements are being conducted to improve and support autonomous mobility control in order to realise the future ITS. Self-control mobilities may move in different street circumstances by the mix of gridlock, development and crash, etc. As a result, it is critical for constant self vibrational modes to be responsible for the information generated from roadside detectors [1]. As a result, a self governing transit guidance process must have been described that provides exact predetermined accessibility influence. The most absolutely vital aspects of recognizing with AMAS are generating an interactive layout. A dynamic map (DM) is essentially that much than a collection which sufficiently but also offers information about road conditions and surrounding scenarios, which will be delivered to autonomous vehicles [2].

The interactive grid is divided into four tiers, each of which is determined by the schedule during which the material must be updated on a constant basis in maintaining the expressway's prominence. The four layers of dynamic map are shown in Fig 1.

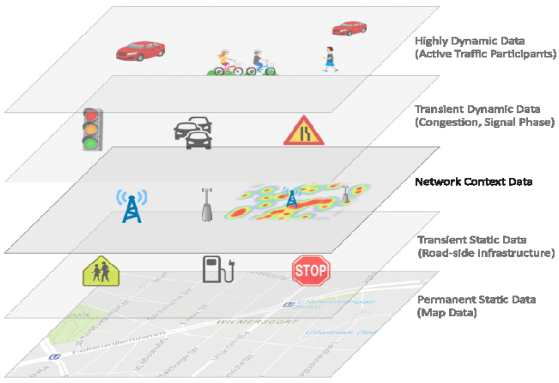

Fig. 1. Dynamic map (DM)

The four divisions are listed below in alphabetical order. Deterministic accessibility information (DAI) is a monthly surface that contains information about vehicular interfaces, pavement sections, and highway configuration, among other things. When making modifications other than congestion management and reactive routing, a surface with information, including post relocation analytics, is continually modified and updated. The surface using especially post accessibility relevant data (mDMI) includes frequent updated information concerning kinds of activities including congestion delays and disasters [3]. Ultimately, additional surface containing evolving accessibility relevant data along each surface gives documentation concerning

instances which adapt rapidly, along with automobile surveillance road users, as well as congestion photon statistics. Everyone's inventiveness is being used to create mobility in all developmental steps of the AMAS, and all four stages have adequate components of that accessible. When you properly retain the actual network characteristics that were required in order to achieve the most up-to-date transportation conditions. This information should be transferred to vehicles through wireless communications; here the entire process should be accomplished as quickly as possible to avoid errors. Because knowledge about the conditions of a road is available in real time, it is interesting to evaluate a system that recognises the roadway. There are, in fact, two ways to receive information on transportation arrangements.One will be through self governing connectivity and an even more one is including the use of nearby detectors [4]. The basic technique provides for every other identity automobile operating upon its expressway using instruments identifies elements mostly on network, provides lane occurrences also including mishaps, structures, delays, other such constraints, so the route details is contributed towards the DM. The recent technique performs additionally towards the subsequent structure, except that transportation systems describe elements mostly on cycle path, simplify the route incident, also modify that DM with this insight. Hazards as well as strategic location, in particular, make it harder for self governing accessibility to establish physical circumstances [5]. A battleground, in addition to being one of the most hazardous and difficult situations for personality movement, is also one of the least transparent. In considerations of route stability, channel conditions, such as those posed by approaching automobiles and individuals, and possibly even the occurrence of interferences, would be conveyed to approaching traffic as soon as possible and as reliably as possible.

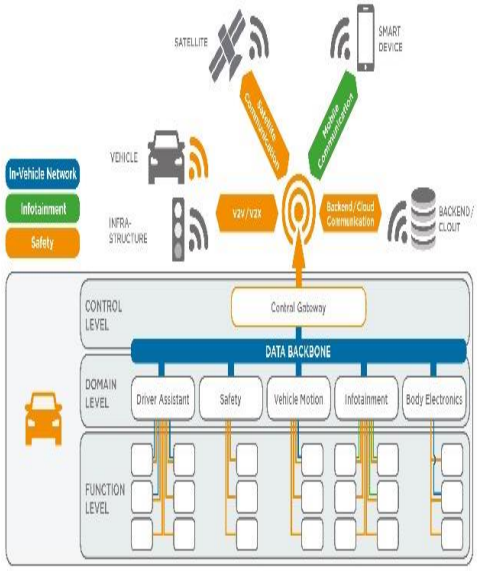

Fig. 2. Automobile intervention method that is simultaneously distinct as well as instantaneous.

The designed roadway detectors for recognising mobility surroundings, specifically when used in conjunction with a transportable computerized flat mirror, that meets the highest standard of service. Besides that, audio amplifiers may track the status of every communication system in important to maintain appropriate data transmission [6]. Transmission detection measures interface reliability and in ensuring adequate connected devices as well for self governing migration. The determination of each and every presently available transmission rate that must be evaluated by the consumer is an example of a substantially widespread, considerable communication guidance. Based on the competence of the transmission line and the connection performance measurement that has been accomplished, only a function is included with a Network adapter as core element. With a stronger RSSI, more or less every configuration could demonstrate an elevated available bandwidth to the assessment, which is referred to those as efficient charge allocation. In addition, the architecture could create a greater transmission distance with the exception of the developer, which is also termed to as efficient charge redistribution. As a result, establishing acceptable interactions in an inconsistently distributed way, such as that found in a wireless arrangement, is frequently not practicable [7]. As a result, the method is unable to identify the source of every single frequency transition because wireless data variance is affected by participation, blockage, or compression when throughput is affected by engagement, obstruction, or deformation. A conscience routing structure made in cooperation with each WETM to exhibit documented transportation events such as automotive as well as network connectivity, the accessibility of challenges, and whatever else is denoted by its examination [23]. The entire system ability to continuously acknowledge every frequency spectrum is dependent around the identification as well as representation of transportation instances. Consequently, each information massive amount must significantly reduce.

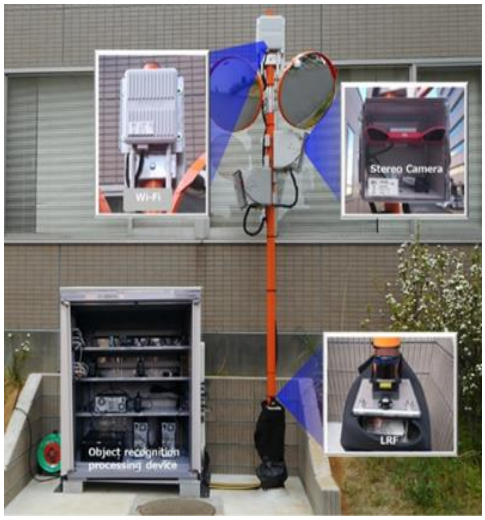

Fig. 3. Automated reflection that has been internet connected

II. Protection Mechanism For Advanced Accessibility

A self-driving accessibility support service seems to be a collection of components that enable continuous operating supervision of identity automobile [8]. Figure 2 displays an AMAS incorporating transportable monitors, a powerful computational infrastructure, terminals, and an interactive

map, all of which are depicted in detail (DM). The three significant procedures successful accomplishment of AMAS are just the acquisition of assets, the provision of services, and the availability of data. Using monitors incorporated into identity instruments, permeation might be a means of acquiring extra data on various road circumstances and afterwards communicating that material to a hypervisor through the use of a wireless networking approach. The procedure by something that monitoring processors evaluate transportation instances and modify content concerning network circumstances for DM is known as preservation. Last but not least, composition appears being the technique employed by some who believe that perhaps the uninterrupted data transfer mechanism allocates the resulting sensory information to conscience interoperability handsets mostly through communications networks as quickly and efficiently as possible in attempt to provide testing.

III. Connectivity Interactive Congestion Represent With Pavement Detector

Zeren et al [9] explicitly stated that there will be instances of methods to gain information on traffic patterns using external monitors. The confluence has also been defined as a crossroads wherever two or more roadways come together in an area wherever that is a considerable danger of collision involving self-driving automobiles due to a lack of visibility.

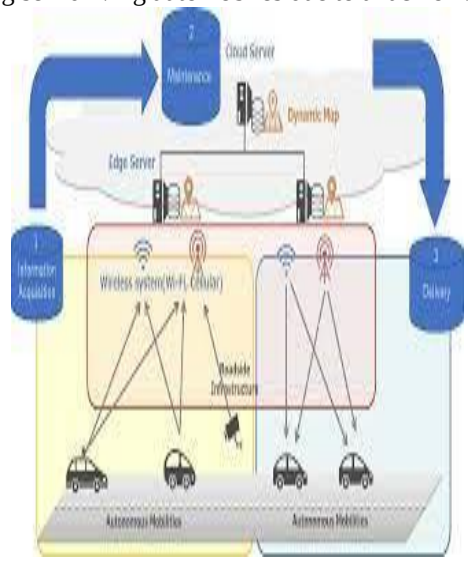

Fig. 4. Mechanism for feature extraction as well as modifying surface parameters

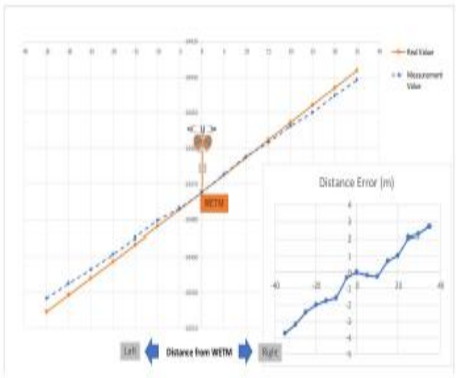

Fig. 5. WETM detects a proximity defect.

The premise of a sport utility vehicle, the responses of such an individual, and also the activation of boundaries are all necessary to assure preservation during the exchange in gathering exterior necessities as quickly and permissibly as possible. Therefore, scientists developed a second device to be used with the mobility geiger counter, which they characterise as beyond just a clever programmed projection. Figure 3 depicts the WETM that has been created, which includes characteristics such as an embedded detector, wireless routers, and edge detection technologies.

A. Component detection and adoption

Using a continuous chart, Figure 4 illustrates the methodology for exhibiting features on paving along with producing chrome plating for WETM beyond a variety of terrain types. The WETM utilises the projection screen as a biosensor, allowing it to compile information describing occurrences on this channel over a long duration using the beam. Each of these photographs are being captured on a constant basis through the webcam. Moreover, photos of automobiles operating on the roadway, pedestrians, as well as indicators are taken into consideration [10]. In terms of information recovery, the imagenet dataset communication systems infrastructure was also used to accomplish this task. Towards further distinction, treatment system a development tools assessment way to address every vicinity surrounding the destination or even the WETM, and then maybe the regularity, which includes its pledged location. This methodology is illustrated in Figure 5. Once at distance of 30 metres outside the WETM, the functional assessment is about equal to or same to 3 metres.

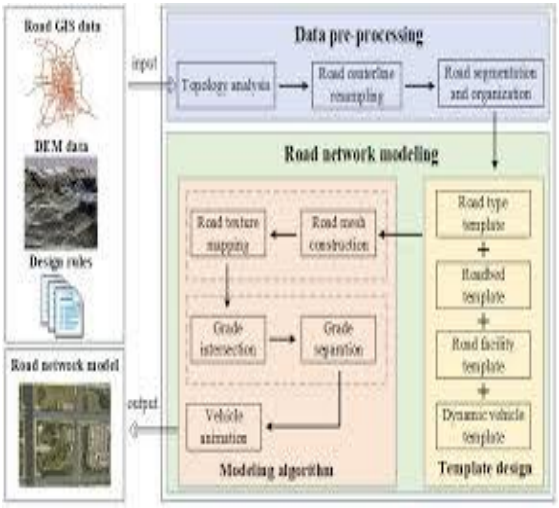

Fig. 6. Preservation of documentation

B. Preservation And Transfer Of Data

It is possible to identify faults caused by detectors per each representation obtained by WETM because every image includes data about the vehicle. This enables the customers to understand the condition of the main street exactly and to identify any inconsistencies by detectors. Therefore, the photos must be provided online [11]. Consider an exterior study in which all the visuals retrieved using a photodiode consume 1.4 Gbps of available bandwidth, comprising four input data streams of 1.2 million pixels as well as 30 frames per second, and even

where particular views collected using an imaging system use 1.4 Gbps of fading channels. In order to take advantage of the local network size restrictions made accessible during transmitted data, the depiction output rate needs constantly be reduced by a significant amount. Data compression is one approach for reducing the amount of data. Each treatment method is a procedure for eliminating non-essential elements from a collection of data, allowing just the most important information to be retrieved as a result. Only the photos of the things that are necessary are taken into consideration, with the rest being ignored. This information compression method is called as region of interest (ROI). Figure 6 depicts a ROI pictorial reduction demonstration. The WETM obtains portraits of numerous items mostly on path, including a commuter, an automobile, as well as other vehicles [12]. This means that the return on investment (ROI) for each webpage that contains a defined imagery with dimensions of 1280*960 density should be fallen drastically, by almost 20%.

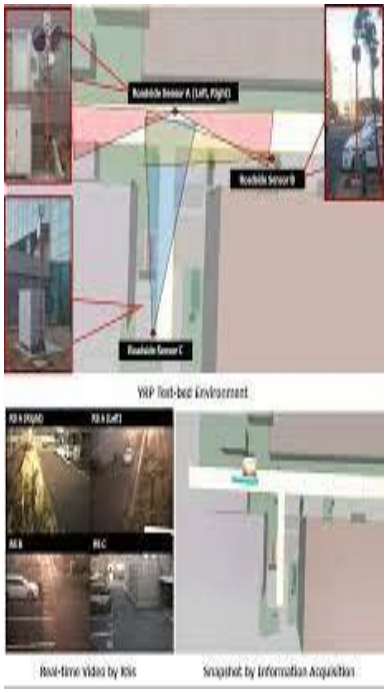

Fig. 7. A demonstration surface AMAS

IV. Connectivity Systems Are Supervised In Real-Time

The statistics acquired from the road surface incorporating detectors may be required to regulate conscience density through an independent as well as instantaneous movement protection scheme, where such information must continuously verified with the device and delivered to transitions over wireless connections [13]. Regarding the security purpose, the best wireless connection should be provided by assistance system. In order to ensure effective network connectivity, electronic devices continuously evaluate the available bandwidth [6]. Wireless network assessment determines network efficiency in order to ensure effective access points enabling self governing movement. Generally, significant physical layer assessment would be the identification including its actual transmission capacity being delivered to the user. Throughout implementation, such process generates every individual with a broadband system depends on the characteristics of every communication system, including certain obtained spectral efficiency notification (RSSI). Consequently, the operation will further require significantly more data throughput for the implementation with such a higher RSSI, referred as the state responsibility utilisation, and even the detector should choose another other comparatively high signal quality for the observer other than even a tougher RSSI, and thus a massively better network utilization for such viewing audience [14]. ARS is appropriate for persons with stable connectivity. In any case, it is hard to give sufficient connectivity over wireless medium in an unpredictable wireless environment [22]. This is due to delay in selecting quality wireless channels thereby the transmission rate becomes inappropriate. Additional factor contributing towards the difficulty in delivering the requisite wireless communication is the mobility of items and impediments on the road surface. There are specific steps that must be performed while selecting the bitrate [15]. The street acknowledgment and ongoing remote channel checking is very valuable for the future ITS framework advancement.

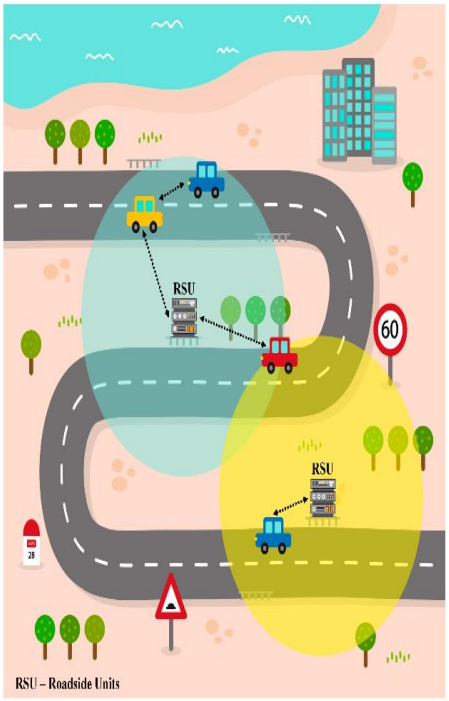

Fig. 8. The transportation recognition surveillance and wireless transmission maintenance are illustrated.

The discovery establishes a demand values observation set of mechanisms in collaboration with the WETM as well as produces comprehensive estimates across the AMAS congested specific situation [16]. The WETM would therefore also demonstrate different path circumstances including accessibility, inconveniences, as well as lateral movement, among other things. Meanwhile the occurrences of both the physical layer alteration are being determined.

V. Interventions In The Domain

As seen in Fig. 7, a prototype outer layer AMAS is being created to collect lane markings through the use of WETM

technology.

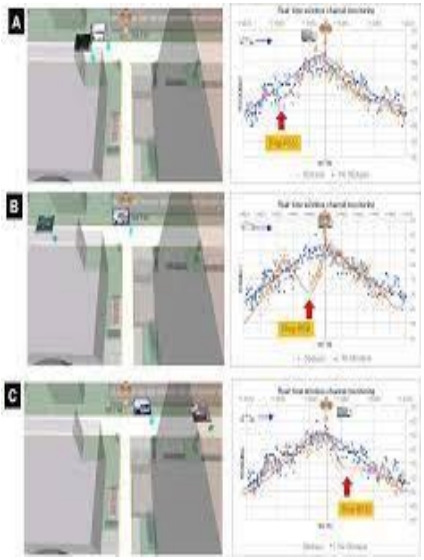

Fig. 9. Visual representation using data about signalized intersections (A), WETM is situated in the front of the building (B), and placed within 10 metres of WETM (C)

During the field testing, the low bandwidth detection method with either a roadway categorization technique is proven to be effective [19]. Based on the configuration of the lane as well as structural constraints, it must to deploy the sensors at a height of 2.4 metres or higher to monitor the precise surface [17]. Fig. 8 shows the transportation recognition surveillance and wireless transmission maintenance is illustrated. The movement of mobilities will be recognized by sensors and this collected information will be transferred to the vehicles moving on a road [23]. In the lower portion of Fig. 8, it is demonstrated that WETMs are used to identify and gather intelligence on road surfaces, as well as connection intelligence gathered by a car travelling down the road at the same time. The description of roadway information and the variation in RSSI during in the migration of potentials are depicted in Fig. 9, respectively [18]. In fig. 9, designers get that a red line within that illustration shows RSSI significance whereas a vehicle slows down and sometimes an automobile makes its way, as well as a blue line indicates RSSI rating if a transportation passes left to right also on lane independently. The RSSI significance is immediately lowered throughout the findings, as analysed. It seems to be challenging to figure out how the network performance is diminishing due to a reduction in RSSI caused by a variety of factors.

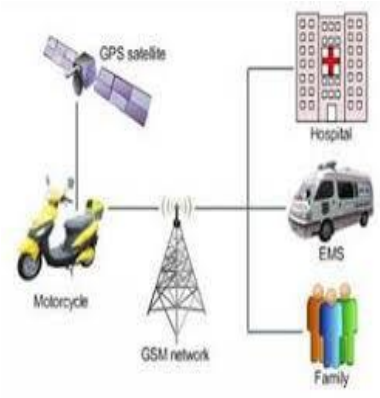

Fig. 10. The variations in data transmission as well as the transportation circumstances are depicted.

The tracking of wireless channel with WETM gives the accurate information on road conditions (the left figures) [20]. The tracking near AP leads to RSSI level deduction which in turn produces the interference between AP and vehicle [21]. Figure 10 depicts the state of the vehicle together at rear end of something like the lane along with RSSI improvements. Assume a circumstances upon its expressway where the automobile mostly on opposite side of the WETM seems to have a frequency spectrum compared to the channel intensity without restrictions, but really the indication extent demonstrates that the automobile re-visits the transmission rate without interferences as it moves towards the adequate direction of such WETM. The actual wireless channel tracking with WETM gives away the precise image information on roadway conditions and explains the reason behind the change of wireless channel when a vehicle is moving behind a truck.

VI. Conclusion

By incorporating detectors anywhere along wayside, it is necessary to construct a foundation for analysing layout for identifying the route, but now with the collaboration of radio connectivity, the intelligence is delivered to personality vibrational modes. The WETM technique, which has been implemented in conjunction with the proving ground structure, is intended to allow for the effective updating and transmission of data acquired and assessed by the sensors. In additionally, the investigation was designed to determine how effectively bluetooth connectivity functioned in conveying the attributes retrieved from the itineraries when they were delivered. In this step, the image collected information is reduced in order to lower the capacity of the communication. The proposed autonomous flexibility assistance process is very crucial for further Integrated Transportation Mechanism construction in sufficient quantity to enhance network connectivity worldwide and optimize autonomous charge density.

References

[1] IEEE Std 802.11p, Wireless LAN Medium Access Control (MAC) and Physical Layer (PHY) Specifications, Amendment 6: Wireless Access in Vehicle Environments", 2010

[2] IEEE Std 1609.4 TM-2010, IEEE Standard for Wireless Access in Vehicular Environments (WAVE)-Multi-channel Operation", IEEE Vehicular Technology Society, February 7, 2010.

[3] ETSI TR 102638, Intelligent Transport Systems (ITS); Vehicular Communications; Basic Set of Applications; Definitions",2009

[4] 5GAA Whitepaper, "Toward fully connected vehicles: Edge computing for advanced automotive communications", 2017.

[5] T.D.Subha, T.D.Subash, K.S.Claudia Jane, Devadharshini.D, Dhanya and Francis, 2020 "Autonomous Under Water Vehicle Based on Extreme Learning Machine for Sensor Fault Diagnosistics", Elsevier-materials today proceedings-24, pp. 2394-2402.

[6] Cross-ministerial Strategic Innovation Promotion Program, Dynamic Map, http://www.sip-adus.go.jp/rd/.

[7] T.D.Subha, T.D.Subash, Elezabeth Rani and P.Janani, 2020 "LiFi: A Revolution in Wireless Networking", Elsevier-materials today proceedings-24, pp. 2403-2413.

[8] S. Chen et al., "LTE-V: A TD-LTE based V2X Solution for Future Vehicular Network", IEEE Internet of Things J., vol. 3, no. 6, pp. 997-1005, Sept. 2016.

[9] T.D.Subha and V.D.Reshma, 2017 “A study of Non-invasive Heart Rate Monitoring System by using FPGA”, Elsevier-materials today proceedings-4, pp. 4153-4168.
[10] M. Kihl, ”3GPP LTE Downlink Scheduling Strategies in Vehicle-to-Infrastructure Communications for Traffic Safety Applications”, IEEE Symp. Computers and Commun., 2012.
[11] Arya, Jaqualin, Nimmi, Sonali, Amrutha, Hega & Subha, 2016, “Transition Mechanisms from IPv4 to IPv6 Addresses”, Journal of Web Engineering & Technology, vol.3, no.2, pp.21-27, ISSN: 2455-1880.
[12] Changwoo Pyo, Homare Murakami, Kentaro Ishizu, and Fumihide Kojima ”Field-Test of Road Information Recognition and Transmission by Road-Side Sensors to Support Autonomous Mobility System”, IEICE Tech. Rep., vol. 118, no. 57, SR2018-15, pp. 87-94, May 2018.
[13] T.D.Subha, T.D.Subash, K.S.Claudia Jane, Devadharshini.D, Dhanya and Francis, 2020 “Study and Analysis of Suppress of Surface Wave Propagation in Microstrip Patch Antenna”, Elsevier-materials today proceedings-24, pp. 2414-2423.
[14] J. Redmon, S. Divvala, R. Girshick, A. Farhadi, ”You Only Look Once: Unified real-time object detection”, IEEE Conference ComputerVision and Pattern Recognition (CVPR), 2016.
[15] K.S.Swetha and T.D.Subha, 2020, “A Novel Approach to White Light Radiation from Silicon Based Tunnel”, Trends in Opto-electro & Optical Communication, vol.10, n0.1, pp.1-13, ISSN:2231-0401.
[16] G. Leen and D. Heffernan, “Vehicles without wires,” Computing & Control Engineering Journal, vol. 12, no. 5, pp. 205–211, 2001.
[17] Eugene Peter, T.D.Subash, T.D.Subha, Alsufiyan Nazim, 2020 “Utilizing Radiant Nanoparticles in Silicon for Balanced White Color Adaptors”, International Journal of Silicon, Springer.
[18] A. F. Molisch, “Ultrawideband propagatiton channels-theory, measurement, and modeling,” IEEE Transactions on Vehicular Technology, vol. 54, no. 5, pp. 1528–1545, 2005.
[19] M. Z. Win, F. Ramirez-Mireles, R. A. Scholtz, and M. A. Barnes, “Ultra-wide bandwidth (UWB) signal propagation for outdoor wireless communications,” in Proceedings of the 47th IEEE Vehicular Technology Conference (VTC ’97), vol. 1, pp.251–255, Phoenix, Ariz, USA, May 1997.
[20] M. Moharrum and A. Al-Daraiseh, "Toward Secure Vehicular Ad-hoc Networks: A Survey," IETE Technical Review (Medknow Publications & Media Pvt. Ltd.), vol. 29, no. 1, pp. 80-89, Jan/Feb 2012.
[21] S. Zeadally, R. Hunt, Y.-S. Chen, A. Irwin and A. Hassan, "Vehicular ad hoc networks (VANETS): status, results, and challenges," Telecommunication Systems, vol. 50, no. 4, pp. 217-241, August 2012.
[22] G. Caizzone, P. Giacomazzi, L. Musumeci and G. Verticale, "A power control algorithm with high channel availability for vehicular ad hoc networks," in IEEE International Conference on Communications, ICC 2005, May 2005.
[23] Intelligent Transportation Systems (ITS); Performance Evaluation of Self-Organizing TDMA as Medium Access Control Method Applied to ITS; AccessLayer Part, Tech. Rep. DTR/ITS-0040021, European Telecommunications Stan-dards Institute, 2011-12.

Forecasting The Sea Level Rise Using ARIMA Model

Methini M[1], Mohana Priya T.R.[2], Sruthika M[3], Suryadharshini S[4]

[1-4]Electronics and Communication Engineering, Sri Sai ram Engineering College, Chennai, India

[1]methini.ece@sairam.edu.in, [2–4]e8ec181@sairamrap.edu.in

***Abstract*—In recent years, global warming and rising sea levels are of more concern. Predicting the increased sea level becomes a complex task for the scientific community. Existing local and global changes in sea level are monitored by tidal stations and satellite radar altimeters. However, these tools are not designed to forecast a potential sea-level rise scenario. The proposed project tends to provide a solution to this issue. The idea is to gather information on the sea-level rise which is the measure of height from an existing mean sea level value in a specific location. The descriptive analysis is done on the collected input to identify the flawless model to predict future values. The proposed system uses a machine learning model ARIMA (Auto-regressive Integrated Moving Average). The gathered information can be used as a predictor of future values. This approach is more precise than the altimeter forecast.**

***Keywords*—sea-level rise, machine learning, ARIMA model.**

I. INTRODUCTION

In recent years persistent increase in earth's temperature has led to greater than average summer melting. The sea-level rise is seen to be higher in inland forests and coastal wetlands that play a major role in the ecosystem. It also helps in understanding more about sea-level rise [1]. The sea-level rise may lead to floods and there are methods to find about early floods and it gives prior information to the respected department and people [2]. The rising of sea level is one of the climatic changes and average sea levels have increased by over 8inches and every year it rises by 13 inches [3]. Since the start of the 20th century, the Global Mean Sea Level (GMSL) has risen by about 16-21cm, with more than 7 cm of this occurring since 1993. Sea level rise can be due to a variety of reasons like sinking land, a slowing gulf stream, and ice melting.

The sea-level rise may have a great impact on human life as almost half of the population resides near the coastal region.

Some other effects include rising the frequency and intensity of flooding due to shoreline increases.

The socio-economic consequences of Sea Level Rise include water and soil quality degradation, loss of lives, and properties, damage to infrastructures, and depletion of agricultural resources.

The proposed project uses machine learning algorithms to develop models and predicts sea level accuracy.

Empirical values are collected and sorted and they are plotted to get a high level of accuracy. These methods have higher accuracy than the tide gauges. Machine learning was used to just plot the graph of mean sea level to study the variations [4].

Machine learning can speed up the data process. It is a promising tool to model and anticipate sea-level changes in the coming years, which is crucial for near-term decision-making and strategic planning about coastal protection measures.

II. SPECIFICATIONS

The specifications of the proposed system are described below.

A. Software Specification

GOOGLE COLABARATORY is also known as GOOGLE COLAB is an online simulator developed by Google and was released in the year 2017. Fig 1 shows the sample of how the google colab works. It created a great impact on machine learning, artificial intelligence, and data science. It uses python for the coding. The coding is done to train the model and make it suitable according to our needs. The colab is designed in a way that it has a great memory which is said to be 12GB of RAM so that a lot of data can be stored and it is known that machine learning works great when the input data is huge.

Also, the colab has a maximum running limit of up to 12 hours. The google colab pro gives extra features like 25GB of RAM and 24 hours of run time which becomes an added advantage for those who use machine learning, deep learning, A, I, and data science. It accepts the input in form of both images and CSV. The google colab can be easily integrated with PyTorch, Tensor Flow, and Open CV.

Google Colab saves the trouble of having to set up a local environment and maintaining all the dependencies, along with free access to faster GPUs and TPUs, so it reduces the risk of hanging due to workload.

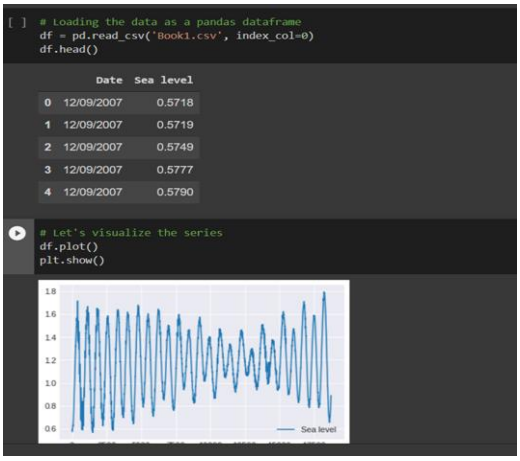

Fig 1 Plot Between Mean Sea Level Value And Time In Google Colab

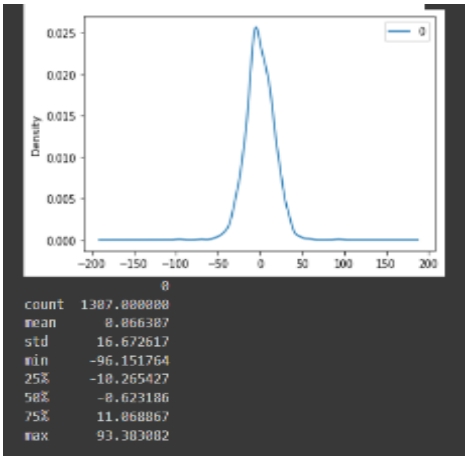

Fig 2 Descriptive Analysis Plot

B. Design Specification

This section describes the model and algorithms used for this project.

ARIMA MODEL known as Auto-Regressive Integrated Moving Average is used for time series analysis which can predict the future values from the given input values. Initially, the input data is given and a graph is plotted as shown in Fig 3 to find whether the graph is stationary or not.

If it is stationary the parameters are found else the input is stationary using the differencing method.

Differencing method is done by finding the difference between the previous input and the present input which reduces the fluctuations and makes it stationary. It has three parameters (p,d,q) which are used to predict the values.

- p- It is the Auto Regression part where it gets the input data given by the user.
- d- It is the degree of difference used to make the input stationery if it's not stationary.
- q- It is the moving average part. It defines the window size to find the moving average.

These parameters are found by running the ACF Autocorrelation function, and the PACF Partial Autocorrelation function. The model is trained by using some data which is split using the sorting method and the rest of the data is used to test the model at the final step, it shows the future values that are needed.

III. Execution And Operation

The mean sea level value is observed using two methods tide gauge and satellite altimeter. The measurement of satellite altimeter gives higher accuracy than the tide gauge method [5].

The other methods by which the sea level rises were linear models, regression models, and neural networks, and they all show similar outcomes [6]. Thus, ARIMA MODEL is used to forecast future values.

The descriptive statistics are done on the collected input as shown in Fig 2 to find the mean, mode, median, covariance, skewness, kurtosis, range-maximum, and minimum to understand the data and apply the suitable algorithm.

In this project according to the descriptive data ARIMA MODEL is chosen to predict the future values.

The first part is to initialize the google colab and import all the necessary libraries such as tensor flow, pandas, matplotlib, NumPy, etc.

These functions are developed to work with traditional machine learning, for large computations, to do all the descriptive statistic functions.

The next part is to load the collected mean sea level data as a .csv file and derive a graph to view whether the inputs are stationary or not.

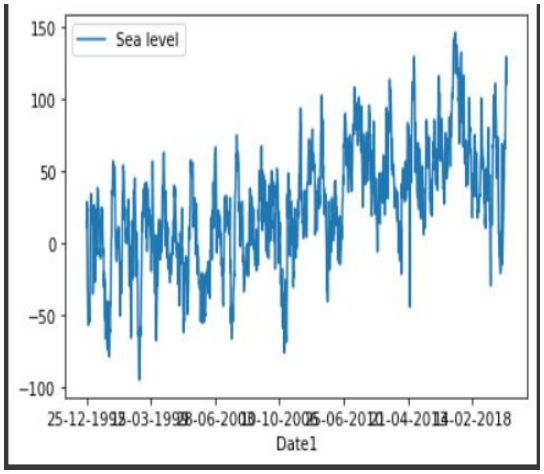

Fig 3 Plot between the input data and date to find stationarity

From the graph shown in fig 3, the input given seems to be not stationary which makes the prediction hard.

Thus, the next part is to make it stationary and the flow is shown in the flowchart in fig 4

The 96% of the dataset is split into the training part the and remaining 4% of the dataset is the set as the validation part.

If stationary, then the p, d, and q values are found using the autocorrelation method. Else, there will be a differencing part where the previous input value and the present values are subtracted to form it stationary.

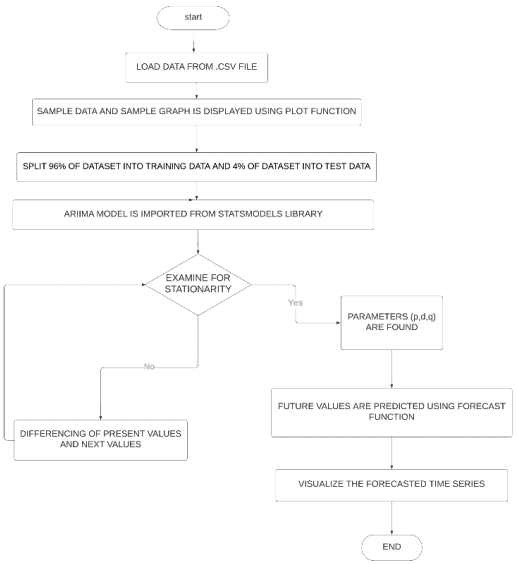

Fig 4 Flowchart

After the parameters are found the final prediction is done by the in-built function present in the stats model library. The prediction can be done to any extent in this project we have predicted monthly month data.

The final predicted output is shown in figure 5

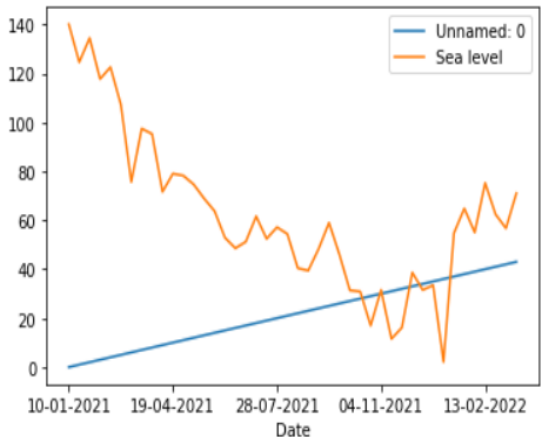

Fig 5 Final predicted outcome

IV. Outcomes And Discussion

The proposed system is used to predict the future values of sea-level rise using the mean sea level data and the time series analysis that is done by implementing the machine learning models.

In this paper, the data till 2020 is used, and predicted the next 1 year of data using the ARIMA MODEL.

The arrived accuracy was about 80%. The dataset can be changed easily hence the prediction can be done without any strains.

This will be useful to know how much the sea level may rise and can be used to take precautions if the level is known to be dangerous.

Thus, it is concluded that this method is easy and even layman can understand what is been done to predict the future values.

Reference

[1] Charles S Hopkinson, Ariel E lugo, Merryl Alber, and Skip J Van bloom, “Forecasting the effects of sea-level rise and windstorms on coastal and inland ecosystems” Research gate-Article Frontiers in Ecology and the Environment 6(5), June 2018.

[2] S.karthick, Maruthi Shankar, ManjPatnaik, and S.karthikeyan Tegil J John, “IoT Based smart flood forecasting and early warning system”, 5th International Conference on Computing Methodologies and Communication (ICCMC), 2021.

[3] D. Deva Hema, Anirban Pal, Vineet Loyer, and

[4] Rajeev Gaurav, “Global Warming Prediction in India using Machine Learning”, International Journal of Engineering and Advanced Technology (IJEAT) ISSN: 2249-8958 (Online), Volume-9 Issue-1, October 2019.

[5] Maritsa Faridatunnisa, and Leni Sophia Healing, “ Study of Sea Level Rise Using Tide Gauge Data Year 1996 to 2015 at Semarang and Parigi Stations”, 4th International Conference on Science and Technology (ICST),2018.

[6] Vivien Lai, Ali Najah Ahmed M.A. Malek, Haitham Abdul Mohsin Afan, Rusul Khaleel Ibrahim, Ahmed El-Shafie, and Amr El-Shafie, “Modeling the Nonlinearity of Sea Level Oscillations in the Malaysian Coastal Areas Using Machine Learning Algorithms” Research gate-article (Sustainability 11 (17):4643,2020.

[7] Adam àyszkowicz, and Anna Bernatowicz, “Geocentric Changes of the Mean Sea Level of the Baltic Sea from Altimeter and Tide Gauge Data”, Baltic Geodetic Congress (BGC Geomatics), 2018.

[8] Magnus Hieronymus, Jenny Hieronymus, and Fredrik Hieronymous, “On the Application of Machine Learning Techniques to Regression Problems in Sea Level Studies”, Journal of Atmospheric and Oceanic Technology 36(9),2019.

[9] Md.Riftabin Kabir, Nazmus sakib borso Sifat momen, and Sazzad Hossain, “Forecasting sea level rise using machine learning techniques” Research gate-Article, December 2019.

[10] Rifat Tur, Erkin Tas, Ali Torabi Haghighi, and Ali Danandeh Mehr, “Sea Level Prediction Using Machine Learning”, Research gate-Article Water 13(24):3566, December 2021.

A New Paradigm of COVID ChamberUsing Raspberry PI

Mahalakshmi[1], G. Sasikala[2], Nookala Sai Venkata Raghavan[3], Shaik Nasir[4], Reddy Veerendranath[5]

[1-5]Department of ECE. Vel Tech University,Chennai, India

[1]maha.88.ece@gmail.com, [2]gsasikala@veltech.edu.in, [3]raghavannookala@gmail.com, [4]nasirshaik0620@gmail.com, [5]rvnreddy66@gmail.com

***Abstract*—In 2019, the world was affected by the deadly virus called corona. This virus can transmit from person to person via sneezing, coughing as the infection can go through the droplets. Since its outbreak, to ensure safety to everyone, it is necessaryto wear the face mask to protect ourselves from the covid19. As the surfaces are also contaminated by the virus it is not safe for us to come in contact with the contaminated surfaces. So, hand sanitization should be done frequently in order to protect from the corona. The main symptom for the covid19 is high bodytemperature. So, in many public plac-es like hospitals, airports, railway stations hand sanitization temperature checking and face mask detection is done manually which causes risk for the person who is doing it. The body temperature, sanitization and face mask de-tection should be automated using raspberry pi. If the body temperature is normal and face mask is detected then the servo motor rotates which will open the doors. Then the programmed sanitizer disinfects the whole body of the individual in the type of mist. If any condition is not satisfied then the doors are remained closed and the automated systemwill inform the authori-ties as the person should be tested for the virus. By this way, the human presence can be reduced to screen individuals who are affected with the virus or not whichis not safe.**

***Keywords*—Mask detection, Raspberry pi, Computer vision, Automatic hand sanitizing, Contactless temperature sensing , Buzzer.**

I. INTRODUCTION

Covid19 has changed our lives a lot. Everyone is trying to isolate in order to protect themselves from the virus. Most people are avoiding public transport, ritual gatherings, travelling etc. Majority of the corona victims have no symptoms like fever, breathing problem, cough, and severe cold due to their immunity. The results of the rapid antigentest are also not accurate which is a serious problem. There are so many frontline workers who are risking their livesworking day and night in order to control the covid19. Under the WHO guidelines wearing face mask, frequent hand sanitizing, maintain social distancing are the key one. In the public areas checking of body temperature, hand sanitization, mask checking is done manually by the workers which arerisk for their lives. So, all these processes should be done without the need of human. The temperature checking can be achieved by using MLX90614 non-contact temperature sensor. By utilizing pi cam face cover is distinguished. The disinfection is finished utilizing the programmed fog sprayer. All these hardware components are connected to the raspberry pi which is brain of the system. Mainly this system is used at the entrances of the public places where there is too much crowd. The people should enter one by one at a time wherethe system first detects the presence of the person.

II. LITERATURE SURVEY

Nagrath, Preeti[1] proposed a framework that utilizes profound learning, Tensor Flow, Keras, and OpenCV for facial covering and Single Shot Multibox Detector as a face indicator and the MobilenetV2 structure as a lightweight separator and can be utilized even on implanted gadgets like the NVIDIA Jetson Nano, Raspberry pi.

Kailasam Selvaraj[2] proposed a framework in which man-made reasoning is uti-lized to perceive the surface of the appearances and changed shapes. This framework likewiserecognizes the appearances from the video sources. The identified face is checked inside the data set. Assuming that the face is on the site the framework gives admittance to the room or is denied. The program is made utilizing an openCV discussion. The benefit of this framework is that we have some control over our office and home from anyplace. Entirely solid, quick viable and secure also. Really awful the framework some of the time neglects to identify faces because of specific issues.

Akash Thakre[3] proposed a framework in which it will check temperature, facial covering and in the event that the internal heat level is typical and individual wear-ing the facial covering, he will be allowed in and get cleaned by the sterilization machine to guarantee the Coronavirus wellbeing. Assuming that anybody recognized without facial covering or the temperature surpasses as far as possible the system cautions the covid19 wellbeing focus. The raspberry pi camera module identifies the people wearing veil or not utilizing the OpenCV and tensorflow. The fundamental expectation here is to stop the spreading of Coronavirus - 19 with this framework.

NaveenKumar[4] proposed a Computer Vision mechanization program that spot-lights on constant facial acknowledgment of individuals to find both facial covering and internal heat level openly puts. The incorporated Pi camera is utilized to distinguish facial coverings and the MLX90614 sensor isutilized to screen internal heat level as indicated by WHO guidelines. Here profound learning has

been utilized to prepare the framework with a lot of pictures with and without facial coverings in the data set.

Nicholas Wei-Jie Goh[5] proposed an aurdino based computerized IR thermometer with distance change utilizing the MLX90614 IR thermometer and the HC-SR04 ultrasonic sensors. IR thermometers under the most recent innovation estimations are impacted by an assortment of variables, for example, perspiring in the sweat-soaked region and the deliberate region of the temple. The supportive of presented framework defeats those mistakes and can give precise temperature readings. Additionally with the consequences of temperature tests taken without perspiring on the temple, the temperature contrast among wet and dry brow was from 3.06 ± 0.00 to 2.85 ± 0.02 ° C.

Sivasankara Rao[6] proposed a framework with facial covering recognition with sound reaction and contactless disinfection and temperature estimation. The pro-found learning calculation utilizing Tensorflow, Keras libraries and MobileNetV2 that intends to recognize an individual wearing a facial covering in a picture. Con-tactless Sanitization is performed after temperature estimation. The framework then gives sound result regardless of whether the individual is wearing a facial covering as well as an individual's temperature perusing.

Rosepreet Kaur Bhogala[7] proposed a framework that will permit individuals pro-vided that they have ordinary body temperature and face mask. The program utilizes OpenCV, Convolutional Neural Networks (CNN), Keras, TensorFlow and Mo-bileNetV2 engineering for face location. Just the significant piece of the picture is recognized to limit the components of the picture to diminish the intricacy. The info is taken from the webcam and resizes it to 224*224. In this framework Arduino UNO, the MLX90614 called non-contact temperature sensor and LCD show are uti-lized.

R. Syafeeza[8] proposed effective entryway opening framework by utilizing face acknowledgment. To utilize face acknowledgment proficiently they utilized raspber-ry pi with profound learning joined with Internet of Things(IoT). Here profound learning is the primary key to coordinate the face which has been put away in data set with the caught face by the pi camera. The creator men-tioned that by utilizing profound learning the machine constantly develop by catching the appearances eve-ryday and don't bother dreading of face maturing in light of the fact that it will keep each little change and store in information base. In this manner, here is the motiva-tion behind profound learning is to empower the machine to accurately characterize pictures. The justification behind utilizing raspberry pi facial acknowledgment is that, it has a high administration limit, minimal expense, and its volume is changed in an assortment of altering techniques.

Z Wang[9] proposed three kinds of covered facial informational indexes and of that Real-world Masked Face Recognition Dataset (RMFRD) is the biggest data set. The different face veiled acknowledgment framework accomplishes 95% exactness. It just sees if an individual is wearing a facial covering or not. To forestall the insur-ance of contacts in broad daylight places they have fostered this model.

Militante[10] proposed framework utilizes inside and out perusing strategies to recognize facial acknowledgment and decide if an individual is wearing a facial cover-ing or not. The gathered information contains 25,000 pictures utilizing 224x224 pixels remedy and accomplished a precision of 96% with the presentation of a pre-pared model. The framework upgrades the consideration of the Raspberry Pi-constant facial gleam and catches a facial picture when the individual istracked down not wearing a cover.

III. Proposed Model

The object detection, sterilization, and the temperature checking are done physically by the front-end laborers. For location of internal heat level, temperature weapons are utilized. The issue with these weapons is, they won't give precise understanding when measured from the distance past its cutoff points. Additionally the specialist who checks the temperature ought to be adequately close to the individual whose temperature is being checked which abuses the social distance. To shield ourselves from the Coronavirus following the precautions is especially significant. People are more inclined to manual mistakes contrasted with PCs. The sterilization is done exclusively for the hands. Yet, the Covid can get by on the surfaces of the garments, packs, etc which isn't protected. To guarantee wellbeing the absolute body disinfec-tion is finished by utilizing the fog sprayers. clamor.

IV. Methodology

The individual ought to enter the Coronavirus chamber which is introduced at the passages of the public spots. Just a single individual ought to enter at a time. At first, the doors are shut. The individual identification is done on first stage. In the event that the individual is available close the chamber, the individual is identified by the IR sensor. IR sensor conveys message to the grate berry pi board which affirms the individual close by. Then the chip provides orders to the pi cam. The motivation behind the pi cam is to distinguish the facemask of the individual remainingin front it. In the event that an individual wears a facial covering appropriately, one is al-lowed to really look at the second stage temperature. The internal heat level check-ing is finished utilizing MLX90614 non-contact temperature sensor. This sensor is additionally between confronted with the pi board. In the event that the internal heat level is ordinary thatis 38°C or beneath, the individual will get sterilization by the fog sprayer. In the event that an individual doesn't wear aveil or his internal heat level is better than average, then an individual isn't permitted to enter that region. The ringer will deliver the sound which thus cautions the specialists. On the off chance that the over two measures are fulfilled, the doors open. The door activity is constrained by the servo engines which are connected to the pi board. The internal heat level, facial covering identification, states of the entryway is shown through the LCD.

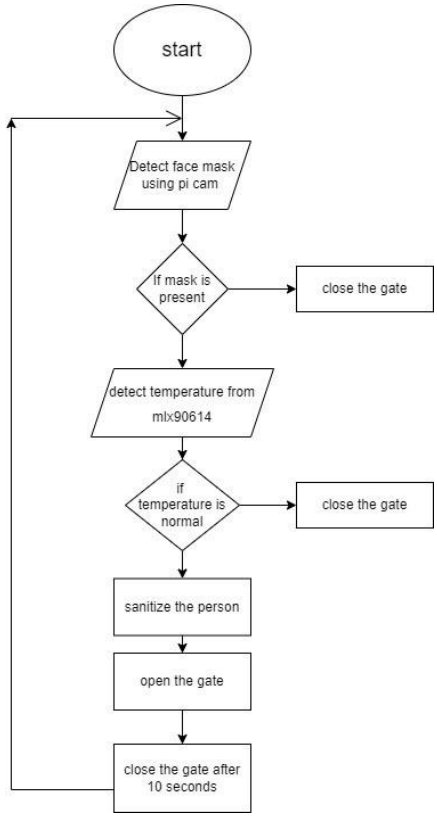

Fig. 1. **Flow chart**

V. Block Diagram

The beneath block diagram Fig. 2 shows the rundown of interacting gadgets with raspberry pi board. The raspberry pi board takes the contributions from the web camera and temperature sensor (MLX90614). A web camera is utilizedto identify an individu-al's facial covering and a temperature sensor is utilized to distinguish an individual's temperature. The result interfaces for the raspberry pi board are servo engine, LCD show, ringer and the fog shower. The servo engine is utilized to lift the entryway all over, so the individual can head inside. The LCD show and signal is utilized for the showcase and gives blare sound as a caution. The fog shower is utilized for disin-fecting the people who are entering in to the chamber.

The power supply for the raspberry pi is 5 to 9 volts dc,2 amp. The power supply for residual parts is taken from raspberry pi board which is of 3.3V - 5V. In the event that engine driver is utilized rather than servo engine, outside power supply ought to be given to engine relying on its ability.

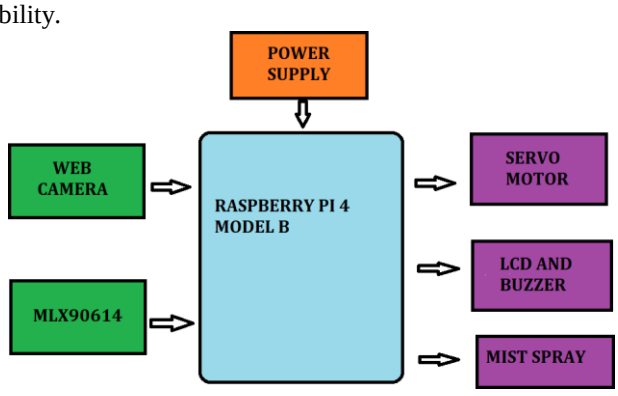

Fig. 2. Block Diagram

VI. Procedure

- Open proteus simulation software and select new project.
- Select the board as raspberry pi model b or b+ in the creating project window.
- Pick the required components from the library like servo motor or motor driv-er, LCD display, buzzer, compim, mcp3208, mlx90614 or LM35 temperature sen-sor.
- Connect the components to the raspberry pi board according to the GPIO pin numbers assigned to the components in the programming code.
- Download the Virtual Serial Port Emulator (VSPE) and setup new connection.
- Enable the connection in the VSPE and make sure the status should be started.
- Compile the face mask detection code in the Python IDE using OpenCV and Tensor flow.
- Now go to the source code in the proteus and dump the code for the connec-tions in the proteus.
- Run the simulation in the proteus.

VII. Working

- Run the simulation in proteus, connect the VSPE and runthe face mask detec-tion code in the python IDE.
- Firstly, the raspberry pi board detects the face of theperson through webcam connected to VSPE.
- Then it will detect when the person is wearing mask or not.
- If face mask is not detected, the pi board will display "please wear mask" with beep sound.
- If mask is detected and the temperature of the person is too high. Then the gate remains closed and the pi board will display "High temperature" with beep sound.
- If mask is detected and temperature is normal, then gate opens and the mist module start working.
- When the person gets inside the chamber then the person gets sanitized completely.

VIII. Simulation Result

A. Proteus Raspberry Pi Interfacing Pi Camera

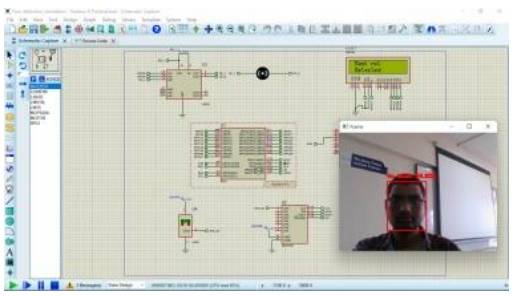

Fig. 3. Detection of non wearing a face mask

In Fig.3 the person is not wearing the mask. So it is showingmask not detected and gate remains closed.

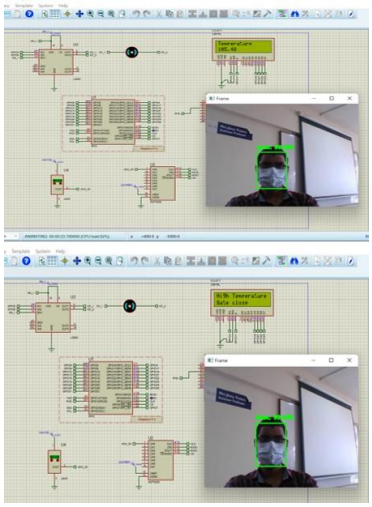

Fig. 4. Detection of a face mask and high temperature

In Fig.4 the person is wearing the mask but the temperature is so high. So it is showing mask detected and temperature is high so, gate remains closed.

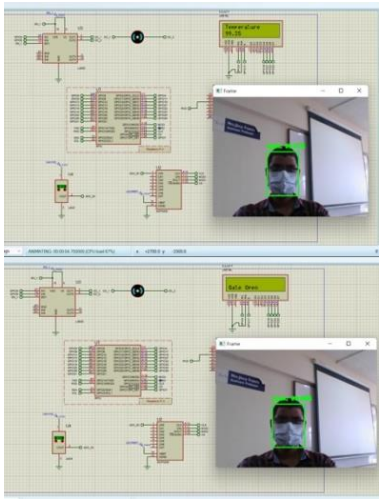

Fig. 5. Detection of normal temperature and face mask

In Fig.5 the person is wearing mask and the temperature isnot normal. So it is showing mask detected and temperatureis normal so, gate opens.

IX. CONCULSION

By utilizing this framework Covid conventions can be kept up with and observed precisely. Transmission of the infection starting with one individual then onto the next can be decreased. This mechanized framework can lessen the human endeavors and manual mistakes. It is additionally utilized for studying reason to recognize the level of individuals affected with infection. Thus, that the public authority can take proper measure inside no time. It is extremely smaller and modest. It very well may be utilized openly places, for example, theaters, stores, medical clinics, train stations, and so on.

REFERENCES

[1] Nagrath, Preeti, et al. ”SSDMNV2: A real time DNN-based face mask detec-tion system using single shot multibox detector and MobileNetV2.” Sustaina-ble cities and society 66 (2021): 102692.

[2] Selvaraj, Kailasam, Saravanan Alagarsamy, and M. Dhilipkumar. ”Raspberry Pi based Automatic Door Control System.” 2021 3rd International Conference on Signal Processing and Communication (ICPSC). IEEE, 2021.

[3] Thakre, Akash, et al. ”Face Mask Detection and Sanitizer Despenser with Tem-perature Detection.” (2021).

[4] Naveenkumar, K., et al. ”Automatic Covid-19 Face Mask And Body Tempera-ture Detection With.” vol 9: 255-259(2021).

[5]]Goh, Nicholas Wei-Jie, et al. ”Design and Development of a Low Cost, Non-Contact Infrared Thermometer with Range Compensation.” Sensors 21.11 (2021): 3817.

[6] Rao, M. Sivasankara, et al. ”Real Time Face Mask Detection and Thermal Screening with Audio Response for COVID-19.” REVISTA GEINTEC-GESTAO INOVACAO E TECNOLOGIAS 11.4 (2021): 2703-2714.

[7] Bhogal, Rosepreet Kaur, et al. ”Corona virus disinfectant tunnel using face mask detection and temperature monitoring.” 2021 5th International Conference on Intelligent Computing and Control Systems (ICICCS). IEEE, 2021.

[8] Radzi, Syafeeza Ahmad, et al. ”IoT based facial recognition door access control home security system using raspberry pi.” International Journal of Power Elec-tronics and Drive Systems 11.1 (2020): 417.

[9] Wang, Zhongyuan, et al. ”Masked face recognition dataset and application.” arXiv preprint arXiv:2003.09093 (2020).

[10] Sammy V., and Nanette V. Dionisio. ”Real-time facemask recognition with alarm system using deep learning.” 2020 11th IEEE Control and System Grad-uate Research Colloquium (ICSGRC). IEEE, 2020.

[11] Meenpal, Toshanlal, Ashutosh Balakrishnan, and Amit Verma. ”Facial mask detection using semantic segmentation.” 2019 4th International Conference on Computing, Communications and Security (ICCCS). IEEE, 2019.

Depiction of User Clustering algorithm in MIMO - NOMA for 5G and Beyond

C. Elayaraja[1], C. Amali[2]

[1]Anna University & AP/Dhaanish Ahmed College of Engineering

[2]Department ECE, SRM Valliammai Engineering College (autonomous), Anna University, Chennai

[1]elayaraja.c@dhaanishcollege.in, [2]amalic.ece@valliammai.co.in

Abstract—As 5G and beyond, targets the higher spectral utilization, high data rate, robustness, minimum latency, good reliability, massive connectivity, all could achievable in the best rated by combining Multiple-Input Multiple Output (MIMO) and Non Orthogonal Multiple Access (NOMA). The proposed user-clustering algorithm of MIMO-NOMA system suggests the parameters of sum rate, user capacity, ergodic sum capacity, inter cell interference, Signal to Interference Noise Ratio (SINR) and Symbol Error Rate (SER), which are paramount to conventional MIMO-OMA. Precisely, the MIMO-NOMA receiver comprise of Maximum Ratio Combiner (MRC), Zero Forcing (ZF) that are convert the combined signal into disseminated low-complexity calculations. Also, the techniques of Successive Interference Cancellation (SIC), Inter Cluster Interference and Intra Cluster Interference at the receiver of MIMO-NOMA, outfits for 5G beyond. The theoretical and simulation results are compared to ensure the performances that suits the 5G beyond network requirements.

Key words—SINR, SER, low complexity, SIC, interference

I. INTRODUCTION

History of the wireless communication evolution is as shown in Fig.1. As if the generation grown in terms of data rates requirements, the corresponding techniques also suitably fixed till. The expectation of the present technology is to have higher data rates, lower latency, accommodate higher capacity [1], power and spectrum efficiency. These are the motivated factors to initiate the researchers to achieve higher end technologies growth exponentially. Based on the concentration of spectrum utilization with performance achievements has been a greater motivation to adapt the inevitable wireless systems techniques similar as MIMO, massive MIMO, mm-Wave MIMO, NOMA, Device to Device FBMC and Cooperative communication, full duplex, Light waves cognitive radio as 5th generation and beyond communication. Motivation of this paper to achieve better performance of MIMO-NOMA than the conventional methodologies are opted until 4G communication. A system, which is designed in a manner that multiple users are arranged in non-overlapping time slots or frequency bands by the transmission. This system is called Orthogonal Multiple Access technique (OMA). The Conventional OMA techniques covers TDMA, FDMA, CDMA and OFDMA. These techniques have principle that serves a single user in each orthogonal resource block. Hence, 'n' - no. of users (n=1,2,…..N) are scheduled for transmission over a time period 'T', where the period T has less than the coherence time of the channel and each user transmits only T/N times of the total transmission period. The entire transmit power Ps depicted to that particular user. MIMO-NOMA schedules transmission by multiple users above the entire transmission period and bandwidth on the same resources. In general, these multiple users been categorized in the Power domain [2] and Code domain under NOMA. Since the total transmit power Ps must be shared between all 'n' users and a portion of $n \in (0,1)$ of the transmit power which is allocated to user n, and Ps. Hence, MIMO-NOMA has inter cell interference, Intra Cluster Interference, Inter cluster interference, Successive Interference Cancellation (SIC) are active at the receiver to remove the interferences of the signal from the users with lower channel gains. MIMO-NOMA provides prime guaranty that each user to achieve a minimum capacity, which is higher than MIMO-OMA. Non Orthogonal Multiple access (NOMA) has been retaining attention recently owing to its superior spectral efficiency. Specifically, at the transmitter of MIMO-NOMA adopts Superposition Coding (SC) and at the receiver, it has a technique of Successive Interference Cancellation (SIC).

This paper concept flows as follows: Section II depicts the related works on MIMO NOMA concepts. Section III elaborates the system model of MIMO-NOMA both uplink [6] and downlink using user clustering algorithm with successive interference cancellation (SIC) receiver, **Maximum Ratio Combiner (MRC), Zero Forcing (ZF)** power allocation methods. In Section IV explains the results of MIMO-power domain NOMA and the parametric simulations analysed on channel gain and SINR, SER [5] finally Section-V concludes the MIMO-NOMA fitness.

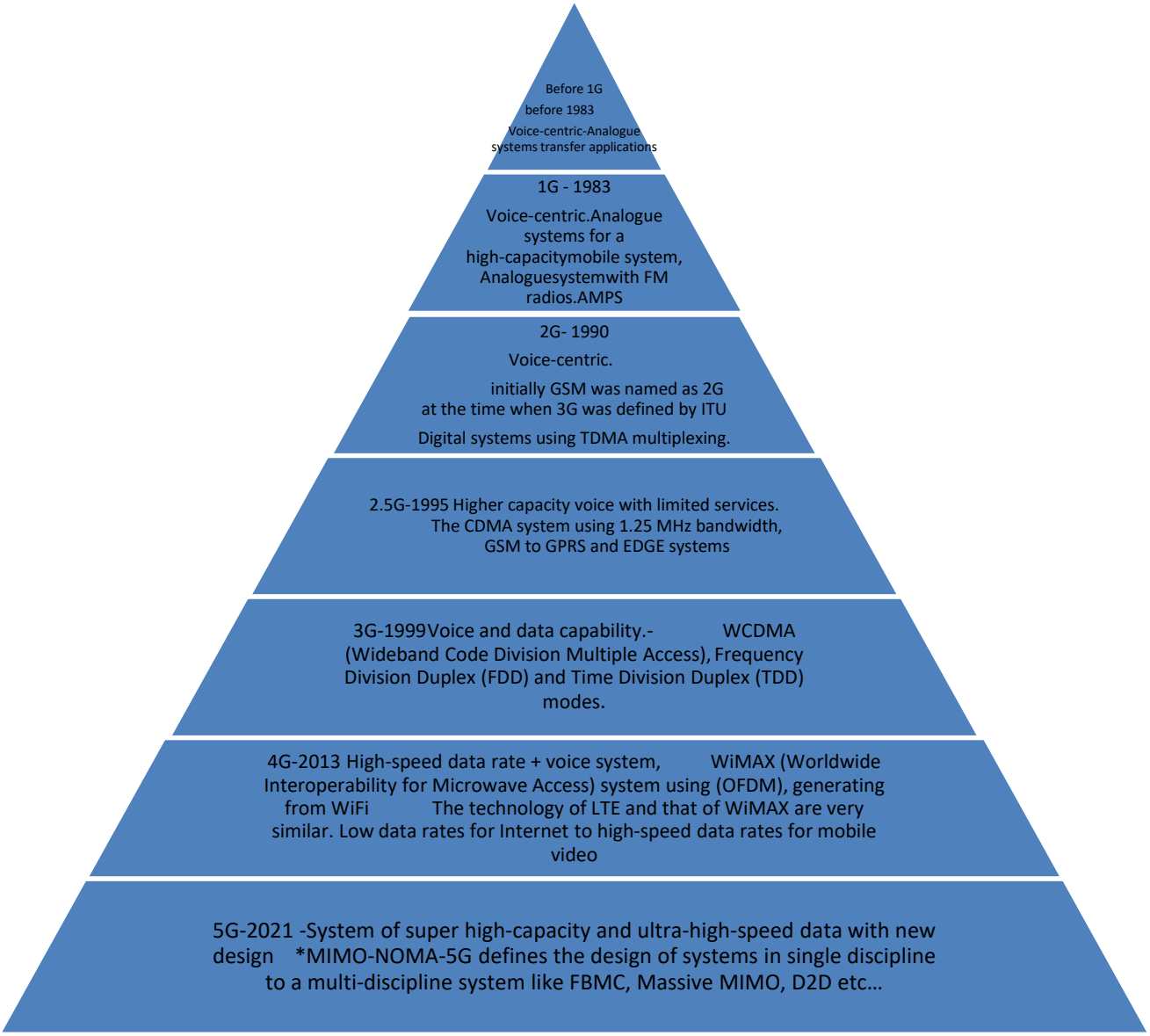

* requisite technique

Fig.1. Progression of wireless communication networks - before 1G, 1G, 2G, 3G, 4G and 5G and beyond.

II. Related works on MIMO-NOMA:

Superposition coding (SC) and Successive Interference Cancellation (SIC) are the adaptive techniques in MIMO-NOMA transmitters and receivers. Focus on the Channel capacity improvement [1]-[4], power profile [2]; throughput, fairness have been compared between the MIMO-NOMA and MIMO-OMA[1]. By the way of allocating power factor coefficients [2][3], that allow all of the participating users to achieve capacity at least as good as OMA. Using Superposition Coding for future wireless cellular networks has indicated to increase single user rates by comparing the CDMA. The proficient approach to communicate the information with more antennas [3] both UL and DL[11] with in the cell. Asymptotic Performance Analysis[4] to achieve good capacity, with low complexity[16] input-output variance-transfer curves of ZF, LMMSE detector in MIMO-NOMA. The key trends for evolving wireless systems like 5G and beyond focus towards the high data rates and error-rate [5] performance approaching close to theoretical limits. Joint interference alignment and power allocation [7] for NOMA - based multi-user MIMO systems provides an right analysis on the interference cancellation. In view of sum channel capacity and ergodic sum capacity are analysed [8] in mathematical format and demonstrated that the more users are admitted to a cluster, the lower is the achieved sum rate. Having the Channel State Information (CSI) for uplink and downlink of NOMA, performance of has described in [6] [9][10]. Power allocation coefficients has derived by the proposed optimization algorithm for a broadcast MIMO-NOMA [12] system with N base-station antennas serving 2N simultaneous users, where user pairing has based on clustering [12]. By creating a two-stage, beamforming approach with MIMO-NOMA, such that closed-form solutions to the power allocation coefficients derived. Energy efficient sub-channel assignment strategies are proposed to conclude the amount of spectral efficiency and energy efficiency [13][14]. MIMO NOMA system[15] ergodic capacity has calculated when the base-station has only statistical Channel State Information[16][17].

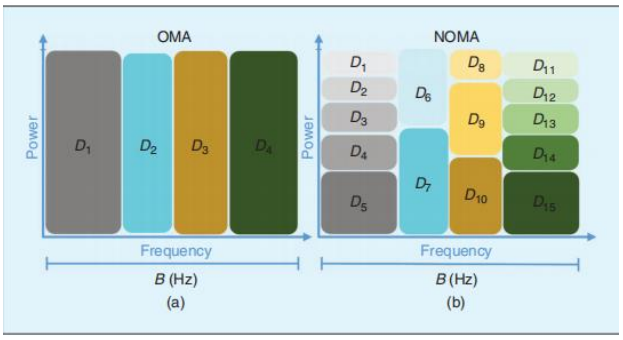

Fig.2. OMA Vs NOMA schemes

The objective of this paper is to develop a system model of MIMO-NOMA by appropriately choose the parameters in such a way that provides good performance of MIMO-power domain NOMA in analytical and simulation methods. In addition, by proposing a new algorithm of user cluster based to minimize the interferences of the beams, cells/cluster and to improve the power level profile and decoded result are very close to the input sequence. On comparing the MIMO-NOMA and MIMO-OMA systems with the above objectives, to identify which combination is closely maps to 5G requirements.

III. SYSTEM MODEL

A. MIMO-Power domain NOMA: Ergodic sum capacity Vs Transmit Power:

The base station consist with N antennas, and K users in a cell. Each user (receiver) have a single antenna. This formation is different from the traditional MIMO-OMA technology. Here, the system has the objective to increase the number of service users, by opting each transmit antenna can support two and above users. In this case, up to N user groups scheduled at the same time. For simplicity, we assume that there are two users in a cluster, and N beams can support 2N users. For two users in the same cluster, the user with large channel gain as strong user, and the user with small channel gain as weak user.

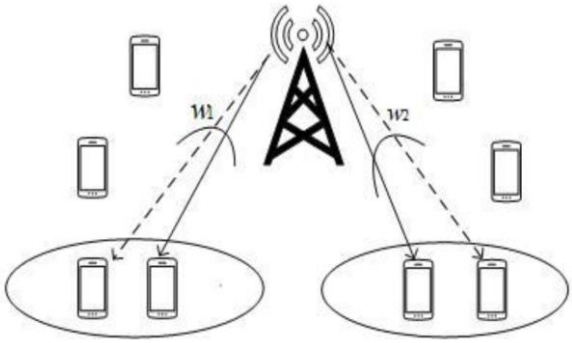

Fig.3. MIMO-NOMA Channel Model.

User Xi input are consider with power allocated to the particular user1 and user2 equation 1 and equation2

$$X_i = \sqrt{\alpha_{i,1} P_i} s_{i,1} + \sqrt{\alpha_{i,2} P_i} s_{i,2} \tag{1}$$

With $E\left\{\left|s_{i,j}\right|^2\right\} = 1 \text{ for } j = 1,2 \,.\, P_i$

Output matrix

$$y_{n,i} = h_{n,i} \sum_{k=1}^{N} w_k x_k + n_{n,i} \qquad i = 1,2 \tag{2}$$

Channel matrix has the coefficients with weighing function is as follows equation 3, equation 4.

$$\mathrm{H} = \left[h_{1,1}^T \ldots h_{N,1}^T \right]^T \tag{3}$$

$$\mathrm{W} = \left[w_1 \ldots w_N \right] = \left(\mathrm{H}\right)^{\dagger} = \left(\mathrm{H}\right)^{*} \left(\left(\mathrm{H}\right)\left(\mathrm{H}\right)^{*} \right)^{-1} \tag{4}$$

The received signal is calculated from the following equation 5.

$$y_{n,2} = h_{n,2} w_n \sqrt{\alpha_{n,2} P_n} s_{n,2} + h_{n,2} w_n \sqrt{\alpha_{n,1} P_n} s_{n,1} + h_{n,2} \sum_{k=1, k \neq n}^{N} w_k x_k + n_{n,2} \tag{5}$$

$$\mathrm{SINR}_{n,k} = \frac{\left|(d_{n,k}\mathbf{h}_{n,k})\mathbf{m}_n\right|^2 p_{n,k}}{\underbrace{\left|(d_{n,k}\mathbf{h}_{n,k})\mathbf{m}_n\right|^2 \sum_{j=1}^{k-1} p_{n,j}}_{\text{Intra-beam interference}} + \underbrace{\sum_{i=1, i \neq n}^{N} \left|(d_{n,k}\mathbf{h}_{n,k})\mathbf{m}_i\right|^2 p_i}_{\text{Inter-beam interference}} + \underbrace{d_{n,k} z_{n,k}}_{\text{Noise}}} \tag{6}$$

The signal to Interference Noise Ratio is calculated with the inter cell and intra cell interferences using equation 6.

TABLE 1: ERGODIC SUM RATE CAPACITY-CALCULATION PARAMETERS

No. of User: 2
No. of cells:19
Frequency 1.8GHz
Propagation model: Okumura model
Total Transmit Power : 40Watts
Cell radius: 1Km
Total Transmit Power (NEU): 0.1
Total Transmit Power (FEU): 0.9
Base station height: 20 meters
Mobile station height : 1.5meters
Bandwidth = 15MHz
Cell radius: 1000 meters

By the way of choosing user1 and user 2 who are placing very near to the base station and far distance from the base station with their power level as shown in Table 1. MIMO-NOMA and MIMO – OMA are analysed with the same parameters, as Okumura model, frequency, transmitter power, cell radius, antenna heights, and bandwidth. The simulation results are shown MIMO-NOMA is superior than the MIMO-OMA in Ergodic Sum Capacity (bits/s/Hz) as in Fig.4.

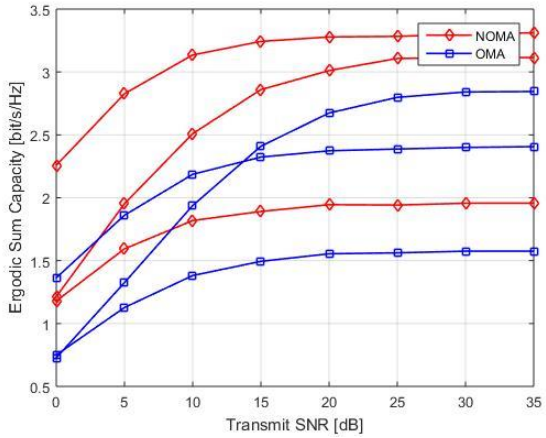

Fig.4. Comparision of MIMO-NOMA Vs MIMO OMA in Ergodic sum capacity

User Capacity (bits/s/Hz) is also is better for NOMA than on OMA shown in fig.5. With respect to the density of the cells available in a particular geometric area, it found sum capacity decreases while the no. of cells increases as in fig.6 and fig.7. Signal to Interference Noise Ratio (SINR) in dBm is drastically reducing if number of cells increasing. OMA also provides equivalent result on this SINR for the near user and far user cases, but relatively NOMA performs superior as in fig.8.

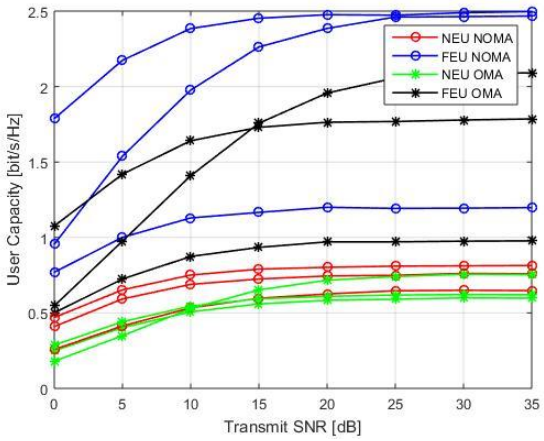

Fig.5. Comparision of MIMO-NOMA Vs MIMO OMA in User capacity

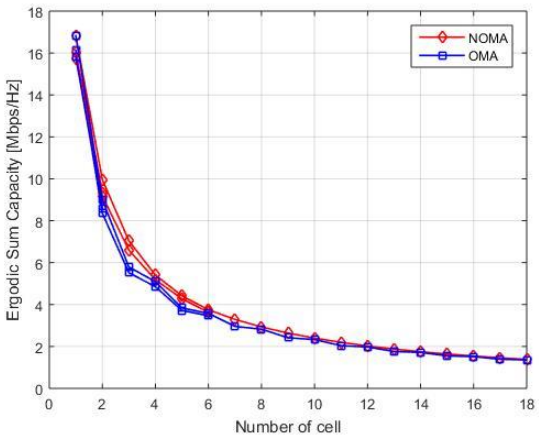

Fig.6. Comparision of MIMO-NOMA Vs MIMO OMA in Ergodic Sum capacity with increased cells

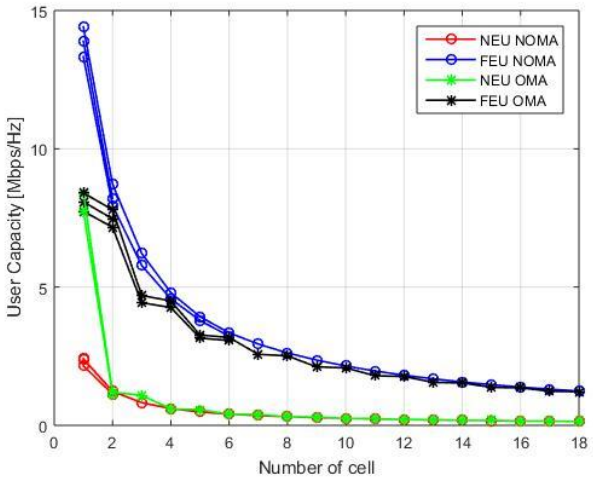

Fig.7. Comparision of MIMO-NOMA Vs MIMO OMA in User capacity Vs Transmit SNR

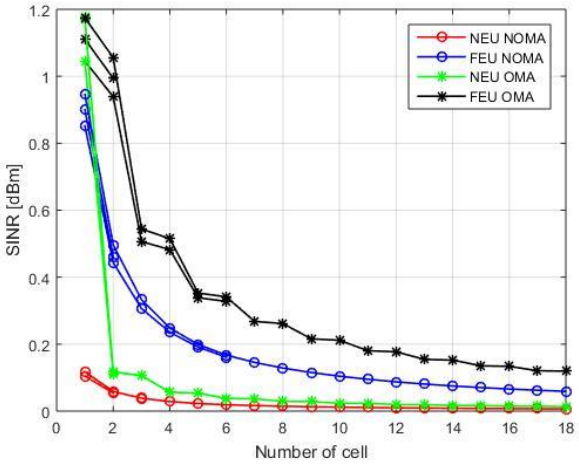

Fig.8. Comparision of MIMO-NOMA Vs MIMO OMA in Signal to Interference Noise Ratio as equation (6).

B. User clustering algorithm for correlated and uncorrelated users are as follows:

The spectral efficiency is the right constraint in the MIMO-NOMA technique, which provides a right solution to the application of wireless cellular system. The total number of UE receive antennas in a cell is much higher than the number of BS transmit antennas. The receiver antennas are formed into a number of clusters and each cluster of MIMO-NOMA is assisted by one MIMO beam, which is perpendicular to the other clusters beams, which means to non over lapping each other. By NOMA based allocation of power to all users in a cluster and further scheduled is formulated as model for the user clustering [12] is shown in fig.9, which has 3 base stations with 3 clusters heads, 6 user equipment.Thick line indicates the MIMO beam, interfered MIMO beam is as dotted line. Distributed area of cluster heads and other users are discriminated with the hexagonal shapes different colours.

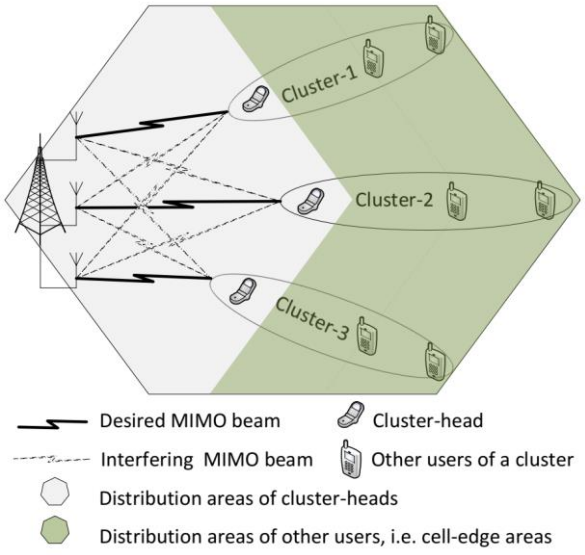

Fig.9.Model for the User clustering.

B-1 User - Cluster algorithm (correlated and non-correlated):

1. Channel gain - ascending order based Sort the users: h1 ≥ h2 ≥ · · · ≥ hi, hi = i-th user.
2. Choose the total no. of clusters and cluster-heads: Number of MIMO-NOMA clusters is N, and the nth higher channel gain user in a cell is the cluster-head of nth MIMO-NOMA cluster.
3. Adding of second users into each cluster: Initiate user sets: A ={ 1; 2; · · · ; Ng}, B ={ N +1; N +2; · · · 2, 2N}; Ri;j = correlation coefficient between hi, and hj.(a) Clustering of users with correlated channel gains: for i = 1 : N ; for j = N + 1 : 2N ; if (Ri,j >Ri,k ≥ ρ, ∀j ∈ B AND Ui is not equal to Uj) include j-th user into i-th cluster, update A ← A − {i}, B ← B − {j}. end ;end ;end
(b) Clustering of users with uncorrelated channel gains: for i = 1 : N ; for j = N + 1 : 2N ; if (i ∈ A AND j ∈ B AND Ui = Uj), include j-th user into i-th cluster, update A ← A − {i}, B ← B − {j}. end ; end ; end
4. Include k-th users into each cluster: Repeat Step 3, while 3 ≤ k ≤ K; set i = 1 : N, j = kN-N+1 : kN, A=(1; 2; ⋯ ; Ng), B= (kN - N + 1; kN - N + 2; · · · ; kN) end; end.
5. Final MIMO-NOMA clusters: while k ≥ 1; C0(t) = [A_0(k); B_0(k)], update: t-> t + 1; k k – 1.

If the Base station antennas are increased then results in high inter-cluster interference, and experiences the number of beams are proportional to increases the interference. Here, new inter-beam and intra-beam cluster are eliminated by zero-forcing beamforming [12] technique MRC decoding for downlink MIMO-NOMA discussed. Inter-cluster interference are minimized, when the more individual channel gain users clusters. A positive solution is provided towards the dynamic power allocation for inter cluster and intra-cluster power in downlink MIMO-NOMA system. This technique mitigate the Inter Cluster Interferences, and provide optimum solution for intra-cluster power allocation. In this way, the system throughput maximized. Multi-cell system increases the inter cluster interferences,

The sum rate of MIMO-NOMA with perfect Channel State Information evaluated for multi users scenario.

B.2.massive MIMO sum rate with perfect CSI:

The capacity of desired rate of user 1 is greater than the Sum rate capacity as in equation 7, 8 then,

$$C_{u1}^{x1} = \log_2(1 + \gamma_{u1}^{x1}) < R_1 \quad (7)$$

$$\log_2(1 + \frac{a_1\rho_s\beta_1}{a_2\rho_s\beta_1+1}) < 2^{R_1} - 1 = R_1 \quad (8)$$

where $\beta_1 < \frac{R_1}{(a_1 - a_2 R_1)\rho_s}$, the probability of outage for the user 1 and user 2 are as in equation 9,10,11 respectively.

$$Pr\left\{\beta_1 < \frac{R_1}{(a_1 - a_2 R_1)\rho_s}\right\} = 1 - \exp(-\frac{R_1}{(a_1 - a_2 R_1)\delta_1^2\rho_s}) \quad (9)$$

Probability of outage for user 2 is decoding fails if either decoding of x_1 or x_2 fails.

$$Pr\{C_{u2}^{x1} < R_1 \; added \; with \; C_{u2}^{x2} < R_2\} \quad (10)$$

$$Pr\left\{\beta_2 < \max\left\{\frac{R_1}{(a_1 - a_2 R_1)\rho_s}, \frac{R_2}{a_2\rho_s}\right\}\right\} = 1 - \exp\left(-\frac{1}{\delta_2^2} max\left\{\frac{R_1}{(a_1 - a_2 R_1)\rho_s}, \frac{R_2}{a_2\rho_s}\right\}\right) \quad (11)$$

By increasing the SNR values, the resultant becomes better in MIMO-NOMA compared to the conventional MIMO-OMA techniques.

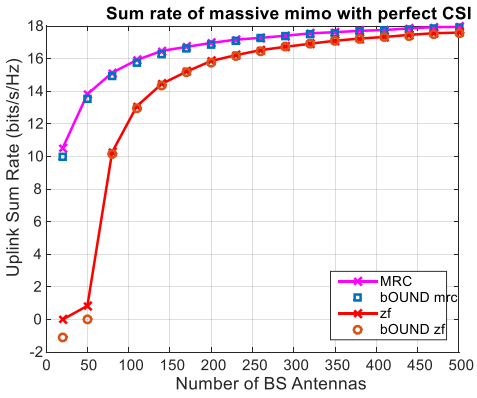

Fig.10. Sum rate (bits/s/Hz) for different MRC, ZF

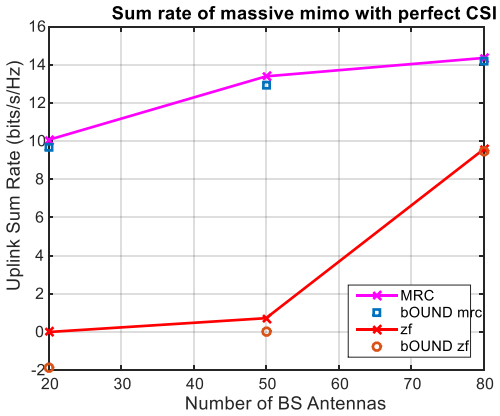

Fig.11. Sum rate (bits/s/Hz) for different MRC, ZF with less no.of Base station antenna.

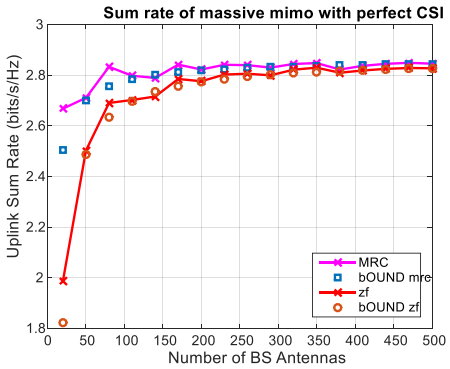

Fig.12. Sum rate (bits/s/Hz) for different MRC, ZF with high no. of Base station antenna.

Uplink sum rate is derived for less no. of base station antennas as in fig.11, and more no. of base station antennas as in fig.10 and fig.12. The simulation results arrived with different coding techniques like Maximum Ratio Combiner, Zero Forcing with the theoretical comparison. If the number of antennas ae increasing from 100, the uplink sum rate is maintaining saturation. SNR value are less while less amount of antennas are placing at the base station. Probability of outage has calculated for the ordered NOMA to uplink and downlink scenarios are discussed further in next section.

IV. Result and Discussion

Uplink MIMO-NOMA employs superposition coding for transmission and Successive Interference Cancelation considered at reception downlink. Where the 50% of channel capacity power loss is high in OMA based MIMO systems, whereas in NOMA performs better in terms of 5G requirements. Through put is high in MIMO NOMA, fitness parameters has improved by using the correlated and uncorrelated 2 user and 3 user cases in cluster-based algorithm. With Rayley fading channel sum capacity is rely on the SNR and channel gain. If SNR increases from 10 dB to 20 dB and further, the sum capacity increased proportionally. This implied that MIMO-NOMA has high closeness towards the 5G techniques as massive connectivity, fairness to the user and maximum sharing of resources. In addition, simulation results implied in MATLAB is to identify the correlation of the sum capacity as if calculated in theoretical output. The results paramount fit as both in simulation and theoretical on the sum capacity, ergodic capacity, SNR, SINR for near user case and far user cases.

V. Conclusion

MIMO-NOMA model allocated with more than one antennas at transmitter as well as receiver. This model can extended to any no. of users on both transmitter and receivers as shown in the simulation results. For simplified version the model has two users for both NOMA and OMA and analysed on the uplink and downlink scenarios. Where, it founds the MIMO-NOMA performs well in all throughput, quality of service, robustness, sum capacity, connectivity, re-configurability, minimum latency than MIMO-OMA. User-Cluster based approach reduces the inter beam and intra beam interference cancellation for both correlated and uncorrelated users. Massive MIMO-NOMA combination performances extremely outfit for the 5BG. Once no. of cells increases then subsequently interference ratio also increases largely, this motivate the researchers to find suitable cancellation techniques through which the leakage of power reduced significantly. In the hardware implementation RF chains performances are degrade the throughput and power profile. Need new implementation techniques to resolve it. High-speed networks like vehicular communication, Internet of Things (IoT) [9] services has been resolved using MIMO-NOMA techniques.

References

[1] Al-Eryani, Y., & Hossain, E. (2019). The D-OMA method for massive multiple access in 6G: Performance, security, and challenges. *IEEE Vehicular Technology Magazine*, *14*(3), 92-99.

[2] Oviedo, J. A., & Sadjadpour, H. R. (2019). Fundamentals of power allocation strategies for downlink multi-user noma with target rates. *IEEE Transactions on Wireless Communications*, *19*(3), 1906-1917.

[3] Senel, K., Cheng, H. V., Björnson, E., & Larsson, E. G. (2019). What role can NOMA play in massive MIMO?. *IEEE Journal of Selected Topics in Signal Processing*, *13*(3), 597-611.

[4] Chi, Y., Liu, L., Song, G., Yuen, C., Guan, Y. L., & Li, Y. (2018). Practical MIMO-NOMA: Low complexity and capacity-approaching solution. *IEEE Transactions on Wireless Communications*, *17*(9), 6251-6264.

[5] Rizk, M., Baghdadi, A., & Jézéquel, M. (2019). Computational complexity reduction of MMSE-IC MIMO turbo detection. *Journal of Circuits, Systems and Computers*, *28*(13), 1950228.

[6] Aldababsa, M., Toka, M., Gökçeli, S., Kurt, G. K., & Kucur, O. (2018). A tutorial on nonorthogonal multiple access for 5G and beyond. *wireless communications and mobile computing*, *2018*.

[7] Rihan, M., Huang, L., & Zhang, P. (2018). Joint interference alignment and power allocation for NOMA-based multi-user MIMO systems. *EURASIP Journal on Wireless Communications and Networking*, *2018*(1), 1-13.

[8] Zeng, M., Yadav, A., Dobre, O. A., Tsiropoulos, G. I., & Poor, H. V. (2017). Capacity comparison between MIMO-NOMA and MIMO-OMA with multiple users in a cluster. *IEEE Journal on Selected Areas in Communications*, *35*(10), 2413-2424.

[9] Liu, Y., Qin, Z., Elkashlan, M., Ding, Z., Nallanathan, A., & Hanzo, L. (2017). Non-orthogonal multiple access for 5G and beyond. *Proceedings of the IEEE*, *105*(12), 2347-2381.

[10] Ding, Z., Lei, X., Karagiannidis, G. K., Schober, R., Yuan, J., & Bhargava, V. K. (2017). A survey on non-orthogonal multiple access for 5G networks: Research challenges and future trends. *IEEE Journal on Selected Areas in Communications*, *35*(10), 2181-2195.

[11] Tabassum, H., Ali, M. S., Hossain, E., Hossain, M., & Kim, D. I. (2016). Non-orthogonal multiple access (NOMA) in cellular uplink and downlink: Challenges and enabling techniques. *arXiv preprint arXiv:1608.05783*.

[12] Ali, S., Hossain, E., & Kim, D. I. (2016). Non-orthogonal multiple access (NOMA) for downlink multiuser MIMO systems: User clustering, beamforming, and power allocation. *IEEE access*, *5*, 565-577.

[13] Fang, F., Zhang, H., Cheng, J., & Leung, V. C. (2016). Energy-efficient resource allocation for downlink non-orthogonal multiple access network. *IEEE Transactions on Communications*, *64*(9), 3722-3732.

[14] Luo, F. L., & Zhang, C. J. (Eds.). (2016). *Signal processing for 5G: algorithms and implementations*. John Wiley & Sons.

[15] Sun, Q., Han, S., Chin-Lin, I., & Pan, Z. (2015). On the ergodic capacity of MIMO NOMA systems. *IEEE Wireless Communications Letters*, *4*(4), 405-408.

[16] Bai, L., Choi, J., & Yu, Q. (2014). *Low complexity MIMO receivers*. Springer International Publishing.

[17] Kaltenberger, F., Ghaffar, R., & Knopp, R. (2009, September). Low-complexity distributed MIMO receiver and its implementation on the OpenAirInterface platform. In *2009 IEEE 20th International Symposium on Personal, Indoor and Mobile Radio Communications* (pp. 2494-2498). IEEE.

A review of data security challenges in Wireless Sensor Networks(WSN)

R.K. Sharma

United University, Prayagraj, India

rajiballa@rediffmail.com

***Abstract*—Wireless Sensor Network (WSN) is a combination of hardware and software network that uses a system of sensors to detect physical phenomena. WSN is being widely used in industrial and consumer applications. Privacy is a key factor of WSN, it is imperative to secure data that is used, transmitted, or stored. Data security is a major challenge in today's world of the information age.The control of equipment from a remote location requires a wireless network, like the internet, IoT, in the whole process we need various sources, types of data to be transported over communication channels utilizing various protocols, The modem receives data through different passages which may be corrupted and damage our system, consequently may be a threat to security. This paper introduces various challenges and methodology to protect the data from a facility to be transported from source to destination.**

***Keywords*—Wireless Sensor Network (WSN) Internet of Things IoT, General Data Protection Regulation(GDPR), California Consumer Protection Act(CCPA)Sarbanes Oxley Act(SOX), Health Insurance Portability and Accountability Act(HIPAA),**

I. INTRODUCTION

Wireless Sensor Network (WSN) is a combination of hardware and software network that uses a system of components and sensors to sense the physical parameters, this massive digital data is shared all over the world through router and gateways. Smart systems like IoT using web network with devices and sensors to share the data with other systems.

Data security is a big challenge in an industrial environment because the sensor produces very highly sensitive data to control the process, this data is when converted into packets according to protocols of the channel, and transported over the media, then there are chances of data corruption. The data security can not be detected at the source, hence the error correction code is required to be augmented with the data at the source itself. Thereafter proper decoding checksum is to be used to get the data in its original form. In a long-distance wireless communication system, Sometimes noise is introduced with the message transmitted over the channel. Proper clipper and clamper should be applied to increase the strength of the signal.In this paper challenges and measures like cryptography , Data aggregation, firewall ,AI , Multicloud, data erasure, are explored and various Regulating agencies are reported.

II. COLLECTING -PARAMETERS

The device parameters like temperature, voltage, and current are in analog form at the initial stage,which is being converted into a suitable digital form and suitable communication protocol. Wireless media supports IoT, remote monitoring, telemedicine, telerobotics, etc.

The sensor gives analog data which loses its originality during conversion from analog to digital at the source or digital to analog at the destination,which is corrected by data conditioning.

III. IMPORTANCE OF DATA SECURITY

Digital information is affecting every walk of life and business today from the Internet of Things (IoT) sensor to Robot and Energy generation process control to Smartgrid End-users. It is required to protect digital information from corruption. unauthorized access, cybercrime, human error, etc.Data security involves creating tools and technologies, for protection like the Masking of data, encryption-decryption, and automation of feedback to streamline the whole process under regulatory requirements like IEEE standards of protocols, this complexity creates more chances of an attack on data as digital information is vulnerable in the public cloud.

IV. REGULATORY AGENCIES

It has become a need to make consumers aware of challenges in data security and governance; this creates an exhaustive need to take initiative in the protection of data. So many data protection and privacy regulation are urged as per demand by business enterprises and consumers. A few of them are Europe's General Data Protection Regulation(GDPR), California Consumer Protection Act(CCPA)Sarbanes Oxley Act(SOX), Health Insurance Portability and Accountability Act(HIPAA), and protection from accounting errors and financial frauds, etc.

V. TECHNIQUES OF DATA SECURITY

a) Encryption:It is a basic transformation of digital information into an unreadable format using various algorithms. It generates a key public or private so that only an authorized person can decrypt the data in its original form. database encryption solution serves as a back-end defence for sensitive volume by utilizing

encryption tokenization, and security key management solutions.

b) Data erasure: it utilizes some software to completely overwrite the data on any storage device to verify the data is unrecoverable. It is more secure than data wiping.
c) Data Masking: It allows the teams to develop applications using real data.it protects personally identifiable information (PII)
d) AI:cognitive computing which is a subset of AI, is used to protect the data. but AI used data from human processes through a large number of inferences which requires more sensitive cognitive capabilities.
e) Multicoud computing:Now the process is required not to protect data only but a large number of applications spanned over various clouds run by business operations which may be public or private.
f) Quantum: Latest technology for data protection provides teeth to the encryption of data in a business environment.

VI. Comprehensive Method Of Data Protection

It involves people, technologies, organizations, and processes to establish policies making information security a buzzword amongst all stakeholders. some as follows

a) **Physical security:**Generally,our data is stored in memories, devices, on-premises, in data centers, or the public cloud there must be adequate facilities to secure against intruders, .climate control and fire suppression method.
b) **Less privilege Access:** This principle should be followed by each organization in the IT world. It means allows minimum people to access the information of database, network, administrative account
c) **Backups:** always keep Thoroughly tested backup copies of all important and relevant data,in a separate main / cache memory. Back again requires the same physical and logical control of security algorithms.
d) **User training:** It is an important practice of imparting education to users about security practices, password hygiene, and awareness about social cyber-attacks .so they can make a human firewall to safeguard the data.

VII. Information Security In Homogeneous Sensor Network

Geo-metrical models[7] of different shapes with real information nodes and Bonds are applied to analyze the best possible route of information with secured data. The optimal network model is used to analyze the change in signal parameters.some important geometric models used to analyze the wireless sensor network are,

1. Simplex diamond with one real information node
2. Simplex diamond with two real information nodes
3. Simplex diamond with three real information nodes

Under these geometrical models, the escalation of predefined real nodes determines the best way of functional bond lengths, for the security of data.

VIII. Conclusion

Information security in homogeneous wireless sensor networks is of utmost requirement meant for the source of information and user as well. The paper has reviewed various measures that should be taken into account before commissioning any wireless sensor network system. The paper also reports different methodologies to provide cyber security of data transported over world wide web.

REFERENCES

[1] Akyildiz, I. (2002). A survey on sensor networks. IEEE Communications Magazine, (pp. 102–114)
[2] Arduino.cc. (2018). Arduino - Introduction. https://www.arduino.cc/en/Guide/Introduction
[3] Adafruit (2018). Adafruit Industries, Unique & fun DIY electronics and kits. https://www.adafruit.com/
[4] Instructables.com. (2018). AT Command Mode of HC-05 and HC-06 Bluetooth Module. http://www.instructables.com/id/AT-command-modeof-HC-05-Bluetooth-module/
[5] Horbaty, S. (2018). Security in distributed systems https://www.slideshare.net/EngHaitham/security-indistributed-systems
[6] Oppenheimer, P. (2018). Security Mechanisms Developing Network Security Strategies, http://www.ciscopress.com/articles/article.asp?p=1626588&seqNum=2
[7] Marek Aleksandera , Mikolaj Karpinskib*a Ternopil Ivan Puluj ,Information Security Measures in Homogeneous Wireless Sensor Networks 5th International Conference on Knowledge-Based and Intelligent Information & Engineering Systems

For MIMO OFDM Systems, the Design of A New MRMDF Structure-Based FFT Processor

Nancy W[1], Deepika V[2], Shobana L[3], Satvika V[4], Saitharun KB[5]

[1-5]Jeppiaar Institute of Technology, Chennai, India

***Abstract*—This research proposes a 128/64-point fast Fourier transform processor (fft-processor) to accommodate future generation Multiple input systems. Base band processor for IEEE 802.11n wireless local area network (WLAN) with multiple output orthogonal frequency multiplexing (MIMO OFDM). A pipelined mixed radix multipath delay feedback (MRMDF) FFT design is given to attain a higher throughput rate. The recommended CPU meets IEEE802.11n requirements by providing FFT operations in 128 and 64 points, as well as varying throughput rates for 1-4 simultaneous data sequences. The mixed radix algorithm is used in this FFT processor. The radix 8 and radix 2 algorithms were chosen as a result. At a clock rate of 300 MHZ, our proposed processor can perform 128-point FFT with four distinct data sequences in 3ns, meeting the requirements in IEEE802.11n criteria.**

***Keywords*—Multiple-input multiple-output (MIMO), orthogonal frequency division multiplexing, 802.11n, Fast Fourier transform (FFT), multiple-input multiple-output (MIMO) (OFDM).**

I. INTRODUCTION

Wireless communication has become more ubiquitous in people's lives in recent years. The improvement of wi-fi conversation technology and generation has been quite rapid thanks to VLSI generation. Several sophisticated communication device designs have been demonstrated to be feasible.

A high-speed, environmentally friendly, and dependable virtual communication device with the purpose of guiding multimedia transmission that includes great voice, video, and other capabilities is in unexpectedly high demand.

(OFDM) is a powerful modulation technology that can be utilised to meet the need. This is a complex modulation technology that efficiently expands channel utilisation while minimising inter-image interference (ISI) and inter-provider interference due to the multi-course effect (ICI).

The multiple-entry multiple-output (MIMO) signal processing technology has been integrated with OFDM for next-generation wi-fi communication devices to improve link performance and transmission robustness over a frequency selective fading channel. The physiological layer of the WLAN/IEEE 802.11n standard was created during this time. It's a project to figure out how to design the physical layer of a MIMO OFDM device with the least amount of hardware complexity and power consumption, with a concentration on VLSI implementation.

The FFT/IFFT processor is one of the most computationally demanding physical layer modules in the IEEE 802.11n standard. According to the IEEE802.11n standard, multiple antennas can send or receive up to four statistics sequences at the same time. As a result, if the traditional approach to solving numerous statistical sequences at the same time is adopted, many FFT/IFFT processors are required within the physical layer of a MIMO OFDM machine. As a result, a MIMO OFDM machine's body layer hardware complexity could be quite high.

This project proposes an FFT/IFFT processor with a single multipath pipelined topology to handle the problem of numerous information sequences in MIMO OFDM applications. The 128/64-factor FFT/IFFT with 1–four simultaneous information sequences could be accommodated inside the recommended CPU with low hardware complexity. Furthermore, a superior radix FFT technique can be used to save strength intake.

The block diagram of a common IEEE 802.11n receiver is shown in Figure 1. There are four RFs, four ADCs, four FFTs, a MIMO equaliser, four de-qam and de-interleaver, a de-spatial parser, a de-puncture, a channel decoder, a synchronisation block, and a channel estimation block. Depending on the selected statistics fee, the modulation approach may be binary section shift keying (BPSK), quaternary section shift keying (QPSK), or quadrature amplitude modulation (QAM) with 1–6 bits. The throughput of this device ranges from 54 Mb/s to over 600 Mb/s, and the execution time should be calculated between 3.6 and four zero seconds.

Due to enhanced VLSI technology, the Fast Fourier Transform (FFT) and Inverse Fast Fourier Transform (IFFT) have been applied in the area of virtual sign processing (DSP) applications. The FFT/IFFT within the OFDM could be crucial for modern-day verbal exchange systems. FFT/IFFT is utilised to accomplish bottom band multicarrier demodulation and modulation since it is the most important computation block in the OFDM system.

The complicated multiplication operation in the FFT processor uses a lot of electricity. A larger radix set of rules has fewer complex multipliers. To keep electricity dissipation to a minimum, better radix FFT set of rules [4] can be used. To keep complicated multiplications under control, our structure employs a three-step radix-eight set of rules.

An N-Points discrete Fourier transform (DFT) is defined as for a sequence x(n).

$$\mathbf{X[K]} = \sum_{n=0}^{N-1} x(n) W_N^{nk} \qquad \text{k=0,1,2,3.....127}$$

Where x(n) and X[K] are complex numbers. The twiddle factor is

$$W_N^{nk} = e^{j2\pi nk/N} = \cos(2\pi nk/N) - j\sin(2\pi nk/N)$$

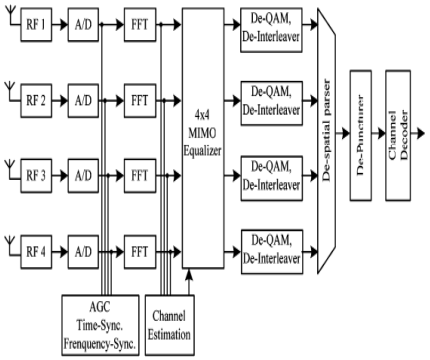

Figure 1. Block diagram of the receiver for IEEE 802.11n standard

Furthermore, the MIMO OFDM device will have far more computational and hardware difficulties than today's SISO OFDM device. A green FFT/IFFT processor can now manage high speeds with reduced hardware complexity, as well as having a cheap hardware cost and a high throughput rate. The excessive radix approach can be used to reduce electricity consumption.

II. FFT Processor For MIMO OFDM Systems

Memory-based FFT architectures and pipeline-based FFT architectures are the two types of FFT architectures. Single reminiscence architecture, twin reminiscence architecture [7], and cached reminiscence architectures [8] are the most often used reminiscence architectures. Those reminiscence architectures, on the other hand, no longer overlook high throughput rates. As a result, this research focuses on pipelined FFT architectures. The two types of pipelined architecture are single path delay feedback (SDF) [2] and multipath postpone commutator (MDC) pipelined architecture. In this paper, we integrated the SDF and MDC. Because SDF uses feedback to lower the memory length, MDC uses multipath to boost the throughput rate.

Because 128 is not a power of 8, we can divide it into 2 8 8. As a result, both the radix 8 and radix 2 methods are used in this application. If we utilise 64-point, this indicates that we only use these 8 8. As a result, for our project, we chose the mixed radix technique (radix 2 and radix 8).

A. Algorithm

Since the mixed radix algorithm is derived in detail [5], First let

$N=128$

$n=64n1+n2 \quad \begin{cases} n1=0,1 \\ n2=0,1,\ldots..63 \end{cases}$

$K=k1+2K2 \quad \begin{cases} k1=0,1 \\ k2=0,\ldots..63 \end{cases}$

To create a radix-8 FFT technique more efficiently, we divide the butterfly of the radix-8 FFT method into three phases and use it as a radix-23 FFT process.

III. For MIMO OFDM Systems, A Proposed Processor Has Been Proposed

The architecture of a 128/64 FFT processor is proposed in this paper. It combines the properties of SDF and MDC systems and consists of four modules, two multiplexers, conjugate blocks, and a division block.

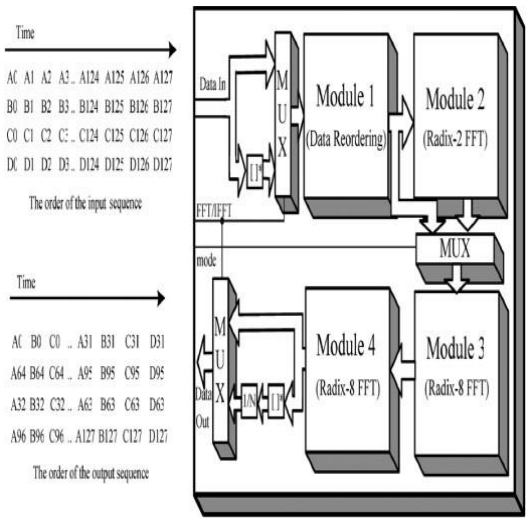

Fig.2. Block diagram of the proposed 128/64-point FFT/IFFT processor

MUX is employed in the block diagram above (Fig2) to assess whether the FFT (or) IFFT processor is required. The conjugate block selection approach is used to carry out IFFT. Module 1 is used for the rearranging of records. If we wish to employ a 128-factor FFT processor, we must finish Modules 2, 3, and 4. We can skip module 2 and focus on modules three and four if we want to employ a sixty-four factor FFT approach. As a result, the second MUX is used to choose an FFT processor with 128 factors (or 64 factors). The manage signal is used to control this MUX. Each 128-factor and 64-factor FFT frequently uses Module 1.

The input order of data in a sequence

	a[6]	a[5]	a[4]	a[3]	a[2]	a[1]	a[0]

Data path	a[0] n	a[1] n					
1st	0	0	a[2]	a[3]	a[4]	a[5]	a[6]
2nd	0	1	a[2]	a[3]	a[4]	a[5]	a[6]
3rd	1	0	a[2]	a[3]	a[4]	a[5]	a[6]
4th	1	1	a[2]	a[3]	a[4]	a[5]	a[6]

The output order of data in a sequence

Fig .3. Relation between the input order and the output order

To use the IFFT method, first choose the conjugate block in MUX, and it will function similarly to the FFT. The FFT output statistics' complicated conjugate can then be taken once more. Then it's divided by the FFT factor quantity, using approach 128 (or) 64 dependent on the actions of the 128/64 factor processor. Module 2 contains the implementation of the radix 2 technique. Modules 3 and 4 are used in the three-step radix 8 approach. However, unique schemes are employed in modules 3 and 4.

The entrance and output sequences are in the correct order inside the proposed FFT architecture. In the diagram above, the letters A, B, C, and D signify exceptional entry sequences, which have an index that calculates the number

of FFT points. The index for 128- and 64-point FFTs is 0 to 127 and 0 to 63, respectively.

The order of the output sequences is influenced by the FFT method, the number of statistical paths, and the FFT architecture. The relationship between the enter and output order of statistics is shown in Fig.3 for each statistics series.

A. Module 1

Module1 is used to rearrange the statistics. Because the four entry sequences come from unusual phases. Procedures such as relocating and switching are included in Module 1. A single put off unit was used to separate the four neighbouring sequences at first. Using the switch's best operation, the segregated statistics might then be reordered across four sequences. Finally, the isolated statistics might be changed using the set off elements.

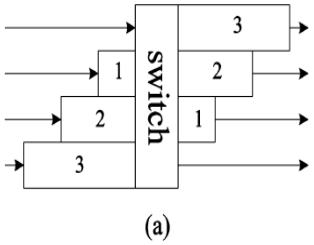

Fig 4 (a): Block diagram of Module 1

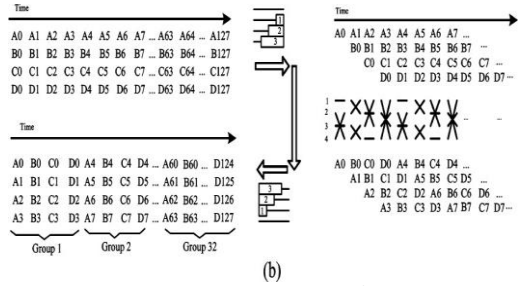

Fig 4(b). Data scheduling and grouping concept of Module1

The reordered facts can be separated into 32 or sixteen agencies for 128- or 64-point. Each institution carries four fact sequences: A, B, C, and D. As demonstrated in Figure 4, any data collection within a single institution has the same FFT index (b). The FFT's operation is fact-dependent in general. The range of factual sequences determines the range of operations in any institution. The institution's range of operations will be one if there is only one way to collect data; if there are three or four ways to collect data, the institution's range of operations will be three or four. Using these facts reordering and grouping methods, FFT/IFFT effectively enforces multiple fact collections.

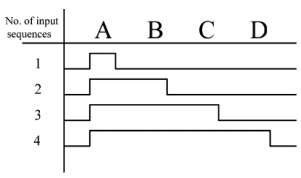

Fig 5. Relation between the number of operation and the number of input sequence in a group.

B. Module 2

This module can be used to function 128-point FFT techniques; nevertheless, we can pass this module if our scheme method uses 64-point FFT methods. Four complex multipliers are utilised in four parallel approaches to implement the radix-2 method. However, the grouping concept and rescheduling the timing of the complex multipliers [5] illustrated in fig.6 are required in our technique to obtain the most effective complicated multipliers. Module 2 is illustrated as a block diagram in Fig. 7 with a memory, four radix-2 FFT technique butterfly gadgets (BU 2), complex multipliers, ROMs, and a few multiplexers.

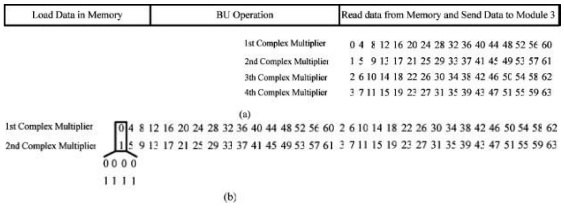

Fig 6. scheduling of the twiddle factors. (a)traditional 4 parallel architecture with 4 complex multipliers, (b) proposed approach with 2 complex multipliers.

The use of four data paths in this module necessitates the use of four memory banks

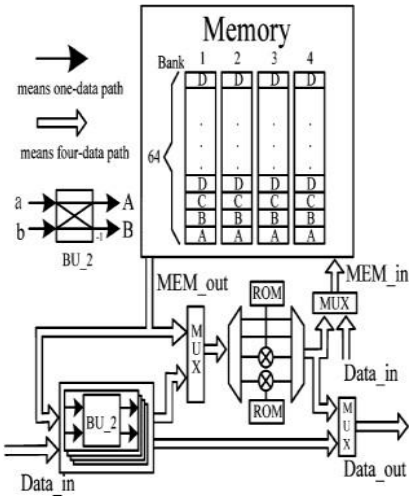

Fig 7. Block diagram of module 2

Four data from memory are transmitted to BU 2 at the same time. The memory size enables for 16 groups of 256 complex data to be stored. BU 2 cannot start until both the input sequences x(n) and x(64+n), with n=0 63, have been received, due to the use of the radix 2 algorithm.

1/8 length cosine and sine waves are preserved in ROM, and those saved values can be used to construct different length waveforms. The first sixteen corporations' records are kept in memory in accordance with the institution's records format. When the records of the following 16 firms are fed into Module 2, the 8 enter records are loaded into four BU 2s, four from the recollection and four from the enter. How BU 2 operates in an institution is determined by the number of records sequences available.

Using the radix-2 FFT approach, four BU 2s yield eight output records; four output records can be sent directly to Module 3, while the other four output records can be stored in memory. Following the BU 2 procedure, Module 3 receives 16 agencies, which are then fed back into memory.

C. *Module 3*

Module 3 contains three levels and a complex multiplier; in our method, four input records from the previous module are simultaneously transferred into Module 3. The specific record sequences A, B, C, and D are considered a group in Fig. 8. The length of the postpone detail in three tiers is 32 (8 group), 16 (4 group), and eight (as shown in Fig. 8). (2 group).

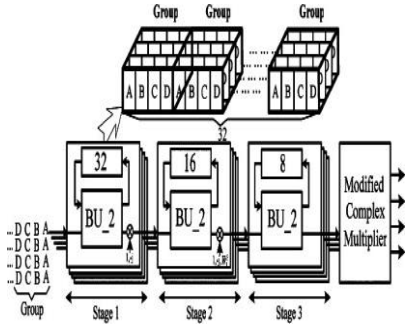

Fig 8. Block diagram of module 3

The put off detail is utilised to store the enter data until the BU 2 operation obtains the opposite available enter data. BU 2 activities at each level, which are the same as BU 2 activities in Module 2. (see Fig. 7). Within the first stage (or) second stage, the trivial twiddle elements are subsequently used to enlarge the output facts obtained with the help of the BU 2. However, by applying the nontrivial twiddle elements concurrently within the adjusted difficult multiplier [5], the four output data from Module 3's third stage must be raised.

D. *Module 4*

Figure 9 shows the block diagram for Module 4. The three-step radix-8 FFT set of rules is revealed in Module 4. The second and third stages of Module 4's plan differ from Module 3's in that the two available BU 2 information are contained within the atypical information paths. Before being transmitted to the next phase, some of the output data created by the BU 2 inside the first and second stages is accelerated by the nontrivial twiddle components.

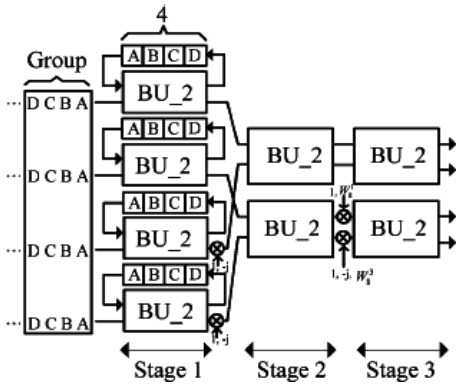

Fig 9. Block diagram of Module 4

IV. Results Of The Simulation

In this architecture, the information phrase duration is 8 bits. At a 300MHZ operation clock rate, a 128-point FFT/IFFT with four data sequences takes roughly 3ns to compute. The high throughput charges of our suggested processor can be calculated using this calculation.

4R operating ratio = effective throughput price

The number of various information sequences divided by four is the operation ratio. As a result, our proposed processor's throughput rate is around 1.2Gsamples/s.

Module 1 simulation findings suggest (data reordering)

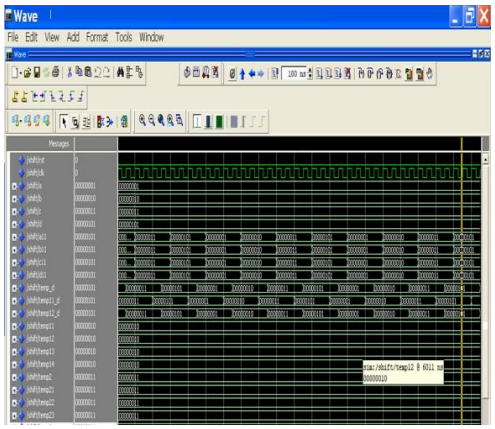

Fig 10. Simulation results for module 1 (data reordering)

V. Conclusion

To boost throughput rate in MIMO OFDM systems, the pipelined blended radix multipath put off feedback (MRMDF) structure has been proposed as a novel 128/64-point FFT/IFFT processor. To lower the quantity of energy consumed, the number of advanced multipliers can be reduced. Using this blended radix (radix-8 and radix-2) strategies, we can reduce the number of challenging multipliers in our proposed work.

References

[1] Mujtaba et al., IEEE 802.11 Task Group 2005, TGn Sync Proposal Tech. Specification, IEEE 802.11-04/0889r3.

[2] H. Shousheng and M. Torkelson, "Designing pipeline FFT processor for OFDM (de)modulation," in Proc. URSI Int. Symp. on Signals, Syst, Electron., vol. 29, pp. 257–262, URSI International Symposium on Signals, Syst, Electron., Oct. 1998, vol. 29, pp. 257–262.

[3] "A 200 MIPS single-chip 1 k FFT processor," in Proc. IEEE Int. Solid-State Circuits Conf., 1989, vol. 36, pp. 166–167, 327; J. O'Brien, J. Mather, and B. Holland, "A 200 MIPS single-chip 1 k FFT processor," in Proc. IEEE Int. Solid- State Circuits Conf., 1989, vol. 36, pp. 166–

[4] W.-C. Yeh and C.-W. Jen, "High-speed and low-power split-radix FFT," IEEE Trans. Acoust., Speech, Signal Process., vol. 51, no. 3 (March 2003), pp. 864– 874.

[5] [5]Y.-W. Lin, H.-Y. Liu, and C.-Y. Lee, "A 1 GS/s FFT/IFFT processor for UWB applications," IEEE J. Solid-State Circuits, vol. 40, no. 8, August 2005, pp. 1726–

[6] 1735.

[7] IEEE J. Solid-State Circuits, vol. 19, no. 10, pp. 702–709, Oct.1984. E. E. Swartzlander, W. K. W. Young, and S. J. Joseph, "A radix 4 delay commutator for rapid fourier transform processor implementation," IEEE J. Solid-State Circuits, vol. 19, no. 10, pp. 702–709, Oct.1984.

[8] S. Magar, S. Shen, G. Luikuo, M. Fleming, and R. Aguilar, "An application specific DSP chip set for 100-MHz data rates," in Proc. Int. Conf. Acoustics, Speech, Signal Process., vol. 4, pp. 1989–1992, in Proc. Int. Conf. Acoustics, Speech, Signal Process., Apr. 1988, vol. 4, pp. 1989–1992.

[9] B. M. Bass, IEEE J. Solid-State Circuits, vol. 34, no. 3, pp. 380–387, Mar. 1999, "A low-power, high-performance, 1024-point FFT processor."

Smart Agriculture

S. Palvesh[1], M. Meena[2], G. Nixon Samuel Vijayakumar[3], A.Vijayalakshmi[4]

[1]Computer Science and Engineering R.M.K. Engineering College, Kavaraipettai-601206, India

[2-4]Department of Science and Humanities R.M.K. Engineering College, Kavaraipettai-601206, India

[1]palv21342.CS@rmkec.ac.in, [2]mm.sh@rmkec.ac.in, [3]gns.sh@rmkec.ac.in, [4]avl.sh@rmkec.ac.in

***Abstract*— From prehistoric times onwards, farmers have always been the backbone of agriculture. Farmers working in the fields, producing food for the world. Farming used to be an extremely time-consuming and labour-intensive way of production. As years progresses, labour-intensive procedures are replaced by capital-intensive processes that produce more with less effort. In India, smart farming or smart agriculture is required to help farmers increase their production and income. This analysis delves at the many sensing devices used in smart farming and their benefits and drawbacks.**

***Keywords*—IoT, sensor, precision, impacts**

I. Introduction

Modern technologies are utilised to increase the efficacy of agricultural products. The agriculture industry requires infrastructure to measure, monitor, automate, and analyse processes using new technology such as big data, the cloud, and the internet of things (IoT). Modern Information and Communication Technologies (ICT) are being applied to agriculture[1], resulting in a Third Green Revolution. Agricultural sensors provide data that allows farmers to monitor and optimise their crops by adapting to environmental changes. The agriculture firm needs such sensors in weather stations, drones, and robotics. Farmers should move away from old farming paradigms and toward a data-driven strategy by using agricultural sensors. They can increase their return on investment by tailoring their yield to market demands and reducing any expenses that could impact their rate of interest. Sensors also let farmers apply an analytical mindset to every phase of the crop's life cycle, from seed selection to harvesting.

II. Objectives Of Smart Farming

- Increasing agricultural productivity and incomes in a sustainable manner.
- Adapting to climate change and increasing resilience
- Whenever possible, reducing and eliminating greenhouse gas emissions.

III. Precision Farming

Precision farming is one of the most common IoT applications in smart agriculture. This farming method is based on data and analytics collected through IoT sensors and devices deployed on farm equipment and surveillance devices [1]. Achieving the target will necessitate climate-smart agriculture. It is a powerful tool in food-insecure nations when applied efficiently and based on local crop and site-specific characteristics. As a nutshell, in less-developed areas, the adoption of new approaches should begin with a simple, inexpensive, and successful mix of technologies and practices.

A. IoT sensors

An IoT smart farming solution is a platform that uses sensors to track crop development and control irrigation systems ((for example, sunlight, moisture, temperature, soil humidity, crop yield, etc.). Farmers can examine their fields from any location [2]. Farmers can employ sensors to figure out how efficient their fertilisers are. Alternatively, livestock farmers can employ IoT sensor data analysis to track animal habits including eating patterns and sleeping cycles, which can reflect diseases or stress levels.

Sensors of many types are used in agriculture to include smart agriculture. In India's agriculture sector, the following are the most widely used contemporary instruments and sensors.

- Sensors that detect location
- Sensors that detect light.
- Chemical sensors

- Mechanical sensors.
- Airflow sensors and dielectric soil moisture sensors

B. Location Sensors

GPS-based sensors, GIS-based sensors characterize the land with the help of drones [3], thus helps in knowing the soil composition and other relevant details.

C. Optical Sensors

These sensors help in analysing the light reflected back from the crop yield, thus gives an interpretation on components of soil and its quality. This also helps in finding the nutrient deficiency of the soil.

D. Chemical Sensors

Change in pH levels of the soil affects the growth and quality of the plants. These chemical sensors alleviate the problem by signalling the conditions of the soil at the right time.

E. Mechanical Sensors

No till farming explains the sustainable development. So with the help of mechanical sensors, the amount pressure required to till the land can be determined. These sensor preserves the land by the forceful excursion on pressure on the soil

F. Dielectric Soil Moisture Sensors

The humidity level of the soil can be best understood with the advancement in technology. The moisture sensors help in preserving the soil from excess water and also indicates exact amount of water needed for the healthy growth of plants.

G. Air Flow Sensors

Air pockets in the soil helps in irrigation and indicates health of the soil. Based on the texture of the soil and air pockets existing in the soil, required amount of nutrients can be supplied to the crops at the needy times.

IV. Positive Impacts Of Smart Farming

- The benefits of smart agriculture may be easily quantified by enhancing the efficiency with which fertilisers and insecticides [4] are applied to crops.
- As per an Iranian case study, it was found that using smart agriculture farming lowered input costs. There were also some positive environmental effects.
- Energy resources were conserved 90.7 percent of the time when precision agriculture was implemented. Furthermore, 99.2 percent of the time, when subsurface and surface water use decreased.

V. Negative Impacts Of Smart Farming

- One major problem of smart farming is that it requires an endless or constant internet connection to be successful, which makes it impractical to use in rural communities [5], particularly in developing nations where mass crop production is common.

VI. Conclusion

Smart farming is a wonderful solution for the farmers in many ways starting from saving electricity to nutrient supply. The technology enabled tools reduces the man power and also helps in cost cutting. It saves farmers money by reducing the amount of money they spend on maintaining capital-intensive technologies. In smart agriculture, artificial intelligence is employed to improve wireless monitoring, regulation, and data collection. With these inputs, high-quality crop production is possible in the near future. Smart farming, on the other hand, employs high-end technologies that require technical expertise and precision to succeed. Many farmers, however, lack these skills. It's difficult, if not impossible, to find someone with this degree of technical knowledge. And for many promising farmers, this can be a hindrance to embracing it.

REFERENCES

[1] A. Chakraborty, A. Banerjee and S. Saha, “"Sensors in precision agriculture: a survey on application, security and privacy”, Advances and Applications in Mathematical Sciences Volume 18, Issue 9, July 2019, Pages 949-957 © 2019 Mili Publications

[2] M. Ayaz, M. Ammad-Uddin, Z. Sharif, A. Mansour and E. -H. M. Aggoune, "Internet-of-Things (IoT)-Based Smart Agriculture: Toward Making the Fields Talk," in IEEE Access, vol. 7, pp. 129551-129583, 2019, doi: 10.1109/ACCESS.2019.2932609.

[6]

[3] P. K. Reddy Maddikunta et al., "Unmanned Aerial Vehicles in Smart Agriculture: Applications, Requirements, and Challenges," in *IEEE Sensors Journal*, vol. 21, no. 16, pp.17608-17619, 15 Aug.15, 2021, doi: 10.1109/JSEN.2021.3049471.

[4] https:// www.mouser.in/applications/smart-agriculture-sensors/

[5] https://www.rfwireless world.com/ Terminology/ Advantages-and-uses-of-Agriculture-Sensors.html

Fingerprint Based Person Authentication System Using Siamese Resnets

J. Jeffrey Joan, Naveen Sriram R., Uma Maheshwari D., Prithiviraj V.S., Dr. Veluchamy

Department of Electronics and Communication Engineering and Computer Science Engineering, Sri Venkateswara College of Engineering

I. INTRODUCTION

Authentication is one of the key features in security. Biometric authentication is considered to be the speedy investigation as its unique to each person. Still, there are numerous ways of the inputted ***fingerprint [1]*** image to degrade the image quality. Poor image quality when fingers are wet or dirty, and false positives due to the ease of forgery are two prevailing issues. Capacitive sensors' performance decreases when common contaminants are present, e.g., water, lotion, condensation, etc. The recently developed ultrasound fingerprint reader addresses the shortcomings of current technologies. In the paper there is two major neural networks being used ***Siamese [2]*** and ***residual network [3]*** (ResNets) is being used to find the similarity in the varied finger print due to the above-mentioned poor image quality factors.

II. RESIDUAL NETWORK:

In order to fully learn the intricate features, we build a very deep neural network. Very deep neural networks are prone to vanishing gradients and exploding gradients. In order to avoid this phenomenon, we use a residual network as our base network.

III. SIAMESE NETWORK:

The purpose of using a Siamese network is to calculate the similarity score between a pair of inputs. It is generally used when there are plenty of classes and very little and very less training data for each of the classes. It is generally used in One-Shot learning. Here, we take two of the above residual networks as the model in the left side and right side. The Siamese network takes a pair of images as input for both the residual base networks. Each model outputs a vector the Euclidean distance between both the vectors is calculated. The loss function used here is ***contrastive loss[4].***

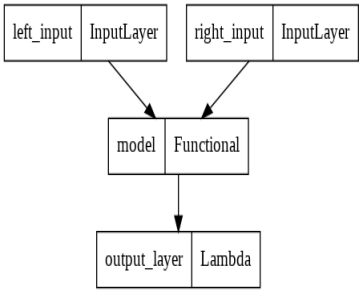

IV. CONTRASTIVE LOSS

The loss which is generally used for a Siamese network is Contrastive loss. It basically minimizes the Euclidean distance between similar pairs of inputs and maximizes the distance for dissimilar pairs of inputs. Below is the formula for the contrastive loss function

L = Y * D^2 + (1-Y) * max (margin — D, 0) ^2

were, Y - True label value of the sample

D - Euclidean distance between the outputs of the base networks

max - takes largest value of the parameters margin - The margin defines a radius around the vector space around the sample.

V. SOCOFING DATASET:

The SOCOFing dataset contains 6,000 fingerprints belonging to 600 African subjects. There are 10 fingerprints per subject and all subjects are 18 years or older. SOCOFing contains unique attributes such as labels for gender, hand and finger name. Moreover, synthetically altered versions of these fingerprints are provided with three different levels of alteration for obliteration, central rotation, and z-cut using the STRANGE toolbox. STRANGE is a unique framework for the generation of realistic synthetic alterations on fingerprint images. Alterations were done using easy, medium and hard parameter settings in the STRANGE toolbox over than a 500dbi resolution images. Therefore, we receive a total of 17,934 altered images with easy parameter settings, 17,067 with medium settings, and about 14,272 with hard parameter settings. In some cases some images did not meet the criteria for alteration with specific settings using the STRANGE toolbox, hence the unequal number of altered images across all three alteration categories.

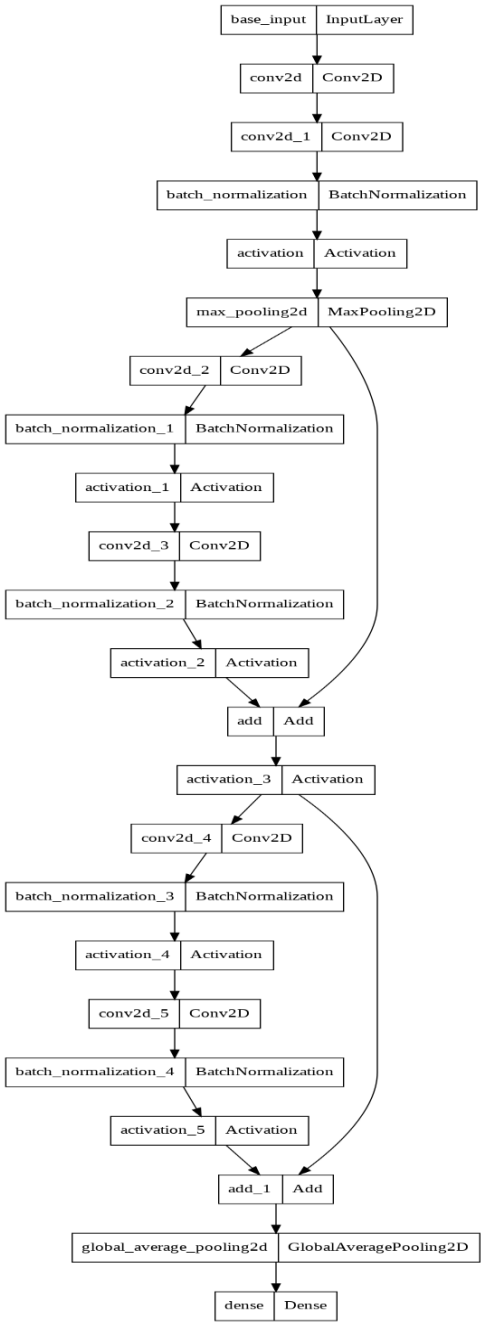

VI. Conclusion

By taking threshold value of 0.5 for final sigmoid layer we are able to classify into original and forgery thumb prints. There is significant accuracy, recall and precision with notifiable accuracy of more than 95% in the test set. The following Siamese resonates model has surpassed various other previous model's bench mark.

References

[1] https://www.kaggle.com/datasets/ruizgara/socofing

[2] https://proceedings.neurips.cc/paper/1993/file/288cc0ff022877bd3df94bc9360b9c5d-Paper.pdf

Secured Dynamic Substitution box Design using Linear Trigonometric Transformation

B. Sarala, G.A. Sathish Kumar, A. Shalini, A. Subhapriya, T. Thivya

Department of Electronics and Communication Engineering,
Sri Venkateswara College of Engineering, Sriperumbudur, Kancheepuram District, Tamil Nadu, India.

***Abstract*— In today's developing world, digitization plays a major role. Though the world has becoming fully digitalized, there is a negative side on it, which is data theft. When the confidential data is shared over the internet, it is unsafe to attack by the hackers. This type of data theft leads to misuse of data of the individual. To prevent and protect these attacks in an effective way, substitution boxes are being used. In this paper, to strengthen the data security and protect it from the attackers, dynamic improvised substitution box is generated by using linear trigonometry transformation. Standard strength analysis is pertained to the proposed s-box to prove the cipher strength.**

I. INTRODUCTION

Modern world has made many changes in the data communication. Nowadays data transformation mostly happens over the internet. Each and every firm of technology needs data and that data is used for several purpose .Data and documents are most important properties of any firm or organization. Protection of those data from the attackers is another issue due to this developed technology. The attackers easily intrude over the network by breaking all the security walls. Taking all these into account they have introduced a term called cryptography which is actually derived from the Greek word 'Kryptos' that means hidden. The main aim of this cryptography is to hide and protect the data from the intruders.This technique has further more developed and is still developing, contributing its best to protect and secure the data. Cryptography uses ciphers to hide the original information from the network invaders. These ciphers are categorized into two: stream ciphers and block ciphers. In stream ciphers.encryption is done in bit by bit. But the speed is lesser than the block ciphers. Stream ciphers are used where the system has very least computational resources. Stream ciphers are taken into account when efficiency is not considered. Block ciphers transform the data in block wise.The block length is predefined in nature. Cryptography has major divisions (i.e.) symmetric cryptography, asymmetric cryptography, hashing. Symmetric cryptography utilize single key for both encipher and decipher process,whereas asymmetric uses one key for the encipher process and another key for the decipher. Hashing uses one algorithm and not a key. In block ciphers, substitution is the important element and s-box takes part in producing a non-linear relation between the plain and cipher text. The plain text denotes the original information which is to be sent to receiver and the cipher text denotes the one which gets shuffled or rearranged or enciphered by the s-box. More stronger the s-box more security is furnished for the data transformed.

II. PROPOSED S-BOX

The Substitution box is designed to make a confusion between the plain and cipher text which creates difficulty for the invaders to know the original information sent .It prevents the attackers by increasing the complexity of the s-box generation. In this paper, to make the s-box more efficient and dynamic, a linear trigonometric method is used. By using this method for the generation of s-box increases its non-linearity characteristics. The s-box is generated in two stages. The s-box is first generated by applying the transformation which results in the initial s-box and then shuffling is applied to the preliminary s-box which produces final s-box with improved non-linearity and complexity.

III. TRIGONOMETRIC TRANSFORM METHOD:

The given s-box is of n x n s-box which has n=8.the parameters involved in the transformation are a ,b ,c and x. the number of parameters used in the transformation makes it more complex.

Stage 1: Initial s-box is formed with the linear trigonometric transformation.The algorithm for the s-box generation is given below and it is also represented in the figure 1.

The mathematical representation:

$T(z) = \cos((A + B) * X * z + C)$

where, $0 < X < 1$, $0 \le z \le (2n - 1)$,B * z, and A,C = { 1, 3, . . . , 2 n − 1}

IV. ALGORITHM 1

Preliminary n x n s-box
Input parameters:
n= 8 // for n × n S-box
x // 0 < x < 1
a, c // a, c 10 { 1, 3, ..., 2 n - 1 }
b //b ∈ { 0, 1, 2, ..., 2 n - 1 }
Output parameters :
S//preliminary n x n s-box
Initialization:
g ← 0
For h=1:256

```
r= (a+b)*x
K(h)=cos(r*h+c)
  if(x>0.5)then
     x=x*x
  else
     x=x*1.75
  finish
h++//h=h+1
Finish
g++//g=g+1
For g=1:256
 min =k(1)
 loc=1
 h=1
For h=1:256
  If(min>k(h))then
     Min=k(h)
     Loc=h
  Finish
   H++//h=h+1
Finish
S(g)=loc
K(loc)=111
g++//g=g+1
Finish
   Return s
```

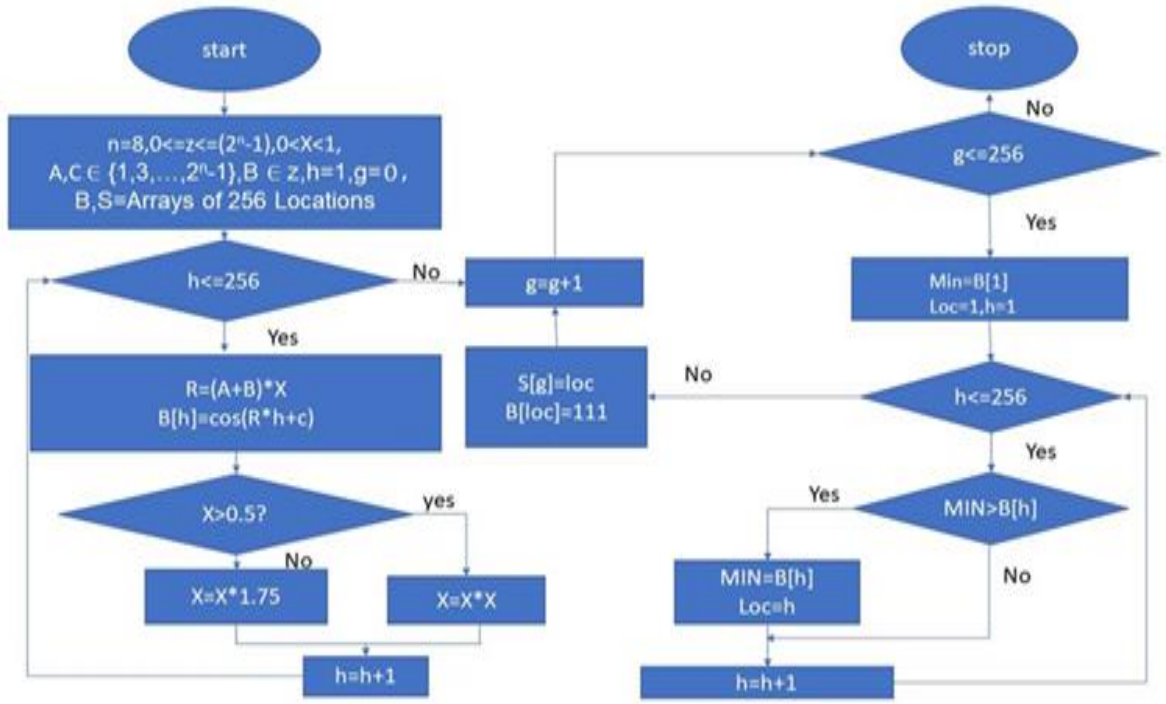

Figure 1 : Flow chart for the generation of preliminary s-box

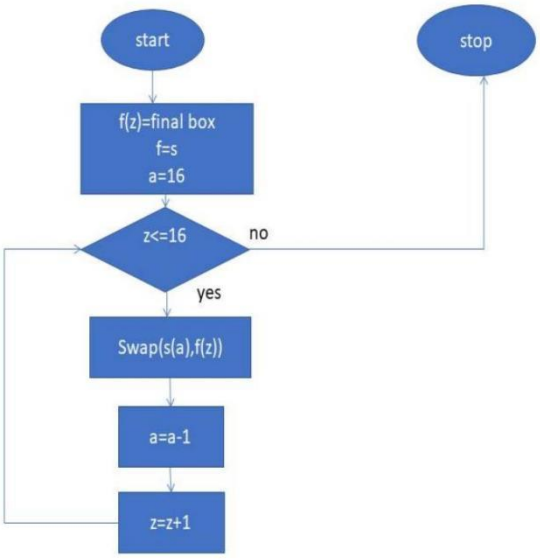

Figure 2: Flow chart of final s-box

Stage 2: Final s-box

The initial s-box gets shuffled by swapping the s-box values in the first row and this makes the proposed s-box more dynamic and improvises its non-linearity. The algorithm for the improvised s-box is given for the first row and the same set of process should be done for the remaining number of rows .finally all the rows of the preliminary s-box gets shuffled and results the final s-box. Flow chart of final s-box is shown in figure 2. The output for the final s-box is also shown by providing inputs for the parameters.

Algorithm : Final s-box

a=16//denotes the number of s-box elements in row 1
Output parameter : f//final s-box
Initialization:
a=16//denotes the number of s-box values in row 1
F=s
for z=1:16
T=s(a)
S(a)=f(z)
F(z)=t
A--//a=a-1
Z++//z=z+1
Finish

Strength analysis of the proposed s-box:

There are certain standard analysis to analyse the security in quantitative and qualitative manner. The proposed s-box satisfies the criteria in an elegant manner.

1. Bijectivity:

Bijectivity criterion necessitates that a unique k-bit input for a n x n s-box should result in a unique k-bit output and also similarly it should have a unique k-bit input for the outputs produced in the n x n s-box. The propounded s-box satisfies this criteria and an example with different parameter values is displayed in figure 1.

2. Non-linearity:

Non-linearity criterion is the one which creates a link between the n-bit inputs and the n-bit outputs. When there is a linear function between input data and output,the data cannot be ptotected from the attacks and its cryptographic strength is very less. But this propounded s-box has its non-linearity property to the maximum level as it has no linearity between the given inputs and outputs. Thus the s-box satisfies this criteria in a graceful manner.The graph shown in figure 3.

3. Bit independence criterion:

Any two bit gets changed in the output bit when there is a modification in one bit even. The given s-box gets satisfied to this criteria in an efficient manner.

4. Strict avalanche criterion:

When the single input bit changes in the input,then half of the output bits get changed. This s-box fulfills this criteria in a graceful manner.

TABLE 1: S-BOX WITH PARAMETERS A =1,B=3,C=7,X=0.1

162	59	203	4	169	36	81	113	222	141	184	129	32	74	211	224
212	131	18	201	115	9	253	21	90	93	130	219	216	134	158	61
180	84	26	51	37	121	232	144	17	16	240	210	194	112	43	147
205	230	41	128	75	250	150	178	108	151	30	248	71	69	56	192
254	8	95	185	13	239	168	223	177	163	11	127	24	241	233	136
171	135	214	146	15	175	220	189	27	52	25	142	89	234	111	228
101	132	160	170	78	197	227	164	143	46	231	86	167	73	237	2
193	31	103	204	96	179	123	124	102	173	80	92	174	66	3	140
198	72	7	54	154	100	105	246	48	152	215	226	14	126	70	22
182	242	87	176	209	23	44	236	256	187	35	156	148	88	57	85
79	68	159	221	137	191	208	251	225	181	145	238	200	206	138	172
247	98	106	114	19	45	139	38	65	109	125	63	47	183	83	1
188	235	255	53	77	42	157	20	199	217	29	213	252	58	34	49
10	28	118	116	190	166	161	82	33	202	55	12	76	117	196	67
140	3	66	174	92	80	173	102	124	123	179	96	204	103	31	193
149	91	229	122	155	120	110	133	207	195	244	165	119	97	40	107

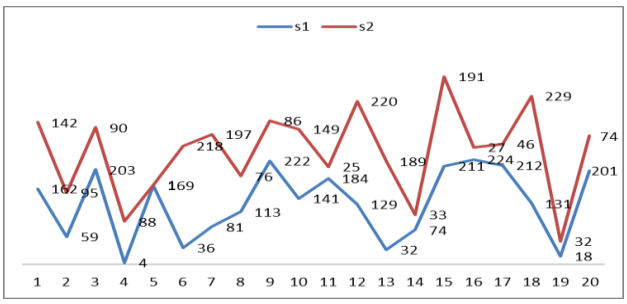

Figure 3: Non-linearity of proposed s box.

V. CONCLUSION

With the help of trigonometric transformation and diffusion process, this research constructed a simple dynamic substitution box. A new dynamic performance improvisation strategy is proposed to improve the nonlinearity score of a preliminary S-box constructed using a novel trigonometric transformation. Dynamic nature of linear Trigonmetric transformation and improvised s- box, use various parameters in their evolution, and cypher key uses the values to the respective parameters. Each time the cypher key is changed, the parameter values change, and a new nonlinear S-box is created. Comparative analysis helps to the construction of dynamic and stable S-boxes.

REFERENCES

[1]. X. Yan, S. Wang, A. A. A. El-Latif, and X. Niu, ''Visual secret sharing based on random grids with abilities of AND and XOR lossless recovery,'' *Multimedia Tools Appl.*, vol. 74, no. 9, pp. 3231–3252, May 2015.

[2]. M. Tanveer, G. Abbas, Z. H. Abbas, M. Waqas, F. Muhammad, and S. Kim, ''S6AE: Securing 6LoWPAN using authenticated encryption scheme,'' *Sensors*, vol. 20, no. 9, p. 2707, May 2020.

[3]. L. R. Knudsen and M. J. B. Robshaw, *The Block Cipher Companion*. Berlin, Germany: Springer-Verlag, 2011.

[4]. A. A. El-Latif, X. Niu, and M. Amin, ''A new image cipher in time and frequency domains,'' *Opt. Commun.*, vol. 285, nos. 21–22, pp. 4241–4251, Oct. 2012.

[5]. M. M. Lauridsen, C. Rechberger, and L. R. Knudsen, ''Design and analysis of symmetric primitive,'' Tech. Univ. Denmark, Lyngby, Denmark, Tech. Rep. 382, 2016.

[6]. L. Li, B. Abd-El-Atty, A. A. El-Latif, and A. Ghoneim, ''Quantum color image encryption based on multiple discrete chaotic systems,'' in *Proc. Federated Conf. Comput. Sci. Inf. Syst.*, Sep. 2017, pp. 555–559.

UI Based Solution for XSS Vulnerability Detection and Report Analysis

Yukesh Kumar S,* Sneha S, Sujitha R, Sakthi M, Vaishnavi M, Sathya Priya S, T.J. Jeyaprabha

Department of Electronics and Communication Engineering, Sri Venkateswara College of Engineering, India
**yukeshkumar622@gmail.com*

***Abstract*— 'No website is secure'. All websites we encounter everyday has certain bugs, which may lead to malicious attacks. Bugs can seriously impact your company's growth. Just one bug could have a far-reaching impact on your bottom line which causes a business downtime. It may lead to defacing websites, complete takeover of websites, phishing and also company's data and reputation losses. Customers usually prefer to use websites and apps that are secure and bug free. So, we have come up with an effective web application that tracks the status of bugs present and report the same to the client. Here the client who seeks to secure their website, post their domain in our web application. Our technology examines the client's website for flaws, resolving their effects, and finding their sources. A script enumerates subdomains, filters out living hosts, scans for vulnerabilities, and checks for cves. On the server side, we employ bash scripting and Golang tools to pen test the website. The obtained findings are then compiled into a report and delivered to the customer for review. The program includes capabilities for evaluating major patterns, which development teams may use to avoid reoccurring difficulties that cause process disruptions. It offers a centralized case workflow where problems can be tracked and fixed in real time. Businesses may handle all of their defects in a single interface, cooperate effectively, and save time using this strategy.**

***Keywords*—Cybersecurity, web application, bugs, XSS vulnerability, payload.**

I. INTRODUCTION

In today's environment, a user can send and receive data in the form of audio, video, and pdf with the touch of a button, without knowing how safe the data is. Securing a user's private information and privacy is becoming increasingly difficult. Because of loopholes in the system or server, cybercrime is on the rise. A spammer commits cyber-crime in order to steal a company's crucial information or private information. Many large corporations and government agencies are taking numerous precautions to secure private information and avoid cyber-crime. Cyber security can help prevent a cyber-attack. Practical measures to secure information, networks, and data from internal and external threats are included in cyber-security. Professionals in cyber-security safeguard networks, servers, intranets, and computer systems. This ensures that only those who are permitted have access to the information.

II. MORE ON BUGS AND ITS DETECTION

Software bug is a mistake, error, or flaw in computer software that causes it to generate an inaccurate or unexpected result, or act in unexpected ways. Bugs can seriously impact company's growth. It may lead to malicious attack. Just one bug could have for reaching impact on your bottom line when they cause business downtime. It may lead to defacing websites, complete takeover of websites, phishing, company's data and reputation losses. For example, in case of payment application, if website is insecure the user credentials may be retrieved by hackers and it may lead to loss in reputation of company. Customers want to visit websites that are safe and free of bugs.

According to research, 65 percent of customers will not return to a site if their credentials are compromised.

A bug tracking system (also known as a defect tracking system) is a web application that tracks website issues and reports them to the client.

A bug tracking system is typically a required component of a professional software development infrastructure, and its constant use is regarded as one of the "hallmarks of a strong software team".

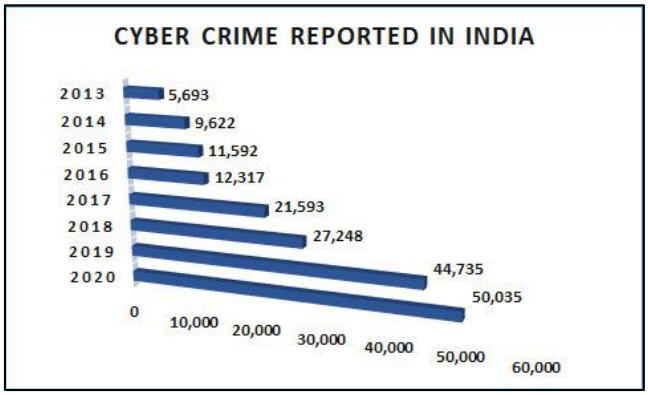

Source: (Cyber Crimes in India Spiked Nearly Nine Times Since 2013, UP Topped Chart in 2020: Data (news18.com))

III. MORE ABOUT XSS

A. Cross site scripting:

A online security issue known as cross-site scripting (XSS) allows an attacker to alter user interactions with a vulnerable application. It enables an attacker to circumvent the same origin policy, which is intended to keep websites separate. Cross-site scripting flaws allow an attacker to impersonate a target user and execute any activities or access any of the victim's data. If the victim user has privileged access to the application, the attacker may be able

to take complete control of the app's functionality and data.

B. Working:

Cross-site scripting is carried out by injecting malicious JavaScript into a vulnerable website. When malicious code is executed in a victim's browser, the attacker has total control over how they interact with the application.

C. Impacts:

The severity of an XSS attack is usually determined by the compromised user's status. For instance: When all users are anonymous and all information is public, the impact is frequently minor in a brochureware application. The impact on an application that stores sensitive data, such as banking transactions, emails, or medical information, is frequently significant. The impact will usually be serious if the affected user has elevated rights inside the program, allowing the attacker to gain complete control of the vulnerable application and compromise all users and their data. Preventing cross-site scripting can be simple in some cases, but it can be much more complicated in others, depending on the application's sophistication and how it handles user-controllable data.

D. Prevention:

In general, avoiding XSS vulnerabilities will almost certainly need a mix of the following measures:

On arrival, filter the input. At the point where user input is received, filter as precisely as possible depending on what is expected or legitimate input. Encode the data on the output. To avoid being mistaken as active content, encode user-controllable data in HTTP responses. A combination of HTML, URL, JavaScript, and CSS encoding may be necessary depending on the output context.

IV. Benefits Over Existing System

Bugs discovered by testers during the software testing process are reported to the Project Manager and Developer via shared lists and emails. The majority of businesses communicate this information via a document called a "defect report." Because there is no specific tracking system in place, this technique is prone to errors, and there is a good probability that some defects will go unnoticed. Every member of the software development life cycle team should be informed of the status of every defect that has been reported. The current system falls short of this need, affecting each team member's productivity and accountability**.**

The current system is slow and will only scan Vulnerability for a single URL. However, if the domain is provided, our suggested method will return all susceptible URLs.

V. Deeper Insights On Our Ui Design

A website serves as a link between technology and scavenging minds. It allows us to enjoy the experience of identifying our satisfying need. Similarly, our user interface is meticulously designed to be simple to understand and is developed in an uncluttered manner. The frontend is built primarily with HTML, CSS, BOOTSTRAP, and JAVASCRIPT. They are perfectly blended together to improve the user's experience. To begin, our homepage is designed to entice users to embark on a journey with our process (figure 1). It has a navigation bar that allows you to quickly navigate to the desired location. Then, to get a sense of our scripts and technology, our essential features are shown in a concise manner (figure 2). The scanning section (figure 3) is then submerged, where the user inputs the domain name (example: www.domain.com) and begins the process of identifying the issue. The susceptible parameters are presented correctly when our scripting process compiles successfully, allowing the user to work on the vulnerability easily. Then, in order to understand our working domain, our functionality and specializations are addressed (figure 4). Finally, because users are our first concern, a full-featured contact section is available to maintain flawless dual-way communication and to address constructive criticism for user issues (figure 5).

(Figure 1)

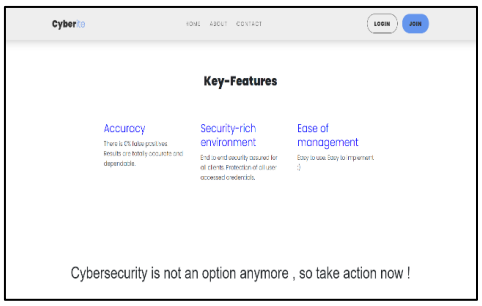

(Figure 2)

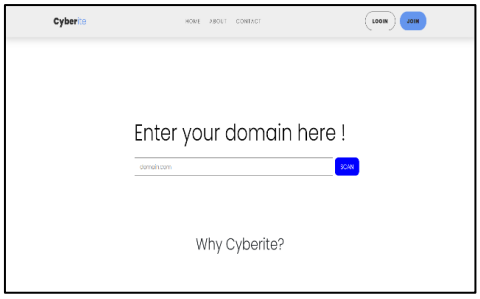

(Figure 3)

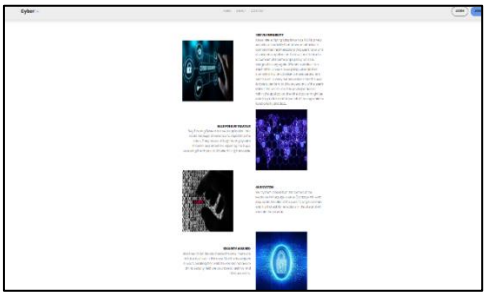

(Figure 4)

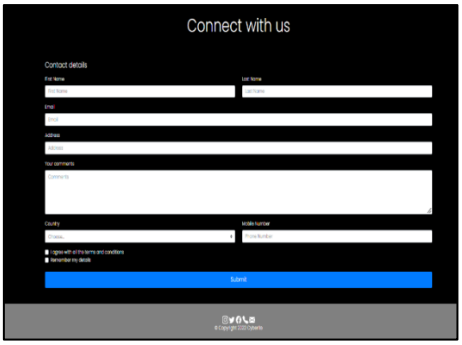

(Figure 5)

VI. Our UI's Unique Features

1) It is incredibly user friendly and automated, with nearly little manual laborious work or procedures.
2) A one-stop solution that provides a virtual platform to help all growing brains uncover vulnerabilities with ease and speed, as well as a broader range of accuracy.
3) A completely synchronized online station for resolving vulnerability issues with corrective actions in a few steps.

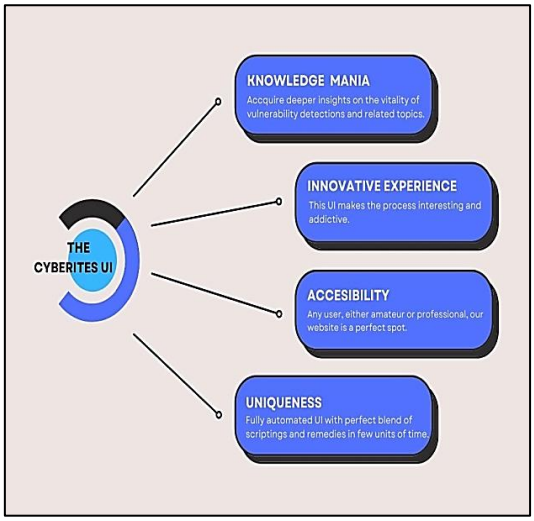

(A CRISP FLOWCHART TO KNOW MORE ABOUT OUR UI DESIGN)

VII. Our System in Action

Python Flask is used for backend scripting. It's where we blend html, CSS, and JavaScript files that went into making the user interface. Bash scripting is used to automate the process of filtering out susceptible URLs. We have a field on our website dedicated to getting the user's domain. The bash script starts to run when the user presses the 'SCAN' button.

The automation uses the 'Request and Response' approach. The fundamental idea behind this automation is that every susceptible URL within a domain has a '=' parameter that can be exploited to verify the website's reliability. We include payloads and check for vulnerabilities using these settings. Generally speaking, secure websites do not enable such payloads to be mirrored on the webpage, however URLs with an XSS vulnerability do not sanitize inputs and allow malicious code to run.

1) 1)First, we use the 'waybackurls' command to get all the URLs in the provided domain.
2) This displays a list of all the website's URLs. We then filter out all URLs that have the '=' argument. We run our payload through this parameter. The acquired results are saved in a file.

```
waybackurls domain.com | grep "=" | tee urls.txt
```

3) Then, next to the '=' argument, we apply payloads to each and every URL. The payload we're using here is an alert message that appears when an image is missing.

There are two probable outcomes:

- The current URL is not susceptible when the payload is not reflected in the webpage, hence it skips to the next URL
- Another option is for the payload to be run in the webpage and the alert message to be displayed. If that's the case, malicious code could be delivered over such URLs. This shows the presence of an XSS vulnerability and such vulnerable URL is printed.

  This procedure is repeated until all URLs have been scanned.

4) Finally, we'll be able to see a list of all URLs that are vulnerable to XSS (Figure 6). This can be checked by going to any URL and manually putting any payload next to '?param=' and seeing how it changes the page. (Figure 7).

By providing a list of susceptible URLs inside a domain, the concerned business or customer will be able to better comprehend the impact of bugs that disrupt processes and take the required steps to avoid them.

The following is a flow diagram of how our system filters out such URLs.

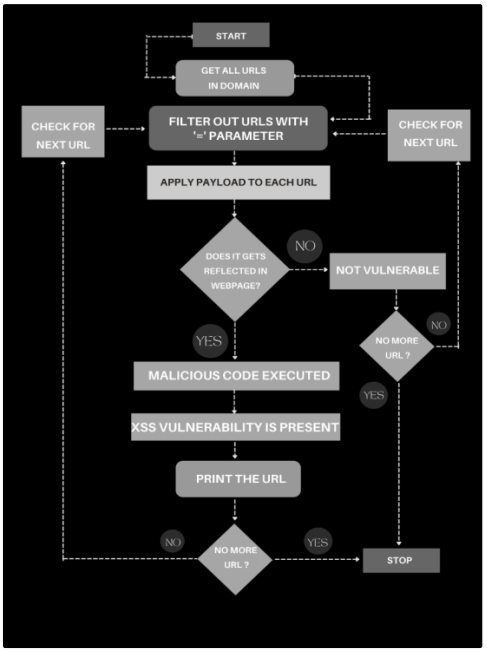

A. *Future enhancements*

This bug tracking system currently detects an XSS Vulnerability. This can be tweaked and improved to detect variety of bugs. Report generation is our future update.

When a bug is discovered, a bug report is generated that includes the severity of the bug, the cause of the bug, bug mitigation, and so on. Each client is also given their own account, which they may access at any time and use to view their previous reports. In the future, we will offer clients memberships with additional benefits such as limitless bug scanning, scanning of higher priority bugs, and so on. Bugs discovered by testers during the software testing process are reported to the Project Manager and Developer via shared lists and emails. The majority of businesses communicate this information via a document called a "defect report." Because there is no specific tracking system in place, this technique is prone to errors, and there is a good probability that some defects will go unnoticed. Every member of the software development life cycle team should be informed of the status of every defect that has been reported. The current system falls short of this need, affecting each team member's productivity and accountability.

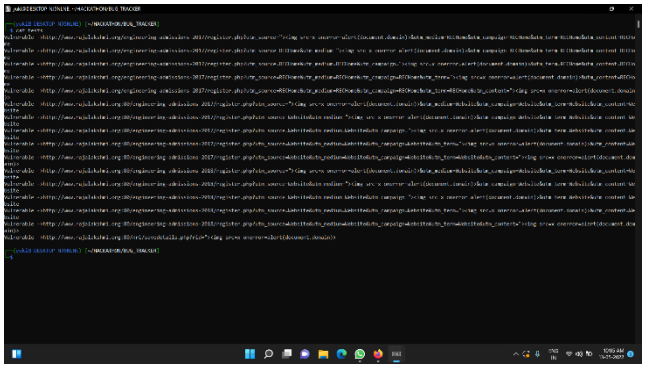

(Figure 6)

VIII. CONCLUSION

The materialistic universe eventually evolves to accommodate current technological advances. One such rapidly evolving technology is cybersecurity. Our technology is intended to detect historical flaws in order to improve the smoothness of the present, which improves the futuristic approach. It is meticulously designed to meet the ease-of-use factor, which is extremely important in today's technological field. Furthermore, our unique magical touch is defined by its speed and accuracy. As a result, until the world evolves, the process of improving the system will be never-ending. Thus, the desire to update it would last forever. Hence, this system is expected to have a significant future impact.

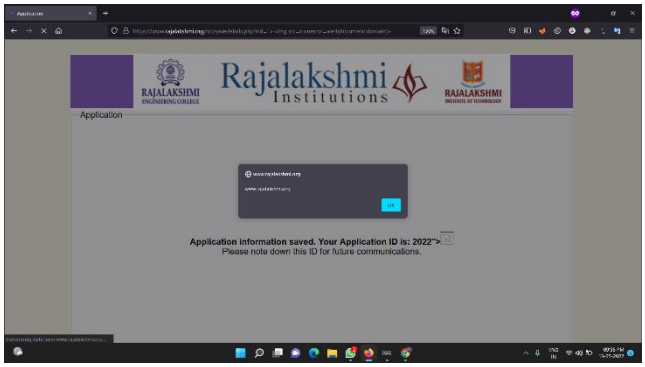

(Figure 7)

REFERENCES

[1] Portswigger.net. https://portswigger.net/web-security/cross-site-scriptin

[2] Acunetix.com. https://www.acunetix.com/websitesecurity/cross-site-scripting/

[3] Research Paper on cybersecurity. https://www.researchgate.net/publication/352477690_Research_Paper_on_Cyber_Security/

[4] Bug tracking system. https://www.geeksforgeeks.org/bug-tracking-system/

[5] A comprehensive review of cyber-attacks. www.sciencedirect.com

THE INSTITUTION OF ELECTRONICS AND TELECOMMUNICATION ENGINEERS

CHENNAI CENTRE

37, Conran Smith Road, Gopalapuram, Chennai-600066